UNCLASSIFIED

AD **400 507**

Reproduced
by the

ARMED SERVICES TECHNICAL INFORMATION AGENCY
ARLINGTON HALL STATION
ARLINGTON 12, VIRGINIA

UNCLASSIFIED

63 - 3 - 1

TRANSLATION

METHODS FOR A DETAILED STUDY OF SEISMICITY

By

V. I. Bunz, M. V. Gzovskiy, et. al.

FOREIGN TECHNOLOGY DIVISION

AIR FORCE SYSTEMS COMMAND

WRIGHT-PATTERSON AIR FORCE BASE

OHIO
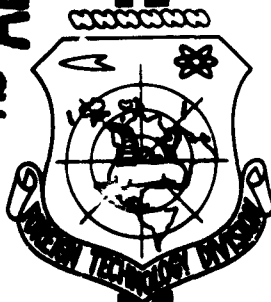
UNEDITED ROUGH DRAFT TRANSLATION

METHODS FOR A DETAILED STUDY OF SEISMICITY

BY: V. I. Bunz, M. V. Gzovskiy, et. al.

English Pages: 544

PREPARED BY:

TRANSLATION SERVICES BRANCH
FOREIGN TECHNOLOGY DIVISION
WP-AFB, OHIO.

Date 28 Feb 19 63

8

METODY DETAL'NOGO IZUCHENIYA SEYSMICHNOSTI

FTD-TT-62-269/1+2

TABLE OF CONTENTS

FOREWORD

This book, dealing with methods for the detailed study of seismicity, is an exposition of the principal results of the work of the Tadzhikskaya Complex

Seismological Expedition (TKSE) of the Institute of the Physics of the Earth, Academy of Sciences USSR, and the Institute of Seismology, Academy of Sciences Tadzhikskaya SSR which was undertaken in the years 1955 to 1957.

The foundation for these investigations was laid by G. A. Gamburtsev, who was Chief and Scientific Director of the TKSE from the moment of its organization to his death on 28 June 1955. His ideas have found embodiment and development in all the principal aspects of subsequent work of the TKSE.

A large body of scientific workers of the institutes mentioned took part in the execution of the described investigations; a number of other Union and republic organizations also participated.

The monograph describes the seismic apparatus used for detailed investigations. It describes new methods for the large-scale determination of the coordinates of earthquake foci worked out on the basis of experience in seismic exploration and detailed methods for determination of the structure of the earth's crust on the basis of earthquake observations by a network of stations. Some results of these determinations are given. Methods are described for determination of seismic energy which allow for the extremely substantial influence of dissipation and absorption of energy, expecially important in the epicentral zone. An analysis is given of the dependence of the dominant frequencies of oscillations during earthquakes on the seismic energy of the focus. Frequency selection apparatus is described and some of the results derived by its use are presented. The results of determination of the dynamic parameters of earthquake foci in the Garmskiy region are given with the statistical processing of the data derived. Estimates and computations are given for the

parameters of earthquake foci and displacements in foci as functions of earth-
quake energy. A method is discussed for use in the study of the seismic regime,
and the results of the use of this method are applied to observational data
relating to the seismicity of the Garmskiy and Stalinabadskiy regions. The
geological structure of the Garmskiy region and the history of its development
are examined. In conclusion, a comparison is made of the spatial distribution
of seismicity with the geological-tectonic structure of the region under investi-
gation.

The individual sections of the monograph were written by the following
persons: Introduction and Chapter 1, by I. L. Nersesov and Yu. V. Riznichenko;
Chapter 2, by I. L. Nersesov; Chapter 3, by I. L. Nersesov and T. G. Rautian;
Chapter 4 by T. G. Rautian; Chapter 5, by K. K. Zapol'skiy and V. I. Khalturin;
Chapter 6, by V. I. Keylis-Borok, L. N. Malinovskaya, G. I. Pavlova, and V. I.
Khalturin; Chapter 7, by V. I. Bune, I. L. Nersesov, and Yu. V. Riznichenko;
Chapter 8, by M. V. Gzovskiy, V. N. Krestnikov, and G. I. Reysner; and Chapter 9,
by V. I. Bune, M. V. Gzovskiy, V. N. Krestnikov, and I. L. Nersesov.

The general editing was done by Yu. V. Riznichenko, who also wrote indi-
vidual passages in various sections of the monograph.

INTRODUCTION

In periods when science is faced with the need for formulating and solving major new problems or more effectively solving old ones, the need always arises for devising new methods of research and for improving those already existing. Present-day seismology is at this stage. Prevailing conditions have imposed on seismology two problems of fundamental scientific and practical importance: a) the geophysical substantiation and improvement of methods of seismic zoning with increasing emphasis on the role of a more objective quantitative approach and b) the search for ways to predict strong earthquakes. Indeed these two problems are the most important of all those in seismology insofar as the national economy is concerned.

Both of these problems, being of a complex nature, require that seismic, geological, and other methods be employed, theory and experimentation be applied, and laboratory and field observations be made. But, to be sure, the basic requirement is systematic and detailed observation and the study of the peculiarities of the nature of earthquakes directly in the regions where they occur — in epicentral zones. The development and improvement of the methods for such research is the subject of this monograph. The actual solution of the two above-mentioned problems, however, is beyond its scope.

History of the Organization of Research

The study of the seismicity of particular epicentral zones has been undertaken repeatedly by the seismologists of a number of countries: the USSR, the United States (California), Japan, and others. The investigations described here constitute an organic continuation of earlier national work in this field in the direction of more detailed study.

The detailed study of relatively small areas within the limits of individual seismically active regions was done earlier in the Soviet Union only sporadically, by means of conducting brief seasonal investigations of an expeditionary character. Such work has already been done for decades, but the

number and scale of investigations increased substantially after the destructive Ashkhabad earthquake of 1948.

The principal objective of such work during the past decade has been the refinement of data on the seismicity of individual particularly active regions. These data were used to explain the relationship between earthquakes and active tectonic structures for the purposes of seismic zoning and for making regional travel-time curves more precise. These data are used by the network of permanent stations for the determination of epicenters and the depths of earthquake foci, etc.

Examples of the largest scale seasonal investigations of this type include work in the vicinity of Ashkhabad and in western Turkmeniva, on the Akhalkalakskoye (Dzhavakhetskoye) Plateau, and in the Shemakhinskaya epicentral zone of the Caucasus, as well as in the Garmskaya region of the Tadzhikskaya SSR. Particular note should be made of the work of the Garmskaya Expedition of the Geophysical Institute, Academy of Sciences USSR (later renamed the Academy's Institute of the Physics of the Earth—IFZAN). This [expedition] served as the basis for the subsequent organization of the TKSE. The activity of the Garmskaya Expedition has been described in detail in a number of articles and reports [1 to 8][1]. The results of its scientific activity have been summed up in an article by Professor V. F. Bonchkovskiy, chief of the expedition [8].

As a result of seasonal work, a type of apparatus has been developed which is suitable for seismic observations in epicentral zones (the D. A. Kharin regional seismographs and a series of high-frequency instruments developed by G. A. Gamburtsev and others). The so-called correlation method for the study of earthquakes—KMIZ—was developed on the basis of such research. The accuracy of interpretation of observations has been increased (thus, the accuracy of determination of the hypocenters of local earthquakes in the course of detailed

---

[1]Reports of the Garmskaya Expedition during 1948-1953, in the archives of the Institute of Physics of the Earth of the Academy of Sciences.

work is about 2-5 km in lieu of the 20 to 50 km which is possible with the usual network of seismic stations). Detailed seismic maps have been compiled for individual regions (the Bogdanovskiy and Shemakhinskiy regions in the Caucasus, western Turkmeniya, the vicinity of Ashkhabad, etc.). As a rule, the only weak spot in these investigations was the qualitative interpretation of the results. This was due to the lack at that time of developed quantitative criteria for seismicity.

Seasonal expeditionary investigations were and still remain an important means for the study of the present-day seismic activity of regions. However, such investigations are inadequate for the study of the nature of earthquakes. The nature of this inadequacy is that in seasonal investigations of the long-term seismic process occurring in a particular region only a particular stage is examined. This stage is brief even in comparison with the known mean period of recurrence of strong earthquakes. This does not make it possible to systematically trace the development of the mutually related seismic processes transpiring in the region in space and over time and to derive a full idea concerning the seismic regime of the particular region. This shortcoming can only be eliminated by the organization of long-term uninterrupted observations.

The continuous study over time of earthquakes in individual regions has long been practiced in the USSR and is continuing, as is also true in a number of other countries. These observations are made by regional networks of seismic stations. But for the most part, the data from such networks apply only to rather strong earthquakes which occur relatively rarely. This makes their study difficult. Not only that, but information on the distribution of the foci of observed earthquakes in space, based on the data of regional networks of stations, is derived with a low accuracy which is often inadequate for reliable comparison with the regional peculiarities of the geological structure and structural development and with local geophysical fields and processes. This shortcoming can be eliminated by the organization not only of lont-term observations, but by

5

more detailed seismic observations as well.

Particular emphasis should be given to the superiority of detailed obser-
bations. These offer an opportunity to study not only the rare strong earth-
quakes but weak earthquakes as well, which exceed the former many times in number.
The study of all earthquake events in a rather wide range of energy, including
weak ones, will in principle make it possible to formulate the problem of explain-
ing the laws which govern the distribution of earthquakes of different energies.
In addition, weak earthquakes felt over small areas can sometimes serve as a sort
of model of seismic processes of greater energy which affect larger areas. This
makes possible with reasonable limitations the extrapolation of the manifested
laws. This method for the study of earthquakes can substantially speed up the
revelation of the general laws governing seismic processes, including those which
are most important for practical purposes—the laws governing the origin of strong
earthquakes.

It follows with complete clarity from these considerations that the study
of the nature of earthquakes requires the establishment of a system of obser-
vations which will permit the study of the seismic process with sufficient
continuity over time and in space and with greater accuracy and detail and in a
wider range of earthquake energies than is done by the usual regional networks
of seismic stations. These principles were formulated for the first time by
Academician G. A. Gamburtsev in his report to a session of the Council on
Seismology of the Academy of Sciences USSR at Stalinabad in October 1953 [9-10].

A permanent year-round Tadzhikskaya Complex Seismological Expedition (TKSE)
was organized in February 1954 by a resolution of the Council on Seismology for
the implementation of the work program assigned to it. The Institute of Seis-
mology of the Tadzhik Academy of Sciences took part in the work of this expedi-
tion on an equal basis with the Institute of the Physics of the Earth. Groups
of scientific workers and individual scientists of other Union and republic
organizations have participated in individual phases of the work of the

expedition. The collaboration of organizations participating in the TKSE has proven productive and in many was has facilitated the successful accomplishment of the tasks which it has been assigned. In the implementation of the work of the expedition, especially during the period of its organization, a great deal of assistance was rendered by the Central Committee of the Communist Party and the Council of Ministers of the Tadzhikskaya SSR. I. L. Nersesov has been chief of the TKS3 since 1955. The scientific director is Yu. V. Riznichenko.

The general work program of the expedition, laid down by its first chief and scientific director, Grigoriy Aleksandrovich Gamburtsev, has retained its significance at all times since its formulation, although to be sure in individual cases it has been repeatedly better defined and expanded. The overall objective of the newly organized expedition from the very beginning of its activity was the study of the nature of earthquakes—their special characteristics and the conditions under which they occur. At first a variety of geophysical and geological methods were employed in the solution of this problem. Later those methods were retained which appeared most promising under specific conditions. These methods were seismological and geological.

Because of the novelty of the general character of the work and its exceptional scope (every year it was necessary to cope with several thousand earthquakes of different intensity within a small area), the workers of the expedition had to revise virtually all of the traditional methods, seismological concepts, and methods used in observing earthquakes and had to analyze earthquake data and adapt them to the solution of new problems. This revision ranged from the elementary concepts of geometric seismics to the methods of earthquake dynamics and statistics. During the years 1955-1958 seismological work was conducted along the following lines: 1) the large-scale determination of the epicenters and depth of foci of earthquakes with an appropriate degree of accuracy, as well as their times of occurrence; 2) the study of the structure of the media in which seismic processes occur; 3) large-scale determination of

7

the seismic energy of earthquake foci and study of the character of attenuation of the energy of seismic oscillations with increasing distance from the focus in dependence on geological conditions and the direction of propagation; 4) the study of the spectrum of oscillations at different distances from the focus under different conditions and for earthquakes of different energy; 5) the determination of the mechanism of the earthquake process at the focus and the ascertainment of its effect at the surface; 6) the most important aspect of the work of the expedition, the study of the seismic regime—ascertainment and study of generalized indices characterizing the totality of the earthquakes of a particular region in space and over time.

Geological and geomorphological work was conducted on a systematic basis in 1955-1957 in conjunction with seismological research. The principal objective of this work was the study of the history of development of seismically active structures and present-day tectonic movements in the southern part of Central Asia. An important characteristic of these investigations was the endeavor to characterize tectonic movements quantitatively. This is necessary for a constructive and effective comparison of tectonics with the quantitative indices of seismicity.

In addition to the execution of a program of seismological and geological research, the expedition engaged in work associated with the development and testing of new kinds of seismic apparatus.

The results obtained in all these fields are described in the sections of the monograph which follow. The systematic aspects of these results can be of interest for detailed investigations of seismicity not only in this and nearby regions of Central Asia, but in other regions of the Soviet Union as well. It is to be hoped that these results will help in forming a geophysical basis of the quantitative methods for seismic zoning which are now being worked out and will contribute to the clarification of the directions which if followed may show promise of solution of the problem of prediction of the places and times of

strong earthquake events. In addition, the new data collectd by the expedition, which reveal the details of the distribution of seismicity in the Garmskiy and Stalinabadskiy regions of the Tadzhikskaya SSR and in certain other regions of Soviet Central Asia, may prove to be of independent interest.

•

CHAPTER 1

GENERAL INFORMATION

In the selection of the Garmskiy and Stalinabadskiy regions of the Tad-
zhikskaya SSR as the principal area for conducting work on the detailed study
of earthquakes, the Council on Seismology was guided by considerations of both
a scientific and practical character. On the one hand, it was necessary to
select a region with high seismicity which would provide a solution to the
problems included in the program in the shortest time possible. On the other
hand, it was desirable that this work could yield results useful for the nation-
al economy of the country, and in the immediate future—while the research
program was still in progress—without awaiting its completion. For this to be
possible, the work area should include areas which stand in need of major anti-
seismic construction work and because of this more precise and detailed data
on its seismicity. The combination of the two regions mentioned—Garmskiy and
Stalinabadskiy—well satisfies these two scientific and practical requirements.
The Garmskiy region is one of the most seismically active continental mountainous
regions of the USSR. Moreover, it is thinly populated, and consequently it is
relatively free of industrial and other artificial interference. The area is
well exposed for geological investigation.

The region of the capital of Soviet Tadzhikistan—the city of Stalinabad—
and its environs is far less seismic than the Garmskiy region, and ther is more
interference to clear geophysical observations. However, the detailed study
of its seismicity is an important practical problem in view of the major hy-
draulic engineering, industrial, and housing construction which is in progress
or is planned here. On the other hand, the Garmskiy region will in the not too
distant future be the scene of hydroelectric power construction work.

Also of fundamental interest for seismology is the opportunity of com-
paring the highly seismic Garmskiy region with the neighboring "normally"
seismic Stalinabadskiy region. A practical aspect of this work was the pos-

sibility of application of several of the general laws established on the basis of the abundant data from seismic observations in the Garmskiy region to the conditions of the Stalinabadskiy region. It had been difficult to derive such laws with sufficient clarity in the latter area because of the relative infrequency of seismic shocks.

Work Area

The Expedition's work area is situated in the central and western parts of the Tadzhikskaya SSR. It has the form of a zone extending in a latitudinal direction and bounded by the coordinates 38°20' to 39°30' N and 68°00' to 71°30'E. (Fig. 1). This area includes the following administrative rayons: Dzhirgatal'-skiy, Garmskiy, Komsomolabadskiy, Obi-Garmskiy, Tadzhikabadskiy, Fayzabadskiy, Ordzhonikidzeabadskiy, Stalinabadskiy, Varzobskiy, and Gissarskiy. The capital of the republic, Stalinbad, is situated in the western part of the studied region.
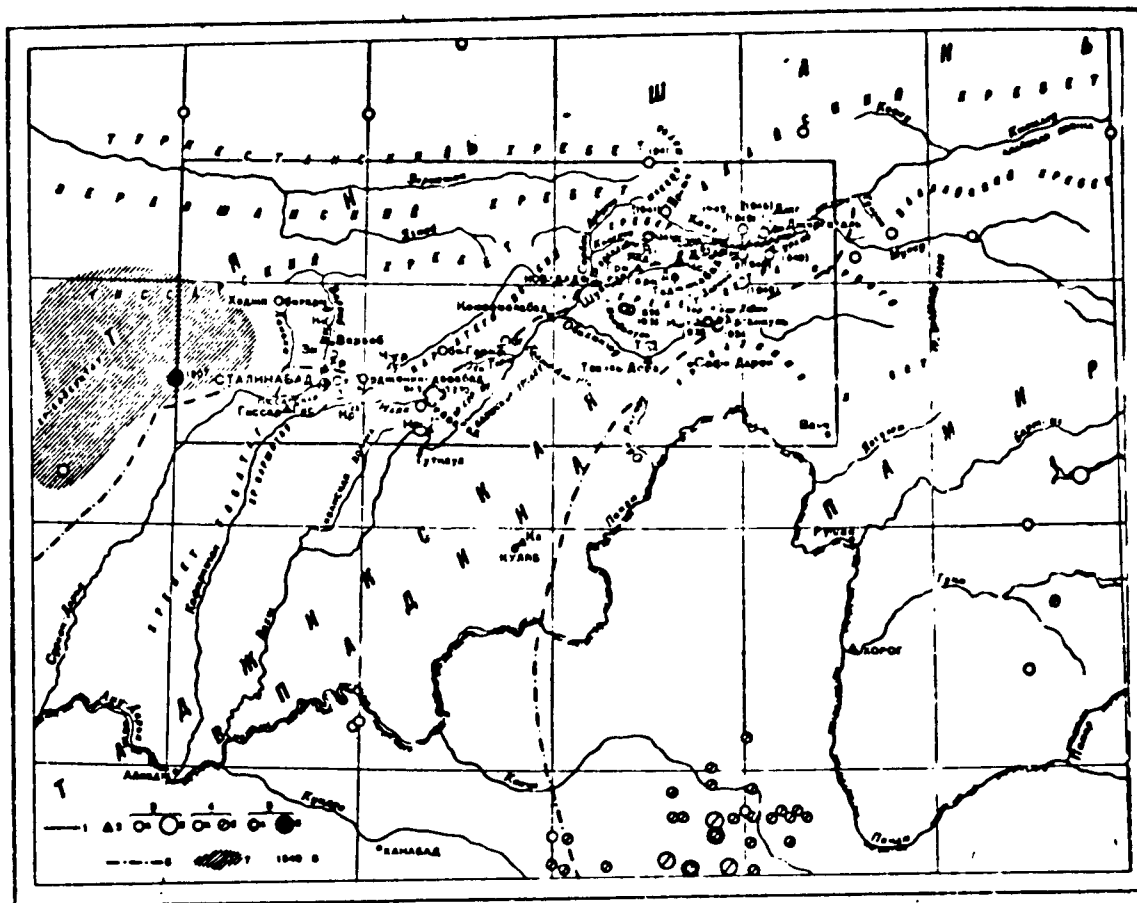
Fig. 1. Location of the work area and seismic stations of TKSE 1-limits of the work area; 2-seismic stations (Boldface numbers refer to full names given in Table 2.); 3-earthquake epicenters (as shown in the Atlas of the Seismicity of the USSR): a - M from 5 to 7, b - M>7; 4-focal depth: a - in the earth's crust, b - under the earth's crust; 5-intensity of the major earthquakes at the epicenter according to macroseismic observations: a - approximate intensity of 8 to 9, b - greater than 9; 6-limits of the Tadzhikskaya depression; 7-areas within the intensity-8 isoseist for the strongest earthquakes; 8-year of occurrence (Parentheses denote repeated events).

Topography

The greater part of the area of the regions under study constitute highly mountainous and strongly dissected terrain, gradually dropping downward toward the west, where the major mountain ranges are replaced by low mountains and piedmont plains. The Expedition's work area includes parts of three of the most important elements of the relief of Soviet Central Asia: the Tien Shan, the Pamirs, and the Tadzhikskaya depression. It is therefore naturally divided into three parts.

The first part, which belongs to the system of ranges of the southwestern Tien Shan, extends in a SW-NE zone along the northern boundary of the region. Within its boundaries in the east there is located the western tip of the Alayskiy Range; in the Matcha Mountain complex this branches westward into the Turkestanskiy Range (the more northerly) and the Zeravshanskiy Range (the more southerly). Elevations in the Matcha complex and in the Turkestanskiy and Zeravshanskiy Ranges exceed 5000 m above sea level. The next most southerly of the ranges, part of the Tien Shan, are the Karateginskiy and Gissarskiy Ranges. Both exceed 4000 m. The eastern part of the Gissarskiy Range runs parallel to the Karateginskiy Range somewhat to the west of it; the former branches off from the eastern part of the Zeravshanskiy Range. The western part of the Gissarskiy Range has a latitudinal orientation, parallel to the Zeravshanskiy Range. The Baysuntau Range gradually drops downward toward the southwest from the western end of the Gissarskiy Range.

The major ranges of the southwestern Tien Shan, enumerated above, posses extraordinarily complex relief. Each of them constitutes a system of ranges and valleys of different orientation. The Gissarskiy and Karateginskiy Ranges have the most complex topography. The peaks of the smaller range of which they consist can in many places be mentally connected by planes which are slightly tilted to the south. Several of these ranges have flat plateaulike tops.

The Gissarskiy and Karateginskiy Ranges are distinctly bounded by major topographic scarps constituting canyon walls or the steep slopes of the valleys of large rivers--the Yagnob, Sorbog, etc.

The second part of the region is its southeastern corner, constituting a part of the Pamirs. This is the location of the Darvazskiy Range with peaks exceeding 4000 m, which is oriented in a SW-NE direction. To the southeast, in the Vanchskiy, Yazgulemskiy, and Akademiya nauk Ranges, as well as northeastward in the eastern part of Petr I Range, the relief rises and the peaks attain heights of more than 6000 to 7000 m.

The third part of the region, with an interior location with respect to the others, consists of the major Tadzhikskaya intermontane depression. Its southern half is located in Afghanistan. Its lowest elevations (300 to 600 m) are found along the axis of the depression, which is followed by the Amu-Dar'ya River and which passes along the National boundary. The relief therefore in general rises to the northward, and the area constitutes a complex of broad valleys separated by ranges with elevations up to 2000 m and sometimes somewhat higher. These valleys and ranges extend from south to north with a slight deviation in a NE-SW direction. On approaching the Tien Shan, the valleys become narrower and the ranges become broader. About 10 to 30 km from the Tien Shan, the ranges are sharply deflected northeastward and join with one another. A zone of low relief extends between their northern ends and the Tien Shan and has a SW-NE orientation. It consists of a chain of isolated valleys with broad flat floors or of hilly and mountainous sectors in which the peaks attain lesser elevations than in the more southerly and northerly sections. The valley of the Surkhan-Dar'ya River is the most westerly link of the chain; it is located near the western boundary of the Tadzhikskaya depression, where it merges with the Baysuntau Range. The Gissarskaya valley, at whose center Stalinabad is situated, is located farther to the east along the northern boundary of the depression where it merges with the Baysuntau Range. Several rivers flow through

14

this common valley in different directions. This is followed by the valley of the headwaters of the Ilyak and Obi-Garm Rivers, which flow in opposite directions. The valley of the headwaters of the Vaksh and Surkhob, in which Garm is located, is situated in the eastern part of the region and belongs to this same chain.

The general northward rise of that part of the Tadzhikskaya depression belonging to the USSR is accompanied by increasing elevations and intensification of the dissection of its relief from southwest to northeast. As a result, the northeastern corner of the depression possesses mountainous relief with absolute elevations of 4800 m; this is the western half of Petr I Range. The valley of the Surkhob region is situated to the northwest of these mountains and the valley of the Obikhingou is situated to the southeast.

Although the eastern half of Petr I Range is topographically connected with its western half, it differs from it by having far greater elevations and a different general orientation. It already constitutes part of the Pamir mountain system.

On the whole the relief of the region is characterized by large relative relief and strong erosional dissection; this makes it quite inaccessible. These factors, in combination with severe continental climatic conditions, are responsible for the good exposure of geological structures.

Some Information on Tectonics

The tectonics of the work area are different in its various parts and reflect the complex history of its geological development. During the Paleozoic the territory of the southern part of Soviet Central Asia constituted a geosynclinal area; that is, it possessed great mobility. Then, during the Mesozoic and the greater part of the Paleogene, the entire territory of the work area, with the exception of the Pamir section, constituted part of an extensive, less mobile platform region which developed after the Hercynian tectonic stage (an epi-Hercynian platform). A part of the region, now occupied by the present-day Tadzhikskaya depression, was distinguished primarily

by downwarping in comparison with the less subsident Tien Shan part of the
region. The Pamir section was part of the Alpine-Himalayan geosynclinal region
characterized by high mobility of the earth's crust.

The next stage in the development of Soviet Central Asia began at the end
of the Paleogene, and this is continuing at the present time. Tectonic move-
ments again became extremely intensive over its entire area. The southwestern
Tien Shan and the Pamirs, which are in part included in the region studied,
are being strongly uplifted although the rate of movement is uneven over time
and varies from place to place. The most important role is played by displace-
ments of slightly folding blocks bounded by fractures in rocks of Paleozoic
age. In the Tadzhikskaya depression area the earth's crust is in some places
experiencing downwarping, while elsewhere the process is one of uplifting,
although is is slower than in the Tien Shan and the Pamirs. Thick deposits
of Tertiary and Quaternary deposits have therefore accumulated in the Tadzhi-
kskaya depression. These strata reveal numerous folds which are continuing to
develop at the present time.

Thus, the three main parts of the region differ from one another in relief
and have different histories of tectonic movements and different present-day
structures. They are separated by large zones of tectonic fractures which
extend to great depths. Great numbers of fractures are also present elsewhere.
Because of this and alo because of high and sharply differentiated mobility,
the entire region as a whole is characterized by high present-day seismicity.

The Most Intense Earthquakes

In seismic respects, the region selected for conducting detailed expe-
ditionary investigations is a single unit and is clearly separated from the
territories which surround it.

On all general seismic maps it stands out due to an unusually dense con-
centration of epicenters of strong earthquakes. Fig. 1 shows the epicenters
of strong earthquakes for this region and surrounding areas on the basis of

data contained in the Atlas of Seismicity of the USSR, in which earthquakes are classified by "magnitudes" M. (For epicenters situated within the boundaries of the Expedition's work area, there is also indicated the intensity of earthquakes by the unit scale.) Here the epicenters are for the most part distributed in a zone which extends from southwest to northeast along the southern boundary of the Tien Shan. On the east it touches the northern boundary of the Pamirs. This zone passes through Stalinabad and stops 150 km to the southwest of it and 250 km to the northeast of it. An exceptionally large number of epicenters of weaker earthquakes is concentrated in this same zone. The density of epicenters decreases in all directions from the work area. The next closest concentration of epicenters is situated far to the northeast (in the eastern part of the Fergana Valley and its mountainous borders) and to the south (on the northwestern slope of the Hindukush) of the work area. In the Fergana concentration, the density of epicenters of strong earthquakes is less than in the work area, but in the Hindukush it is greater [11].

The focal sites in the earth's crust were determined for all of the strong earthquakes in the area under study. In this respect, a similarity was noted with the earthquakes of eastern Fergana. However, the foci of many strong earthquakes in the Hindukush are at a depth of 200 to 300 km beneath the earth's crust and therefore differ substantially from the foci in the work area.

Twelve strong earthquakes have been recorded in this region since the end of the 19th century (Table 1). Besides the strong earthquakes enumerated in Table 1, there also occurred during this same period of time a great number of weak earthquakes with an intensity of 7.6 or less. Their epicenters usually virtually coincide with the epicenters or are grouped near them.

As can be seen from the list, strong earthquakes have occurred at intervals of time from several days to 12 years. There are cases of the repeated occurrence of strong earthquakes at the same places after 44 years (Karateginskiye), after 13 years (Fayzabadskiye), after 1 year (Argankul'skiye), several months

TABLE 1. Regional Earthquakes From 1895

Earthquake	Date	Intensity	Magnitude*
First Karateginskoye	1895	8-9	-
First Karatagskoye	21 Sep 1907	10	-
Second Karatagskoye	27 Sep 1907	9	-
First Fayzabadskoye	1930	8-9	5 1/2
First Argankul'skoye	1934	8-9	6
Second Argankul'skoye	1935	8-9	-
Second Karataginskoye	1939	8	5 3/4
Garmskoye	1941	8-9	6 1/2
Second Fayzabadskoye	1943	8-9	6
Khaitskoye	1949	10	7 1/2
First Tovil'-Dorinskoye	8 Aug 1950	7-8	-
Second Tovil'-Dorinskoye	17 Nov 1950	7-8	-

*M magnitudes after S. L Solov'yev.

(Tovil'-Dorinskiye), and several days (Karatagskiye).

Among the strong earthquakes mentioned, those which have received the greatest attention are the Garmskoye and Khaitskoye earthquakes and the group of earthquakes which have occurred at various times around Stalinabad.

The Garmskoye earthquake of 20 April 1941 was centered with a maximum intensity of 8 to 9 at a distance of 20 km to the northeast of Garm. Its intensity at Garm was estimated at 7 to 8. The territory encircled by the isoseismal line for intensity 7 occupies an area of about 4000 square kilometers. This earthquake was accompanied by the formation of fissures on the earth's surface, landslides, and rockfalls. The energy of the main shock of 20 April 1941 is estimated at 10^{15} J (10^{22} ergs) with M = $6\frac{1}{2}$. This earthquake was followed by many aftershocks during 1941 which attained intensities of 6 and 7.

The Khaitskoye earthquake, with an intensity of 10, occurred on 10 July 1949. Its energy was of the order of 10^{17} J (M = 7.5). It was preceded by a tremor of 8 July with an intensity as great as 8 (M = $5\frac{1}{2}$). The epicenter of the Khaitskoye earthquake was situated 40 km to the east of Garm. The zones of maximum intensity of the Khaitskoye and Garmskoye earthquakes in part overlap one another. During the Khaitskoye earthquake seismic waves caused the collapse of a considerable part of a mountain at whose foot the city of Khait was situated; it was destroyed. There were landslides of unconsolidated soil on many slopes in the vicinity of Khait. Mudflows were formed in the valleys. The territory surrounded by the isoseismal line for intensity 7 constitutes an area of about 6000 square kilometers.

A series of strong earthquakes has occurred near Stalinabad. Fifty kilometers to the west of the city is the epicentral site of one of the strongest earthquakes of Soviet Central Asia—the Karatagskoye earthquake of 21 October 1907—with an intensity of 10. It was felt at Stalinabad with an intensity of 7 to 8. The territory surrounded by the isoseismal line for intensity 7 con-

stitutes an area of approximately 80,000 square kilometers, that is, close to the area of the Pamirs. At the same distance as the Karatagskoye earthquake epicenter, but to the east of Stalinabad, are located the epicenters of the two Fayzabadskiye earthquakes of 1930 and 1943; these were of intensity 8 to 9. Their regions of maximum intensity were small: The territories bounded by iso-seismal lines for intensity 7 only constitute about 40 square kilometers in each case. Many shocks with an intensity as great as 7 have arisen at various times at distances of 10 to 20 km to the wouth of Stalinabad. Finally, in 1952, there was a local earthquake of intensity 7 in Stalinabad itself. These phenomena in conjunction with the geological peculiarities of the region are considered indices of the great seismic danger in the vicinity of Stalinabad.

In conjunction with the normal depth of the foci, the zones of maximum intensity of strong earthquakes in the work area usually are of only insigni-ficant length, not exceeding 50 km (often 10 to 20 km) and are small in width (less than 20 km), the usual long and narrow shape of zones of maximum intensity.

The chief peculiarity of the seismicity of the region is the occurrence of strong earthquakes predominantly near the southern boundary of the Tien Shan. This is due to the fact that this boundary is not only orographic but tectonic as well, and there are many tectonic fractures now developing along it. One of the principal tasks of the geological work, forming part of a unified complex with detailed seismic research, is investigation of the details of the problem of the relationship between seismicity and the pecularities of tectonics, especially the problem of seismogenetic zones of fractures of different orders in connection with their degree of mobility.

Location of Seismic Stations

The selection of points for making seismic observations in the Garmskiy region was conducted on the basis of the work experience of the Garmskaya Expedition in past years and in the Stalinabadskiy region on the basis of seeking to determine more complete data on the seismicity of the environs of Stalinabad.

The selected distribution of observation stations (Fig. 1) makes it possible to solve two problems: first, the making of observations over the entire territory which is situated between Dzhirgatal' and Stalinabad as a whole (work at a medium scale), and second, the making of especially detailed observations in the small but most active region of this territory, Garm-Khait.

Six seismic stations had been established in the Garmskiy region by October 1954: Yaldymych, Yangalyk, Nimich, Chusal, Tovil'-Dora, and Ishtion. Four stations in the Stalinabad area were completed and began to operate by the end of December 1954: Karasu, Gissar, Khorongon, and Kon-Dora. In addition, the Garmskaya Geophysical Station and the Dzhirgatal' Seismic Station were transferred to the control of the expedition.

In 1956 the Yangalyk station was transferred to the village of Dzhafr and the Nimich station to the neighborhood of Stalinabad in the village of Chuyangaron. These changes in the distribution of stations were made at the request of the Presidium of the Tadzhik Academy of Sciences in order to intensify seismic observations in the vicinity of Stalinabad. The Kon-Dora seismic station was transfered to the village of Zimchurud late in 1956.

Table 2 gives data on the code designations of stations and the dates operations began and ended. This same table lists the stations of the regional network of Soviet Central Asia whose data have been used systematically in the analysis of the observations of the Expedition.

TABLE 2. Stations of the TKSE Network (1-16) and Nearby Stations of the Regional Network

No.	Station	Symbol	Period of Operations	
			Begun	Ended
1.	Garm	Grm	1 Jan 1949	
2.	Yaldymych	Yald	1 Jan 1955	
3.	Yangalyk	Yang	1 Jan 1955	10 May 1956
4.	Dzhafr	DF	20 Jul 1956	
5.	Nimich	Nm	1 Jan 1955	12 Jun 1956
6.	Chusal	Chs	1 Jan 1955	
7.	Dzhirgatal'	Dzhg	1 Jul 1950	
8.	Tovil'-Dora	T-D	1 Jan 1955	
9.	Ishtion	Isht	1 Jan 1955	
10.	Karasu	Kr	1 Jan 1955	
11.	Gissar	Gis	1 Jan 1955	
12.	Khorongon	Khr	1 Jan 1955	
13.	Kon-Dora	Kh	1 Jan 1955	25 Jul 1956
14.	Chuyangoron	Chngr	1 Sep 1956	
15.	Zimchurod	Zmch	20 Oct 1956	
16.	Nurek	Nrk	27 Sep 1956	11 Oct 1956
17.	Stalinabad	St	-	
18.	Obi-Garm	Obg	-	
19.	Kulyab	Kl	-	

References

1. Nersesov, I. L. Opyt izucheniya mestnykh zemletryaseniy (Experience in the study of local earthquakes). Moskva, 1953. Candidate's dissertation, Institut fiziki Zemli.

2. Kharin, D. A., V. I. Keylis-Borok, and S. D. Kogan. On methods of seismic observations in the epicentral zone and their interpretation. IN: Akademiya nauk SSSR. Geofizicheskiy institut. Trudy, no. 21 (148), 1953, 27-42.

3. Nersesov, I. L., and L. N. Rykunov. On the processing of [data from] local earthquakes of Garmskaya oblast'. IN: Akademiya nauk SSSR. Geofizicheskiy institut. Trudy, no. 21 (148), 1953, 19-26.

4. Kharin, D. A., and S. I. Masarskiy. Study of epicentral areas through regional seismic stations. IN: Akademiya nauk SSSR. Geofizicheskiy institut. Trudy, no. 25 (152), 1954, 97-112.

5. Keylis-Borok, V. I., and A. V. Vvedenskaya. Stress investigations at hypocenters of the Khaitskaya epicentral zone. IN: Akademiya nauk SSSR. Geofizicheskiy institut. Trudy, no. 25 (152), 1954, 113-123.

6. Bonchkovskiy, V. F. Sloping of the earth's surface as a potential indicator of earthquakes. IN: Akademiya nauk SSSR. Geofizicheskiy institut. Trudy, no. 25 (152), 1954, 134-153.

7. Antsyferov, M. S. On the use of geoacoustic methods in the solution of problems of earthquake forecasting. IN: Akademiya nauk SSSR. Geofizicheskiy institut. Trudy, no. 25 (152), 1954, 157-161.

8. Bonchkovskiy, V. F. Results of the work of the Garmskaya expedition. IN: Akademiya nauk SSSR. Sovet po seysmologii. Byulleten', no. 1, 1955, 31-39.

9. Gamburtsev, G. A. Present state and prospects in earthquake forecasting. IN: Akademiya nauk SSSR. Sovet po seysmologii. Byulleten', no. 1, 1955.

10. Gamburtsev, G. A. Synopsis of the report "On earthquake forecasting." IN: Akademiya nauk SSSR. Izvestiya, Seriya geofizicheskaya, no. 3, 1955.

11. Vvedenskaya, N. A. Methods and results of generalization of seismic-network observations for 1950-1953. IN: Akademiya nauk SSSR. Izvestiya. Seriya geofizicheskaya, no. 6, 1954.

Chapter 2

SEISMOGRAPHIC EQUIPMENT

In a detailed study of earthquakes, high requirements with respect to maximum sensitivity, dynamic range, accuracy, type of frequency characteristic, identity of similar instruments, and economy are imposed on seismographic equipment in the epicentral zone.

In the projects to be described, special equipment was used at all stations, and this equipment was developed earlier for an instrumental study of weak local earthquakes. To improve quality of registration in the equipment, certain design changes and additions were introduced during field trips; in addition to other features, these provided for simplicity and reliability in the identification of seismographic instruments and made it possible to employ a simple stability-control system. This equipment is described in the first section of this chapter. The second section describes new developments in equipment, said developments worked out in the field.

The recording portion of the equipment must provide for recording resolution making possible the reliable determination of time of initiation for various types of waves as well as to carry out a correlation of the vibrations. An important requirement imposed on the recording portion is the one relating to recording economy, a high coefficient of photographic-material utilization, and a low coefficient of electric power consumption.

In addition to seismographic equipment intended for direct recording of earthquakes, special equipment for a frequency analysis

24 .

of seismic vibrations were tested in the field; this equipment was developed by K. K. Zapol'skiy. The description of this equipment is presented in the fifth chapter, together with the observation results obtained through the frequency analysis.

§ 1. Standard Seismographic Equipment

Basic Seismographic Equipment

The selection of equipment is determined primarily by the need for the proper reproduction (with distortion control) of soil vibrations during earthquakes at small epicentral distances. As this requirement was satisfied, it became possible to resolve problems relating to the study of the frequency composition, the amplitudes, and similar dynamic characteristics of vibrations. Seismographic instruments must provide for the recording both of strong as well as of extremely weak earthquakes. It is, for all intents and purposes, impossible to accomplish this with a single set of instruments. Therefore, it became necessary to provide several instruments at each observation point, and these instruments had to have a wide frequency passband, reproducing soil vibrations with small amplitude distortions within a wide dynamic range (with magnification from 10 to 10^5).

In this connection, each seismic station was equipped with a set of VEGIK [not identified in standard references] seismographs by means of which three or four components of shifts in soil were recorded (magnification $V = 20,000$), a less accurate VEGIK channel ($V = 1000$), and a D. A. Kharin vibrograph ($V = 80$-50).

The following instruments, and these proved themselves in operation, were selected as the basic links in the receiving-recording channel: the VEGIK seismograph, the GB-IV galvanometer, and the RS-II oscillograph. Such a complex of instruments is not heavy nor too large

25

in size, it is simple and reliable in operation, it is inexpensive, economic in its use of electric power, and can be adapted easily to the solution of a wide range of problems in regional seismology.

The VEGIK seismograph [13] was selected as the sensing element to detect shift. This choice was based on the following considerations. Because of poor magnification, particulary in high-frequency regions, SGK and SVK [not identified in standard references] [14] were not suitable for the recording of weak earthquakes. On the other hand, the GSKh and VSKh [not identified in standard references] instruments [15], although meeting the requirement of being able to record weak local earthquakes, cannot be used on an inclined installation. In addition, they cost substantially more than the VEGIK instruments. Neither could the KMIZ [not identified in standard references] equipment [16] be used in the given investigations, because it was impossible to carry out continuous re- cording of earthquakes over extended periods of time at moderate expenditures of manpower and resources.

According to its parameters, the VEGIK is similar to the VSKh, but its dimensions are smaller and it weighs less. The VEGIK may be used in its horizontal, inclined, and vertical versions. Depending on the supporting and coil springs used, the proper period of the seismograph may vary within wide limits, ranging from 0.5 sec to 3-4 sec. The seismometer (seismograph) is damped electrodynamically. The design data for the instrument are as follows: length, 30 cm; width, 14 cm; height, 12 cm; total weight, 8.0 kg; weight of inert mass, 1.5 kg; reference length, 9.4 cm; distance from axis of rotation to center of coil, 17.0 cm; magnetic-field strength in the gap of the magnet, approximately 3000 oersteds. The instrument has three

coils situated in the cylindrical gap of the magnet. One of the coils is used for purposes of recording, the other for damping, and the third for the excitation of pendulum oscillations in the daily checking of the equipment.

At first (January 1955 to June 1956) the VEGIK seismographs were used as a four-component inclined (45°) azimuthal installation [17, 18]. From the second half of 1956 on, the azimuthal installations were replaced with three-component units (North to South, East to West, and vertical [Z]).

Individual stations had additional seismographic units: general-type seismographs (SGK and SVK) — the stations at Garm and Dzhirgatal'; there were mechanical seismographs (SMR-II and SRZ [not identified in standard references]) employed at the stations at Garm and Chusal. In addition to these permanent installations, the stations employed other types of seismic receivers during various periods of recording — the MPS-1, the VSN [not identified in standard references], etc.

The GB-IV galvanometer, used by the expedition, is somewhat different from the standard model described in the literature [19]. The magnetic gap of this galvanometer is expanded, and the width of the frame has been increased (up to 2 mm), and the mirror surface has been increased substantially (1.5 x 3 mm). These changes have made it possible to reduce the natural frequency of the galvanometer, to reduce its sensitivity to external tremors, and to employ a weaker light source. All of the galvanometers are placed within a common permanent magnet, a GB-9 or a GB-12 block [20], which makes it possible to carry out recording simultaneously over nine or twelve channels, respectively.

The frequency characteristic of a system with selected values

for seismograph and galvanometer constants is almost flat within a range of 1.5 to 50 cps. This provides a sufficiently precise reproduction of a shift in soil, within the limits of the frequencies generally encountered in the recording of local tremors (see Chapter 5). The flatness of the characteristic substantially facilitates and makes more reliable the strength (energy) classification of the tremor. A standard frequency characteristic for the instrument set is shown in Fig. 2. The calculation of the frequency characteristics and their identification were carried out according to the method described in reference [15]. The absolute magnification of the channel was $(2.0 - 2.5) \cdot 10^4$ at the stations of the Garm District [rayon] and somewhat lower $(1.2 - 1.5) \cdot 10^4$ at the Stalinabad Stations. The latter is attributed to the high level of interference in the Stalinabad District.
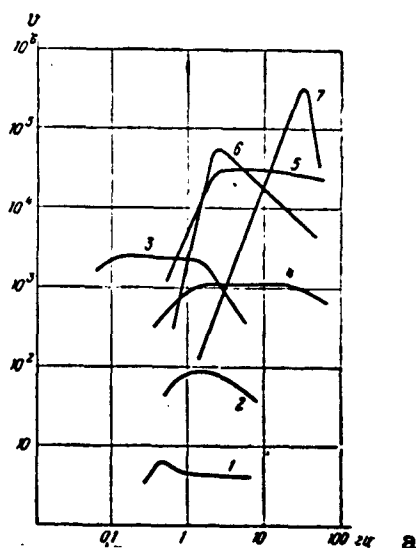
Fig. 2. Typical frequency characteristics of seismic-recording devices. 1) Mechanical seismograph, SMR-II; 2) Kharin vibrograph; 3) Kirnos [sic] seismograph (SGK) [seismograph Kirnos]; 4) shunted VEGIK; 5) standard VEGIK; 6) Kharin seismograph (GSKh); 7) MPS--I seismograph; a) 100 cps.

We must bear in mind that the above discussion involved frequency characteristics for stationary processes. The characteristics for a transitional regime differ quite substantially from these. For example, for the first maximum the amplitude distortions

28

TABLE 3

	1 Параметр	2 Сейсмограф	3 Гальванометр
4	Собственная частота, гц	$f_1 = 1,25$	$f_2 = 12$
5	Постоянная затухания	$D_1 = 0,4$	$D_2 = 3,0$
6	Момент инерции, кг·м²	$K_1 = 9,8·10^{-3}$	$K_2 = 1,1·10^{-11}$
7	Сопротивление рабочей катушки, ом	$r_{12} = 47$	$r_g = 38$
8	Сопротивление катушки затухания, ом	$r_{11} = 47$	—
9	Токовая постоянная рабочей катушки, а на мм на м	$P_{12} = 1,3·10^{-4}$	$P_2 = 5·10^{-6}$
10	Токовая постоянная катушки затухания, а на мм на м	$P_{11} = 1,4·10^{-4}$	—
11	Коэффициент затухания, ом	$a_{12} = 34$	$a_2 = 490$
12	Коэффициент затухания, ом	$a_{11} = 30$	
13	Коэффициент связи системы		$\sigma^2 = 0,2$
14	Увеличение системы		$\bar{V} = 2,0·10^4$

1) Parameter; 2) seismograph; 3) galvano-
meter; 4) natural frequency, cps; 5) at-
tenuation constant; 6) moment of inertia,
kg-m²; 7) resistance of operating coil,
ohm; 8) resistance of attenuation coil,.
ohm; 9) current constant of operating coil,
amps/mm/m; 11) coefficient of attenuation,
ohm; 12) coefficient of attenuation, ohm;
13) coupling coefficient of the system; 14)
magnification (amplification) of the system.

may reach as high as 60 per cent. For all intents and purposes,
it is only with the third maximum that the oscillation amplitude
begins to correspond to the calculated amplitude.

As an example of constants for the system employing the
VEGIK seismograph and the GB-IV galvanometer, used at a conventional
seismic station such as used by the TKSE [Tadzhik Integrated Seis-
mological Expedition], we will present these values (Table 3) for
the Z-component channel of the station at Tovil'-Dor.

Small values of the coupling factor σ^2 enhanced the correct
reproduction of soil vibration [21].

As was pointed out above, for purposes of expanding the dy-
namic range, a MPS-1 seismograph ($\bar{V} = 2·10^5$), D. A. Kharin's vibro-
graph, a VEGIK seismograph ($\bar{V} = 10^3$) coarsened by a factor of 20,

and the logarithmic device by A. N. Vetchinkin were used in addition to the VEGIK seismograph. The total dynamic range of the above-enumerated instruments reaches 10^6.

A MPS-1 seismograph [22] with a natural frequency of 11 cps and low attenuation was connected to the GB-IV galvanometer whose natural frequency is 20-25 cps. This channel exhibited a sharp-resonance characteristic with magnification of $\bar{V} = 200,000$ in a narrow frequency band of 20-30 cps. This band was intended for the recording of extremely weak and nearby tremors. In practice, it turned out, however, that this channel did not provide the necessary quality of recording, and because of the sharp-resonance characteristic its effective magnification was less than nominal. Therefore, after a year and a half (January 1955-June 1956) the use of this channel was curtailed.

For the recording of strong tremors (up to 6 points) all stations have been provided with vibrographs employing the D. A. Kharin system (VKh) [Kharin vibrograph]. This vertical pendulum has a natural period of about 1.5 seconds and an attenuation constant of $D_1 = 0.6$. This device is connected to the GB-III galvanometer whose natural period is 0.3 sec, and the attenuation constant $D_2 = 10$. Both the seismograph and the galvanometer are extremely stable with respect to external vibration. The total magnification of this unit is 50 to 80 in the frequency range from 0.7 to 3 cps, predominant (see Chapter 5) in the spectrum of perceptible earthquakes.

Since there is a substantial discontinuity between the magnification of the VEGIK channel and the VKh vibrograph, all stations introduced an intermediate magnification of the order of 1000. For this purpose, one of the attenuation coils from the VEGIK was connected by means of a shunt to the GB-IV galvanometer. The light

beam from this galvanometer impinges on a narrow screen installed on the recording lens. In the case of small soil-vibration amplitudes, this component produces no recording. With larger amplitudes, however, where the recording of the basic channels cannot be seen (washed out), the coarsened channel may be used to determine the necessary kinematic and dynamic recording features. Examples of earthquake records by means of the coarsened channel are shown in Fig. 62, Chapter 5.

The frequency characteristics of all seismic-recording equipment, used by the expedition, are shown in Fig. 2.

In order to expand the dynamic range of one set of instruments, an attempt was made to use an electron-tube amplifier whose quiescent point was situated in the nonlinear portion of the characteristic. This amplifier, suggested by A. N. Vetchinkin and called "logarifmator' [sic], was connected between the sensing element and the galvanometer. The quiescent point of the amplifier was selected so that the small amplitudes would not be distorted, and the large amplitudes would be recorded proportionally to their logarithms. A specimen of earthquake records by means of and without a "logarifmator' is presented in Fig. 3. By means of the "logarifmator," the dynamic recording range is expanded up to 1000, and this substantially exceeds the possibilities of conventional photographic recording. A shortcoming of this instrument is the somewhat low change in amplitude recording of large vibration amplitudes, as a result of which it proved to be impossible to use these earthquake records (produced with the "logarifmator") for dynamic problems. The presence of a radio circuit in the seismograph-galvanometer link reduced the stability of the set and increased the quantity of electric energy consumed. Therefore, after a number of months, recording by means
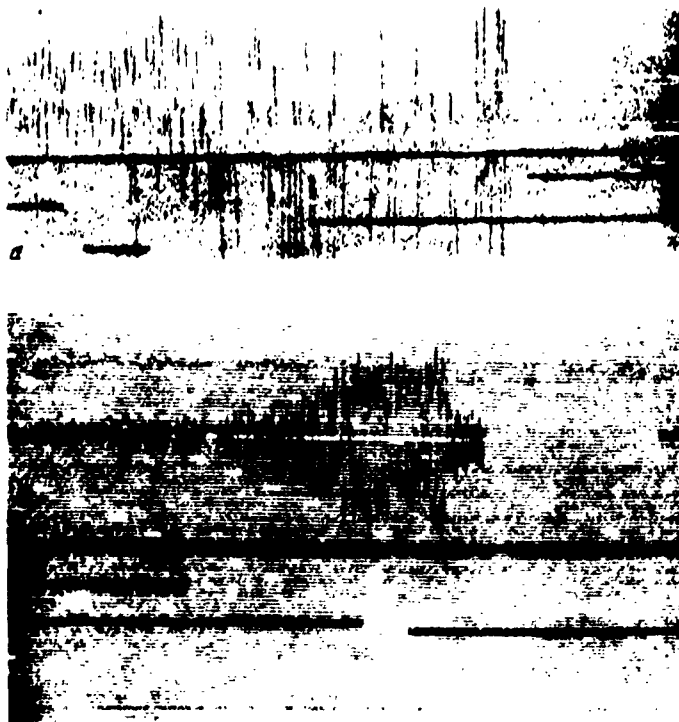
Fig. 3. Recording examples of same tremor.
a) Straight-line recording; b) logarithmic
recording.

of the "logarifmator" was curtailed. Nevertheless, it should be stressed that for purposes of observations in which only the kinematic recording elements are employed, this instrument is of definite interest.

The recording system is based on the use of RS-TI station recorders. However, in comparison to a conventional model, the relationship between the pinions in the head of the clock mechanism were changed so that the guide pinions, designed in a standard head for a speed of 120 mm/min, the clock mechanism runs down at 240 mm/min. The pitch of the lead screw was reduced to 0.5 mm. Using photographic paper 28 cm wide it is possible to record four components in a period of eight hours. The optical recording system

involves autocollimation [23], and the distance between the gal-
vanometer and the recorder is 600 mm.

To resolve certain special problems associated with the study
of oscillation spectra during earthquakes, as well as with a study
of the features encountered in recording shapes, particularly with
respect to various ground conditions, recording devices were employed
in which the "running-down" speed was increased to 35 mm/sec. A re-
cording in this manner is either carried out in short intervals of
time (two hours) or the device is turned on only at the instant that
the earthquake takes place. In the latter case, the first entries
on the record are lost.

Auxiliary Equipment

MGPA. For purposes of monitoring the frequency characteristics
of channels and to check their identity, we make use of a magnetic
constant-amplitude oscillator (MGPA) [24]. This device is connected
to the third coil winding of the seismograph. Moreover, there may
be an irregular pulse on this coil. During the monitoring process,
all auxiliary coils of the seismographs being checked are connected
in series.

Fig. 4. Recording specimen
of MGPA.

A MGPA recording is shown in
Fig. 4. The frequency characteristic
of the channel can be constructed
from this recording [25]. Once a day,
the MGPA signal is transmitted to the
tape. In addition, in the case of azi-
muthal observations, channel identity
if verified by setting up all of the
instruments on the same azimuth, and
this is done for two to three days

Fig. 5. Recording specimen during identity check. Instruments are set on a single azimuth
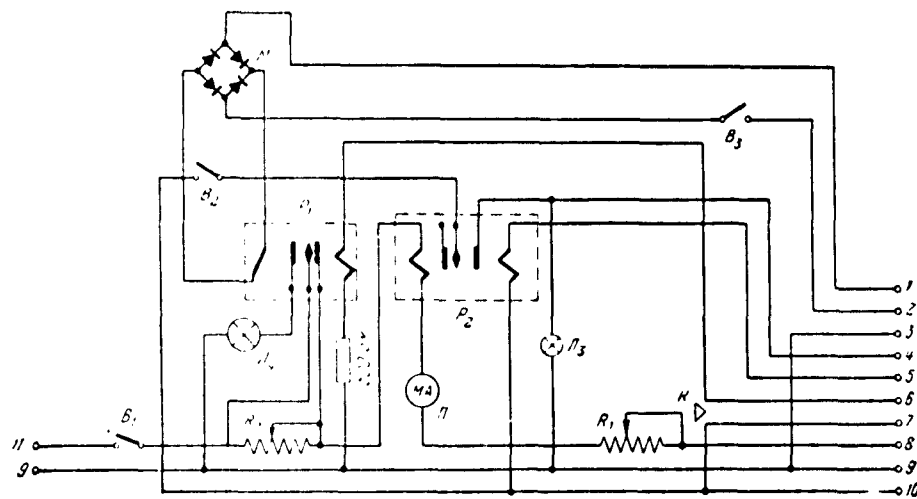
Fig. 6. Main control-panel circuit. П) Milliammeter in galvanometer-light source circuit; M) DGTs bridge for time-signal rectification; K) "start" and "stop" buttons; V_1) general switch; V_2) "emergency" signal switch; V_3 receiver-signal switch; L_4) signal light of time marker; L_3) emergency signal light; R_1) rheostat control of galvanometer light filament; R_2) rheostat to extinguish time marker; P_1) time-marker relay; P_2) "emergency" signal relay; terminals: 1,2) amplifier output of time-signal receiver; 3,4) "emergency" signal output; 3,5) to pendulum post of recorder; 6,7) to chronometer; 8,9) to

galvanometer light; 9,10) to overillumination device; 9,11) common battery terminals.
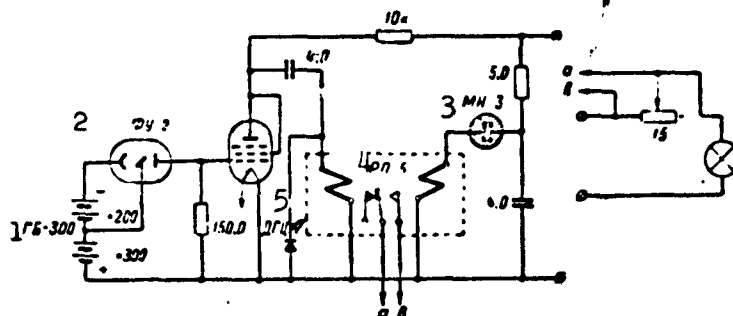
Fig. 7. Brightness-amplifier circuit. 1) GB-3;
2) FU-2; 3) MN-3; 4) RP-5; 5) DGTs.

each month (Fig. 5).

The control panel of a seismic station (Fig. 6). The following operations can be handled from a control panel: 1) time markings are provided by a minute contact chronometer; 2) the light filament can be controlled; 3) the extinguishing of the light channel can be controlled at the instant of time marking; 4) filament voltage is monitored by means of a special receiver for the internal time-marking system; 5) a "Rodina" radio receiver is used to transmit precise time signals to the tape; 6) an audiosignal can be sent in case of an operating malfunction of the station (stoppage of recorder or burning out of light bulb); 7) automatic switching on and off of the special receiver by means of the minute chronometer; 8) the time-marker relay can be shut off during adjustments for the special receiver.

Each station was equipped with a "Rodina" radio receiver and a special receiver for the reception of telegraphic time signals from the expedition base.

The overillumination device. To improve recording quality,
all stations were equipped with special photoelectric devices,
amplifying the brightness of the light source, when the oscilla-
tion amplitude on the recording exceeds a particular value. The
circuit of such a brightness amplifier is shown in Fig. 7. This
device operates in the following manner: the light from a special
light source impinges on one of the operating galvanometers at an
angle different from the angle produced by the basic light source;
from the operating galvanometer the light is reflected to a narrow
screen that has been installed in front of the FEU-2 photo copier.
When the oscillation amplitude reaches the point at which the
light moves beyond the limits of the screen and impinges on a
photocell, the circuit is actuated and switches on an auxiliary
ligh-source power supply. With sufficiently great oscillation am-
plitudes, the switching lag for the entire device, on the average,
comes to 0.1 to 0.3 sec. Specimens of corresponding recordings of
seismic vibrations are shown in Fig. 62, Chapter 5.

Time Service

Seismic expedition stations maintain a time service through
the employment of MKh-1 marine chronometers that have a minute
contact. At least five acurate time signals were received daily.
Thanks to the excellent thermal insulation and periodic checking
of the chronometers, the rate was accurate to within 0.2 to 0.5 sec
per day.

As a rule, the error in the reading of absolute times for the
initiation of seismic waves does not exceed 0.2 to 0.3 sec. The
primary factors responsible for reduced time-reading accuracy are
variations in chronometer rate and nonuniformity of recorder rate.

In order to increase time-determination accuracy, an internal

-36

time service was set up. An MRK-0.5 radio station was set up at the expedition base to transmit precise-time signals. The signals were transmitted only during daylight hours, since at night the passage of radio signals was generally extremely poor.

The circuit functioned in the following manner. The basic chronometer at the Garm station actuated a secondary clock. The contact device of the secondary clock was regulated so that on the 29th minute of each hour a motor was actuated, which in turn actuated a disc on which the call letters of the radio stations had been recorded. At the same time, a power relay switched on the transmitter. On the 30th minute, the transmission of the call letters was stopped and the secondary clock actuated the second chronometer. Breaks in chronometer contact were transmitted for periods of 50 sec. An extended break, corresponding to the beginning of a minute, served as a mark for all stations. After the transmission of the signal, the radio station was shut down. The second chronometer of the radio station was checked against the precise-time signals. Two minutes prior to the transmission, the minute chronometer at the seismic stations was used to start up the telegraphic receiver, tuned to the transmitting radio station. The transmitted signals were picked up on tape. Although the transmission of signals was not always satisfactory, in many instances the recording was sufficiently good and made it possible to determine reliably the kinematic characteristics of the earthquake, to an accuracy of up to 0.05-0.1 sec. A comparison of the recordings of this internal signal against the chronometer rate determined in accordance with the precise-time signals, indicates that the difference rarely exceeded ± 0.1 sec.

From 1956, the internal precise-time radio service no longer

functioned, since it was a rather laborious measure to maintain, and there was doubt as to whether it was justified in terms of the comparitively small refinement of the earthquake observation material.

The experience gained in the utilization of the typical seismic and auxiliary equipment used by the expedition for a period of two years demonstrated that the equipment is sufficiently reliable and operationally convenient and more suitable for the solution of problems dealing with regional seismology than had been the case with the equipment generally used at regional seismic stations in the USSR.

§ 2. Development of New Equipment

In conventional earthquake recording, the greater part of the photographic paper is expended not on the recording of earthquakes, but on the anticipation of earthquakes. Therefore, the thought naturally arises that it would be expedient to develop an automatic device to switch on the recording unit at the instant that the seismic vibrations are initiated.

The direct solution of the problem — the switching on of the recorder motor at the instant that the first seismic waves are received — cannot be satisfactorily achieved because of the lag that is inherent in any mechanical system, and the beginning of the record in this case will, of necessity, be lost.

One of the realistically attainable solutions to the problem of automatically switching on the recording unit in sufficient time is the use of memory cells for the preliminary recording of seismic vibrations, in order to "delay" them, with the subsequent reproduction of the vibrations (oscillations) oscillographically at any desired recorder speed. Such memory cells may be based on

the use of magnetic recording.

Equipment based on this principle has already been in regular use for approximately 10 years for special seismological investigations in Vituotersrand [Witwatersrand] (South Africa). This equipment was used for the precise determination of time and point of origin of a tremor, similar to a nearby earthquake, and we have reference here precisely to the underground blasts that take place in regions of deep gold-bearing mines. A description of the equipment is given in article [26] and in a series of other reports. We would point out that this equipment, in addition to its use for the purposes for which it was originally intended, also makes up part of the automatic station complex used for deep seismic soundings of the earth's crust. In this case, seismic field stations are set up some 400 to 500 km from the epicentral zone of the underground blasts which the stations use. Equipment based on the principle of magnetic memory is also used in Japan [27] for the recording of nearby earthquakes.

The operating principle of such equipment involves the following. The basic unit is a uniformly moving ring made of ferromagnetic tape. The recording and play-back heads are set up at some distance from each other along the tape channel. Electrical oscillations, subject to delay for a predetermined interval of time, are transmitted to the recording head and correspondingly magnetize the recording carrier — the ferromagnetic tape. After a given interval of time, determined by the distance between the heads and the speed of the recording carrier, these oscillations are picked up from the play-back head. With continued forward motion, the recording on the tape is removed by means of the erase head and the tape is again ready to record and "remember" the subsequent oscillations. Thus we obtain an unbroken delay cycle

for all of the oscillations that arrive at the recording head. The delay time (memory) is set to be somewhat higher than the time required to establish the operating regime of the recorder whose mechanism is started at the instant that the first oscillation arrives at the recording head. As a result, the entire process will be recorded, and its beginning will not be lost on the record.

The following technical requirements were taken into consideration in the design of this equipment: the frequency range - from 7 to 20 cps (preferably from 2 cps); dynamic range (i.e., the ratio between maximum reproduced signal and installation noises) - 40 db; nonlinear distortion not to exceed 10%; a chronometer second marking must be provided; the installation must operate from the VEGIK vibrograph to the loop oscillograph; the number of channels is 6, including the time-marker channel; the installation must consume a minimum quantity of energy.

The utilization of a magnetic memory cell requires the magnetic recording and reproduction of electrical oscillations of seismic frequencies, lying in the infrasonic range. However, in the case of magnetic recording, the emf induced in the play-back head is directly proportional to the frequency, as a result of which it becomes so small in the case of the direct reproduction of the seismic oscillations that it is extremely difficult to amplify the signals. Moreover, a certain measure of complexity is encountered in correcting the frequency characteristic of the reproduction amplifier as a result of the need to raise it substantially in regions of low frequencies.

For the recording and reproduction of infrasonic frequencies, we generally employ methods based on the conversion of infrasonic oscillations into oscillations at higher frequencies, and these can

be recorded and reproduced easily by conventional methods of magnetic recording. This conversion can be reduced to the modulation of the carrier frequency by means of infrasonic oscillations. For this purpose, the received signal is transmitted to the input of the modulator where the carrier frequency from the oscillator is modulated by the input signal. The resultant modulated oscillations are recorded on the ferromagnetic tape. On reproduction, the emf developing on the winding of the play-back head are amplified, and the initial signal is separated after rectification from the modulated oscillations.

In the described design, a method of frequency modulation was employed in which the carrier frequency is changed as a result of the seismic signal. These frequency changes are directly proportional to the magnitude of the modulation-signal amplitudes.

A drum mechanism was used as the magnetic memory cell. This drum mechanism is a freely rotating massive brass drum covered with a ferromagnetic layer on its outer surface. The recording and play-back heads are placed a short distance from the ferromagnetic layer by means of adjustment screws, but the heads never come into contact with the ferromagnetic layer. The ferromagnetic layer, applied by galvanization, is a layer of cobalt 7μ thick, without seams or splices, and it therefore produces no pulse-like interference. The uniformity of the linear motion of the surface of the massive drum with respect to the heads is sufficiently great, particularly in the case of the oil shock absorber used in the mechanism; the energy used on the rotation of the drum is sufficient only to overcome the friction in the bearings and in the present design does not exceed 1 watt. The basic difficulty in the utilization of the drum mechanism is the fabrication of the drum itself

to the high degree of precision required. For satisfactory operation, it is necessary for the distance between the recording carrier and the heads (the eccentricity) to change by no more than 10 μ.
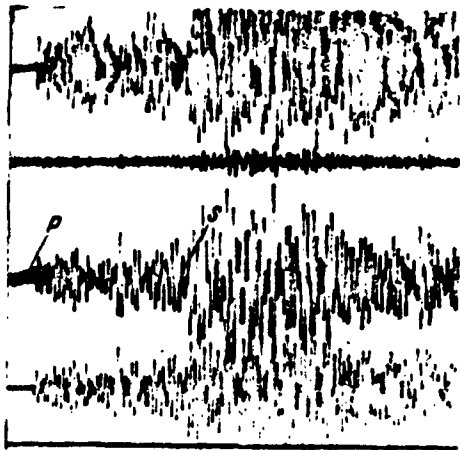
Fig. 8. Example of seismogram obtained by means of magnetic-memory equipment.

As a result of the theoretical and experimental work that was carried out, a circuit and design was worked out for the radio-technical portion of the installation, said section consisting of a frequency modulator and demodulator. The basic modulator link is the so-called sweep oscillator. This is an oscillator of sinusoidal oscillations, the frequency of the first harmonic of which depends on the amplitude of the transmitted seismic signal. The output stage of the oscillator is connected to the recording head and the voltage taken from the play-back head is passed on to an amplifier-limiter and then to the demodulator. The output stage of the demodulator is loaded on the galvanometer of the oscillograph through the transformer.

The testing of the first experimental specimen, developed and designed by A. N. Vetchinkin and G. I. Aksenovich, was carried out in Garm and produced satisfactory results. Figure 8 shows an example of an earthquake record produced by an installation with magnetic memory.

We can depend on the fact that this design will serve as the basis for the future development of automatic seismic stations.

Chapter Three

STRUCTURE OF EARTH'S CRUST AND METHOD OF PROCESSING

SEISMIC OBSERVATIONS

The structure of the Earth's crust was studied in the regions in which the expedition* was operating in order to resolve two problems.

The first problem involved the possibility of providing a method for the reliable and sufficiently accurate determination of the coordinates for earthquake foci. This determination is, in practical terms, possible only with a sufficiently clear idea of the structure of the medium in the region being studied, of the thickness of the Earth's crust, of the seismic velocities within the crust, as well as of the upper portions of the subcrustal layer. Good information as to the coordinates of the foci (epicenters and depths) provides the basis without which all of the remaining seismological problems could not be resolved: the study of the seismic regime governing the distribution of earthquakes with respect to time and space, the study of the spectral quantitative relationships governing vibrations during earthquakes, the study of the association between seismic and tectonic phenomena, etc. In this sense, a study of the structure of the Earth's crust and the subcrustal layer is a problem within the over-all complex of seismological investigations.

The second problem, involving a study of the Earth's crust in the working region — the intracontinental zone, primarily the zone

of Alpine folding — is of independent interest as a portion of the over-all geophysical problem of studying the structure of the Earth's crust on continents.

In principle, the solution of the first problem is possible through the recording of earthquakes directly in the region being studied, in this case, the Garm-Stalinabad region. However, the complexity of geologic structure in this mountainous region, the great number of local nonuniformities in the composition of the rocks, and the presence of numerous discontinuities frequently makes it impossible to obtain a clear picture of the over-all quantitative relationships governing the plutonic structure of the given region through the study of local earthquakes alone. Therefore, an easier, and yet more reliable, method of resolving the problem is the method which involves the obtaining of a general idea as to the structure of an extensive region and to use these data to refine the structural features of local sections. This is how the work was carried out.

To the extent that this was possible, a seismographic-prospecting method of processing the observations was employed in interpreting the data: overtaking and oncoming, as well as differential and vertical hodographs were constructed, and the well-known "t_0 method" was employed to determine the thickness of the Earth's crust, and the amplitude characteristics of the waves were determined. Then, on the basis of all obtained data as to the structure of the Earth's crust, a perfected isochronous method was worked out for the determination of earthquake-foci coordinates.

§ 1. Horizontal Hodographs

Method for the Construction of Horizontal Hodographs. Kinematics

In seismological investigations, it is general practice in the

construction of hodographs for a given region to use a series of epicenters. Either individual hodographs are prepared for these epicenters, and these hodographs can subsequently be used for the construction of an averaged hodograph for the given region, or a single averaged hodograph is immediately constructed for all of the epicenters under consideration [28]. In this case, a number of difficulties arise, and these, in considerable measure, restrict the possibility of interpreting the results of such a procedure. These difficulties are caused by the following circumstances.

The accuracy with which the coordinates of the epicenters that have been used were determined rarely exceeds ± 10 km, and the depths of the foci are generally unknown or determined in extremely approximate fashion; the identification of the arrival of various types of waves, at various stations, given a small recording time sweep and inadequate time-service accuracy, are by no means always uniquely defined. Additional difficulties arise as a result of the fact that, as a rule, in the preparation of the hodograph it becomes necessary to use data from stations located at various azimuths from the epicenter, and situated under the most varied geologic conditions. It frequently turns out that the seismic beams, as they are propagated, cut through sections of the medium that have extremely varied structures. A change in the thickness of the Earth's crust in various directions may result in a pronounced variance in the apparent velocity of the head waves from the Mohorovicic discontinuity or some of the other boundaries (discontinuities) within the Earth's crust. These structural features of the Earth's crust, as a rule, cannot be ascertained in setting up an average hodograph.

Finally, it should be pointed out that in this seismological-

ly conventional construction of hodographs, the dynamic character-
istics of waves were almost not used at all.

The observation system employed by the expedition in Tadzhikis-
tan and Kirgiziya made it possible to undertake the preparation and
processing of hodographs in a more efficient and detailed manner,
particularly insofar as this applies to the utilization of pros-
pecting methods for the interpretation of the observations [29, 30].
The possibility of such an approach can be attributed to the fol-
lowing circumstances. The seismic stations of the expedition (Dzhi-
rgatal' [Джг], Chusal [Чсл], Nimich [Нмч], Dzhafr [Дф], Yangalyk
[Янг], Yaldymych [Ялд], Garm [Грм], Obi-Garm [Обг], Chuyangaron [Чнгр],
Karasu [not given], Khorongon [Хр], Gissar [Гис]) are positioned in
a chain extended in an approximate latitudinal direction and form
an almost "straight line" of stations, approximately 200 kilometers
long. The epicentral zone, bordering Yuzhnyy Tyan'-Shan' [Tian Shan]
on the south, is situated far to the east and west of this chain of
stations, within the confines of this 200-km line. Such a distribu-
tion of stations with respect to the epicentral zone provides for
observations along a single azimuth, and earthquakes along various
portions of the line make it possible to set up a system of oncoming
and overtaking hodographs.

The work on deep seismic sounding (GSZ) carried out in the
Alayskaya Valley in 1955, within the confines of the Southern Tian
Shan epicentral zone [31] makes it possible for us to coordinate the
data obtained through explosions with the data obtained from earth-
quakes, and to extend substantially the line along which the inves-
tigations were carried out. Figure 9 shows the distribution of earth-
quake epicenters, used for the construction of the oncoming hodo-
graphs, and the GSZ section of the line.

The existence of seismic stations in Tadzhikistan, Kirgiziya*, and in the Ferganskaya Valley (Fergana [Фг], Namangan [Нмг], Andizhan [not given]) makes it possible to construct oncoming hodographs in the other direction (Stalinabad - Frunze) as well. A diagram of the location of the stations and earthquake epicenters for this line is also shown in Fig. 9.

The comparatively small distances between the stations of the expedition, and the large recording time sweep, as well as the excellent time service, all serve to make it possible reliably to ascertain and determine the absolute time of arrival for the waves, and in individual cases, to correlate these. Finally, the epicenters and depths of the foci in Kirgiziya and the Garm and Stalinabad regions covered by the expedition can be determined with increased accuracy.

In addition to the basic data produced by the expedition, additional data was also employed in the processing, said data produced by the Central Asian seismic stations of the Southern group: Khorog [Xp], Kulyab [Кб], Murgab [Mr], Tashkent [Тшк], Samarkand [not given]. For one earthquake (18 April 1955) use was also made of records produced by the seismic stations of the northern group: Alma-Ata [Ал], Kegen' [Кн], Przheval'sk [Прж], Fabrichnyy [Фбр], Ili [Или], Chilik [Члк], Chimkent [Чм]. In individual cases, information was taken from the Bulletin of Seismic Stations USSR for the period 1955-1956.

Regional seismic-station records were used to confirm the validity of the interpretation of the waves from the Mohorovicic discontinuity. Primarily, these records were used for an evaluation of recording features in other directions, said directions not coincident with the direction of the main station line. The basic in-

Fig. 9. Diagram of earthquake-epicenter distribution, used for.
construction of overtaking hodographs, following the Gissaraskaya
[Gissar] Valley — Alayskaya Valley (lower dashed-dotted line) and
the Stalinabad — Frunze line (upper dashed-dotted line). 1) Perma-
nent stations of the network; 2) temporary TKSE stations; 3) earth-
quake epicenters; A) GSZ section of the line (1955).

formation on the earthquakes for which the hodograph was construct-
ed along the first line (Gissarskaya Valley - Alayskaya Valley) are
shown in Table 4, and the data for the hodograph of the second
line (Stalinabad -Frunze) are presented in Table 5. The distance
between the extreme earthquake epicenters on these lines is approx-
imately 700 km.

The epicenters and depths of the earthquake foci, situated
close to the seismic stations of the expedition, were determined
by methods proposed by Wadati and Isikava [sic], the method of
average lines, and a method involving an isochrone transparent

TABLE 4

List of Earthquakes Along the Line Gissar-
skaya — Alayskaya Valley (From West to East)

1 Дата	2 Часы, мину-ты, секунды	3 Координаты		6 h, км	K*
		4 с. ш.	5 в. д.		
3.VI 1956	16 06 00	38°02'	67°40'		10
13.IV 1955	16 35 00	38 29	68 34,2	15	9
22.XI 1956	15 54 23	38 27,5	69 17,5	5	13
28.I 1957	21 01 41	38 27,5	69 17,5	5	12
11.IV 1956	01 26 50	38 27,5	69 17,5	5—10	12
11.IV 1956	01 45 16	38 51	70 25	5—10	:3
1.III 1956	05 44 13	39 04	70 32,5	4—5	11
1.II 1955	09 04 42	39 00	70 50,5	5—10	10
15.VI 1955	01 03 54	39 00	71 36	5—10	13
18.I 1955	02 45 09	39 26	72 36		12
19.I 1955	01 19 00	39 26	72 36		12
18.IV 1955	05 04 39	39 55	74 36		

*K is the number of the earthquake classifica-
tion, K = log E joule. See Chapter 4 for addi-
tional details.

1) Dates; 2) hours, minutes, seconds; 3) coor-
dinates; 4) North latitude; 5) East longitude;
6) h, km.

TABLE 5

List of Earthquakes Along Line Stalinabad - Frun-
ze (From South-West to North-East)

1 Дата	2 Часы, мину-ты, секунды	3 Координаты		6 h, км	K
		4 с. ш.	5 в. д.		
28.I 1957	21 01 41	38°27'	69°17,5'	3—5	12
7.I 1958	06 05 09,6	38 54	70 20	3—5	13
12.V 1957	20 09 23,5	39 30	72 06		12
25.V 1957	01 14 31	39 13	71 41		11—12
22.VII 1957	16 05 10	40 40	73 24		12
16.XI 1957	16 37 55	41 57	72 40		12—13
8.V 1957	14 25 34,2	41 34	74 40	15	13
12.V 1957	17 25 58	41 34	74 40	10—15	10—11
23.X 1957	23 20 11,4	41 34	74 36	15	10—11
12.IX 1957	16 09 57	42 38	74 43	10	10—11
12.VI 1957	06 42 14	39 05	71 55		11

1) Dates; 2) hours, minutes, seconds; 3) coor-
dinates; 4) North latitude; 5) East longitude;
6) h, km.

sheet divided into squares (see § 3). The earthquake epicenter situated far beyond the limits of the line Gissarskaya Valley - Alayskaya Valley were taken from the Bulletin of the Seismic Network of the USSR.

The determination of the depths of earthquakes occurring beyond the limits of the operating regions of the expedition, as will be demonstrated below, is not significant. The time in the focus for all earthquakes was determined according to the Wadati curve or taken from the Bulletin of the Seismic Network of the USSR. For strong earthquakes, occurring close to the seismic stations of the expedition, the amplitudes obtained on the records produced by the VEGIK seismograph were somewhat large and, therefore, the records of the coarsened components were used.

An individual hodograph was constructed for each epicenter, and here the position of the station relative to the epicenter was taken into consideration. For the most part, longitudinal waves were used, since the determination of the arrival of transverse waves, particularly at great distances, involves considerable difficulties and it was possible to determine these only for individual earthquakes along the line Stalinabad - Frunze.

Generally, the records showed clearly two, and rarely three, arrivals of longitudinal waves. This division becomes clearest at distances beginning on the order of 100 kilometers from the epicenter. The arrival of waves can be noted clearly at all stations. Even close to the zone of interference, the separation of the waves was marked with sufficient clarity as a result of the increased time sweep. The interference zone for the head waves from the Mohorovicic discontinuity and the direct waves for earthquakes with shallow foci (0-15 km) is situated approximately 220 km from the
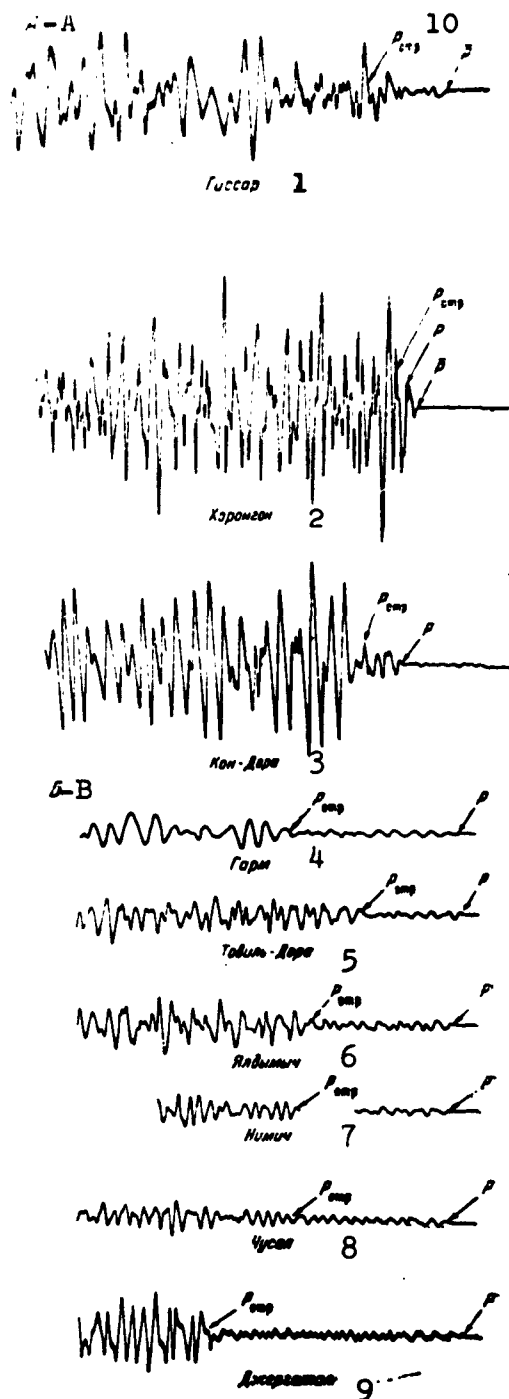
Fig. 10. Recording specimens of reflected longitudinal wave. Earthquake of 3 June 1956, 16:06 hours. A) Before the zone of interference; B) after the zone of interference; 1) Gissar; 2) Khorongon; 3) Kon-Dora; 4) Garm; 5) Tovil'-Dora; 6) Yaldymych; 7) Nimich; 8) Chusal; 9) Dzhergatal; 10) P_{otr}.

focus.

Individual hodographs make it possible to determine reliably three types of waves: direct and head waves from the Mohorovicic discontinuity, as well as waves which, on the basis of their kinematic and dynamic indicators, may be classified with the reflections from that same discontinuity. We did not succeed in isolating any refracted waves associated with the intermediate boundaries (for example, with the Konrad [sic] "granite" — "basalt" boundary). If such refracted waves exist here, they, apparently, interfere with the reflected waves. Earthquake-recording specimens, obtained at the stations of the expedition, are presented in Fig. 10.

Extremely intensive arrivals were observed at individual stations, and these arrivals, in terms of their kinematic indicators, might be included among the "exchange" waves.

However, in view of the fact that it was not always possible reliably to carry out the correlation of these arrivals between the various stations, these occurrences, as a rule, were not plotted on the hodograph. The single exception is the earthquake of 18 April 1955 for which an "exchange" wave was clearly noted at many stations in Central Asia. Apparently, this wave belonged to the type $S_1P_2P_1$, i.e., this wave is an "exchange" head wave at the Mohorovicic discontinuity.

For straight-line longitudinal waves in the granite layer, a speed of 6.0-6.1 km/sec was obtained; for transverse waves, the speed was 3.53 km/sec. In readings taken above the epicenter, the points t_0 at which the straight-line waves intersect the time axes of the hodographs lie at a level of 1.0-1.5 sec. The experimental points close to the epicenters are situated on a branch of lower speed, corresponding approximately to 5.0 km/sec. These data, obtained from longitudinal hodographs, indicate that there is a decline in speed close to the Earth's surface, and this is in good agreement with the change in velocity indicated by the vertical hodographs (see § 2). The arrivals of a straight-line wave at station situated on the mesozoic-cenozoic series of the Tadzhik Depression (Tovil'-Dora, Ishtion, Gissar) are delayed by approximately one second in comparison to arrivals at the remaining stations.

The apparent velocities of the head waves kept under observation by means of the hodographs change within a wide range, and this, apparently, is associated with the relief of the underside of the crust. On the average, the apparent velocity of longitudinal head waves is 7.9 km/sec, and for transverse waves, 4.6 km/sec. For a longitudinal wave reflected from the Mohorovicic discontinuity, in the case of observations at epicentral distances of 150 to 300 km,

the apparent velocities range from 6.8 to 6.3 km/sec.

Velocity V = 5.6 km/sec, corresponding to the velocity in the "granite" layer according to the hodograph prepared by Ye. A. Rozova, did not appear on our hodographs.

Oncoming and Overtaking Hodographs

After the final processing, all of the individual hodographs were compiled into a system of oncoming and overtaking hodographs for the refracted and reflected waves. The scale used in the construction of the hodographs was 1:1,000,000 for distance, and for time, 1 cm - 2 sec. The system of oncoming and overtaking hodographs along the line Gissarskaya - Alayskaya Valley is shown in Fig. 11.

To obtain summary overtaking hodographs for all earthquakes on each line, we selected two for which we were able to establish depths with some measure of reliability. The earthquakes of 28 January 1957 and 1 March 1956 were chosen for the line Gissarskaya - Alayskaya Valley, and for the line Stalinabad - Frunze, we selected the earthquakes of 28 January 1957 and 23 October 1957. These earthquakes occurred in the immediate vicinity of the station; therefore, it was possible to determine their depth with a high degree of accuracy, by using the transparent grid paper employed for the theoretical hodographs (see § 2). These basic earthquakes on the first line were referred to a zero depth, and for the second line the earthquake of 23 October 1957 was referred to the depth of the quake which took place on 28 January 1957. The summary oncoming hodographs were constructed in terms of the basic earthquakes, in accordance with the conventional rules of seismic prospecting, to the extent that this was at all possible under seismological conditions.
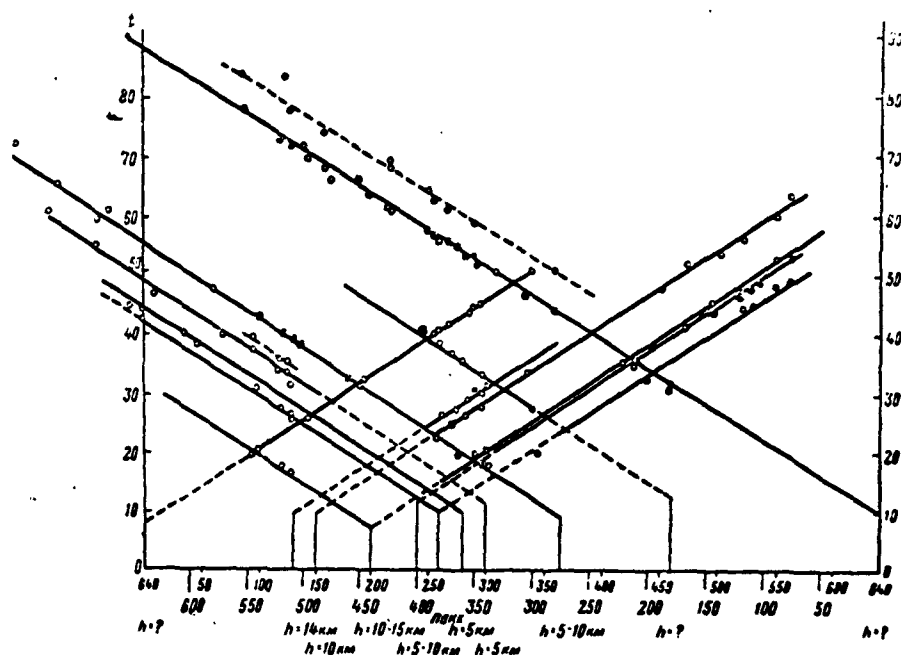
Fig. 11. System of oncoming and overtaking hodographs of refracted
head waves from the Mohorovicic discontinuity, along the line
Gissarskaya Valley - Alayskaya Valley.

Summary overtaking hodographs were constructed for longitudinal

head waves along both lines (Fig. 12), and for the transverse head

waves - such hodographs were constructed only for the second line

(Stalinabad - Frunze). Figure 12 shows for the end of the straight-

line hodograph of the first line a dense cluster of points obtained

in the deep seismic sounding (GSZ) carried out in the Alayskaya

Valley in 1955 [31]. For the second line, averaged hodographs of

longitudinal (Fig. 13) and transverse waves reflected from the

Mohorovicic discontinuity were constructed.

Since the foci of the earthquakes employed here were situated

along approximately the same longitudinal lines, any errors in

the determination of their depth had no effect on the resultant

velocity for the refracted head waves, since an inaccuracy in

.54
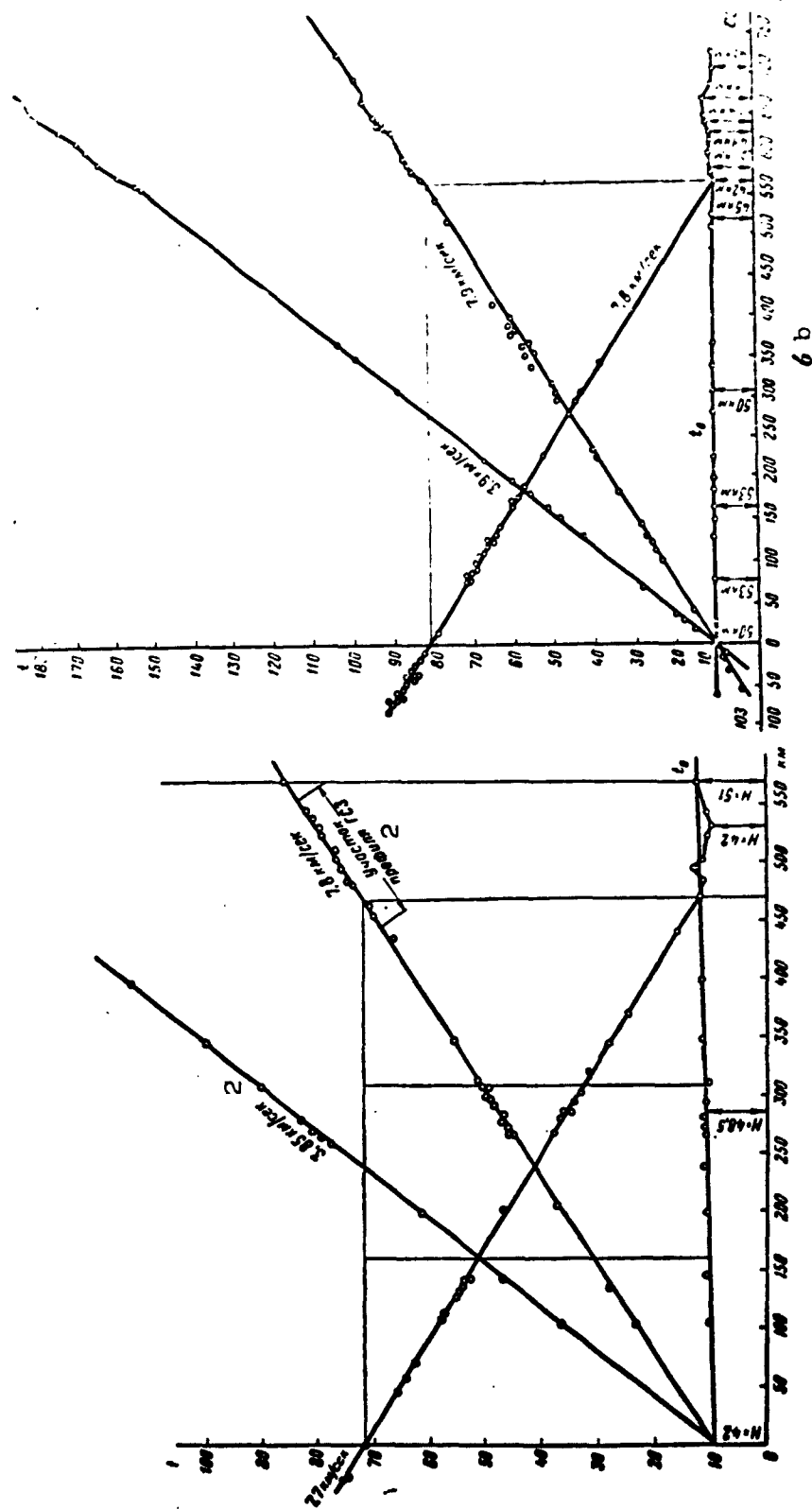
Fig. 12. Averaged oncoming, overtaking, and differential hodographs
of refracted head waves from the Mohorovicic discontinuity, and
the values of t_0. a) Gissarskaya Valley – Alayskaya Valley; b)
Stalinabad – Frunze; 1) 3.85 km/sec; 2) GSZ line section.

55
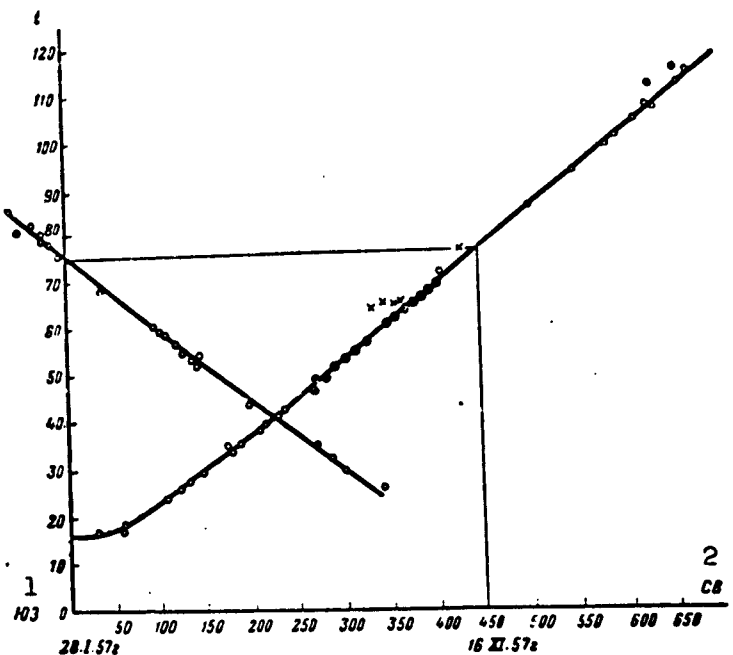
Fig. 13. Averaged hodographs of reflected
waves

Direction Stalinabad - Frunze
1) Southwest; 2) Northeast.

depth, in this case, results only in a parallel shift on the
hodographs for these waves along the time axis, without intro-
ducing any changes in apparent velocity. The time difference for
common points on the eastern and western branches of the oncoming
hodographs did not exceed 0.3 sec. If we take into consideration
the limited accuracy of the seismic observations employed, such
a degree of coordination for common points may be regarded as
good.

The summary oncoming and overtaking hodographs of the head
waves exhibited experimental points that were generally quite well
distributed along straight lines. The section of the line inter-
secting the northern Tien Shan is an exception. Here we find a pro-

.56 .

nounced deviation of the points from the straight line. Individual points, corresponding to the stations Andizhan, Namangan, and Tashkent did not line up well on the hodograph lines, and this also applies to the data for the expeditionary time stations situated in the district around the city of Tashkent.

Differential Hodograph and Structure of Earth's Crust

In accordance with the summary oncoming hodographs, a differential hodograph was constructed and the values of t_0 for both lines were determined (see Fig. 12, a, b). On the eastern section of the line Gissarskaya - Alayskaya Valley, the differential hodograph was extrapolated in the assumption that it was a straight line to the end of the GSZ line. For this section, t_0 was determined in accordance with the differential hodograph and the GSZ section of the line. Deviations in the points of the t_0 line, from a straight line, were insignificant along the entire line and did not exceed the limit of observation accuracy, which points to the relative evenness (for the given degree of detail) of the relief of the Mohorovicic discontinuity along this line. The thickness of the crust was determined according to the following formula [30].

$$H = \frac{Vt_0}{2 \sin i},$$

where i is the critical angle, V is the velocity in the covering layer. The resultant data indicate that the thickness of the crust increases from West to East; at the extreme western end of the line, the crust is 46 km thick, it is 48 km thick in the Garm district, and it is 50 km thick at the extreme eastern end of the line.

The t_0 for the second line (Stalinabad - Frunze) exhibit little change in the southwestern part of the line. In the Northeast, be-

-57

fore the Fergana Range, the t_0 value is somewhat lower, and further on in the region of the Fergana and then in the region of the Kirgiz Ranges, this value increases, only to diminish again at points beyond. The numerical values of the thickness of the Earth's crust along the line, which correspond to these t_0, are presented in Fig. 12 in the line $\overset{\bullet}{t_0}$. The maximum thickness (58 km) corresponds to the axis of the Kirgiz Range.

The values for the thickness of the Earth's crust on the southwestern sector of the second line, in the region Garm – Stalinabad, came out somewhat higher than for the same sector on the first line. The greatest divergence, determined for the two lines in coincident sectors, comes to 5 km. This gives us some idea as to the accuracy with which the thickness of the Earth's crust can be determined by the method outlined here. On the whole, the thickness of the Earth's crust varies, approximately, from 40 to 60 km on all of the line sectors in Central Asia under consideration. In the overwhelming majority of cases, the thickness is close to 50 km.

Summary Experimental Hodograph of the Line Stalinabad – Frunze

Figure 14 presents experimental data based on an overtaking system of hodographs for longitudinal and transverse, straight-line, reflected, and head waves for the line Stalinabad – Frunze. The hodograph for the reverse direction is similar, with the exception of the sector corresponding to the Northern Tien Shan. In Fig. 14, the straight-line hodograph of the head wave for this sector is represented by a dashed-dotted line, and the reverse hodograph is represented by a simple dashed line. The numerical values for the arrival time of all indicated waves for these averaged hodographs are presented in Table 6.

The use of this hodograph for the processing of earthquakes
(the determination of the focal coordinates) for the region of
the Fergana Range yielded better results than the hodograph by
Ye. A. Rozova that had also been used for this purpose.
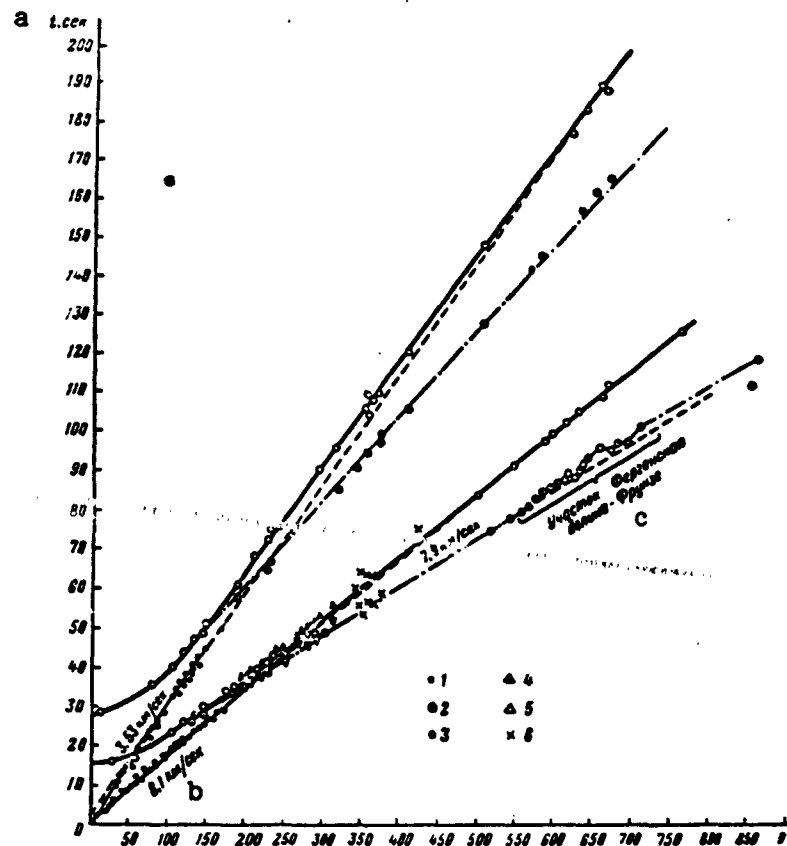
Fig. 14. Experimental and theoretical hodographs of longitudinal
and transverse waves, as well as of head and reflected waves from
the Mohorovicic discontinuity, along the line Stalinabad - Frunze.

Constructed in accordance with the straight-line overtaking system
of observations. Experimental data from the TKSE network: 1)
straight-line wave; 2) head wave from the Mohorovicic discontinuity;
3) reflected wave from the Mohorovicic discontinuity. GSZ data:
4) head wave from the basalt discontinuity; 5) head wave from the
Mohorovicic discontinuity; 6) data from stations not on the line.
Theoretical hodographs: thin line) straight-line wave; dashed-dotted
line) head wave from the Mohorovicic discontinuity; solid heavy
line) reflected wave from Mohorovicic discontinuity; the dotted line
on the extension of the hodograph for the straight-line waves in-
dicates that a wave reflected beyond the maximum angle could easily
be confused with a straight-line wave; a) t, sec; b) 6.1 km/sec;
c) the Ferganskaya Valley - Frunze sector.

TABLE 6

Tabular Values of Hodographs for Straight-Line, Reflected, and Head Longitudinal P and Transverse S Waves

д. км	P_I	P_{II}	P_{III}	P_{III} Ст.-Фр.	S_I	S_{II}	S_{III}
0	1,4 (0)	16,0			2,0 (0)	27,7	
10	3,0 (1,9)	16,0			4,8 (3,3)	28,0	
20	4,7 (3,8)	16,2			7,7 (6,6)	28,6	
30	6,3 (5,6)	16,6			10,6 (10,0)	29,4	
40	8,0 (7,5)	17,0			13,3 (13,3)	30,4	
50	9,6 (9,4)	17,8			16,2	31,6	
60	11,3 (11,3)	18,4			19,0	32,8	
70	12,9	19,4			21,8	34,2	
80	14,5	20,4			24,7	35,8	
90	16,2	21,6			27,5	37,2	
100	17,8	22,8			30,3	39,2	
110	19,5	24,0			33,2	41,0	
120	21,1	25,4			36,0	43,4	43,4
130	22,8	26,8	26,6		38,8	45,6	45,6
140	24,4	28,3	27,8		41,7	48,0	47,7
150	26,0	29,7	29,1		44,5	50,2	49,9
160	27,7	31,2	30,3		47,3	53,0	52,0
170	29,3	32,6	31,6		50,2	55,4	54,2
180	31,0	34,0	32,8		53,0	58,0	56,3
190	32,6	35,5	34,1		55,9	60,7	58,5
200	34,3	37,0	35,3		58,7	63,4	60,6
210	35,9	38,4	36,5		61,5	66,1	62,8
220	37,6	39,8	37,8		64,4	68,8	64,9
230	39,2	41,3	39,0		67,2	71,6	67,1
240	40,8	42,8	40,3		70,0	74,3	69,2
250	42,5	44,2	41,5		72,9	76,0	71,4
260	44,1	46,0	42,8		75,7	79,7	73,5
270	45,8	47,6	44,0		78,6	82,4	75,7
280	47,4	49,2	45,2		81,4	85,1	77,8
290	49,1	50,7	46,5		84,2	87,8	80,0
300	50,7	52,3	47,7		87,0	90,6	82,1
310	52,3	53,9	49,0		89,9	93,3	84,3
320	54,0	55,5	50,2		92,7	96,0	86,4
330	55,6	57,0	51,5		95,5	98,7	88,6
340	57,3	58,6	52,7		98,4	101,4	90,8
350	58,9	60,2	53,9		101,2	104,1	92,9
360	60,6	61,8	55,2		104,0	106,8	95,1
370	62,2	63,3	56,4		106,9	109,5	97,2
380	63,8	64,9	57,7		109,7	112,2	99,4
390	65,5	66,5	58,9		112,5	114,9	101,5
400	67,1	68,0	60,2		115,4	117,7	103,7
410	68,8	69,6	61,4		118,2	120,4	105,8
420	70,4	71,2	62,6		121,1	123,1	108,9
430	72,0	72,8	63,9		123,9	125,8	110,1
440	73,7	74,3	65,1		126,7	128,6	112,3
450	75,4	75,9	66,4		129,6	131,2	114,4
460	77,0	77,5	67,6		132,4	133,9	116,6

TABLE 6 (Continued)

	P_1	P_{11}	P_{121}	P_{121} Ст-Фр	S_1	S_{11}	S_{121}
470	78,7	79,1	68,9		155,2	136,6	118,7
480	80,3	80,6	70,1		158,1	139,3	120,9
490	81,9	82,2	71,3		160,9	142,1	123,0
500	83,6	83,8	72,6		148,7	144,8	125,2
510	85,2	85,4	73,8		146,6	147,5	127,3
520	86,9	86,9	75,1		149,4	150,2	129,5
530	88,5	88,5	76,3		152,2	152,9	131,6
540		90,1	77,6		155,1	155,6	133,8
550		91,8	78,8		157,9	158,3	136,0
560		93,4	80,0	80,0	160,7	161,0	138,1
570		95,0	81,3	81,8	163,6	163,8	140,1
580		96,6	82,5	83,3	166,4	166,5	142,3
590		98,3	83,8	85,2		169,2	144,5
600		99,9	85,0	86,6		171,9	146,6
610		101,5	86,3	87.7		174,6	148,8
620		103,2	87,5	88,2		177,3	150,9
630		104,8	88,8	89,8		180,0	153,1
640		106,4	90,0	92,4		182,7	155,2
650		108,1	91,2	94,0		185,4	157,4
660		109,7	92,5	95,2		188,2	159,5
670		111,3	93,7	96,0		190,0	161,7
680		113,0	95,0	96,2		193,6	163,8
690		114,6	96,2	97,2		196,3	166,0
700		116,2	97,4	98,6		199,0	168,1
710		117,8	98,7	100,2			170,3
720		119,5	100,0	101,8			172,4
730		121,1	101,2	103,0			174,6
740		122,7	102,4	104,3			176,7
750		124,4	103,7	105,6			178,9
760		126,0	104,9	106,8			
770			106,2	108,1			
780			107,4	.109,3			
790			108,7	110,6			
800			109,9	111,9			
810				113,1			
820				114,4			
830				115,6			
840				116,9			
850				118,1			
860				119,4			

Note. P_1 and S_1 are straight-line waves, P_{11} and S_{11} are reflected waves from the Mohorovicic discontinuity, P_{121} and S_{121} are head waves from the Mohorovicic discontinuity, P_{121} St-Fr represents the experimentally determined duration of the head waves at the Fergana Valley sector. The duration of the waves, corresponding to a straight-line wave in the "deposition" layer, are shown in parentheses; Ст- Фр= St-Fr = Stalinabad-Frunze.

We can see from the example presented that with a special system of earthquake observations, employing seismic-prospecting methods for processing these results, we can obtain more detailed data as to the structure of the Earth's crust in large regions, than is possible with conventional seismological methods. The accuracy in the determination of the thickness of the Earth's crust with these constructions (of the order of ± 5 km), possibly approaches the accuracy of the results obtained by the GSZ method, which employs a version of the "piece-continuous profiling" method. For the solution of similar problems, a combination of seismological (earthquake observation) and GSZ (observation of explosions) methods is most expedient.

Amplitude Characteristics for Various Types of Waves

In the identification of waves and the construction of horizontal hodographs, even in the case of comparatively favorable observation conditions, the same kinematic criteria may generally be inadequate. In view of this, in the preparation of individual hodographs, we made use of dynamic (amplitude) wave features as well.

1. Experimental amplitude curves. Together with the determination of the arrival time for various waves, the average amplitude of the wave arrival was also measured, said time reliably determined on the basis of kinematic indicators. For this purpose, as a rule, only recordings from the expedition stations equipped with similar frequency-characteristic equipment was employed. As an exception, records of regional stations from the Fergana Valley were used, and here the arrival amplitudes on the records of these stations, taking into consideration the frequency characteristics of the instruments, were magnified 20,000 times, the standard mag-

nification of the instruments employed by the stations of the expedition. The values for the average arrival amplitudes were recorded on an individual hodograph for each point, corresponding to the arrival time of a given wave, determined according to kinematic indicators. It should be pointed out that, in the majority of cases, corresponding amplitudes on the records of regional seismic stations, equipped with SGK and SVK seismographs, were anomalously large and the results were unsatisfactory in the attempt to coordinate these data with the records produced by the expedition stations equipped with VEGIK seismographs. This is, apparently, associated with the fact that the frequency ranges of the equipment employed by these stations do not coincide. ·

The further processing involved the following. The amplitude values were plotted on a curve which was constructed on a double logarithmic scale (the axis of abscissas represented the distances, and the axis of ordinates represented the amplitudes, in mm, of records produced by the VEGIK). Such curves were constructed for each individual earthquake (Fig. 15, a) or for several earthquakes of similar intensity classification (K = 12), whose amplitude curves coincided on a single curve (Fig. 15, b).

2. Theoretical amplitude curves. In order to have some idea as to the magnitude of the amplitudes of various types of waves, at various distances from the source, theoretical amplitude attenuation curves were calculated at the request, to the expedition, of LOMI* coworkers A.V. Manukhov and M.V. Vasil'yeva, for different orientations of dipole-type sources with moment (a model of the earthquake focus).

The calculations were carried out in the assumption that the Earth's crust was uniform and nonabsorbing, with the velocity val-

ues and crust thickness values attained by the TKSE in accordance
with the horizontal and vertical hodographs (§ 1 and 2). A change
in wave amplitude was examined in a direction perpendicular to the
extension of the discontinuity in the focus for a case in which the
discontinuity plane was oriented vertically or at an angle of 45°
to the daylight surface.

On the theoretical amplitude curves obtained (Fig. 16, b, c)
our attention is first caught by two circumstances: first of all,
the extremely strong dependence between the amplitude curves and
the position of the discontinuity plane; and secondly, by the
great intensity of the reflected waves beyond the critical angle,
said intensity exceeding the intensity of straight-line waves,
sometimes by orders of 2 to 3. The latter wave becomes substantial-
ly weaker than all of the remaining waves, as a rule, at a short
distance from the source. The exchange wave of the type $S_1P_2P_1$ is
commensurate in intensity with a reflected wave. .
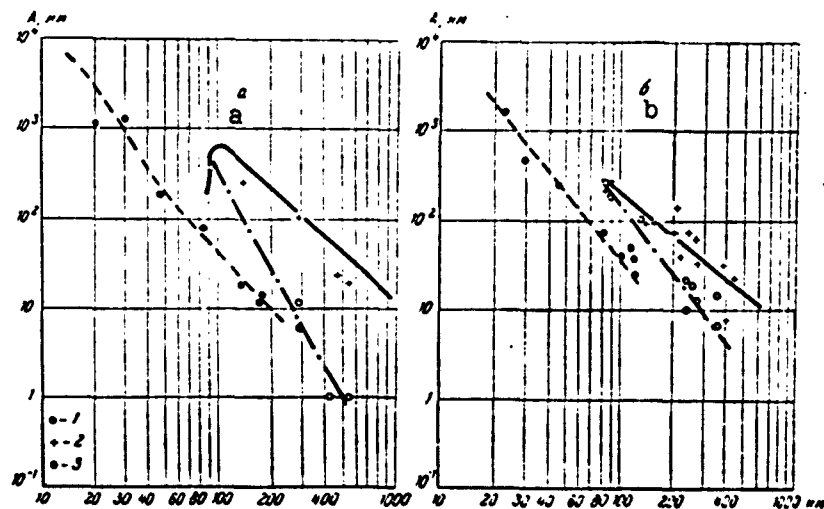
Fig. 15. Experimental curves for the attenuation of longitudinal
straight-line, reflected, and head waves. a) For the earthquake
on 7 January 1958 (K = 13); b) for the group of earthquakes of
intensity classification 12. 1) Straight-line; 2) reflected; 3)
head wave.
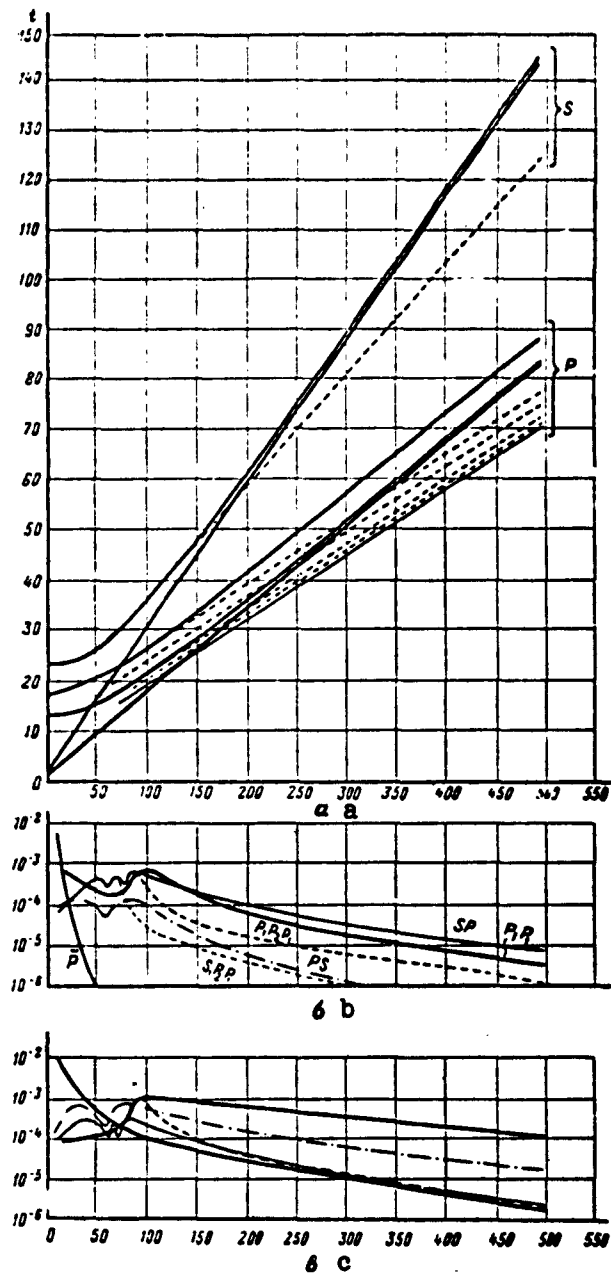
Fig. 16. Theoretical hodographs and amplitude curves for longitudinal and transverse waves of various types (thickness of Earth's crust, 45 km; focus at a depth of 5 km). a) Kinematic hodographs; b,c) amplitude curves for vertical discontinuity plane (b) and discontinuity plane inclined at an angle of 45° (c). Wave type: SP, PS, P_1P_1 - reflected; $P_1P_2P_1$ - head; $S_1P_2P_1$ - exchange head; $\overline{P}$ - straight-line.

An examination of the results obtained in these calcula-
tions leads us to the following conclusions: a) with obser-
vations along various azimuths from the source, wave inten-
sity of a given type of wave may vary by a factor of more
than one order of magnitude; b) a straight-line wave may be
noted only close to the source, up to the zone of inter-
ference with the head wave, so long as it appears in the
first arrivals, and it is more difficult or, for all intents
and purposes, impossible to note such a wave beyond the zone
of interference on the background of the records of other
more intensive waves; c) beyond the zone of interference,
we can reliably note a reflected wave which, in terms of inten-
sity, predominates over all other types of waves, or we can find
an exchange wave of the type $S_1P_2P_1$ which can be distinguished
easily from a reflected wave by its kinematic indicators. An im-
portant criterion in the identification of waves, a criterion
which follows from the same theoretical curves, is the differ-
ence in the attenuation of straight-line, head, and reflected
waves. Thus, amplitude characteristics of waves lead to a sub-
stantial expansion of the possibilities of interpreting these
observed data.

A comparison of the degree of attenuation with the dis-
tance of straight-line, head, and reflected waves for theoretical
(Fig. 16) and experimental (Fig. 15) curves produces satisfactory
agreement. Insofar as the amplitude relationships are concerned,
the amplitude of reflected waves, on experimental curves, exceed
the amplitude of straight-line waves by no more than 1 to 1.5
orders of magnitude, whereas this difference in the case of
theoretical curves (Fig. 16) reaches, in individual cases, 3 to

4 orders of magnitude.

The attenuation of the vibration amplitude on the summary experimental curve (Fig. 15, b) is more intensive for all waves than is the attenuation on the theoretical curves. Apparently, this difference can be explained by a significant absorption effect. On the basis of the divergence between the theoretical and experimental attenuation curves, the amplitude values for the absorption decrement were calculated. For straight-line and reflected waves, the decrement was 0.03. This value is somewhat higher than the value for the Earth's crust that is usually assumed ($\varepsilon = 0.01$) and cannot be regarded as reliable in view of the inadequate number of experimental data.

It should be stressed that the results, cited here for the theoretical calculations of amplitude curves, pertain only to the simplest case of single-layer "granite" nonabsorbing crust. As the calculations of a number of examples for multilayer "granite-layer basalt" crust have demonstrated, the reflection from the Mohorovicic discontinuity remains more intensive in this case as well. A great variety of relationships between intensities of reflected and refracted (head and penetrating "refracted") waves is possible in media which exhibit discontinuous-continuous changes of parameters (medium gradients, transitional layers, etc.). Taking into consideration the absorption whose magnitude is greater in the crust than directly beneath the crust, we find that there is a relative strengthening of refracted waves in comparison to reflected waves. The intensity relationship between reflected and refracted waves also changes as a function of the position of the source and the point of observation.

Thus, the results cited in this section, on the study of the

- 67

structure of the Earth's crust, said study undertaken by means of horizontal hodographs for earthquake waves, these waves obtained and processed with the use of methods similar to seismological prospecting and partially supported by dynamic calculations, have not yet made it possible to detect, in the Earth's crust of the given region, basic layers other than the "granite" layer, which exhibits a velocity of approximately 6.0 km/sec. A further discussion of the problem dealing with the velocity structure of the Earth's crust and the subcrystal layer in the regions being investigated, will be presented in the following section.

§ 2. Vertical Hodographs

<u>Transparent Sheets of Graph Paper for Theoretical Hodographs</u>

The determination of the velocity boundary within the Earth's crust, i.e., the nature of the distribution of seismic velocities within the crust, as is well known, presents considerably greater difficulties than an estimate of some average velocity and the total thickness of the crust. While seismologists at the present time are more or less in agreement with respect to the structure of the crust beneath the oceans, this primarily of "basaltic" composition, with respect to the structure of the continental crust, we encounter the following disagreements (see, for example, the summary by B. Gutenberg [32], as well as the work by Teytel and T'yuv [33]).

Some researchers are still of the opinion that there is a more or less pronounced separation of the continental crust, beneath the sedimentary layer, into two major strata "granite" and "basalt," ([34-37] etc.), whereas others maintain that the structure of the earth is substantially uniform and may exhibit a constant rise in velocities from the depths ([33] etc.). Some

have noted waveguide channels within the crust where the velocities are lower, whereas others have found no bases for maintaining that such zones exist [38].

In investigations involving great explosions, it was generally concluded that the power of resolution of the methodology and equipment presently in use is not equal to the stratification of the crust which sometimes exhibits a great number of layers. In the latest works dealing with great explosions (including nuclear explosions), at certain points the conclusion was reached that the crust consisted of a single layer, whereas at other points the conclusions drawn indicated that the crust was stratified. In works in which a more detailed study of the structure of the Earth was undertaken, and this by means of small explosions, carried out in the USSR in accordance with the method of deep seismic sounding (GSZ) ([31] etc.,) on continents, as well as in inland seas and seas close to continents (the Caspian Sea, the Black Sea, and the Sea of Okhotsk), a "granite" and a "basalt" sedimentary layer was generally noted, and only in individual local cases, in the presence of a thick sedimentary layer, did the investigations fail to reveal the presence of one of the major crustal layers ("that of the granite layer"), while at other points the thickness of the "basalt" layer diminished markedly. There were points at which the separation of the crust into individual layers was more pronounced, particularly in the Pamiro-Alayskaya zone, adjacent to Garm [31], where "basalt" was divided into two sublayers: an upper layer - with a lower velocity, and a lower layer - with a greater velocity. It is important to note that in all of the GSZ projects the crust was found to be nonuniform and a basalt layer was found to exist above the Mohoro-

vicic discontinuity, said layer having a velocity greater than through granite. In this case, the boundary of separation for the layers within the crust was not always clearly delineated. It is possible that in a number of instances, the boundaries of separation could be replaced by smooth transitions.

Finally, some contemporary seismologists take an agnostic position, sometimes with complete justification pointing to the absence of sufficient argumentation in the given works to accept particular conclusions with respect to the stratification of the Earth's crust.

With such complex circumstances, new investigations are necessary, these directed toward a more thorough study of this important problem. Below we discuss such an attempt, proceeding from the kinematic position and based on the concept of a possibility of distinguishing "strata" and "discontinuity" velocities in the Earth's crust.

We would first like to point out that seismic velocities determined on bases of, on the one hand, primarily horizontal extended lines, and on the other hand, on primarily vertical lines, can differ substantially in the presence of a velocity stratification of the medium even if this medium is macroisotropic (the latter assumption is sufficiently valid insofar as it pertains to large rock volumes) [39]. In "major" seismology, conclusions as to the velocity structure of the Earth's crust were, until recently, based on waves that are primarily propagated in a horizontal direction. Correspondingly, the determination of velocities was carried out in accordance with conventional horizontal hodographs of straight-line and refracted waves. This pertains both to earthquake observation as well as explosions that served seismological purposes

rather than prospecting goals.

Moreover, we know from experience gained in seismological prospecting that "horizontal" systems for the observation of straight-line and refracted waves yield the possibility, in principle, of determining only discontinuity velocities with some reasonable degree of reliability, whereas strata velocities [39, 40] can be determined with only a small degree of reliability by these methods.

In seismological prospecting, strata velocities can be determined with sufficient accuracy according to "vertical" drillhole observations, which may be supplemented or partially replaced, under appropriate conditions, by appropriate methods of observation and interpretation of conventional horizontal hodographs for reflected waves, through the construction of vertical hodographs of seismic waves. Methods similar to the latter may be employed in seismology for the determination of the velocity structure of the Earth's crust, in accordance with observations of near-by earthquakes. Such methods were proposed by Yu.V. Riznichenko [41]. These methods consist in the use of transparent grid paper for theoretical hodographs of straight-line or passing refracted waves, as well as in the use of vertical hodographs for these waves.

For the determination of a velocity discontinuity according to seismological data (for the joint determination of focal depths of earthquakes, average velocities, and times t_z along the vertical) we can use the same transparent grid sheet for the theoretical hodographs of reflected waves as was used in seismological prospecting. The difference here lies in the fact that in seismology the source of the excitation, the focus, is situated not at the surface as is the case with a seismic-prospecting explosion, but

at a substantial depth $\underline{h}$, and here we must determine the distance from the surface not to the reflection discontinuity, but to the focus. In actual practice, this difference is taken into consideration in the interpretation of earthquakes by the fact that the depth scale of the prospecting grid sheet must be changed by a factor of two. Further, the prospecting grid sheets are plotted for the case in which the distance from the explosion point to the extreme observation point does not exceed the depth of the reflection discontinuity. Since these conditions are rarely satisfied in the case of seismological observations, the grid sheet must be extended for greater epicentral distances, and then all existing observation stations may be employed in the determination. Although the more distant stations do not, in this case, make it possible to determine the depth of the focus, they do, however, make it possible to achieve more reliable coincidence between the theoretical curve and all of the observation points used.

A specimen of a seismological grid sheet for theoretical hodographs, calculated for the determination of foci of small depth $\underline{h}$, is presented in Fig. 17. In the case of deep earthquake foci, when the conditions of the prospecting case are satisfied, the prospecting grid (Fig. 18) yields high accuracy, and its use is preferred.

Calculation Procedure

On a piece of tracing paper, laid over the transparent grid, crosshairs are laid out and these represent the vertical time axis which coincides with the axis of symmetry of the transparent grid and the horizontal distance axis which is situated at mark 1.0 when times t_p - t_Q are used, or at mark 0.7-0.8 (in accordance with the

relationship between velocities of longitudinal and transverse waves, on the basis of the Wadati curves,(see § 3) when times $t_s - t_p$ are used. Here t_Q is the time at the focus, t_p is the arrival time of the longitudinal waves, and t_s is the arrival time of the transverse waves. In this coordinate system, however, the "observed" points are plotted with the coordinates: epicentral distance, determined by the isochrone method (see § 3), and time. Further, keeping the corresponding axes parallel, the tracing paper is moved across the transparent grid for plotting of all observed points on one and the same theoretical curve of the transparent grid. Now, according to the position of the curve minimum, approximating the observation hodograph, the focal depth is marked off on the vertical scale, and the initial horizontal axis of the tracing paper determines the average velocity on this same scale. For a reading of t_z, the time of duration at the epicenter along the vertical, this same horizontal line is made to coincide with the initial grid line: the distance from this line to the minimum point of the theoretical curve, plotted on the tracing paper along the observed points, determines time t_z along the same vertical scale. The most reliable result is obtained if the stations are situated approximately along the same straight line, on various sides from the epicenter, but the transparent grid may be employed even if the stations are situated on only one side with respect to the epicenter. In an area positioning of the stations, i.e., in different directions with respect to the epicenter, the data from the stations situated on one side of any conventional line dividing all of the stations into two groups, can be plotted on the left-hand side, and the data from the stations lying on the other side of the line can be plotted to the right of the axis.

·73·

of symmetry of the transparent grid.

Further processing of the resultant data can be reduced to the construction of a vertical hodograph. Two axes are plotted on a piece of graph paper: the horizontal axis is the time axis t_z, and the vertical axis represents the axis of depths. Points with the coordinates obtained for a series of earthquakes at various depths are plotted on a curve; the sequence of these points — it can be expressed by a smooth curve or a broken line — forms the vertical hodograph.

Having carried out the graphical differentiation of this curve, we obtain the values for the strata velocities for various depths, and by drawing a line from point (h = 0, t_z = 0) which intersects each point along the curve of the vertical hodograph in succession, we obtain the values for the average velocities to the corresponding depths. The same curve can be constructed for fictitious t_s - t_p waves. The above method was employed to obtain the vertical hodographs for the Garm and Pamiro-Gindukushskiy regions.

In determining the strata velocities according to the vertical hodograph we must bear in mind that their values, obtained by means of graphical differentiation, may be reliable only if the detected strata are sufficiently thick. In thin layers, strata velocities cannot, for all intents and purposes, be determined from the vertical hodographs. This restricts the possibilities for this given kinematic method. It is possible that certain dynamic methods may exhibit greater power of resolution in this respect.

Accuracy in Determination of Depths and Velocities by Means of Transparent Grid of Theoretical Hodographs

Errors in the determination of depths and average velocities
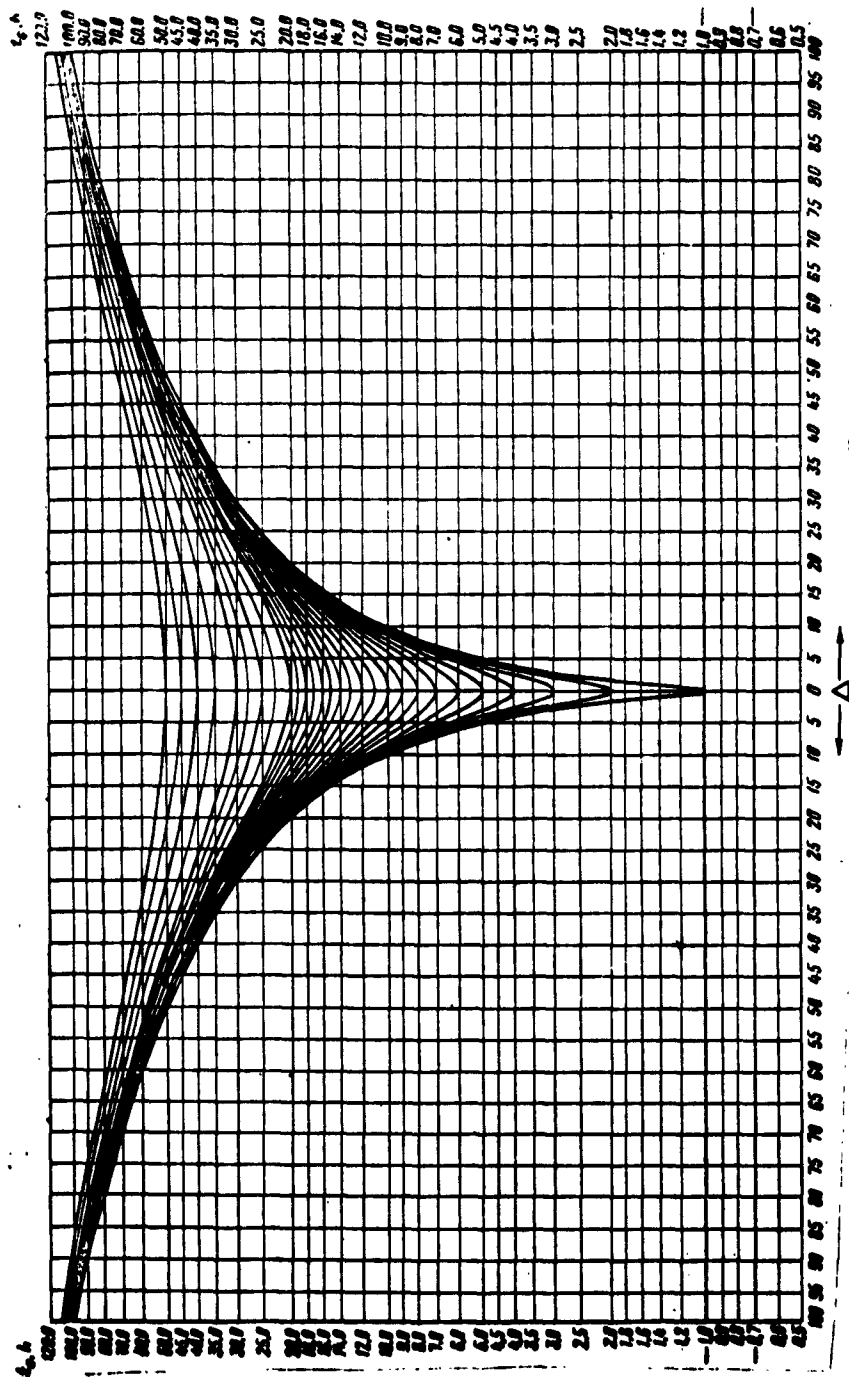
Fig. 17. Transparent grid of theoretical hodographs for combined
determination of focal depths and average propagation velocities
for seismic waves.
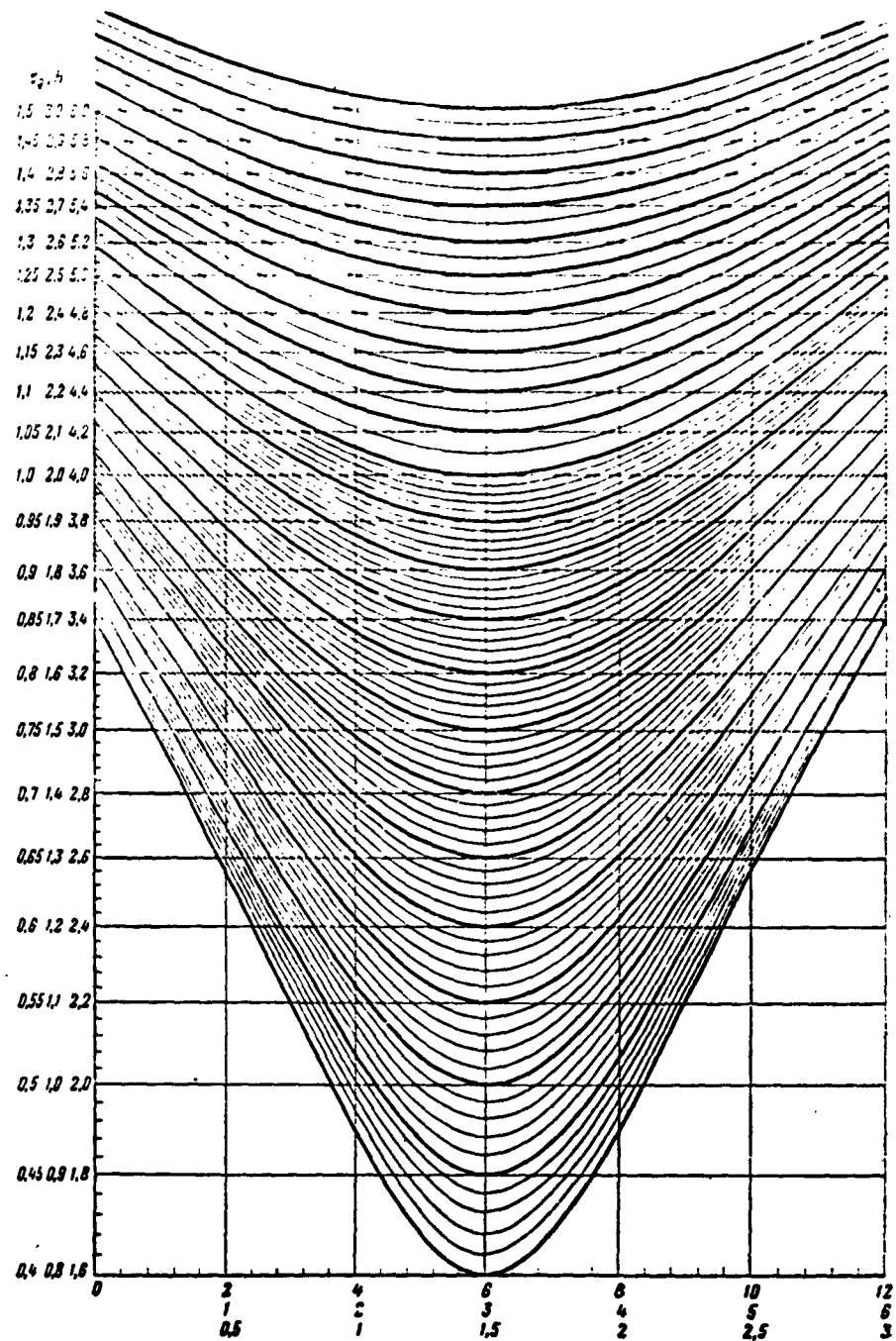
Fig. 18. Prospecting transparent grid of theoretical hodographs for joint determination of focal depths and average propagation velocities for seismic waves, said transparent grid used for deep earthquakes.

of seismic waves may be random or regular. Here we will dwell on an examination of only the latter. These may arise as a result of the fact that the transparent grid of the theoretical hodographs is intended for a uniform medium and only then does the "effective" velocity, determined according to the transparent grid, coincide exactly with the average velocity in the vertical direction. In actual fact, we are dealing here, in the first approximation, with a medium in which the wave velocities change with depth (a horizontally stratified medium).

In this connection, the effective velocities V_e and correspondingly h_e are somewhat overestimated in comparison with the actual average velocities V_m and depths $\underline{h}$. The relative systematic overestimation of velocities and depths

$$ \gamma = \frac{V_e - V_m}{V_m} \Bigg| = \frac{h_e - h}{h_e} $$

depends on the length of the hodograph, and increases with this length.

It is well known [30] that the effective velocity, determined from the entire hodograph, does not exceed

$$ V_{e,\,\text{max}} = \sqrt{V^* \frac{\Delta_{\text{max}}}{t}} , $$

where Δ_{max} is the maximum epicentral distance, and $\underline{t}$ and V^* are the corresponding values of time and apparent velocity according to the hodograph, at the point farthest from the epicenter. If the medium is made of layers having parameters h_1, V_1, h_2, V_2,...., h_n, V_n (h_k is the thickness of the layer, V_k is the velocity within the layer), we have the following relationships:

$$ h = \sum h_k; \quad V_m = \frac{\sum h_k}{\sum \frac{h_k}{V_k}} ; $$

---

*tg = tan

$$V^* = \frac{V_1}{\sin i_1};$$

$$\Delta_{max} \quad \Sigma h_k \operatorname{tg} i_k; \quad t \quad \Sigma \frac{h_k}{V_k \cos i_k}.$$

where i_1, i_2,..., i_n are the angles which the seismic rays make with the vertical: along one and the same ray $(\sin i_k)/V_k = $ const, summation Σ is carried out for all values, 1, 2,... n.

The cited relationships make it possible to determine the value of $V_{e,max}$ and to evaluate the corresponding maximum error $\gamma = \gamma_{max}$, if the structure of the medium is given, i.e., if the magnitudes of h_1, V_1, h_2, V_2,... are given. For this purpose, it is enough to substitute the values of V^*, Δ_{max}, written above, into the formula for $V_{e,max}$, and then the values of $V_{e,max}$ (instead of V_e) and to substitute V_m for γ in the formula.

The minimum systematic (but therefore highly random) error is obtained with an extremely short hodograph, if we can assume that $\cos i_k \to 0$. In this case,

and then

$$V^2_{e,min} = \frac{\Sigma V_k h_k}{\Sigma \frac{h_k}{V_k}}$$

$$\gamma_{min} = \frac{\sqrt{\Sigma V_k h_k \Sigma \frac{h_k}{V_k}}}{h} - 1.$$

It is interesting that in the limiting case at $\Delta = 0$, the quantity $\gamma_{min} \neq 0$.

In the case of layers, the minimum error values of γ are determined and presented graphically for various ratios $m = h_2/h_1$ and $n = V_2/V_1$ in the reference [30]. For a determination of the maximum values of γ in the case of two layers, we will use the following formulas [30]:

$$V_m = V_1 \frac{1-m}{1 + \frac{m}{n}},$$

$$V_e = V_1 \left(\frac{\frac{1}{\cos i_1} - \frac{mn}{A}}{\frac{1}{\cos i_1} - \frac{m}{nA}} \right) V_1,$$

where $A = (1 - n^2 \sin^2 i_1)^{1/2}$. The angle i_1, is apparently equal to zero at the epicenter, and approaches the magnitude arc sin (V_1/V_2) as it moves away from the epicenter.

The values of $\gamma = \gamma_{max}$ were calculated in the assumption that $n = (V_2/V_1) = 1.2$ for angles i_1 from 0 (at the epicenter) to 56° (at an epicentral distance of $\Delta \sim 10$ h), for various ratios of $m = h_2/h_1$. At $i_1 < 50^o$, the quantity γ does not exceed 2.5%; at $i_1 = 56^o$, it reaches 7%. This degree of accuracy may be regarded as fully adequate, particularly at distances where $\Delta \sim$ h.

Vertical Hodographs for the Garm District

The vertical hodographs for the Garm district were constructed on the basis of observations taken in the period 1955-1956, for four separate sectors.

The first sector was the most favorable for the construction of hodographs - an earthquake strip extended along the line of the northern stations on the right bank of the Surkhob. Here, a great number of earthquakes was recorded, and their coordinates were determined with great accuracy (according to the isochrone method, see § 3). The focal depths in this sector ranged within rather wide limits: from 2-3 to 40 km. The observation conditions here (extremely small epicentral distances and a great depth interval) are closest to the seismic prospecting conditions with respect to the method of reflected waves. Vertical hodographs, constructed for these earthquakes, are shown in Fig. 19, a. The hodographs of

longitudinal $(t_p - t_Q)$ and fictitious $(t_s - t_p)$ waves are plotted
on the curve, as are the strata velocities of the longitudinal
waves and the average velocity of the longitudinal and fictitious
waves $(S - P)$. The hodograph was constructed to a depth of 40 km,
although the last sector was not too reliable. Along this entire
hodograph, with the exception of the upper·part, the strata vel-
ocity was 6.05 ± 0.05 km/sec for longitudinal waves (V_p) and 8.3
km/sec for fictitious waves (V_f). Close to the surface, the vel-
ocity V_p dropped to 5.0 km/sec. The over-all thickness of the
surface layer here is small and amounts to 2-3 km.

The second sector, for which the vertical hodograph was con-
structed, is a strip of epicenters between the axial portion of
the Peter I range and the bed of the Surkhob River. The resultant
vertical hodograph differs little from the preceding one (Fig. 19,
a), but exhibits a somewhat lower velocity in the zone adjacent
to the surface. In this sector, there are outcroppings of sedi-
mentary rocks at the surface, and the resultant hodograph shows
them to be of comparatively limited thickness.

The following, the third, sector coincides with the axial
portion of the Peter I range. The hodograph for this sector is
shown in Fig. 19, b. It is of the same general nature as the
hodograph for the first sector (Fig. 19, a), but the surface layer
with a velocity of $V_p = 5.0$ km/sec exhibits far greater thickness
here: up to 9 - 10 km.

A similar hodograph was obtained for the last, the fourth,
sector - the valley of the Obikhingou River.

A simultaneous examination of the vertical hodographs that
we obtained indicates that there is a substantial increase in the
thickness of the surface layer with an average velocity of about
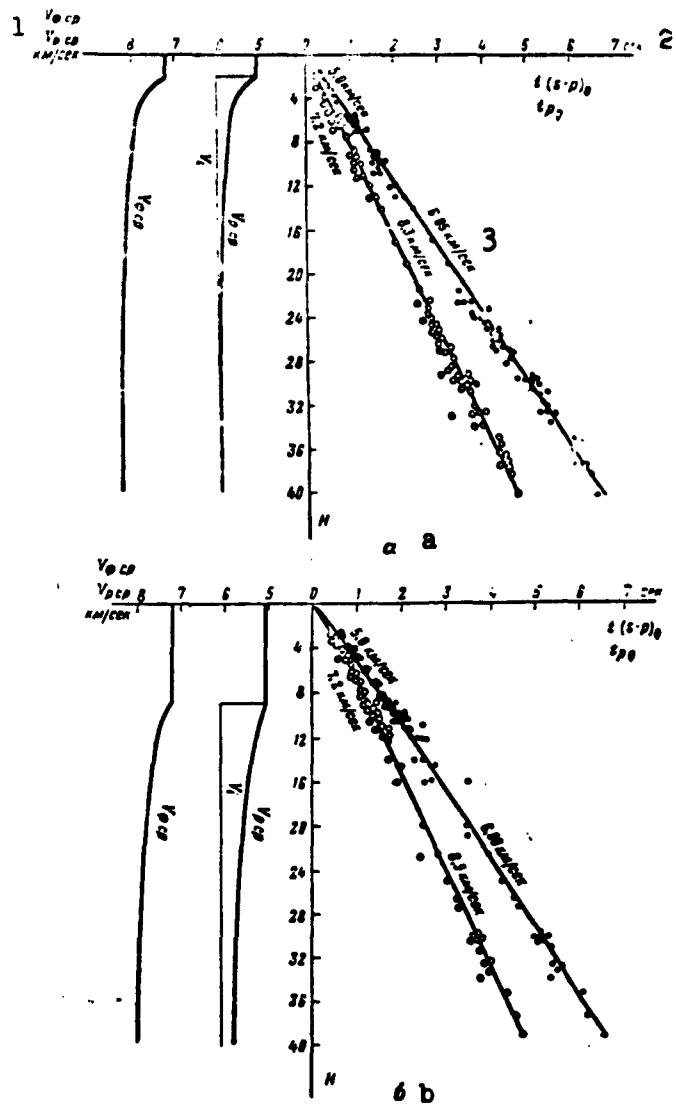
Fig. 19. Vertical hodographs along the northern-station line. a) The sector of the Surkhob River Valley; b) axial portion of the Peter I Range. The open circles correspond to times $t_s - t_p$; the solid circles correspond to times $t_s - t_p$ [sic]; 1) $V_{f,sr}$, $V_{p,sr}$, km/sec; 2) sec; 3) 6.05 km/sec.

5 km/sec from 2 - 3 km to the north of and up to 9 - 10 km to the
south of the axial portion of the Peter I Range. The change in
the thickness of this layer is rather pronounced, and the under-
side is shown to be a steeply inclined discontinuity which sub-
sequently levels off to the south at a depth of 9 to 10 km. This
structure of the upper layers of the Earth's crust in the region
of the Peter I Range, obtained from seismological data, are in
good agreement with the geological data obtained by an entirely
different method (see Chapter 8).
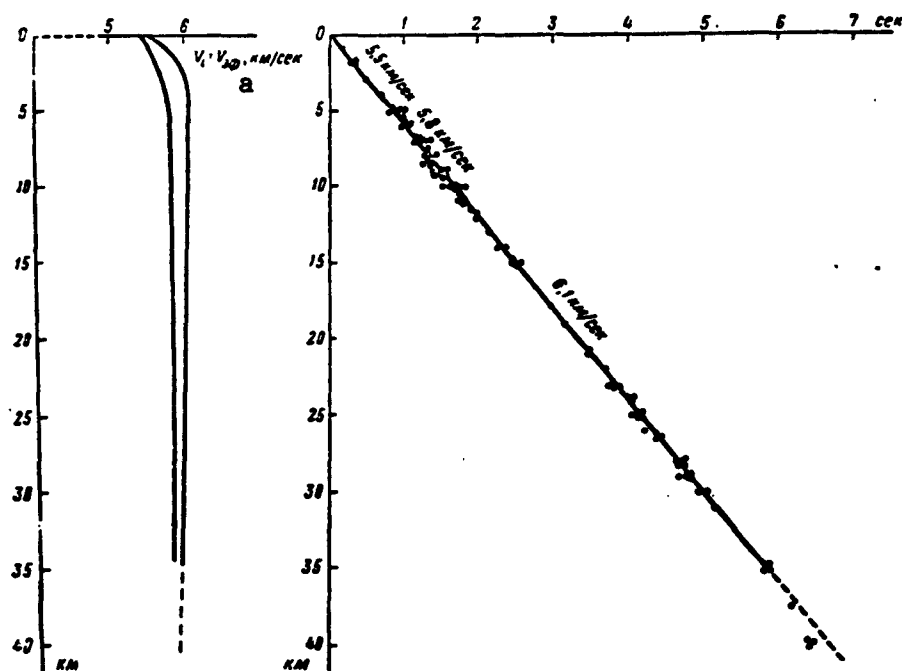
Fig. 20. Generalized vertical hodograph along northern-station
line 1955-1957 observations. a) $V_1 = V_{ef}$, km/sec.

Figure 20 shows a vertical hodograph which generalizes the
most reliable data for the Garm district. This hodograph applies
to both sectors (Fig. 19, a) of the northern group of stations
and includes the 1957 observations in addition to the 1955-1956 ob-

servations. In the construction of this hodograph use was made of the transparent grids of the theoretical seismological hodographs (somewhat refined), as well as of the prospecting hodographs. The mean error in the determination of the coordinates of the observed point on this hodograph does not exceed 2 to 3 per cent, so that the construction accuracy is sufficiently high. On this vertical hodograph, as well as on the earlier ones, only the strata velocity of the "granite" layer is determined with complete reliability; this velocity was determined to be 6.10 ± 0.05 km/sec. For all intents and purposes, this velocity coincides with the discontinuity velocity determined from the horizontal hodographs (§ 1). In addition, the vertical hodograph for the surface zone clearly shows a decrease in velocity. However, strata velocities inherent in the "basalt" layer are not detected to depths of the order of 35 km. Unfortunately, the small number of earthquake foci in the depth range of from 30 to 40 km and the complete absence of such foci at depths beyond 40 km makes it impossible to obtain sufficiently reliable data on the strata velocity for the depths between the Mohorovicic discontinuity (which here lies at a depth of 45 to 50 km) and the most reliable points of the vertical hodograph, corresponding to a depth of 35 kilometers. This leaves unresolved for this region, the problem of the absence or existence of a layer with "basalt" velocity, and here this layer can, apparently, have only a comparatively limited thickness.

Within the limits of the layer with a velocity of $V_p \approx 6.1$ km/sec, the hodograph (Fig. 20) shows no deviations in the points which would confirm the existence of the layer, suggested by B. Gutenberg, exhibiting a low velocity in the lower portions of the granite layer.

Insofar as a drop in velocity close to the surface is concerned, a drop which is clearly exhibited on all of the cited vertical hodographs, this fact has been well established for the Earth's crust both by means of seismological-prospecting projects carried out throughout a great many districts in the USSR (see, for example, [39, 42]) and other countries, as well as from laboratory experiments on the study of change in velocities V_p in various rocks, with increasing pressure ([43] etc.). However, this is also indicated by the high values of the outcrop angles, said values obtained at all stations of the expedition, regardless of the points at which the stations were situated with respect to the epicenter (see Chapter 4). The over-all reduction in velocities V_p on the line to the surface of the Earth in the zone of small depths can take place both comparatively gradually as well as in sudden jumps - in the case of pronounced changes in composition, and sometimes in the state of the rocks. Sharp velocity jumps in this zone (Fig. 19) and their gradual reduction (Fig. 20) are shown only conditionally: the accuracy of determination does not make it possible to choose a given version here.

The above-described results, obtained in the Garm district, represent the first attempt to use the method involving transparent grids of theoretical hodographs and the method of vertical hodographs for the direct determination of strata velocities in the Earth's crust on the basis of earthquake observations.

Vertical Hodograph for the Pamiro-Gindukush Zone

The operating region of the expedition is situated close to the epicentral zone of the Pamiro-Gindukush earthquakes, the focal depths of which attain values of 300 km. It was regarded as possible to construct a vertical hodograph for these earthquakes by using

the same method. The interest in the determination of strata vel-
ocities and the direct determination of the velocity structure of
the subcrustal layer in general is, from the geophysical standpoint,
obvious. To carry out this project, the expedition undertook special
seismic observations in Pamir.

Close to the epicentral zone of the Pamiro-Gindukush earth-
quakes, there is situated the Khorog seismic station of the cen-
tral Asian region network. To the north, there are stations be-
longing to the expedition that are equidistant from the deep-focus
earthquakes. Farther north, there are the seismic stations of the
Fergana Valley, which are approximately 400-500 km from the epi-
central zone. Such a distribution of stations is not favorable for
the processing of observations in accordance with the method de-
scribed, since in this case it would, for all intents and purposes,
be possible only to obtain three individual points or dense clus-
ters of points on the transparent grid of the theoretical hodo-
graphs. Therefore, the expedition provided for the recording of the
earthquakes under investigation at an additional two points in
Pamir: at Vanch and Rushan. Near these two populated areas, mobile
seismic stations, mounted on trucks, were set up in September 1957.
The distances between the stations Khorog, Rushan, Vanch, and Garm
were approximately identical. In the interval between the stations
Garm and Vanch, closer to Garm, we find the station Tovil'-Dora.
The line of five stations is terminated on the east by the Dzhir-
gatal' station, and in the west by the stations of the Stalinabad
division of the TKSE; as a result, it was possible to carry out
the processing of the observations with a sufficient degree of
accuracy, said observations having the purpose of obtaining a
vertical hodograph, although this observation system provided only

for onesided positioning of the line with respect to the epicentral zone. Figure 21 shows the positioning of the expeditionary stations and the regional network, as well as the position of the earthquake epicenters which were employed for the construction of the vertical hodograph.

The earthquake epicenters were determined once again by means of transparent isochrone grids (see § 3). All of the determinations according to the transparent grid of the theoretical hodographs were carried out six times by independent observers; the average values of the six observations were plotted on the hodograph. An estimate of the accuracy in the determination of V and $\underline{h}$ indicates that the errors do not exceed 3-5 per cent for earthquakes with a focal depth of from 100 to 175 km and do not exceed 5-6 per cent for deeper earthquakes. The determination of the depth and of t_Q were carried out with respect to the time difference $t_s - t_p$. The values of the velocity ratio V_p/V_s of the longitudinal and transverse waves were preliminarily determined for all earthquakes according to the Wadati curve. For earthquakes with depths ranging from 100 to 200 km, this ratio turned out to be equal to 1.73 ± 0.03, whereas for deeper earthquakes, the figure was 1.77 ± 0.02. A change in the velocity ratio takes place at a depth of from 200 to 220 km, said change occurring in the form of a jump. The resultant values for the velocity ratios were also used for the selection of the origin on the theoretical transparent grids. In the processing, both the prospecting transparent grid (Fig. 18) and the transparent grid intended for earthquakes (Fig. 17) were used.

The resultant vertical hodograph is depicted in Fig. 22. Points from the vertical hodograph shown in Fig. 20 and for the Kulyaba
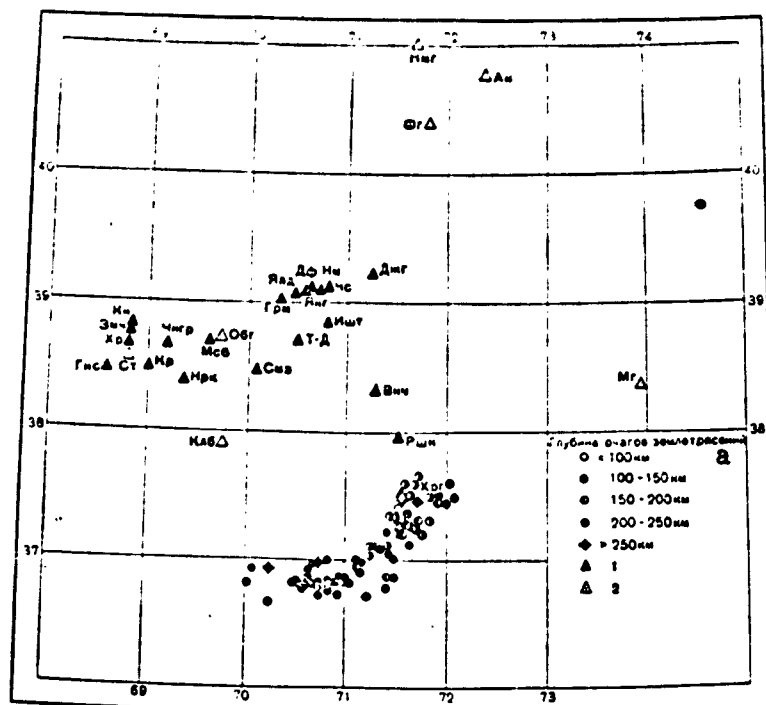
Fig. 21. Position of deep Pamiro-Gindukush earth-
quake epicenters, used for the construction of
the vertical hodograph. 1) TKSE seismic station;
2) seismic stations of the regional network; a)
depth of earthquake foci.

earthquake of 5 October 1957 have been plotted on the same hodo-
graph; the epicenter and depth of the Kulyaba earthquake were de-
termined with a high degree of reliability. Such coincidence for
the vertical hodographs obtained in various regions where the
structure of the Earth's crust may be varied, of course, makes it
possible to obtain only a general picture of the velocity structure
of the Earth, to rather great depths (of the order of 250 km) in
the subcrustal layer, but it was precisely this which was of in-
terest in the given investigation.

The cross section of the subcrustal layer, obtained according
to the vertical hodograph, yields the following values for the
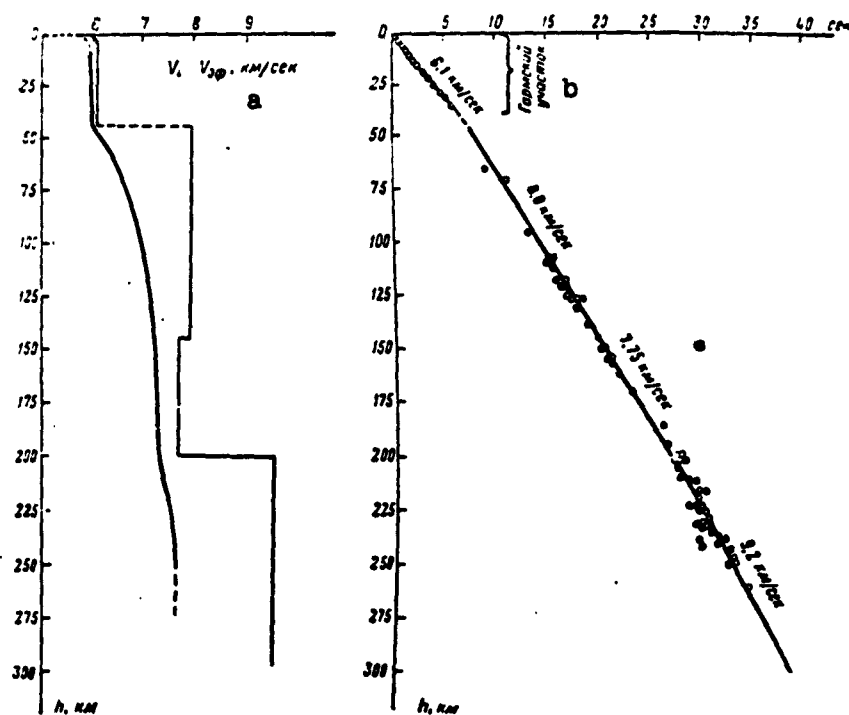
Fig. 22. Vertical hodograph for Pamir, constructed
on the basis of deep Pamiro-Gindukush earthquakes. a)
$V_1 \cdot V_{ef}$, km/sec; b) Garm sector.

strata velocities of longitudinal waves. Close to the underside of

the crust and up to a depth of 150 to 175 km, the velocity is

8.0 to 8.1 km/sec. From this depth, we note a sector with reduced

velocity of the order of 7.7 to 7.8 km/sec. At a depth of approx-

imately 220 km, we note an increase in velocity, possibly up to

9.0 to 10.0 km/sec. Since this sector is not supported with a

sufficient number of points at great depth, we can speak of this

change in velocity and the presence here of a discontinuity only

in hypothetical terms. The results are, as yet, only the first at-

tempt at processing the earthquakes. The depth limitations of earth-

quakes in the Pamiro-Gindukush zone make it difficult to obtain

reliable data for great depths here. Apparently, the best result

may be anticipated from the observations of deep earthquakes in the Pacific Ocean belt.

For an additional check on the data obtained as to the existence of a separation boundary at a depth of 220 km, longitudinal waves were used to construct horizontal hodographs. For this purpose, three earthquakes were employed: 25 May 1955, at 12:28 hours; 9 September 1955, at 21:46 hours; and 5 March 1956, at 07:12 hours. The coordinates of these earthquakes were taken from the bulletins of the seismic networks of the USSR and Czechoslovakia. The utilization of these earthquakes has the advantage that their foci are situated in the east (in China) and lie approximately along the line of the stations of the Tadzhik TKSE network. Therefore, inaccuracies in the determination of the epicenters of these earthquakes will have no effect on the magnitude of the apparent velocities, determined according to the hodograph. The distance from the epicenters of all three earthquakes to the first eastern station (Dzhirgatal') is 500 to 600 km. According to calculations, it is approximately at these distances that the headwave from the layer at a depth of 220 km must be initiated in the first arrivals. And indeed, in the sector of the summary hodograph of these three earthquakes, on the line Dzhirgatal'-Gissar, a wave with a velocity of 9.6 km/sec is observed. In the second arrivals, we can note with sufficient accuracy (on the basis of the earthquake of 5 March 1956) a wave with a velocity of 7.9 km/sec, said velocity corresponding to the velocities of the head waves from the Mohorovicic discontinuity. For purposes of checking these data, the earthquake of 5 October 1957 was also employed. For this earthquake a hodograph of the reflected longitudinal wave was constructed on the basis of the clear arrivals. This hodograph coincides well

wit the theoretically calculated hodograph of the reflected wave from this same discontinuity.

If by way of experiment the vertical hodographs of shallow earthquakes in the Garm district and of deep Pamiro-Gindukush earthquakes are made to coincide, and if we assume the absence of a "basalt" layer, the intersection of the branches of these hodographs, with velocities of 6 and 8 km/sec, will determine the thickness of the Earth's crust in the region of central Pamir. The data thus obtained indicate that the thickness of the crust here must be 45 ± 5 km, and this is close to the values obtained in accordance with the longitudinal hodographs for the Garm district. The assumption of the presence of a "basalt" layer led to greater values for the thickness of the crust for central Pamir. It is interesting to note that these, as yet, coarse approximate constructions will, nevertheless, lead to sufficiently reasonable results.

Thus the example of processing deep Pamiro-Gindukush earthquakes demonstrated the practical possibility of the direct determination of strata velocities in the ground by this method, not only for the Earth's crust, but for the subcrustal layer as well. We may anticipate that the introduction of this method into practical seismology will enable us markedly to expand and refine our knowledge as to the velocity structure of the Earth in this important depth zone, where earthquake foci are encountered.

§ 3. Method for the Determination of Position of Earthquake Foci
General Characteristic of Methods Used to Determine Focal Coordinates

In all seismological investigations, the primary goal is the determination of the epicentral coordinates (x, y) and the focal

depth (h) of the earthquakes. These magnitudes are initial data for all further operations. It is evident that all subsequent constructions and conclusions depend in great measure on the reliability of the results obtained in the determination of these quantities. The process involved in the determination of the basic geometric quantities x, y, and h is extremely laborious. In view of all of this, particular significance has always been placed on the selection of efficient methods for the determination of focal coordinates.

Let us take a brief look at the methods used in seismology for the determination of focal coordinates, or to be more precise, for the determination of the coordinates of the hypocenter. These methods can conventionally be divided into three groups.

1. The methods for which use knowledge of the propagation velocities of elastic waves in the region being studied is not required (said methods sometimes inappropriately referred to as "objective methods," as if all remaining methods were "subjective"). Of these, the Wadati [44] method is regarded as classical. In recent years, other methods have been proposed: an epicentral method [45], Yevseyev's method [46], and an isochrone or mean-line method [47]. We can also include in this group the method which involves the determination of the epicenter according to the azimuth of the first arrival, said method proposed in 1910 by Academician B. B. Golitsyn and subsequently developed in the work carried out by Academician G. A. Gamburtsev [48], the latter's work devoted to the corrolation method of studying earthquakes. An evaluation of the accuracy of the methods included in this group is undertaken in the following works [49-51].

2. The methods for whose use it is necessary to know the

velocities of seismic waves in the region being studied. These
methods include the hyperbolic method, the Kaloi, Isikava, and
Inglad method [34], as well as the hypocentral method [52]. We
can also include in this group the intersection method with a
given hodograph. An evaluation of the accuracy of this intersection
method is presented in the work [53].

The above-enumerated methods are based on the assumption that
the medium being studied is either uniform or, in certain cases,
horizontally stratified.

3. The third group of methods includes those which take into
consideration the horizontal nonuniformity of the structure of
the medium in the region being studied. These include: the re-
duction method [54], and the method of iso-surfaces after S.S. An-
dreyev [55]. It makes sense to use these methods when the velocity
structure of the medium is known to a high degree of accuracy. The
graphic analytical method [3] can also be included in this group,
and to employ this method we need not know the velocities in
the region being studied. However, this method is restricted in its
application, since it requires a specific system for the position-
ing of the stations relative to the separation boundary for two
media and since it necessitates rather cumbersome and laborious
calculations. The latter circumstance makes it little suited for
mass processing.

Methods based on the assumption that velocities are constant,
in essence, represent a variety of methods for the solution (gen-
erally graphically) of the system of equations

$$(x - x_i)^2 + (y - y_i)^2 + (h - z_i)^2 = V^2 t_i^2, \qquad (1)$$

where x, y, h are the coordinates of the focus, x_1, y_1, z_1 are the

coordinates of the ith station, t_i is the time required for the wave to reach the ith station, and V is the propagation velocity of a specific type of wave. All of the graphical methods of solving the system of equations can be reduced to the successive processing of observations from several pairs of stations, as a result of which the earthquake epicenter is determined as the intersection of any lines: a hyperbola, a cord of the circumference, etc. This system of equations, generally speaking, may be solved analytically; however, in view of the cumbersome calculations required, analytical methods have found almost no application in practice.

A shortcoming of the graphic methods is the impossibility of carrying out the following operations: a) to process jointly and simultaneously all of the similar observation data, including excess data; b) easily to evaluate the coincidence of all observation data, to select and reject those data which contain serious errors; c) to evaluate the consistency and accuracy of the results; d) to process the observations simply and efficiently, which is a point of particular importance in the processing of mass material.

Under the conditions of high seismicity in the Garm district and the great magnification of the seismic equipment, the stations of the expedition recorded tens of earthquakes per day. Existing methods were inadequate to process this material with the required efficiency and accuracy. Therefore, a special method was developed for the primary use of the expedition, said method involving transparent isochrone grids, and this method was, for the most part, devoid of the above-enumerated shortcomings, and what is most important, it provided for sufficient efficiency and accuracy in the processing of the observation data. This method was proposed by Yu. V. Riznichenko [41] for the case of a uniform or horizontally

stratified medium. Under the conditions prevailing in the Garm region, in the presence of pronounced nonuniformities in the medium, in the horizontal direction, (close to the vertical boundary of separation), it was necessary to generalize the method for the case of an arbitrary structure of the medium.

We will dwell briefly on the essence of this method and its application for various structures of the medium, in particular in its application in the Garm district.

The Isochrone Method for a Uniform Medium

Let us consider a uniform half-space, for which the propagation velocity of seismic waves is known. The earthquake focus will be assumed as given by coordinates x, y, and z = h. In this case, as any value of h, it becomes possible to calculate the longitudinal hodographs of straight-line waves at the boundary of the half space. As is well known, these hodographs for various focal depths will make up a set of hyperbolas. The isochrones of the time field within the half space will be spheres or exhibit spherical surfaces, and at the boundary of the half space, concentric circles with their centers at the epicenter of the earthquake. Evidently, a change in focal depth will result in a corresponding change in the radius of the circle (Fig. 23).

The set of concentric circles of the isochrone for various focal depths, is constructed on tracing paper or any other type of transparent material, to the scale of the chart being employed, and will serve as the transparent grids for the determination of the position of the earthquake epicenter and the focal depth.

The transparent isochrone grids, generally speaking, can be constructed by using velocities V_p, V_s, V_f for longitudinal P, transverse S, or fictitious $(t_s - t_p)$ waves. The fictitious vel-

ocity is determined by the following formula:

$$V_\phi = \frac{V_p \cdot V_s}{V_p - V_s}.$$

In all subsequent considerations we will regard the velocity V as being precisely the velocity of the fictitious waves and this velocity will be employed for the construction of the transparent grid. This is associated with the fact that at small epicentral distances (up to 50 to 70 km) the difference between the instants of arrivals for longitudinal and transverse waves can, in the majority of cases be obtained with the highest accuracy.

The selection of the depth intervals in the construction of the transparent grids must be based on the true accuracy of the determination of the depths, and this depends on the density of the seismic-station network, the positions of the epicentral zones relative to the stations, the accuracy of the time service, etc.

The techniques in working with transparent grids can be reduced to the following. The transparent grid is superimposed on the chart (on which the seismic stations have been plotted) in such a manner that each seismic station coincides with the circle that corresponds to the value of $t_s - t_p$ at this station (Fig. 24.). When this position is determined, the isochrones of the transparent grid coincide with the isochrones of the earthquake-time field, and the transparent-grid center coincides with the earthquake epicenter on the chart. It is clear that if the focal depth of the earthquake coincides with the depth which we initially used in the construction of the transparent grid, such a coincidence will also be possible in the case of three stations that do not lie, separately, on a single straight line. If, however, the depth of the earthquake is different from the depth which was assumed in the construction of the transparent grid, such coincidence
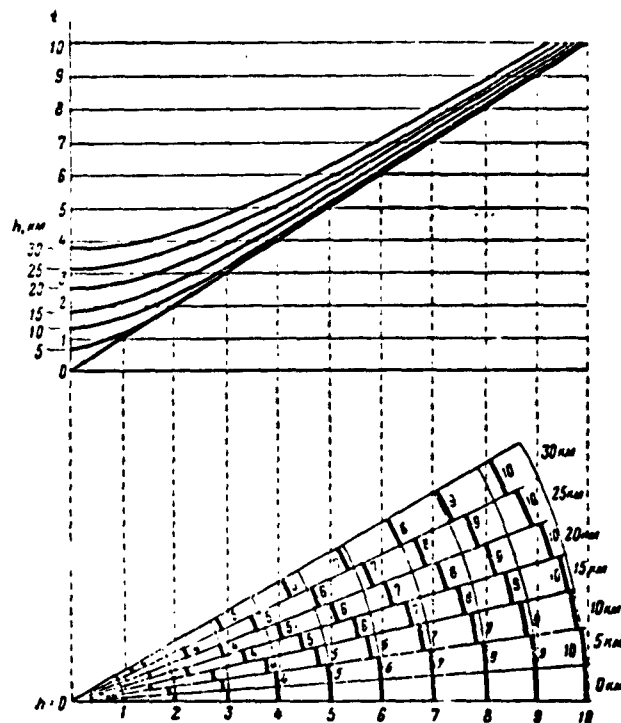
Fig. 23. Hodographs and transparent-grid
sectors of isochrones for various focal
depths in a uniform medium.

will be completely impossible. By superimposing transparent grids

for various depths on the chart, we can find the depth for which

such coincidence is possible, and in this way we determine the

position of the epicenter and the focal depth. In practical work,

when we generally have to deal with an excessive number of data

(when there are more than three stations), the determination of

depth can be reduced to the selection of the particular transpar-

ent grid for which it is possible to obtain the best agreement

between the data received from the various stations.

The basic advantage of the transparent-grid isochrone method

is its efficiency and lack of difficulty: in using transparent

grids, there is no longer any need to carry out any calculations
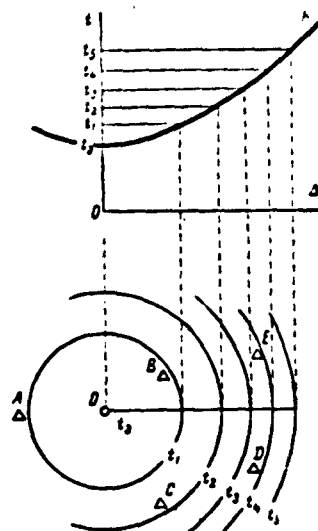
Fig. 24. Diagram of
operations with
isochrone transpar-
ent grid.

or to perform any graphical constructions.
Moreover, the isochrone method makes it
possible to determine the extent of agree-
ment between all of the data, and to re-
ject those of the data which contain gross
errors. It is also not difficult to deter-
mine any systematic variance in data from
individual stations, said variance possi-
bly related to the nonuniformity of the
structure at specific sectors in the re-
gion under investigation.

The Isochrone Method for a Nonuniform
Medium

Given a horizontal-stratification struc-
ture of the medium, the time field will no
longer be spherical, but the isochrones at the surface will remain,
as before, concentric circles. If the velocity cross section of
the operating district has been determined, for example, by means
of vertical* or longitudinal hodographs, it will be possible to
construct the time field for the foci situated at various depths.
The cross section of these time fields at the surface will serve
as the isochrone transparent grids for the determination of focal
positions, and here the technique of working with transparent
grids remains the same as in the case for a uniform medium.

We encounter a different situation if there are nonuniformi-
ties in the medium not only in a vertical direction (horizontal
stratification), but in the horizontal direction (for example,
vertical or inclined boundaries of separation in the form of planes
or surface curves). In this case, the shape of the isochrone will

· 97 ·

change as the seismic ray intersects the boundary of separation. If the focus and the observation station are on one side of the boundary of separation, the isochrone system will correspond to a uniform medium; if, however, the focus and the observation station are situated on opposite sides of the boundary, the time field will depend not only on the focal depth but on the position (x, y) of the epicenter. In other words, for various foci, situated at one and the same depth, but $\hat{b}$n opposite sides relative to the boundary of separation, the isochrone system will be varied.

In order to construct a transparent grid in this case, said grid to be useful for the determination of the epicentral position at any point in the region being studied, we will use the principle of reciprocity. We will assume that the point coinciding with the seismic station is itself a source of the perturbation. We will construct a time field for this fictitious source. This field characterizes the time required for the wave to cover the distance between the fictitious focus and any point in the medium and back from any point to the given station.

Let us consider a case in which the boundary of separation takes the form of the vertical plane MN, separating region I, where velocity $V = V_1$, from the region II, where velocity $V = V_2$ (Fig. 25). For the sake of determinacy, we will assume that $V_2 < V_1$. Let there be four seismic stations, each in a different position relative to the boundary of separation: station A in region I; station B, at the boundary of separation; stations C and D, in region II, all at various distances from the boundary of separation. Situating the fictitious focus, successively, at the points where the seismic stations are located, we will construct the time fields for these sources (Fig. 25).
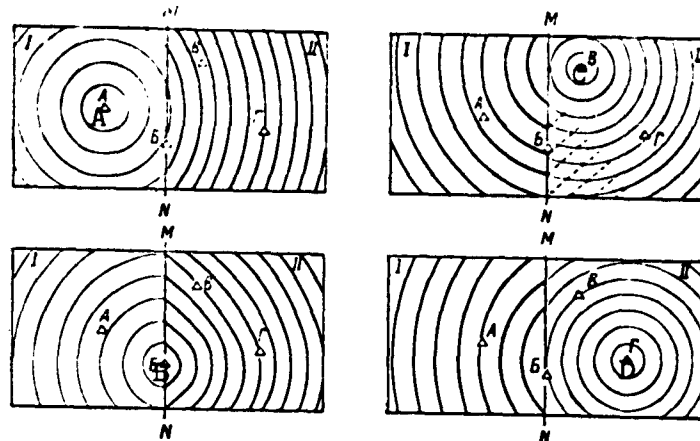
Fig. 25. Time fields for stations A, B, C, and D. Fine lines represent straight-line waves; bold-face lines represent refracted waves; dashed lines represent head waves.

Let us take one of the time fields constructed on the tracing paper; for example, let us take the set of isochrones for station C. Let us position this field on a chart of the region, said field naturally drawn to the same scale, and then we will line up the transparent grid, keeping the lines MN on the chart and on the transparent grid parallel. We will select some arbitrary point O (epicenter) on the chart. Then we will turn the transparent grid 180° in the horizontal plane (about its vertical axis), i.e., so that the line NM on the transparent grid again becomes parallel to the line MN on the chart. Then, by parallel translation (without rotation) we will cause the center of the transparent grid to coincide with the arbitrarily selected point O.

In accordance with the principle of reciprocity, the time required for the wave to move between the focus and the station, in this case, remains the same and this means that station C lies on the isochrone corresponding to the time required for the wave to move from this focus to station C, although, generally speaking, the
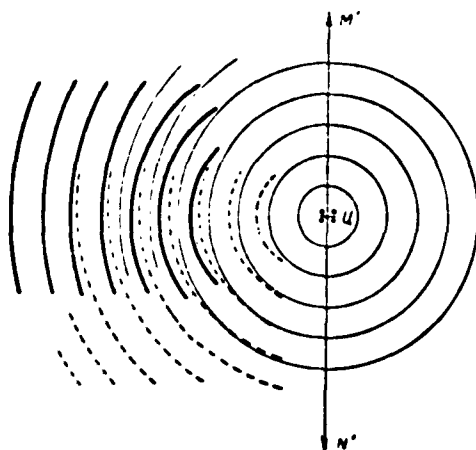
Fig. 26. Coincidence of time
fields for various stations.
Tnin lines represent the iso-
chrones of stations A and B;
dashed lines represent the
isochrones for the station C;
and the bold-face line rep-
resents the isochrone for
station D.

Ц = Tsentr = Center

isochrones of the transparent
grids, in this case, do not coin-
cide with the isochrones for the
time fields of the focus. In oth-
er words, if only the time field
(turned through an angle of 180°)
of any station is subjected to
parallel translation on the
chart, the given station, in this
case, will always lie on the iso-
chrone which corresponds to the
time required for the wave to
pass to this station from the
epicenter which is coincident
with the translated time field.
What has been said above is valid
for any position of the epicenter, but only for the given station.

In order to make use of the data from all stations simultan-
eously, parallel translation must be employed, i.e., without rota-
tion, to cause the centers of the time fields of various stations
to coincide, and then execute a 180° turn. This plotting of several
(in terms of the number of existing stations) isochrone systems may
serve as the transparent grid for the determination of the position
of the epicenter at any given point in the given region. Each sta-
tion produces its "own" isochrone system with such a transparent
grid. With the utilization of a transparent grid, each station
must be made to coincide with the corresponding isochrone of its
system (i.e., obtained by turning the time field of this station).
Since the isochrones in a nonuniform medium are not circles, the
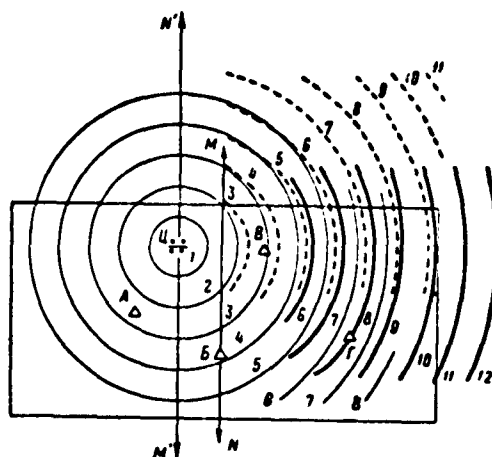
Fig. 27. Example of determination of epicenter, by means of transparent isochrone grid for nonuniform medium. Isochrone denotations the same as in Fig. 26. The difference $t_s - t_p$ (in seconds): for seismic station A, 2.6; B, 3.9; C, 3.4; D, 8.0.

transparent grid may not be turned, but must be subjected to a parallel translation. For this, in the construction of the time fields, some direction line must be marked both on the chart and on the transparent grid and care must then be taken so that these lines are kept parallel on the chart as well as on the transparent grid. This line may be a meridian or the known vertical boundary.

A transparent grid consisting of a system of several superimposed time fields is difficult to read. It is more convenient to construct individual transparent grids for the determination of foci in various regions, i.e., on one or another side of the boundary of separation. As an example, let us undertake a detailed examination of the transparent grid for the determination of the foci situated in region I, with the stations positioned as indicated as in Fig. 25. For simplicity, we will assume that parameter h is equal to O.

The construction of the transparent grid is handled in the following sequence. The center of the final transparent grid - point Ц - is marked on the tracing paper, and the straight line M'N' (Fig. 26) is drawn through this point. Then point Ц on the tracing cloth is made to coincide with the center of the time field of one of

the stations - for example, station C - so that the straight line M'N' is parallel to the boundary of separation MN, and that portion of the time field of station C, which lies within the limits of the selected sector is transferred to the tracing cloth; in this particular case, the selected sector is the region I (with the use of transparent grids, these isochrones are employed for purposes of coincidence with station C). Then, by means of parallel translation, the tracing cloth is successively superimposed on the time fields of other stations, and point Ц is made to coincide with the centers of these time fields, and while the straight line M'N' and the boundary of separation MN are kept parallel, those sectors of each of the time fields which pertain to the region I are plotted on the tracing cloth, with conventional denotations. It is clear that the isochrones in this sector, for stations A and B, will be the same as for a uniform medium in which the velocity $V = V_1$, whereas for stations C and D the shape of the isochrones is not that of a circle. The isochrone system thus obtained is shown in Fig. 26. To convert this system into a transparent grid for the determination of epicenters, we need only turn it through an angle of 180° in the plane of the drawing.

The determination of the position of the epicenters, said determination accomplished by means of the transparent grid that we obtained, is handled in the following manner. The transparent grid is superimposed on the chart and moved along the chart, keeping the boundary of separation on the chart and the straight line N'M' on the transparent grid parallel. In this case, and in this case alone, as each station on the chart is made to coincide with the isochrone of the isochrone system for this particular station, the center of the transparent grid (point Ц), corresponding to a value of $t_s - t_p$

at this station, will coincide with the earthquake epicenter. Figure 27 shows an example of the determination of an epicenter by means of a transparent grid.

Similar methods are employed for the construction and application of transparent grids for the other sector on the chart of region II. In the case under consideration, we assume the depth of the focus $h = 0$, i.e., we solved a two-dimensional problem. In order to construct the transparent grid for a focal depth of $h = h_1$, other than zero, it is, apparently, necessary to replace the isochrone systems shown in Fig. 26 with other systems which show a cross section of the spatial time fields of several stations as a horizontal plane lying at a depth of $h = h_1$.

A similar method for the construction of transparent grids may be employed for any other shape of the boundary of separation — inclined planes or curved surfaces — as well as with a continuous change in velocity.

The isochrone transparent grid method, in this generalized form, may be employed in cases in which the stations are situated not only at the surface but deep within the Earth, at depths comparable to the focal depths (for example, in studying the position of feeble pulses and mine blasts in shafts, where seismic receivers may be installed not only at the surface but deep underground).

Isochrone Transparent Grids for the Garm District

The velocity cross section of the medium in the Garm district, obtained from the vertical hodographs (§ 2) is close to the case of nonuniformity which was examined above. Along the axial portion of the Peter I range there is a boundary of separation between the mesozoic-cenozoic sedimentary layers ($V_f = 7.2$) to the south and the crystal bedrock of the range ($V_f = 8.3$) to the north. This
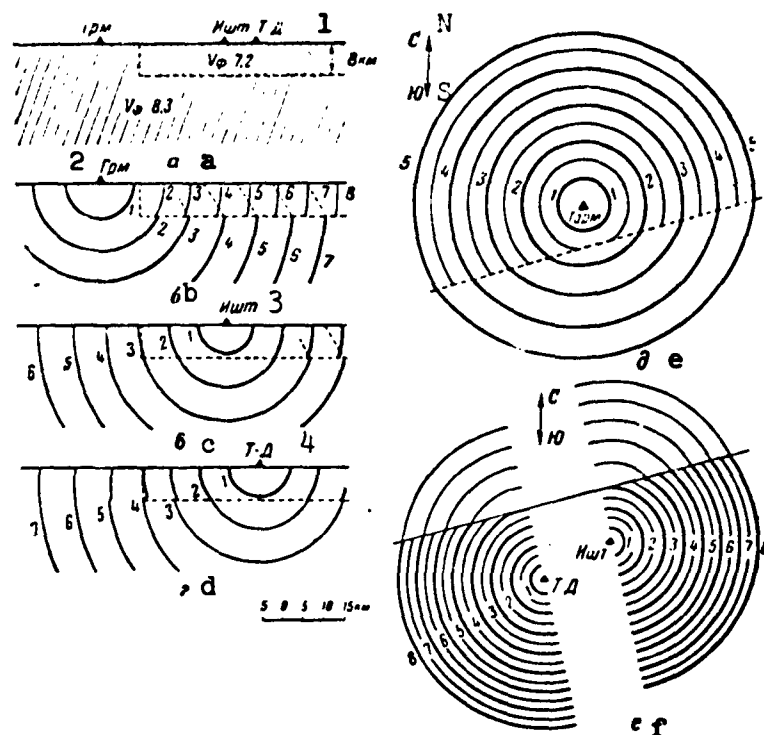
Fig. 28. a) Velocity cross section of medium in Garm district; b - d) time fields for stations in vertical plane; b) for the Garm station or any other station of the northern group; c) for the Ishtion station; d) for the Tovil'-Dora station. Isochrones f and e of the time fields in the horizontal plane at depth h = 5 km; bold-face lines represent the isochrones for the time field of a straight-line wave; the thin lines represent the isochrones of the time field for a refracted wave; and the dashed lines represent the isochrones for the time field of a head wave; 1) Isht-T-D [Ishtion-Tovil'-Dora]; 2) Grm [Garm]; 3) Isht [Ishtion]; 4) T-D [Tovil'-Dora].

boundary is steeply inclined close to the surface, and evens out markedly at a depth of 8 to 10 km, thus forming a "step."

This structure is schematically presented on the vertical cross section of the Peter I Range (Fig. 28, a). Apparently, for foci at a depth of h < 8 km, this cross section matches the vertical plane boundary whereas for foci with depths of h > 8 km, the
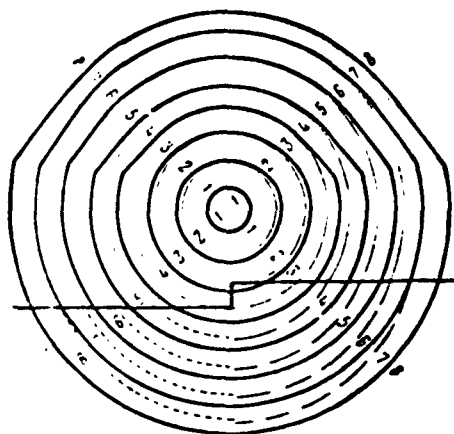
Fig. 29. Transparent grid for the determination of epicenters throughout the Garm district. h = 5 km
Bold-face lines represent the isochrones for the time field of the group of northern seismic stations; the thin lines represent the isochrones of the time field for the Ishtion and Tovil'-Dora stations, in the region to the north of the axial portion of the Peter I range; the dashed lines represent the isochrones for the time field of the Tovil'-Dora station, in the region to the south of the axial portion of the Peter I range; the dashed-dotted (short dashes) line represents the same for the Ishtion station.

cross section is equivalent to a uniform medium (for the northern stations) and to a horizontally stratified medium (for the southern stations). The time fields for the stations Garm, Tovil'-Dora and Ishtion are shown in Fig. 28, b - 28, d for this velocity cross section in the vertical plane, and in Fig. 28, e - 28, f in the horizontal plane, at a depth of h = 5 km.

The northern group of stations (Garm, Yaldymych, Yangalyk, Dzhafr, Nimich, Chusal, Dzhirgatal') extends along the boundary of separation. All of these stations are approximately equidistant from the boundary, but in any case the difference in these distances falls within the limits of accuracy with which the position of the boundary has been determined. Therefore, the time fields for the northern stations are practically identical. The distances from the stations of the southern group (Tovil'-Dora and Ishtion) to the boundary, show pronounced divergence.

Having caused the three time fields to coincide so that their centers coincide, and having turned them through an angle of 180°, we obtain a transparent grid (Fig. 29) that is suitable for the de-

termination of positions of epicenters at a depth of h = 5 km, throughout the entire Garm district. The transparent grids for a depth of h = 5 km were constructed separately, in their working version, for epicenters to the north and south of the axial portion of the Peter I Range. Moreover, several simplifications have been introduced into these working transparent grids, said simplifications having as their goal the more convenient reading of the grids. Since the boundary of their separation in our case is flat, the time fields of the Tovil'-Dora and Ishtion stations will be symmetrical relative to the straight line passing through the center of the transparent grid and perpendicular to the boundary of separation. It has therefore proved to be possible to draw only half the time fields of these stations on the transparent grid, and as a result they do not overlap.

For foci deeper than the thickness of the layer with velocity V_p = 5.0 (V_f = 7.2), the transparent grids are simpler, since this case approaches the case of horizontal stratification. The cutting of the time fields (Fig. 28, c, d) with horizontal planes h = 10, 15, 20,..., 40 km, will yield circular isochrones both for the northern as well as for the southern stations. However, the radius of the corresponding isochrones for the northern and southern stations will vary somewhat as a result of the difference in the thickness of the sedimentary layers (V_p = 5.0), through which the seismic waves pass on their way to the northern (thickness not more than 2 to 3 km) and the southern (thickness approximately 8 to 10 km) stations. The determination of focal depth is accomplished just as in the case of a uniform medium by selecting the transparent grid which yields the best agreement between the data of the various stations.

Similar transparent grids were constructed for the Stalina-bad district.

We spoke above of the fact that transparent grids, as a rule, are constructed for fictitious waves, since at small distances the difference $t_s - t_p$ is determined with greatest accuracy. However, for earthquakes in individual districts (for example, the Obi-Garm district), for which extremely unclear arrivals of transverse waves are characteristic, it became necessary to construct the transparent grids according to times $t_p - t_Q$ (here t_Q is the time at the focus). In using such transparent grids, we must know the time t_Q for the occurrence of the earthquake. Generally, this time is determined according to the Wadati curve. Knowing the mean velocity ratio between the longitudinal and transverse waves ($k = (V_P/V_S)$), obtained from a great quantity of material for the Garm district ($k = 1.73 \pm 0.02$ for crystaline rocks and $k = 1.78 \pm \pm 0.02$ for sedimentary rocks), we can determine t_Q with sufficient reliability according to the data of one or two stations alone, if the values of t_p and $t_s - t_p$ have been determined for these stations.

Isochrone transparent grids were used for the determination of the hypocenters of all earthquakes occurring in the Garm, Obi-Garm, Stalinabad, and other areas in which the expedition was engaged. During the period from 1955 to 1958, this method was used to carry out approximately 15,000 determinations.

Transparent Grids with Various Types of Waves

Isochrone transparent grids can be used successfully for the determination of epicenters of so-called near-by shallow earthquakes, i.e., earthquakes situated at distances of $\Delta \sim 100$ to 700 km, for example, in Central Asia. In this case, for various

distances we may employ various types of waves which can best be distinguished and identified on the seismograms. Thus, for example, transparent grids can be constructed according to fictitious waves $t_s - t_p$ at distances of $\Delta \leq 70$ km, and for great distances we can use the time difference $t_{s_{11}} - t_{p_{11}}$ for the arrival of very intensively reflected waves. We can construct transparent grids over the arrival times of the longitudinal wave which arrives first (initially a straight-line wave, then a head wave). The transparent grid can be constructed of several sectors, each for a certain type of wave.

As an example we will present a transparent grid (Fig. 30) for the determination of the epicenters of shallow earthquakes, for the region of the Fergana Range, said transparent grid constructed on the basis of the experimental hodograph (Fig. 14) obtained for the line Stalinabad - Frunze. Here, the isochrones for the various sectors of the transparent grid are in correspondence either with the time differences $t_s - t_p$ of the straight-line or reflected waves, or with the time $t_p - t_Q$ of the first arrival of the longitudinal waves: at first straight-line, and then head waves.

If there are any particular features encountered in the structure of the Earth's crust at individual points, these may be taken into consideration in the construction of such transparent grids through the application of the principle of reciprocity, similar to the way that this was done for the case of a vertical boundary of separation.

Transparent Grids for Deep Earthquakes

Isochrone transparent grids may be successfully used for the determination of the position of deep-earthquake foci. The velocity cross section of the crust and the subcrustal layer, at depths up

108

to 250 km (see Fig. 22) serves as the basis for the construction of the isochrone transparent grids for this case.

In the construction of these transparent grids, use was also made of the principle of reciprocity. Instead of constructing various time fields for the foci situated at various depths $h = h_i$, a single time field was constructed, with the center of this field lying at the surface (Fig. 31). The intersection of this time field by horizontal planes, at various depths $h = h_i$, will result in isochrone time grids for the determination of the epicenters of the foci of the corresponding depth. The use of these transparent grids in the processing the Pamiro-Gindukush earthquakes, employing the difference $t_s - t_p$ proved to be an extremely effective step and made it possible to attain high accuracy in the determination of epicenters and earthquake depths.

The Accuracy of the Isochrone Transparent-Grid Method

The accuracy of the determination of focal position depends on the number of stations, the location of the focus relative to the station network, and on the error δr in the determination of the hypocentral distance in the data from each of the stations. In the case of a uniform medium, the quantity δr is composed of the errors resulting from the determination of time $t_s - t_p$ at the given station and the error in the determination of the propagation velocities for elastic waves in the given district:

$$\delta r = \frac{\partial r}{\partial t} \, \delta t + \frac{\partial r}{\partial V} \, \delta V. \qquad (2)$$

It is generally regarded that the second term is substantially smaller than the first term and it may therefore be neglected. This is valid so long as the error δt is sufficiently great. Thus in the determination of epicenters according to the data produced by the regional network, as a rule, $\delta t > 1$ sec. For the observations of

the expedition, under conditions of great recording time sweep and a good time service, the quantity δt does not exceed 0.2 sec, and then the second term of Expression(2) becomes comparable to the first, and it must be taken into consideration.

Formula (2) is valid under the conditions of a uniform medium. If, however, the medium is nonuniform, and consists of two media, with a flat vertical boundary between them, the error δt will, in addition, be a function of the error δb in the determination of the position of the boundary of separation. Taking these errors into consideration, we obtain the following formula for the maximum error value:

$$\delta r = \frac{\partial r}{\partial t}\, \delta t + \frac{\partial r}{\partial V_1}\, \delta V_1 + \frac{\partial r}{\partial V_2}\, \delta V_2 + \frac{\partial r}{\partial b}\, \delta b, \qquad (3)$$

where V_1, V_2 are the velocities of the seismic waves in regions 1 and 2, $\underline{t}$ is the time required for the wave to reach the given station, $\underline{b}$ is the distance from the station to the boundary of separation, and δV, δt, δb are the errors in the determination of these quantities. The first term may be modified

$$(\delta r)_1 = \frac{\partial r}{\partial t}\, \delta t = V \delta t,$$

and if, for simplicity, we assume $\delta V_1 = \delta V_2 = \delta V$, the second and third terms may be transformed as follows:

$$(\delta r)_2 = \frac{\partial r}{\partial V_1}\, \delta V_1 + \frac{\partial r}{\partial V_2}\, \delta V_2 = t \delta V.$$

Let us evaluate the magnitude of the last term, associated with the position of the refraction boundary. It is not difficult to demonstrate that

$$(\delta r)_3 = \frac{\partial r}{\partial b}\, \delta b = \frac{V_1 - V_2}{V_1} \cdot \frac{\cos \frac{i_1 - i_2}{2}}{\cos i_1}\, \delta b,$$

where V_1 and V_2 are the wave velocities on various sides of the

110

vertical boundary, and i_1 and i_2 are the angles of incidence and refraction. It is clear that in a uniform medium this term vanishes. Thus, the error quantity δr is equal to

$$\delta r = V \delta t + t \delta V - \frac{V_1 - V_2}{V_1} \cdot \frac{\cos \frac{i_1 - i_2}{2}}{\cos i_1} \cdot \delta b.$$

The errors δV_1 and δb, in essence, reflect not only the error in the determination of the quantities V and $\underline{b}$, but the extent to which there are local deviations from the average values in these quantities. Let us evaluate the value of δr under the specific conditions of the Garm district. The error δt in the determination of times generally does not exceed 0.2 sec, diminishing for extremely close earthquakes (at r = 10-15 km) to 0.1 and even 0.05 sec.

Thus,

$$(\delta r)_1 = V \delta t = (0.4 \div 1.6) \text{ km.}$$

The error δV in the determination of velocity does not exceed 0.1 km/sec. Accordingly, t = 1-10 sec,

$$(\delta r)_2 = t \delta V = (0.1 \div 1.0) \text{ km.}$$

The velocities of the seismic waves in the Garm district are equal to V_1 = 8.3 km/sec to the north, and to V_2 = 7.2 km/sec to the south of the vertical boundary. Then

$$\frac{V_1 - V_2}{V_1} = 0.13.$$

The angles i_1 and i_2 are associated by the expression

$$\frac{\sin i_2}{\sin i_1} = \frac{V_2}{V_1} = 0.87.$$

Consequently, with a change in angle i_1 from 0 to 90°, angle i_2 changes from 0 to 60°, since

$$\arcsin \frac{V_2}{V_1} = \arcsin 0.87 = 60°$$

111
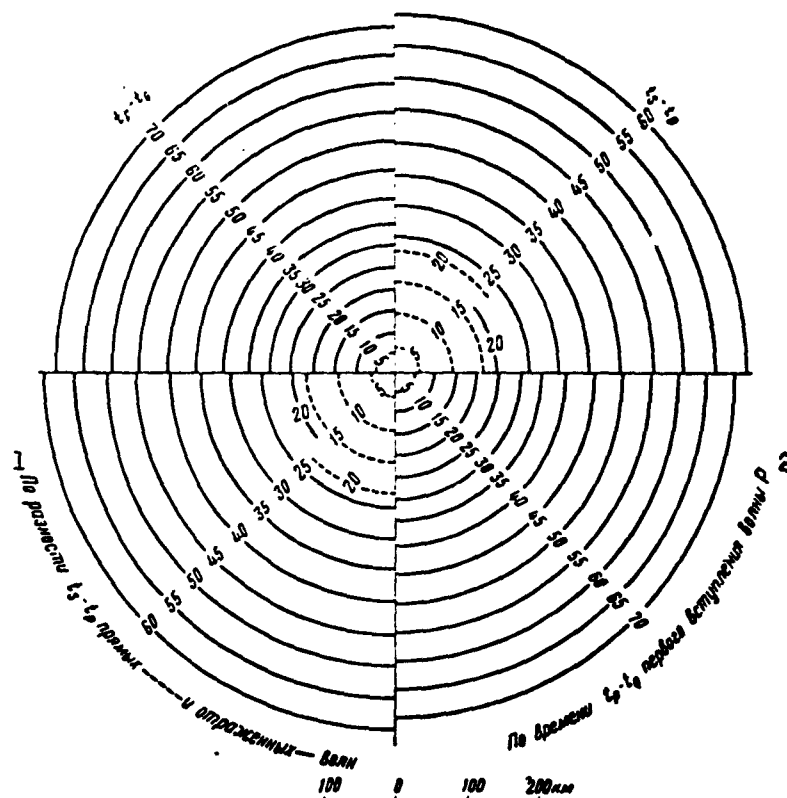
Fig. 30. Transparent grid for the determination of epicenters at
$\Delta \leq 500$ km, said transparent grid constructed in terms of the
time difference for straight-line and reflected waves as well as
over the time of the first arrival of the longitudinal waves. 1)
Over the difference $t_s - t_p$ for straight-line ----- and reflected
_____ waves; 2) over time $t_p - t_Q$ of the first arrival of the P
wave.

and the coefficient

$$\frac{\cos \frac{i_1 - i_2}{2}}{\cos i_1}$$

is equal to 1 at $i_1 = 0°$ and changes from 1 to 1.5 for angles
$0 < i_1 < 60°$. With a further increase in the angles i_1, this
factor may increase, attaining 3 at $i_1 = 70°$. Thus, the third
term of Expression (3) is equal to
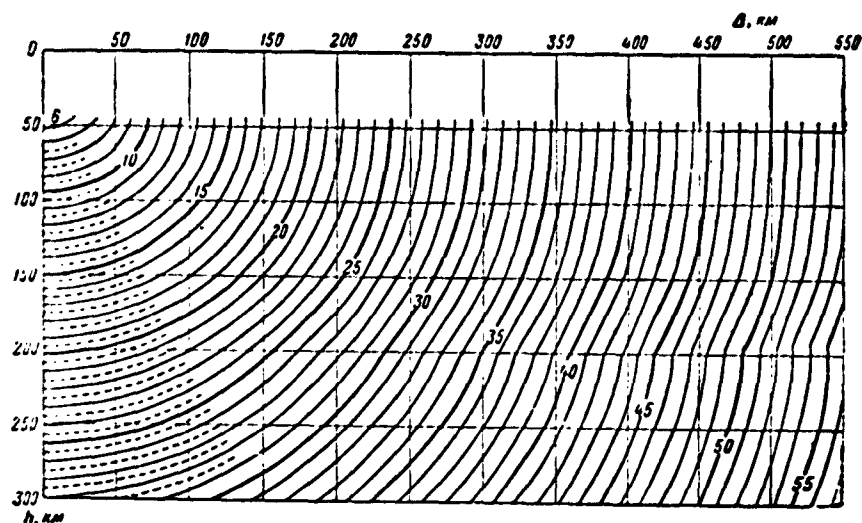
Fig. 31. Time field in vertical plane at depths up to 300 km, said time field used in the construction of transparent grids for the determination of the hypocenters of the deep Pamiro-Gindukush earthquakes.

$$(\delta r)_3 = \frac{V_1 - V_2}{V_2} \cdot \frac{\cos \frac{i_1 - i_2}{2}}{\cos i_1} \, \delta b = (0{,}1 \div 0{,}4)\, \delta b$$

The position of the boundary of separation may be regarded as determined to an accuracy of up to 2 km, and consequently,

$$(\delta r)_3 = (0{,}2 \div 0{,}8) \text{ km.}$$

The total error δr, evidently, is composed of $(\delta r)_1$, $(\delta r)_2$, and $(\delta r)_3$. A simple sum of these quantities will result in the maximum magnitude of error. Since the partial errors are independent and may be of different sign, the average error is most properly evaluated in terms of the magnitude of the square error

$$(\delta r)_{KB} = \sqrt{(\delta r)_1^2 + (\delta r)_2^2 + (\delta r)_3^2.}$$

In accordance with the estimates made above, the square error $(\delta r)_{kv}$ ranges from 0.5 to 2.0 km, and the maximum error ranges from 0.7 to 3 km.

Let us now examine the magnitude of the "error region" as a
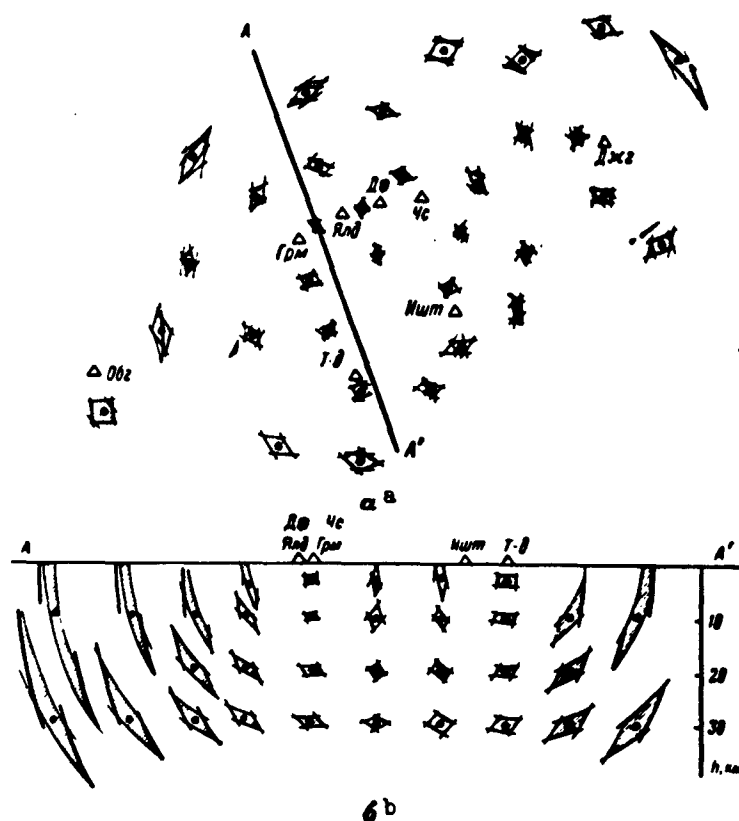
Fig. 32. Dimensions of the error region as a function of the position of the focus relative to the TKSE stations. a) in the horizontal plane; b) in the vertical plane. The triangles represent the seismic stations; the cross hatched areas represent the error regions.

function of the number of stations and their mutual disposition.

N. A. Vvedenskaya [53] presented some formulas by means of which it is possible, in terms of the magnitudes of δr, to evaluate the dimensions of the error regions when there are three stations, assuming that the wave front may be regarded as plane. The latter condition is not satisfied at small distances from the focus. Moreover, Vvedenskaya's formulas are comparatively simple for the case in which the stations are situated in a symmetrical pattern. It is inconvenient to use these formulas in practice, since it is necessary to carry out a calculation for a position of 27 points to

determine the error region of a single focal position alone, and this must be done for various combinations of positive, negative, and zero values of the error δr at each station. With a large number of stations, the calculations become even more cumbersome.

It is simpler to estimate the magnitude of the error region graphically, constructing a system of intersections, with two intersections for each station, and the intersection radii are to be chosen equal in magnitude to the radii $r + \delta r$ and $r - \delta r$ of the spheres cut by the horizontal plane $z = h$, corresponding to the focal depth of the given earthquake. The region, bounded by these intersects from the various stations, will be the error region. In similar fashion it is possible to estimate the error in the determination of the focal depth, constructing the intersects in the vertical plane. Such an estimate was carried out for foci at various positions relative to the station network (Fig. 32). The errors in the determination of the focus surrounded by the stations does not exceed 1 to 2 km, but it increases to 3 to 5 km beyond the limits of the network, and at the edges of the drawing board, the determination error reaches 5 to 10 km.

Thus if the hypocenter is well surrounded by the stations, the error region, for all intents and purposes, does not exceed the magnitude of δr, i.e., errors in the determination of the hypocentral distance, in terms of data provided by an individual station. If, however, the epicenter falls within the group of stations, the error region will be considerably greater in dimension than the magnitude of δr.

We are interested in an individual estimate of the extent of increased accuracy which we attain by taking into consideration the nonuniformity of the medium. For this, we will compare the magni-

tude of a certain hypocentral distance r_1, calculated with consideration of the nonuniformity, and r_2, calculated in the assumption that the medium is uniform and that the velocity of the seismic waves within this medium is equal to the wave velocity in "granite" ($V_f = 8.3$). Then the difference

$$\Delta r = r_1 - r_2 = (t_1 V_1 + t_2 V_2) - (t_1 + t_2) V_1 = t_2 (V_2 - V_1)$$

(t_1 and V_1 represent the time and velocity, respectively, required for the wave to pass through the "granite layer," t_2 and V_2 represent the respective figures in sedimentary rocks) will provide some idea as to the magnitude of the additional error, which may arise if the nonuniformity of the medium is neglected. Under the conditions prevailing in the Garm district, time t_2 required for waves to pass through the sedimentary layer generally ranges from 2 to 4-6 sec. Accordingly, the error Δr lies within the following limits:

$$\Delta r = (2 \div 7) \text{ km,}$$

which is approximately three times greater than had the nonuniformity been taken into consideration, in which case the error would not exceed two kilometers.

Under the conditions prevailing in the Garm district, an estimate of determination accuracy for the coordinates of earthquake foci was also undertaken in a purely experimental manner, according to specific earthquakes. The technique involved in this evaluation can be reduced to the following. If an earthquake took place close to one or two of the stations (time $t_s - t_p$ at the stations did not exceed 1.0 - 1.5 sec), the use of the observations obtained at the remaining stations made it possible to determine the position of the hypocenter and to check this determin-

116 -

ation at nearby stations. For earthquakes farther removed from the closest stations, the accuracy evaluation was handled in the following manner: the position of the hypocenter was determined according to various station "triplets" of a total number of 7 to 8 stations, recording this earthquake, and the error region was estimated according to the scattering of the resultant points.

The results obtained in a check of this type indicated that the determination accuracy for the position of epicenters and focal depths corresponds to the theoretical calculations.

FOOTNOTES AND TRANSLITERATED SYMBOLS

Manu-script Page No.	
20	*In this chapter, we have used TKSE observations for the years 1955-1957, not only from the Garm-Stalinabad station network of the expedition, but from the Kirgiz stations as well.
24	*Seven stations of the Narynskiy section of the TKSE have been functioning in central Kirgiziya since May 1957.
40	*Leningrad Department of the Mathematics Institute of the Acad. Sci. USSR.
57	$V_{\Phi} = V_f = V_{f,iktivnaya}$ (volna) $= V_{fictitious}$ (wave)
58	$V_{\Phi,cp} = V_{f,sr} = V_{f,srednyy} = V_{f,mean}$
59	$V_{\vartheta\Phi} = V_{ef} = V_{effektivnyy} = V_{effective}$
74	*Let us take note that for the construction of vertical hodographs involving the use of transparent grids for theoretical hodographs (§ 2) it is necessary to have sufficiently exact advance knowledge of the epicentral position alone, the focal depth not being required. Having determined the epicenters according to the iso-chrone transparent-grid method, with a sufficiently dense network of stations, it is enough to make use only of the circular symmetry of the isochrones, for which the velocity cross section need not be known in advance.

Manu-
script
Page
No.

90      $(\delta r)_{\text{КВ}} = (\delta r)_{kv} = (\delta r)_{\text{kvadratichnaya (oshibka)}} =$

     $= (\delta r)_{\text{square (error)}}$

Chapter Four

THE ENERGY OF EARTHQUAKES

In an earthquake, the stressed-state potential energy of the rock mass, which has accumulated in the process of continuous tectonic movement, is liberated very rapidly, undergoing conversion into the energy of seismic waves and other forms of energy. Thus, energy characterizes the very essence of the earthquake phenomenon. The energy of an earthquake is one of the major physical characteristics of the focus. Knowledge of this energy, together with other characteristics of the focus, makes it possible to approach the problem of creating a physical model of the focus and to gain familiarity with its nature. Without classifying earthquakes on the basis of their energies, it is impossible to study the seismic regime. Data concerning the energy of earthquakes and the conditions under which it propagates are those that present direct practical interest: this information, together with the coordinates of the foci, make it possible to estimate the possible disruptive effect of the earthquakes at the Earth's surface.

The present chapter undertakes to describe a classification of earthquakes on the basis of the energy flow through a sphere having a definite radius - the "reference sphere" - and the relationship between the total seismic energy emanating from the earthquake focus and the flow of energy through the reference sphere. The following methodological problems are considered: determination

of the energy density at the observation points, the diminution of energy density with distance (calibration curve), construction of working alignment charts, and problems of the accuracy with which the energy can be determined. Then we proceed to a comparison of energy values obtained by the method described with energy values obtained by the Golitsyn-Gutenberg-Richter method. In conclusion, we present an evaluation of the shape of the isoenergetic lines on the basis of the observed diminution properties of seismic-wave energy density during propagation of these waves along and across the trends of basic geological structures.

§ 1. Basic Foundations for Energy Classification of Earthquakes

In addition to the point system for classifying earthquake intensities, two methods making use of instrumental data have recently come into being. The first method, which was first proposed by Golitsyn [56] and elaborated by a series of other authors [57-61], consists in estimating the energy of the seismic waves emanated by the focus. In the second method, which was proposed by Richter [62], earthquakes are compared with one another on the basis of the highest peak amplitudes that they produce on seismograms (or the ratio of the amplitude to the oscillation period) obtained with the aid of a specified apparatus and reduced to a certain standard distance from the focus; this resulted in the introduction of the "earthquake magnitude*" concept, which is a certain arbitrary dimensionless quantity. The second classification method has thus far come into more widespread use and is, at the present time, officially recommended. There are different varieties of the magnitude scale, each constructed for certain types of "volume" and surface waves and for different distances from the focus [63-67]. As one example, the Soviet Union employs the M magnitude scale, which is based on

comparison of the peak-amplitude ratios in surface waves to their period [68-70].

The high popularity of the M scale as compared with the energy-based classification is accounted for not so much by its obvious advantages, simplicity, and unequivocal nature as by formal circumstances. Gutenberg and Richter, who introduced this scale, computed the magnitudes of a considerable number of severe earthquakes over the entire territory of the Earth's surface. In many of these cases, it is also found convenient for pusposes of comparison to evaluate the magnitude of the earthquake at the same time; this applies particularly to severe earthquakes. Nevertheless, it can be stated with certainty that the future belongs precisely to the energy classification of earthquakes.

The expedition's system of observation - which disposed over a far-flung network of stations located directly in the epicentral zone and apparatus with a wide dynamic range - made it possible to study the attenuation curves of the seismic waves at distances ranging from 3 - 4 to 700 km from the focus. This was used as a basis for refining an energy-measurement technique, and a concrete physical significance is conferred upon its value as determined.

Basic Determinations

Of the total quantity of energy liberated in the focus at the time of an earthquake, only that part which is converted into elastic-wave energy - the seismic energy E of the earthquake - is taken into account. Its magnitude may be characterized by the seismic-wave energy flux through a certain closed surface (it is more convenient to take a sphere for the sake of simplicity) within which the focus is located, taken over the entire time τ during which vibrations take place, i.e.,

$$E = \int_0^\tau dt \int_s (\vec{E} \mathbf{n}) ds,$$ (4)

where $\vec{E}$ is the energy-flow density vector (the Umov vector) at the points of the surface S at the instant of time t and $\vec{n}$ is the unit vector normal to the elementary area ds of the surface S over which integration is performed.

As we recede from the focus, the energy-flow density $\vec{E}$ diminishes as a result of divergence (the increase in the wave-front area [71]) and the absorption of elastic energy by the nonideally elastic medium [72] or scattering of this energy on small, "structural" nonuniformities of the medium (quasi-absorption). Moreover, the duration τ of the vibrations also varies with increasing distance from the focus, chiefly as a result of the appearance of secondary waves associated with the nonuniformity of the medium. This gives reason to speak of the variation with distance not only of the energy-flow density $\vec{E}$, but also that of the integral of this quantity over the entire time during which the vibrations take place:

$$\mathcal{E} = \int_0^\tau (\vec{E} \mathbf{n}) dt.$$ (5)

It is clear from (4) and (5) that the quantity $\underset{\circ}{E}{}^*$ is equal to $\partial E / \partial s$, i.e., is equal to the energy flow during the entire time of vibration referred to the unit surface area. We shall henceforth designate the quantity $\underset{\circ}{E}$ in this sense to be the energy density.

We shall apply the term attenuation to the over-all diminution effect shown by the quantities $\underset{\circ}{E}$, $\vec{E}$, or the amplitude A as a result of both the increase in the wave-front surface (divergence)

[Translator's note: text occurrences of displayed script letters ($\mathcal{E}$) are typed $\underset{\circ}{E}$.]

and absorption and scattering; the distance function $\psi(r)$, which characterizes this decline with increasing distance quantitatively and is given by the formula

$$\frac{E(r_1)}{E(r_2)} = \frac{\psi(r_1)}{\psi(r_2)},$$ (6)

where $E(r_1)$ and $E(r_2)$ are the energy densities of a given earthquake at distances r_1 and r_2 from the focus, respectively, will be referred to as the attenuation function.

In the case of an infinite, uniform, ideally elastic medium, the attenuation will reduce to the spherical divergence, i.e.,

$$\psi(r) = \frac{1}{r^2}.$$

and the value of the integral (4) will not depend in this case on the radius taken for the sphere of integration.

Under real conditions, the attenuation differs considerably from the spherical. As we know [71, 73, 74], the presence of the half-space boundary and other boundaries, as well as transitional layers, results in an energy exponent n in the divergence function $\psi(r) = 1/r^n$ other than n = 2. Thus, for example, in the case of a uniform half-space and a shallow focus, we have from theory n = 4 for longitudinal and transverse waves at the half-space boundary. Experimental study of divergence in seismic prospecting [75] also arrived at a value n = 1.5 to 2 for the amplitude divergence exponent and, consequently, n = 3 to 4 for the energy exponent.

Due to its nonideal elasticity, the real medium also possesses significant absorption [72, 76]. Moreover, the energy-density attenuation is complicated by the appearance of secondary (reflected and head) and surface waves at certain distances. The horizontal stratification of the real medium has as one of its consequenc-

.123

es that the energy density not only of the surface, but also of the "volume" waves is different at points lying at the same distance from the focus in the interior of the Earth and on its surface.

As a result, the energy-flow density $\vec{E}$ and the energy density E are attenuated along the Earth's surface in accordance with a functional relationship $\psi(r)$ other than $1/r^2$. Consequently, the value of the integral (4) will depend on the integration surface selected.

It is necessary to note that all of these generally well-known facts are generally nevertheless ignored in energy determinations in seismology. Thus, it is customary to consider that energy absorption may be disregarded. This attitude has taken shape because registration of earthquakes has generally occurred at relatively long distances from the focus, where frequencies of the order of one cycle or fractions of a cycle, for which the absorption exponent is very small [77] prevail in the recorded vibration spectrum, while higher-frequency vibrations, which are already highly attenuated by absorption, have not been registered.

As regards the divergence, this is generally assumed to be spherical. The formula of B.B. Golitsyn [56] is based on this assumption. V.I. Bune [61] also employed the same presentation. In the paper by Ye.F. Savarenskiy and E.A. Dzhibladze [78], the authors referred to the classical work of Lamb [73] and to empirical attenuation determinations [79] which had given near-to-theoretical results, nevertheless compute the energy by the use of Golitsyn's formula, although they note that the energy computed by this formula is not equal to the elastic-wave energy. S.I. Sol-

ov'yev also regards the Golitsyn formula to be highly approximate, estimating the possible error at three orders [69]. And indeed, this is justifiable even for the single reason that the use of the Golitsyn formula is equivalent to making the surface of integration (a sphere with a radius equal to the hypocentral distance) different in each individual determination.

In order to render the result of a seismic-energy determination for the earthquake focus itself independent of the usual hypocentral-distance value of r, it is necessary to know the attenuation curve of energy density with distance in order to reduce the energy-density values $E(r)$ measured from the seismogram at any distance r to their values at a certain known distance R taken as the radius of the integration sphere.

The energy-density attenuation function cannot yet be indicated with sufficient accuracy by purely mathematical means. This is a consequence of the fact that the intensity calculations for various types of waves, which may be carried out using solutions of the appropriate dynamic problems in elasticity theory [80], frequently become quite complex, and are usually carried out using only approximate, assymptotic formulas [81], as well as for a rigorously idealized structure of the medium and frequently without taking the nonideal elasticity into account. Furthermore, the calculations may yield the attenuation function not for the entire ensemble of waves, but only for certain specific wave types, which it is frequently difficult to isolate and identify on the earthquake record.

For this reason, it can now be considered more rational to use an attenuation law obtained empirically from the earthquake traces of seismic stations located at various distances from the

- 125

focus. Such an empirical attenuation function is obviously determined not only by the divergence and absorption for frequencies that appear on traces at observation stations, but also by the decline in energy density as a result of absorption of the higher frequencies present in the vibration spectrum for all practical purposes only in the region near the focus [1, 4, 82, 83]. Since absorption depends on vibration frequency, the empirical attenuation function may be found to vary in accordance with the frequency range of the apparatus used. Also reflected in the form of the empirically-obtained attenuation function will be the relative increase in energy density as a result of the appearance of secondary (refracted and reflected waves) at certain distances.

Integration over the surface S is the most complex problem. First, we are not in a position to integrate in the strict sense, since the energy-density distribution over the entire sphere is unknown. It is normally assumed that integration over a spherical surface can be replaced by multiplication by its area i.e., that

$$\int_s \mathscr{E}ds = 4\pi R^2 \mathscr{E}(R). \qquad (7)$$

It is thereby implied that the value of $\dot{E}(R)$ obtained by averaging the data of several stations located on various azimuths on the surface of the Earth may be regarded as the average energy-density value for the entire sphere, i.e., not only for the surface, but also in the interior of the Earth. This assumption may be regarded as approximately valid only for small r, of the order of the depth h of the focus. The energy density at these distances is transferred by straight-line waves having a spherical wave front.

Replacing $\dot{E}(R)$ in Formula (7) by its value from (6), we obtain

tain

$$E = 4\pi R^2 \frac{\psi(R)}{\psi(r)} \ell_s(r).\qquad(8)$$

As concerns selection of the radius R of the integration sphere, there are two fundamentally different approaches possible here; these result in different systems of classification. In one of these, earthquakes are classified by the magnitude of the seismic-wave energy flux E through a certain fixed-radius sphere - the reference sphere. This classification is quite simple and reliable, since it rests upon an empirically established calibration curve, and is found to be quite convenient in solving a number of problems, e.g., in evaluating the seismic effects of earthquakes at the Earth's surface. The radius R of the reference sphere may be selected at will within certain limits, with the lower limit defined by those distances to which it has been possible to determine the attenuation function reliably, and with the upper limit determined by the distances at which it can still be assumed that the wave front has a near-spherical shape and the energy density on the surface does not differ from the energy density at the same distances in the interior of the Earth. On the basis of these considerations and consideration of the conditions under which the expedition was working, the radius of the reference sphere was set at R = 10 km.

The second type of classification is based on comparison of earthquakes as regards the magnitude of the total seismic energy E_0 emanated by the focus. If the boundary separating the breakdown and residual-deformation zone (the actual zone of the focus) from the zone of primarily elastic deformations external to the focus, where the seismic waves propagate, is referred to as the

surface of the focus, the energy flow through the focus surface S_0 may be regarded as the __total__ seismic energy E_0 of the earthquake:

$$E_0 = \int_{S_0} \mathscr{E} ds. \tag{9}$$

In this case, the focus surface S_0, which, generally speaking, differs from the spherical, is taken as the surface of integration. In the zeroth approximation, it may, however, also be regarded as spherical, and the radius r_0 of this sphere can be taken as a quantity characterizing the size of the focus. In this case, Expression (9) takes the form

$$E_0 = 4\pi r_0^2 \mathscr{E}(r_0) = 4\pi r_0^2 \frac{\psi(r_0)}{\psi(r)} \mathscr{E}(r).$$

Determination of the total seismic energy E_0 requires knowledge of the size r_0 of the focus and the seismic-wave attenuation in the vicinity of the focus surface at distances commensurable with its radii. Thus far, information of this type has only been accumulated, but nevertheless certain approximate evaluations can be carried out on the basis of estimated earthquake-focus radii listed in Chapter 6 of the present monograph, as well as on the basis of extrapolation of the energy-density attenuation function as determined empirically in the direction of small r, right down to the very surface of the focus, i.e., to $r = r_0$.

The ratio E/E_0 of the energy flows through a reference sphere of radius R and through the surface of a focus of radius r_0

$$\frac{E}{E_0} = \left(\frac{\mathscr{R}}{r_0}\right)^2 \frac{\psi(\mathscr{R})}{\psi(r_0)}. \tag{10}$$

For weak earthquakes with various focal radii $r_0 \le R$, the fraction of the energy absorbed within the reference sphere will obviously also differ, and this difference will be larger for wider

deviations of the attenuation function $\psi(r)$ from $1/r^2$. For these weak earthquakes, both energy evaluations (E and E_0) have a quite definite physical significance. For severe, destructive earthquakes, when $r_0 > R = 10$ km, the seismic-energy flow E through a reference sphere of radius $R = 10$ km has only a formal significance. The quantitative relationship between E and E_0 will be considered below in § 4.

Classification of earthquakes on the basis of E_0 is of the greatest physical interest and is absolutely necessary in study of processes that take place in a given focus, whether of a severe or a weak earthquake, as well as in consideration of single seismic events in an entire seismically active zone, its energy balance, etc.

Thus, computation of the seismic energy of an earthquake reduces to the following stages: 1) determination of the energy density E at the point of observation from a seismogram; 2) reduction of the quantity $E(r)$ to its value at a distance R (or r_0) selected as a radius of integration, using the empirical attenuation curve of Formula (6), and 3) calculation of the earthquake energy E – on the reference sphere – or E_0 – the total seismic energy at the surface of the focus:

$$E = 4\pi \mathcal{R}^2 \mathscr{E} (\mathcal{R}), \qquad (8')$$

$$E_0 = 4\pi r_0^2 \mathscr{E} (r_0). \qquad (9')$$

Let us consider each of these stages in detail.

§ 2. Calculation of Energy Density at Point of Observation

The energy density at the point of observation is determined by integrating the energy-flow density over time:

$$\mathscr{E} = \int_0^\tau (E \cdot n)\, dt, \qquad (5)$$

. 129 .

where

$$E = \rho V \left(\frac{dx}{dt}\right)^2. \qquad (11)$$

Here, ρ is the density of the medium, V is the velocity of propagation of the seismic waves under consideration in the medium, $x(t)$ is the amplitude and dx/dt is the velocity of vibration in the falling wave, and $\vec{n}$ is the unit vector of the normal to a sphere of radius $\underline{r}$ equal to the hypocentral distance.

Simplification Assumptions

It is difficult to obtain an exact determination of the integral (5). We must adopt certain simplifications. Thus, although in the existing recording system it is, in principle, possible to determine the magnitude of the scalar product $(\vec{E}\cdot\vec{n})$, but in practice, for simplicity, instead of this magnitude we determine only the modulus of the vector $\vec{E}$ of the energy-flow density. Close to the focus this assumption may be regarded as sufficiently valid, since the wave front of straight-line waves is virtually coincident with a sphere. However, at great distances from the focus, there is an increase in the importance of secondary waves, whose fronts are substantially unlike a sphere, and then the assumption $(\vec{E}\cdot\vec{n}) = \vec{E}$ loses its effect. However, the errors associated with this can partially be taken into consideration by the vibration-attenuation curve with an increase in the hypocentral distance.

Further, shifts in the soil during earthquakes are quasi-periodic vibrations and may be represented, in approximate terms, in the form of the superposition of several sinusoids

$$x(t) = \sum a_k e^{-2\pi j f_k t}, \qquad (12)$$

where f_k is the frequency and a_k is the amplitude of the shift in the incident wave, corresponding to the aforementioned frequency.

In this case, differentiating with respect to $\underline{t}$ and squaring (12), after substitution into (11) and (5), we obtain

$$\mathscr{E}(r) = 4\pi^2\rho \sum_{i,k} V_i \int_0^{\tau_{ik}} (a_{ik}/f_{ik})^2 e^{-4\pi j f_{ik}t}\,dt.$$

where $i = p,s$; $k = 1, 2, \dots$ Here we will replace the complex expression $e^{-4\pi j f_{ik}t}$ with the mean value of its real portion during time τ_{ik}. If $\tau_{ik} \gg 1/f_{ik}$, this mean value is equal to 1/2, and this with a sufficient degree of accuracy. Then, integrating with respect to $\underline{t}$, we will obtain the following approximate calculation formula for the density of energy E which passes (during time τ, during which the vibrations take place) through a unit of surface on a sphere with radius $\underline{r}$ equal to the hypocentral distance

$$\mathscr{E}(r) = 2\pi^2\rho \sum_{i,k} V_i (a_{ik}/f_{ik})^2 \tau_{ik}. \tag{13}$$

To calculate $\dot{E}$ according to this formula it is necessary to carry out a frequency analysis of the soil shift. This can be done most conveniently by instruments. There is an apparatus, developed especially for purposes of seismic prospecting [84] and the continuous recording of earthquakes (Chapter 5), said apparatus making it possible to undertake an analysis at precisely the instant at which the vibrations are recorded. It is possible also to record a soil shift on magnetic tape (see Chapter 2) with a subsequent analysis of the recording under laboratory conditions. However, the observation system of the expedition generally employed wideband equipment, but experiments on the frequency analysis of soil shifts were nevertheless carried out.

The seismograms obtained by means of the wideband equipment show, almost without distortion, the soil vibrations within the passband of the instrument, whereas the vibrations which exhibit frequencies outside of this band are virtually not recorded by the instrument. There-

fore, the energy density calculated according to the seismogram pertains to the frequency range determined by the position and passband width of the instrument.*

A harmonic analysis [85] of the seismograms produced by wideband equipment (VEGIK, SGK, and SVK) can be carried out graphically or analytically. In principle, these methods of analysis may yield sufficiently complete and precise data, yet because of the amount of work required for these methods they are not suitable for extensive energy calculations. Therefore, in actual practice, instead of spectral decomposition, the seismogram is visually approximated with sinusoidal segments superposed on one another or with one behind the other, and the frequencies and amplitudes of these sinusoids are evaluated in approximate terms. This corresponds to the fact that the spectral decomposition is limited to several of the highest terms.

Frequency Determination

The dominant frequency seen on the recording is defined as the number of maximums per unit time on the sinusoidal segment which approximates the sector of the seismogram. For the observed vibration shapes the dominant frequency corresponds approximately to the frequency of the greatest term of the shift spectrum. This correspondence was verified through a comparison of approximately 400 earthquakes, recorded at the same point of observation by wideband equipment (VEGIK) and the frequency-selection equipment (ChISS) of K.K. Zapol'skiy. The comparison demonstrated that the dominant frequencies on the VEGIK seismograms are, on the average, in sufficiently good agreement with the position of the maximum of the conventional shift spectrum, constructed according to the ChISS seismograms (see Chapter 5, §1).

The greatest term of the velocity spectrum rather than of the shift spectrum carries the basic vibration energy; the velocity spec-

- 13² -

trum exhibits a slight shift toward the higher frequencies in compari-
son to the maximum of the shift spectrum. Therefore, we would be mak-
ing a systematic error, underestimating the energy density as a result
of losing the high-frequency terms if we restrict ourselves, in Expres-
sion (13), to the single decomposition term with the dominant shift
frequency. The magnitude of this error was evaluated by comparing the
energy density determined according to the VEGIK seismogram against
the energy density of the ChISS seismogram, said density defined as
the sum of the energy densities on various channels

$$\mathcal{E}_{\text{ЧИСС}} \sim \sum_{k=1}^{n} (a_k/\hbar)^2 \tau.$$

Here $\underline{n}$ is the number of channels. All in all, 80 earthquakes were proc-
essed, these earthquakes having been recorded at a single point by
both of the instruments — the VEGIK and the ChISS. The results of the
comparison are presented in Fig. 33. Here, E_{ChISS} is plotted along the
axis of abscissas, and E_{VEGIK} has been plotted along the axis of or-
dinates. The curve shows that the earthquake energy E_{VEGIK} referred to
the dominant frequency, on the average, amounts to approximately 70%
of the energy E_{ChISS}. This means that if we restrict ourselves to the
single decomposition term, in Formula (13), with the dominant frequency,
we tolerate a systematic reduction in energy by approximately 30%.

On the average, the observer's error in the determination of the
dominant frequency in these evaluations comes to 15%.
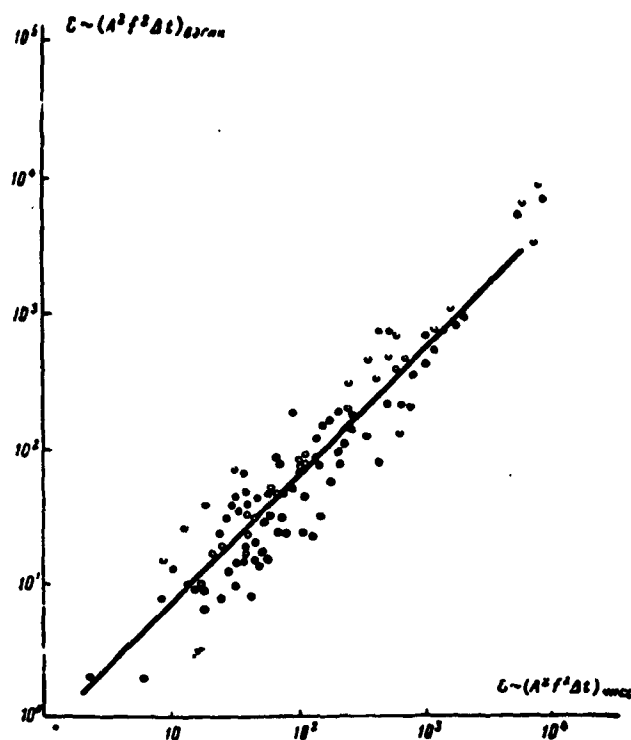
Fig. 33. Comparison of density of energy
E, determined at a single observation
·
point, according to VEGIK and ChISS seis-
mograms.
ВЭГИК = VEGIK; ЧИСС = ChISS.

Determination of Amplitudes

The quantity $\underline{a}$ in Formula (13) stands for the amplitude of the
shift $x(t)$ in the incident wave. It should be borne in mind, however,
that seismic equipment is set up at the surface (the boundary of the
half space), in connection with which the soil vibrations $\xi(t)$ recorded
by the seismic equipment result from the interference of the incident
wave with the waves reflected from the half-space boundary.

The calculations [86] indicate that the ratio $\xi(t)/x(t)$ for the
SH wave is constant at any angles of incidence and equal to two. For P
and SV waves, at angles of incidence $i \leq 70°$ this ratio exhibits lit-
tle change — ranging from 1.8 to 2.3. The angles of incidence for seis-

mic radiation, observed for local earthquakes, as a rule, vary from 0 to 60° and do not exceed 65°. Therefore, we may hold that the ratio of soil shifts to shifts in the incident wave is approximately equal to two (with an accuracy of up to 10%). If we take into consideration the increase in $\overline{V}$ of the seismic equipment, we obtain $a_k = A/2\overline{V}$, where A is the amplitude of the total vector on the seismogram.

If the recordings are made on a three-component installation, the calculation of the amplitude A of the vector sum is not difficult:

$$A = \sqrt{(A_k^{(v)})^2 + (A_k^{(v)})^2 + (A_k^{s})^2}.$$

When we have an azimuthal installation with four or more inclined instruments, the calculation of the amplitude of the vector sum is made more difficult by the need to take into consideration the sign of each shift. In this case, it is more convenient to measure the amplitude A_k^{max} on one of the components alone, and this component will be the one on which the shift is greater, and consequently, closer to the vector sum. Here, the appropriate correction is introduced into the formula. As has been demonstrated by special measurements, the quantity A_k^{max}/A, on the average, is equal to 0.76 for many measurements, or approximately

$$\frac{A_k^{max}}{A} \simeq \frac{1}{\sqrt{2}}.$$

Thus the amplitudes a_k of shift in the incident wave are expressed in terms of amplitude A^{max} of the shift on the seismogram

$$a_k \simeq \frac{A}{\sqrt{2}\,\overline{V}}.$$

Then Expression (13) for the density of energy E takes the form

$$\mathcal{E} = \pi^2 \rho \sum_{i,k} V_i \left(\frac{A_{ki}^{max}/\mu}{\overline{V}}\right)^2 \tau_{ik}; \quad i = p, s; \quad k = 1, 2, \dots \tag{14}$$

If we use wideband equipment, $\overline{V}$ may be regarded as a constant quantity and taken out from under the summation sign.

Since the squared amplitude enters into the expression for the energy density E, in approximating the seismogram by one or several sinusoids, it is necessary to assign values to the amplitudes A_{1k} of each sinusoid, said values equal to the mean-square values of the oscillation amplitudes of given frequency, observed in the recordings. In accordance with the evaluations that have been carried out, the observer's error in a visual averaging of the amplitudes comes to approximately 15%.

Determination of Duration of Vibration

In essence, this operation involves the isolation of certain sectors from the entire recording, said sectors corresponding to P and S waves, according to which the energy density is determined, and the operation further involves the measurement of the length of these sectors. The selection of these sectors is conventional to a great extent. It is possible, for example, to measure the energy density E only on the recording sector that corresponds to straight-line waves. In this case, the quantity τ may virtually be identical at any distance from the focus and equal to the duration of the vibrations of straight-line waves at extremely small distances, of the order of the reference-sphere radius. We can determine the energy density throughout the entire recording for the entire period of time during which the vibrations take place, regardless of the type of wave involved. In this case, the quantity τ will vary at different distances from the focus and the energy density E will correspond to various sets of waves as a function of r.

The selection of τ has an extremely substantial effect on the nature of the attenuation function, but close to the focus the quantity E in actuality is independent of the τ chosen. We have reference here to the fact that in the zone close to the epicenter ($r < 20$ km) the

earthquake recordings, as a rule, have the characteristic of exhibiting extremely clear arrivals and low total vibration duration. The first few vibrations (straight-line waves) generally exhibit amplitudes substantially in excess of the following vibrations and, therefore, almost all of the energy is contained in the straight-line waves.

Since it is difficult to isolate reliably a recording sector corresponding precisely to straight-line waves, it was decided subsequently to measure the energy density for the entire recording, rather than for any individual sectors. Only surface waves were excluded from consideration, since the general-type SVK and SGK seismographs are still extremely unstable in their recording of surface waves at distances of $r = 200$-300 km, and on the earthquake recordings produced by the basic equipment used by the TKSE, the VEGIK surface waves do not appear at all.

Thus the measurement of the energy density at the observation point is carried out by means of an approximation of the entire earthquake recording through one or several sinusoids, one behind the other, or one superposed on the other. Then the duration τ_{1k} is determined, this time to correspond to each segment of the sinusoid, its frequency, and its amplitude, the last on one of the components: on the component exhibiting the greatest shift.

The value of ρ is assumed to be equal to the density of granite ($\rho = 2.7$ g/cm^3) and the magnitude of the rate of wave propagation is equal to the velocity in granite $V_p = 6.0$ km/sec and $V_s = 3.5$ km/sec.

Accuracy in the Determination of Energy Density

Errors in the determination of $\underset{\bullet}{E}$ at a given point are composed of the errors associated with certain assumptions adopted in the given method, and of measurement errors.

In making the transition from the basic formula (5) to its calcu-

lation version (9) it was assumed that the projection of the vector $\vec{E}$ for the energy-flow density to the normal $\vec{n}$ can simply be replaced by the modulus of the quantity $\vec{E}$, i.e., $(\vec{E}, \vec{n}) = |\vec{E}|$, and that the soil vibrations, reflected in the seismogram, could be replaced by segments of the sinusoid. It is extremely difficult to take account of the error resulting from the first assumption; we can only say that the smaller the hypocentral distance, the closer the wave front to the sphere and, consequently, the smaller the sphere.

We can make an indirect judgment as to the order of magnitude of the error resulting from the second assumption on the basis of the relationship between the energy densities E measured by the VEGIK and the ChISS. As was pointed out above, the ratio E_{ChISS}/E_{VEGIK} is equal to 1.3 on the average.

With respect to errors in the measurement of E according to the adopted method, these can easily be evaluated. The quantity $\delta E/E$ is composed of the errors produced in the determination of frequencies ($\delta_1 \simeq 15\%$) and the errors resulting in the determination of amplitudes: in averaging ($\delta_2 \simeq 15\%$), as a result of inaccurate data regarding the magnification of the equipment ($\delta_3 \simeq 10\%$), in replacing the vector sum $\vec{A}$ with the amplitude A^{max} on one component ($\delta_4 \cong 10\%$), and in accounting for the effect of the earth's surface ($\delta_5 \simeq 10\%$). The total error $\delta E/E$ in the measurement of energy density can be evaluated through a calculation of the mean-square error

$$\delta E/E = 2\sqrt{\overline{\sum_{j=1}^{5} \delta_j}} \approx 0.55.$$

Thus errors in the determination of energy density for a given point are comparatively small.

When we are confronted with the problem of determining the energy E of earthquakes, it is not so much the determination of the energy

density $\underset{\bullet}{E}$ at the point of observation as it is that we must determine

the value of $E(r)$ for the given distance which represents the mean

magnitude of $\underset{\bullet}{E}$ over the entire sphere of the given radius $\underline{r}$. At the

same time, the various soil conditions resulting in amplitude and fre-

quency distortion, the nonuniformity of the radiation in various direc-

tions from the source, as well as the nonuniformities of the medium

along the wave path, all lead to various energy densities at the

points lying at equal distances from the focus, but on various azi-

muths.

1. The effect of the soil conditions at the points of observation

on amplitudes and oscillation frequencies, said effect associated with

the interference phenomena in the surface layers [87], was studied by

special observations carried out at the Chusal station. Identical in-
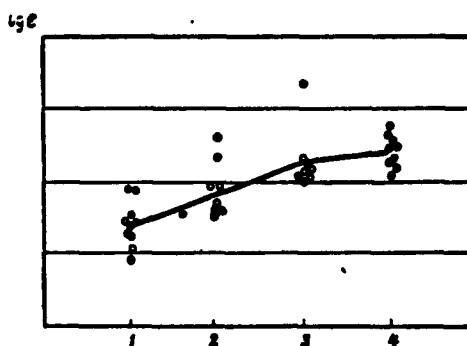
Fig. 34. Summary curve for
change in energy density, said
change associated with various
soil conditions.

struments were set up there under various soil conditions: on rocks

occurring in their places of origin; on an incline at which the deposi-

tion thickness is at a minimum — of the order of a half meter; in the

eastern section of the slope, on a deluvial layer approximately 10-15 m

thick; in the central portion of the slope, where the deluvial layer is

at its thickest (50-100 m). The distances between the individual obser-

vation points did not exceed 0.5 km, and this made it possible to neglect the difference in epicentral distance.

A comparison of the records for one and the same earthquake at various observation points demonstrated that with an increase in the thickness of the deluvial layer both amplitudes and the vibration duration increase, and there is a slight reduction in the oscillation frequency. There is more detailed examination of these results in Chapter 5. Here, we will only undertake an evaluation of the association between the observed quantity $\Sigma A^2 f^2 \tau$ and the soil conditions at the point of observation.* The quantity $\Sigma A^2 f^2 \tau$ of the S waves at various observation points was determined for tens of earthquakes. The results are presented in a summary curve (Fig. 34). Here, the above-enumerated observation points (1-4) are plotted along the axis of abscissas, and the quantity proportional to $\Sigma A^2 f^2 \tau$ is plotted along the axis of ordinates. An examination of this curve indicates that the difference in soil conditions may result in a change in the magnitude of $\Sigma A^2 f^2 \tau$ by a factor of 10, i.e., by an order of magnitude.

This difference may be taken into consideration, and the effect of the various soils can be eliminated by introducing the appropriate corrections. To realize this possibility, special research is required.

2. Nonuniformity of emission. The foci of all tectonic earthquakes can be modeled, with a certain degree of accuracy, by a double force with moment [88]. The nature of emission directivity from a source of this type is examined theoretically by V. I. Keylis-Borok [89].

Asymptotic formulas of shift intensity as functions of the mutual orientation of source and point of observation are presented in the article by K. I. Ogurtsov, I. N. Uspenskiy, and N. I. Yermilova [90], and these formulas are valid for considerable distances from the focus. In accordance with these formulas, the emission intensity is a function
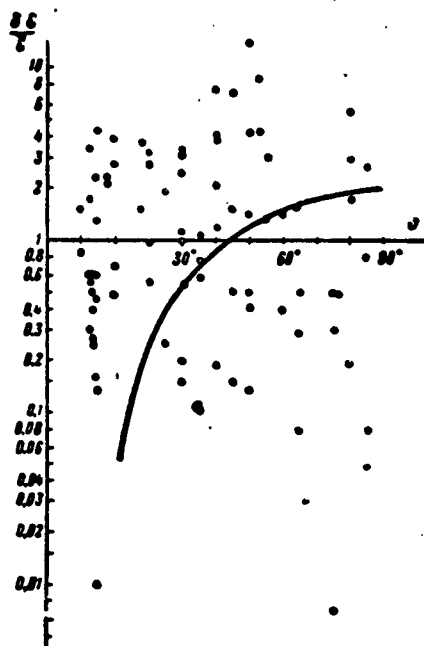
Fig. 35. Distribution of relative deviations $\delta E/\bar{E}$ in energy density from the mean values of $\bar{E}$ as functions of the angle ϑ between the direction of the discontinuity plane and the direction to the seismic station, according to observation data.

of direction, and in several directions — in the nodal planes — the intensity is equal to zero.

We attempted empirically to derive the relationship between intensity and the mutual orientation of the focus and point of observation. For this purpose seven earthquakes were selected, and for these we determined the dynamic focal parameters. The discontinuity plane for each of these earthquakes, within the limits of determination error, can be regarded as vertical. The earthquake foci were situated in the Peter I Range and are rather uniformly surrounded by seismic stations. The curve (Fig. 35) shows the observed values of $\delta E/\bar{E}$ as functions of the angle ϑ, read in the horizontal plane from the direction

of the discontinuity plane

$$\frac{\mathcal{E}'}{\bar{E}} = \frac{\mathcal{E}(\vartheta) - \bar{E}}{\bar{E}},$$

where $\underset{\bullet}{E}(\vartheta)$ is the energy density in the direction ϑ; $\underset{\bullet}{\bar{E}}$ is the mean value of energy density in various directions.

The theoretical directivity diagram is symmetrical with respect to two axes lying in the horizontal plane; one of these axes coincides with the direction of the shift plane, and the second axis is perpendicular to the first. Therefore, for purposes of compactness all observation points were plotted in only a single quadrant. The light (open) circles indicate the energy deviations $\delta E/\underset{\bullet \, \bullet}{\bar{E}}$ in calculating energy for an extremely short interval of time after the arrival of the S waves — no more than 0.2 sec. During this time, a total of only 1 to 3 vibrations could occur. The intensity of this group of vibrations must be stronger functions of the azimuth for the station. The dark (solid) circles denote the deviations $\delta E/\underset{\bullet}{\bar{E}}$, determined from a group of more enduring vibrations ($\tau \sim 1\text{-}3$ sec). The solid line shows $\delta E/\underset{\bullet \, \bullet}{\bar{E}}$ as function of ϑ.

An examination of the curve shows that no systematic relationship exists between $\underset{\bullet}{E}$ and ϑ and, consequently, it is impossible to undertake any attempt to take into consideration the nonuniformity of source emission by means of conventional simplified theoretical concepts as to the conditions of wave propagation and "the mechanism of the focus." This result is not unexpected. In fact, the theoretical directivity diagrams are valid only for a uniform medium and are made only for straight-line waves (the first arrivals). In an actual medium, however, the deviation from ideal conditions — a great number of discontinuities at which refracted, head, reflected, and multiple-reflected waves [91-92] can occur — substantially complicates the picture. The secondary

waves, observed at any point, correspond to the various courses and directions of egress from the source. As a result, the energy density of the total waves observed at the given point is substantially a weaker function of direction. Insofar as actual movements within the focus are concerned, these, apparently, are considerably different from the idealized mathematical model. If we had found only an empirical relationship between emission intensity and the mutual orientation of the focus and the station, it would have been virtually impossible to use this relationship for the determination of the energy because to the present time it has been possible to determine the dynamic focal parameters (the orientation of the discontinuity plane and the shift direction) for very few individual earthquakes, amounting to no more than 2-3% of the total number, and here the error in the determination of the dynamic parameters is quite great — of the order of 5 to 20°.

Thus it turns out that the energy density at the given point can be determined with sufficient accuracy (the error is, on the average, 50 to 60%). However, the over-all effect of the various soil conditions, the nonuniformity of the medium, and the nonuniformity of emission result in the fact that at one and the same distance from the focus, energy density $\overset{.}{E}$ at various stations may exhibit pronounced variation. The magnitude of this variation, as can be seen from Figs. 34 and 35, considerably exceeds the measurement error and is, on the average, equal to ±0.5 of an order of magnitude, sometimes reaching as high as ±1 order.

§3. DAMPING OF SEISMIC WAVES WITH DISTANCE

The damping of seismic waves at a distance $\underline{r}$ from the focus was studied empirically within a range of distances from 3-4 km to 600-700 km. The earthquake recordings produced by the VEGIK and VKh seis-

mographs at the expeditionary stations located in the regions of Garm, Stalinabad, Tashkent, and Naryn served as the basic material for the damping study. In addition, seismograms from general-type SVK and SGK instruments were also used; these instruments had been set up at the stations Garm and Dzhirgatal', as well as at seismic stations in Central Asia.

For a comparison of the attenuation curves, 40 comparatively powerful earthquakes were processed (with energy not below 10^9 joule), recorded by an average of 15 seismic stations situated at distances from 7 to 730 km from the focus. Moreover, approximately 150 weaker (with an energy ranging from 10^4 to 10^8 joule) earthquakes were processed, and these have been recorded by the seismic stations of the Garm region. The hypocentral distances in this case changed from 3 to 15 to 50 to 100 km. One earthquake (22 June 1955, 13:28 hours) was recorded at a distance of only about 0.8 km from the focus ($t_s - t_p = 0.1$ sec).

We examined the attenuation of three quantities: a) energy density E; b) the maximum value of the modulus of energy-flux density $\vec{E}$, proportional to the product $A^2 f^2$ and determined on the basis of the group of vibrations in which this product attains its maximum, regardless of the type three-dimensional waves to which it belongs; and c) the sum of the maximum amplitudes $A_p + A_s$, regardless of their period. For each of the earthquakes individual attenuation curves were derived for each of these three quantities. The curves were constructed in a double logarithmic scale.

The comparison of the summary attenuation curves made on the basis of the curves obtained for individual earthquakes was handled in the following manner. Initially, individual curves were separated into groups with approximately identical hypocentral distances: from 3-5 to

50 km; from 10-30 to 300-400 km, from 50-100 to 500-700 km, and from 10-20 to 700 km. Subsequently, by shifting along the axis of ordinates, individual curves of each group were made to coincide with one another. And, finally, from the summary curves for each group, an over-all summary curve was constructed by causing the overlapping sections to coincide.

During the construction of the curves certain attenuation features were revealed and these are associated with the differing frequency ranges in the equipment employed. These features are of special interest both from the standpoint of energy distribution between the frequency ranges of various instruments (SGK 0.08-2 cps, VEGIK 1.5-50 cps), as well as for the purpose of obtaining an energy classification that can be applied to observations of expeditionary and regional stations equipped with a variety of equipment.

Empirical Data on Attenuation (Damping)

Empirical data on the damping of E, A, and $|\vec{E}|$ are presented in Figs. 36-38. The curves marked $\underline{a}$ in each of these figures represent the data of only the high-frequency instruments — the VEGIK and the VKh — and the averaging curves $A(r)$, $|\vec{E}|(r)$, and $E(r)$.

As can be seen from these curves, the damping of seismic waves is substantially unlike a sphere (proportional to $1/r$ for amplitudes or $1/r^2$ for energy). At distances of $r < 50$ km, the maximum amplitudes on VEGIK seismograms diminish proportionally to $1/r^{2.1}$, energy density $E(r) \sim 1/r^{4.5}$ and $|\vec{E}| \sim 1/r^{5.5}$. Then, in the range of distances from $r = 50$-250 km, attenuation diminishes and the curves smooth out. With a further increase in distance ($r = 250$-700 km) damping again increases sharply: $A \sim 1/r^3$; $E \sim 1/r^{5.7}$; $|\vec{E}| \sim 1/r^7$.

The curves $\underline{b}$ in Figs. 36-38 show the position of the points obtained from SGK and SVK data relative to the curve which averages the

VEGIK data, said curve shown by the solid line. From an examination of these curves we can see that values of the quantities E, $|\bar{E}|$, and especially of A, in general exceed the corresponding values obtained from the VEGIK; in this case, for the VEGIK and the SGK, earthquakes can be divided into two types on the basis of the nature of the relationship between these quantities. If a shallow "step" can be detected on the attenuation curves produced by the VEGIK at distances of $r =$ = 100-300 km, the SGK data for these distances of earthquakes of the first type yield points that form an even more pronounced "step" (these data are shown by light (open) circles). The points of earthquakes of the second type (shown by asterisks) form a "hump" on the attenuation curve, with a maximum at distances of $r = 150$-200 km. The amplitude of this "hump" relative to the attenuation curve for $E_{.VEGIK}$ comes approximately to one and a half orders of magnitude.

It was noted that the epicenters of the first type of earthquake, as a rule, are situated in root crystalline rocks (Gissar Range, the crystalline base of the Peter I Range, and the ranges of Kirgiziya). The foci of earthquakes of the second type generally lie in the meso-cenozoic sedimentary layer (the Tadzhik Depression, the Peter I range, and the Fergana Valley). Sometimes, violations of this rule can be noted.

The drop in attenuation, seen in the curves in Figs. 36-38, from the VEGIK data for distances of 100 to 200 km and a certain increase in energy density in the form of a "hump" on the curves constructed according to the SGK data are, apparently, associated with the appearance of secondary waves which exceed the straight-line waves in intensity. Close to $r = 100$ km lies the initial point for the hodograph of the headwaves from the underside of the crust. At distances of 100 to 300 km we should find the rather intensive waves reflected from the
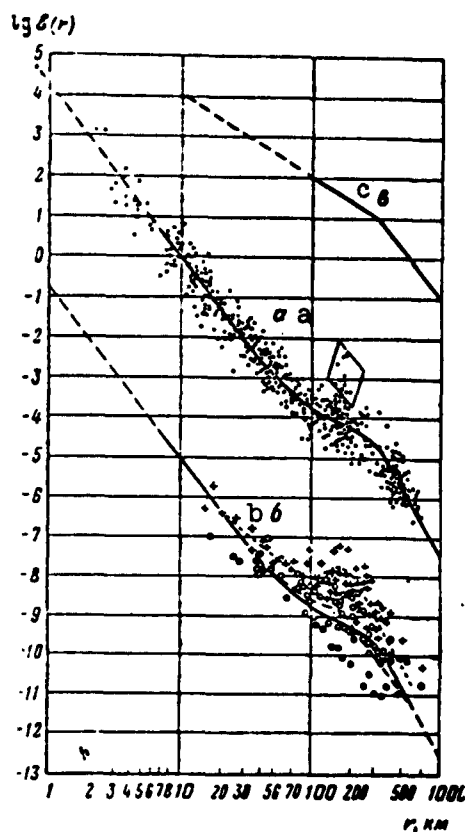
Fig. 36. Summary attenuation
curve for energy density E(r):

a) according to VEGIK and VKh;
b) according to SKG; c) according to data by Bune [61].

Mohorovicic discontinuity at an angle greater than the critical.

The reason for the observed difference in attenuation for earthquakes of various types has as yet not been made clear. We may assume that in the case of earthquakes whose foci are situated in the sedimentary layer, there will appear extremely intensive waves that have been reflected [91-95] repeatedly within this layer. This problem requires continued and more detailed study. In any event, in calculating the energy we must take this difference into consideration.

At small distances from the focus (r = 15-30 km) the quantities E and |Ē|, determined according to SGK seismograms, generally coincide

- 147 -
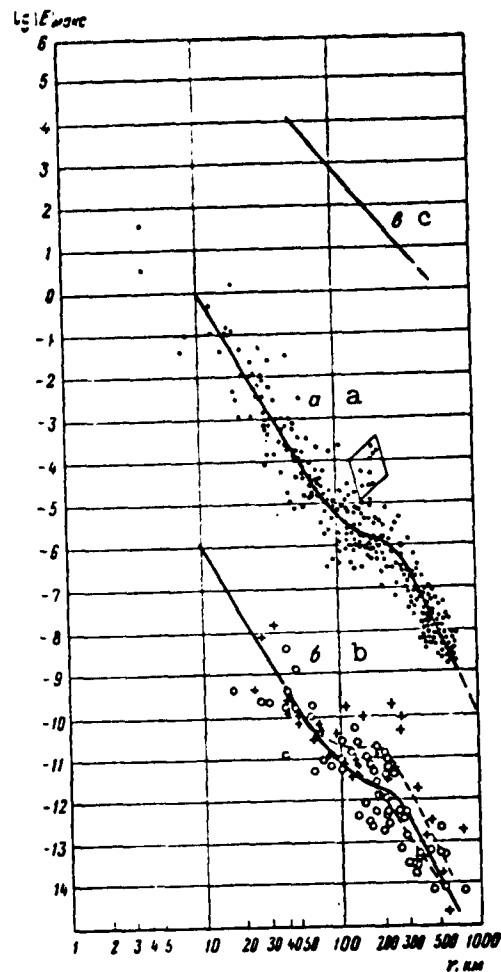
Fig. 37. Summary attenuation
curve for maximum energy-flux
density $|\vec{E}|_{\text{maks}} \sim A^2 f^2$: a) ac-
cording to VEGIK; b) according
to SGK; c) according to data
by Solov'yev and Dzhibladze [79].

with the VEGIK data for earthquakes of both types. The latter circum-
stance is extremely important from the standpoint of determining energy,
and therefore this point has yet to be verified with additional ma-
terial.

The attenuation curves described above, for the range of dis-
tances from 7 to 700 km, served as the calibration curves for the de-
termination of the energy flow through the reference sphere.
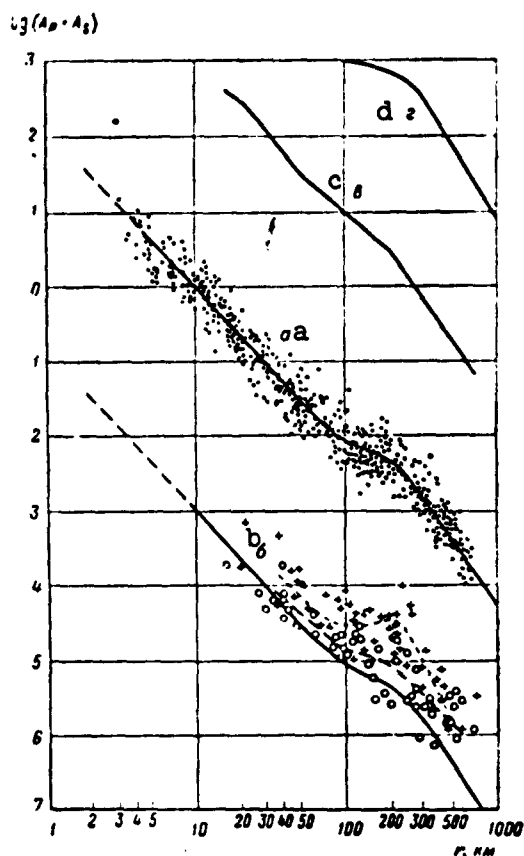
Fig. 38. Summary attenuation curve for maximum amplitude $A_p + A_s$: a) according to VEGIK; b) according to SGK; c) according to data of Gutenberg [96]; d) according to data of Kawasumi [97].

Scattering of Points on Attenuation Curves

This scattering, for all intents and purposes, does not exceed one order of magnitude. Several points on the attenuation curves for $E(r)$ and $|\overline{E}|(r)$ in Figs. 36-37 are an exception, since these points lie above the averaging curve by one or two orders of magnitude and are enclosed in a rhombic-like frame. These points correspond to data from the Zimchurud station and deviate from the remaining data primarily as a result of extremely high frequencies (approximately 10 cps instead of 1-2.5 cps at the remaining stations). Possibly these devia-

tions are associated with certain local features of the medium in the vicinity of the Zimchurud station.

The probable deviation of individual points from the averaged curve is ±0.5 of an order of magnitude. It is possible to maintain that this value for the deviation characterizes the relative accuracy of energy determination on the basis of data produced by a single station.

The attenuation curve for $|\vec{E}|(r)$ is characteristic of a comparatively limited scattering of points at considerable distances ($r > 200$ km), where the greatest deviation does not exceed one order of magnitude. At small distances ($r > 100$ km) the total scattering of the points is quite great and individual points deviate by 1.5-2 orders of magnitude. The less stable behavior of $|\vec{E}|$ in comparison with E and A at small distances makes this quantity inconvenient for the determination of energy.

The points on the curves which correspond to the SGK data exhibit greater scattering than the VEGIK data, and this corresponds to a lower energy-determination accuracy for SGK seismograms than for VEGIK seismograms. The reasons for this are not yet clear.

Relationship Between Direction of Seismic-Wave Propagation and Attenuation

Attenuation of seismic waves as a function of the direction of the seismic waves perpendicular or parallel to the direction of the basic geologic structures is of considerable interest from the standpoint of seismography. An attempt was made to establish such a relationship, although the position of the stations in the Garm district is not too favorable for the solution of such a problem.

Thirty earthquakes whose epicenters are situated on the line of stations Ishtion-Tovil'-Dora-Sultan-Mazar (the line along the extent
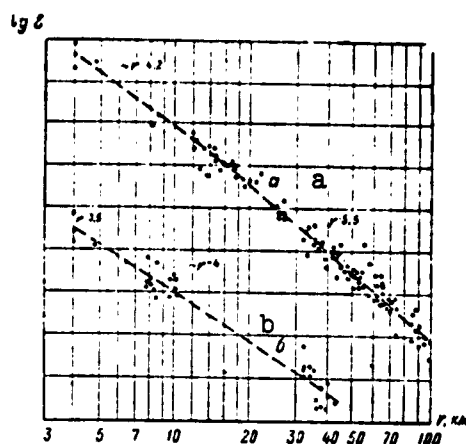
Fig. 39. Summary attenuation
curves for energy density at
distances of $r = 4$-100 km for
various directions of seismic-
wave propagation: a) across;
b) and along the Peter I Range.

of the Peter I Range) were selected, as were 19 earthquakes along the

line stations Garm-Tovil'-Dora, Yaldymych-Tovil'-Dora, and Chusal-

Ishtion (the line perpendicular to the Peter I Range).

The summary attenuation curves for $\underset{.}{E}(r)$, corresponding to the

various propagation directions, are shown in Fig. 39.

The attenuation along the line of the Peter I Range is propor-

tional to $1/r^4$ (lower curve) and proportional to $1/r^{5.5}$ (upper curve)

for the line perpendicular to the range, i.e., the difference in at-

tenuation magnitude is quite perceptible. The greater damping of energy

in the propagation of waves perpendicular to the structures is appa-

rently associated with the dissipation of energy in refracted and re-

peatedly reflected waves at discontinuities exhibiting various elastic

properties. The obtained results are preliminary and require further

detailed study in conjunction with a greater amount of material, a

greater number of stations, and in other areas as well.

The Relationship Between the Damping of Seismic Waves and the Energy of Earthquakes

We can expect that such a relationship exists, since the spectrum of vibrations in the case of powerful earthquakes shifts toward the lower frequencies and in accordance with this the absorption of energy for strong earthquakes must be somewhat lower.
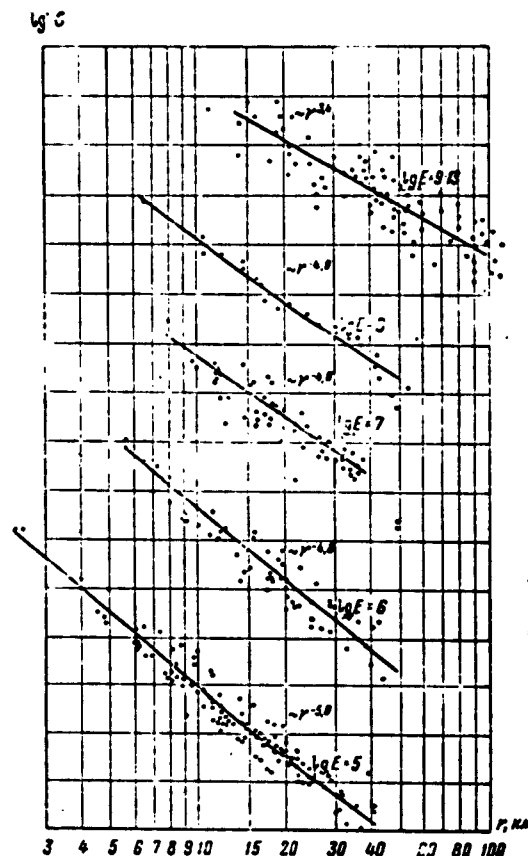
Fig. 40. Energy-density attenuation curve for earthquakes of various energies.

Figure 40 shows the summary attenuation curves for earthquakes with energies ranging from 10^5 to 10^{13} joules. We can see from the curves that, indeed, the attenuation for strong earthquakes is generally somewhat lower than in the case of weak earthquakes. However, this

difference is comparatively small. In view of this, the middle curve was selected as the calibration curve for the determination of energy, since it is the same for both the weak and the stronger earthquakes.

Data on the Nature of Attenuation, Said Data Obtained by Other Authors in Various Regions

This information is generally close to the data that we obtained in Central Asia. The attenuation of the energy-density flow was examined by S.L. Solov'yev and E.L. Dzhibladze [79] on materials for earthquakes occurring in the Great Caucasus. In accordance with the data that they obtained, the attenuation of the energy-flow density at distances from 50 to 500 km is proportional to $1/r^{3.8}$ (curve $\underline{c}$ in Fig. 37), and this is close to the damping values that we obtained, and is proportional approximately to $1/r^{3.5}-1/r^{4.0}$ at these distances.

Richter and Gutenberg used the attenuation of the maximum three-dimensional-wave amplitudes as the basis for the M scale [62]. Figure 38 shows Gutenberg's and Richter's [96] calibration curve (curve $\underline{c}$) which we converted from epicentral distances to hypocentral distances.* The general nature of the curve that we obtained for the earthquakes of Central Asia is close to the calibration curve derived by Gutenberg, differing from the latter by a somewhat smaller attenuation at distances of r > 100 km. The observed difference is small and it is difficult to say whether it is attributable to the structural features of the earth's crust in Central Asia and California, or whether it is associated with the difference in frequency characteristics for the equipment employed, or possibly a result of the methods employed to interpret the seismograms.

The attenuation of the maximum amplitudes was also studied by Kawasumi for shallow earthquakes occurring in Japan. The curve A(Δ) (Fig. 38, curve $\underline{d}$), that he obtained on a section ranging from 100 to

400 km, is in sufficiently good agreement with the corresponding section of a curve which we obtained for Central Asia (Fig. 38, curve a) by means of the VEGIK.

V.I. Bune [61] examined the attenuation of energy density through the records of the Stalinabad earthquake of 1952, said records produced by the seismic stations of Central Asia (curve c in Fig. 36). The closest observation point — the Obi-Garm station — is located at a distance of $r \simeq 90$ km from the epicenter. According to these data, the attenuation of energy density at distances from 100 to 300 km is proportional to $1/r^2$, whereas at distances of $r > 300$ km it is proportional to $1/r^4$. A comparison shows that Bune's data (curve c) does not contradict the curves that we obtained (curves a and b) on the section $r > 100$ km. However, as can be seen from a comparison of the curves, it is impossible to extrapolate the Bune attenuation curve in the form $1/r^2$ in the region of small r (the extrapolation is shown by the dashed line which is the extension to curve c), since in the region of small r the attenuation increases significantly (up to $1/r^4$).

Evaluation of the Role Played by Deviation and Energy Absorption in the Over-All Attenuation of Energy at Small Distances from the Focus

We spoke earlier of the fact that in order to establish the relationship between energy flow E through the reference sphere and the total seismic energy E_0 it would be necessary to know the type of function for attenuation at small distances from the focus and to evaluate the role played by absorption and deviation, factors which make up the total attenuation.

1. The deviation in seismic waves is a function of the structure of the medium and the type of wave. Close to the source, at distances r from the focus comparable to the depth of the focus, i.e., at $r \simeq h$, the amplitude deviation will not be more pronounced than $1/r - 1/r^{1.5}$.

For the density of the energy flow $\vec{E}$, proportional to the square of the amplitude, the deviation at these distances does not exceed $1/r^2$ — — $1/r^3$. A comparison of this magnitude of deviation against the mean empirical curve $|\vec{E}|(r) \sim 1/r^{5.5}$ leads one to the conclusion that a single geometric deviation cannot produce the observed attenuation of energy-flow density, particularly at distances of $r \leq 40$ km from the focus. The fact that the attenuation of energy density $\dot{E}$ is somewhat weaker than the attenuation of $|\vec{E}|$ is apparently a result of the increased vibration duration τ with an increase in the distance from the focus.

2. Absorption. At the present time, there are two popular theories on the absorption of elastic waves: there is the theory of viscous friction and the Deryagin theory that is based on the phenomena of elastic aftereffects [72]. For rocks, the latter is, apparently, in better agreement with experimental results [76]. In accordance with this theory, the amplitude absorption factor q for transverse waves is equal to

$$q = \frac{\pi^2}{2\lambda}\beta$$

or

$$q = \frac{\varepsilon}{\lambda},$$

where λ is the wavelength, β is the constant for the material in question and ε is the absorption decrement that is independent of vibration frequency within a wide range of frequencies. The material constant and its proportional absorption decrement for various materials and rocks may exhibit rather pronounced differences.

We did not undertake any quantitative separation of the deviation and absorption. It is doubtful whether any such distinction could be reliable in view of the great scattering of observed points on the at-

tenuation curves. Moreover, it makes sense to determine the absorption factor for a certain frequency, while the existing data indicate that in the case of earthquake records produced by wideband equipment the dominant vibration frequencies undergo pronounced changes with dis-. tance [98].

A sufficiently great amount of work has been done to determine the absorption decrement ε in rocks in their natural state or in rock
• specimens [76, 99-105], and these yield a value of ε ranging from 0.008 to 0.04. The absorption factor q per unit length is associated with the decrement ε, the wavelength λ, the velocity V of wave propagation, and the frequency f for the vibrations by the following functions:

$$q(f) = \frac{\varepsilon}{\lambda} = \frac{\varepsilon}{V} f. \qquad (15)$$

Knowing the frequency composition of the vibrations, characteristic for local earthquakes of the Garm region, and having assumed a certain value for the attenuation decrement, we can arrive at an estimation of the extent to which the absorption affects the over-all attenuation of energy under local conditions within the range of hypocentral distances from 5 to 80 km in which the TKSE station network generally records earthquakes.

If for these calculations we assume ε = 0.01 we will, apparently, at the same time set the lower limit of energy absorption. Substituting the value of ε = 0.01 and V = 3.5 km/sec for granite into Formula (15), we will obtain

$$q(f) = 0.0028f \text{ km}^{-1}.$$

Figure 41 shows the drop in amplitudes A and the density of the energy flow |$\vec{E}$| in the case of seismic waves of various frequencies with distance for plane waves, i.e., only as a result of absorption.

These curves have been constructed in a double logarithmic scale. From an examination of the curve (Fig. 41) we can see easily that the absorption of vibrations with frequencies of the order of 1 to 3 cps, at r < 100 km, can have no substantial effect on the total energy attenuation, whereas frequencies of the order of 10 to 20 cps and higher experience extremely intensive absorption.

The actual shape of the total energy-absorption curve is a function of the vibration spectrum. For an evaluation of this portion of total energy attenuation, which is determined by absorption, it is evidently necessary to be familiar with the spectrum of earthquakes occurring close to the focus, for example, at distances of 5 to 10 km, and, assuming a certain value for the absorption decrement, to calculate the energy-attenuation curves individually for each frequency as well as a summary curve for all frequencies.

The seismograms of the ChISS installation served as the initial data for these calculations. On the basis of eighty earthquake recordings in which the epicenters were situated 8 to 12 km from the Chusal station, curves were constructed for the distribution of shift amplitudes for the frequency interval corresponding to the various channels of the ChISS installation. These curves, constructed in a double logarithmic scale, will henceforth, for simplicity, be referred to as spectra (for additional details, see Chapter 5). The averaged spectrum, constructed according to these 80 individual earthquakes (for additional details on the averaging of the spectra, see Chapter 5, §1), functioned as the basis for the calculation of absorption, wherein it was assumed that the absorption decrement $\varepsilon = 0.01$.

Figure 42 shows the energy-absorption curves for individual frequencies as well as the summary curve for the absorption of energy-flow density for all frequencies, the latter curve denoted on the

Fig. 41. Curve of drop in amplitude A and density of energy flow $|\vec{E}|$ as a result of absorption, for various frequencies.

Fig. 42. Curve of energy absorption for various frequencies.

graph by Σ. The latter curve, in double logarithmic scale, is closer to a straight line than the curve for individual frequencies. This is associated with the fact that the summary curve seems to serve as a type of envelope for the exponential curves of the various frequencies.

The function $1/r^2$ corresponds approximately to the slope of the summary absorption curve in the double logarithmic scale. If we take into consideration the deviation in energy, proportional at these distances to $1/r^2-1/r^3$, we will find that the total attenuation of density for the energy flow at $\varepsilon = 0.01$ must be proportional to $1/r^4-1/r^5$, and

this is close to the observed attenuation of $|\vec{E}|$, proportional to $1/r^{5.5}$, and close to the observed attenuation of $\dot{E}$, proportional to $1/r^{4.5}$. This indicates that the value of the absorption decrement $\varepsilon =$ $= 0.01$ does not contradict the attenuation pattern for seismic waves of various frequencies under the conditions prevailing in the Garm region, given the condition that the deviation is proportional to $1/r^2$- $1/r^3$.

There is another way of estimating the agreement between the selected value of $\varepsilon = 0.01$ and the actual absorption, without any reference to the nature of the deviation, i.e., according to the deformation of the vibration spectrum with an increase in distance from the focus. The coincidence of the calculated (assuming $\varepsilon = 0.01$) and actually observed deformation of the spectrum can serve as a qualitative confirmation for the evaluation accuracy of the importance of absorption in the total attenuation of energy.

Figure 43 shows the calculated and actual deformation of the spectrum with distance. Unfortunately, in 1955 to 1957, there was only a single frequency-selection station; therefore it was impossible to verify the actual deformation of the spectrum with distance for precisely those specific earthquakes whose spectra at close distances served as the basis for the calculation. It was necessary to use the average spectra of various earthquakes in order to judge the actual deformation of the spectrum with distance; the hypocentral distances from these various earthquakes to the Chusal station ranged from 8-10 to 80-100 km. A comparison of the calculated (curve a) and the observed (curve b) deformation of the soil-shift spectra with distance from the focus indicates that they are in good agreement with one another. This again serves to confirm the accuracy of the cited evaluations of ε.
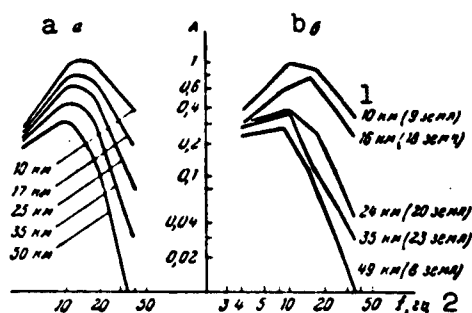
Fig. 43. Deformation of shift spectrum as a result of absorption, with increasing hypocentral distance: a) theoretical (calculated); b) actual; 1) 10 km (9 earthquakes); 2) f, cps.

Thus the energy absorption, particularly for vibrations of high frequencies, plays a substantial role in the total attenuation of energy close to the focus.

§4. GRAPHICAL METHODS OF CALCULATING EARTHQUAKE INTENSITY (ENERGY)

Basic Nomograms

The calculation of earthquake energy E (or E_0) according to Formulas (8) and (9) is most conveniently carried out graphically, by means of nomograms constructed according to the following principle. If the family of curves obtained by means of parallel translation along the axis, log E of the calibration curve E(r) is constructed on a graph in a double logarithmic scale (log r — log E), and this family of curves will represent the energy scale.

Let us select a rational method of dividing this scale and let us also select the value of the ordinates for the curves at r = R. Earlier (§3), the accuracy of the energy determination was evaluated in terms of the mean magnitude of deviation from the averaging curve for the individual points on the summary attenuation curve for E(r). This mean deviation is equal to ±0.5 of an order of magnitude. In this connection, it is sufficient to set one order of magnitude as the divi-

- 160 -

sion for such a logarithmic scale.

So that the whole values of the energy logarithms will correspond
to the center of the interval between the two curves, we will select
such values of energy density $\dot{E}$ on a sphere of radius $\dot{R}$ = 10 km, at
which the energy logarithm is equal to some half number, i.e.,
log E joule = K $\pm$ 0.5 or log Eerg = K + 7 $\pm$ 0.5, where K = 1, 2, ...,
as the initial ordinates of these curves. In this case, at points $\dot{R}$ =
= 10 km, the energy density must satisfy the equality

$$\log \dot{E} \text{ erg/cm}^2 = K + 7 - \log (4\pi\dot{R}^2) \pm 0.5.$$

Into this equation, in the place of $\dot{R}$, substitute its value of $\dot{R} = 10^6$
cm, and we will obtain

$$\log \dot{E} \text{ erg/cm}^2 = K - 6.1 \pm 0.5.$$

This principle was employed in the construction of the nomograms
that were used in connection with the SVK, SGK, and VEGIK equipment.
Certain additions and changes were introduced into the working ver-
sions of the nomograms, and these had the purpose to achieve the
greatest possible simplification of all calculations.

1. The hypocentral distances in the range from 1 to 150 km were
plotted not only in kilometers but in units of $(t_s - t_p)$ seconds, meas-
ured according to the seismogram. The magnitude of the energy density
$\dot{E}$ is not plotted in ergs per cm^2, but in the units of the quantity
$\Sigma A^2 f^2 \tau$, where A is taken in millimeters on the seismogram. In this
case, the initial ordinates are determined in the following manner:

$$\lg \left[\sum_k (A_k^2 f_k^2 \tau_k)_s + \frac{V_p}{V_s} \sum_k (A_k^2 f_k^2 \tau_k)_p \right] =$$

$$= K + 7 - \lg \left(4\pi^3 \mathcal{R}^2 \frac{\rho V_s}{V^2} \right) \pm 0.5, \qquad (16)$$

$$\text{at } t_s - t_p = 1.2 \text{ sec.}$$

We will calculate the ordinates of the curves for the nomograms
(Fig. 44) constructed for the earthquake recordings produced by the

VEGIK seismograph. The values of the constants in Formula (16) are as follows: $\overline{V} = 2 \cdot 10^4$ cm/cm or if amplitudes are being measured in mm, $\overline{V} = 2 \cdot 10^5$ mm/cm; R = 10^6 cm; ρ = 2.7 g/cm^3; V_S = 3.5$\cdot$10^5 cm/sec. Hence,

$$4\pi^3 \mathscr{R}^2 \rho \Gamma_s \frac{1}{\overline{V}^2} = 2.9 \cdot 10^9;$$

$$\lg \sum A^2 f^2 \tau = K + 7 - 9.5 \pm 0.5 = K - 2.5 \pm 0.5.$$

Correspondingly, for the SGK (SVK) seismographs, assuming a magnification of $\overline{V}$ = 1000 cm/cm or $\overline{V}$ = 10,000 mm/cm, we have

$$4\pi^3 \mathscr{R}^2 \rho \Gamma_s \overline{V}^{-2} = 1.2 \cdot 10^{12};$$

$$\lg \sum A^2 f^2 \tau = K - 5.1 \pm 0.5.$$

2. Since earthquakes whose foci are situated in sedimentary and base rocks differ in nature of attenuation, two systems of calibration curves, corresponding to two types of attenuation, have been plotted on the nomogram (Fig. 45) constructed for the seismograms of the SGK.

3. In order for the energy scale on the nomogram to represent a family of straight lines (in this case, it is more convenient to undertake the averaging of the data from various stations), the scale of the axis of abscissas is deformed somewhat in order to transform the calibration curves into straight lines.

4. For convenience in the calculation of the quantity A^2f^2 on the basis of the values of amplitude A and frequency $\underline{f}$ there is an additional nomogram to the left of the basic nomogram, this additional nomogram consisting of three vertical scales: A, $\underline{f}$, and A^2f^2. Plotting the recording values of A in mm on the extreme scales and the vibration frequency $\underline{f}$ in cps, we can link the obtained points by a straight line. The intersection of this straight line with the center scale yields the square of the product of these quantities $(Af)^2$; the multiplication by τ and the addition of the quantities $A^2f^2\tau$ for longitudinal and transverse waves is carried out mentally.
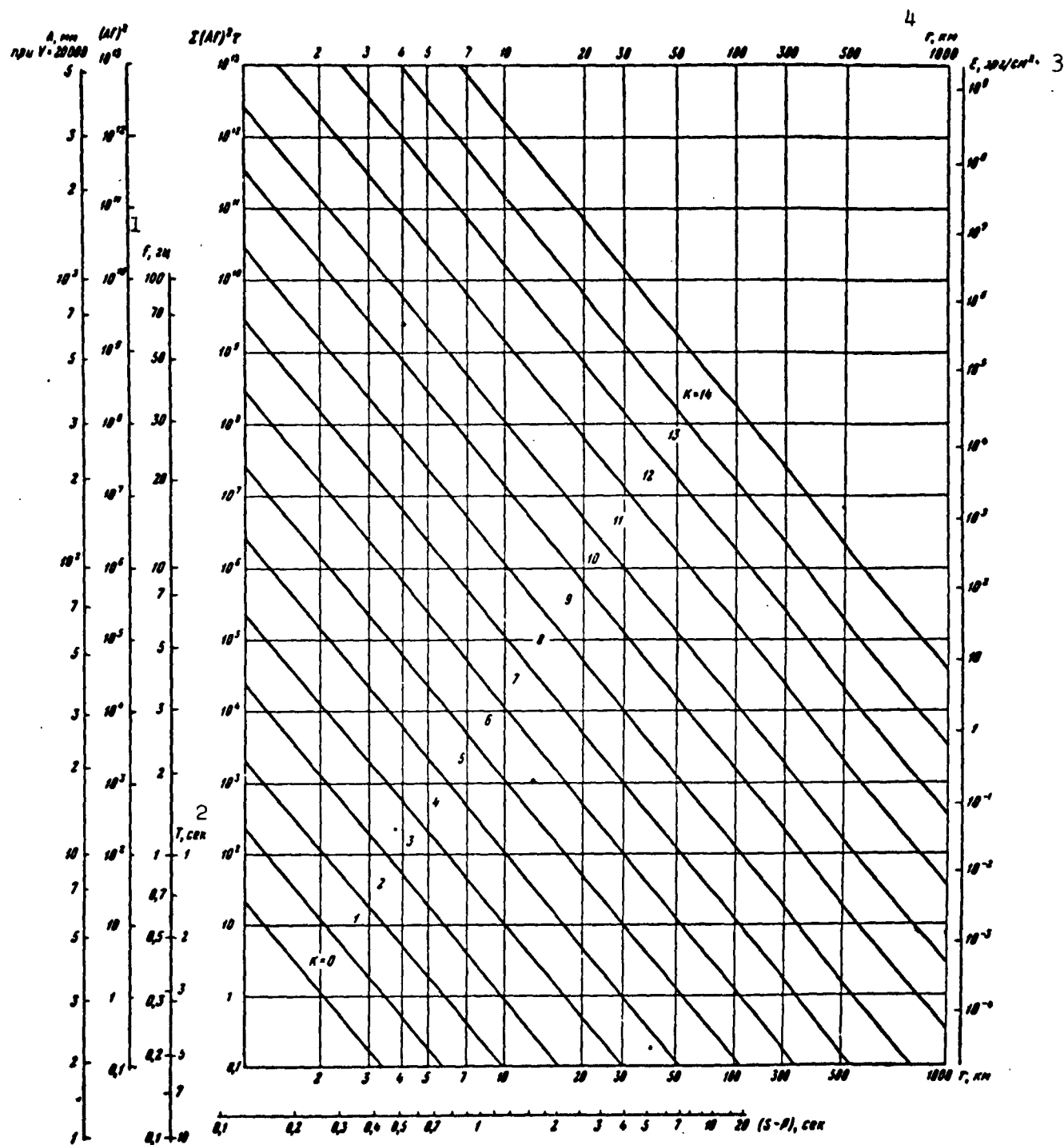
Fig. 44. Nomogram for calculation of earthquake energy according to VEGIK seismograms. 1) f, cps; 2) T, sec; 3) ε, erg/cm²; 4) r, km.

The further determination of energy according to the nomogram can be reduced to the following. Let certain quantities

$$\sum (A^2/t_s)_s + \frac{V_p}{V_s} \sum (A^2/t_s)_p$$

be determined on the seismograms of several stations in mm^2/sec and $(t_s - t_p)$ in sec or $\underline{r}$ in km. Plotting these values on the nomogram, we will obtain a series of points lying within a certain band. The energy corresponding to the center of this band is ascribed to the earthquake.

In addition to expressing energy in joules, energy classes have been introduced, since these are more convenient in practical operations. Denoting the class number by K, we will determine this number according to the formula $E = 10^K$ joules, and

$K = \log (E$ joule$) \equiv \log (E$ erg$) - 7 \equiv \log (E$ megajoule$) + 6.$

Scale of Total Seismic Energy

Earlier (§1) it was mentioned that an energy scale could be constructed on the basis of the energy flow E_0 through a sphere of variable radius, equal to the focal dimension r_0, i.e., on the basis of the magnitude of total seismic energy. The ratio between the quantities E and E_0 for one and the same earthquake is expressed by the following formula:

$$\frac{E_0}{E} = \left(\frac{r_0}{\mathcal{R}}\right)^3 \frac{\psi(r_0)}{\psi(\mathcal{R})}.$$

In order to estimate the magnitude of this ratio quantitatively, we must make certain assumptions pertaining to the focal dimensions r_0 and the nature of attenuation close to the focus.

The empirical determination of the attenuation function for small distances (1-50 km) demonstrated that the attenuation function at these distances has the form of a power function

$$\psi(r) = \frac{1}{r^n}.$$

The exponent n of the attenuation function at these distances is equal to 4-4.5, and in this case we do not observe any drop in the magnitude of n as we approach the focus. The data of N.V. Shebalin [106] on the values of I_0 of earthquakes at the epicenter as functions of depth h

$$I_0 \sim \frac{1}{h^{3.6}}$$

permit us to maintain that energy density declines with distance r at r $\geq$ h, according to a law close to $1/r^4$.
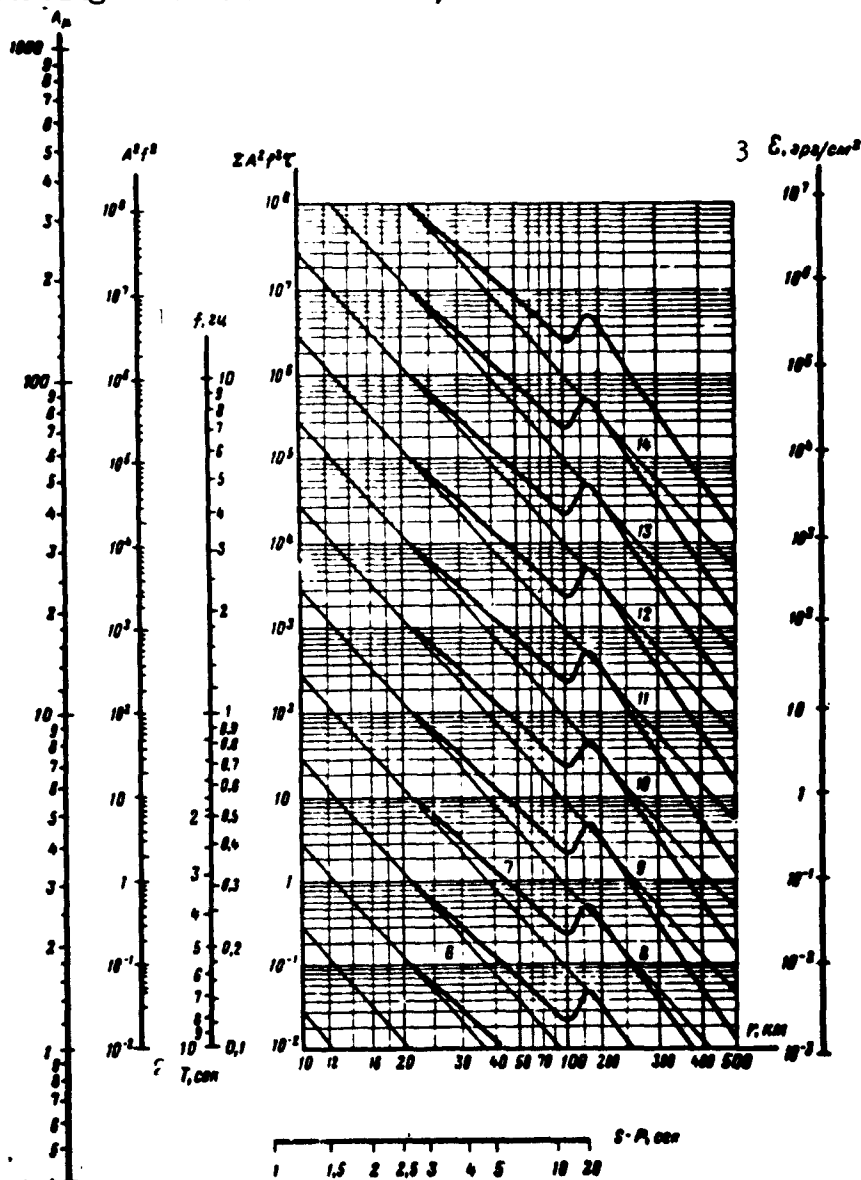
Fig. 45. Nomogram for calculation of earthquake energy according to SGK seismograms. 1) f, cps; 2) T, sec; 3) E, erg/cm².

-140-

Relying on these data, we will maintain that the law governing the attenuation of energy density at all distances down to the focal boundary remains constant even at $r = 1$-50 km, and we will assume

$$\psi(r) = \frac{1}{r^4}.$$ (17)

An evaluation of the focal dimensions for earthquakes of various strength is carried out in Chapter 6, where we obtained the following relationship:*

$$r_{0,M} = 15 \sqrt[3.3]{E} \text{ Joule}.$$ (18)

We will use Expressions (17) and (18) in order to estimate the relationship between total seismic energy E_0 and the energy flow E through the reference sphere of radius $R = 10$ km. Instead of $\psi(r)$ and r_0, let us substitute their values from (17) and (18) into (10) and taking the logarithms, we will obtain

$$\lg E_0 = 5.64 + 0.62 \lg E.$$ (19)

An examination of Expression (19) indicates that the total energy E_0 of weak earthquakes is substantially greater than the flow of energy E through the reference sphere. And only for earthquakes with energies of $E = 10^{14}$ joules for which $r_0 = 10$ km $= R$ does the total energy E_0 coincide with the energy E on the reference sphere.

For more powerful and destructive earthquakes, the quantity E has no physical significance. As has already been pointed out (§1) such earthquakes should be classified according to the energy flow E_0 of three-dimensional waves through the surface S_0 of the focus. However, the calculation of this quantity for powerful earthquakes encounters a series of difficulties. First of all, the assumption adopted above that the surface of the focus is a sphere in the case of powerful earthquakes is not valid. We know that the foci of shallow powerful earthquakes frequently are quite extended in a given single horizontal

direction, whereas the zone of destruction in the vertical direction
may possibly not extend beyond the boundaries of the earth's crust
(30-45 km). Therefore, an evaluation of the focal dimensions r_0, as
carried out in Chapter 6, can also be extended conventionally to the
region of powerful earthquakes, if a sphere of radius r_0 is assumed
approximately to be equal to the volume of the focus. Then, using the
relationship between r_0 and E_0, as obtained in Chapter 6,

$$r_{0,\text{м}} = 0.27 \sqrt[3.2]{E_0} \text{ Joule},$$

we will calculate E_0 as the flow of energy through the sphere of vari-
able radius r_0. Correspondingly, the initial ordinates for the curves
on the nomogram for the calculation of the energy of powerful earth-
quakes are not calculated for $r = 10$ km, but for $r_0 > 10$ km

$$\log \underline{r} \ m = \tfrac{1}{3.2}(K \pm 0.5) - 0.57.$$

Amplitude Nomogram

The energy density determined according to the seismogram depends
on the amplitude A, frequency $\underline{f}$, and on the duration τ of the vibra-
tions. Observations indicate that the vibration duration is determined,
primarily, by the hypocentral distance $\underline{r}$. The dominant frequency $\underline{f}$ also
depends primarily on the energy of the earthquake and the hypocentral
distance. Generally, with constant amplitude and hypocentral distance,
the energy density of various earthquakes, as a function of frequency
and vibration duration, may vary by no more than 0.3-0.5 of an order
of magnitude. In other words, the energy at this distance from the
focus is primarily determined by the amplitude.

This circumstance makes it possible to determine approximately
the energy of earthquakes on the basis of amplitudes alone, without
taking into consideration frequency and vibration duration, by estab-
lishing a correlative relationship between amplitude, distance, and

earthquake energy. Such an evaluation of energy would serve as a type
of "express" method, making it possible rapidly and with comparatively
limited work, to achieve the energy classification of all recorded
earthquakes, without exception. The amplitude method of estimating
energy requires no great skill on the part of the observer and may be
employed with a small recording time sweep, which would not permit a°
determination of vibration frequency.

The basis of the nomogram for the determination of energy in ac-
cordance with the sum of maximum amplitudes is the curve presented
above (Fig. 38) for the attenuation of amplitudes with distance and
the correlation curve between the sum of the maximum amplitudes, re-
ferred to a certain fixed distance, and the earthquake energy deter-
mined in accordance with the system described earlier. For the con-
struction of the curve of the latter approximately 800 earthquake re-
cordings with energies ranging from 10^4 to 10^{13} joules were processed.
Figure 46 shows the results of these measurements. The earthquake en-
ergy E has been plotted in logarithmic scale along the axis of abscis-
sas, and the sum of maximum amplitudes $A_p + A_s$ shown in mm on a VEGIK
seismogram, referred to a certain fixed distance r' according to the
amplitude-attenuation curve (Fig. 38), has been plotted along the axis
of ordinates. The following equation corresponds to the averaging
curve, a straight line,

$$\lg E = 1.8 \lg (A_p + A_s)_r \div C(r').$$ (20)

The quantity C, determined from the curve, will vary as a function of
r'. Thus at r' = 10 km, C will be equal to 3.9; at r' = 100 km, C = 7.5.

The amplitude nomogram for the determination of energy (Fig. 47)
represents a family of curves for the attenuation of maximum amplitudes
$(A_p + A_s)_{VEGIK}$, constructed in a coordinate system in which, in loga-
rithmic scale, the maximum vibration amplitudes in mm on the VEGIK

seismogram have been plotted along the axis of ordinates, and the hy-
pocentral distances have been plotted along the axis of abscissas. As
in the basic nomogram, the scale along the axis of abscissas is loga-
rithmic, deformed so that the calibration curve is converted into a
straight line. The divisions of the scale are chosen so as to be equal
to a single order of magnitude in energy, and this corresponds to 0.56
of an order of magnitude in amplitude. The initial ordinates of the
curves are determined by Eq. (20) under the condition that the center
of the interval between the two curves corresponds to the whole value
of the logarithm of K for energy

$$\lg(A_p \div A_*) = 0.56(K \pm 0.5 - C) \qquad K = 1, 2, \ldots$$

For example, the curves which constitute the upper and lower bounda-
ries of the nomogram band corresponding to an energy of $E = 10^6$ joules
$(K = 6)$, have the following ordinates at $r' = 10$ km and, this means,
at $C = 3.9$:

$$\lg(A_p \div A_*) = 0.56 \cdot (6 - 3.9 \pm 0.5) = 1.17 \pm 0.28,$$

i.e., at $r' = 10$ km the maximum earthquake amplitudes of the sixth en-
ergy classification range from 7 to 25 mm.

The determination of energy according to maximum amplitudes, natu-
rally, is less exact than the determination of energy involving a con-
sideration of frequency and vibration duration. The magnitude of the
energy errors associated with this method can be estimated in accordance
with the scattering of the points on the correlation graph relative to
the averaging curve. On the basis of the magnitudes of energy deviation
$\delta \log E$ from the average relationship $E = E(A)$

$$\delta \lg E = \lg E - \lg E(A)$$

the curve $N = N(\delta \log E)$ was constructed for the distribution of the num-
ber of deviations (Fig. 48). It follows from an examination of the
curve that the probable error in the determination of energy according

$lg(A_p \cdot A_s)$
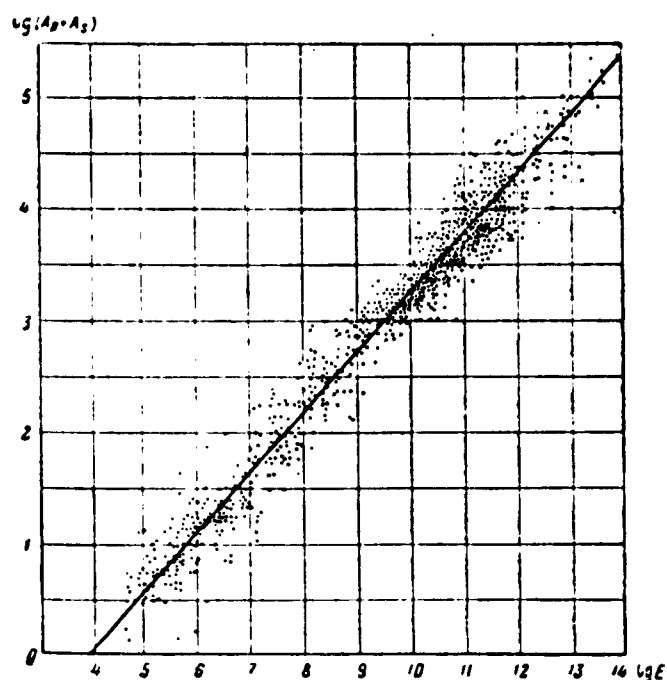
Fig. 46. Correlation graph between magnitudes of maximum amplitudes at distance of r' = 10 km and earthquake energy.

to the maximum amplitudes amounts to 0.4 of an order of magnitude, and here the maximum value of the error does not, for all intents and purposes (in 97% of all cases), exceed one order of magnitude.

We may maintain that the determination of energy according to the maximum amplitudes will introduce no great error and this method can be recommended as an "express" method for purposes of energy classification, primarily for the numerous weak earthquakes.
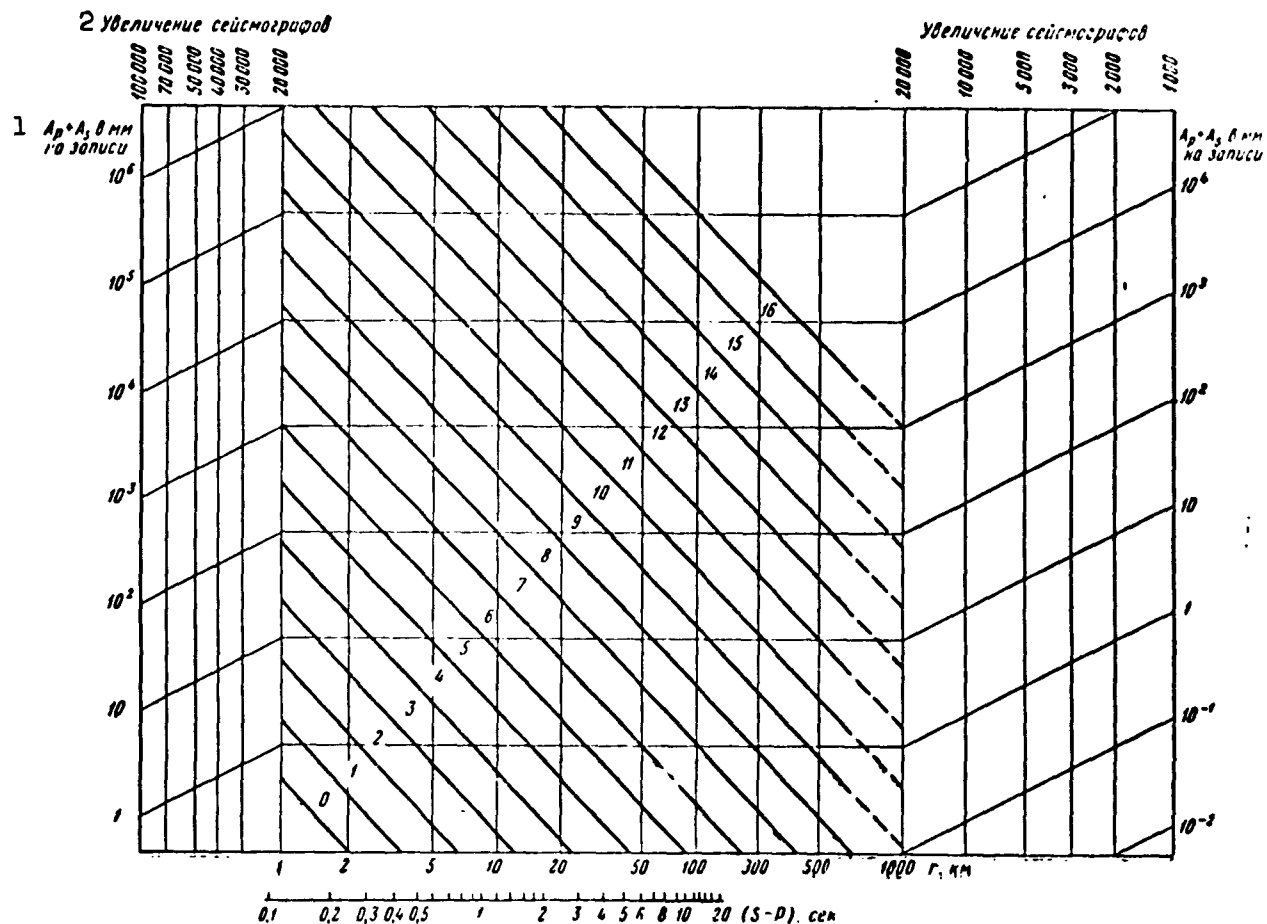
Fig. 47. Nomogram for the determination of energy according to maximum VEGIK amplitudes. 1) $A_p + A_s$ in mm, on recording; 2) seismograph magnification.

§5. COMPARISON OF VARIOUS ENERGY CLASSIFICATIONS

The energy classification described above is based on the empirical damping function determined by shape and on the fixed magnitude of the integration sphere. It is therefore natural that both a change in the radius of the integration sphere as well as the assumption of a different nature for the damping function (one not confirmed by experience) will result in substantially different values for the magnitude of energy E.

Below we present a comparison of the TKSE energy classification
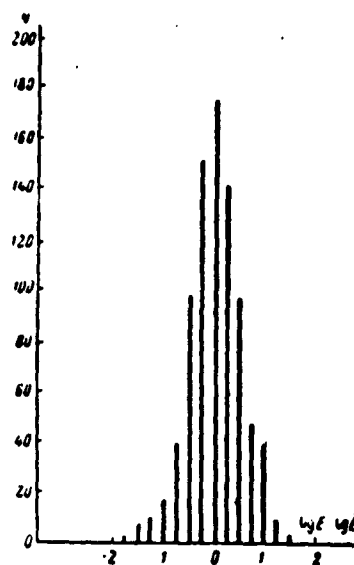
Fig. 48. Distribution of earth-
quake-energy deviations, from
the mean correlation E = E(A),
calculated by means of the
nomogram presented in Fig. 47.
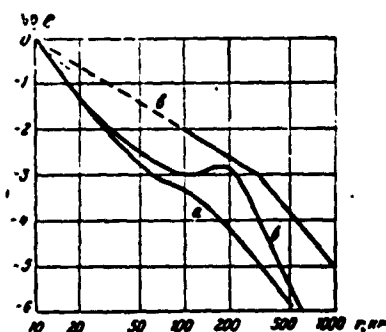
Fig. 49. The difference Δ log E
between the energy flow through
the reference sphere and the
energy calculated according to
the Golitsyn-Bune formula.

with certain other energy classifications, as well as with a relative

scale of "magnitudes" — the scale M.

Energy According to the Gutenberg Formula

Energy according to the Gutenberg [63] Formula is, in essence,

equal to the energy flow through the sphere having a radius equal to

the focal depth $\underline{h}$

$$E = 3\pi^3 h^2 \rho V s \left(\frac{A_0}{T_0}\right)^2 t_0.$$

In using this formula, we assumed the magnitude $\underline{h}$ to be equal to the average depth of the California earthquakes, i.e., h = 16 km.* Gutenberg's and Rikhter's method of determining energy density at the epicenter is somewhat different from the one described above. For example, it is maintained that T and $\underline{t}$ are virtually independent of distance and only the amplitude A is referred to its values A_0 at the epicenter according to the calibration curve $A = A(\Delta)$, which is extremely close to the amplitude-attenuation curve that we obtained from observations of earthquakes in Central Asia. We can maintain that, despite small methodological differences, the determination of energy (according to the Gutenberg formula and the method employed by the expedition) is essentially similar and the two methods should yield quantitatively close results.

Energy According to Golitsyn's [56] Method

In essence, this energy is a flow of energy of elastic waves through a sphere with a radius equal to the epicentral distance Δ to the station at which it is calculated: ·

$$E = 2\pi^3 \Delta^2 \rho V \sum \frac{A^2}{T^2} \tau.$$

However, because the actual damping of seismic waves differs from the adopted quantitative relationship $1/\Delta^2$, the magnitude of energy calculated according to this formula loses its specific physical sense: for one and the same earthquake, the energies calculated according to data from stations lying at various distances from the focus prove to be varied as well.

In order to be able to compare data on the flow of energy through a sphere with radius R = 10 km against the data for earthquakes whose

energy was determined according to the Golitsyn formula (for example, [12, 68] and [61, 107]), it is necessary to estimate the magnitude of the systematic energy discrepancy, determined according to each of the methods, as a function of hypocentral distance. In determining energy according to Golitsyn's formula, the authors mentioned above generally made use of SGK and SVK seismograms with which the Central Asian stations had been equipped; here, the epicentral distances lie within limits of from 50 to 300 km. Therefore, for a quantitative evaluation of the magnitude of energy discrepancy Δ log E = log E_{TKSE} -
- log E_{Golits}, which can be anticipated if the TKSE method and the Golitsyn formula are used, we will use the damping curves constructed according to the SGK seismograms.

The quantity Δ log E as a function of distance $\underline{r}$ can be calculated by a simple graphical method that is illustrated in Fig. 49. Here, with a double logarithmic scale, are presented the curves ($\underline{a}$ and $\underline{b}$) for damping according to SGK data for two types of earthquakes (see page 140), and the magnitude of the energy density $\underset{.}{E}$ at r = 10 km (initial ordinate) is assumed to be unity. The graph of the function $1/r^2$ (curve $\underline{c}$) was constructed from this same initial point for r = 10 km. Evidently, the difference in the ordinates of the empirical attenuation curve and the curve $1/r^2$ at any distance r > 10 km will be equal to Δ log E. As can be seen from the curves, for earthquakes of the first type (curve $\underline{a}$) the magnitude Δ log E on the average attains 1.5 orders, dropping to one order of magnitude at r = 30 km. For earthquakes of the second type (curve $\underline{b}$) this difference is smaller and attains a single order of magnitude only at distances ranging from r = 50 to 100 km. At distances of r = 150 to 250 km, where there is a "hump" on the damping curve, this difference decreases to 0.5 to 0.2 of an order of magnitude. On the average, in the range of distances from 10 to 300 km,

energy determined according to the Golitsyn formula is approximately smaller by one order of magnitude than the energy determined by the TKSE method.

The estimates of magnitude $\Delta \log E$ obtained above represent systematic deviation. The observed values of $\Delta \log E$ obtained in practice may even be somewhat greater (approximately up to 2.5 orders of magnitude) as a result of random deviations.

Thus if we use the earthquake energy data determined according to the Golitsyn formula in the works cited above and in similar projects, it is necessary to bear in mind that the obtained energy magnitudes are, on the average, lower by approximately one order of magnitude than the energy flow through the sphere with radius $R = 10$ km.

The above refers to comparatively weak earthquakes ($\log E \leq 14$), for which the classification with respect to the magnitude E is applicable. For more intense earthquakes, the magnitude of possible deviations, apparently, may be smaller. This is associated with the fact that for powerful earthquakes the focal dimension $r_0 > 10$ km and their energy E are calculated by integration over the sphere with radius $r_0 > R$. However, the attenuation curve from the SGK data becomes markedly smoother beginning at distances $r = 80$-50 km, forming a "step" or "hump" on approaching $1/r^2$.

Relative Scale of Magnitudes M

The relative scale of magnitudes first introduced by Ch. Richter [62] has now come into widespread use. The magnitude M of an earthquake is the logarithm of the ratio between the maximum amplitudes of the threedimensional waves of the given earthquake and the amplitudes of the same waves for a "standard" earthquake for which $M = 0$ at one and the same distance from the focus. The calibration curve (the relationship between amplitudes and the epicentral distance Δ) and the level

of the curve (at r = 100 km, the amplitude on the recordings produced by the Vud-Andersen [sic] seismograph is equal to 1 μ) are given.

Subsequently, the M scale was generalized for greater epicentral distances [66, 67]. At the present time, there are methods for the determination of M on the basis of threedimensional and.surface waves, according to maximum amplitudes on recordings produced by a certain instrument, or according to the amplitudes of soil shifts, as well as on the basis of the ratio of maximum amplitude to period. A detailed analysis of these methods, as well as a description of the M scale worked out by S. L. Solov'yev and N. V. Shebalin (utilized in the USSR) can be found in References [68-70].

Since for many problems the expression of earthquake magnitude in the dimensionless relative scale is inadequate, attempts are being made to find a relationship between magnitude M and seismic earthquake energy E. The authors who derived the M scale [63, 65, 96, 108] and other investigators [109-111] present a great number of empirical formulas relating these magnitudes and they are of the following form

$$\lg E = a + b M \qquad (21)$$

(sometimes, a term with M^2 is also introduced). The values of each of the parameters a and b frequently exhibit pronounced divergences for various authors. These divergences may be the result of features contained within the energy-calculation method or may be a result of the fact that formulas of the type (21) average a cluster of points that frequently have a comparatively small interval of change for the two quantities M and E and yet differ in a large scattering of points as a result of various determination errors. In view of the latter circumstance, formulas that exhibit pronounced differences can, within a certain range of changes in M, yield close results. Therefore, in order to compare the formulas of the various authors it is most convenient
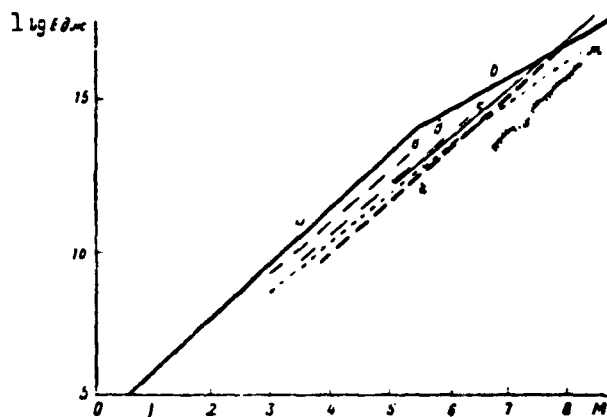
Fig. 50. Relationship between energy E joules and magnitude M according to data of various authors. a) TKSE ($\log E = 4 + 1.8\,M$); b) TKSE ($\log E_0 = 8 + 1.1\,M$); c) Solov'yev [12] ($\log E = 4 + 1.7\,M$); d) Solov'yev [12] ($\log E = 3 + 1.7\,M$); e) Bune [61] ($\log E_0 = 3.5 + 1.7\,M$); f) Gutenberg [63] ($\log E = 4 + 1.6\,M$); g) Gutenberg [96] ($\log E = 2.4 + 2.14\,M - 0.054\,M^2$); h) De Noyer [109] ($\log E = 0.76 + 1.87\,M$); 1) $\log E$ joules.

to present graphically the relationship between M and E that they have derived. Figure 50 shows Function (21) according to the data from a series of foreign and Soviet authors.

There are various possible methods of carrying out a comparison of the M scale with the energy classification adopted by the TKSE. The first of these involves a comparison of data from many earthquakes for which energy has been determined according to the TKSE method and in which the magnitude M has been determined according to the method proposed by S.L. Solov'yev. However, unfortunately the magnitude M is not given for all earthquakes cited in the Bulletin of the Seismic Network of the USSR. From 1956 on, when the low-sensitivity VKh seismograph went into operation, said seismograph making it possible to determine reliably the energy of comparatively powerful ($E = 10^{11}$-10^{13} joules) earthquakes according to data from near-by stations, by 1958 it had

been possible to obtain joint data only for 27 earthquakes. The extremely small range of changes in E and M, in which lie the existing points, do not permit the drawing of any reliable curve.

The second method is based on the initial determination of the M scale presented by Richter [62] (the so-called M_L scale), and it has the advantage that it makes it possible to use a greater volume of material for purposes of comparison because it can employ the data from a great many weak earthquakes. There is also the important fact that the magnitude of maximum amplitude serves as the basis for the initial determination of M for a comparatively small distance of $r = 100$ km, and this is close to the distances at which earthquakes are generally recorded under TKSE conditions.

The relationship between M and E was sought in the form of (21). The values of the coefficients a and b were found in the following manner. Apparently, the coefficient b characterizes the slope of the averaging straight line in Fig. 46 where, the earthquake energy and the logarithm of the amplitude at a fixed distance from the focus are plotted along the axes. The latter quantity is proportional to M. The value of the angular coefficient of the curve in Fig. 46, on which there are approximately 300 points for earthquakes with energies ranging from 10^4 to 10^{13} joules, is equal to b = 1.8.

The parameter a in Eq. (21) is the logarithm of earthquake energy with a zero value for M. By definition, an earthquake of this type has its maximum amplitude on the recordings produced by the Andersen-Vud [sic] seismograph ($A = 1 \mu$ at $r = 100$ km). The frequency characteristics of the VEGIK and the Andersen-Vud [sic] seismographs are sufficiently close. The magnification of these instruments for the maximum of the frequency characteristics is equal to 20,000 and 2800, respectively. We should also bear in mind that in the method employed by the

expedition it is not the maximum wave amplitude A_s that is generally determined, but rather the total of maximum wave amplitudes A_p and A_s, said total approximately 1.3-1.5 times greater than the amplitude of the S waves. In this case, we may state that an earthquake with a zero value of magnitude ($M = 0$) at a distance of 100 km will show a total of maximum amplitudes $A_p + A_s$ on the VEGIK seismogram that is equal to 10 μ, i.e., 0.01 mm. In accordance with the energy-determination amplitude nomogram presented in Fig. 47, an energy of $E = 10^4$ joule corresponds to this type of earthquake, i.e., $a = \log E_{M=0} = 4$ or if energy is measured in ergs, then $a = 11$.

Thus we obtain a relationship between magnitude M and energy flow E through the sphere with radius R = 10 km which takes the form

$$\log E \text{ joules} = 4 + 1.8\ M$$

or

$$\log E \text{ erg} = 11 + 1.8\ M. \tag{22}$$

Earlier (§3) we spoke of the fact that the Gutenberg and Richter [96] calibration curve ($A = A(\Delta)$) is little different from the attenuation curve for the maximum VEGIK amplitudes that we obtained. We may therefore maintain that deviations from Eq. (22), associated with this small difference between calibration curves, will be insignificant.

Equation (22) was constructed on the basis of earthquakes with energies ranging from 10^4 to 10^{13} joules and, consequently, is valid for that range of energies. Figure 50 shows curve $\underline{a}$ as corresponding to this equation. The joint earthquake data for which we know both the energy E determined by the methods employed on the expedition as well as the magnitude M determined on the basis of surface waves by means of the method proposed by S.L. Solov'yev do not contradict the function $\log E$ joules $= 4 + 1.8$ M. The graph in Fig. 50 also shows curves $\underline{c}$ and $\underline{d}$ calculated according to S.L. Solov'yev's [12] formulas for weak (c) and strong (d) earthquakes, as well as curve $\underline{e}$ calculated according to

the Bune [61] formula. The latter is almost coincident with the curve
(f) derived by Gutenberg and Richter for powerful earthquakes [65]. As
can be seen from an examination of the graph in Fig. 50, curve a which
corresponds to the relationship between M and E, said relationship ob-
tained by us, lies above the curves c-e. This is a completely valid
reflection of the fact that in determining energy according to Golitsyn's
method, the method employed by the authors who derived the formulas
for c-e, underestimated energy values are obtained (on the average,
lower by an order of magnitude).

Let us now examine the relationship between the total seismic en-
ergy E_0 and M. Instead of the quantity E we will substitute into Ex-
pression (19) which relates E_0 and E, the value of E from Formula (21).
We will obtain

$$\log E_0 \text{ joules} = 8 + 1.1 \text{ M} \qquad (23)$$

or

$$\log E_0 \text{ ergs} = 15 + 1.1 \text{ M}.$$

The last formula can be used for the transition from M to the
energy of the threedimensional waves for more powerful and destructive
earthquakes, classified on the basis of total seismic energy E_0. The
values of energy E_0 as obtained by means of this formula for powerful
earthquakes (M $\geq$ 5.5) are close to the energy obtained by the formulas
derived by Gutenberg and Richter [96] (curve g) and the formula derived
by De Noyer [109] (curve h). For earthquakes with maximum magnitude M =
= 8.6, Formula (23) yields an energy of $E_0 = 10^{17.5}$ joules. This coin-
cides with the earthquake-energy estimates made by Bullen [110] and
Tsuboi [111].

§6. THE SHAPE OF ISOENERGY LINES

In studying the attenuation of energy in seismic waves at small
distances from the focus it turned out that there is a substantial dif-

ference in attenuation for seismic waves propagated along and across the basic geologic structures. This phenomenon was noted in macroseismic observations; for example, the observations carried out by G.P. Gorshkov [112], et al. The factor responsible for this divergence in attenuation is the varied scattering of elastic waves in the stratified medium, in the directions along and across the layers, a phenomenon of the so-called seismic quasi-anisotropy [113]. The evaluation of the effect that this difference in attenuation has on the shape of the iso-energy lines, and consequently, to a great extent on the shape of the isoseists, is of great practical interest.

The sufficiently complete theoretical solution of this problem for an actual extended focus whose mathematical model is the double force with moment at distances comparable to the focal dimension is an extremely complex independent problem even in the case of a homogeneous and isotropic medium. Under conditions of quasi-anisotropy, however, resulting from the stratification, the calculations would prove to be extremely cumbersome [114].

Here, we will limit ourselves only to simplified concepts for the very coarsest evaluation of the effect on the shape of the isoenergy lines: a) exhibited by the shape of the source and b) by the varying attenuation of seismic waves in different directions. It would be interesting to undertake an examination of the effect that these factors have individually as well as jointly.

Effect of Attenuation Difference

Let the source be in the shape of a sphere of small radius r_0, and let the energy density per unit of sphere surface be constant over the entire surface of this sphere during the time in which the vibrations took place. The focal depth will be assumed to be equal to 0, 5, 10, 20, and 40 km.
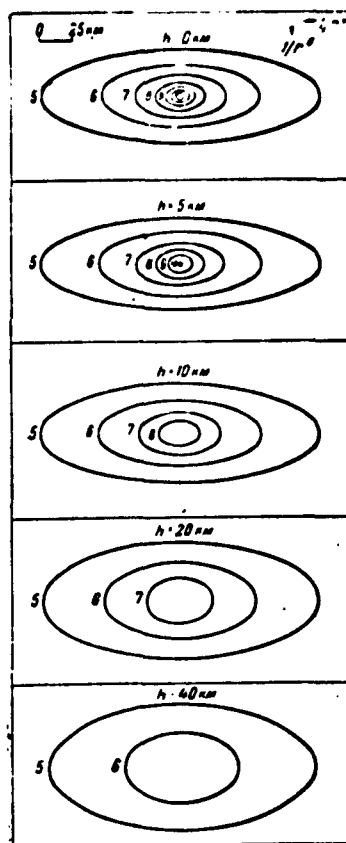
Fig. 51. Calculated isoenergy
lines for a spherical focus in
the case of damping, dependent
on the direction of seismic-
wave propagation.

We will hold that the attenuation of energy density, associated
with divergence, absorption, and scattering, in the propagation of
seismic waves along the basic geological structures as well as vertic-
ally, takes place proportionally to $1/r^4$, and that the attenuation
across these structures is proportional to $1/r^6$. The values of the ex-
ponent $\underline{n}$ of the attenuation function $\psi(r) = 1/r^n$ are 4 and 6, taken in
accordance with the results obtained in §3 on the basis of energy-den-
sity attenuation observations along and across the Peter I Range for
weak earthquakes. The latter circumstance is important with respect to
the fact that the quantity $\underline{n}$, determined on the basis of weak earth-

quakes, has no effect on the shape of the focus, which is sufficiently small in this case, and only attenuation exerts any influence.

Further, we will hold that in the intermediate directions, $\underline{n}$ changes monotonically from 4 to 6. The specific nature of $\underline{n}$ as a function of direction has not been studied experimentally. For purposes of determinacy, we will assume that this function is represented graphically by an ellipse. In essence, however, for such coarse calculations it is sufficient for us to estimate only the total extent of elongation for the isoenergy lines in the main directions.

Then, if the origin of the coordinate system is made to coincide with the center of the source, and if the $\underline{ox}$ axis is made to coincide with the direction of least attenuation, and the $\underline{oy}$ axis is made to coincide with the direction of greatest attenuation, obviously the energy density E at an arbitrary point $M(x,y,z)$ must be calculated according to the following formula:

$$\mathcal{E}(r) = \mathcal{E}(r_0)\left(\frac{r}{r_0}\right)^n.$$

where

$$r = \sqrt{x^2 + y^2 + z^2}; \quad n = \frac{r}{\sqrt{\left(\frac{x}{4}\right)^2 + \left(\frac{y}{6}\right)^2 + \left(\frac{z}{4}\right)^2}}.$$

It is not difficult to obtain the equations for the isoenergy lines, if we assume

$$\frac{\mathcal{E}}{\mathcal{E}_0} = \left(\frac{r_0}{r}\right)^n = C_i.$$

where C_i = const. Figure 51 shows the isoenergy lines that have been calculated in this fashion for various focal depths in the assumption that $r_0 = 3$ km. The values of log C_i differ by unity, and this corresponds to a difference in energy density by one order of magnitude for adjacent lines.

The isoenergy lines are markedly elongated along the direction of

least attenuation and have a shape that is close to that of an ellipse. The elongation of the isolines can be characterized by the ratio r_{max}/r_{min} of the isoline semi-axes. The elongation increases with distance from the focus. For the isoline closest to the focus ($c_1 = 10^{-1}$)

$$r_{max}, r_{min} = 1,2,$$

whereas for an isoline $c_1 = 10^{-6}$ the magnitude of this ratio attains 3.

With an increase in focal depth, the elongation diminishes somewhat. For example, for a focal depth of $h = 40$ km, the ratio of the semi-axes for $c_1 = 10^{-6}$ isolines drops to 2, but in the general case, the shape of the elongated isolines and the area which these encompass are a weak function of depth.

Thus the observed difference in attenuation must be related to the pronounced elongation of the isoenergy lines in the direction of least attenuation. As a result, energy density at equal distances from the focus but in different directions may exhibit pronounced differences: by one or two orders of magnitude.

Calculations of this sort are applicable only at distances over which the straight-line waves carry the greatest energy. In the case of greater distances, head waves from the Mohorovicic discontinuity play a greater role, and the intensity of these head waves is less affected by the structural features of the upper layers of the earth's crust.

Influence of Shape and Dimensions of Source

Frequently, the elongation of the isoseists of powerful earthquakes can be explained by the extension of the focus, i.e., the shape of the focus approaches that of a plane (the plane of discontinuity). However, assuming certain simplifying hypothesis, we can demonstrate that if the damping of energy is identical in all direc-

tions, the isoenergy lines quite rapidly approach the shape of a circle with increasing distance from the focus.

If we are to determine the energy density from the extended source of seismic vibrations, meaning thereby, as before, the integral of the energy-flux density over the entire time during which these vibrations take place, we can do without the information on the difference in shift time at various points of the focus and without the difference between the arrival times of the corresponding waves at the point of observation. Moreover, we can do without information as to the nature of shifts in the elements of the focus and the associated emission directivity, bearing in mind that in practice generally no pronounced directivity is noted for the energy of the entire range of observed waves.

Proceeding from these concepts, we will assume that the focus is part of the plane over which the elementary point sources of seismic energy are distributed uniformly with a density E_0 = const, with the point sources exhibiting spherical characteristics of directivity. We will calculate the energy density at the point of observation by making use of the elementary formulas of the theory of potentials for static fields for the distributed sources [115]. At first, let us position the coordinate origin at any point on the surface. Let us denote the coordinates of the points in the focus by ξ, η, ζ, and the coordinates of the points in the remaining space by $\underline{x}$, $\underline{y}$, and $\underline{z}$. Let the focus be a rectangle lying in the plane $\underline{x}$, $\underline{z}$ and passing through to the surface, so that $\xi_1 \leq \xi \leq \xi_2$; $\eta = 0$; $0 \leq \zeta \leq \zeta_2$.

The energy density at the surface of the source, by convention, is constant and equal to E_0. The energy dE_0, emitted by an element of source surface $ds = d\xi d\zeta$ is equal to

$$dE = \mathscr{E}_0 d\xi d\zeta.$$

If the damping of the energy density is proportional to $1/r^n$ with distance, at any arbitrary point $M(x, y)$ on the surface of the earth, the energy density of the waves from the element of source surface ds will be equal to

where

$$d\mathscr{E}(x, y) = \frac{\mathscr{E}_0}{4\pi r^n} d\xi d\zeta, \qquad (24)$$

$$r = \sqrt{(x - \xi)^2 + y^2 + \zeta^2}.$$

To calculate the energy density from the entire focus at point $M(x, y)$, Expression (24) must be integrated over the entire surface of the focus

$$\mathscr{E}(x, y) = \frac{\mathscr{E}_0}{4\pi} \int_{\xi_1}^{\xi_1} \int_0^{\zeta_2} \frac{d\xi d\zeta}{r^n},$$
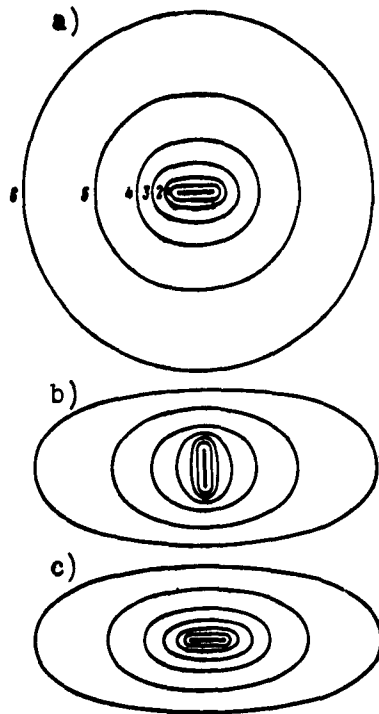
Fig. 52. Calculated isoenergy lines for an extended focus. a) In the case of damping independent of direction; b) and c) in the case of damping dependent on direction and in · the case in which the focus is extended in the direction of the least (c) and the greatest (b) damping.

where n = const. Hence, assuming $E/E_0 = C_1$ = const, we will derive the equation for isoenergy lines. It is convenient to select such values of C_1 that log $C_1 = -1, -2, -3$, i.e., so that the energy density on the adjacent isolines exhibits a varience of one order of magnitude.

Figure 52 shows the isoenergy lines of a plane (flat) focus with dimensions of 20 x 20 km, passing through to the surface, so that

$\xi_1 - \xi_2 = 20$ km; $\zeta_2 = 20$ km; $\eta = 0$; and $n = 4$ in the case of damping, regardless of the propagation direction of the seismic waves. We can see from Fig. 52 that the elongation (extension) of the isoenergy lines

is associated with the shape of the focus, and the elongation quickly diminishes with distance from the source, and in this particular case as early as $r \cong 3$ $(\xi_1 - \xi_2)$, i.e., at distances exceeding the dimensions of the focus by a factor of only 3, the isolines are virtually indistinguishable from circles.

Isolines of an Extended Focus in the Case of Damping that is Dependent on Direction

Let us now write the equations for the isoenergy lines of an extended focus for the case of various focal orientations with respect to the directions of least and greatest damping. As before, let the damping in directions $\underline{x}$ and $\underline{z}$ be proportional to $1/r^4$, in direction $\underline{y}$ proportional to $1/r^6$, and in the remaining directions the subscript $\underline{n}$ in the damping function $1/r_n$ assumes values varying between 4 and 6. Let us examine the cases in which the focal plane coincides a) with the plane xz and b) with the plane yz. We will take the same focal dimensions as in the case examined above. The equations for the isolines in case a) will be

$$\frac{1}{4\pi}\int_{\xi_1,0}^{\xi_2,\zeta_2}\frac{d\xi \, d\zeta}{r^n} = C_i, \tag{25}$$

where

$$r = \sqrt{(x-\xi)^2 + y^2 + \zeta^2}; \quad n = \frac{r}{\sqrt{\left(\frac{x-\xi}{4}\right)^2 + \left(\frac{y}{6}\right)^2 + \left(\frac{\zeta}{4}\right)^2}};$$

and in case b)

$$\frac{1}{4\pi}\int_{\eta_1,0}^{\eta_2,\zeta_2}\frac{d\eta \, d\zeta}{r^n} = C_i, \tag{26}$$

where

$$r = \sqrt{x^2 + (y-\eta)^2 + \zeta^2}; \quad n = \frac{r}{\sqrt{\left(\frac{x}{4}\right)^2 + \left(\frac{y-\eta}{6}\right)^2 + \frac{\zeta}{4}}}.$$

The isoenergy lines calculated according to Formulas (25) and (26) are shown in Fig. 52. A comparison and examination of these lines with the isolines shown in Fig. 51 demonstrates that the effect of focal elongation, shape, and orientation, and the shape of the isoenergy lines is restricted to a small area in the immediate

vicinity of the focus. However, at great distances $\underline{r}$, with $r \gg \underline{l}$ ($\underline{l}$ is the dimension of the source), the isolines are extended along the direction of least damping regardless of focal orientation.

Since there is a definite relationship between the density of the energy and the scale point [106, 116], the isoenergy lines obtained above can be compared with the isoseists. Generally, the isoseists of powerful earthquakes are extended along the basic geological structures, and at no point are they extended across the structures, so that the extension by no means diminishes with distance from the focus.

The isoseists of the Krasnovodsk earthquake of 1895 [86] are quite characteristic in this regard. From the south, where the Kopet-Dag and Elbrus ranges are located, the isoseists seem to converge on the focus, whereas from the north, from the side of the plateau, the isoseists approximate in shape the arc of a circle and encompass tremendous areas.

This effect — the elongation of the isoenergy lines along the extent of the basic geological structures, associated with the least attenuation in this direction — must, of necessity, be taken into consideration in a detailed seismic study of the region. In those cases in which the region under study is separated from the seismic-active zone by mountain ranges, more pronounced damping in this direction will result in a lessening of seismic danger. If, however, the region for which this seismic study of the region is being carried out is situated in the same zone of geological structures as the seismic-active zone, it becomes necessary to take into consideration the increase in seismic danger, regardless of the anticipated orientation of the discontinuity planes in the case of powerful earthquakes in the given seismic-active region.

It should be stressed that evaluations of this type can be employed in the practice of a detailed seismic regional study. However, for this it is necessary to carry out additional work on refining and clarifying details of the relationships between energy-density attenuation and the elastic properties of the rocks which make up the geological structures, taking into consideration in this case the problems of quasi-anisotropy. On the other hand, we must take into consideration the relationship between energy density and the earthquake intensity scale. For this reason, there is some interest in a quantitative analysis of the effect that the magnitudes of maximum amplitudes, dominant frequencies, duration of vibrations, as well as soil velocities and accelerations have on the intensity scale — let us say, in the case of a fixed density of seismic energy.

Chapter 5

FREQUENCY OF SEISMIC VIBRATIONS

We are interested in a study of the frequency of vibrations in the case of earthquakes of various intensities, on the one hand, to establish the focal properties and to understand the processes taking place within the foci. In this connection, probably the most important is the relationship between the frequencies and the seismic energy of the focus and the focal dimensions. With an increase in energy, there is an increase in the volume of the region in which the energy liberation is accompanied by a disruption of continuity, i.e., the volume of the focal region [7, 9, 82, 89, 110, 117-124]. In turn, an increase in the dimensions of the source must result in a lowering of the dominant frequencies of the seismic waves being emitted and this, as a rule, is actually what is observed.

On the other hand, a study of the vibration frequencies in the case of earthquakes over a wide range of energies is important in seismic regional studies. To evaluate the disruptive effect of an earthquake of given energy it is necessary to know the spectral composition of the vibrations of a powerful earthquake under specific geological and soil conditions which have a pronounced effect on the composition.

However, a study of the connection of all of these circumstances with the frequencies of the seismic vibrations on the basis only of rare powerful earthquakes would postpone the solution of this problem

indefinitely. It is for this reason that we are here, as well as in many other projects of the expedition, approaching the problem from the position that we can undertake a study of the basic quantitative relationships by examining a great number of weak earthquakes, then to establish means and methods of extrapolating these quantitative relations for the area of more powerful earthquakes.

The observation system employed for the case in which the station network is positioned directly in the epicentral zone makes it possible to examine a great number of earthquakes over a wide dynamic range and yields favorable conditions for the solution of this problem.

As is well known, soil vibrations in the case of earthquakes at some distance from the focus consist of a series of jolts or "arrivals" of individual waves (longitudinal, transverse, etc.). Each of these waves is generally presented on the seismogram as quasisinusoidal oscillations restricted in time. Taking into consideration the nonsteady nature of the latter, we can speak of the spectral composition of the entire succession of vibrations for the given earthquake (at the given point of observation, and for specific components of the mixing vector, etc.) or of the spectral composition of the vibrations for the given wave; other generalized concepts of the frequency composition of seismic vibrations are also possible.

The spectral composition of vibrations at the point of observation, apparently, is a function of the spectral composition of the vibrations in the focus, as well as a function of the conditions under which seismic waves are propagated over paths to the point (region) at which they are received and a function of the conditions prevailing in the reception region, including the interaction between

the seismic installation and the soil. Finally, the spectrum of the vibrations seen on the seismogram depends on the frequency properties of the very equipment, and what is most important, depends on the width of the frequency passband.

The standard wideband equipment (without special attachments for frequency analysis) makes it possible directly to determine only the dominant vibration frequencies — the magnitudes that are the inverses of the apparent dominant oscillation "periods" on the seismogram. The utilization of this primitive method of studying frequencies, despite all of its shortcomings and limitations, exhibits the advantages of great simplicity, and this makes it possible to use the entire mass of seismic observations carried out by standard wideband equipment. The results obtained in the utilization of this method of "dominant" frequencies by the expedition are described in Sections 1-3 of this chapter.

In order to undertake a more detailed study of vibration frequencies, we employed the frequency-selective seismic station (ChISS), developed by K.K. Zapol'skiy. The results obtained in the utilization of this method of "frequency-selective seismology" are described in Sections 4-6 of this chapter. Equipment of this type was tested here and was employed to evaluate (process) the still limited volume of observations. Under these conditions, the comparison of some data obtained by both methods simultaneously proved to be quite useful.

§1. POTENTIALS OF USING WIDEBAND EQUIPMENT TO STUDY THE FREQUENCIES OF SEISMIC VIBRATIONS

Earthquake recordings by wideband equipment may yield, at least in principle, a sufficiently complete picture of the vibration spectrum of some groups of waves or sections of recordings.

To obtain a frequency spectrum from wideband recordings, we can employ, first of all, one of the well-known methods of approximate harmonic analysis (for example, [125-126]). In its application to seismology this method is described in references [127-129]. Among the other calculation methods, we would note the method of "periodogram" analysis [85, 130], used in works [128-129]. The general shortcoming of these methods is the fact that they require a great deal of work.

Apparatus methods, presently concentrating on the utilization of electrical analysis devices, show the greatest promise [84, 131-135]. These methods call for a primary vibration record in reproducible form. The system of wideband vibration recordings on magnetic tape have proved quite successful. Systems of this type have found widespread application in seismic surveying and the regular utilization of these systems is quite desirable in seismology for the study of earthquakes, but this is still something for the near future.

Apparatus analysis methods may be used for the processing of seismograms recorded by conventional oscillography. However, such seismograms must be re-recorded in an electrically reproducible form such as, for example, by blacking out the film on one side of the vibration recording track in order to obtain the pattern of a type of "transverse" sound recording for subsequent reproduction by means of a photocell. In view of the laboriousness of this procedure, this method is justified in practice only to process selected and particularly important recordings such as, for example, the seismograms of individual powerful earthquakes.

In connection with all of the foregoing, for the mass utilization of conventional wideband seismograms in the solution of problems involving frequencies, we have limited outselves to the determina-

tion of only the dominant frequencies. Naturally, this restricted
the problems on which we touched to only those which can be solved
without a detailed knowledge of the entire vibration spectrum.

Correspondence Between Dominant Frequency and Position of Spectrum Maximum

The examination of a great quantity of seismograms indicates
that the recording of local earthquakes, particularly in the case
of small hypocentral distances, has the form of a group of quasi-
periodic damped oscillations the maximum of the spectral function of
which is approximately coincident with the value of the dominant
frequency apparent from the recording [84, 105, 133-136]. Character-
izing the spectrum by the value of one or two dominant frequencies,
we restrict ourselves, at the same time, to the one or two greatest
terms in the spectral decomposition.

In order to carry out a quantitative evaluation of the degree
of coincidence between the dominant frequency and the position of
the maximum of the spectral curve with respect to specific earth-
quake conditions in the Garm region, the following project was under-
taken. On the basis of recordings for one and the same earthquake
at one point of observation (Chusal) by two types of equipment — the
wideband (VEGIK) and the frequency-selective (ChISS) units — the
dominant frequencies (from the VEGIK seismograms) were compared
against the amplitude distribution for the frequencies (on the ChISS
recordings). This comparison was carried out for 400 local earth-
quakes (r < 50 km), and the measurements were made for the groups
of greatest amplitudes in straight-line longitudinal P and trans-
verse S waves.

The dominant frequencies in the VEGIK recordings were measured
with respect to four components with subsequent averaging. The method

employed to measure the dominant frequency is described below ($ 2). The dominant frequency and its amplitude was measured on the basis of ChISS recordings on each of four channels. A graph was constructed for each earthquake according to these data, and the frequency f was laid off along the axis of abscissas, and the amplitude A was plotted along the axis of ordinates. A logarithmic scale was selected for both of these quantities, since such a scale for the amplitudes makes it possible to compare the shape of the spectrum regardless of the amplitude level, and for frequencies the logarithmic scale corresponds to the constancy of the relative error in the measurement of the frequency (for a more detailed discussion of the construction of these graphs, see **page**).

This amplitude distribution on the basis of frequency intervals, a crude simulation of the shape of the spectrum, served as the basis of the comparison. The maximum of such a conditional spectrum was compared against the dominant frequency of the VEGIK recordings. For a quantitative evaluation of this coincidence, graphs of the type shown in Fig. 53 were constructed. Here, the dominant VEGIK frequencies were plotted along the axis of abscissas, and the frequencies that correspond to the maximum of the conditional ChISS spectrum were plotted along the axis of ordinates, and this for each individual earthquake. The relative probable deviation of the individual measurement determined according to the distribution curve for the number of deviations with respect to their magnitude, amounts to 15%. Generally, the dominant frequencies are somewhat lower in comparison with the position of the maximum. The magnitude of such a systematic deviation lies within limits of random errors and is, on the average, equal to 10%.
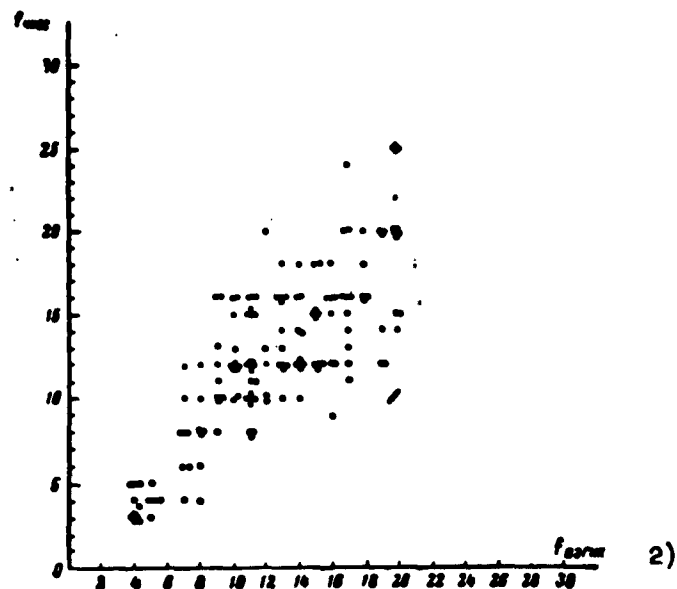
Fig. 53. Comparison of dominant VEGIK frequencies
with maximum of conditional ChISS spectrum for
individual earthquakes. 1) f_{ChISS}; 2) f_{VEGIK}.
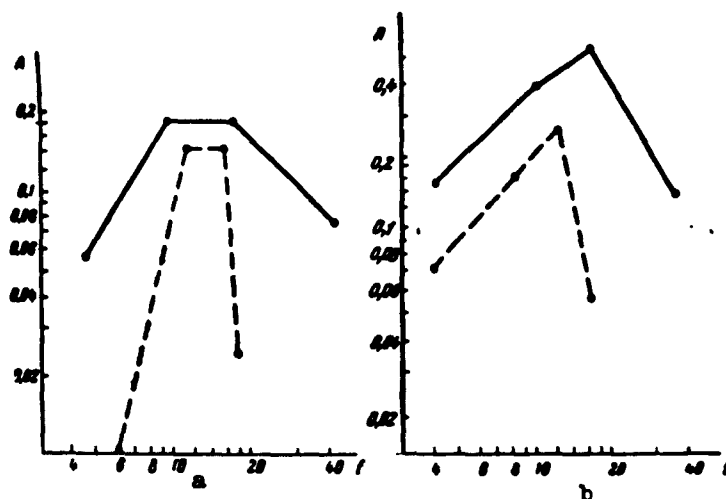
Fig. 54. Comparison of average ChISS spectrum (solid line)
with distribution of dominant VEGIK frequencies (dashed
line) for various groups of earthquakes in the interval of
hypocentral distances from 14 to 20 km. a) Energy class
K = 3; b) K = 4. For the construction of the average spec-
trum, 25 earthquakes of energy class 3 and 30 earthquakes
of energy class 4 were employed.

In view of the fact that the method employed to study the re-
lationship between the frequencies and the energy involved the pro-
cessing of a great number of earthquakes, it became of interest to

establish the degree of correspondence between the values of the dominant frequencies and the maximum of the conditional spectrum, averaged for groups of similar earthquakes. Approximately 20 to 30 earthquakes of one intensity classification (K) entered into each group; the hypocentral distances of these earthquakes did not exceed the given interval Δr. To construct the average spectrum of each group on the basis of the ChISS seismograms, we calculated the arithmetic mean of the logarithms of the amplitudes in the frequency interval equal to the passband of each of the four channels. This value was ascribed to the arithmetic mean frequency of the interval. As a result of the fact that the conditional spectra on individual earthquakes were constructed in logarithmic scale it was easy to carry out the graphical averaging of the shapes of individual earthquake spectra alone, so that the difference in amplitudes did not result in any advantage for earthquakes exhibiting great amplitudes. At the same time, a curve for the distribution of dominant frequencies according to VEGIK records was constructed simultaneously on the graph for the averaged conditional spectrum of each group of earthquakes. The frequency was plotted along the axis of abscissas and along the axis of ordinates we plotted the number of earthquakes whose dominant frequencies fall within the frequency interval equal to the width of the ChISS channel.

Figure 54 presents an example of such a graph for two groups of earthquakes. The solid line on these graphs shows the average ChISS spectrum, and the dashed line indicates the corresponding distribution curve for the number of earthquakes on the basis of the dominant VEGIK frequencies for the same group of earthquakes. These and similar graphs serve to convince us that the maximum of the ChISS spectrum is, in all cases, in sufficiently good agreement

with the distribution maximum according to the VEGIK (the probable deviation amounts to approximately 8%, whereas the systematic (regular) deviation amounts to about 10% toward reducing the VEGIK frequencies in comparison with the maximum obtained with the ChISS equipment).

Thus for the characteristics of the position of the maximum on the vibration spectrum in the case of earthquakes under the given conditions, as a rule, we can use the dominant frequencies that are apparent from the earthquake recordings of the VEGIK with sufficient accuracy for practical purposes.

§ 2. INITIAL MATERIAL AND METHODS FOR THE DETERMINATION OF DOMINANT FREQUENCIES

Selection of the Initial Material and the Principles Involved in the Evaluation (Processing) of this Material

To bring out the function $f(E)$ of the dominant frequencies $\underline{f}$ of seismic vibrations and seismic energy E in the focus, we made use of the recordings of local earthquakes by the Garm network of seismic stations in the expedition. This observation material has the following properties that are favorable for the solution of the problem before us; identity of seismic-recording equipment at the stations of the network; readability of recordings of earthquakes differing in intensity by as much as 11 orders of magnitude; the extensiveness of the material, etc. The latter circumstance is of significance because we can only bring out the quantitative relationships (of interest to us) against a background of other data, and this is possible only through the statistical evaluation of a great quantity of recordings.

Under the conditions prevailing in the Garm Region we note a pronounced variation in the nature of the recordings and dominant frequencies of the earthquakes whose foci lie in markedly diverse

geological structures: 1) in the sedimentary deposits of the mezo-
cenozoic strata of the Peter I Range and the Tadzhik Depression,
and 2) in the ancient paleozoic metamorphosed rocks and granites of
the Gissar Range and the crystalline base of the Peter I Range. It
is for this reason that the study of the frequency relationships of
interest to us was carried out separately for these two groups of
foci.

We took the recordings of local earthquakes whose hypocentral
distances amounted to, on the average, 20 to 40 km with extreme
limits of 15 and 50 km as the initial material. We would point out
that these differences correspond approximately to the dimensions
of the zone in which the destructive effect of powerful earthquakes
makes itself felt. The function $f(E)$, derived below, belongs to
this range.

The dominant frequencies f of the vibrations at the point of
observation are functions of, in addition to energy E, many factors
whose importance is difficult to account for in the shaping of the
spectrum. It is for this reason that in the initial stage it seemed
convenient to investigate the aggregate of earthquakes of various
intensities, said earthquakes representing the successive jolts of
one and the same powerful earthquake, observed from one and the same
station. The foci of such earthquakes frequently coincide with one
another in space with an accuracy of up to 2-3 km, and the times of
initiation are quite close. Under these conditions, extraneous
circumstances that are difficult to control are kept in approxi-
mate identity.

The series of observations that correspond to various focal
positions and points of observation will, naturally, show the varia-
tions that are functions of the structural features of the media at

the foci, at the points at which the stations are located, and along the paths of wave propagation. It is not so much on the shape of the f(E) curves as on their "levels," which are determined by absolute frequency values, that we can anticipate some special influence of these factors. The f(E) curves averaged over several series of observations in the given region do not exclude the influence of these factors, but only make it possible to obtain the relationship that is characteristic for certain "average" conditions for the given region.

If we compare the f(E) curves among each other for the various stages of the averaging process, we can estimate, in advance, the importance of certain particular factors in the shaping of the spectrum.

Frequency and Dynamic Ranges

The investigated seismograms were obtained by means of equipment having three levels of magnification: a) the three-component VEGIK installation with a magnification of 20,000 in the frequency range of 2 to 50 cps; b) the shunted VEGIK channel with a magnification of 1000 in the same frequency range; and c) the Kharin vibrograph with a magnification of 50 to 80 in the frequency range from 1 to 5 cps. The difference in the frequency characteristics of this equipment does not disturb the correct reproduction of the shifts over the entire frequency range of interest to us, since in the case of feebler earthquakes the recorded frequencies generally exceed 2 cps and fall into the plateau part of the VEGIK characteristic; however, for the evaluation of spectra of more powerful earthquakes whose frequencies, in the majority of cases, are below 4 to 5 cps, we most frequently employ the recordings produced by the Kharin vibrograph, which properly reproduces the shifts in this frequency

range.

Frequencies below one cycle per second cannot, for all intents and purposes, be determined by our equipment. Therefore there arises the natural question as to the feasibility of eliminating the lowest-frequency part of the spectrum, at least in the initial stages. Instruments that are capable of recording low frequencies ranging from 2 to 0.1 cps — Kirnos seismographs — have been installed only at two stations of the expedition, in Garm and in Dzhirgatal. A study of local-earthquake recordings produced by these instruments showed that vibrations with periods ranging from 2 to 6 sec are encountered on the recordings rather frequently. However, these vibrations are completely irregular and, at times, their apparent arrivals vary for various components, changing from earthquake to earthquake, even for earthquakes from one and the same focus. The magnitude of the period changes within wide limits for earthquakes of identical intensity and is a weak function of this factor. Great vibration periods are generally found in the case of shallow foci (h = 5-10 km) and are more frequently encountered in earthquakes having foci situated in the Peter I Range. The long wavelength (several tens of kilometers) that corresponds to such long-period vibrations, even in the case of relatively weak earthquakes (K = 7-10), and the absence of a clearly defined relationship between periods and earthquake intensity, allows us to assume that the formation of such waves is associated not so much with the features of the foci themselves as with the features of the structure of the medium in which the vibrations are propagated. It is possible that these vibrations of low frequency are waves resulting from interference and are caused by the stratification of the medium; we observe these waves at various stages of their shaping [137-138]. The sedimentary layers of the

Peter I Range, for example, may be the layers that cause the appearance of these interference waves.

In addition, these low frequencies may possibly be of less interest from the engineering standpoint, since in view of the great vibration periods the seismic disturbances produced by these waves are insignificant in the majority of cases.

In any event, at the present stage of the study of the relationship between the dominant frequencies and energy we have limited ourselves to frequencies above 0.8-1 cps. The study of lower vibration frequencies, requiring special observation means, must remain a matter for the future.

Measurement Method

To reduce the volume of measurements, we rejected the idea of studying frequencies over the entire seismogram and measured only the most characteristic sections: in the region of the first arrival and the group of maximum amplitudes. The first arrivals, to a greater extent than the vibrations of other sections of the recording, are determined by processes taking place within the focus, whereas the group of maximum amplitudes is of great interest from the standpoint of the seismic effect of the earthquake.

The following quantites were measured directly on each of the seismograms: f_{max}, the dominant frequency of one, or less frequently, of two vibrations with great amplitude; f_1, the frequency of the first arrival; and $\bar{f}$, the mean frequency for the group of vibrations which carry the basic energy (the duration of this group is generally 1 to 2 sec). The measurement of these frequencies was carried out individually for longitudinal and transverse waves on each of the components, with subsequent averaging of the frequency values obtained for the various components.

The utilization of the concepts "period" and "frequency" for vibrations of improper shape is somewhat conditional. In the measurement of the frequencies f_{max}, f_1, and $\bar{f}$ we adhere to the following system. The frequency $\bar{f}$ was defined as the number of maxima per unit time on the selected section of the seismogram having a duration τ. In this case, the quantity τ and the estimate of $\bar{f}$ remain the same as in the calculation of earthquake energy (see Chapter 4, § 2).

The frequency f_1 of the first arrival was conditionally defined as the reciprocal of twice the time from the instant of first arrival to the instant of passage through the equilibrium position. In the case of pronounced first arrivals with sufficient amplitude such measurements are single valued. If, however, the first arrival was very smooth, and the instant of arrival quite indeterminate, f_1 was defined as the reciprocal of the time between the first and third extremums.

The frequency f_{max} was determined, as a rule, on the basis of a group of two-three of the greatest vibrations in P and S waves. If a single vibration having an amplitude exceeding the rest by no less than half was clearly brought out, the frequency of only this vibration, the reciprocal of the period, was measured.

Sometimes we encounter recordings in which a higher frequency is superposed on the basic low frequency. Generally, this frequency is less not only with respect to the amplitude A of the shift but also with respect to the amplitude $A\omega$ of velocity. In such cases, this frequency was neglected. If, however, this superposed frequency had the same velocity amplitude as the basic frequency, it was regarded on a par with the basic frequency.

Accuracy of Frequency Measurements

The error in the measurement of the dominant frequency is composed of several errors: 1) the subjective error of the observer in approximating the section of the recording of a given sinusoid; 2) the measurement error caused by the quality of the photographic recording and the measuring instruments; and 3) the errors introduced by the nonuniformities of the recorder drive.

The first error is the most serious. As was shown in the estimates carried out, this error is equal to 15% in the case of measurements of T (see Chapter 4, § 2), and is equal to 10% in the case of measuring f_{max}.

In essence, the second and third errors are results of absolute errors in the measurement of the time interval. In the measurement of frequencies on the basis of a small number of vibrations, the relative errors of this type increase with an increase in frequency and total some 5% for frequencies of up to 5 cps; the errors total some 8% for frequencies ranging from 5 to 10 cps, and amount to 10-12% for frequencies ranging from 10 to 12 cps. These results have been obtained in calculating the mean error in the measurement of the frequencies of various recording sections of a vibration jolt, said recordings produced by an MGPA oscillator exhibiting a great moment of inertia. It was assumed that on these recordings the frequency changed linearly with respect to time within the limits of the selected sections in 15 to 20 vibrations.

Subsequently, depending on the evaluation of frequency-measurement accuracy that was carried out, the following values (in cps) were rounded off to the nearest whole number: 0.8, 1.0, 1.2, 1.5, 2.0, 2.5, 3, 4, 5, 6, 8, 10, 14, and 20.

§ 3. DOMINANT FREQUENCIES AS A FUNCTION OF EARTHQUAKE ENERGY

The details discussed in this section and the examples of the results obtained in the determination of the function $f(E)$ between the dominant frequencies f of the vibrations and the seismic energy E of the earthquake pertain, primarily, to foci lying in the sedimentary layers of the Peter I Range.

The Function $f(E)$ According to a Series of Weak and Strong Repeated Jolts

In accordance with the procedure described above, we evaluated the repeated jolts of seven powerful earthquakes. The most representative was the swarm of repeated jolts produced by the earthquake of the 12th intensity classification that occurred on 13 November 1955 north-east of Stantsia Ishtion. In this swarm, there is a complete range of jolts with intensities from 4 to 11 inclusive, i.e., the dynamic range was composed of eight orders of energy. In the remaining cases, the dynamic range was composed of 5 to 7 orders of energy. The distribution of the number of jolts with respect to the energy in each swarm is shown in Table 7.

TABLE 7

Distribution of Number of Repeated Jolts with Respect to Energy

1) Дата	2) Время 3) ч. мин.	4) Классы энергии землетрясений									
		13	12	11	10	9	8	7	6	5	4
13.XI 55 г.	7 27	—	—	1	3	4	9	13	27	19	13
11.IV 56 г.	1 45	—	1	—	—	3	3	14	40	42	—
16.VI 56 г.	1 20	—	—	—	—	1	2	4	13	29	—
22.IX 56 г.	14 02	—	—	—	—	—	—	1	10	14	11
25.X 56 г.	3 50	—	—	—	2	—	1	4	4	—	—
5.XI 56 г.	20 01	—	—	—	1	—	—	—	2	5	21
13.I 57 г.	11 38	—	—	—	1	—	1	3	13	24	50

1) Date; 2) time; 3) hours, minutes; 4) earthquake energy classification.
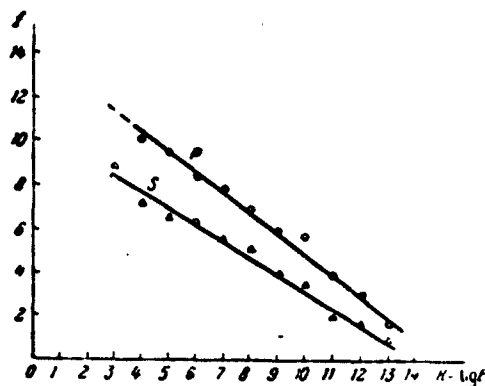
Fig. 55. Summary curves of dominant frequencies f as functions of energy E joules according to observations of a series of repeated jolts for longitudinal P and transverse S waves.

The summary curves of the relationship between the dominant frequencies and energy (averaged over all points of observation and seven series of repeated jolts) is presented in Fig. 55 in a logarithmic-linear system of coordinates log E and $\underline{f}$. Here, the earthquake energy classifications (K = log E joules) have been plotted along the axis of abscissas, and the frequency $\underline{f}$ cps is plotted along the axis of ordinates.

Appropriate markings (circles for the longitudinal P waves and triangles for the transverse S waves) have been used to plot the frequency values, averaged for all of the processed earthquakes of a given energy classification. In the range of K = 3-13, i.e., all eleven observed classifications, the points line up well on straight lines

$$ f = f_\bullet - b' \lg E, \tag{27} $$

where for the longitudinal waves $f'_0 = 14.3$ and $b' = 0.94$, and for the transverse waves $f'_0 = 10.6$ and $b' = 0.76$.

We see that within this energy range there is observed a stable reduction in dominant frequencies with an increase in energy. The frequencies of the P waves on the average are greater by 30 to 40% and diminish more rapidly with energy than the frequencies of the S waves. We can judge the extent to which the observed points line up well on straight lines by the magnitudes of standard deviations: for the P waves these deviations amount to 0.25 cps, while for S waves they amount to 0.3 cps.
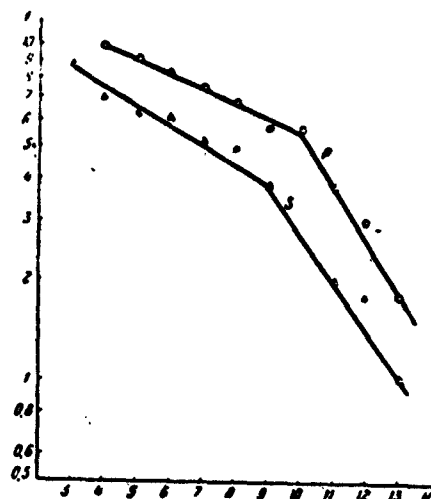
Fig. 56. Summary curves of the function in Fig. 55 in a double logarithmic scale.

1) Интервал энергии K	2) Тип волны	f_0	b
4÷10	P	15	0,04
3÷9	S	13	0,06
10÷13	P	280	0,17
9÷13	S	66	0,14

1) Energy interval, K; 2) wave type.

On the basis of the curves shown in Fig. 55, we can expect dominant frequencies of 1 cps and lower for the stronger earthquakes. However, the empirical relationship f(E) obtained in the form of (27) cannot, in practice, be extrapolated toward very much greater energies than those observed. In actual fact, from (27) for K = 14 we would obtain f = 0, whereas for K > 14 we would obtain f < 0, which lacks any physical significance. It is natural to anticipate that in the case of more powerful earthquakes, the linear function (27) is disrupted.

To avoid similar misunderstandings, we can attempt to approximate the observed sequence of points f(E) by a straight line, as before; however, under conditions of a graphical presentation of these points in a double logarithmic system of coordinates K = log E, log f (Fig. 56). If this were done, it would turn out that the observed points are well approximated by straight lines in accordance with the following equation:

$$\lg f = \lg f_0 - b \lg E. \tag{28}$$

The various values of the parameters f_0 and b, in Formula (28), in the region of weak and relatively more powerful earthquakes,

indicate that at low K the increase in frequency is explicitly less pronounced with a drop in energy. This can be explained if we take into consideration the effect of selective absorption of high frequencies.

The f(E) Function for Weak Earthquakes

It has been noted previously that for weak, higher-frequency earthquakes, the dominant frequencies observed depend to a considerable degree upon the hypocentral distances, and these frequencies are
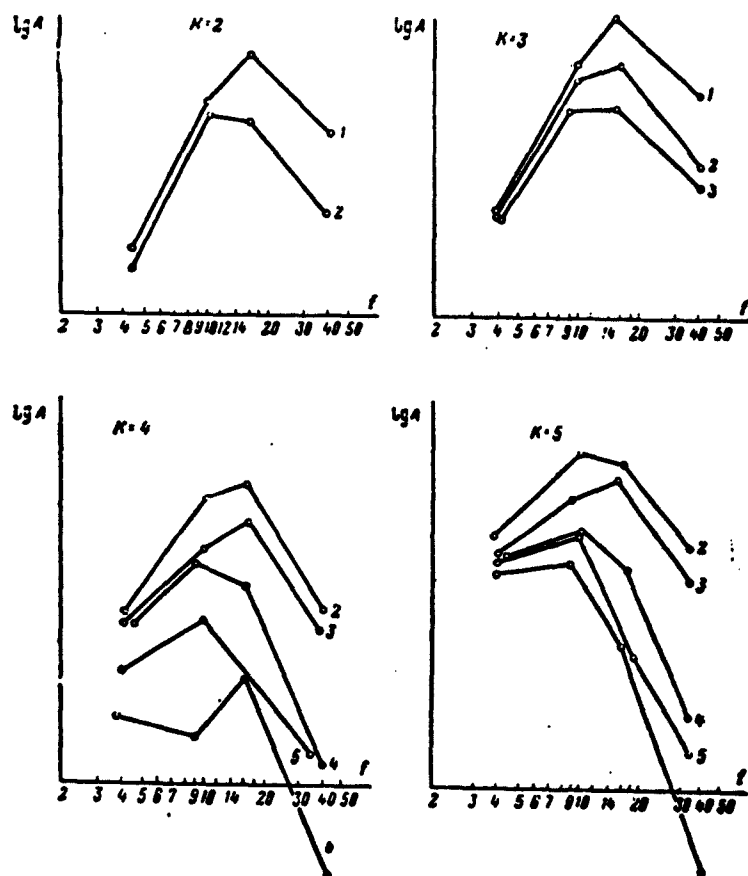
Fig. 57. Average spectra for groups of earthquakes of different K classes of energy $E = 10^K$, and for different hypocentral distances. 1) $r = 4-7$ km; 2) $r = 8-12$ km; 3) $r = 13-19$ km; 4) $r = 20-30$ km; 5) $r = 31-46$ km; 6) $r = 47-70$ km.

higher near the focus than those observed for distances of the order of 20-40 km. Owing to the selective absorption of high frequencies

with increasing distance from the focus, the spectrum maximum is shifted toward the lower frequencies. The low dominant frequencies at 1-4 cps, which are characteristic of the more severe earthquakes (K = = 9-13), are less liable to absorption, and thus in the high-energy region, the function $f(E)$ is subject to very little distortion over the first tens of kilometers.

The magnitude of the variation in the dominant frequency of vibrations (the shift in the spectrum maximum) depends on the degree of absorption, characterized by the value of the absorption decrement ε, and upon the shape of the spectrum. If near the focus the shifted spectrum drops off sharply toward the low frequencies, the dominant-frequency shift with distance due to absorption will be slight, while where the drop is gradual, it will be quite noticeable. A rough calculation of the change in spectrum shape with distance is given in Chapter 4, §3. To perform these calculations, we must know the shape of the spectrum at the observation point, and the magnitude of the absorption decrement. Average spectra obtained from recordings of ChISS, for groups of earthquakes belonging to the same energy class K, but different ranges of seismic-center distances $\underline{r}$, are used to judge the spectrum shape.

Figure 57 shows these spectra for each of the following energy classes: K = 2; K = 3; K = 4; and K = 5. The numbers given for each spectrum indicate the range of hypocentral distances $\underline{r}$, which here vary from 4 to 70 km. In accordance with Chapter 4, §3, we take $\varepsilon =$ = 0.01 for the value of the absorption decrement. A rough estimate, made directly from the material of the charts (Fig. 57), yields a magnitude of the same order ($\varepsilon = 0.011 \pm 0.003$).

An evaluation of the change in shape for the average spectra indicates that the hypocentral distances of 20-30 km are quite adequate

to produce the weak-earthquake dominant frequencies having the values obtained from Formula (28).

Such estimates, naturally, are quite arbitrary. For a more trustworthy estimate of the frequencies that might be expected near the focus, it would be necessary to observe the variation with distance r in the shape of spectra for individual earthquakes. To solve this problem, it is necessary to have frequency-selective apparatus at several observation points; this was not done by the expedition. Thus, we shall assume that absorption is a possible, although perhaps inadequate, explanation for the flatter linear relationship between log f and log E in the weak-earthquake region.

Accepting the explanation given, we will thus assume that for weak earthquakes (K = 7-3, or below), observed for hypocentral distances r of from 20 to 50 km, the vibration frequencies continue to rise with decreasing energy in accordance with a linear law. In other words, extrapolating Function (28), which was constructed from frequencies observed at distances r = 20-50 km for more intense earthquakes, we obtain hypothetical values for the vibration frequencies at the focus for weak (K < 7) earthquakes.

So far, we have discussed the function f(E), averaged over various focus positions and observation points. The effect of these and certain other factors may be evaluated by examining similar graphs for various stages of averaging.

The Scatter of Dominant Vibration Frequencies for Earthquakes

We examine such scattering for conditions under which the locations of the focus and observation points are fixed. Figure 58 gives graphs of the mean vibration frequencies for successive shocks of the Ishtion earthquake of 13 November 1955 for the P and S waves from observations at three stations: a) Ishtion (r = 25 km), b) Yaldymych
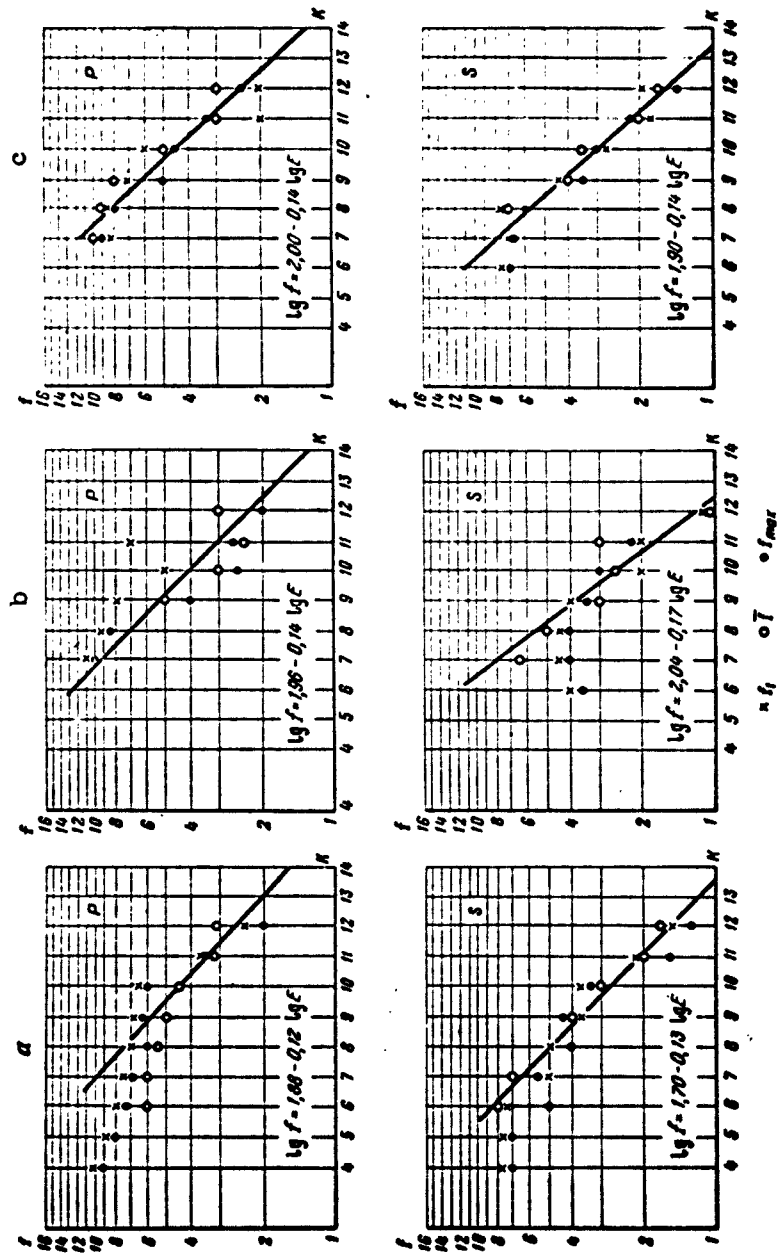
Fig. 58. Dominant frequencies as a function of energy for repeated shocks of Ishtion earthquake of 13 November 1955, obtained from observations at a single station. a) Ishtion; b) Yaldymych; c) Garm.

(r = 50 km), and c) Garm (r = 60 km). On each of the graphs, the straight line shows the appropriate function f(E) in the form (28) for the strong-earthquake region (K = 7-13). It is clear from the graphs that, as a rule, the dominant frequencies f_1 of the first arrivals (crosses) are somewhat higher than the frequencies $\bar{f}$ — the mean frequencies for the vibration groups carrying the maximum energy (open circles), while the frequencies f_{max} for the vibrations with the greatest amplitudes (solid circles) are somewhat lower than those for $\bar{f}$. The general shape of the function f(E) is nearly the same, however, for all three categories of frequencies.
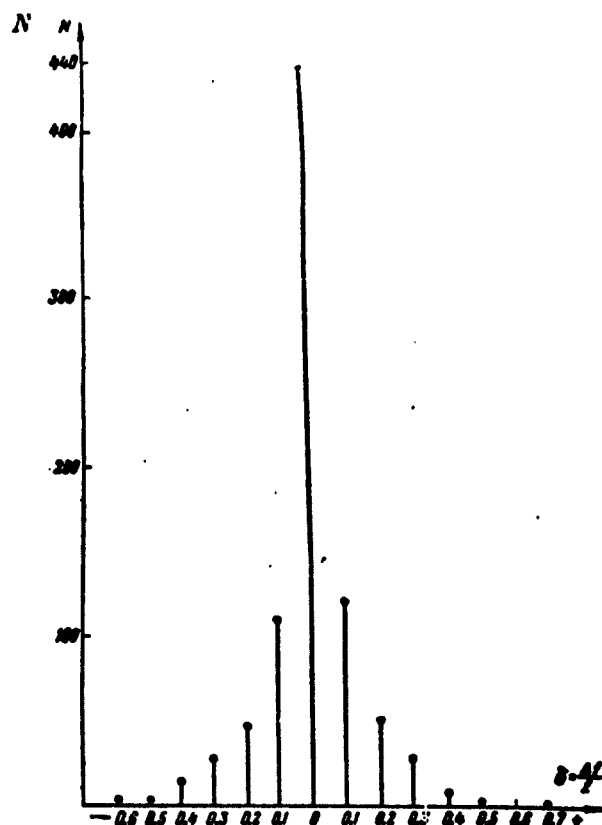
Fig. 59. Total distribution of relative deviations $\delta = \Delta f/f$ of vibration frequency f from mean value for equal energy, with the same focus and observation point. N — Number of observations.

On the graphs considered, it was the mean values of the vibration

frequencies for many earthquakes that were considered. We will now look for the spread around the center values of the dominant frequencies for individual earthquakes. Figure 59 shows the total distribution of relative deviations from the center frequency for constant energy, with the locations of focus and observation point fixed. This graph was obtained by summing the partial distributions for all cases for which the number of averaged earthquakes of the same energy, written at the same station for precisely the same focus was greater than ten. The spread of frequencies, as we see, is not very large. No less than half of the separate measurements differ from the arithmetic average of the given series by no more than 10%. The distributions $\Delta f/f$ constructed separately for transverse and longitudinal waves are very nearly coincident. The distributions $\Delta f/f$ for various foci are also identical. The mean relative deviation of $\Delta f/f$ also does not exceed 10% for these cases.

The considerable individual deviations far exceed the limits of experimental error. This may be caused by changing conditions at the focus, such as a difference in the velocities of disturbances, etc. The fact that the sign of the first arrival of P waves for successive shocks does not remain the same can serve as indirect evidence for the fact that the dynamic parameters of the successive shocks are not identical. In addition, considerable variations in the amplitude ratios for arrivals of longitudinal and transverse waves are observed.

An analysis of the distribution curve makes it possible to draw certain conclusions with respect to the velocity of a disturbance at the focus. If the disturbance velocity is close to the S-wave propagation velocity V_S, there should be a Doppler effect [139-140]. This would lead to a considerably greater spread in frequencies with respect to the center frequency, and to the appearance of high frequencies for

earthquakes of any energies. In this case, the distribution curve should be asymmetric. The small amount of frequency spread testifies to the fact that the velocity of a disturbance is evidently considerably less than $\vec{V}_s$.

The Effect of Conditions at Station Sites

Comparing the graphs of $f(E)$ for the aftershocks of the same earthquake, for example, the Ishtion earthquake of 13 November 1955 (Fig. 58), plotted from the data of various stations, we are able to judge to what degree this function is stable for various observation points. Table 9 gives numerical values for the parameters f_0 and $\underline{b}$ of formula (28) for various stations according to the series of repeated shocks from this earthquake.

TABLE 9

Values of Parameters f_0 and $\underline{b}$ for Aftershocks of Ishtion Earthquake for Various Observation Points

1 Станция	$f_{o,p}$	$f_{o,s}$	b_p	b_s	$\bar{\eta}_p$	$\bar{\eta}_s$
2 Гарм	100	·80	0,14	0,14	0,10	0,06
3 Ядымыч . . .	90	110	0,13	0,16	0,17	0,10
4 Янголык . . .	90	100	0,14	0,18	0,21	0,09
5 Нымич . .	35	70	0,09	0,15	0,06	0,10
6 Чусал	45	85	0,00	0,13	0,13	0,11
7 Иштиоя . . .	75	50	0,12	0,13	0,05	0,06

1) Station; 2) Garm; 3) Yaldymych; 4) Yangolyk; 5) Nimich; 6) Chusal; 7) Ishtion.

The two last columns of this table give values of $\bar{\eta}$ for the average departure of the logarithms of the observed frequencies from the values of the logarithms of frequencies corresponding to a function of the form (28), which is linear in a double-logarithmic coordinate system. For the station closest to the focus (Ishtion, in this case), $\bar{\eta}$ is at a minimum. For this station, the parameters f_0 and $\underline{b}$ are normally close to the average values for all the observation points. At greater

distances, the f(E) dependence becomes less clearly defined, the spread of points around the line becomes greater, and the parameters f_0 and $\underline{b}$ depart more sharply from their mean values over all stations. In order to discover systematic spectrum distortions introduced by observation-site features, the mean frequencies for a specific group of earthquakes are compared for the various stations. Five groups of earthquakes were selected: 1) all of the earthquakes falling into the seventh energy class occurring among the repeated shocks of the earthquake of 16 June 1956; 2) the same group for the earthquake of 13 November 1955; 3) the same groups, but for class eight repeated shocks; 4) the same, for class nine shocks; 5) all 27 class nine earthquakes occurring in 1955-1956 in the Peter I range.
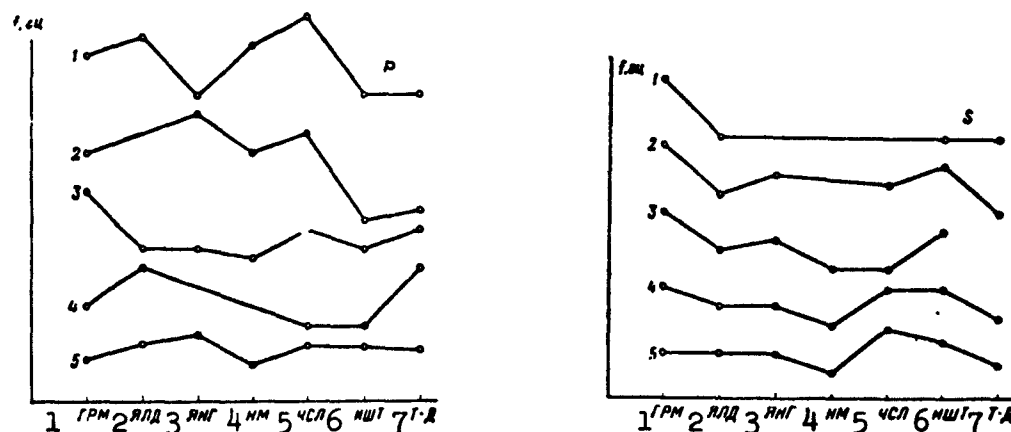
Fig. 60. Effect of observation site on dominant vibration frequency for arrivals of longitudinal (P) and transverse (S) waves. 1) Garm; 2) Yaldymych; 3) Yangolyk; 4) Nimich; 5) Chusal; 6) Ishtion; 7) Tovil'-Dora.

Figure 60 shows the results of a comparison for the f_1 vibration frequencies in the arrivals of P and S waves. Here, the stations are arranged arbitrarily along the axis of abscissas, while the axis of ordinates is a linear frequency scale with the origin shifted somewhat for each of the five earthquake groups mentioned. No sharp anomalies — peaks or dips connected with the observation sites and common to all

five graphs — are to be seen. There is a certain noticeable increase in S-wave frequency at the Garm station, and a general drop in frequency at the southern stations: Tovil'-Dora and Ishtion. This may be explained by the fact that these stations are founded upon sedimentary material, many kilometers thick, which has a greater coefficient of absorption than the rocks of the crystalline and metamorphic "basement," upon which the remaining, northern stations are established.

The absence of large spectral anomalies connected with observation sites is natural, since all of the seismic stations under consideration are located on lithified Paleozoic (northern stations) or densely cemented Mesozoic or Cenozoic bedrock (southern stations).

Effect of Loose Soil

It is known that a layer of loose deposits at an observation point can cause a change in the frequency composition of seismic vibrations. In seismology, however, the existence of such a layer is taken into account, as a rule, only in evaluating the amplitude variation of such vibrations [87, 141]. It is of interest to use experimental data to obtain even an approximate estimate of the effect of ground conditions upon the dominant vibration frequencies, and, incidentally, upon their amplitude and duration. Such an investigation was carried out in the region of the Chusal seismic station.
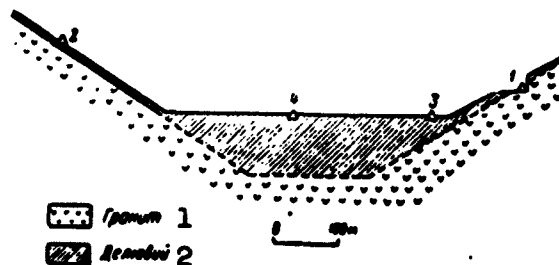
Fig. 61. Diagram showing seismograph placement for recording earthquakes under various ground conditions at Chusal station. 1) Granite; 2) talus.

Here identical VEGIK seismographs were installed at various points:
1) on bedrock; 2) on a mountain slope where the layer of detritus
(talus) amounted to 1-2 m; 3) in the eastern portion of the gully,
with a depth of 20 m; 4) in the center of the gully, where the thick-
ness of the layer of detritus reaches 60-100 m. A diagram showing the
placement of the instruments is given in Fig. 61. The distances between
the individual observation points did not exceed 200 m. This made it
possible to assume that for any given earthquake, the hypocentral dis-
tances to each of the observation points were practically identical,
so that differences in the dynamic features of the seismic vibrations
at these points could be associated only with a difference in ground
conditions.

The vibrations arriving at the various points were recorded on a
single strip. The time sweep was speeded up by a factor of 2.5-3 over
the normal rate, and reached 10-12 mm/sec, which made it possible to
obtain good resolution on the records, and quite high precision in fre-
quency determination.

Figure 62 shows two examples of earthquake records for different
thicknesses of the detritus layer. The recordings are numbered in ac-
cordance with the numbering of the observation points (Fig. 61), so
that as the number goes up, the layer thickness increases. It is clear
from the recordings that for the same earthquake, an increase in layer
thickness leads to a well-defined increase in vibration amplitude and
duration, and to a decrease, on the average, in the vibration fre-
quencies.

The maximum displacement amplitudes rose, on the average, by fac-
tors of 1.9, 3.1, and 3.6 for points 2, 3, and 4 with respect to point 1.

For a quantitative evaluation of the increase in vibration length
Δt, we define the length as the time over which vibrations are observed

- **217** -

at an amplitude of no less than $A_{max}/2.7$. Then at points 2, 3, and 4, the length turns out to be greater than at point 1 by factors of 1.2, 2.4, and 2.7, respectively. The length increase at points 3 and 4 is associated with the appearance of a set of several vibrations of roughly constant period in place of the one-two vibrations at point 1.

The dominant vibration frequencies at the various points were compared for three vibration groups: 1) for the short-wave group, beginning with the arrival of the S waves, and lasting about 0.1-0.5 sec; 2) for the longer-wave group following the first group, and 3) for the maximum displacement, regardless of the time of arrival. A comparison of the dominant frequencies for each of these sections at all of the four observation points showed the following.
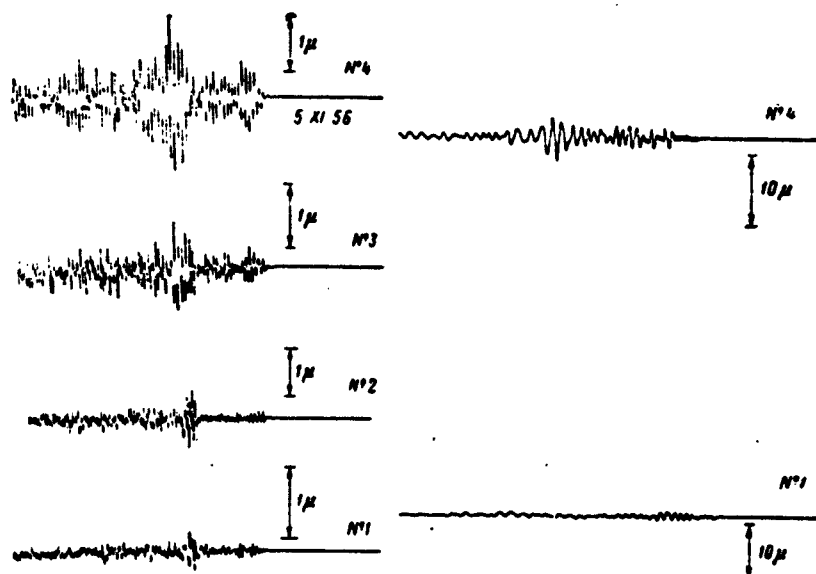
Fig. 62. Examples of earthquake records for various detritus depths.

1. The vibration frequencies in the S-wave arrival region at all four points were nearly the same. The values of the frequencies at points 2, 3, and 4, however, fluctuated in both directions from the value at point 1 by roughly 20-30%.

2. The frequencies of the second group, normally carrying the main portion of energy for the disturbance were, on the average, lower than the frequencies of the first arrivals by 20-40%. But while this decrease was stable at the first point (on bedrock), at the other points (on detritus), it was observed against a background of great scatter (60-80%).

3. As a rule, the frequency in a region of maximum displacement for bedrock coincides with the frequency of the first-arrival group, since at such a point the vibration maximum normally occurs precisely with the first-arrival group. At points 3 and 4, where the thickness of the layer of detritus reaches several tens of meters, the displacement maximum in the majority of records moves to the region of subsequent vibrations. With this change, the frequency in this region at points 3 and 4 will be less in comparison with that at point 1, for example, it will have half the value.

Thus, ground conditions have comparatively little effect upon the dominant frequencies of the main group of vibrations near the arrival of the S waves. Greater frequency variations are found on the later portions of the record. A certain systematic drop in frequencies may be observed on these sections, appearing against a background of extremely large scatter. Basically, the effect of the layer of detritus reduces to a sharp tightening up of the record, and the appearance of a set of vibrations in normal form at relatively low frequency. This corresponds, as is known, to a compression of the frequency spectrum and to the appearance of a resonance peak on the spectrum curve in the dominant-frequency region.

Function f(E) for Earthquakes with Various Focal Locations within Sedimentary Bed

So far, we have examined graphs of f(E) for the dominant vibra-
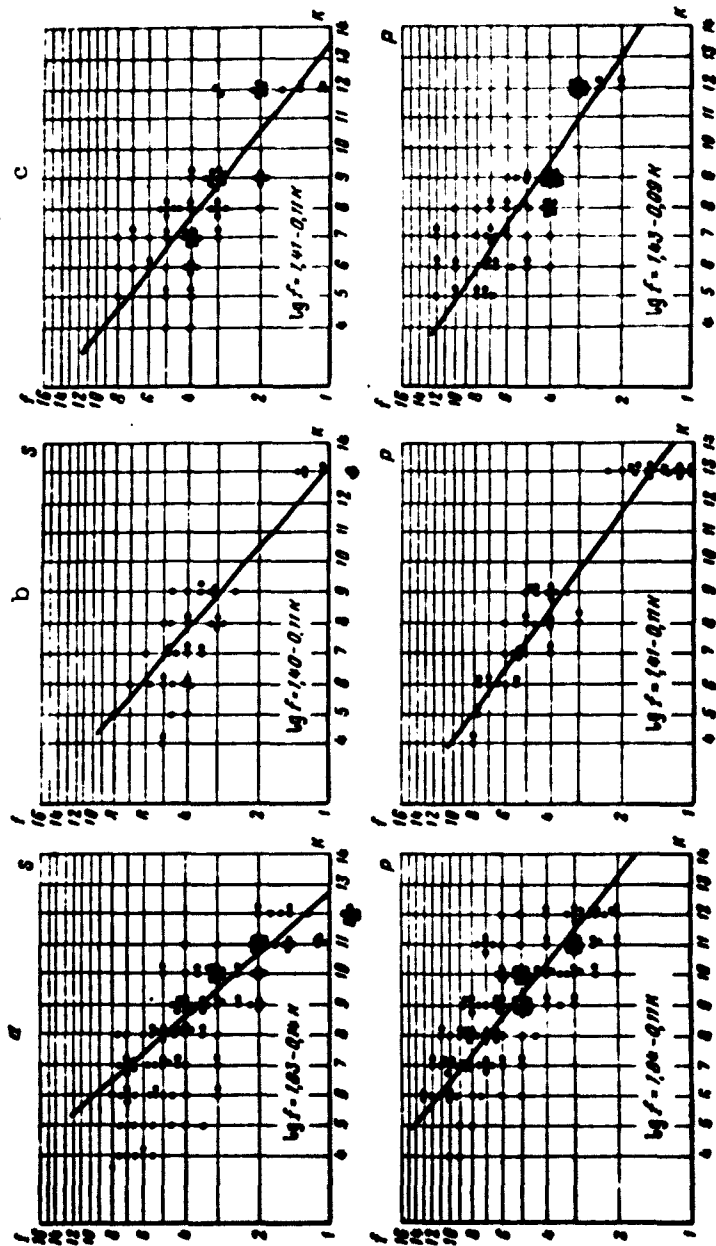
Fig. 63. The function f(E). a) From earthquake of 13 November 1955 and its aftershocks; b) from earthquake of 11 April 1956 and its aftershocks; c) from earthquake of 16 June 1956.
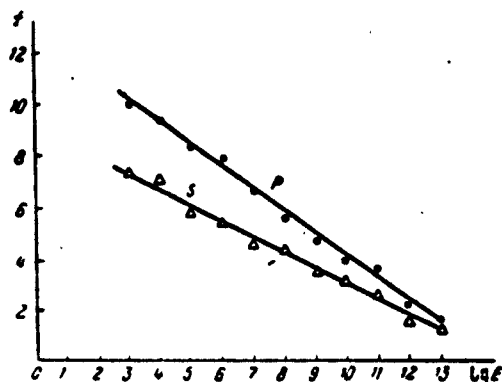
Fig. 64. Graph of the function
f(E), plotted from observations
of dominant earthquake frequen-
cies, disregarding location of
the focus within sedimentary
bed of Peter I Range.

tion frequencies $\underline{f}$ as a function of the seismic energy E of the focus,
plotted from observations of repeated shocks from precisely the same
focus. We now turn to graphs of f(E) based on data for the dominant
frequencies of repeated shocks from other foci (Fig. 63). Comparing
these graphs, we see that when the focal position changes (within the
strata of the Peter I Range), the dominant frequencies will differ by
20-30%, on the average, and the position of the focus will affect the
shape of the $\underline{f}$ vs. E function in about the same way as the observation-
point position. This last conclusion is extremely important, and makes
it possible to plot the function f(E) from observations of the dominant
frequencies for various earthquakes in the Peter I Range without refer-
ence to the positions of their foci.

In order to do this, 20 earthquakes were selected from each energy
class from K = 3 to K = 10, and all earthquakes of higher classes oc-
curring in the Peter I Range in the 1955-1956 period were taken: eight
earthquakes of K = 11, six of K = 12, and three of K = 13. The dom-
inant frequencies were measured on all records of these earthquakes,
using the method described above (§2).

As a result, for each energy class we obtained the value of the dominant frequency, averaged for various recording sections, all observation points, and different foci. This averaging was carried out separately for the longitudinal and transverse waves. Figure 64 shows the measurement results over the entire energy range from K = 3 to K = 13 (the graphs are plotted in a logarithmic-linear coordinate system). The results are described quite well by the following functions for the longitudinal (P) and transverse (S) waves:

$$f_p = 13 - 0.89 \, K.$$

$$f_s = 9 - 0.69 \, K.$$

(29)

If we attempt to approximate these results by a step function, which corresponds to drawing the averaging line in a double logarithmic coordinate system, we will find that for weak earthquakes of K = 3-10, the frequency will drop off in inverse proportion to the fifteenth root of the energy, while for stronger earthquakes of K = 9-13, it will decrease in inverse proportion to the eighth root of the energy.

Comparing these results with the similar results obtained from several series of repeated shocks, we see that, on the whole, they agree satisfactorily.

Comparison with Data on Vibration Frequencies Occurring during Destructive Earthquakes

It is desirable to connect and fit together our data on the vibration frequencies for weak (and moderate) earthquakes with the results of similar investigations for strong destructive earthquakes, in order to investigate the possibility of extrapolating the functions f(E), obtained for weak earthquakes, to strong earthquakes.

As we ourselves do not have observational material on strong earthquakes available, we turn to the works of other authors. Here we are faced with well-known difficulties. Data on vibration frequencies

available in the literature for strong earthquakes must be selected very critically, in view of the differences among the apparatus employed, the frequent lack of the information required for a sufficiently definite evaluation of earthquake energy, and in view of the normally large epicentral distances at which the observations were carried out. In nearly all the studies, the earthquakes are not classified in terms of the energy E, but by the magnitude M, where various modified M scales are used. In analyzing the studies of other authors, we have converted their results to our E energy scale. To do this, we made use of the results of a comparison of the M and E scales (Chapter 4, §5), and a correlation formula (20), connecting the maximum amplitudes with the hypocentral distance and the energy E of the earthquake.

The article [132] gives results of a spectral treatment by Tomoda's method [142] of more than 100 earthquake records from Japan. The results of this work are extremely well-grounded and reliable. The following relationship between M and T was obtained for groups of earthquakes having foci that were not too deep

$$\lg T = -1.35 + 0.3 M. \tag{30'}$$

Assuming in accordance with Formula (22) that M = 0.55 K − 2.2, we obtain

$$f = \frac{100}{\sqrt{E}}.$$

Figure 65 shows the dominant frequencies $\underline{f}$ plotted as a function of the earthquake energy E in joules, found in accordance with the data of this article.

The relationship between the period T of the maximum amplitudes and the earthquake intensity M has also been studied in [63]. The authors arrived at the following formula:

$$\lg T = -1.5 + 0.22 M. \tag{30''}$$

Converting from M to E, and substituting $1/f$ for T, we obtain

$$f \quad \frac{10^{\cdot}}{\sqrt{E}}.$$

In [143], a relationship was obtained between the period T of longitudinal (P) waves and the earthquake magnitude M from observations of several destructive (K = 14-17) Japanese earthquakes. This study is
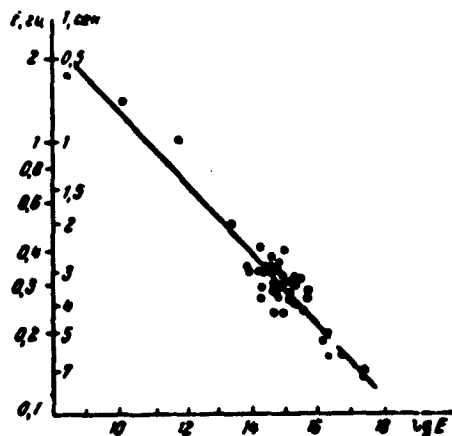
Fig. 65. Dominant vibration frequencies from data of Aki [130].
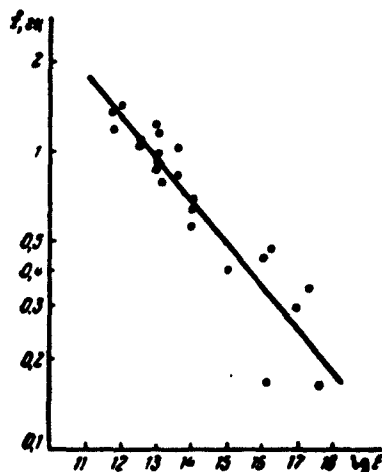
Fig. 66. Dominant vibration frequencies for strong earth-quakes from data of several authors.

supplemented by [119], which gives the results of dominant-frequency

measurements for P and S waves for four weaker (K = 11-14) earthquakes in the same region. The frequency data·given in these two articles correspond approximately to the following function

$$f = \frac{\text{const}}{\sqrt[4]{E \partial x}}.$$

Separate unrelated data on the dominant frequencies for strong earthquakes, obtained from [14, 97, 144-149], and based to a large extent upon direct measurements, are shown graphically on Fig. 66. Despite the considerable spread of the individual points, which is quite natural in such cases, the increase in period with rising energy is evident. The equation of the line in double logarithmic coordinates, which is the best means for averaging these data, takes the form

$$\lg f = 1.8 - 0.14 \lg E \, \partial x. \qquad\qquad (30''')$$

or

$$f = \frac{60}{\sqrt[7]{E}}.$$

Finally, let us summarize (in the form of the graph of Fig. 67) the relationships between the dominant frequencies f and the earthquake energy E; the relationships are based upon our data for weak earthquakes of K = 4-13, and the relationships for perceptible and destructive earthquakes of K = 12-17, on the publications mentioned above. On the overlapping section for K = 11-13, the graph for the data of the expedition basically agrees with data obtained in other studies, but the mean slopes of the average curve differ to the right and to the left of this section. In the strong-earthquake region, the average curve is steeper, and the frequencies vary more sharply with energy, $f \sim E^{-1/5}$, than in the weak-earthquake region where $f \sim E^{-1/8}$. The summary graph (Fig. 67) is approximated over the entire energy range by the function
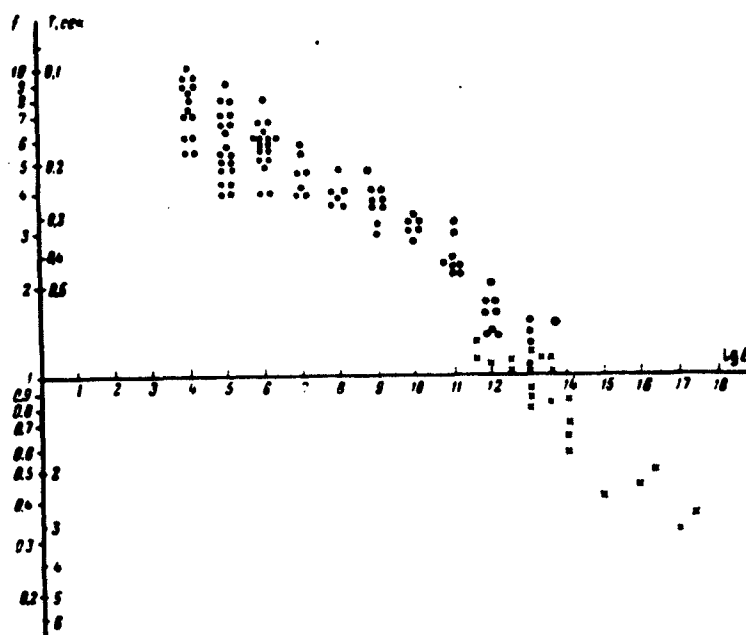
Fig. 67. Summary graph of f(E) from materials of
TKSE (dots) and data published in the literature
(crosses).

$$ \lg f = 0.79 + 0.047 \lg E - 0.0078 (\lg E)^2 . \qquad (31) $$

This is an empirical formula, and may be utilized for a rough,
approximate estimate of dominant vibration frequencies $\underline{f}$ for strong
earthquakes, using observations of weak-earthquake frequencies, i.e.,
it tends to confirm that the desired extrapolation is possible. We
should also note the desirability of further refinements and more de-
tailed work in this region. To do this, it is first of all necessary to
continue the experimental investigation of the dominant frequencies of
seismic vibrations over a broad range of earthquake energies, and for
various focal conditions, and to investigate the wave-propagation
paths in the detection region.

§4. APPARATUS FOR FREQUENCY-SELECTIVE SEISMOMETRY

The principle of parallel analysis of an oscillation through si-
multaneous recording of the oscillation by a set of frequency-selective
channels operating in various sections of the range under investigation,

a principle well known in electroacoustics, forms the basis for the method of frequency-selective seismometry. For this purpose, the ChISS-1954 fixed frequency-selective seismic station was developed in 1954; the station was designed to study the frequency composition of seismic waves occurring during earthquakes, and for absolute measurements of the basic ground-vibration parameters: displacements, velocities, and accelerations.

The apparatus of the ChISS station represents a further development of the earlier high-sensitivity universal type VUSS seismic station, which was designed to measure the frequency spectra of short-period microseisms and the physical characteristics of the seismic waves observed in seismic prospecting [150, 272]. The frequency range of the ChISS station, and its magnification in fixed recording were chosen on the basis of experience gained by the Garm expedition of 1952-1953 in recording near-by earthquakes with a special spectral device.*

Operating Principle of Frequency-Selective Station

The following considerations were involved in the choice of the simultaneous frequency-analysis principle to investigate near-by earthquakes. When analyzing records of such earthquakes, we are involved, as a rule, not with a single disturbance, but with a series of separate seismic waves, arriving at irregular and sometimes very short time intervals. A study of seismic-wave frequency composition presupposes the possibility of first isolating these waves from the general complex disturbance. Experience gained in seismic prospecting shows that one of the most effective means for isolating waves is the deliberate introduction of certain controlled frequency distortions; various types of distortion may be required in this case to extract the different waves. The simultaneous frequency-analysis method makes it possible to

do this directly, solving two problems by a single method: the isolation of the seismic waves, and the determination of their frequency composition.

We note that the application of the principle of step-by-step analysis of a broad band recording, well-known from electroacoustics, for these same two purposes would require the additional procedure of rerecording the primary seismogram to make copies.

The choice of bandwidth in the set of selective channels for the ChISS is intimately associated both with the amount of detail desired from the analysis, and with the resolving power of the apparatus with respect to the isolation of separate waves. It would evidently be necessary to decrease the bandwidth of a tuned filter in order to increase analysis detail; this would require a corresponding increase in the number of selective channels over the given range. A decrease in bandwidth will inevitably lead to an increase in the length of natural oscillations in the filter circuit, however, and will consequently hinder the time separation of successive waves. In addition, an increase in the number of channels will complicate the equipment and the processing of the observations. In practice, the selection of a reasonable bandwidth for the selective channels is determined by the frequencies to be analyzed, and by the minimum time intervals between the wave pulses that must be differentiated. Experimental recording of near-by earthquakes using sets of frequency-selective channels having relative bandwidths of from 10% to 400% has shown that the best filters have bandwidths of about 100% (this is the same bandwidth normally used in seismic prospecting by the refracted-wave correlation method, and in deep seismic sounding of the earth's crust).

Initially, tuned filters were used for this purpose. Subsequently, they were replaced, in the ChISS station, with band-pass octave fil-

ters, which have the advantage that on single-channel records, over the flat part of the characteristic, it is possible to differentiate vibrations from the frequency of the various wave pulses, which is visible on the seismogram.

The ChISS-1954 Frequency-Selective Seismic Station

This station was specially designed for the quantitative study of seismic-wave dynamic characteristics for near-by earthquakes.

The basic difference between this station and normal equipment for broadband earthquake recording is the addition of a third intermediate filter-amplifier stage to the two-section seismic transducer-galvanometer system; this makes it possible to control the frequency-selective properties of the channel, and its magnification. Another important function of the filter-amplifier section is to isolate the seismic transducer from galvanometer reaction. The frequency response of each detector-recording channel will in this case be the product of the frequency responses of its series-connected sections. This circuit makes it possible to control the frequency responses and magnifications of the channels, and also permits an increase in station sensitivity over the entire range of frequencies to values close to the theoretical limit associated with the existence of thermal fluctuations. The frequency characteristics may be monitored under field conditions.

The ChISS station is equipped with five separate filter-amplifier — galvanometer channels using a common seismic transducer as the sensor. The inputs of all of the filter-amplifiers are connected in parallel. The basic block diagram of the station is shown in Fig. 68. An RS-II station recording device is used for the recording system.

A filter-amplifier may be connected to either an integrating or differentiating circuit, which makes it possible to choose between measurements of ground displacement x, velocity $\dot{x}$, or acceleration $\ddot{x}$.

In order to expand the over-all dynamic recording range a nonlinear element may be introduced into the intermediate circuit; this element acts to produce a logarithmic function of the vibration process recorded.

Basic Sections of a Seismic Channel

These sections include: the seismic transducer, a filter-amplifier, and the galvanometer.

1. The seismic transducer. The ChISS-1954 station made use of D.A. Kharin's VSKh-1 dynamic device as the seismic transducer; this device has a pendulum-oscillation period $T_1 = 1$ sec. The amount of damping
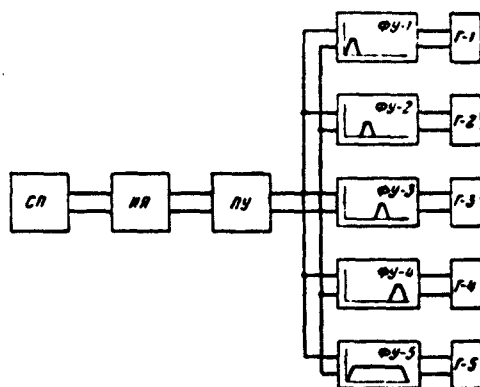
Fig. 68. Block diagram of ChISS-1954 frequency-selective seismic station. SP) Seismic transducer; IYa) integrating circuit; PU) preamplifier; G1-5) galvanometers; FU 1-5) filter-amplifiers.

was chosen on the basis of experiments using a vibrating platform; the amount of damping was so calculated that over the 1.25 to 40 cps band, the instrument characteristic was a linear function of frequency within the permissible limits of error. In this case, the seismic transducer acts as a velocity sensor. The seismic transducer was calibrated in absolute units. The characteristic for this instrument is shown in Fig. 69. The platform-vibration frequencies f, in cps, are plotted along the horizontal axis of this graph, and the amplitude A of the emf fluctua-
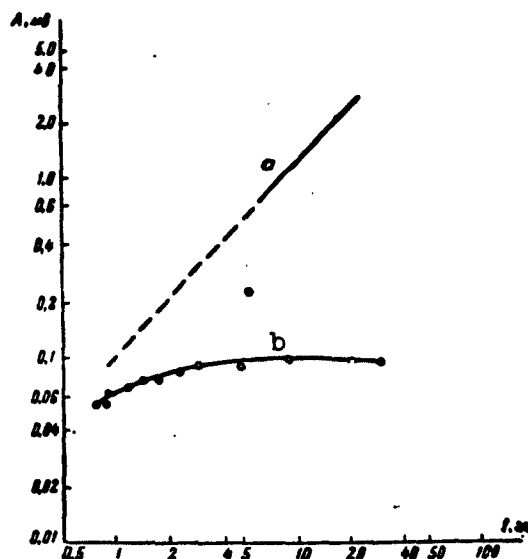
Fig. 69. Seismic-transducer frequency
responses. a) Without integrator
(velocity sensor); b) with integrat-
ing circuit (displacement sensor).
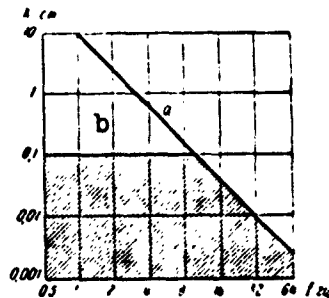
Fig. 70. Region of
seismic-transducer
dynamic-range line-
arity.

tions across the seismic-transducer terminals
is plotted along the vertical axis, in milli-
volts per micron of platform displacement.

Curve a gives the voltage directly across
the seismic-transducer terminals (displace-
ment-velocity measurement), and curve b, the
voltage across the terminals of the integrat-
ing RC circuit connected in series with the
seismic transducer (displacement measurement).

We can calculate the frequency response of the seismic transducer
if we know the electromechanical coupling coefficient (KEMS), which is
easily obtained by the static method. There is an advantage in the di-
rect determination of its frequency response with the aid of a vibrat-
ing platform, lying in the fact that it is possible to uncover (and
eliminate) possible sources of spurious resonances, and substantially to
refine the characteristic at frequencies close to the resonant frequency

of the seismic transducer.

In addition to finding the frequency response, it is quite important to determine the upper limit of linear operation for the instrument. There may be two factors causing nonlinear distortion in the seismic transducer: vibration of individual mechanical elements at sufficiently high accelerations, and the limited operating range of the uniform magnetic field in the magnet gap. With the help of the vibrating platform, it has been established that nonlinear distortions appear at an acceleration of 0.4 g. For various frequencies, this corresponds to ground-displacement amplitudes that may be determined from a chart (Fig. 70). Thus, at a frequency of 1 cps, an acceleration of 0.4 g corresponds to a 100-mm displacement, at 10 cps to 1 mm, and at 30 cps to 0.1 mm (curve a); on the other hand, displacement amplitudes for the seismic-transducer coil exceeding 1 mm will be subject to distortion owing to the nonuniformity of the magnetic field (curve b). Thus, the dynamic range of vibrations recorded turns out, in reality, to be quite limited at both low and high frequencies. The hatched section on the graph of Fig. 70 indicates the dynamic range for linear operation of the seismic transducer at frequencies of from 1 to 64 cps.

Seismic transducers of other types may be used as the sensor for the ChISS station, provided that the frequency responses and impedances are matched.

2. The filter-amplifier. This is a complex four-terminal network, consisting in general of n series-connected single-stage amplifiers and coupling (intermediate) circuits (Fig. 71). The following simple elements of this four-terminal network may be isolated.

a) An RC integrating circuit, which performs the function of signal frequency division (see Fig. 71, left side). In this case, the RC circuit represents the load on the seismic transducer, and it is de-

signed with an eye to the internal resistance. If the impedance of the
seismic transducer equals r_{sp}, and the permissible error in the divider
does not exceed 10% (here we do not allow for the voltage drop across
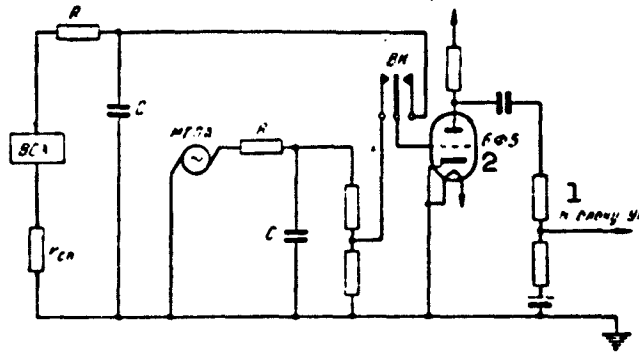
Fig. 71. Circuit of preamplifier PU.
VSKh) Seismic transducer; RC) integrat-
ing circuit; MGPA) monitoring generator.
1) To amplifier-galvanometer unit; 2)
6F5.

the sensor coil), then the total divider-circuit impedance should be
at least 10 r_{sp},

$$R - \frac{1}{\omega C} \geqslant 10\, r_{cn},$$

where ω is the angular frequency.

For the integration error to stay below or at 10%, the reactance
over the entire working frequency range should be no more than one
tenth the divider-circuit impedance

$$\frac{1}{\omega C} < 0.1 \left(R + \frac{1}{\omega C} \right).$$

If this condition holds at low frequencies, it will certainly hold at
higher frequencies. Consequently, it is sufficient to ensure that this
condition is fulfilled for the lower frequency boundary of the working
range ($f \approx 2$ cps, where $\omega = 12.5$)

$$\frac{1}{12.5 C} = 0.1 \left(R + \frac{1}{12.5 C} \right),$$

$$R + \frac{1}{12.5 C} = 10\, r_{cn} = 1400\ om.$$

233

Solving these two equations, we find the values of R and C for the integrating circuit: R = 1260 ohms, C = 570 μf.

Figure 69 shows the characteristic of the seismic transducer with integrating circuit; it reflects the self-evident relationship

$$\frac{LC}{R \cdot LC} = \frac{\frac{1}{\omega C}}{\frac{1}{\omega C} - R} = \frac{1}{1 + \omega RC} \cdot$$

Where ωRC ≫ 1, we may substitute the expression

$$\frac{1}{1 - \omega RC} \simeq \frac{1}{\omega} \cdot \frac{1}{RC} \cdot$$

for it. This means that the signal taken from capacitor C will always be smaller than the signal appearing in the seismic-transducer coil; here the magnitude of the signal will be inversely proportional to the frequency.
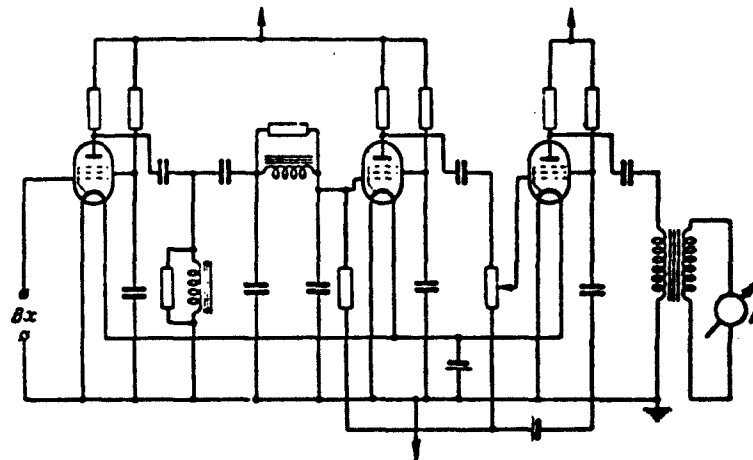
Fig. 72. Circuit of filter-amplifier.
Vkh) Input; G) galvanometer.

The lower the permissible integration error, the smaller the amount of the signal supplied to the next stage in the form of a useful signal. Thus, it is necessary in practice to tolerate the presence of deviations from ideal integration, and in particular, in the design of extremely sensitive circuits, where the useful signal may prove to

be comparable in magnitude with the fluctuation noise.

b) The preamplifier PU, which acts to magnify the signal, uses a
single 6F5 tube, is a broad band amplifier, and does not introduce
frequency distortion (Fig. 71). A special feature of the preamplifier
power supply is the reduced heater and plate voltage, resulting in al-
most complete absence of grid-current fluctuations; this ensures a low
internal-noise level; this level, which determines the maximum sensi-
tivity for each channel does not exceed 0.1 μv at the output over the
working frequency band. The preamplifier has a gain of roughly 10-15.

c) The filter-amplifier proper, whose transfer function is a def-
inite function of frequency, also determines the characteristics of the
channel as a whole. The gain of this unit may be adjusted; it is thus
possible to establish the required channel magnification. The filter-
amplifier output-circuit impedance is matched to the load, i.e., to
the galvanometer resistance.

Figures 72 and 73 show circuits for two filter-amplifiers. The
three- and four-stage circuits use the low-power-drain 1B1P tubes,
which are pentode-connected. 6D4Zh diodes are used in the logarithmic
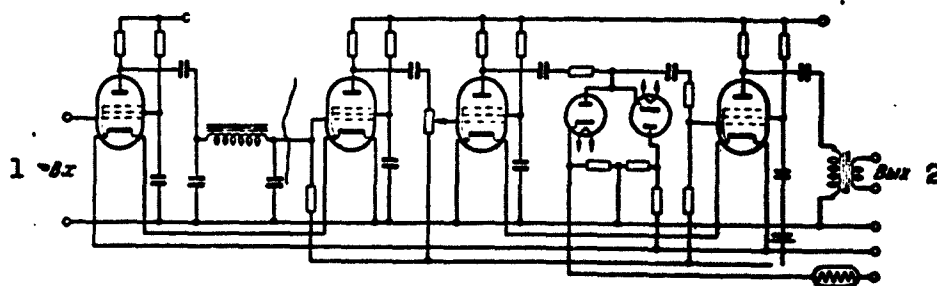
Fig. 73. Circuit of filter-amplifier with loga-
rithmic circuit. 1) Input; 2) output.

circuit. A type 0.425B 5.5-12 current-regulator tube is used to stabil-
ize the heater current. The basic LC filter circuit is located between
the first and second stages, and its over-all impedance is designed to
allow for the constants of the first filter-amplifier stage: the filter

is the load for the first stage. We arbitrarily consider the first stage with the filter circuit to be the filter proper. Thus, the circuit of the actual filter-amplifier will be considered to consist of the filter proper and the amplifier proper.

The circuit sections enumerated are connected in series; it is thus in principle possible to rearrange the elements, provided that certain technical operating features for the different type of circuit are taken into account. Here it is necessary to reckon with limitations upon the choice of the linear operating sections of the several circuits. Thus, for example, an element containing inductances and radio tubes has a more limited linear characteristic section for the transmission of electrical signals, than elements consisting solely of a capacitance and resistors.

In the general case, the complex four-terminal network (filter-amplifier), connected between two-terminal networks (the seismic transducer and galvanometer), is designed with an eye to both the frequency responses required for the circuit as a whole, and the amplitude range of the signals which the given circuit is supposed to transmit.

3. The galvanometer. Two types of galvanometer are used in the ChISS station: GB-IV galvanometers [19, 20] and the strain-gauge-type galvanometers of the "Geofizika" Plant. The parameters for both types of galvanometers are about the same: resonant frequency 70 cps, sensitivity $0.4 \cdot 10^{-6}$ amp/mm for an optical lever of 0.4 m, galvanometer resistance 40 ohms. Thus, the galvanometer voltage sensitivity will equal $0.4 \cdot 10^{-6}$ amp/mm $\cdot$ 40 ohms $= 1.6 \cdot 10^{-5}$ v/mm. The maximum useful signal (100 mm amplitude on the recording) corresponds to a current of $0.4 \cdot 10^{-4}$ amp in the galvanometer circuit with an output voltage of $1.6 \cdot 10^{-3}$ v. Type BG-9 or BG-12 permanent-magnet units are used with the galvanometers.

The damping was so chosen by experiment that over the entire working range of the station, the galvanometer sensitivity was nearly frequency-independent, while outside the working frequency range, the damping fell off.

Station Frequency Characteristics

The over-all frequency range of the ChISS-1954 station extends from 1.5 to 40 cps. It is divided into four ranges of roughly an octave each, corresponding to the four filter channels of the station: the first channel covers 1.5 to 4 cps, the second 4.5 to 9 cps, the third 10 to 20 cps, and the fourth 20 to 40 cps. In addition, there is a fifth broad band channel which comprehends the entire working range of
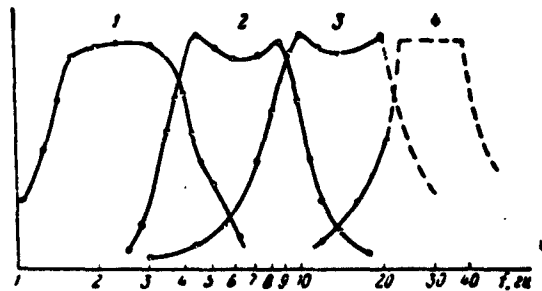
Fig. 74. Frequency characteristics of amplifier-galvanometer channel. 1-4) Numbers of channels.

the station. The frequency curves for the ChISS station were taken separately for two sections of the channel. For the seismic transducer, or for the transducer with integrating circuit, they were determined by means of a vibration platform; they have been given before in Fig. 69. The characteristics of the remaining channel section (amplifier-galvanometer) were determined with the aid of a special electrical generator of seismic frequencies. These curves are shown in Fig. 74.

Under field conditions, the frequency characteristics of the amplifier-galvanometer channel sections were regularly monitored as follows. At the beginning and end of each seismogram, a generator furnish-

ing constant-amplitude (voltage) electrical signals (MGPA) with an integrating circuit was connected to the input of the amplifier-galvanometer system in place of the seismic transducer. The frequency of the signals was varied continuously from 50 to 1/2 cps, while the absolute value (in microvolts) of the signal was known. This signal was recorded by all channels on the seismogram. On the basis of the resulting record, the relationship between the signal amplitude on the record and the voltage in microvolts at the input was established for each trace, and for any frequency in the range under investigation.

The magnitude of the emf per unit ground displacement for the various frequencies is known from the seismic-transducer characteristic. The record of the monitoring-generator signals furnished the amplitude corresponding to a specific signal in microvolts applied to the input of the amplifier-galvanometer system. These data served as the basis for determining the parameters of ground vibration for any known frequency.

The sensitivity of the ChISS station is limited by the internal noise level (electrical fluctuations) of the amplifiers; with a PU preamplifier using a 6F5 tube, and the passband selected, the level was equivalent to an electrical signal with an amplitude of 0.1 μv appearing at the input of the PU. On the basis of the permissible measurement error of 10%, the minimum useful signal from the seismic transducer should equal 1 μv. It follows from the seismic-transducer frequency curve that a signal having amplitude of 1 μv at a frequency of 1 cps will appear for a ground displacement of roughly 0.01 micron. At a frequency $f = 10$ cps, the signal from the seismic transducer will be ten times greater than the signal at $f = 1$ cps for the same ground displacement (seismic transducer without integrator). Correspondingly, the minimum measured displacement at $f = 10$ cps will not equal 0.01

micron, but 0.001 micron, etc.

As the permissible error is increased, station sensitivity rises
in proportion. Data on ChISS sensitivity to displacement for various
permissible errors are shown in Table 10.

TABLE 10
Minimum Ground-Displacement
Amplitudes Measurable for a
Given Error

1 Допусти- мая по- грешность, %	2 Смещения (в 10⁻⁷ см) на частоте (в гц)			
	1	3	10	30
10	10	3,3	1	0,33
20	5	1,6	0,5	0,16
50	2	0,6	0,2	0,06

1) Permissible error, $\%$; 2)
displacements (in 10^{-7} cm) at
frequency (in cps).

Station velocity sensitivity in recording without an integrator
is frequency-independent. For a 10% permissible error, the minimum use-
ful signal equals $6.28 \cdot 10^{-6}$ cm/sec, and at 50%, $1.25 \cdot 10^{-6}$ cm/sec.

The maximum useful station amplification is determined by the ra-
tio of the amplitude on the record to the amplitude of ground vibra-
tions. Remembering that an amplitude no smaller than 1 mm can be read
from a seismogram with a 10% error, we find that the maximum possible
over-all magnification for a channel of a ChISS station will be

at a frequency of 1 cps, $V = 1 \text{ mm}/0.01 \ \mu = 10^5$

at a frequency of 10 cps, $V = 1 \text{ mm}/0.001 \ \mu = 10^6$, etc.

With this magnification, an electrical-noise level equal to 0.1 of the
useful signal will equal 0.1 mm on the record, i.e., it will in prac-
tice stay within the thickness of the light-trace line (0.13 mm).

There are other noise sources in addition to internal electrical
noise; they limit the maximum useful magnification of the apparatus.

In earthquake recording, this type of noise primarily includes micro-seisms. In the majority of cases, it is the microseism level, rather than electrical fluctuations, that determines the working magnification of a station. In practice, most of the observations with the ChISS station in 1955-1956 were carried out at magnifications (arbitrarily referred to 1 cps) equal to 17,000, 25,000, and 50,000.
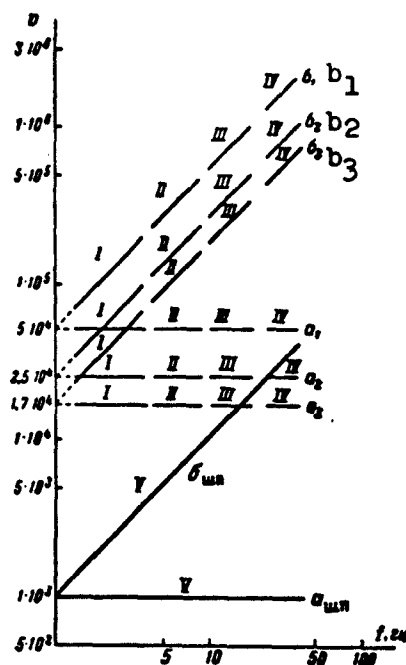
Fig. 75. Absolute magnification of ChISS-1954 station. I-IV) Number of selected channels; V) broad band channel; a_1, b_1) for sensitivity of amplifier-galvanometer channels of 10 mm on the record for a voltage across the seismic-transducer terminals of 20 μv; a_2, b_2) the same, for 40 μv; a_3, b_3) for 60 μv; a_{shp}, b_{shp}) for 1000 μv.

Figure 75 shows absolute curves of effective station magnification

for these three values of amplifier-galvanometer-circuit gain and for the single broadband channel. The curves b correspond to operation without the integrating circuit, for which the amplitude on the record is proportional to the velocity of ground displacement; for curves a, the integrating circuit is in use, and the amplitude on the record is proportional to displacement.

§5. OBSERVATION METHOD AND TREATMENT OF DATA FROM ChISS

The investigation of earthquake frequency spectra using the ChISS-1954 station is the first work of this type carried out by means of a specialized fixed installation. This work was experimental in nature, and was carried out in order to evaluate the potential of the given equipment in studying spectral composition and measuring the dynamic characteristics of ground vibrations (displacements, velocities, and accelerations) during earthquakes. The fact that only a single ChISS station was in existence at the time placed a substantial limitation upon the potential of the investigation. Nonetheless, an attempt was made, on the basis of the materials obtained, to evaluate, albeit qualitatively, the general picture of the variation in vibration frequency compositions during earthquakes as a function of the location and depth of focal zones, and of the earthquake energy and epicentral distances. The absolute values of the three kinematic magnitudes (displacements, velocities, and accelerations) were also determined for perceptible earthquakes.

Method of Observation

Generally speaking, the method of observation used to solve the problems mentioned should have been based upon simultaneous recording of earthquakes by several stations of the ChISS type, located at various points in the zone being investigated. Owing to the fact that only a single station of this type was available, however, protracted ob-

servations were carried out in turn at two points: at the Garm geophysical station (from 1 January to 17 July 1955) and at the Chusal station (from 1 January to 1 July 1956). Both of these stations, located 40 km apart, are founded upon Paleozoic bedrock outcroppings, which to some degree equalizes the conditions at the observation points.

Round-the-clock observations were carried out at both points both with and without an integrating circuit, i.e., both the displacements and velocities of ground vibrations were recorded.

The absolute magnifications were chosen on the basis of preliminary measurements of microseisms; the microseism level was greatest at the low frequencies of the working range. Noise amplitude on the record sometimes reached 0.3 mm at a frequency $f = 1$-2 cps (first trace) for a magnification of $V = 50,000$. This also limited the useful sensitivity of the equipment. The most favorable conditions for realizing the possible useful magnification of the equipment occurred in velocity recording, i.e., in operation without the integrating circuit, where the magnification rises in proportion to the frequency. The possibility of increased magnification at high frequencies is explained by the fact that the microseism level within the frequency band under consideration, as was shown experimentally, drops off rapidly as the frequency rises (more rapidly than $1/f$). In this connection, for velocity recording, the maximum equipment magnification ranged from 50,000 at $f = 1$ cps to 2,000,000 at $f = 40$ cps.

Method of Processing

The method of processing the observations consisted in constructing individual seismic-wave spectra, and generalizing them further.

First, vibrations corresponding to individual waves were isolated on the seismographs, and the arrivals of identical waves were identified on all traces. Next, the vibration period and maximum amplitude

were measured on all traces in the region including the arrival and maximum amplitude of the wave. The reference-signal recording was used as the basis for a determination of the soil-vibration amplitude, in absolute or relative units. The measured amplitude and frequency values were plotted on a graph of $A = A(f)$, which also represented the so-called individual wave spectrum. This graph gives a general idea of the amplitude-distribution features in the frequency range under investigation (1.5-30 cps).

In operation with the integrator, the amplitude on the record is proportional to the ground displacement, and the individual spectrum plotted correspondingly is a displacement spectrum. The spectrum constructed from observations without the integrator is a velocity spectrum. Henceforth, we shall basically be concerned with the displacement spectra.

One of the basic characteristics of the individual spectrum for a particular wave is the dominant frequency f_{pr}, which corresponds approximately to the maximum on the spectral curve $A(f)$. A comparison of the spectra was carried out in order to generalize the observations; it was basically the dominant-frequency values that were compared. For cases in which the dominant frequency could not be clearly distinguished from the graph, it was taken as the geometric mean of the frequencies at the amplitude level $A_{max}/\sqrt{2}$, where A_{max} is the maximum amplitude of the spectrum curve.

The individual spectra were constructed for earthquakes having known focal coordinates, with data obtained from expedition bulletins for weak, near-by earthquakes, and from bulletins of the seismic-station network of the USSR for more remote earthquakes. The spectra were constructed chiefly for longitudinal and transverse waves. For earthquakes with small epicentral distances $\Delta < 150$ km, as a rule,

these were the $\bar{P}$ and $\bar{S}$ waves (according to the terminology employed in "large-scale" seismology); for the deep Afghan earthquakes, they were the "direct" P and S waves; for earthquakes having foci in the earth's crust at $\Delta > 150$-200 km, where diffracted waves appear on the records, the spectra were normally constructed for the most intense waves, and in isolated cases, for several waves.

§6. RESULTS OF INVESTIGATION OF VIBRATION FREQUENCIES FOR EARTHQUAKES WITH THE AID OF ChISS

Frequency Spectra for Earthquakes from Different Focal Zones

As a result of the processing of the 1955-1956 materials, 300 individual earthquake spectra were constructed: 175 from observations made with the ChISS station at Garm, and 125 with the ChISS station at Chusal. Most of the spectra constructed relate to earthquakes in the Garm region and the Pamir-Hindu Kush zone, and some to earthquakes in the Fergana Valley, Southern Tadzhikistan, and Central Tien Shan. The epicenters of the earthquakes for which the displacement spectra were constructed are plotted on the map of Fig. 76.

The dominant frequencies f_{pr} in the individual spectra for all earthquakes were divided into four groups: 1) $f_{pr} \leq 3$ cps, 2) 3 cps $\leq$ $\leq f_{pr} > 6$ cps, 3) 6 cps $< f_{pr} \leq 12$ cps, and 4) $f_{pr} > 12$ cps. Figures 77-78 show examples of the individual displacement spectra and the seismograms corresponding to them. Individual larger-scale maps have been plotted for earthquakes in the Garm region, from observations with the ChISS station at Garm (Fig. 79a) and with the ChISS station at Chusal (Fig. 79b).

It is easily seen from the charts given that there are noticeable deviations for the various focal zones, against the background of a general decrease in the dominant frequencies with increasing epicentral distance. Three basic zones having characteristic earthquake fre-

quency-spectrum features may be distinguished: 1) a zone of deep Hindu Kush earthquakes $(80 < H < 300$ km); 2) the Tovil'-Dora zone and 3) the earthquake district of the Chusal station.

The deep Pamir-Hindu Kush earthquakes are characterized by relatively high dominant frequencies. The epi- and hypocentral distances for these earthquakes from the Garm station range from 200 to 300 km. At such epicentral distances, earthquakes with foci in the earth's crust have dominant frequencies, as a rule, of less than 2-3 cps, while for deep earthquakes, this frequency basically ranges from 6-10 cps, and drops below only in isolated cases.

Especially low-frequency spectra predominate for earthquakes of the Tovil'-Dora district, having foci in the earth's crust; this may be seen clearly from Fig. 79a. For epicentral distances of 30-50 km, frequencies of $f \leq 3$ cps are dominant in the earthquake spectra of this zone. For other shallow-focus earthquake districts, the dominant frequencies basically range from 6 to 12 cps at these epicentral distances.

Earthquakes in the region of the Chusal station are characterized by higher dominant frequencies of 10-14 cps.

The features of frequency spectra for earthquakes having different focal zones may be associated both with the conditions under which the earthquakes appear, and with the seismic-wave propagation conditions along the path from the focus to the point of observation. For deep earthquakes, characterized by relatively high dominant frequencies, the elastic waves propagate basically in the layer beneath the crust, where the high frequencies are considerably less subject to absorption than in the earth's crust. The foci of the Tovil'-Dora earthquakes, characterized by especaally low frequencies, are located in the earth's crust, basically at shallow depths and mostly in sedimentary rock.
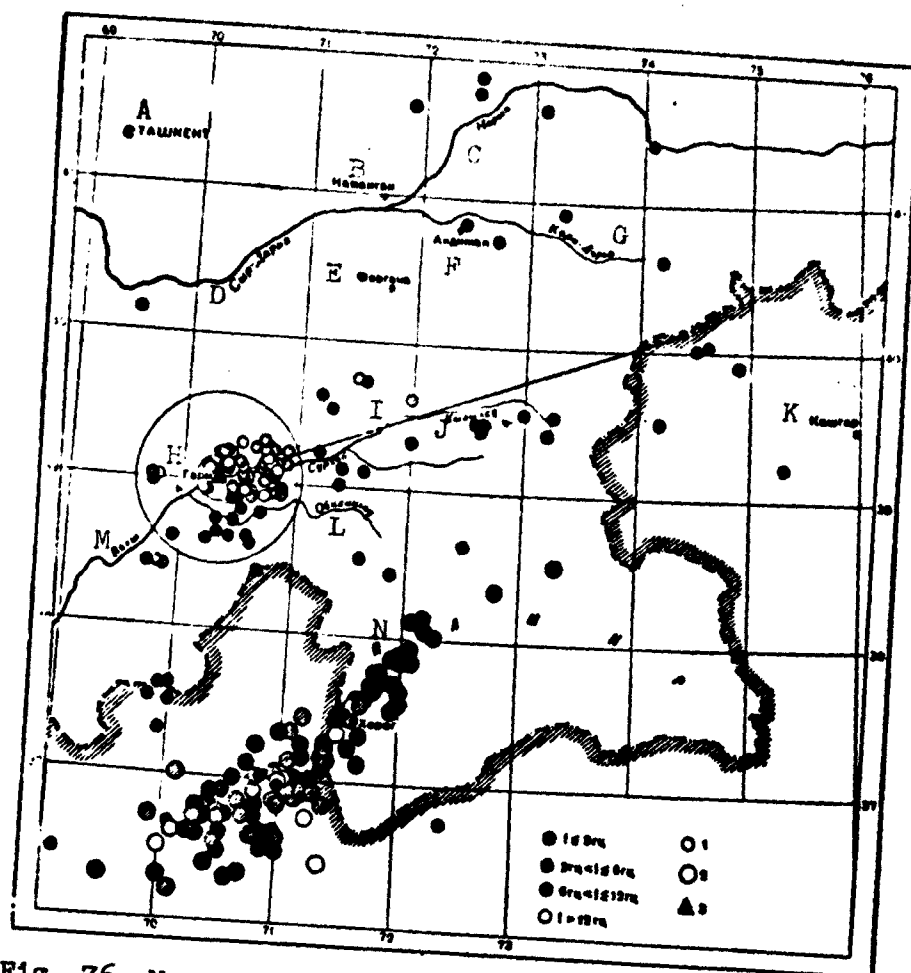
Fig. 76. Map showing distribution of dominant frequencies f_{pr} for earthquakes in Central Asia from observations of the ChISS at Garm. 1) Focus in earth's crust; 2) focus under earth's crust; 3) Garm seismic station. A) Tashkent; B) Namangan; C) Naryk; D) Syr-Dar'ya; E) Fergana; F) Andizhan; G) Kara-Dar'ya; H) Garm; I) Syrkhob; J) Kyzylsu; K) Kashgar; L) Obi-khinyuu; M) Vaksh; N) Pamir; O) Khorog.

Trends of major tectonic structures lie across the propagation path for the waves from these foci to the Garm station. In this last case, the tectonic boundary between the crystalline rocks of Tien Shan and the sedimentary deposits of Pamir can also affect spectrum formation during propagation; when elastic waves propagate along the boundary, they may lose high frequencies owing to diffraction.

Observations indicate that variations in earthquake spectral fea-

- 246 -
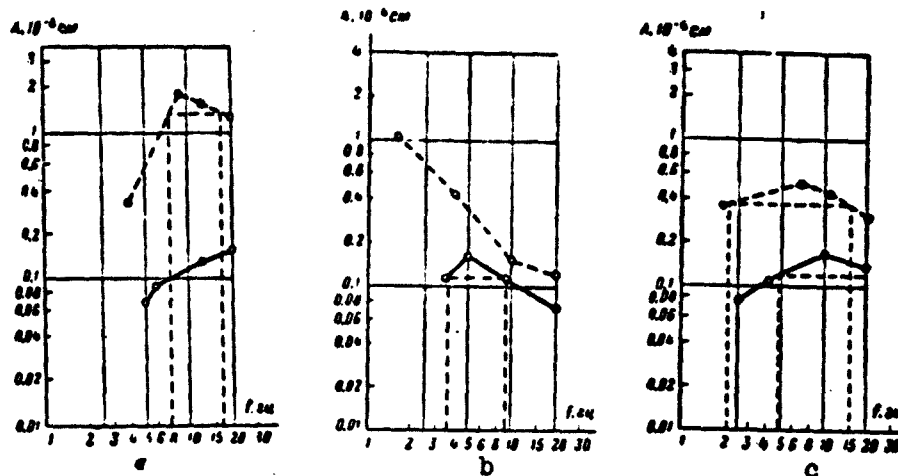
Fig. 77. Examples of displacement spectra for various earthquakes from seismograms obtained from Garm ChISS. a) Earthquake of 12 January 1955; focus coordinates: $\varphi = 39^{o}07'$ N; $\lambda = 70^{o}23'$ E; h = 10 km. t_p = 22 hr 33 min 17.4 sec. $t_s - t_p$ = 2 sec; b) earthquake of 2 February 1959, epicenter in Fergana Valley, $\varphi = 40^{o}.7$ N; $\lambda = 72^{o}.7$. t_p = 21 hr 26 min 34 sec. $t_s - t_p$ = 37.95 sec; c) earthquake of 3 February 1955. Focus coordinates: $\varphi = 37^{o}.9$ N; $\lambda = 72^{o}.1$ E; h = 200 km; t_p = 22 hr 30 min 18 sec; $t_s - t_p$ = 29.5 sec. Solid line — longitudinal P waves; dashed line — transverse S waves.

tures associated with the territorial arrangement of foci, may be quite considerable, which complicates the study of other general factors affecting the general composition of seismic shocks. Thus, in the general study of earthquake spectral peculiarities, it is first of all necessary to isolate spectral variations associated with features of the focal zones. When an estimate is made of the nature of the way in which spectral composition depends upon earthquake energy and focal depth, territorial distortions may be eliminated in practice by utilizing earthquakes from narrow local epicentral zones.

The anomalous spectral peculiarities of individual focal zones, which are obstacles to the study of general laws, at the same time are of independent interest. A study of the connection of these anomalies with the conditions for the appearance of earthquakes and the propaga-
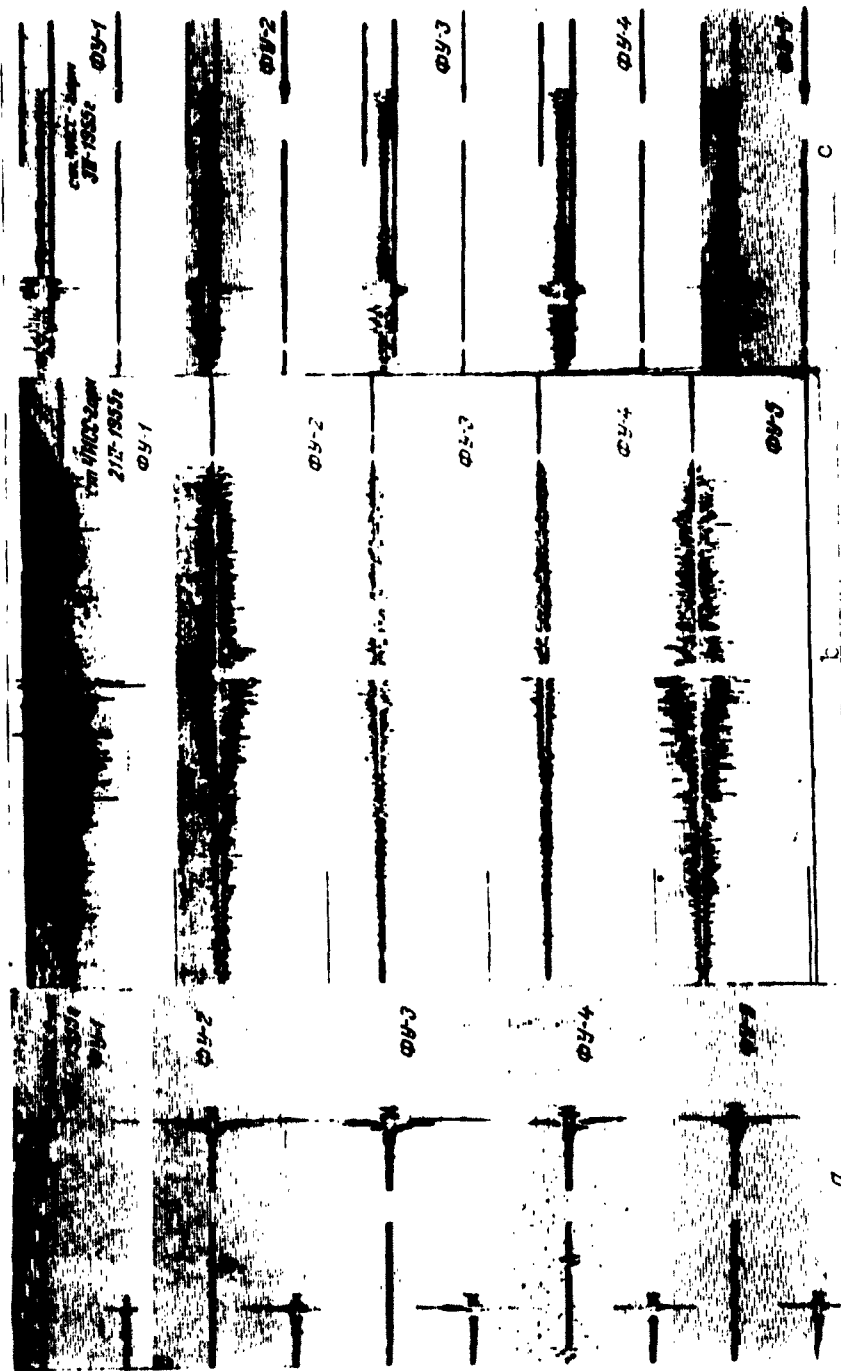
Fig. 78. Earthquake records from ChISS-1954 stations. 1-5) Number of channels (see Fig. 68). Basic earthquake data a, b, c) given in legend for Fig. 77.
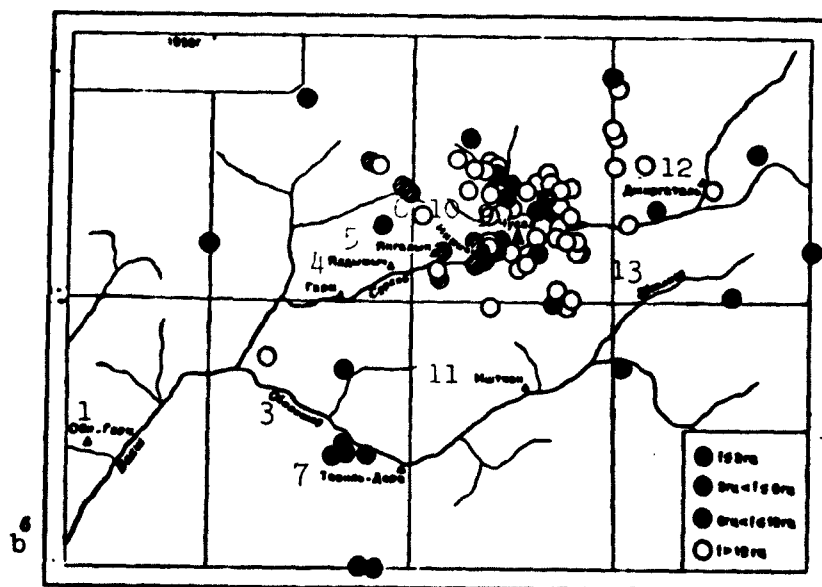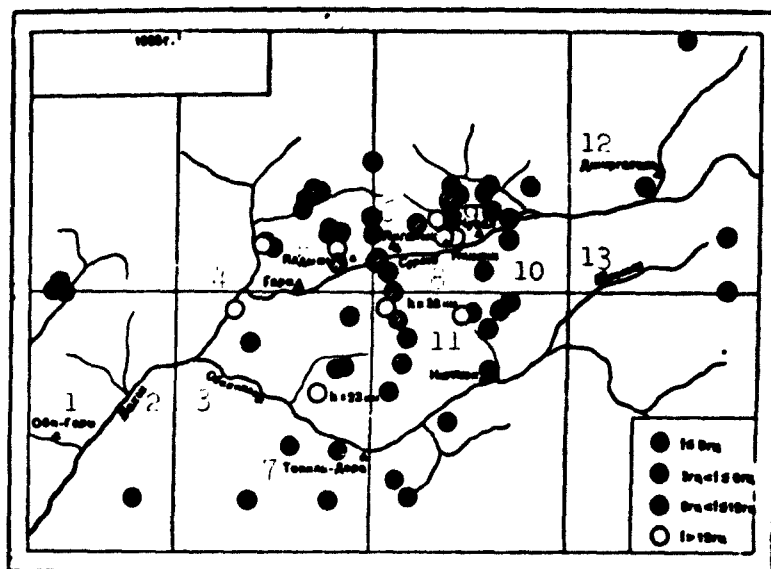
Fig. 79. Map showing distribution of earthquake
dominant frequencies. a) From observations of Garm
ChISS station; b) Chusal ChISS. h) Depth of focus.
1) Obi-Garm; 2) Vakhsh; 3) Obikhinyuu; 4) Garm; 5)
Yaldymych; 6) Yangalyn; 7) Tovil'-Dora; 8) Surkhob;
9) Chusal; 10) Nimichi; 11) Ishtion; 12) Dzhir-
gatal'; 13) Shaklisy.

tion of elastic waves may be used, in particular, for contouring of in-
dividual tectonic zones.

249

Vibration Frequencies as a Function of Depth of Focus

Attempts to find such a relationship have been made from determinations of the dominant frequencies f_{pr} for weak $(K = 4\text{-}5)$ earthquakes of the Chusal epicentral zone for focal depths $\underline{h}$ ranging basically from 2-5 km to 10 km $(h = 20$ km in one case), and for earthquakes of the Pamir-Hindu Kush zone with $K = 11\text{-}12$, and a focal depth $\underline{h}$ ranging from 80 to 240 km. Figures 80$\underline{a}$ and $\underline{b}$ show charts of $\underline{f}$ as a function of $\underline{h}$ for earthquakes of both zones.

Judging from these graphs, $\underline{f}$ does not appear to depend noticeably upon $\underline{h}$ in either case. It is probable that this negative result is associated with the inadequate precision with which the compared values of $\underline{f}$ and $\underline{h}$ are determined.

Fig. 80. Dominant frequencies as a function of depth of focus. a) For earthquakes in the Chusal zone; b) Pamir-Hindu Kush earthquakes.

A well-defined relationship between seismic-vibration frequencies and depth of focus was noted only for the case in which there was a qualitative variation in the properties of the medium containing the earthquake foci together with a variation in focal depth. Thus, for example, in the region of low-frequency earthquakes for the Tovil'-Dora district, an earthquake was detected that had an anomalous high-frequency spectrum; the depth of focus for this earthquake equaled 23 km. Clearly, in contrast to most of the earthquakes in the Tovil'-Dora district, whose foci were located in a sedimentary stratum, the focus of this earthquake was located in a crystalline layer.

The same pattern is observed for Afghan earthquakes for which the focus lies outside of the earth's crust, under the Mohorovicic discon-

tinuity. For earthquakes of this district having foci within the earth's crust, the dominant frequencies, as a rule, are less than 3 cps, while for deep foci, as a rule, they exceed 6 cps.

Vibration Frequencies as a Function of Earthquake Force

The relationship between the dominant frequency f_{pr}, corresponding to the maximum ground displacement x_{max} in an S wave, and the quantity x_{max} itself, has been investigated, using investigations of earthquakes in the local Chusal zone. For this purpose, 50 earthquakes were selected for which $t_s - t_p$ amounted to 2-2.5 sec at the Chusal ChISS station. The dominant frequencies $\underline{f}$ were determined on the basis of displacement spectra constructed for these earthquakes.
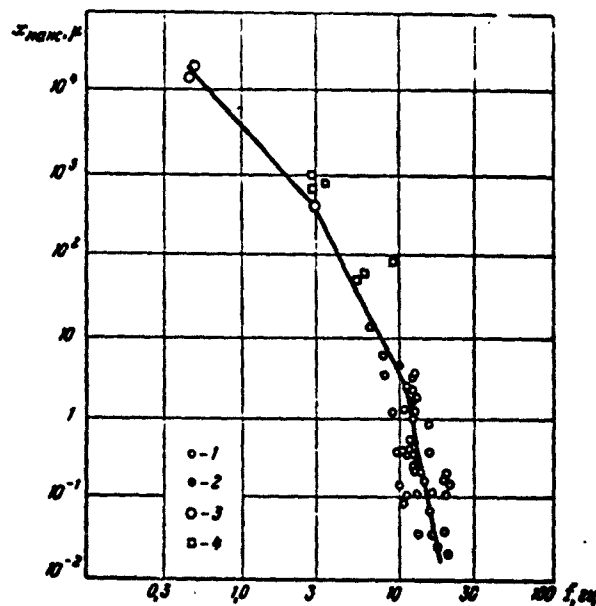
Fig. 81. Dominant frequencies $\underline{f}$ as a function of maximum displacements x_{max} in epicentral district. 1) Dominant frequencies in displacements from observations of ChISS station (Chusal); 2) average values of dominant frequencies (from data of the same station); 3) frequency from observations of displacement meter (data for strong earthquakes in the USA during 1952); 4) displacement frequencies corresponding to maximum accelerations (data the same as for 3).

The maximum ground displacements for the earthquakes observed here varied from 10 microns to 0.01 micron, corresponding to weak and very weak earthquakes. In order to evaluate the way in which the dominant frequency f depends upon vibration amplitude in the epicentral zone over a wider dynamic range, including strong earthquakes, results of displacement measurements for perceptible and destructive earthquakes, taken from sources in the literature [151] were brought in. Here only observations for very close earthquakes were selected.

On the basis of this data, a summary graph was also compiled for the desired function $x_{max} = x(f)$, which is shown in Fig. 81. This graph is drawn in double logarithmic coordinates. The maximum ground displacements x_{max} are plotted along the vertical axis in microns, and the corresponding displacement frequencies f along the horizontal axis in cycles per second.

As the graph shows, for strong earthquakes the variation in dominant frequencies with a change in maximum displacements at the epicentral zone is considerably more noticeable than with weak earthquakes. The straight segments of the broken average line on this graph correspond to the following indices: in the region of very weak earthquakes, for epicentral-zone displacements of from 0.01 to 3 microns, the frequencies range from 20 to 11 cps, with the approximate proportion $x \approx f^{-8}$ holding; for stronger earthquakes with displacements in the epicentral zone ranging from 3.0 to 500 microns, the dominant frequencies range roughly from 11 to 3 cps, and the line has a slope corresponding to roughly $x \approx f^{-4}$. For destructive earthquakes, where the displacements in the epicentral zone range from 500 microns to 10 mm, and the dominant frequencies from 3 to 0.5 cps, the function $x \approx f^{-2}$ is observed to hold.

There is a very large scatter of the points in the lower section
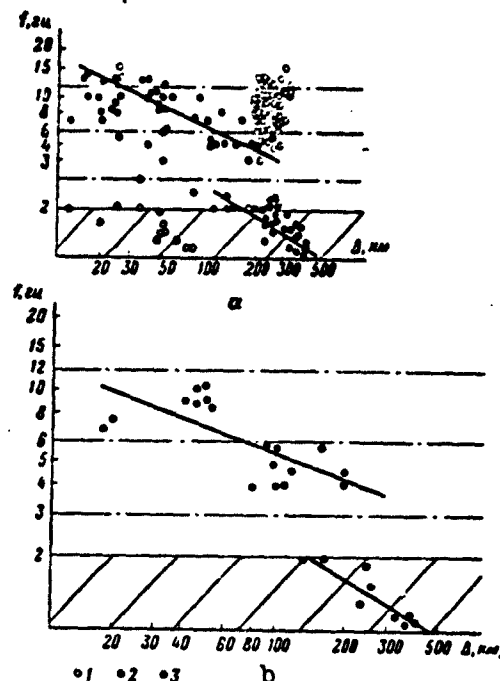
Fig. 82. Dominant frequencies
as a function of epicentral
distance. a) For different
foci; b) for foci lying on pro-
file along structure in South
Tien Shan. 1) Deep-focus Pamir-
Hindu Kush earthquakes; 2)
earthquakes from Tovil'-Dora
district; 3) other earthquakes
in Central Asia; the hatched
region corresponds to area in
which low-frequency portion of
the spectrum is not determined
reliably.

of the graph of Fig. 81 for the region of very weak earthquakes, where

the number of observations is quite large. This is evidence for the

instability of the dominant frequency for earthquakes of roughly the

same force, at least in this region.

Vibration Frequencies as a Function of Epicentral Distance

It is known that distant earthquakes, as a rule, are characterized

by lower dominant frequencies than near earthquakes, and that this is

associated with the greater absorption of high frequencies upon propa-

gation of elastic waves through actual media. The nature of the varia-

- 253 -

tion in seismic-wave frequency spectra as a function of distance has so far been little investigated, however. The difficulty lies in the fact that the earthquake spectra depend not only upon distance, but also upon the conditions in the focus; in addition, as has been indicated above, the territorial distribution of focal zones has a large effect upon spectrum formation, as do differences in conditions along the seismic-wave propagation paths.

Figure 82a shows a chart for the dominant frequencies f_{pr} of transverse waves as a function of the epicentral distance Δ; the graph is plotted from observations of the Garm station, with no allowance for the force or territorial distribution of foci (transverse waves are characterized by maximum intensity on the seismogram). Two anomalous regions are clearly distinguishable on the chart, corresponding to the foci of low-frequency Tovil'-Dora earthquakes and the high-frequency, relatively distant deep (h > 60 km) Pamir-Hindu Kush earthquakes. In order to determine the nature of the frequency spectrum vs. distance function, these two groups of earthquakes were excluded from consideration. The remaining points were approximated by means of two lines as shown on the graph. The first line, corresponding to small values of Δ characterize the variation in the spectrum with distance for direct waves propagating basically in a "granite" stratum; the second line, corresponding to epicentral distances ranging from 100 to 400 km are clearly associated with the appearance on the records of waves propagating in deeper layers. The exclusion of the basic anomalous focal zones from consideration, however, does not completely eliminate the effect upon the frequency spectra of the territorial focal distribution.

An attempt has been made at a more rigorous approach to finding the relationship between the dominant frequency and distance, by the.

possible elimination of the effect of irrelevant factors. To do this, earthquake records where chosen for foci located along one direction only: to the east-north-east of Garm (line AB on Fig. 76). In this case, seismic waves propagated from the earthquake foci to the observation point under relatively uniform conditions, along the south Tien Shan structure. We considered relatively distant earthquakes to be precisely those whose epicenters lay within a band of about 100 km width along the direction selected. Earthquakes located south of the Surkhob River were excluded from the near-by earthquakes of the Garm region. In order to eliminate the influence of shock intensity, only earthquakes of about the same energy were considered: classes K = 10-11 (class IV according to Bune [152]). As an exception, several weaker earthquakes were investigated (class III according to Bune) from the Chusal group; an appropriate correction to the dominant frequency was introduced in these cases, however, on the basis of a curve for the dominant frequency as a function of earthquake intensity.

The graph constructed as a result for the function $f(\Delta)$ is shown in Fig. 82b. On this drawing, the average line, corresponding to small epicentral distances $\Delta < 150$-200 km, has a lower slope than the preceding line (Fig. 82a). This is connected with the fact that weak near-by earthquakes are excluded in this case; they are characterized by especially high vibration frequencies. It should be noted, that owing to the insufficient number of observations, the slope of both lines of this graph is not determined with certainty.

Relationship of Frequencies of Longitudinal and Transverse Waves for Different Epicentral Distances

A comparison of the spectral curves for longitudinal P and transverse S waves for foci located at various distances from the station shows that the ratio of the dominant vibration frequencies f_p and f_s

for these waves is not constant, but varies noticeably with the epicentral distance Δ. In order to find the nature of the variation in the ratio f_p/f_s with the distance Δ, the spectra for the P and S waves were determined for 50 earthquakes having epicentral distances ranging from 5 to 400 km. As a result of averaging the values for f_p/f_s for four intervals of Δ (5-20 km, 20-60 km, 60-180 km, and 180-400 km), corresponding values were obtained for f_p/f_s of 1.10, 1.19, 1.43, and 1.84.
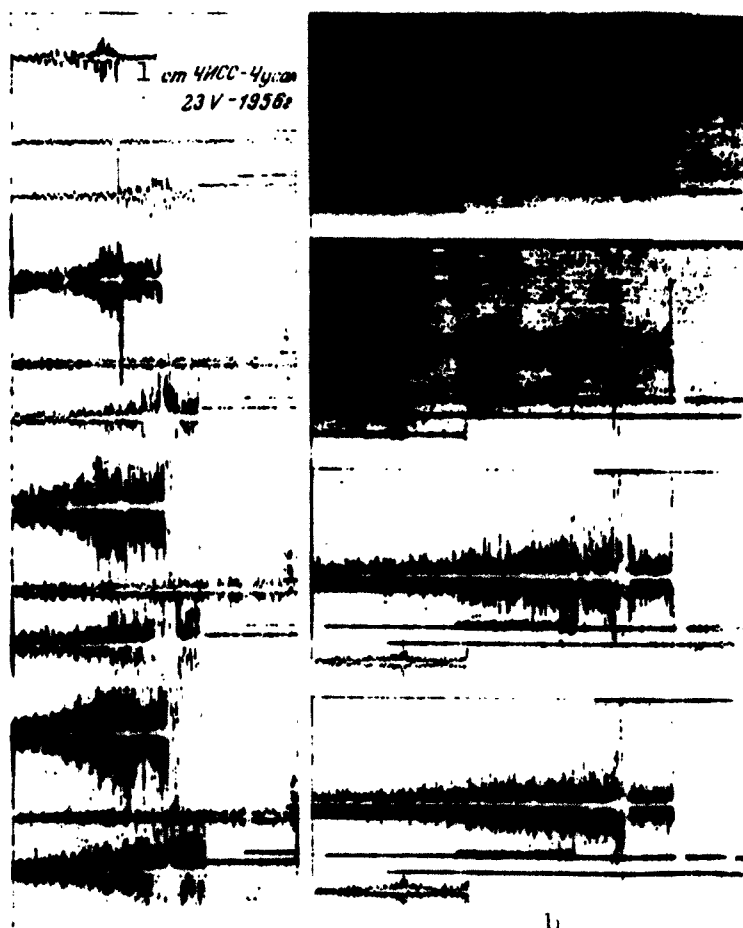
Fig. 83. Records of perceptible earthquakes for Chusal ChISS station. a-b) (see Table 11). 1) Chusal ChISS station, 23 May 1956.

There is a large scatter of points within the averaged values for individual intervals. It may be seen that in some cases, this spread

was caused by the characteristic features of the territorial focal-zone arrangement with respect to the observation station. Thus, for example, the Tovil'-Dora district focus group was characterized by a large value of the ratio f_p/f_s, characteristic of more distant earthquakes.

Absolute Displacement, Velocity, and Acceleration Spectra for Perceptible Earthquakes

In 1956, the ChISS station (at Chusal) registered local earthquakes (Fig. 83) which were perceived in the station area as of intensity 4.5: they were accompanied by breaking of glass, ringing of dishes,

TABLE 11

Values of Maximum Amplitudes for Displacement x_{max}, Velocity $\dot{x}_{max}$, and Accelerations $\ddot{x}_{max}$, and Their Dominant Frequencies f for Weak Perceptible Earthquakes in Chusal in 1956

1 Дата и ощутимость в эпицентре	2 Смещение				3 Скорость				4 Ускорение			
	f, гц		x_{max}, мк		f, гц		$\dot{x}_{max}$, мк/сек		f, гц		$\ddot{x}_{max}$, мк/сек²	
	P	S	P	S	P	S	P	S	P	S	P	S
a) 25.V 1956 г. P : 16 ч. 28 м. 20 с. S — P = 1,7 сек. Слабый толчок, если бы ре было гула, не обратили бы внимания	10	2,5	0,134	0,6	10	9	9,2	20	20	10	825	1150
б) 23.V 1956 г. P : 15 ч. 37 м. 17 с. S — P = 1,9 сек. Гул со стороны Хаита, без ощущения	12	3—18	0,33	0,17	13	>30	20	24	13	>30	1630	4050
в) 12.V 1956 г. P : 12 ч. 10 м. 54 с. S — P = 3,4 сек. Гул без ощущения	12	10	0,26	0,38	12	20	11	24,2	13	>30	1750	2000
г) 14.V 1956 г. P : 15 ч. 37 м. 05 с. S — P = 2,1 сек. Ощутимое землетрясение с гулом	6	13	0,29	0,4	16	13	22,4	3,28	16	13	2240	2880

1) Date, perceptibility at epicenter; 2) displacement; 3) velocity; 4) acceleration; a) 25 May 1956, P: 16 hr 28 min 20 sec. S-P = 1.7 sec. Weak shock perceptible only as a rumble; b) 23 May 1956, P: 15 hr 37 min 17 sec. S-P = 1.9 sec. Rumble from Khayt, imperceptible; c) 12 May 1956, P: 12 hr 10 min 54 sec. S-P = 3.4 sec. Rumble, imperceptible; d) 14 May 1956, P: 15 hr 37 min 05 sec. S-P = 2.1 sec. Perceptible earth tremor with rumble.
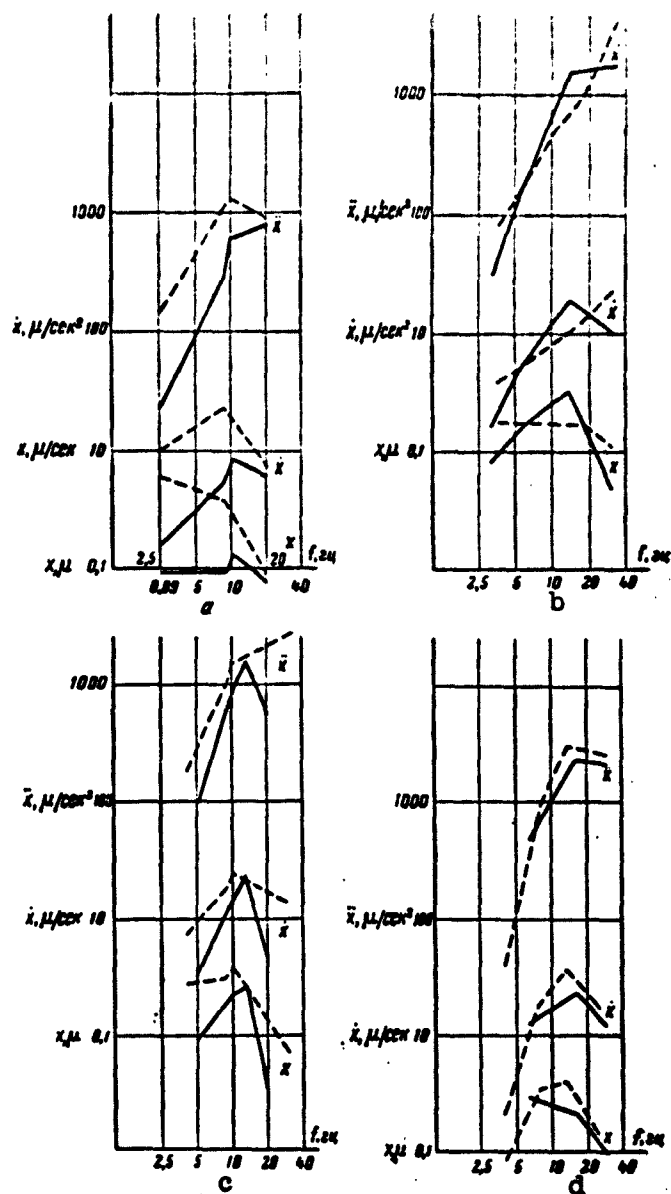
Fig. 84. Spectra for displacements x, veloc-
ities x, and accelerations x for perceptible
earthquakes according to seismograms of ChISS
(Chusal). a-d) (see Table 11). Solid lines —
for longitudinal waves; dashed line — for
transverse waves. Logarithmic scales used.

and rumbling of various intensities. It is interesting to compare the

results of a quantitative measurement for the absolute values and spec-

tral features for the displacements x, velocities x, and accelerations

- 258 -

$\ddot{x}$ for these earthquakes with the intensity determinations carried out, as is usual, by means of descriptive qualitative indices.

To do this, individual spectra were constructed for the given earthquakes; they are shown in Fig. 84a-d. Here, the frequency f is plotted along the horizontal axis in cycles per second, and the values of x, $\dot{x}$, and $\ddot{x}$ along the vertical axis in microns, microns/sec, and microns/sec^2, respectively. The scale of x displacements is shifted upward by a single decade with respect to $\dot{x}$ and $\ddot{x}$. Numerical data on the extremum values for x, $\dot{x}$, and $\ddot{x}$ are given in Table 11. Direct recording was carried out for velocities, while displacement and acceleration were computed.

The featured characteristic of the spectra for the perceptible earthquakes is the increase in acceleration toward the high-frequency end of the range under investigation, toward 20-30 cps to values exceeding 1000-4000 microns/sec^2. The weakest of these shocks (a) is characterized by the following maximum-acceleration values: 1150 microns/sec^2 at a frequency of 10 cps for S waves and 900 microns/sec^2 at a frequency of 20 cps for P waves (Fig. 84a). The further increase in acceleration for the P wave toward the audio frequencies beyond the measurement range is noteworthy. The strongest of these shocks (d), which was perceptible, and accompanied by audible rumbling, is characterized by accelerations in the P and S waves of 2240-2880 microns/sec^2 (0.22-0.29 gal). The absolute values of ground displacement vary from 0.13 to 0.4 micron at frequencies corresponding to the maximum values of velocity and acceleration.

On the basis of these data, the conclusion may be drawn that at frequencies of the order of 20 cps and above, a perceptible effect may be caused by ground oscillations with an amplitude equal all-in-all to only 0.1 micron, which corresponds to a velocity of 13 microns/sec and

an acceleration of 1600 micron/sec². A seismic rumble without per-

ceptible mechanical vibrations is observed in the case of even

higher frequencies for deviations of less than 0.1 micron.

Manu-
script   [Footnote]
Page
No.

202   See K.K. Zapol'skiy, I.M. Mel'nikova. Spectral Components of
         Near-by Earthquakes from Data of a Frequency-Selective Sta-
         tion, IFZAN Fund, 1953; Report of Garm Expedition of 1952,
         IFZAN Fund.

Manu-
script   [List of Transliterated Symbols]
Page
No.

200   дж = dzh = dzhul = joules
201   lg = log
208   сп = sp = seysmopriyemnik = seismic transducer
215   шп = shp = shirokopolosnyy = broadband
219   пр = pr = preobladayushchaya (chastota) = dominant (frequency

Chapter 6

EARTHQUAKE FOCI

An earthquake focus is defined as a region within which faulting
and intensive inelastic deformations of the medium occur, leading to
the earthquake. Thus, the focal region is defined as a portion of
space containing both the basic fault causing the earthquake, and the
secondary faults directly associated with it in time, and the rapid
continuous movements of the medium – plastic or otherwise – that are
irreversible, or very slowly reversible. The portion of space where
the deformation is continuous and chiefly reversible and elastic is
considered to lie outside the focus; this is the region in which elas-
tic seismic waves propagate.

The focus of an earthquake may either lie on the earth's surface,
as in the case of several strong earthquakes, or lie completely under
the surface, as in the case of all weak earthquakes.

As of the present, only very scanty data from direct measurements
[86, 121, 153, 154] have been obtained on the magnitude of disloca-
tions and surface faults occurring during strong, destructive earth-
quakes. Direct measurement of focal dimensions and dislocations is
clearly impossible for weak earthquakes. Nonetheless, it is important
to know the order of these magnitudes, even if approximately, and the
way in which they depend upon energy. This makes it possible to evalu-
ate the role of weak earthquakes in the general process of deformation
of the earth's crust, and permits a quantitative comparison of seismic
and geodesic observations for periods in which only relatively weak

earthquakes are observed. Seismic-wave observations make it possible to evaluate certain important properties of the foci for weak (as well as strong) earthquakes that are hidden under the ground.

At the beginning of the present chapter, we will make use of various methods to evaluate focal dimensions, and the magnitude of dislocations within foci, depending upon earthquake energy. In the first section, these estimates are obtained by means of a theoretical analysis of the stress fields in the region surrounding the focus, before and after the earthquake. Here, computational methods are used and improved that have been developed in the theory of stress concentration. In the second section, these estimates are made in simpler fashion, using general physical concepts, and certain empirically established laws.

The next section of the chapter gives results of a determination of the so-called dynamic focal parameters: the orientation of the fault plane, and the direction of focal dislocations, for earthquakes in the Garm region.

§1. EVALUATING FOCAL CHARACTERISTICS ON THE BASIS OF STRESS FIELDS

By carrying out a theoretical analysis of the static-stress fields within the earth before and after an earthquake, we are able to determine many focal characteristics. The results thus obtained should be connected with observations on the basis of the fact that the difference in energy for the fields considered will determine the energy of the seismic waves observed with an accuracy to within the energy expended on irreversible processes. This way of setting up the problem was proposed, and carried out with great success, in the works of P. Bayerli [155] and L. Knopov [124]. The main advantage of the method lies in the possibility of dispensing with the complicated investigation of the wave excitation process in faulting.

Knopov considered a two-dimensional focal model, with the displacements occurring perpendicular to the plane in which the solution is sought; this problem is associated with the study of strong earthquakes having a horizontal dislocation in the focus. In the present paragraph, we consider a three-dimensional model of the focus, which may be of interest in the study of weak earthquakes.

Defining the Problem

We are given a homogeneous isotropic ideally elastic space with Lame constants λ and μ. We define the initial homogeneous stress field

$$\tau_{xy} = p; \ \tau_{xz} = \tau_{yz} = 0; \quad \sigma_x = \sigma_y = \sigma_z = 0, \tag{32}$$

where τ and σ are, with the appropriate subscripts, the shear and normal stresses, p is a constant. The results to be obtained will not be affected if we introduce the hydrostatic pressure

$$\sigma_x = \sigma_y = \sigma_z = -P,$$

where P is a constant. The stresses (32) correspond to a displacement

$$u_x = C_1 y, \quad u_y = C_2 x, \tag{33}$$

where u_x is the displacement component along the $\underline{x}$ axis, C_1, C_2 are constants (clearly, $C_1 + C_2 = P/\mu$).

Let us consider the ellipsoid

$$\frac{x^2}{a^2} + \frac{y^2}{a^2} + \frac{z^2}{b^2} = 1 \quad (a < b). \tag{34}$$

In the elliptical coordinates $\underline{u}$, $\underline{v}$, $\underline{w}$, where

$$x = \frac{b}{\operatorname{ch} u_0} \operatorname{ch} u \cdot \sin v \cdot \cos w, \ y = \frac{b}{\operatorname{ch} u_0} \operatorname{sh} u \cdot \cos v,$$
$$z = \frac{b}{\operatorname{ch} u_0} \operatorname{ch} u \cdot \sin v \cdot \sin w, \tag{35}$$

the equation (34) takes the form $u = u_0$, and $a/b = \tanh u_0$.

We define the final displacement and stress field, which coincides at infinity with the initial field, while at $u = u_0$, the condition $\tau_{uv} = \tau_{uw} = \sigma_u = 0$ is satisfied. We find the following quantities: the stresses σ and τ in the final field ; the differences δu_u, δu_v,

and δu_w between the displacement components in the initial and final fields; the difference ΔE in the energies of the initial and final fields.

In using the results obtained, we will assume that (34) is a model of the focus, and that the final state was produced from the initial state as a result of the earthquake — of the elimination of the stresses at the focus boundary. In this case, the fault plane in the focus will be identical with the circle $y = 0$, $x^2 + z^2 = b^2$ — the major section of the ellipse. The ellipsoid itself is identified with the zone of break-down and plastic flow which, as in the case of a fault, may relieve the shear stresses. At $a = 0$, the ellipsoid (34) reduces to the circle mentioned before. It is desirable to consider all cases for which $0 \leq a \leq b$.

This approach to the problem contains two basic simplifications: first, phenomena associated with permanent set in the focal zone are neglected, in particular the fact that the focal boundary may not be as well-defined; second, it is assumed that the stress field prior to the earthquake is homogeneous, and that after the earthquake, it does not vary beyond the focus. The second simplification is plausible only for earthquakes that are not very strong, and that are not of the surface variety. In addition, there is no physical reason that obliges us to assume that $\sigma_u = 0$ and $u = u_0$. It is not impossible, for example, that the stress σ_u will be redistributed, with a change in the hydrostatic pressure P. There is still no point, in investigating such fine effects, however.

Stresses

The final field defined above has been examined previously [156]. Formulas for these stresses may be obtained directly from the formulas given in [156] after quite simple manipulations.

$$\sigma_u = \frac{p}{h^3}\,\mathrm{sh}\,2u\cdot\sin v\cdot\cos v\cdot\cos w + p\,\frac{C}{h^3}\Big[q\,(T\,\mathrm{sh}\,2u - 2\,\mathrm{ch}\,u) +$$
$$+\Big(\mathrm{ch}^2 u_0 + 1 + \frac{a}{2}\Big)\frac{2}{\mathrm{ch}\,u} - \frac{2\,\mathrm{ch}^2 u_0}{\mathrm{ch}^3 u} + \frac{2}{h^2}\Big(\mathrm{ch}\,u - \frac{\mathrm{ch}^2 u_0}{\mathrm{ch}\,u}\Big)\Big]\sin v\cdot\cos v\cdot\cos w; \quad (36)$$

$$\sigma_v = -\frac{p}{h^3}\,\mathrm{sh}\,2u\cdot\sin v\cdot\cos v\cdot\cos w + p\,\frac{C}{h^3}\Big[-q\,(T\cdot\mathrm{sh}\,2u - 2\,\mathrm{ch}\,u) +$$
$$+\Big(1 - \mathrm{sh}^2 u_0 - \frac{a}{2}\Big)\frac{2}{\mathrm{ch}\,u} + \frac{2}{h^2}\Big(\frac{\mathrm{ch}^2 u_0}{\mathrm{ch}\,u} - \mathrm{ch}\,u\Big)\Big]\cdot\sin v\cdot\cos v\cdot\cos w; \quad (37)$$

$$\sigma_w = \frac{2pC}{h^3}\Big[\frac{1 - a}{\mathrm{ch}\,u} + \frac{\mathrm{ch}^2 u_0}{\mathrm{ch}^3 u}\Big]\cdot\sin v\cdot\cos v\cdot\cos w; \quad (38)$$

$$\tau_{uv} = \frac{p}{h^3}\,(-\mathrm{sh}^2 u + \mathrm{ch}\,2u\cos^2 v)\cos w + p\,\frac{C}{h^3}\Big[q\,(\mathrm{ch}\,u - T\cdot\mathrm{sh}^2 u) -$$
$$- 2\,\mathrm{sh}\,u + \Big(\mathrm{ch}^2 u_0 - \frac{a}{2}\Big)\frac{\mathrm{sh}\,u}{\mathrm{ch}^2 u} + \cos^2 v\,(T\,\mathrm{ch}\,2u - 2\,\mathrm{sh}\,u)q -$$
$$- \cos^2 v\Big(\mathrm{ch}^2 u_0 - \frac{a}{2}\Big)\frac{\mathrm{sh}\,u}{\mathrm{ch}^2 u} + \frac{2\,\mathrm{sh}\,u}{h^2}\,(\mathrm{ch}^2 u - \mathrm{ch}^2 u_0)\Big]\cos w; \quad (39)$$

$$\tau_{vw} = \frac{p}{h}\,\mathrm{sh}\,u\cdot\sin v\cdot\sin w + p\,\frac{C}{h}\Big[qS + \Big(\mathrm{ch}^2 u_0 - \frac{a}{2}\Big)\frac{1}{\mathrm{ch}^2 u}\Big]\sin v\cdot\sin w; \quad (40)$$

$$\tau_{uw} = -\frac{p}{h}\,\mathrm{ch}\,u\cdot\cos v\cdot\sin w + p\,\frac{C}{h}\Big[q\,(\mathrm{th}\,u - T\,\mathrm{ch}\,u) + 2\,\mathrm{sh}\,u\,\frac{\mathrm{ch}^2 u_0}{\mathrm{ch}^2 u}\Big]. \quad (41)$$

Here

$$a = \frac{\lambda + 2\mu}{\lambda + \mu};\quad T = \mathrm{arc\,ctg}\,(\mathrm{sh}\,u);\quad h = +\sqrt{\mathrm{sh}^2 u + \cos^2 v};$$

$$S = T\cdot\mathrm{sh}\,u - 1;\quad q = 3\,\mathrm{sh}^2 u_0 + 1 + \frac{a}{2};\quad C = -\frac{\mathrm{ch}^2 u_0}{N};$$

$$N = q\,(T\,\mathrm{ch}^2 u_0 - \mathrm{sh}\,u_0) - 2\,\mathrm{sh}\,u_0.$$

Fig. 85. Graph for function Q(a/b, α) at α = 1.5.

In Formulas (36)-(41), the terms outside the brackets correspond to the initial field, and the terms within the brackets, to the final field.

The maximum shear stress τ_{max}, according to [156], takes the form

$$\tau_{max} = \tau_{xy}\big|_{\substack{z=b \\ x=y=a}} = \frac{p}{Q\,(a_0,\,\alpha)}. \quad (42)$$

where $Q = N \sinh u_0/\alpha$. Figure 85 shows a graph of the function Q(a/b, α) for α = 1.5 (which corresponds to a Poisson ratio ν = 0.25). It is interesting to note that τ_{max} is always larger than 2p.

Displacements

Determining the displacements with an allowance for conditions at

infinity, we find after basically simple, although cumbersome, calculations

$$\delta u_u = \frac{P}{2\mu} \cdot \frac{C}{h} \cdot A_u \cdot \sin v \cdot \cos v \cdot \cos w; \tag{43}$$

$$\delta u_v = \frac{P}{2\mu} \cdot \frac{C}{h} \cdot (A_v + \overline{A}_v \cos^2 v) \cdot \cos w; \tag{44}$$

$$\delta u_w = \frac{P}{2\mu} \cdot C \cdot A_w \cos v \cdot \sin w; \tag{45}$$

where

$$
\left.
\begin{aligned}
A_u &= -(3\,\mathrm{sh}^2 u_0 + 1)(2S \cdot \mathrm{sh}\, u + T) - \mathrm{sh}\, u \frac{\mathrm{ch}^2 u_0}{\mathrm{ch}^2 u} + \alpha(S \cdot \mathrm{sh}\, u - T), \\
A_v &= \left[-K + \alpha\left(S + \frac{1}{\mathrm{ch}^2 u}\right)\right]\mathrm{ch}\, u, \\
\overline{A}_v &= \left[2K + \alpha\left(S - \frac{1}{\mathrm{ch}^2 u}\right)\right]\mathrm{ch}\, u, \\
A_w &= -K - 2\alpha S.
\end{aligned}
\right\} \tag{46}
$$

In particular, the formulas for the displacements at the focus boundary $u = u_0$, where $u_0 = 0$, and the ellipsoid (34) degenerates into a circle, will take the form

$$\delta u_x = \pm \frac{P}{\mu} \frac{4\alpha}{\pi(2+\alpha)} \sqrt{b^2 - \rho^2}; \tag{47}$$

$$\delta u_y = \frac{P}{\mu} \frac{\alpha - 1}{2 + \alpha} x; \tag{48}$$

$$\delta u_z = 0. \tag{49}$$

Here $\rho = \sqrt{x^2 + z^2}$ is the distance from the center of the circle, and the + and − signs in (47) correspond to displacements upward and downward, respectively, for $y \to 0$; thus, the displacements at the edges of our fault-plane model actually experience faulting. It is clear from (48) that this plane also experiences rotation (which restores static equilibrium after formation of a fault). At great distances, the displacements (43)-(45) are the same as those resulting from the superposition of two static mutually perpendicular dipoles with a moment. This confirms the earlier qualitative conclusion [88] that this superposition of dipoles corresponds to shear and rotation.

It is not clear whether or not this rotation actually occurs,

since equilibrium may be established, at least in part, as a result of permanent set. Its possible effect upon a dynamic focus model is also unclear. All the same, it may be assumed that this has no effect upon the order of the quantities studied here.

Displacements on the boundary of a focus (34) will vary sharply from point to point. We will arbitrarily take as a measure of the shift $\underline{1}$ in the focus the slip δy_y of points $y = a$, $x = z = 0$. We have from (43)-(46)

$$l = \frac{p^3}{\mu} L(u_o, a),$$ (50)

where L is a coefficient connecting a focal dimension with the magnitude of the shift,

$$L(u_o, a) = \frac{ch \, u_o}{-2N}(K + 2aS).$$ (51)

Energy

We shall define the energy diffe ence ΔW of the initial and final fields as the work that must be expended to obtain the initial field from the final field. As far as we know, this method was first used in the similar two-dimension problem of Starr [157].

We note that if we were to compute the energy by the normal method — evaluating the work required to obtain the given field from the un-stressed state — it would turn out that the initial-field energy would be less than that of the final field. This is required formally by the fact that in the final field the displacements at infinity are greater than in the initial field.

We represent ΔW in the form

$$\Delta W = \Delta W_i + \Delta W_e.$$

Here ΔW_i and ΔW_e correspond to regions outside and inside the ellipsoid (34). The magnitude ΔW_i is computed by taking half the work of stresses (32) used for the translations (43)-(45). Separating the fac-

tor $(p^2/\mu)b^3$ in the expressions for ΔW_i and ΔW_e, we obtain

$$\Delta W = \frac{p^2}{\mu} \cdot b^3 \left[R_i(\text{th } u_o, \ \alpha) + R_e(\text{th } u_o, \ \alpha) \right], \qquad (52)$$

where R_i and R_e are coefficients determining the way in which the energy is related with the focal dimensions

$$R_i = \frac{\pi}{-2N} \left\{ -Au \cdot \text{sh } 2u \left(\frac{1}{3} + S \cdot \text{ch}^2 u_o \right) - A_e T \text{ sh } u_o + \right.$$
$$\left. + S(\overline{A}_e \text{ sh}^2 u_o - A_e \text{ sh } 2u_o) + \overline{A}_e \text{ ch } 2u \left(\frac{1}{3} + S \cdot \text{sh}^2 u_o \right) - \frac{1}{3} A_u \text{ ch } u \right\}_{u=u_o}, \quad (53')$$

$$R_e = \frac{2\pi}{3} \text{ th } u_o. \qquad (53'')$$

The quantity R_i is less than R_e, even when the focus model is very nearly a sphere.

At large u_0, when the ellipsoid (34) becomes a sphere, it is difficult to calculate the functions Q, R_i, and N from the formulas given above, since when $u_0 \to \infty$, these functions take the form of exponentially decreasing differences of exponentially increasing quantities. G.I. Pavlova has obtained the following asymptotic formulas:

$$N = \frac{-4 - 5\alpha}{15} \frac{1}{\text{sh } u} + \frac{7\alpha - 4}{105} \frac{1}{\text{sh}^3 u} + \frac{13 - \alpha}{35} \frac{1}{\text{sh}^5 u} + \frac{2 + \alpha}{14} \frac{1}{\text{sh}^7 u} + \dots,$$

$$Q = \frac{-4 - 5\alpha}{15\alpha} + \frac{7\alpha - 4}{105\alpha} \cdot \frac{1}{\text{sh}^2 u} + \frac{13 - \alpha}{35\alpha} \frac{1}{\text{sh}^4 u} + \frac{2 + \alpha}{14\alpha} \frac{1}{\text{sh}^6 u} + \dots,$$

$$K + 2\alpha S = \frac{4 + 10\alpha}{15} \frac{1}{\text{sh}^2 u} + \frac{14 - 8\alpha}{35} \frac{1}{\text{sh}^4 u} - \frac{1 + 2\alpha}{7} \frac{1}{\text{sh}^6 u} + \dots,$$

$$\overline{M} = \frac{16 - 40\alpha}{45} \frac{1}{\text{sh}^4 u} - \frac{32 - 84\alpha}{105} \frac{1}{\text{sh}^6 u} - \frac{4 + 16\alpha}{21} \frac{1}{\text{sh}^8 u} + \frac{196\alpha}{735} \frac{1}{\text{sh}^{10} u} - \frac{4\alpha}{35} \frac{1}{\text{sh}^{12} u} +$$
$$+ \frac{2\alpha}{7} \frac{1}{\text{sh}^{14} u} + \dots,$$

where $\overline{M}$ is the expression in braces on the right side of (53').

Two-Dimensional Problems

The foci of strong surface earthquakes are extended horizontally. In studying them, it is of interest to look at solutions of similar two-dimensional problems. With this case in mind, L. Knopov [124] examined the stress concentration in a plane $\underline{xy}$ with a slit $-b \leq x \leq b$, $y = 0$, with the stresses τ_{yz} acting in the initial field (in the absence of the slit). Using the very elegant and, evidently, very fruit-

ful method of hydrodynamic analogies, he obtained

$$a_s = \frac{p}{\mu} \, Im \, \sqrt{w^2 - b^2},$$ (54)

$$\delta u_s = \frac{p}{\mu} \, (Im \, \sqrt{w^2 - b^2} - y),$$ (55)

$$\Delta_z W = \frac{p^2}{\mu} \cdot b \cdot \frac{\pi}{2}.$$ (56)

Here $\Delta_z W$ is the energy per unit length of the $\underline{z}$ axis, $w = x + iy$ on a plane with a section through the slot $\sqrt{w^2 - b^2}$ for $y = 0$, $x > b$.

Starr [157] considered the stress concentration in the $\underline{xy}$ plane with an elliptical opening

$$\frac{x^2}{b^2} + \frac{y^2}{c^2} = 1,$$

in which the stresses τ_{xy} act in the initial field. Making use of Starr's solution [157] in exactly the same way as we used the Neyber solution previously, and correcting certain inaccuracies in [157],* we are able to obtain, following certain calculations

$$\delta u_u = \frac{pb}{\mu} \frac{e^{2u_0}}{4 \, ch \, u_0} \frac{sh \, 2(u - u_0) + a}{\Delta} \, sin \, 2v,$$ (57)

$$\delta u_v = \frac{pb}{\mu} \frac{e^{2u_0}}{4\Delta^2 ch \, u_0} \cdot \frac{[ch \, 2(u - u_0) + a - 1] \cos 2v + a e^{-2u}}{\Delta}$$ (58)

or

$$\delta u_x = \frac{pb}{\mu} \frac{e^{2u_0}}{4\Delta^2 ch \, u_0} \{[sh \, 2(u - u_0) + a] \sin 2v \cdot \sin v \cdot sh \, u +$$
$$+ [ch \, 2(u - u_0) + a - 1] \cos 2v \cdot \cos v \cdot ch \, u + a e^{-2u} \cdot ch \, u \cdot \cos v\},$$ (59)

$$\delta u_y = \frac{pb}{\mu} \frac{e^{2u_0}}{4\Delta^2 ch \, u_0} \{[sh \, 2(u - u_0) + a] \sin 2v \cdot \cos v \cdot ch \, u -$$
$$- [ch \, 2(u - u_0) + a - 1] \cos 2v \cdot \sin v \cdot sh \, u - a e^{-2u} \cdot \sin v \cdot sh \, u\}.$$ (60)

In addition, according to [157], where $a = 0$

$$\Delta_z W = \frac{p^2}{\mu} \cdot b \frac{a(a-1)}{4}.$$ (61)

Here the coordinates $\underline{u}$, $\underline{v}$ are associated with $\underline{x}$, $\underline{y}$ by the relationships (35) where $w = 0$, so that, as previously, $\tanh u_0 = a/b$.

Calculating the Fault Area and Magnitude of Shift

The formulas obtained above make it possible to formulate the problem: on the basis of the total seismic-wave energy E_0, to find the

displacement at the focus $\underline{l}$, the focal dimensions (with the area of the fault plane $S = \pi b^2$ best taken as a measure of the dimensions), and also to find the change in the stressed state appearing as a result of the earthquake. The basic formulas, which may be of interest from the point of view of interpretation, are as follows:

$$S = \left(\frac{E_0}{n} \frac{\mu}{p^2} \frac{1}{R_S \left(\frac{a}{L} \cdot a \right)} \right)^{2/3},$$ (62)

$$l = \frac{p}{\mu} \sqrt{S} L_S \left(\frac{a}{L}, \alpha \right) = \sqrt[3]{\frac{E_0}{n}} \sqrt[6]{\frac{p^2}{\mu}} L_E \left(\frac{a}{b}, \alpha \right),$$ (63)

$$p l S = \frac{E}{n} \frac{L_B}{R_B}.$$ (64)

$$R_S = \frac{R_i + R_e}{\sqrt{\pi^3}}, \quad L_S = \frac{L}{\sqrt{\pi}}, \quad L_E = \frac{L}{\sqrt{R_i + R_e}}.$$

Here R_S is a coefficient determining the relationship of the energy and the focal area; $\underline{n}$ is the ratio of the total seismic energy E_0 to the total energy ΔW expended upon irreversible processes.

The quantity $\underline{n}$ is clearly substantially greater for earthquakes than for explosions [61]. We shall assume that the irreversible processes absorb all of the energy liberated within the model of the focus — the ellipsoid (34), while the elastic energy liberated outside the focus will go completely into the seismic-wave energy E_0, i.e., we discard the quantity R_e in (62) and (64), and assume that $n = 1$.

We recall that $\underline{p}$ is the mean shear stress prior to the earthquake; μ is the shear modulus; $2a/2b$ is the ratio of the fault-plane diameter to the thickness of the plastic-deformation zone in the section perpendicular to the fault (i.e., the eccentricity of the focus model); S is the fault area; $\underline{l}$ is the magnitude of the slip along the fault in the center of the fault surface; R_i and R_e correspond to the energy liberated inside and outside the focus model (so that where $a = 0$, $R_e = 0$); $p^2/2\mu$ is the mean density for the elastic energy of the shear (tangential) stresses prior to the earthquake.
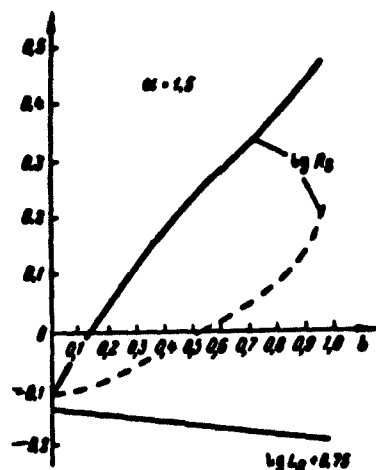
Fig. 86. Graph for the logarithms of the functions R_s and L_s at $\alpha = 1.5$.

Let us consider the problem of choosing the stress values p in the initial field. It was not known earlier what the chief difficulty involved in utilizing formulas (62)-(64) is. It is only possible to state that p is less than the ultimate strength, since it corresponds to the mean stress over a large region.

Benioff [122] evaluated p for the 1952 California earthquake from the formula $E = p^2 HF/2\mu$, where E is the seismic energy; H is the thickness of the earth's crust; F is the area of the aftershock zone. This formula is based upon the assumption that the energy E going into the seismic waves has been accumulated in a zone coinciding with the aftershock zone. He obtained $p = 2.6 \cdot 10^7$ dyne/cm^2. Since the magnitude of E was known for this earthquake ($\sim 5 \cdot 10^{22}$ erg), it is possible to find p from Formula (64). The slip occurred along a fracture 60 km long. Letting H be the depth of the fracture in kilometers, we obtain $S = 6 \cdot H \cdot 10^{11}$ cm^2. Then from Formula (64), where $\mu = 5 \cdot 10^{11}$, H = 15-35 km [122], and a = 0, we obtain $p = (5-9) \cdot 10^7$ dyne/cm^2

Since for this earthquake, the focus was extremely long, it might prove desirable to utilize the formulas for the two-dimensional problems. Assuming in this case that H = 15-35 km, we find from Knopov's Formula (56) that $p = (1.5-3.4) \cdot 10^7$ dyne/cm^2.

We see that the values found for p are of the same order. In the future, we will attempt to use them to study other earthquakes.

The values of the coefficients R_s and L_s are given in Fig. 86 for the case in which $\alpha = 1.5$, corresponding to a Poisson ratio $\nu = 0.25$.

Within reasonable limits ($0.23 \div 0.27$), a change in v has no great effect upon the quantities being determined. The dashed line corresponds to functions in which R_e is neglected.

Using Formula (62) and the graph for R_s, it is possible to find the area of the fault plane S, while from Formula (63) and the graph from L_E or L_s, the slip $\underline{1}$ may be found. In some cases, it is convenient to determine the product plS directly with the aid of (64).

It should be noted that in [122, 123, etc.], the volume of the stress-accumulation region is found from the earthquake energy E with the aid of formulas having the form

$$E = \frac{p^2}{2\mu} V.$$

The quantity V should not be confused with the volume of the model (34). This last may equal zero (where $a = 0$), but the seismic energy E will remain finite in this case. As may be seen from Fig. 86, E is relatively independent of the focus volume. It is basically determined by the fault area, and by the initial stresses $\underline{p}$.

Let us mention still another possible area for the application of Formulas (36) and (41). Using them, it is possible to calculate the effect of an earthquake upon the stress field about the focus. In a small region about (34), the maximum tangential stresses are increased and, consequently, the probability of new earthquakes increases also. This region is naturally identical with the aftershock zone. As is clear from (36)-(41), its linear dimensions are proportional to $\underline{b}$. Moreover, there must be a certain region for which the shear stresses are lowered.

In studying the stresses in the final field, it is of especial importance to allow for nonideal elasticity.

In conclusion, it is of interest to compare Formulas (62), (63)

with data on the probability of earthquakes of various energies. It is known that when the seismic energy E is decreased by a factor of one hundred, the number of earthquakes rises by roughly a factor of ten. In this connection, the contribution of weak earthquakes to the yearly release of seismic energy is very small. When E decreases by a factor of one hundred, however, the total fault area will drop only by a factor of ten and one third, while the total slip, according to (63), may even increase by a factor of ten and one third. Naturally, the fault areas and the slips cannot be added directly in this fashion. These estimates indicate, however, that weak earthquakes may play a substantial role in the formation of major fracture zones, or in dislocations along them.

By making reasonable changes in constants, it is easy to improve the agreement of the calculations cited with empirical data. There is no point to this, however: the indeterminacy in the choice of constants (especially $\underline{n}$ and $\underline{p}$), and the idealization involved in the statement of the problem may lead to large errors. As yet, we cannot do more than state that calculations carried out in accordance with the formulas of this section produce reasonable results, in agreement with data from other methods. This permits us to attempt to utilize the formulas obtained for certain rough estimates.

§2. ESTIMATES OF FOCAL DIMENSIONS ON THE BASIS OF CERTAIN EMPIRICAL LAWS

Despite the rigorousness of the solution to the problem posed, the calculations performed in the preceding section cannot be defended as reliable in view of the large amount of idealization of the earthquake phenomenon itself.

In this connection, it is of interest to find the basic focal characteristics, the linear dimension r_0 and the slip in the focus $\underline{l}$, on the basis of general physical concepts, without getting involved in

- 273 -

complicated calculations, but taking full account of observational data. The results presented below are basically applicable to weak earthquakes, and thus it is weak-earthquake observations that we shall use here.

In all of the findings, it is assumed that the focus is symmetric, and may be represented by a sphere of radius r_0. For weak earthquakes, the spherical-focus supposition is quite acceptable. For strong, destructive earthquakes, where the foci are clearly other than spherical, it is only possible to speak of an arbitrary sphere of radius r_0 equal in volume to the focus.

Energy Evaluation

An energy evaluation of focus dimensions has been employed previously to good effect in calculating the extent of the focal regions for an earthquake of maximum intensity [110, 122, 123, 143, 159, 160]. The method consists in calculating the linear dimension (the radius) of a stressed elastic sphere, which is substituted for the actual focus, sufficient to release an amount of energy upon stress relief to equal numerically the total seismic energy of the earthquake. If we adopt the viewpoint of G.A. Gamburtsev [9, 10], who holds that the intensity of an earthquake is basically determined by the dimensions of the elevated-stress zone, rather than by the stress values themselves, this method for estimating focus dimensions may also be employed for weak earthquakes. The sphere is considered to be ideally elastic, and the earthquake process equivalent to instantaneous relief of a portion of the stresses over the entire volume of the sphere. The total potential energy of elastic strain for such a sphere will equal

$$U_s = \epsilon^2 \frac{\mu V}{2},\qquad(65)$$

where μ is the shear modulus, V is the volume of the sphere, and ϵ is

the strain.

An earthquake occurs when the strains ε in all sections of the sphere reach a certain critical value ε_{krit}. We assume that the earthquake releases only the ωth portion U_0 of the total potential energy U_p, i.e., $U_0 = \omega U_p$, and, in turn, a certain $\underline{n}$th part of U_0 goes into the energy of the elastic waves E_0, so that $E_0 = n\Delta_0$. Then

$$E_0 = \varepsilon_{krit}^2 \frac{\mu V}{2} n\omega. \tag{66}$$

We must now supply the possible ranges of the quantities ε_{krit}, $\underline{n}$, and ω entering into Formula (66).

Judging from data in the literature [110, 122, 123, 143, 158-161], the critical value for the strain ε will evidently lie between 10^{-3} and 10^{-4}.

The coefficient ω, which shows what fraction of the strain energy is released by the earthquake should be less than unity, since in the center of the focus the upper limit will be unity, while on the periphery it should be noticeably less. On the other hand, the nonuniformity of the stress field, and the considerable decrease in the forces of friction at the instant of faulting excludes the possibility of very small values for the coefficient ω. We take the following interval of possible ω values, $\omega = 0.1-0.5$.

The coefficient $\underline{n}$ for the conversion of earth-tremor energy into elastic-wave energy, as before, is assumed to equal $n = 0.1-0.5$.

If we now assume that the quantities ε, ω, and $\underline{n}$ do not range beyond the limits mentioned, the modulus μ will equal $5 \cdot 10^{11}$ dyne/cm^2 [161], and $V = 4\pi r_0^3/3$, and substituting these values into Formula (66), we will obtain the following limits for the focus dimensions r_0 in centimeters, as a function of the total seismic energy E_0 in joules

$$r_0 = (4 \div 30)\sqrt[3]{E_0} \tag{67}$$

Observations, however, may yield not the total seismic energy E_0, but the energy E relative to a reference surface of radius 10 km surrounding the focus (as was assumed in the expedition). In this case, it is necessary to make the following substitution in formula (67). Above (Chapter 4), we have given the relationship between E_0 and E. If we assume that the attenuation of energy density within the reference sphere is proportional to $1/r^4$, this relationship will take the form

$$E_0 = \frac{10^{18}}{r_0^2} E.$$

Substituting the given value of E_0 into Formula (67), we obtain

$$r_0 = (6 \div 20)\, 10^3 \sqrt{E}, \qquad (68)$$

where, as before, r_0 is expressed in centimeters, and E in joules.

Estimate from Wavelength

It is known that the wavelengths, as a rule, depend upon the source dimensions. An increase in the dominant wavelengths of vibrations emitted with increasing dimensions of fractures — fissures, etc. — has been observed experimentally both in laboratory experiments on specimen failure [162, 163], and under natural conditions in the study of shaft pulses [163, 164].

The way in which dominant wavelengths or, in general, vibration form depend upon source dimensions can in many cases also be found from theoretical considerations. In the simplest case, this may be done by examining the solution to the wave equation in the form of the Kirchhoff formula [86]. It follows from this solution that the length of the disturbance at the observation point will equal the time required for the vibrations to propagate through the distributed-source region. In this case, given two sources differing solely in size, the length of the vibrations, and in this connection, the observed periods and vibration wavelengths as well at the corresponding observation

points, will be related as the source dimensions.

An examination of the similar problem for a disturbance due to elastic vibrations of a cavity for an explosion, allowing for radiation [165] also leads to a linear relationship between wavelength and cavity dimensions. The coefficient of proportionality $\underline{m}$ for the cavity diameter and wavelength in this problem depends upon the law governing the variation in pressure with time. Thus, for a sudden application of pressure, we have $m = 3$, while for a pulse, $m = 1-2$. Thus, for this problem, the wavelength obtained is of the order of the explosion-pocket dimension, and rises linearly with it.

V. I. Keylis-Borok [89], investigating sources equivalent to foci, showed that a propagating disturbance contains a damped harmonic oscillation, and that the wavelength of such oscillations is proportional to the dimensions of the source.

In his work, G. I. Gurevich [166] examined the very simple scheme of vibrations appearing in an ideally elastic medium as a result of slip. As is known, this is the main type, and almost the only type, of fracture occurring in earthquakes [88]. Making certain simplifications (two-dimensional case, unbounded ideally conducting medium, instantaneous faulting), Gurevich showed that the wavelength of an observed pulse equals the linear dimension of the region in which stress relief occurred. Where the stress is not relieved instantaneously (duration of the faulting process greater than the period of the observed wave), we will also observe the wave mentioned above, but against the background of a very low-frequency vibration. The wavelength of a basic vibration will remain unchanged in this case, i.e., it will equal the linear dimension of the stress-relief region.

Naturally, Gurevich's scheme is quite idealized. The actual slip process is complicated by inelastic deformations accompanied by a

series of weaker faulting .... but the main phys-

ical import of an earthquake - .... fault surface and

the displacement of masses ....

values — is completely ret.......................

Thus, in first approximation, it may be supposed that the length λ of the emitted wave and the focus dimension r_0 are the same. On the other hand, we assume that the earthquake energy depends solely upon the focus dimensions. Finally, let us make use of the formula (28) obtained above for strong earthquakes, which connects the dominant frequencies f of the seismic vibrations (in the S wave, which bears the maximum energy) with the seismic energy of an earthquake. Let us convert in this formula from the frequency f to the wavelength λ and assume that $\lambda \simeq r_0$. Assuming that the wave propagation rate $V_s = 2.8$ km/sec, we obtain

$$r_0 = 40\sqrt[7]{E},$$ (69)

where r_0 is in meters, and E in joules. This formula also gives the desired focus dimension, obtained from considerations relating to its relationship with the dominant wavelength of seismic waves.

For weak earthquakes (log E joules < 7), this estimate is less reliable than for strong earthquakes, since in the low-energy region in accordance with (28), the observed wavelengths are considerably greater than those obtained by the same relationship for strong earthquakes. High-frequency absorption cannot completely account for this deviation. In order to obtain a more accurate estimate of weak-earthquake focus dimensions, it is necessary to carry out a more detailed investigation of the dominant frequencies of seismic vibrations at minimum hypocentral distances.

Evaluation from Maximum Stresses and Strains

The idea behind this method for estimating focus dimensions, sug-

gested by Yu.V. Riznichenko, consists in the following. A seismic wave is a stress-strain condition of shear or compression, propagating in an elastic medium. The magnitude of the stresses σ and strains ε rises as we approach the focus. By establishing the way in which the quantities σ and ε vary with the hypocentral distance $\underline{r}$, and making a reasonable extrapolation of this function to the region of small $\underline{r}$, we will inevitably be led to the values of $\sigma = \sigma_{krit}$, $\varepsilon = \varepsilon_{krit}$ for which the stress-strain state of the medium will pass through a certain elastic limit or ultimate strength of the material, i.e., we approach the boundary of the focal region from the outside. In the case given, as before, the focal boundary is assumed to be the boundary between the internal region — the focus itself — where faulting and strong plastic and other flows occur in the medium, and the external region where the medium basically behaves elastically, with no faulting or substantial permanent set.

In view of the fact that outside the focus, in the elastic region, there is a one-to-one relationship between σ and ε, the entire discussion to follow can be in terms of one of these quantities, e.g., for the strain ε. In this region, ε and σ are related by Hook's law, with the magnitudes of the elastic constants E and μ determined from the values of the seismic velocities V_P, V_S, and the density. The magnitude of the strain ε at the observation point — at the seismic station — may be found from the seismogram.

For all hypocentral distances $\underline{r}$ that are considerably greater than the observed seismic wavelength λ, which is normally the case for seismic stations, the wave may be considered to be a plane wave. In addition, for the overwhelming majority of earthquakes studied, the vibrations in the maximum-energy and deformation region is approximated by a segment of a sinusoid. For a plane sinusoidal wave

the strain will equal

From which we obtain the

Here the maximum

frequency f are deter

corresponding waves

tion district. We note that

into Formula (70) are the same

mic energy.

As we move away from the focus, ε_{max} will fall off in connection

with the empirically and theoretically established drop in the ampli-

tudes A_{max}, and with the observed, normally far slower, drop in the

frequencies f. The factors responsible for attenuating ε_{max} with dis-

tance are the same as those causing the attenuation of the seismic

energy flux density.

By using earthquake records from several stations lying at dif-

ferent hypocentral distances r, it is possible to establish empirically

a law $\varepsilon(r)$ for the variation in ε_{max} with distance. Constructing such

a function for earthquakes of various energy classes, and extrapolat-

ing it to shorter hypocentral distances, we can find the distances $r =$

$= r_0$, which will differ for earthquakes of different energies, for

which ε reaches the critical value ε_{krit}, i.e., the values correspond-

ing to the ultimate strength. This is the method that we shall use to

estimate focus dimensions.

The legitimacy of extrapolating the observed relationships $\varepsilon(r)$

toward shorter distances is supported by the fact that, as observations
of energy attenuation and, consequently, strain attenuation as well
indicate, these laws, on the average, remain stable over a rather wide
range of distances: from several tens of kilometers to 2 km. There is
no apparent basis for expecting a sharp change in these laws at smaller
hypocentral distances, up to the boundary of the inelastic deformation
region — the focal boundary.

In practice, in order to find the function $\varepsilon(r)$ twenty earthquakes
from each energy class K from $K = 5$ to $K = 10$ were selected, as well
as several earthquakes of greater energies. For all earthquakes, ε_{max}
is determined from the seismograms at each of the stations recording
the earthquakes. To do this, in the maximum-amplitude group, the vib-
ration with the greatest energy is chosen, and the value of ε_{max} is
computed from the measured A_{max} and $\underline{f}$, in accordance with (70). These
quantities are plotted on a graph which has the logarithm of the hypo-
central distance $\underline{r}$ plotted along the axis of abscissas, and log ε for
all earthquakes in each energy class K, from the data of all stations,
plotted along the axis of ordinates.

As an example, Fig. 87 shows the initial data used to plot the
$\varepsilon(r)$ graph for the $K = 6$ and $K = 9$ cases. We see that the "observed"
points lie within a quite restricted band, and in general position,
these points can approximate lines.

For the collection of points corresponding to the various $K = K_1$
($i = 5\text{-}13$), grouping and the method of least squares was used to plot
average lines, satisfying equations in the form log ε = log $\varepsilon_1 - \kappa_1$ log $\underline{r}$
or $\varepsilon = \varepsilon_1 r^{\kappa_1}$, where ε_1, κ_1 = const. Figure 88 shows these lines $\varepsilon = \varepsilon(r)$.
We see that the slopes κ_1 of these lines, at least for weak earthquakes
$K \leq 10$, are nearly the same, and approach $\kappa = 2.4$.

For stronger earthquakes of $K = 11\text{-}13$, the slopes κ decrease no-
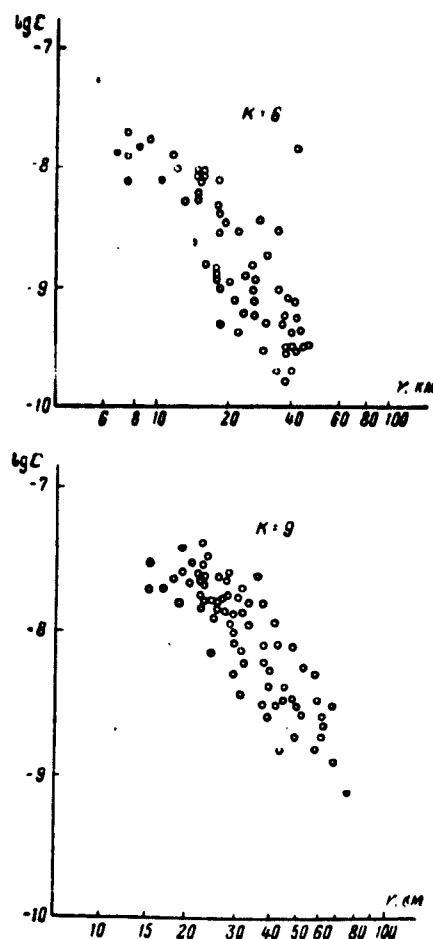
Fig. 87. Maximum strains ε as
a function of hypocentral dis-
tances r̲ for earthquakes in
the energy classes K = 6 and
K = 9.

ticeably. It may be that this is connected with the fact that such
earthquakes are characterized by lower dominant frequencies (of the
order of 1-3 cps), which are strongly attenuated with distance. In ad-
dition, the data obtained for these earthquakes are based upon a small
number of observations, and are thus not completely reliable.

The graphs of Fig. 88, corresponding to earthquakes in the K =
= 5-10 range show, in addition to approximate parallelism of the lines,
approximate equality of the distances between any two neighboring lines
ε(r). In order to determine the focus radius r_0 sought, using the graph

of Fig. 88. it is necessary to plot on it some line $\epsilon = \epsilon_{krit}$ parallel to the horizontal axis. Then the value of r_c for any K_1 should corres- pond to the abscissa of the intersection of this horizontal line and the inclined line $\epsilon(r)$ designated by the given value of $K = K_1$. In view
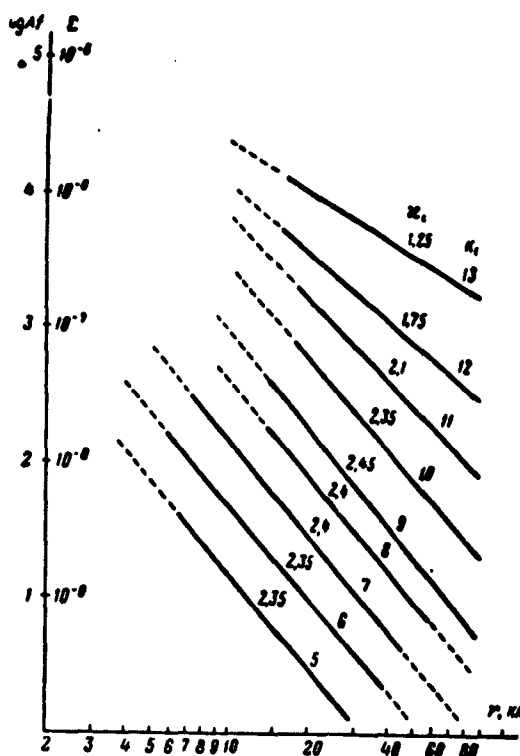
Fig. 88. Average graphs for the max- imum strains ϵ as functions of the hypocentral distances $\underline{r}$ for earth- quakes of various energy classes K. The graphs correspond to the equa- tion $\epsilon = \epsilon_1 r^{K_1}$.

of the fact that the horizontal segments between the lines $\epsilon(r)$ in the coordinate system under consideration are also the same (as is the case for the distances between these lines), we find that the distance r_0 rises as the energy $E = 10^K$ increases, in proportion to some con- stant power of E, and in the given case, roughly as $E^{1/5}$.

In order to carry out a quantitative estimate of the focus dimen- sions r_0, it is necessary to assign a critical value $\epsilon = \epsilon_{krit}$, i.e.,

the strain value for which the elastic state of the medium is noticeably disturbed,and it becomes possible for the continuity of the medium to be destroyed. We note that the choice of different values for ε_{krit} does not change the shape of the function relating the focus dimensions r_0 and energy, but will only increase or decrease the absolute values of r_0 obtained.

It is clear that under natural conditions, the ultimate strength of the rock mass at the sites of foci is noticeably less than the magnitudes determined under laboratory conditions with whole undamaged rock specimens.

Benioff [122], in computing the potential strain energy released during the 1952 earthquake in Kern County (California) estimated the mean elastic strain in the focal region to be $5 \cdot 10^{-5}$. Savarenskiy [86], in evaluating the possibility for the appearance of earthquakes in an elastic-viscous medium, assumed that the critical-strain values ranged from 10^{-4} to 10^{-3}. Kanai and associates [119] using records from several earthquakes to find the strain at the surface of a spherical focus arrived at a value of 10^{-4}. Tsuboi [160], investigating the epicentral zones of Japanese earthquakes occurring in the 1927-1930 period, has shown that the strains do not exceed 10^{-4}. Bath and Benioff [159], studying the series of repeated shocks of the 1952 Kamchatka earthquake, gave a value for the "relieved" elastic strain of $1.2 \cdot 10^{-4}$.

On the basis of these data, we use a strain of $2 \cdot 10^{-4}$ as the critical strain ε_{krit} for our estimate of the focus dimensions. Then the line $\varepsilon = \varepsilon_{krit} = 2 \cdot 10^{-4}$ will intersect the family of average plots $\varepsilon(r)$ of Fig. 88 in points whose abscissas will, in approximation, satisfy the equality

$$r_0 = 10 \sqrt{E \delta \varkappa},$$ (71)

The numerical values for the focus dimensions r_0 corresponding to

- 284

this function are given for various energy classes K of earthquakes in Table 12 (see page 261).

Estimates from Maximum Amplitudes

In this method of estimating focus dimensions, a correlation formula (Chapter 4) is used that connects the maximum amplitude at the observation point A_{max} with the hypocentral distance r and the energy E for the observed earthquake,

$$A_{max} = \frac{10^{5.2} \cdot E^{0.44} \partial x}{r^{3.1} cm}.$$ (72)

Extending this formula to small r and supplying a specific value for the stress σ, we may find the work U carried out to overcome the elastic forces for a translation (pulsation) of A cm of the surface of a sphere of radius r. This work equals roughly $4\pi r^2 \sigma A$. For a focal surface, i.e., for $r = r_0$ and $\sigma = 10^7-10^8$ dyne/cm^2, we obtain

$$U = (10^8 \div 10^9) r_0^2 A.$$ (73)

Since we assume that from the focus surface outward, the deformation is elastic, the work U as a whole will be converted to the energy of elastic waves, i.e., it will equal the seismic energy of the earthquake E_0. We express the magnitude of E_0 in terms of the energy E at the surface of a reference sphere of radius 10 km

$$E_0 \, spz = E \, \partial x \frac{10^{10}}{r_0^2 cm}.$$ (74)

Here as before, we assume that the law governing the energy-density attenuation $\psi(r) = 1/r^4$ holds for all of space outside the focus. Then, replacing the quantity A by its value as found from the correlation Formula (72) in Formula (73), and equating both of the equations of the total energy (73) and (74), we obtain the following equation relating the focal dimensions r_0 (in meters) and the energy E (in joules)

$$r_0 = (3 \div 10) \sqrt[6.3]{E}.$$ (75)

Comparison of Focus Dimensions Obtained from the Various Estimates

Table 12 shows the results of all four estimates. This table gives focus-dimension values as follows: r_0^I, focus dimensions obtained from the critical elastic-energy density per unit volume, Formula (68); r_0^{II}, from the dominant wavelengths λ, Formula (69); r_0^{III}, from the empirical function $\varepsilon(r)$, extrapolated to small $\underline{r}$ all the way to the critical strain values ε, Formula (71); r_0^{IV}, by extrapolating the function $A_{max} = A(r)$ to small $\underline{r}$, all the way to values of r_0 limited by the critical stress value $\sigma = \sigma_{krit}$, Formula (75).

We see that the values of r_0 from estimates based upon basically different assumptions, turn out to agree quite well. In view of the fact that all of these estimates are based upon equally poorly supported assumptions, and that it is difficult to ascribe any overwhelming advantage to any of the assumptions, we may assume that some average of the values of r_0 obtained will be the most probable value. In this connection, the last line of Table 12 gives the arithmetic mean value of r_0 for the values of r_0 found by the different methods for each earthquake energy class K.

TABLE 12

Comparison of Results of Various Estimates of Focus Dimensions r_0 (in Meters) as a Function of the Energy $E = 10^K$ Joules

K	3	4	5	6	7	8	9	10	11	12	13
r_0^I	50	80	130	210	320	520	820	1300	2100	3200	5200
r_0^{II}	110	150	210	290	400	560	780	1100	1500	2100	2900
r_0^{III}	40	60	100	160	250	400	630	1000	1600	2500	4000
r_0^{IV}	30	60	100	180	300	520	870	1600	2700	4900	8200
$\bar{r}_0$	60	90	130	200	320	460	710	1300	2000	3000	3000

We must note that in determining the focus dimensions, each of the estimates carries a somewhat different interpretation of this con-

cept. Thus, for the first estimate, we found the linear dimension of the region in which the major portion of the energy developed during the earthquake was released; for the second estimate, we determined the dimensions of the focus as a radiator; in the third estimate, the region of inelastic deformations was characterized. Despite the fact that we should not expect any great divergence in the dimensions of these volumes, any averaging of the results of these basically different estimates is, naturally, arbitrary.

It follows from Table 12 that the foci for the weakest of the earthquakes considered with $K = 1-4$, have dimensions of the order of tens of meters; the foci of weak earthquakes of $K = 5-10$ are of the order of hundreds of meters, and the foci of perceptible earthquakes of $K = 11-15$ are of the order of several thousands of meters. The data given in the last line of Table 12 may be represented approximately by the following empirical formulas

$$ r_0 = 15 \sqrt[6.3]{E} \quad \text{or} \quad r_0 = 0.27 \sqrt[3]{E_0}, \tag{76} $$

where E is the energy for the reference sphere, E_0 is the total seismic energy.

Extrapolating this function to destructive earthquakes, we obtain a figure of several tens of kilometers, which is in rough agreement with data available on surface faults occurring during strong earthquakes [86, 121, 122, 153, 154]. The problem of faulting during destructive earthquakes, and its connection with energy requires special consideration, however.

Estimating Focal Slip

If we know the way in which focus dimensions depend upon earthquake energy, it is possible to make a rough estimate of the amount of slip in the focus. Here we assume that the elastic strains relieved by

the earthquake lie in the focal region, and that the value of ε for the "relieved" elastic strain, averaged over the entire volume, will equal 10^{-4}. Then, in order to relieve this strain, a displacement in the focus of $\underline{1} = \varepsilon r_0 = 10^{-4} r_0$ is necessary. Substituting the focus-dimension vs. energy function in the form of (76), we obtain

$$l_{cm} = 0.15 \sqrt[3]{E} \ \text{or} \ l_{cm} = 3.7 \cdot 10^{-9} \sqrt[3]{E_e}. \qquad (77)$$

This estimate clearly gives the lower limit of the displacement in the focus, since the volume in which a substantial decrease in elastic strain will occur will be greater than the focus value.

Knowing the lower limit for the slip in the focus, we are able to estimate the amplitude at the focus boundary, i.e., to find the maximum amplitude of the elastic vibrations. To do this, we replace r in formula (72) by the focus dimensions r_0 in the energy function (76); formula (72) relates the maximum amplitude A to the energy E on the reference sphere and the hypocentral distance r. We then obtain a value for the amplitude at the focus boundary as a function of the energy in the form

$$A_{cm} = 0.03 \cdot E^{0.39} \ \partial x. \qquad (78)$$

It is clear that the displacement in the focus will be at least several times greater.

§3. TOWARD A METHOD OF DETERMINING THE DYNAMIC PARAMETERS OF EARTH- QUAKE FOCI

A general description of a method for interpreting seismic observations so as to determine the dynamic parameters of earthquake foci — the orientation of the fault plane and the direction of focal slip — is given in [88, pp. 46-67]; see also [167, 168]. Below, we will describe the features involved in employing this method under the conditions of the Garm region.

For the purposes of interpretation, in this case we made use of

observations from a network of eight stations (Fig. 89) over the period from January 1955 to August 1957. Treatment of the earthquakes was carried out basically from records of four-component azimuth installations of high-sensitivity VEGIK instruments, which had the seismograph axes oriented to the cardinal points of the compass, and inclined at an angle of 45° to the horizon; beginning in July 1956, however, records of normal three-component VEGIK installations were processed.

Practical Interpretation Arrangement

In basic terms, the practical interpretation arrangement reduces to the following. For each station, the sign of the seismic-wave arrivals was determined, as were the directions of the tangents to the rays of these waves at the hypocenter. Stereographic projections of these tangents — arbitrary observation points — were plotted on a Vul'f grid. The sign of the appropriate wave arrival is placed beside each arbitrary point. Next,a system of nodal lines is drawn on the Vul'f grid; these are lines separating regions with different arrival signs. These lines, whose configuration should satisfy certain theoretical conditions, also determine the dynamic parameters of the focus. In particular, the line $y = 0$ at which all waves change sign upon intersection, is the projection of the fault plane; the pole of the line $x = 0$, separating signs of the longitudinal waves only, is the projection of the slip trend (Fig. 90).

In general, it is possible to make use in interpretation of not only the signs, but also the amplitudes of the longitudinal P waves and the two SH and SV transverse-wave components. Under the conditions of the Garm region, not all of this data was determined with sufficient reliability. Thus, we were unable to employ the displacement amplitudes, and could use only their signs; here only the signs of the P and SH waves, which remained constant over their entire path for direct

_ ˙289 _
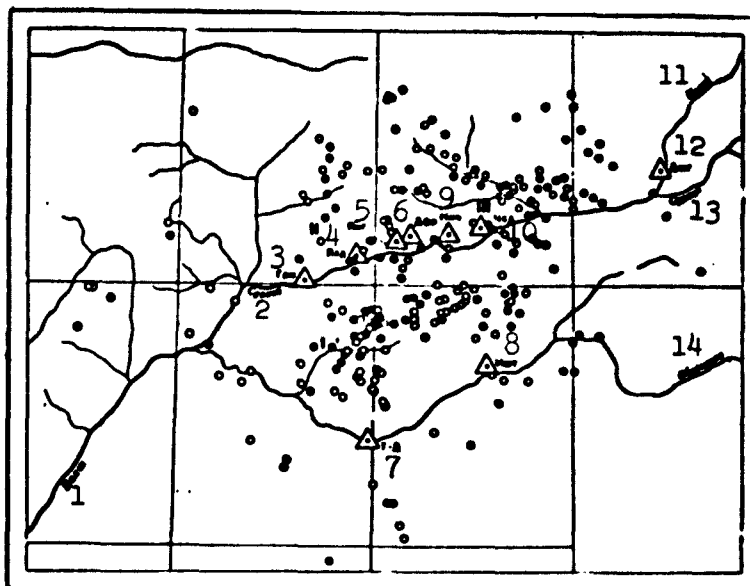
Fig. 89. Map of epicenters for earthquakes in
the Garm district for 1955-1957, for which the
dynamic focus parameters were determined. The
triangles indicate seismic stations; the solid
and open circles show epicenters of earth-
quakes for which the dynamic focus parameters
were or were not determined uniquely, respec-
tively. 1) Vakhsh; 2) Syrkhob; 3) Garm; 4)
Yald.; 5) Yang.; 6) Dfr.; 7) Tovil'-Dora; 8)
Ishtion; 9) Nmch.; 10) Chusal; 11) Koksu; 12)
Dzhail'gan; 13) Surkhob; 14) Obikhinyuu

or refracted waves, as well as for the refracted head waves (possibly
excluding the composite waves). Upon refraction at intermediate bound-
aries, the SV waves may change their sign; this occurs with especial
frequency when the angle of incidence is greater than the critical
angle; thus, we make no use of them.

In addition to the first arrivals (direct or head refracted waves)
it is in principle possible to make use of other waves in the inter-
pretation: reflected waves, various composite waves, etc. Unfortunately,
in the district under consideration, we had almost no success in at-
tempting to isolate waves of this type systematically, although in sub-
sequent arrivals on the records, there are sometimes very distinct
groups of intense and well correlated vibrations.
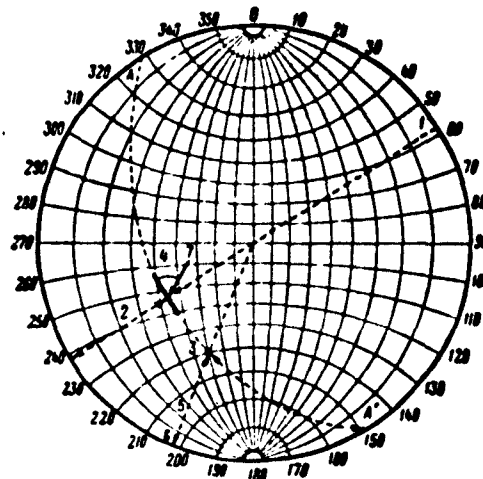
Fig. 90. Representation of dynamic focal parameters on compound stereographic projections. AA') Projection of fault plane; 1) azimuth of fault-plane dip; 2) fault-plane dip angle; 3) stereographic projection of slip direction; 4) angle between slip direction and trend line (measured in dip plane); 5) angle between slip direction and horizontal plane; 6) azimuth of slip direction; 7) arrow from upthrown fault wall (its projection on AA' is directed toward 3).

Thus, in the interpretation, we make use only of the signs of those direct or head refracted P and SH waves that represent first arrivals with respect to the given type of wave.

With the given number and arrangement of stations, it is almost impossible to determine uniquely the type of source (dipole with moment, dipole without moment, simple force, etc.), which acts at the focus. Experience gained in handling earthquakes under other conditions, with a large number of observation points, however, permits us to assume that for all tectonic earthquakes, with very few exceptions, the source will be equivalent to a dipole with moment. We will assume that this is the only type of source to be encountered in the region

- 291 -

under investigation.

Analysis of Observation System: Statement of the Problem

The possibility of uniquely determining the parameters of a previously chosen focus model depends essentially upon the arrangement of the stations with respect to the focus under investigation, and upon the position of the nodal lines. When arbitrary observation points, for example, are located close together on one side of the epicenter it is possible to make a unique determination of the dynamic parameters only for those foci for which the fault plane passes between the arbitrary points. Then all of the foci studied for the given district will have a common fault-plane trend. This will be explained, however, not by the actual predominance of such a trend, but by the fact that for the given station arrangement, other foci cannot be studied owing to the inadequacy of the observations.

In processing observations, and especially in generalizing the results obtained, it is necessary to see whether or not the available observation system limits the possibilities of determining the oriented fault and slip planes in different ways. In the given case, we are concerned with an investigation of such limitations as they apply to the problem of studying earthquakes in the Garm region.

Method of Analysis

The investigation was carried out as follows.

1. For a standard arrangement of the epicenter on a Vul'f grid, the arbitrary observation points were plotted corresponding to the expedition stations and the Central Asia regional station network (it should be kept in mind that the regional stations most frequencly register head refracted P waves as first arrivals; for these waves, the azimuths of the arbitrary points are the reverse of their azimuths at the epicenter).
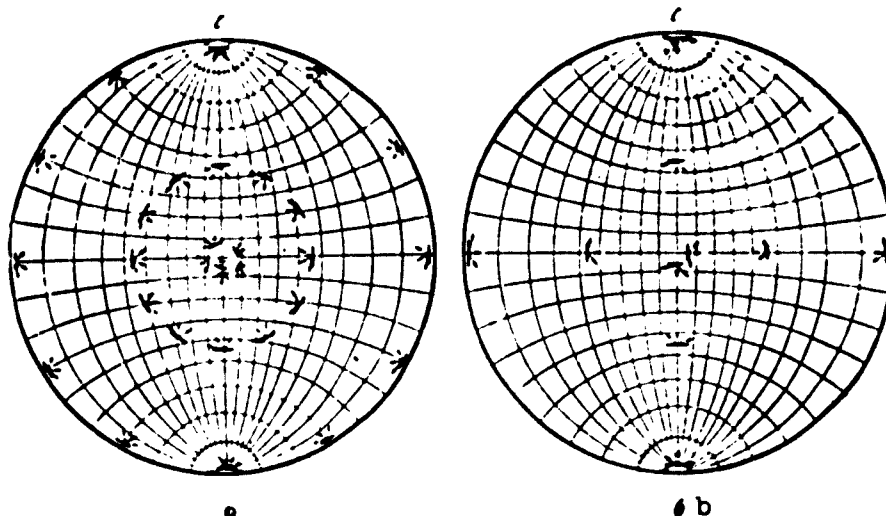
Fig. 91. Variant dynamic focus parameters for which
the possibility of interpretation with the avail-
able observation system was investigated. a) Util-
izing the Garm network and regional stations; b)
using regional stations alone. Given for the cen-
ter of the fault plane (AA' on Fig. 90), for three
possible slip directions.

2. There were 30 possible fault-plane orientation cases, with
three possible slip directions for each case, 90 variants, all-in-all
(Fig. 91).

3. For each of the variants in Fig. 91, nodal lines were plotted,
and the theoretical signs of the P and SH waves were determined at the
arbitrary points.

4. The accuracy and uniqueness of the solution for the converse
problem — the determination of the nodal lines from the given distrib-
ution signs for P and SH — was evaluated. In practice, the given nodal
lines were erased, and the normal interpretation by signs was carried
out again. If the error turned out to be less than $\pm 20°$, it was as-
sumed that the version considered could be determined with the given
observation system.

Such an investigation was carried out for three regions of Fig.
89 in which epicenters were concentrated: I, in the Peter I range; II,

in the Gissar Range, north of Garm; III, in the Khait district. In all cases, the depth of the foci was assumed to be 10 km. The results of the investigations are shown in Fig. 92.

A similar study was carried out by T.I. Kukhtikova for a case in which only regional-station observations were used. These stations were located at greater epicentral distances, and surrounded the district under investigation in more uniform fashion. In this connection,
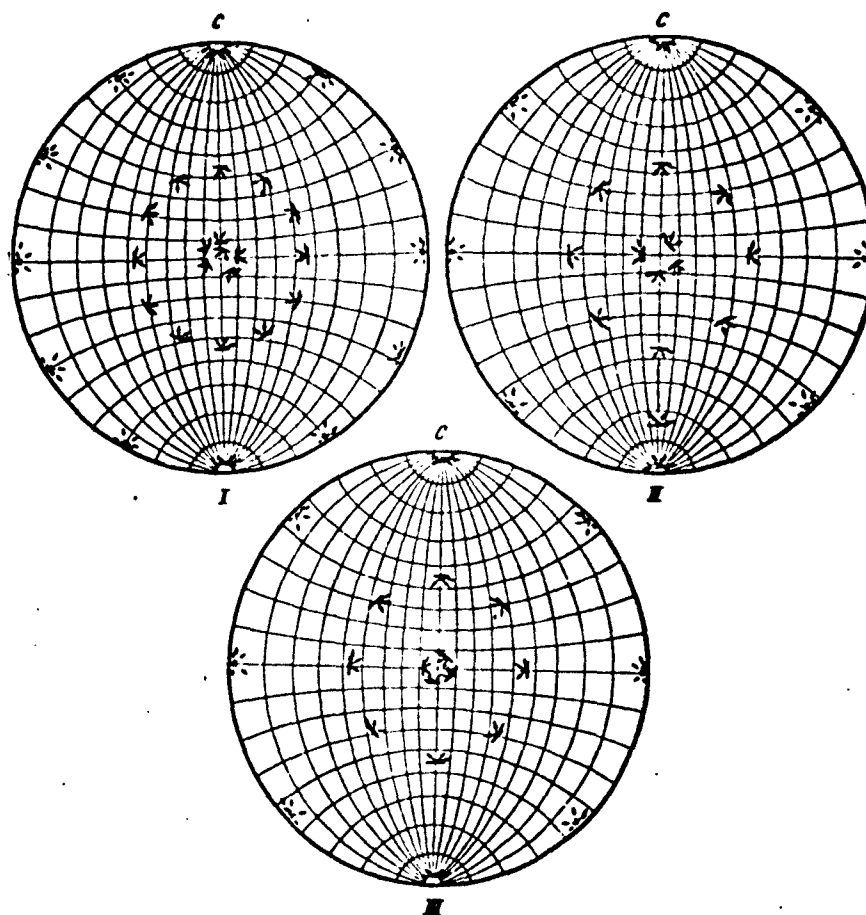
Fig. 92. Summary of dynamic parameters that may be determined from available observation system. Heavy lines indicate versions that may be determined from observations of the Garm TKSE network alone; thin lines show versions determinable from observations of the Garm network and the Central Asia regional stations; the dashed lines indicate versions which cannot be determined from observations of the TKSE and regional stations. a) Epicenter in Peter I range; b) epicenter in Gissar range, north of Garm; c) epicenter in Khait district.

it was sufficient to consider any single epicenter location within the Garm district, and to take into account the 30 variants shown in Fig. 91b. The results obtained are shown in Fig. 93.

Characteristics of Observation System

As a result of the analysis performed, it is possible to draw the following conclusions as to the possibility of studying the dynamic parameters of Garm district foci from the available observation system.
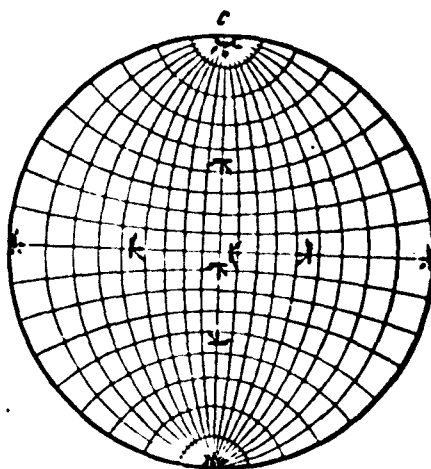
Fig. 93. Summary of dynamic parameters that may be determined from regional-station observations. Solid lines show versions determinable with adequate accuracy; dashed lines show versions that cannot be determined with sufficient accuracy or uniqueness.

In order to investigate group I of foci for the central section of the Peter I range (see Fig. 89), the Garm station network suffices. The region of x-axis emersion — the direction of slip in the focus — is quite well localized in almost all cases. The errors normally do not exceed $\pm 12^o$ for its azimuth, or $\pm 20^o$ for the inclination. The greatest accuracy of determination, up to $\pm 15^o$, is possible for faults with a meridional or north-east trend and a steep dip, exceeding 30°. Faults with a latitudinal or north-east trend and dips greater than 30°

may be found with a large, but permissible error of up to $\pm 22^{\circ}$. Faults with a gentle dip ranging up to 25-30°, cannot be determined with sufficient accuracy, regardless of the trend, but as a rule, the slip direction can be found.

For several of the variants investigated, the solutions did not turn out to be unique; the indeterminacy is easily eliminated by using additional observations from Kulyab station and the southern stations of the Stalinabad network. Treatments of these variants were not encountered in practice.

Partial and very inaccurate determinations of focus parameters for two other sections may be made from observations of the Garm network alone. For the group II foci in the Gissar range north of Garm (see Fig. 89), only faults with meridional and north-west trends and, as before, dips of at least 30° and latitudinal faults with dips from 10° to 20° are determined. Here the north-west observation points are insufficient. Among the group III Khait foci, only faults with northeast trends and dips of at least 30° are well interpreted. Here there are not enough north and north-west observation points. Thus, it is possible, using observations of the Garm network alone, to see whether or not there are faults with some definite orientation in sections II and III, but it is impossible to establish which dips and trends predominate here.

In principle, given good recording equipment, it is possible to study the foci of the entire Garm region from observations of the Central Asia regional stations alone. Experience has shown [169] that the regional stations very clearly record head waves from the subface of the earth's crust for earthquakes in the Garm region. As a rule, it is possible to utilize observations from the stations at Khorog, Murgab, Namangan, Andizhan, Chikment, Naryn, Tashkent, Samarkand, and less fre-

quently, from stations at Fergana, Kulyab, and Stalinabad.

Using records of the P and SH head waves at the majority of these stations, it is possible to obtain quite accurate data on foci having any fault trend, provided that the dip angle is at least 30°. In order to investigate more gently sloping faults, it is necessary to use the direct-wave records at relatively distant stations such as Obi-Garm, Fergana, Kulyab, Kara-Su, etc.

On the whole, the observations of the Garm network alone provide enough information to investigate the dynamic parameters of the foci in the Peter I range zone alone. In order to investigate foci in the entire Garm region, it is necessary to supplement the Garm network so that these stations surround the epicentral sections, or else to utilize observations both from this network and from the regional stations.

At the present time, the regional network records only relatively strong earthquakes from the Garm region, beginning with energy classes $K = 10$ or 11. In this case, however, the use of the records is complicated by the low scanning rate, which makes it difficult to separate the phases in the transverse waves, and also, sometimes, by the inadequate sensitivity of the equipment, which hampers the isolation of longitudinal-wave first arrivals. In order to investigate foci of these earthquakes with the aid of the regional stations, it is necessary to install high-sensitivity equipment, at least at the Obi-Garm, Fergana, Khorog, Murgab stations.

The method discussed in this section for investigating the potential of an observation system may be of interest not only for the Garm region. A similar investigation must be carried out for any large-scale determination of dynamic focal parameters of any district.
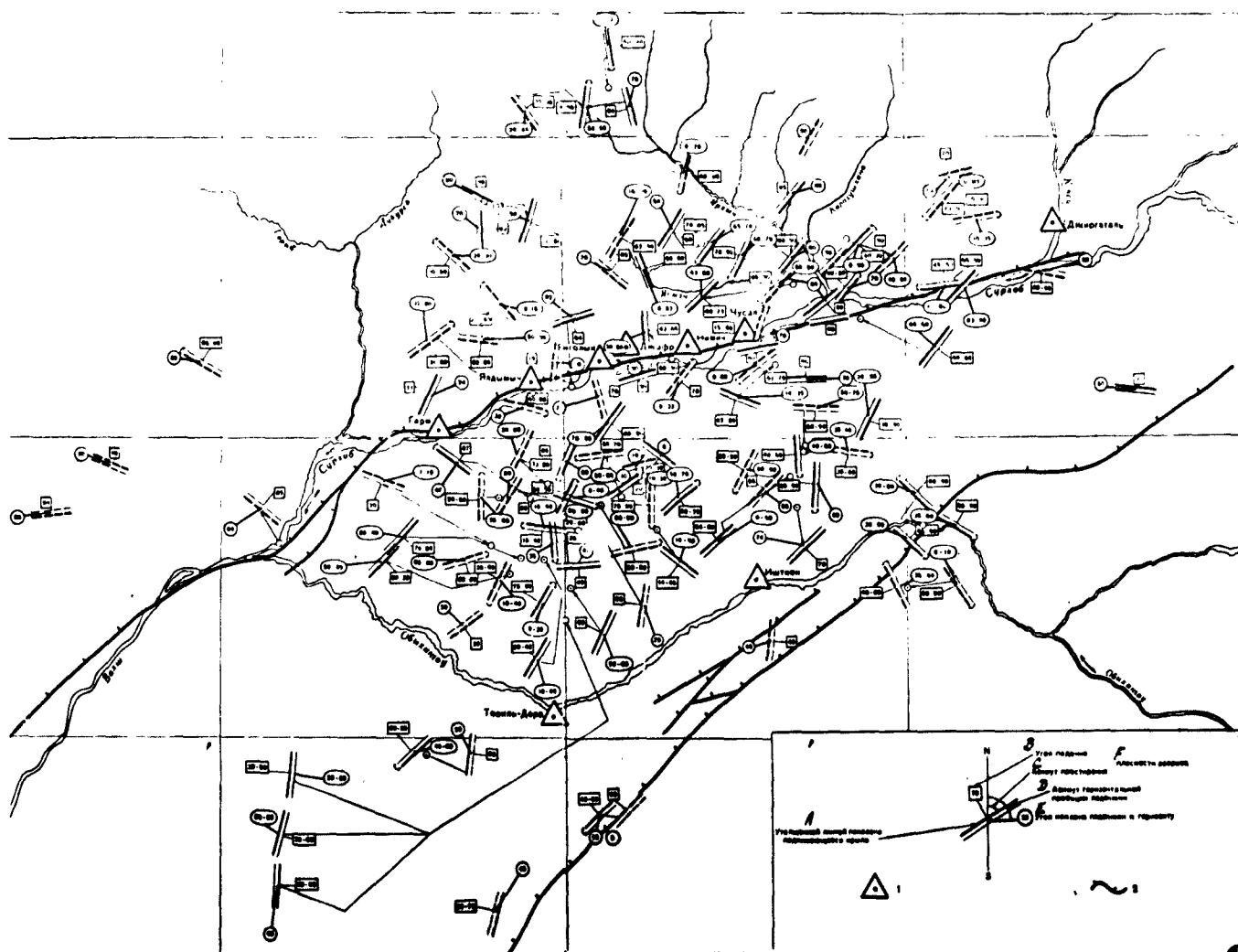
Fig. 94. Dislocation chart for Garm region foci according to data resulting from evaluation of expeditionary observations during January 1955 through August 1957. The dashed lines indicate the foci for which the interpretation is not too reliable. 1) Seismic stations; 2) major faults; A) heavy line shows ascending wing; B) angle of incidence; C) strike azimuth; D) azimuth of horizontal dislocation projection; E) angle of dislocation inclination to horizon; F) discontinuity plane.

- 298 -

§4. DYNAMIC FOCAL PARAMETERS FOR EARTHQUAKES OF THE GARM REGION

Characteristics of Initial Material

Among the observational material from the Garm network, records for earthquakes in the energy classes $K = 7$-9, and for the Peter I range region for the energy class $K = 6$ were examined. Earthquakes of $K = 10$ and higher classes were almost impossible to process, since there is no way of measuring their transverse-wave displacements. All-in-all, 420 earthquakes were examined for the period extending from January 1955 to August 1957. Of this number, 233 earthquakes were selected as suitable for processing (see Fig. 89).

Earthquakes were discarded for which the data was known to be too scanty to permit a unique interpretation, for which it was difficult to establish the nature of the first arrivals for the longitudinal and transverse waves (direct or diffracted) at several stations, and earthquakes for which the nature of the first arrivals was complicated (for example, fine traces prior to the normal wave arrival).

As has been shown before, the observation system utilized is most favorable for studying earthquakes in a section of the Peter I range. Here also, however, there are difficulties. It is possible that for this case, at small epicentral distances, the first arrivals will represent head refracted waves from very fine and, probably, sloping horizons. It is not possible to correlate such waves and establish their nature with accuracy.

A consequence of the difficulties described is the fact that, first, very few of the large number of earthquakes recorded can be interpreted in a well-defined fashion and, second, the earthquakes for which it is possible to determine the dynamic parameters are located irregularly over the area. On the whole, 106 earthquakes were processed in a definite manner, and of these 59 were reliable and 47 not com-

pletely reliable.

Results

The data obtained on dynamic focal parameters of earthquakes are
shown in the form of a map of dislocations on Fig. 94.
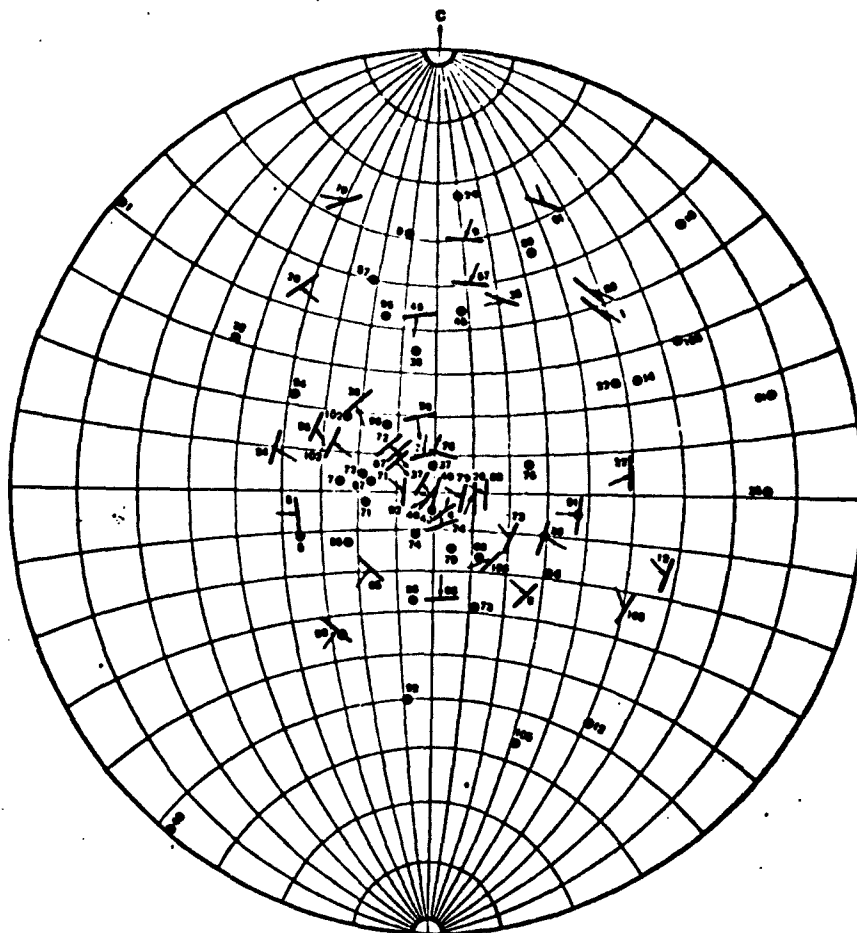
Fig. 95a. Summary of dynamic parameters for earth-
quake foci (Peter I range region) from data of
Fig. 94. (Arbitrary designations the same as for
Fig. 90.)

The dislocations shown on this map are also plotted on the clearer
compound stereographic projection of Fig. 95.

In order to find the general properties of the entire collection
of faults studied in the foci, it is convenient to construct vector
diagrams of the repetition frequencies for the strike azimuths and dip
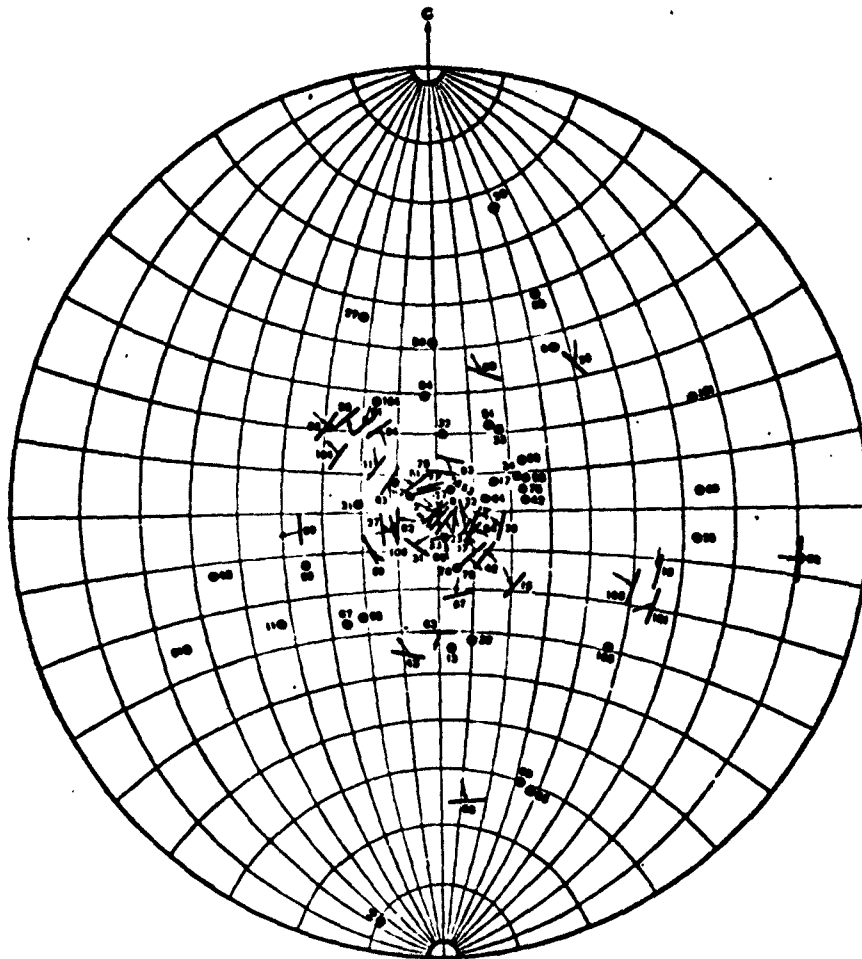
Fig. 95b. Summary of dynamic focal parameters for
earthquakes of the Gissar range region from data
of Fig. 94.

angles of the fault planes.

Figures 96 and 97 also give diagrams constructed from all of the
available reliable materials (Fig. 94 and [88]) for the Garm region as
a whole, and, separately, for the Peter I range section.

We attempted to characterize the general properties of disloca-
tions in the foci studied, first for the entire region as a whole, and
then for the Peter I range section.

Generalized Data for the Garm Region as a Whole

Let us consider the possibility of isolating some of the dominant

fault-plane trend and dip directions, as well as the direction of slip in foci of Garm-region earthquakes.
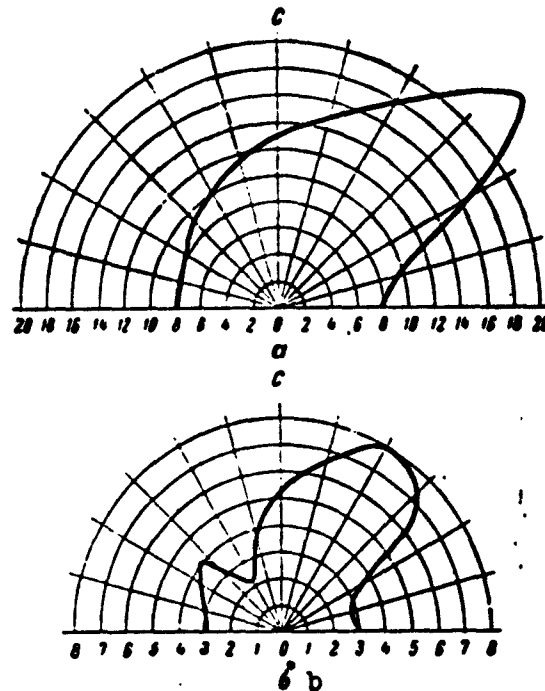
Fig. 96. Vector diagrams of fault-plane trend. a) For entire Garm region; b) for Peter I range region.

1. Dominant trends. Figure 96a clearly shows that trends at 35-45° predominate; they are roughly longitudinal with respect to the trend of the major tectonic structures.

The question arises, however, as to whether or not the irregularity in this diagram is random. Let us first assume that the entire mass of dislocations in the foci of the given region are distributed uniformly over the azimuths, i.e., that any azimuth may be encountered with equal probability, and the vector diagram of the trends for the foci of all earthquakes occurring here over a given period of time will take the form of a circle. We call this assumption the "hypothesis of uniformity." If the hypothesis of uniformity is true, the existence of the maximum on Fig. 96a will be explained as a product of the ran-

dom nature of the process: among the group of foci that could be studied, the majority of foci arbitrarily turned out to have the same definite strike azimuth.

In order to answer the question posed, it is necessary to evaluate the probability that the hypothesis of uniformity is true, and that the observed nonuniformity in the diagram of Fig. 96a, to plot which we selected 122 of the most reliably interpreted foci, appeared as a result of the random choice of the foci to be studied. This probability may be evaluated by using Pearson's χ^2 criterion.
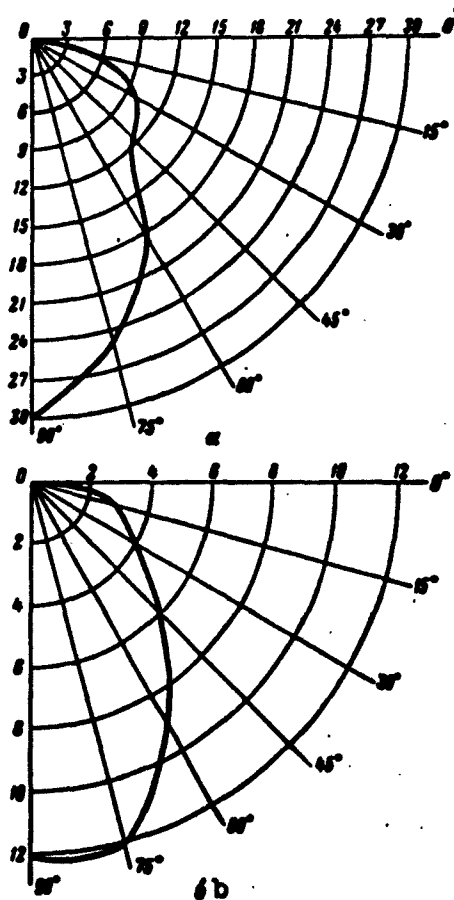
Fig. 97. Vector diagrams of fault-plane dip. a) For entire Garm region; b) for Peter I range region.

In order to do this, we divide the region of strike azimuth varia-

tion A ($0^O < A < 180^O$) into 9 intervals of 20° each. The intervals are numbered in sequence from 1 to 9, and we calculate the quantity

$$\chi^2 = \sum_{i=1}^{m} \frac{\left(v_i - \frac{n}{m}\right)^2}{\frac{n}{m}},$$

where $\underline{n}$ is the number of observations (in our case, n = 122); $\underline{m}$ is the number of intervals mentioned above (in our case, m = 9); v is the number of foci having azimuths falling within an interval with the number $\underline{i}$; n/m is the number of foci which would fall into each of the $\underline{m}$ intervals if the distribution were uniform.

It is easily seen that the magnitude of χ^2 characterizes the uniformity of distribution for the foci studied over the fault-plane strike azimuths. As a matter of fact, for a uniform distribution, $\chi^2 =$ = 0, since all of the v_1 will equal n/m (the number of azimuths in all intervals is the same, and equals the mean value). If all of the azimuths lie in a single interval, then χ^2 will be very large (~1000). In our case, calculations yield $\chi^2 = 30$.

Knowing χ^2 and $\underline{m}$, it is possible, using special tables [170], to find the magnitude of the probability P that the observed, or even larger, nonuniformity in the vector diagram will appear as a result of the random choice of our 122 foci out of the mass of foci distributed uniformly with respect to azimuths. We may interpret P in other terms: P is the probability that the uniformity hypothesis is correct or, more accurately, that if this hypothesis holds, the nonuniformity in the vector diagram will correspond to that shown in Fig. 96a, or be even greater.

We find from the table given in [170] that for $\chi^2 > 26.125$, the value of P is less than 0.1%, i.e., is very small. Consequently, the hypothesis of strike-azimuth distribution uniformity is extremely im-

probable, and the longitudinal trend noted in **Fig.** 96a actually does predominate in the foci. This conclusion is even better grounded owing to the fact that the observation system for weak earthquakes was, as a whole, unfavorable to the detection of longitudinal trends.

In earlier earthquake studies for this region, longitudinal trends were also found on the vector diagrams. The application of the χ^2 criterion to these diagrams does not contradict the hypothesis of uniformity (P turns out to be of the order of 30%). This, naturally, does not mean that faults with transverse trends do not exist: it is quite evident from the maps (Fig. 94 and [88], pp. 86, 87]), that they are very numerous. The question, however, as to what degree the transverse faults may be assumed to predominate remains open, pending the accumulation of additional material.

2. Dominant dips. On Fig. 97a, steep dips of $70\text{-}90^{\circ}$ clearly predominate. Application of the χ^2 criterion shows that the probability for the uniformity hypothesis in the dip-angle interval from 30° to 90° is less than 1%, so that steep dips actually do predominate in this range. According to §3, however, faults having dips of up to 30° are difficult to observe with the observation system in use, so that there may be a second maximum in the 0 to 30° range on Fig. 97a. Judging from the data of [169], however, this is quite improbable.

3. Dominant slip directions (Fig. 94). In separate sections, certain slip directions are noted to predominate; in neighboring grouns of foci, similar directions are observed. It is still difficult, however, to obtain more definite answers.

Generalized Data for Peter I Range Region

The dominant fault-plane strikes in this region, as is clear from Fig. 96b, have azimuths of $20\text{-}50^{\circ}$, differing somewhat from the trend of the range. The χ^2 criterion yields a value $P < 7\%$ for them, so that

- 305 .

these strikes actually do predominate. The maximum in the 300-320° azimuth range is so slight that we need not consider it important. As to the fault-plane dips and the slip directions, we can only repeat what we have already said with respect to the region as a whole.

General Comments on the Determination of Dynamic Focal Parameters for Earthquakes in the Garm Region

Let us briefly list the basic features and results of the determinations discussed in §3 and 4.

From the experience gained in processing data from the Garm region, it was found and shown that for large-scale research into dynamic focal parameters of any region, it is necessary to make a special investigation as to whether or not the available observation system permits a determination of all possible orientations of faults and slip directions. Under unfavorable conditions, entire fault systems may go undiscovered, and observed regularities may prove to be fictitious.

It was found that in utilizing the single Garm station network of the expedition, it was desirable for the Garm region to make a complete study of foci only for the Peter I range section, and for the remaining sections, to study only the slip directions. For a more complete study of Garm region foci, it was necessary to utilize observations from the regional system of stations.

For the Garm region as a whole, dominant faults were found with trends ranging from 30 to 60°, roughly parallel to the trend of the major structures, and with dips that were steep, lying in the 70-90° range. The available material was insufficient, however, to permit a judgment as to the number of gently dipping faults in the 0-30° range. The region also displayed faults with transverse trends, but there is still not enough data to permit a reliable judgment of their relative

number.

In the Peter I range, the dominant fault trend in the foci differed only slightly, by roughly 20-30°, from the general trend of the range and of the tectonic structures.

Manu- script Page No.	[Footnote]
244	Starr allowed for the conditions at infinity for the stresses alone, complicating the direct employment of his formulas for displacements.

[List of Transliterated Symbols]

238	sh = sinh th = tanh ch = cosh
249	п = p = polnyy = total
250	крит = krit = kriticheskiy = critical
260	эрг = erg дж = joules
268	C = S = Severnyy = North
269	ТКСЕ = TKSE = Tadzhik Integrated Seismological Expedition

Chapter 7

SEISMIC REGIME

By the seismic regime of any region, we mean the totality of earthquakes for this region, considered in space and in time [171].

At the beginning of this chapter, we discuss general questions of seismic-regime investigation, indicate the basic characteristics and parameters of a seismic regime, and consider methods for treating and representing seismic-regime material. Next, materials are given dealing with the basic features of the average state and time variation in the seismic regime for the Garm and Stalinabad districts.

Problems dealing with the spatial arrangement of foci in the region under investigation (sections and maps of epicenters, seismic-activity maps), although relating to the seismic regime, are of independent interest. They are considered separately in a special chapter (Chapter 9), where district seismicity characteristics are given in relation with the tectonics of the district.

§1. STATE OF THE PROBLEM

Seismologists are interested in space-time relationships among earthquakes. Repeated attempts have been made to find definite regularities for these complex and intricate relationships. Discovery of such regularities would be extremely helpful in perfecting methods for studying seismicity and defining seismic districts, as well as in seeking methods for predicting intense earthquakes.

In view of the complexity and variety of these relationships, and in connection with the large number of factors upon which they depend,

the problem of studying them in great measure acquires a statistical character. Naturally, this problem should not be limited just to the formal aspect, to the sorting of observational material and superficial comparison of phenomena; the task should also include the establishment of causal connections among earthquakes themselves, and among earthquakes and other phenomena. The establishment of empirical relationships in this little-investigated field is also of great interest, however. Two main trends may be arbitrarily distinguished in the examination of groups cf earthquakes: 1) the study of the temporal course of seismic activity and 2) the study of long-term mean seismicity indices.

The Study of Seismicity Variation in Time

There are numerous studies of seismic statistics and seismic geology where seismicity and its connection with other factors (time of the year, lunar phase, etc.), as well as with geological structure are chiefly examined descriptively [64, 158, 172-186, 187, etc.]. Far fewer studies deal quantitatively with general laws characteristic of a group of earthquakes [107, 188-198].

Among the studies of the latter type, which present the greatest interest to us, we should take note, primarily, of the work of Benioff, who studied several problems dealing with the accumulation and relief of stresses and strains in connection with variations in total earthquake energy with time. In his papers [188, 190] this question is considered with respect to aftershocks of several severe earthquakes, while in papers [191, 192], it is discussed in the light of the most severe earthquakes occurring in the world over the past several decades. The last two articles deal with the alternation of periods of relatively intense and relatively light seismic activity.

Studies basically of a descriptive nature [158, 178-183] also men-

tion many observed facts dealing with the variation in seismic activity for several regions over relatively long periods of time (chiefly decades and centuries).

Detailed instrument observations of seismic-shock sequences in time have been carried out in the USSR by several expeditions; here seismic stations located in the epicentral zones were used to record local earthquakes [1, 4, 199-202, etc.], as well as the regional station network in the Caucasus and North Tien-Shan [203]. Here, no firm connections between sequences of weak seismic shocks and subsequent violent earthquakes were found. Seismic observations were also carried out in studying processes associated with mine shocks, which to a certain degree are similar to tectonic earthquakes [163]. It was found for mine shocks that they normally appear against a general background of increased activity of weaker shocks, but that directly before a major shock, a period of relative calm is observed in the majority of cases. These mine investigations were accompanied by laboratory studies of rock specimens and other materials in accordance with a program similar to that used for detailed field investigations of earthquakes: investigations were made of the sequence of shocks appearing at various stages in the process of specimen destruction by pressure; the shock repetition rate per unit time was determined, as well as the relative energy; the frequency spectra of seismic vibrations were studied [162].

All of these investigations into the temporal variation of seismic properties in which attention is concentrated on the continuous temporal variation in the regime are quite naturally supplemented by investigations into average characteristics that vary relatively little over "long" time intervals.

Study of the Laws of Long-Term Average Seismicity

In this area, there is one very important fact relating to the general properties of a group of earthquakes. It has long been known that, on the average, weaker earthquakes occur more often than stronger earthquakes. Gutenberg and Richter [64] confirmed this fact by a quantitative investigation that made use of statistics for all intense earthquakes occurring in the world for several decades. They plotted graphs of $N(M)$ showing the distribution of the number N for the mean frequency of repetition or recurrence* (i.e., the number in unit time, for example, in a year) of earthquakes in specific magnitude classes M and the depth of focus as functions of the magnitude M itself, which may be connected in a specific way with the magnitude of the seismic energy E at the earthquake focus. They call these graphs "characteristic seismicity curves," although seismicity is normally a much broader concept (this rather unfortunate name for the graphs $N(M)$ is also encountered in the Soviet literature; see, for example, [86], page 32). In the future, we shall here speak of earthquake-recurrence graphs; we shall have in mind their "energy" form $N(E)$, rather than the "magnitude" form $N(M)$.

It was found that when the earthquake recurrence distribution with respect to energy $N(E)$ over several years is represented in a log E, log N coordinate system, the distribution takes the form of a set of points which cluster quite densely, although with a known dispersion, along certain curves, which approximate straight lines over a broad energy range. For shallow-focus earthquakes with foci within the earth's crust, the slope of the curve in the roughly straight-line portion of the graph is $\gamma = -\Delta \log N / \Delta \log E = 0.45$; for intermediate and deep earthquakes, the slopes are close to this value. It is only in the region of maximum earthquake-energy classes that the slopes of the

curves increase noticeably.

V. I. Bune [107, 198] obtained curves of N(E) with roughly the same slopes in the approximately linear sections for moderate and intense earthquakes in several regions of the Tadzhik SSR, using materials from the regional seismic-station network over a 25-year period; for especially strong earthquakes, he also used data not obtained by instruments, for a longer period of time. Kawasumi studied similar relationships in Japan [193, 194].

A theoretical discussion of the question of earthquake recurrence, and many other important statistically oriented problems in the physics of earthquakes are given in the interesting paper of Housner [121]. An examination of strong-earthquake recurrence disregarding energy distribution, and an unsuccessful attempt to construct a statistical prediction method are given in [204]. A statistical examination of earthquake aftershocks is given in [205-209] and several other papers. A survey of the literature and a large bibliography dealing with questions of earthquake statistics are given in the article of Aki [209].

Particularly broad-scale seismic observations in the USSR were undertaken in 1959, under the general leadership of Academician G.A. Gamburtsev [4, 48, 82, 16-18, 200-203, 210-212]. The TKSE investigations, begun under his direct supervision and continued by his students represent a further development of work in this direction. A brief exposition of the results obtained by this expedition in studying the seismic regime in the Garm and Stalinabad districts of the Tadzhik SSR during the 1955-1957 period has been published in [171]. Associated problems were also dealt with in several other articles [213-216]. Below we give a more detailed exposition of problems relating strictly to the seismic regime. Prior to the discussion of the actual material, we will present some of the general ideas and definitions.

§2. GENERAL REPRESENTATION OF SEISMIC REGIME AND ITS CHIEF CHARACTERISTICS

The main, and at the same time simplest, geometric (or kinematic) characteristics of the focus for each separate earthquake are the hypocenter coordinates $\underline{x}$, $\underline{y}$, $\underline{z}$ and the time t_0 at which the earthquake appears.

The chief dynamic characteristic of an earthquake is its seismic energy E, i.e., the energy of the seismic waves leaving the focal region. The set of the five quantities (x, y, z, t, E) gives the simplest quantitative physical description of each individual $\underline{i}$th earthquake with respect to its focus. In this sense, each $\underline{i}$th earthquake may conventionally be represented by a five-dimensional magnitude. In the five-dimensional space Π_5 with measurements of $\underline{x}$, $\underline{y}$, $\underline{z}$, $\underline{t}$, and E, each earthquake may be represented by a point with appropriate coordinates $(x, y, z, t, E)_i$.

It would also be possible to use other quantities, forming a larger or smaller set, to characterize each individual earthquake; thus, for example, it would be possible to add to the five quantities mentioned several other magnitudes determining the dynamic focal parameters, its spectral characteristic, etc.

On the other hand, it is possible to exclude some of the five quantities mentioned in individual cases, for example, the energy E or the focal depth $\underline{z}$. But, for the sake of concreteness, we will assume that we are dealing with a space $\Pi = \Pi_5$ in the sense indicated.

In the space Π, the seismic regime will clearly be represented by the set of all points representing individual earthquakes. These points are discontinuous in the given space; there are open intervals between them.

The problem of studying the seismic regime is now reduced to clarifying the features of this point distribution in the space Π, and to

establishing the laws to which this distribution conforms. This analysis may be carried out either by direct examination of the discrete points themselves $(x, y, z, t, E)_i$ or, more conveniently, by way of certain intermediate functions of the continuous arguments $\underline{x}$, $\underline{y}$, $\underline{z}$, $\underline{t}$, E — the coordinates of the space Π — functions which give the general distribution curve for the points $(x, y, z, t, E)_i$.

Earthquake Density

The most complete characterization of the seismic regime, which reflects directly in generalized form a general representation of the regime as a set of points in the space Π_5, is the density N_* of earthquakes in this space, i.e., the distribution density for the number of earthquake "points" in the physical space $\underline{x}$, $\underline{y}$, $\underline{z}$ in time $\underline{t}$ with respect to energy E. The density $N_* = n/\Delta\Pi$, where $\Delta\Pi$ is some elementary "volume" of the space Π, and $\underline{n}$ is the number of earthquake points falling within this elementary volume. The calculated density values of N_* are ascribed to the centers of the these volumes. In the future, we shall assume by convention that the quantity N_* varies smoothly as a function of the points in the space Π, taking the numerical values in the centers of the volumes $\Delta\Pi$. Thus, the representation of the quantity N_* is smoothed. There are methods for calculating the points and smoothing: the use of partially overlapping or sliding volume elements $\Delta\Pi$ having sharp boundaries (in the one-dimensional case — the sliding-interval method); the method that uses sliding volumes $\Delta\Pi$ with "diffuse" boundaries. The choice of a particular method for calculating the earthquake density N_* should be made on the basis of the actual conditions involved in the geophysical problem of investigating a given set of earthquakes. In particular, in establishing the dimensions and shape of the $\Delta\Pi$ volumes in the physical space $\underline{x}$, $\underline{y}$, $\underline{z}$, it is necessary to allow for the geological and geophysical conditions in the investi-

gated district: the trend direction and dimensions of the tectonic structures of major folded features, deep-fracture zones, etc., the shape and position of earthquake focal zones, etc.

Earthquake Recurrence

The earthquake recurrence N in a specific energy-variation interval in a specific spatial volume $\underline{x}$, $\underline{y}$, $\underline{z}$ is directly connected with the earthquake density N_* in Π_5. If Δt is a unit time interval, the relationship will take this form: $N = \int_\Omega N_* dx \cdot dy \cdot dz \cdot dE$, where the region of integration Ω extends over the given spatial volume $\underline{x}$, $\underline{y}$, $\underline{z}$ and the energy-variation interval E of the earthquakes. The recurrence N thus determined represents an average for the given time interval $\Delta t = 1$.

We let ω be the volume of the entire region Ω in the space $\underline{x}$, $\underline{y}$, $\underline{z}$, E. We then find $N = \overline{N}_* \omega$, where $\overline{N}_*$ is the mean density N_* in this volume. If the region of the physical space $\underline{x}$, $\underline{y}$, $\underline{z}$ and the energy-variation range E is fixed, then the mean density $\overline{N}_*$ for the earthquakes, and their recurrent N, will differ only by a constant factor $\omega = \text{const}$, which will have the dimensions of L^3E.

For a fixed spatial region $\underline{x}$, $\underline{y}$, $\underline{z}$ and various "classes" ΔE of energy E, to each energy class $E = E_i$ [where E_i is some mean energy value within the range ΔE (normally at the central point of the interval on the E axis, with the values of E plotted in a logarithmic scale)] there corresponds a particular recurrence value $N = N_i$, so that $N = N(E)$. This is essentially the same earthquake-recurrence vs. energy relationship studied by Gutenberg and Richter [64, 186], Kawasumi [193, 194], Bune [107, 198], etc.

In place of the recurrence N itself, which is not normalized with respect to a specific area or depth, i.e., with respect to the volume of the region in which the foci are located, it is more convenient in such cases to consider the density N* for recurrence, or the normalized

- 315 .

recurrence, which equals the distribution density for the number of earthquakes in Π_5, per unit element $\Delta\Pi$ of this space, defined by the unit intervals Δx, Δy, Δz, Δt, and the given energy class E. In future, for the sake of brevity, we shall call this simply the <u>recurrence</u>, adding the term "normalized" where necessary.

Going from the nonnormalized recurrence magnitudes to the normalized N*, we make no change in the slope γ of the recurrence distribution curve with respect to earthquake energies, which is plotted in a double logarithmic coordinate system; at the same time, we are now able to compare the seismic activities of the regions, which are determined by the absolute values of the numbers N*.

Recurrence Graph and Recurrence Parameters A and γ

In plotting the recurrence graph, we refer the number of earthquakes to the selected energy-logarithm range, ascribing this number N_K to the geometric center of the interval E_K. For energy-value intervals E'_K, the ordinate N'_K refers to the energy interval having the same width, but with center at point E'_K.

It is necessary to emphasize that in the entire discussion we are speaking of logarithmically equivalent energy intervals: $\Delta \log E = $ $ = $ const. In seismology, as a rule, $\Delta \log E = 1$ and N_K equals the number of earthquakes with energies lying in the range $\log E_K \pm 0.5$. Any other choice of constants will lead to a decrease in the level of the curve N(E). At the same time, any other method of selecting the energy intervals (for example, $\Delta E = $ const), equivalent to classifying earthquakes by some other dynamic parameter -- by the magnitude M, amplitude A, etc. -- will lead to a decrease in the values of γ.

Experience gained in earthquake studies has shown that within the energy-variation range under study, the angular coefficient $\gamma = $ $ = -\Delta \log N^* / \Delta \log E$ is constant.

The lower limit of energy E for which linear interpolation is possible coincides in practice with the minimum energy of those "representative" earthquakes which can be treated completely with the available observation system. The upper limit for E is more difficult to determine, owing to the infrequency of severe earthquakes. It is sometimes indicated by a bend in the curve $N^*(E)$ observed in this region, but most frequently, we simply break off the straight-line curve $N^*(E)$ at some maximum earthquake energy observed in the given district or neighboring districts having similar geological and geophysical conditions. Allowing for these limitations, we may use each $N^*(E)$ curve to determine two quantities: the recurrence value $N^*_{K^{(0)}}$, for each fixed class $K = K^{(0)}$ of earthquake energy, which is best chosen within a region for which the recurrence curve $N^*(E)$ is clearly linear, and the parameter γ.

If the slopes γ of curves $N^*(E)$ for various sections of some spatial region $\underline{x}$, $\underline{y}$, $\underline{z}$ are nearly the same (this is true of the overwhelming majority of sections in the district with which the expedition worked), then in order to compare the characteristics of the mean seismic activities for these regions, it is sufficient to compare the appropriate numbers $A = N^*_{K^{(0)}}$ for the fixed class $K = K^{(0)}$ of earthquake energy. The number $A = N^*_{K^{(0)}}$ which under our conditions represents a general index to the level of seismic activity, or a measure of the seismic activity in the region under consideration, will be called, for the sake of brevity, the "activity."

In practice, it is convenient to determine the activity A for a sufficiently representative earthquake-energy class $K^{(0)}$, i.e., for a class that is sufficiently numerous, and sufficiently free from the influence of station-network arrangement. In this case, the quantity A is determined from the earthquake recurrence not only for the class

$K^{(0)}$, but also with an allowance for other classes, utilizing the average line for the recurrence graph, on its straight-line portion.

We may provisionally compare the seismic activities A of regions even in the case in which the slopes γ of the curves $N^*(E)$ are not the same; here, however, these regions should be characterized by the values of both parameters A and γ, since the ratio of activities will depend upon the choice of the fixed class $K^{(0)}$.

In the general case, the seismic activity A should be referred to some volume in the physical space, $\Delta x \cdot \Delta y \cdot \Delta z$. In this sense, it is possible to speak of the volume seismic activity. But in many cases, where there is no need to consider the way in which A depends upon depth, all earthquake foci can be, as it were, placed in the horizontal plane $\underline{x}$, $\underline{y}$, and the activity A will then refer to a certain area on this plane. In such cases, it is possible to speak, conventionally, of the surface seismic activity.

Under the conditions prevailing in the Garm and Stalinabad districts, where there is a relatively dense network of high-sensitivity stations, and a quite high seismic activity is observed, it is convenient to take as the unit of seismic activity the recurrence $N^*_{K^{(0)}}$ of earthquakes, equal to one class 7 earthquake ($K^{(0)} = 7$) of energy $E = 10^{7\pm0.5}$ joules per year in a volume of $10 \times 10 \times 10$ km^3 for the volume surface activity, and an area $S = 10 \times 10 = 100$ km^2 for the surface activity. We call this unit A_7 (the subscript corresponding to $K = 7$). In view of the fact that in these districts, the zones in which the majority of foci are located at a depth $\underline{z}$ amount to about 10 km, the numbers $A = A_7$ nearly coincide for the volume and surface seismic activity. In this case, clearly, there is no point in specifying at every occurrence precisely which activity we are speaking of, the volume activity or the surface activity. This is necessary, how-

ever, where the earthquake foci range over a broad depth interval, and their depth distribution cannot be excluded from consideration.

In districts having a more tenuous station network provided with the same equipment, for which earthquakes of energy class seven cease to be representative, it is more convenient to select an activity unit that is constructed in accordance with the same general principle as A_7, but which refers to some higher class that is more representative under these conditions. At the same time, it is sensible to increase the reference volume or area. Letting the superscripts (1) indicate quantities in the "old" activity unit, and the superscripts (2) in the "new" unit, it is possible to write the following formula for the relationship between these units

$$\frac{A^{(2)}}{A^{(1)}} = \frac{S_1}{S_2} 10^{\gamma (K^{(2)} - K^{(1)})}. \tag{79}$$

This formula, naturally, may also be employed to construct new activity units applicable to more detailed observations.

Where less detailed observations are available, it is possible to propose the unit of seismic activity A_{10}, which represents a mean earthquake recurrence equal to one class ten earthquake of energy $E = = 10^{10 \pm 0.5}$ joules per year in a volume of 10^4 km^3 for the volume seismic activity, and for an area $S = 1000$ km^2 for the surface activity. Substituting the values adopted for A_7 and A_{10} into the preceding formula and assuming that $\gamma = 0.43$, we obtain $A^{(2)}/A^{(1)} = 1.95$, i.e., the unit A_{10} is roughly twice as large as the A_7 unit. Accordingly, the activity of exactly the same district for which $\gamma = 0.43$ will be expressed in A_{10} units by numbers half as large as those in A_7 units.

The quantity $A = A(x, y, z)$ may be used to construct maps (in the $\underline{xy}$ plane) or sections (in the $\underline{xz}$ plane) of seismic activity, as well as graphs (in the $\underline{xt}$ plane) for the variation in seismic activity with

time $\underline{t}$, and in the space along some line $\underline{x}$. In all of these cases, the points in the $\underline{xy}$, $\underline{xz}$, or $\underline{xt}$ planes are assigned the mean values of A obtained by integration over the volumes enclosing these points. In constructing such maps and other similar graphs, it is possible to make use of data on earthquakes of other classes than the class for which A has been defined formally. Chapter 9 gives concrete methods for constructing seismic-activity maps, allowing for this last fact, and also shows such maps.

Seismic-Energy Density for Earthquake Foci

In addition to the earthquake recurrence N* and associated quantities (the slope γ of the recurrence curve and the seismic activity A), it is possible to use the seismic-energy density E* for earthquake foci in the space Π_5 with coordinates $\underline{x}$, $\underline{y}$, $\underline{z}$, $\underline{t}$, E to characterize a seismic regime. By the density E*, we mean the function E*(x, y, z, t, E), defined as follows:

$$E^* = \frac{\Sigma E}{\Delta \Pi} = \frac{nE}{\Delta \Pi} = \bar{E} N^*,$$

where ΣE represents the sum of the seismic energies for all earthquake foci located in the elementary volume $\Delta \Pi$ of the space Π_5; $\bar{E}$ is the mean energy value for an individual earthquake, corresponding to this volume. The magnitude E* has the dimensions $L^{-3}T^{-1}$.

Associated with E* is the volume work density for the flux of total seismic energy of the earthquake foci in physical space.

$$W^* = \int_{E_1}^{E_2} E^* dE, \qquad (80)$$

where E_1 and E_2 are the limits of that earthquake energy-variation region within which the work is being computed. In the most interesting special case, $E_1 = 0$ and $E_2 = \infty$. It is clear from physical considerations that the quantity W* should be finite in this case.

- 320 -

If in the space $\underline{x}$, $\underline{y}$, $\underline{z}$, we isolate the region V having a volume $\underline{v}$, the work W of the earthquake foci in this volume will equal

$$W = \int_r W^* dx \cdot dy \cdot dz = W^* r, \qquad (81)$$

where W^* is the mean work density in this volume of physical space for the given range of energies E. .

If we arbitrarily place the earthquake foci on the horizontal $\underline{x},\underline{y}$ plane, then, as in the case of the seismic-activity surface dealt with above, it is possible to speak of the surface work density for earthquake foci. This quantity may be represented by an expression similar to (81). In essence, this is precisely the quantity proposed in [217-219] for a quantitative evaluation of seismic regions, and for corresponding mapping; the quantity is determined with no upper limit ($E_1 = 0$, $E_2 = \infty$) of integration, i.e., the quantity involves the summing of the energy of nearly all earthquakes observed. It is possible to use the logarithm of this quantity for the same purpose; this is sometimes called the "coefficient of seismicity" (see [107, 198, 220]). We note that for seismicity mapping purposes, it is also suggested that the square roots of the seismic energies be summed [221-223], in the spirit of Benioff's work [188-192], or that the magnitudes M be employed [224] after Gutenberg and Richter [63, 96]; both of these methods, however, clearly have a less obvious physical interpretation.

A convenient property of the energy quantities E^*, W^*, etc., is their ability to be summed or integrated directly over any energy-change limits, while quantities associated with the recurrence N^*, etc., can reasonably be summed directly only within quite narrow energy-variation intervals. It should be kept in mind, however, that in order to utilize this characteristic of the energy quantities, we must know the recurrence curve $N(E)$ in full, including the region of possible

bends in the curve where $E \to 0$ and $E \to \infty$, and not cnly in the straight-line region γ = const. The fact of the matter is that for the γ = const case, the energy integral

$$W^* = \int_0^\infty E^* dE. \qquad (82)$$

taken over infinite limits, diverges for any numerical values of γ.

Thus, we assume that the work density for the earthquake foci of some fixed class K of energy $E_\bullet$ is a fixed finite quantity $W^*_0 = W^* \frac{E_\beta}{E_\alpha}$, where E_α and E_β are the boundaries for this class. We shall assume, as is normally done, that the classes correspond to orders of magnitude of energy, i.e., the mean energies E for individual earthquakes in two neighboring classes will differ by a factor of 10. Let us initially assume that $\gamma = 1$, i.e., that the number of earthquakes N for neighboring classes also will differ by a factor of 10, but with the converse relationship: there are 10 times fewer strong earthquakes than weak earthquakes. In this case, clearly, the total energy for all the earthquakes will be the same for both classes and equal to $NE = cW^*_0$ (here c = const is a dimensional coordination factor). The same will hold true for any class of this sequence. If the earthquake classes form an infinite sequence in both directions from a given class K, then the total energy of all earthquake classes will rise without limit in both directions from this class (both in the direction of stronger earth-quakes and weaker earthquakes) and, consequently, the integral (82) will diverge. Let us now assume that $\gamma > 1$. This will lead to an in-crease in the numbers of weak earthquakes, which will only intensify the divergence of the energy sums in this direction. In like manner, the assumption that $\gamma < 1$ will lead to an intensification of energy divergence in the strong-earthquake direction. Thus, the energy integ-ral (82) will diverge for any values of γ = const.

Practically speaking, in the linear section of the recurrence curve, the quantity γ will normally amount to $\gamma = 0.4$-0.5 (i.e., $\gamma <$ < 1), so that the energy integral will diverge sharply in the stronger-earthquake direction. This is also associated with the fact that in this energy range, an evaluation of seismicity in accordance with a total energy index is, as a rule, quite unstable: each strong earth-quake will sharply change the estimate of district seismicity. Seis-micity evaluations making use of quantities associated with recurrence (the seismic activity A), are normally incomparably more stable, which represents a clear practical advantage for this method of evaluation, especially for purposes of defining long-term district seismicity.

It is clear from physical considerations that there can be no un-limited work-flux densities W* for the total seismic energy of earth-quake foci. It follows from this that the assumption made as to the infinite linear prolongation of the recurrence curve $N(E)$, i.e., that is a rule that $\gamma = \text{const}$ for $\gamma < 1$ in the strong-earthquake direction, while $\gamma = \text{const}$ for $\gamma > 1$ in the weak-earthquake direction, is a bad assumption.

Here we shall leave aside the question of the behavior of the re-currence curve $N(E)$ in the weak-earthquake region, noting only that for values of γ normally observed, the total effect of all weak earth-quakes upon the general energy balance of earthquakes is slight. Strong earthquakes play a decisive role in this balance, and thus the ques-tion of the behavior of the $N(E)$ curve in this region is in principle of great interest.

For catastrophic earthquakes occurring over the entire world, this question is answered by the graphs of Gutenberg and Richter [64] (see also Fig. 108 in §4 of this chapter). It is still not clear, how-ever, how stable the shape (slope) of the $N(E)$ curve is, especially in

the high-energy region, for different districts. In particular, for the Garm and Stalinabad districts, observational materials obtained by our expedition within a relatively short period of time, and including no reliable information on strong earthquakes naturally can shed no light upon this problem. When the actual behavior of the N*(E) relationship in the high-energy region under the possibly different conditions of individual districts has been clarified, and the function $\gamma = \gamma(E)$ in this region is established with adequate reliability, the integral energy curves for W* of the seismic regime may receive broad practical application.

The work density W* of earthquake foci is associated with the recurrence N* by the following relationship

$$W^* = \int_{-\infty}^{\infty} E N^* dK, \qquad (83)$$

where $N^* = dn/dK$, $E = 10^K$, $\underline{n}$ is the number of earthquakes per unit volume of the space Π_5. As soon as the function N*(E) is known — it is given by the recurrence graph — formula (83) may be used to calculate the mean value of W* with greater stability than is the case for normal "energy flux" calculations for earthquake foci by means of direct summation of the energy E_i for all Q earthquakes observed in a given area S for a given time $\underline{t}$

$$W^* = \frac{1}{St} \sum_{i=1}^{Q} E_i.$$

We note that a similar approach, making use of the law of recurrence, is also possible for calculating the "arbitrary strains" ε, introduced in Benioff's discussion [188-192]. In analogy with (83), we may write for the mean value of ε

$$\varepsilon = \int_{-\infty}^{\infty} \sqrt{V E} N^* dK.$$

- 324.

This formula may be used to obtain more stable mean values of ϵ, replacing the simple summation

$$\epsilon = \frac{1}{N}\sum_{i=1}^{Q} \sqrt{E_i}$$

Of especial importance is the problem of utilizing the energy magnitudes for a clear representation of the seismic-regime time variation, in particular in connection with the arbitrary strains ϵ. A discussion of this problem is given in §3 of this chapter.

R, a Measure of Earthquake Recurrence Scatter

In analyzing a seismic regime by examining the distribution of the points $\underline{x}$, $\underline{y}$, $\underline{z}$, $\underline{t}$, E themselves in the Π_5 space, or by analyzing the functions and parameters N*, A, γ, etc., characterizing this distribution, it is possible to distinguish in conventional manner two seismic-regime aspects, the systematic and the random.

The investigation of the systematic aspect is concerned with the mean values obtained by complete averaging within certain limited regions, or with respect to certain coordinates of formally unbounded regions. Thus, in constructing recurrence curves N*(E) for earthquakes, complete averaging of the observed values of N* over the entire observation time $\underline{t}$ is normally carried out. The same is done in compiling maps of seismic activity A(x, y), etc.

The study of the random aspect is basically concerned with the following problems: the "scatter" of values for N* (as well as other indices for the seismic regime), determined in small volumes of the space Π_5, with respect to the corresponding mean values of $\overline{N*}$ for large volumes, the mutual relationships (regression or correlation) among the parameters characterizing the seismic regime, etc. Such problems are handled in mathematical statistics and the theory of probabilities (see, for example, [85, 225, 226]).

The first and, perhaps most important for practical purposes, is the problem of the degree of scattering for the observed values of the recurrence N* for earthquakes of various energies E in time t — the question of seismic-regime fluctuations. With this question there are the associated problems of evaluating the accuracy and reliability with which long-term seismic-regime average characteristics are determined, characteristics for which the relevant data are gathered by actual observations lasting over a long period of time, and of evaluating the observational periods required to establish these characteristics with the desired accuracy.

In first approximation, seismic-regime fluctuations may be investigated by using the concept of an average regime that is constant with time. The next approximation might be an assumption that the average regime parameters vary linearly with time, or that the regime varies with a long period, etc. In the majority of cases, however, owing to the lack of reliable factual data, it is necessary to restrict the investigation to the first approximation, and in so doing, to employ the simplest methods for analyzing the distribution of random quantities. In this case, the degree of scattering of the values of N* (or of A, etc.), determined over a series of relatively short observation periods, can be evaluated in terms of the standard (mean-square) deviations σ_{N*} of the values of N* with respect to the long-term mean values of these values of N*, which should also be considered to be quite close to the "true" values characterizing the assumed constant average seismic regime. We might use in place of the quantities σ_{N*} other similar quantities known in mathematical statistics and the theory of errors, but this will introduce no essential change.

The quantity σ_{N*}, or other similar quantities, however, will depend upon the observation periods chosen, the dimensions of the regions

under consideration, and upon many other associated circumstances. It is in this sense that these quantities cannot uniquely characterize the scatter of the earthquake process itself.

The quantity $R = \sigma_N / \sqrt{N}$ does not suffer from this drawback; here N is the recurrence itself, or the recurrence density, or a similar quantity, while σ_N is the corresponding standard deviation. Thus, if N is the mean monthly number of earthquakes of a given energy class taken, let us say, from annual observations, then σ_N is the standard error for one determination of this mean monthly number. The quantity R characterizes the spread, the scatter of the recurrence, and in this connection, we call it a measure of the earthquake-recurrence scatter. On the average, for several sections of the district in which the TKSE worked, the scatter measure R turned out to be close to unity, regardless of the observational period, region dimensions, level of seismic activity, or earthquake-energy level, for the energy-variation range $E_{max}/E_{min} > 10^{10}$. The equality $R = 1$ indicates that there is no connection among the instants of appearance of the earthquakes for which the mean recurrence is calculated. In isolated cases, however, in individual sections, and during certain special time periods, for example, in a period during which there are aftershocks from a strong earthquake — the scatter measure displays no visible deviations from the mean value. This will also be associated with other disturbances in the seismic regime, with deviations from the "normal" long-term average regime, and corresponds also to deviations in the values of the parameters A and γ from the long-term mean values. Increased values of R correspond to an increase in instability of the seismic regime in the region under consideration over a given range of variation in the quantities E, $\underline{t}$, etc. The quantity R, together with A and γ, belongs to the group of chief seismic-regime parameters. It characterizes the

"random" aspect, while A and γ characterize the "systematic" aspect.

§3. METHODS OF INTERPRETATION

Let us consider basic methods for processing and representing material on a seismic regime that are employed to systematize the results of expedition observations. The methods are designed to solve the following problems: analysis of the time variation in the seismic regime or the temporal and spatial variation; analysis of the earthquake-recurrence distribution with respect to energies; analysis of seismic-regime fluctuations; analysis of the correlation relationships between the chief seismic-regime parameters.

Analysis of Time Variation of Seismic Regime

The simplest method for representing the time variation of a seismic regime consists, in principle, in representing the arrangement of the discrete earthquake points directly in the five-dimensional space Π_5. Naturally, it is impossible to represent this total pattern on the plane of a drawing, which is only two-dimensional. It is necessary to sacrifice a certain number of the measurements represented, keeping only those most essential to a particular investigation, including, naturally, the time $\underline{t}$. Then the earthquake points in the enclosing region of the space Π_5 will be summed over the coordinates excluded from consideration.

1. Graphs for the temporal variation in the seismic regime $E(t)$ (see Fig. 110). If we fix a specific three-dimensional region of space $\underline{x}$, $\underline{y}$, $\underline{z}$, or a portion of the surface $\underline{xy}$ in plan with corresponding treatment of the volume at the depth $\underline{z}$, we are able to construct for it a graph showing the seismic-regime variation in the coordinate system $\underline{t}$, E. This graph will show all earthquakes whose foci fall within the given spatial volume $\underline{x}$, $\underline{y}$, $\underline{z}$. In this case, where there is no need to isolate a special point in time, the $\underline{t}$ scale is assumed to

be linear. Where there is such a special point, such as the instant of occurrence of a strong earthquake, in order to study the foreshocks and aftershocks, it is convenient to make this scale nonuniform, with the scale increasing as we approach the special point. This scale may be, for example, logarithmic (this is not entirely convenient, since a logarithmic scale essentially has no origin, and the origin must be fixed arbitrarily) or of the type $\sqrt[m]{t}$ where $m > 1$. It is necessary to use nonlinear scales (for example, logarithmic or $\sqrt[m]{E}$) for the energy E, in order to prevent weak earthquakes from escaping consideration, since their energy is very small in comparison with the energies of strong earthquakes shown on the same graph.

2. The space-time graphs for the seismic regime in the x, t plane (see for example, Fig. 109). Diagrams of this type are conveniently used for cases in which the earthquake foci are located in a region that is very extended in one direction, for example, along the axis of a mountain range. In this case, the space coordinate x will correspond to this direction. The foci of earthquakes falling within the strip on the epicenter map through the center of which the x axis runs, are laid off on the x line along the perpendicular. In x, y, z space, this strip corresponds to the specific three-dimensional region with depth z. When the foci are arranged within a relatively narrow depth interval, they are not differentiated with respect to depth. On the drawing, the earthquakes are represented in the x, t plane by black circles whose centers have appropriate coordinates along the space axis x and the time axis t, while the energy E is represented by the radius of the circle.

Where the number of earthquakes treated is large, it is convenient to plot the corresponding points not in terms of the times for each earthquake separately, but by the use of ten-day, semimonthly, etc.

summaries. As a result, the earthquake points on the x, t diagram will lie along lines t = const, spaced at definite intervals Δt. As experience has shown, with a proper choice of intervals Δt, this will not lead to any great distortion in the invisible impression produced by the diagram, but will produce a considerable savings in the time required to prepare the diagram.

In view of the fact that the earthquake-energy classification used is exponential [$E = 10^K$ joules ($K = 1, 2, 3, \ldots$)], the scale of circle radii representing the energy should also naturally be made exponential. It is not possible, however, to make the radii proportional to $\sqrt{E}$ or $\sqrt[3]{E}$, as would be desirable for certain geometric considerations, since in this case, they would rise too rapidly with increasing E. Thus, the scale of radii is suitable for illustrative purposes only. This excludes the possibility of using photometry of the chart obtained in order to average it and thus determine the quantitative indices.

It is evidently impossible to show earthquakes of different energies on a single plane with a graph of the seismic-regime temporal variation in the two-dimensional spatial region x, y. We would require a series of graphs to do this. For this purpose, it is possible to utilize a series of epicenter maps or seismic-activity maps, compiled for a series of successive time intervals.

Attempts have also been made to construct graphs of the type $E = E(t)$ by smoothing the quantities being processed. These graphs do not turn out to be clear. Better graphs may be obtained with smoothed curves for the space-time seismic-regime variation in the xt plane, constructed according to the principle used in the seismic-activity maps (see Chapter 9).

3. Graphs showing the accumulation of arbitrary Benioff strains

[188-192] (see the step curve of Fig. 110). It has been attempted to establish a connection between the energies E_i of individual earthquakes succeeding one another in a certain region, and the strains ε_i appearing as a result of these earthquakes. Benioff has shown that $\dot{\varepsilon}_i \sim$ $\sim \sqrt{E_i}$. In order to obtain the total strain in a given region that appears owing to the action of a series of earthquakes, he constructed the sum $\varepsilon_{\Sigma} = \Sigma C_i \varepsilon_i$, where the C_i are coefficients that depend upon the nature of the focus, and upon the elastic properties of the medium. As a rule, for practical purposes the quantities C_i are neglected, and the simplified formula

$$\varepsilon_{\Sigma} = \sum \sqrt{E_i}. \tag{84}$$

is used.

This formula is used to determine the ordinates of the step curve for the accumulation of some arbitrary "strain," appearing during the excitation of seismic energy for a series of earthquakes. The time t_i at which these earthquakes appear is plotted along the axis of abscissas.

This construction is clearly based upon the assumption that each earthquake of a given sequence creates a strain of identical nature and, correspondingly, causes relative shifts in the medium in the same dirrection: only in this case may the strains be added arithmetically, as is done in Formula (84).

This assumption is quite probable for the strong-earthquake sequences associated with slips along any major fault. It holds very poorly, however, for the numerous weak earthquakes which basically are the subjects of investigation in the study of the seismic regime for a region. Individual points may evidently be associated with different displacement directions in the earthquake foci (see Chapter 6). It is only their combined action, taking effect over some time inter-

val, that may acquire a certain regular nature, amounting, as it were, to plastic flow of the material in some specific direction.

In view of this, it was assumed that within certain short time intervals Δt_k (in practice, over each ten-day period) the strains ε_i are summed not arithmetically in a single direction, but geometrically, as in the case of an orthogonal vector system

$$\varepsilon_{\Sigma_k} = \sqrt{\sum_m \varepsilon_i^2} \sim \sqrt{\sum_m E_i} = \sqrt{E_k},$$

$i = 1, 2...m$; over long time intervals, these total deformations are added in one direction, arithmetically

$$\varepsilon_\Sigma = \sum \varepsilon_{\Sigma_k} = \sum_n \sqrt{E_k} = \sum_n \sqrt{\sum_m E_i}, \qquad (85)$$

where $\underline{m}$ is the number of earthquakes in a ten-day period, and $\underline{n}$ indicates the number of the decade in the total observation period.

This last formula was also used to calculate the ordinates of the corresponding graphs for the accumulation of the arbitrary deformations. Thus, within each ten-day period, the earthquake energies E_i were summed, while among the ten-day periods, the square roots of the values for the total energies E_k were summed. This procedure for constructing the graphs also has the advantage of great simplicity in handling large quantities of material.

We note that the graphs compiled in accordance with this principle, as well as the graphs of Benioff (to a greater extent) which were compiled in accordance with Formula (84) in essence do not yield quantitative values for any actual strains, but represent only a way of illustrating the general trend of seismic-energy release with time. In this respect, the data from the graphs for accumulation of the arbitrary strains are equivalent to the time curves for the seismic regime $E - E(t)$, representing, in a certain sense, their integral form.

4. Graphs for the time variation of seismic-regime parameters. Here we have in mind the representation of the time t dependence primarily for the following main parameters of the average seismic regime: the seismic activity A, the parameter γ, representing the slope of the recurrence curves $N(E)$, and the scatter measure R for the recurrences (see Fig. 110).

In plotting graphs of this type, we should make an evaluation of the accuracy with which the quantities under consideration are determined; if this is not done, random fluctuations in these quantities, associated with errors of determination, may be jumbled up with systematic regular variations in regime characteristics. The elementary time interval Δt over which the quantities A, γ, and R are determined, should be large enough to accommodate the number of observations needed to obtain satisfactory accuracy in the determinations; in addition, these intervals should be small enough with respect to the total observation period to permit changes in regime variation over this period of time to be followed in sufficient detail. As we can see, these requirements for Δt are contradictory. It is easier to satisfy both requirements, naturally, in districts where the seismic activity is greater, where the K earthquake classes are more numerous (i.e., for weaker earthquakes), and for greater areas S (or volumes), and longer observation periods. We note that the same problem exists for areas or volumes as in the case of time intervals. Areas within which averaging is carried out must be taken sufficiently large to prevent averaging out of regime-variation features characteristic of the separate sections.

The chief reason for plotting graphs of the time variation of the various seismic-regime indices is that they make it possible to form an opinion as to the presence or absence of noteworthy features of the

- 333 -

regime prior to strong shocks. The discovery of such features is of
great interest for the purposes of predicting severe earthquakes.

Analysis of Energy Distribution of Earthquake Recurrence

Curves of the recurrence N(E) for large districts and long time
intervals are plotted on the basis of monthly numbers for the earth-
quake recurrence N for various K energy classes. Next, for each K
class, the mean monthly recurrence value $\overline{N} = (\Sigma N)/n$ is found, where $\underline{n}$
is the number of elementary time intervals — in our case, the number
of months — in the total observation period, which in this case is
about two years. Graphs for earthquake recurrence as a function of
earthquake energy are plotted in accordance with the values of N and K
in the form, for example, of Figs. 103-106. The sequence of points ob-
tained was averaged graphically by drawing a straight line. The slope
of this line, in accordance with general considerations, determined
the value of the parameters $\gamma = -\Delta \log \overline{N}/\Delta \log E$, while the value of
the seismic activity A was determined by the point on the line corres-
ponding to K = 7. In determining A, the calculation was carried out,
naturally, for the normalized recurrences N*.

In some cases, other elementary time intervals were employed for
individual sections. Thus, for the Chusal section, recurrence values
for four-hour elementary intervals over a total observation period of
three days were used as the initial data (see Table 19, page   ). In
all cases, precisely the same methods were used to determine the param-
eters γ and A.

The errors in the quantities determined were also shown on the
recurrence graphs. They were given in the form of ellipses whose semi-
axes equaled in the scale of the graph the magnitudes of the errors
for the corresponding coordinate axes. The methods used to evaluate
errors have been described above.

The distribution of the values of A and γ in space (from section to section) and in time for individual sections has been discussed separately for the Garm and for the Stalinabad districts.

Analysis of Seismic-Regime Fluctuations

Here we have in mind the following questions: the evaluation of the accuracy with which the values for the recurrences N^* of earthquakes in the various K classes of energy E are determined; a study of the scatter of the values for N^* in time; a determination of the observation periods required to evaluate the recurrences N^* with the desired accuracy; the establishment of the scatter measure R for earthquake recurrence with an evaluation of the accuracy with which the mean value of this quantity is determined with respect to the large-scale observations. And, finally, the utilization of the quantity R for plotting nomograms for evaluating the observation periods needed for the recurrence of earthquakes in the various energy classes.

1. Evaluation of the accuracy with which earthquake recurrence is determined. To do this, for each K class of earthquake energy E, a series of recurrence values $N = N_i$ ($i = 1, 2, \ldots, n$) is processed; the values are determined in the given district over relatively short time intervals (for example, monthly periods), into which the total longer observation period (for example, two years) is divided. In order to decrease the over-all length of time, the time intervals into which it is divided are also reduced.

The following indices are calculated for the set of values $N = N_i$: the mean value

$$\bar{N} = \frac{\Sigma N}{n},\qquad (86)$$

the standard (mean-square) deviation for a given determination of N

$$\sigma_N = \sqrt{\frac{\Sigma(N-\bar{N})^2}{n-1}},\qquad (87)$$

- 335 -

here σ_N^2 is the variance in the value of N; the standard deviation of the mean value

$$s_N = \frac{s_N}{\sqrt{n}},$$

(88)

here $\sigma_{\overline{N}}^2$ is the variance of the value of $\overline{N}$; the relative deviations: of one determination

$$\delta_N = \frac{s_N}{N}$$

(89)

and of the mean value of $\overline{N}$

$$\delta_{\overline{N}} = \frac{s_{\overline{N}}}{\overline{N}} = \frac{\delta_N}{\sqrt{n}}.$$

(90)

The values of the relative deviations δ_N and $\delta_{\overline{N}}$ remain precisely the same for the quantities N and $\overline{N}$, as for the corresponding normalized recurrence quantities N* and $\overline{N}$*.

The quantity δ_N has the following important sense. It must be taken as the relative error in the determination of the true long-term mean recurrence $\overline{N}$ or $\overline{N}$* of earthquakes in the class under consideration within the given district in accordance with data obtained over the entire actual observation period, provided that the mean seismic regime in this district can be considered to be time-invariant. Here it is of no importance in what units the recurrence considered is measured (whether it is based on the month or the year), or to which area of the district or which volume in the region in which the earthquake foci are located it refers, provided only that the seismic regime is the same for all of these regions.

The magnitude of the error $\delta_{\overline{N}}$ depends upon the total number ΣN of earthquakes for which it is computed. In this connection, it will be lower the greater the over-all observation period, the area S (or volume) in which the observed earthquake foci are located, and the greater the seismic activity of the district. In addition, it depends

upon the degree to which the recurrence diverges from strict periodicity.

2. Investigation of the scatter of the monthly (or other) numbers for earthquake recurrence in time with respect to the long-term mean values. The task of this investigation is to clarify the nature of the observed distribution of recurrence deviations from the mean values for earthquakes in the various energy classes, and a comparison of this distribution with certain theoretical distributions (normal and logarithmic), as well as the determination of the parameters for the corresponding theoretical distributions.

To do this, graphs (histograms) were plotted separately for each class, showing the observed distribution density of the quantity N (Fig. 98) for several relatively large time series of observations for the quantities $N = N_i$ ($i = 1, 2...n$), corresponding to different K energy classes. Along the axes of abscissas on these graphs, the values of the quantity $x = (N - \bar{N})/\bar{N}$ are also plotted, so that these axes are divided into intervals Δx, preferably, but not necessarily, equal to each other. The quantities $y = y_n/(n\Delta x)$ are plotted along the axes of ordinates; here $\underline{n}$ is the total number of determinations of the quantity N and y_n the number of determinations for which the value of $\underline{n}$ lies in a given interval of values of $\underline{x}$. The segments Δx and Δy serve as the base and altitude for the corresponding rectangles which taken together form the step-type distribution curve. With this construction, the area under the curve will equal unity.

This normalization of the distribution curves makes it possible to compare the general nature of the distribution for the quantities N for various earthquake energy classes for which there is very great variation in the number of earthquakes per class within the same district. It is also easy to compare corresponding data obtained in districts that differ in area and seismic activity.

In addition to the curves for the observed distribution of N, theoretical differential curves were also plotted (also normalized) primarily for the appropriate normal distribution in accordance with the well-known formula

$$y = \frac{h}{\sqrt{\pi}} e^{-h^2 x^2},\qquad(91)$$

here $h = (1/\sqrt{2})\delta_N$ is the so-called measure of accuracy. The quantity δ_N is here determined from Formula (89). Tables for the probability density of the normal distribution were used to plot the theoretical curves (see, for example [85]).

A comparison of the observed distribution curves with the theoretical curves gives a clear qualitative picture of the degree to which the observed distributions of earthquake recurrence N conform to the normal law.

To do this, we make use of the method of plotting observed and theoretical cumulative curves (ogives) on probability paper upon which the theoretical curves form straight lines, given a normal distribution (Fig. 99a). As before, values of $x = x_1$ ($N_1 - \bar{N}$) are plotted along the x axes of these graphs, and the observed normalized cumulative recurrence frequencies $y = y_1 = (1/n)\Sigma y_{n_1}$ along the y axes, i.e., the quantities: $(1/n)y_{n_1}$, $(1/n)(y_{n_1} + y_{n_2})$, $(1/n)(y_{n_1} + y_{n_2} + y_{n_3})\ldots$ An averaging line is drawn through the collection of points; it represents the appropriate theoretical normal-distribution law. We note that distance along the x axis between points of this line having ordinates $y = 15.9\%$ and 84.1%, which are symmetric with respect to the center $y = 50\%$, equals twice the relative standard deviation $2\delta_N$, which may be used for graphical determination of the value of δ_N, independent of Formulas (86)-(90).

The following conclusions may be drawn from the distribution

curves, represented in both differential (Fig. 98) and integral (Fig. 99a) form. For the lower earthquake-energy K classes, in the given example for K = 6-10, for which the recurrence values N are relatively large, the observed points fall quite well on the appropriate theoretical graphs for the normal distribution. For higher classes K > 11,
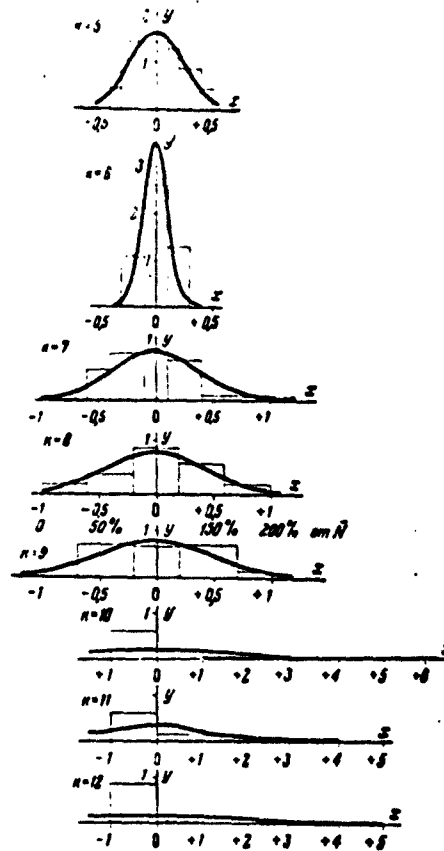
Fig. 98. Graphs showing distribution of earthquake recurrence of various energy classes K in the Garm district in 1955 to 1956.

where the number N drops off sharply, and in several of the time intervals into which the total observation period is divided, these numbers become equal to zero, as is clear from Fig. 98, and the observed distributions become asymmetric, differing substantially from the normal distribution. In addition, the representation of corresponding in-

tegral data on the cumulative curves (Fig. 99a) is complicated or becomes impossible in practice.

A comparison of the observed earthquake-recurrence N distributions for various K classes with the theoretical log-normal distribution, i.e., with the normal distribution for the quantity log N, was carried out on the basis of the following considerations. As is known (see, for example [85]), this theoretical distribution is skew with respect to $\bar{N}$, while the general nature of the skewness is the same as that observed for the graphs of Fig. 98 for the higher classes. The log-normal distribution for N is more convenient to use, in that it eliminates the possible appearance of negative values for N, while with the normal distribution, such values are formally permissible, although they may be quite improbable. From the physical point of view, there naturally can be no negative values for the earthquake recurrence N.

This comparison was carried out by plotting cumulative curves for the observed distributions and for the corresponding theoretical distributions on semilog-probability paper, upon which the theoretical curves for the log-normal distribution takes the form of straight lines. For the graphs of this type shown in Fig. 99b, the x axis is logarithmic. The functional scale log $(x + 1)$ is plotted along it; here, as before, $x = (N - \bar{N})/\bar{N}$; the divisions of the axis represent values of x, as in Fig. 99a, i.e., they characterize the relative deviations of the observed values N from the mean value of $\bar{N}$.

A comparison of the two theoretical [normal (Fig. 99a) and log-normal (Fig. 99b)] with the observed distributions for N leads us to conclude that for the lower K energy classes of earthquakes for which the processed material was quite voluminous, and in this sense completely amenable to statistical treatments, both theoretical distributions agree roughly with the observed distributions. With respect to

- 340 -
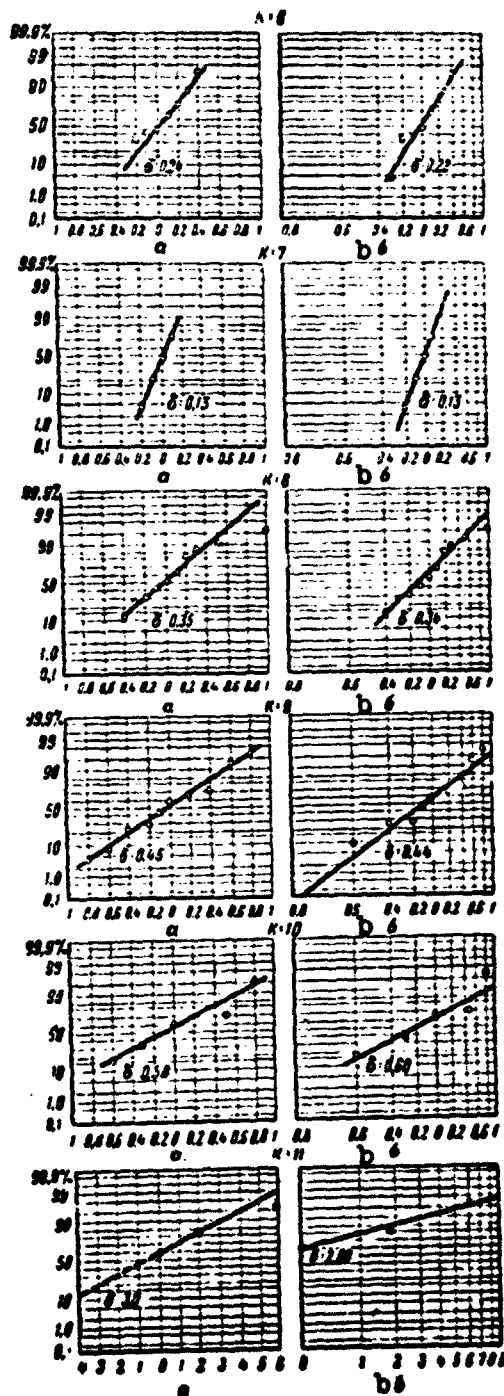
Fig. 99. Cumulative curves for earthquake recurrence. Garm district, 1955-1956. a) On probability paper; b) on semi-log-probability paper.

the higher K classes, where the number of observed earthquakes becomes small, the application of statistical methods, in both versions, produces blurred results with the log-normal distribution clearly giving better agreement with observations in this case.

Thus, in practice, given a number of observations sufficient to permit reliable statistical conclusions, the distribution of the earthquake recurrences N with time may be considered to be a normal distribution for any K energy classes, in first approximation. This does not exclude the possibility that in some cases it might also be desirable to have an approximate picture of the earthquake-recurrence N distribution in time according to the log-normal law. The choice of either of these theoretical laws may be made, in large measure, on the basis of considerations of convenience in the investigation of concrete geophysical problems.

3. Determination of observation periods required to evaluate the mean earthquake recurrence with the desired accuracy. The error δ_N in the determination of the mean earthquake recurrence $\bar{N}$ for any K energy class of earthquakes depends upon two groups of factors. The first group comprises factors which the seismologist may influence to some degree; the observation time $\underline{t}$ and the dimensions of the region covered by the observations (its area S or volume V). The second group of factors cannot be controlled by the seismologist; the normalized recurrence N^* for earthquakes of the given region, which differ for various K classes, and the degree of natural scattering of the earthquake recurrences from the mean values which, generally speaking, may also differ for various K earthquake-energy classes.

Let us assume that for given observation-region dimensions, its area S (instead of the area we might speak of the volume; here it makes no essential difference), and a given seismic activity A in this re-

gion over a observation time $\underline{t}$, the value of the mean recurrence $\bar{N}$ for earthquakes of a given class K has been determined with a relative error δ_N. Keeping in mind that the error in determining the mean recurrence $\bar{N}$ in accordance with Formula (90) decreases as the number $\underline{n}$ of observation increases, as $1/\sqrt{n}$, and that the number $\underline{n}$ increases in proportion to the increase in the observation period $\underline{t}$, we may write

$$\delta_0 = \delta_{\bar{N}} \sqrt{\frac{t}{t_0}},\qquad (92)$$

where δ_0 is the given permissible error in determining the recurrence $\bar{N}$, characterizing the desired accuracy with which this quantity is to be determined. Then, in accordance with (92), the time t_0 required to obtain $\bar{N}$ with this accuracy will equal

$$t_0 = t\left(\frac{\delta_{\bar{N}}}{\delta_0}\right)^2.\qquad (93)$$

Let us give the results of numerical calculations of the time t_K required to determine the recurrences $\bar{N}_K$ with the given accuracy $\delta_{\bar{N}} = = 0.1\ (= 10\%)$, for various K energy classes, using as an example a statistical treatment for results of earthquake observations in the Garm district over the period from February 1955 to November 1956 (see Table 13). Similar calculations were also carried out for the Stalinabad district (see §5).

This table gives nonnormalized mean monthly values for the recurrence $\bar{N}$, obtained over an observation period of 23 months, as well as the relative errors δ_N in the monthly determinations, found from Formula (90) as a result of processing these observations. Table 13 gives the times (in years), computed from Formula (93), required to determine the recurrences $\bar{N}$ (monthly or yearly, nonnormalized or normalized $\bar{N}^*$ recurrence values) with a given relative error $\delta_N = 0.1\ (= 10\%)$. Similar calculations have been carried out for the Greater (area $S = = 14,300\ \text{km}^2$) and Lesser ($S = 4000\ \text{km}^2$) Stalinabad district.

TABLE 13

Determination of the Time t_0 Required to Obtain an
Earthquake Recurrence Value $\bar{N}$ with an Error δ_0 =
= 10%, for Various K Earthquake-Energy Classes us-
ing Observation Data for the Garm District

K	$\bar{N}$	$\delta_{\bar{N}}\%$	$t_{0\,net}$	K	$\bar{N}$	$\delta_{\bar{N}}\%$	$t_{0\,net}$
7	60,6	-,4	0,167	11	0,70	35,2	23,5
8	18,6	7,9	1,16	12	0,48	29,0	16,0
9	7,1	9,3	1,66	13	0,17	47,9	45,5
10	3,2	10,4	2,04				

These results are represented graphically on Fig. 100; Fig. 100a
is for the Garm district, Fig. 100b for the Stalinabad district. The
curves were plotted in logarithmic coordinates with both scales having
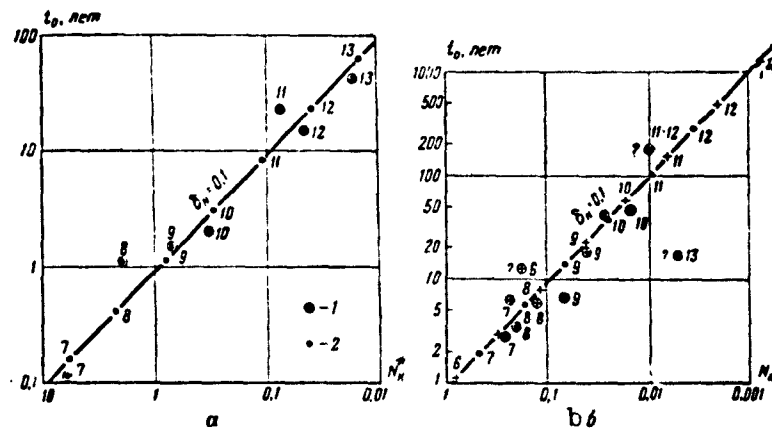
Fig. 100. Graphs of observation time t_0 required to
determine earthquake recurrence N with given accu-
racy of 10%. a) For Garm district; b) for Stalina-
bad district. 1) Observed values; 2) numerical
values. On graph b, points with asterisks are for
the Lesser Stalinabad district, points without as-
terisks for the Greater Stalinabad district.

identical moduli. The numbers $\bar{N}$ are plotted along the x axis from left
to right in a logarithmic scale, and the numbers t_0 (see Table 13)
along the y axis, from bottom to top in the same scale. The pairs of
values $t_0\bar{N}$ for various K earthquake-energy classes represent the coor-
dinates of observation points and are indicated by double circles. We

- 344 -

see that this collection of points lies quite near a certain straight line. The position of the theoretical points (small circles) is determined in accordance with the quantity R (see below).

Sections 4 and 5 give a discussion of these graphs from the point of view of improving earthquake-observation methods. Here we shall concentrate on the other side of the question, namely, on those basic conclusions as to general seismic-regime properties that may be drawn in this case.

4. Establishing the measure R of earthquake-recurrence dispersion. The line used to average the position of points having the coordinates $\log \bar{N} - \log t_0$ on the curves of Fig. 100, as may be seen, lies at an angle of about 45° to the coordinate axes. This indicates that there is a roughly linear relationship between the quantities $1/N$ and t_0 for the various K earthquake-energy classes: $t_{0K} = C/N_K$, or

$$ t_{0K} \cdot N_K = C \ldots, \tag{94} $$

where $C = $ const is a quantity independent of K, while the subscripts (K) on the quantities N and t_0 indicate that both of them belong to precisely the same K class, and vary with variation in K.

Let us turn to Expression (94). The product $t_{0K} \cdot N_K$ has a simple physical interpretation: it equals the total number of earthquakes in the given K class that would be recorded in the time interval t_0 required to determine the recurrence $\bar{N}$ with the given error, identical for all K classes.

We note that the fact that the quantity C remains roughly the same for all K earthquake-energy classes is in this case established empirically, and is not entailed by any logical structures. We might rather expect that the quantity C would depend upon K, i.e., on the earthquake energy. It is possible that over a wider energy range than could be investigated here that this would prove to be the case, and

that the assumption C = const would cease to be valid. According to the data which we have at our disposal, the quantity C remains roughly constant over an energy range covering about 13 orders of magnitude (according to data for the Garm and Stalinabad districts as a whole, K = 7-13, while for the Chusal district (see §4), K = 0-7).

The constancy of the quantity C entails the important conclusion that the error δ with which earthquake recurrence may be determined on the average depends exclusively upon the total number N_Σ of earthquakes for which this recurrence is determined, regardless of the recurrence value, the observation periods, and, the most important point, of the K energy class.

This leads one to believe that the degree of dispersion of the earthquake recurrences for the various K classes, upon which δ depends, remains the same, on the average, if this degree of dispersion applies to sequences of earthquakes for each given class, including sequences having the same number of earthquakes.

Now it is not difficult to arrive at a magnitude associated with the earthquake-recurrence dispersion which should remain nearly constant for all K classes of earthquakes for which Relationship (94) holds in approximation. This quantity — a measure of earthquake-recurrence dispersion — takes the following form:

$$R = \frac{\sigma_{N_\Sigma}}{\sqrt{N_\Sigma}} = \delta_{N_\Sigma}\sqrt{N_\Sigma},\qquad(95)$$

where N_Σ is the total number of earthquakes observed for any K class for which R is determined, while σ_N and δ_N are the corresponding standard deviations (σ_N is the absolute quantity and $\delta_N = \sigma_N/N$ is the relative quantity).

More accurately, the quantity R represents the limit to which Expression (95) tends when $N_\Sigma \rightarrow \infty$. As experience in the application of

Formula (95) to the processing of ɔі ʹɑ:іo:.a1   data has shown, how-
ever, it may also be utilized for comparatively small numbers N_Σ, of
the order of $N_\Sigma = 10$; we shall consider the question of the accuracy
in determination of R below.

We shall show that where the seismic regime remains constant over
the time $\underline{t}$ (or in space, with other evaluations), the quantity R is
independent of the observation periods (or, correspondingly, of the
dimensions of the region in which the observations are made).

Let the observations from which the magnitude of R is determined
be carried out once for a length of time t_a, and once for a length of
time t_b, so that $t_a/t_b = n$. For the sake of clarity, the number $\underline{n}$ may
be assumed to be the number of time intervals t_b into which the total
observation period t_a is divided. The numbers N, σ, R corresponding to
t_a and t_b are denoted by the appropriate subscripts (a), (b). We write
the following relationships which hold for a constant regime and where
the deviations are random and mutually independent

$$N_a = N_b \cdot n \text{ and } \sigma_{N_a} = \sigma_{N_b} \cdot \sqrt{n}. \tag{96}$$

The last expression is completely similar to that used to express
the standard (mean-square) error σ_{N_a} in the determination of the
length of a line consisting of $\underline{n}$ equal segments, where the standard
error for each individual segment, arbitrary in nature, equals σ_{N_b}. In
accordance with (95), (96) we obtain

$$R_a = \frac{\sigma_{N_a}}{\sqrt{N_a}} = \frac{\sigma_{N_b}\sqrt{n}}{\sqrt{n \cdot N_b}} = \frac{\sigma_{N_b}}{\sqrt{N_b}} = R_b,$$

which is what we were to prove. In completely similar fashion, it may
be shown that the values of R found are independent of the dimensions
of the region in which the observations are carried out, and of the
seismic activity.

Thus, the quantity R is determined exclusively by the degree of

dispersion of the earthquake recurrences, which is a characteristic of the process giving rise to the earthquakes which as a group comprise the seismic regime of the given region.

Since for the same N, the dispersion measure is greater the greater the deviations σ_N (or δ_N), this quantity (95) characterizes, on the average, the degree of departure of the earthquake recurrences from strict periodicity.

Let us now determine the mean value of the dispersion measure R, using observational data, and let us evaluate the accuracy of this determination. The calculations were carried out in accordance with earthquake observations for the Garm district over the January 1955 to November 1956 period (Table 14); for similar calculations for the Stalinabad district, see §5.

In Table 14, K is the earthquake-energy class; $\overline{N}$ is the mean monthly recurrence value, determined from observations over a total period of t = 23 montns; $\delta_{\overline{N}}$ is the relative standard deviation for the monthly value of $\overline{N}$. We note that the minimum number of earthquakes observed in a time t = 23 months according to which the value of N was determined was found for K = 13, and equals 4 (4/23 = 0.17). Table 14 gives values of the dispersion measure R_K for various K classes, calculated from Formula (95), and the corresponding standard deviations σ_{R_K} (errors). The latter were calculated from the formula

$$\sigma_{R_K} = \sqrt{\left(\frac{\partial R_K}{\partial \sigma_N}\right)^2 \cdot (\sigma_{\sigma_N})^2 + \left(\frac{\partial R_K}{\partial N}\right)^2 \cdot (\sigma_N)^2}, \qquad (97)$$

where R_K is given by Formula (95). We shall present certain details of the calculations. The quantity σ_{σ_N} was found from the formula, known from the theory of errors, for the standard deviation (see, for example [85])

$$\sigma_{\sigma_N} = \frac{\sigma_N}{\sqrt{2n-1}}.$$

- 348 -

TABLE 14

Value of the Quantities R_K and Errors σ_{R_K} in the Determination of the Dispersion Measure R for the Earthquake Recurrence $\bar{N}$ for Various K Energy Classes

K	$\bar{N}$	δ_N	R_K	σ_{R_K}	ΔR_K
6	115,0	0,238	2,55	0,390	0,690
7	60,0	0,114	0,892	0,134	0,185
8	18,6	0,375	1,62	0,252	0,548
9	7,1	0,449	1,20	0,188	0,432
10	3,2	0,498	0,893	0,142	0,357
11	0,70	1,69	1,42	0,328	1,42
12	0,48	1,39	0,962	0,202	0,812
13	0,17	2,30	0,950	0,269	1,24

In our case, n = 23 (the number of months for which observations were made), so that σ_{σ_N} = 0.151. Now,

$$\frac{\partial R_K}{\partial \sigma_N} \cdot \sigma_{\sigma_N} = \frac{1}{\sqrt{N}} \cdot 0,151 \, \sigma_N = 0,151 \sqrt{N} \, \delta_N,$$

$$\frac{\partial R_K}{\partial N} \cdot \sigma_N = \frac{1}{2} \frac{\sigma_N}{N\sqrt{N}} = \frac{1}{2\sqrt{n}} \frac{(N \cdot \delta_N)^2}{N\sqrt{n}} \approx 0,104 \sqrt{N} \delta_N^2,$$

and then, finally,

$$\sigma_{R_K} = \sqrt{\frac{1}{2(n-1)} N \delta_N^2 + \frac{1}{4n} N \delta_N^4} = \delta_N \sqrt{N (0,027 + 0,0109 \delta_N^2)}. \qquad (98)$$

In examining Table 14, we note the following two facts. First, the exceptionally large range of the quantity R_K, and the large value of σ_{R_K} for K = 6, although this class has the greatest population; second, the very slight over-all increase in the errors σ_{R_K} with increasing K, and, correspondingly, with decreasing numbers N. The small errors for K = 12 and 13 are especially strange, inasmuch as the numbers for these classes are so small that a statistical treatment of the corresponding data was very difficult, as we have seen (see the discussion of Figs. 98 and 99).

The reason for the abnormal behavior of the quantities R_K and σ_{R_K} for K = 6 clearly lies in the fact that they are determined from ob-

servational data that is not of the highest quality: during the calcu-
lation of the earthquake numbers for this class, systematic errors
tending to lower the values undoubtedly were allowed to creep in; more-
over, it is possible that these errors differed for different observa-
tion periods. The fact of the matter is that these weak earthquakes
could not possibly be completely accounted for over the entire dis-
trict under consideration with the existing instrumental sensitivity
and arrangement of the network of stations (the influence of "station
background"). This is shown by the spread for the points $K = 6$, ex-
ceeding the random error, on the recurrence graph, among other things
(see Fig. 103).

In order to verify the general trend of errors in the determina-
tion of R_K for $K = 6$-13, these errors were evaluated by taking loga-
rithms and differentiating. In accordance with (95) we find, using
this method

$$\frac{\Delta R_K}{R_K} = \frac{\Delta \sigma_N}{\sigma_N} + \frac{1}{2}\frac{\Delta N}{N},$$

where ΔR_K, $\Delta \sigma_N$, and ΔN are the errors in the quantities R_K, σ_N, and N,
respectively. Let us assume that $\Delta \sigma_N \approx \sigma_{\sigma_N} \approx 0.151\sigma_N$, and $\Delta N = \sigma_N$. Then,

$$\frac{\Delta R_K}{R_K} = 0.151 + \frac{1}{2}\frac{\sigma_N}{N} = 0.151 + 0.5\delta_N,$$

and, finally,

$$\Delta R_K = R_K (0.151 + 0.5\delta_N). \tag{99}$$

The results of the calculation of the errors ΔR_K from this formula are
shown in Table 14.

A comparison of the errors σ_{R_K} and ΔR_K shows that the general
trend of both quantities is identical with the possible exception of
the values for higher K classes, and in this case we have already com-
mented upon their low reliability for statistical purposes. Both ΔR_K

and σ_{R_K} are characterized by a relatively slight increase in these errors with increasing K, which may serve as indirect confirmation of the correctness of the calculations for the error σ_{R_K}, which were carried out by a more rigorous method.

Let us turn to a determination of the mean value for the dispersion measure R for earthquake recurrence, and to an evaluation of the errors in this quantity, making use of corresponding data for R_K and σ_{R_K} for several K classes.

The mean weighted value of R is determined by the expression

$$R = \frac{\Sigma R_K \cdot w_K}{\Sigma w_K},$$
(100)

where the weighting factors w_K are assumed to equal $1/\sigma_{R_K}^2$. The standard error for R equals

$$\sigma_R = \frac{1}{\sqrt{\sum_k w_k}} = \frac{1}{\sqrt{\sum_k \frac{1}{\sigma_{R_K}^2}}}.$$
(101)

If we make use of the data of Table 14 for all K classes with the exception of K = 6, we then obtain from Formulas (100), (101) R = 1.04 $\pm$ $\pm$ 0.07, while if we also discard the data for K = 12 and 13, making use only of observational material in the most reliable region, we will obtain

$$R = 1.05 \pm 0.08.$$
(102)

We shall now assume that this is the mean value for the earthquake-recurrence dispersion measure for the Garm district from the observations made during the 1955-1956 period. We note that in the case under consideration, the numerical values for R and σ_R remain almost the same whether or not observational data for earthquakes in the higher classes K = 12 and 13 are taken into account. As we see, the mean numerical value for R is close to unity. We shall not, however, assume that it is precisely equal to one; we must remember that this

quantity varies in individual cases, and such variation in this quantity in space or in time may be of special interest.

5. Utilization of the mean value of R to refine estimates of observation periods required. By using Formula (97) and assuming the specific value (102) for R, we may easily compute the number N of earthquakes in any energy class required to enable us to use this number N to characterize the mean long-term value of earthquake recurrence with a predetermined accuracy. This last is characterized by the magnitude of the error δ_N. Assuming various numerical values for δ_N, we obtain the following:

δ_N	1	5	10	20
N	11000	450	110	28

(Here δ_N is given in %)

Thus, if the determination of the mean earthquake recurrence for any given K class with an accuracy of, let us say, 10% requires that about 100 earthquakes be observed, a decrease in the permissible error to 1% would require that more than 10,000 earthquakes of this class be observed.

It is of interest to solve the following question: what should be the observation time $\underline{t}$ in order to determine the mean earthquake recurrence for any given K class with a predetermined error, if we know the area S for the district in which the observations are made or, more accurately, the district in which the foci are located (or the volume $\underline{v}$, in which the foci are located), as well as the seismic activity $\overset{.}{A}$ of this district. This problem represents a natural generalization of the problems whose solutions are given in the graphs of Fig. 100 for the actual conditions of the Garm and Stalinabad districts.

Commencing the solution, we express the total number of observed earthquakes in a given K class in terms of the quantities A, S and

$$N_K = \frac{S \cdot A \cdot t_K}{100} \cdot 10^{-\gamma (K - \eta)}.$$

(103)

Here the area S is given in km^2; A equals, by definition, the number
of earthquakes in the class K = 7 per 100 km^2 per year (in this con-
nection, the number 100 will also appear in the denominator); the quan-
tity γ is a parameter showing the way in which the earthquake recur-
rence drops off with increasing K energy class — it is nearly constant,
and in this case we shall assume that it equals $\gamma = 0.43$. Substituting
(103) into (95), we obtain for t_K the following final formula

$$t_K = \frac{K^2}{t^2} \cdot \frac{100}{SA} \cdot 10^{\gamma (K - \eta)}$$

(104)

In this case, the units of measurement are the same as in (103).
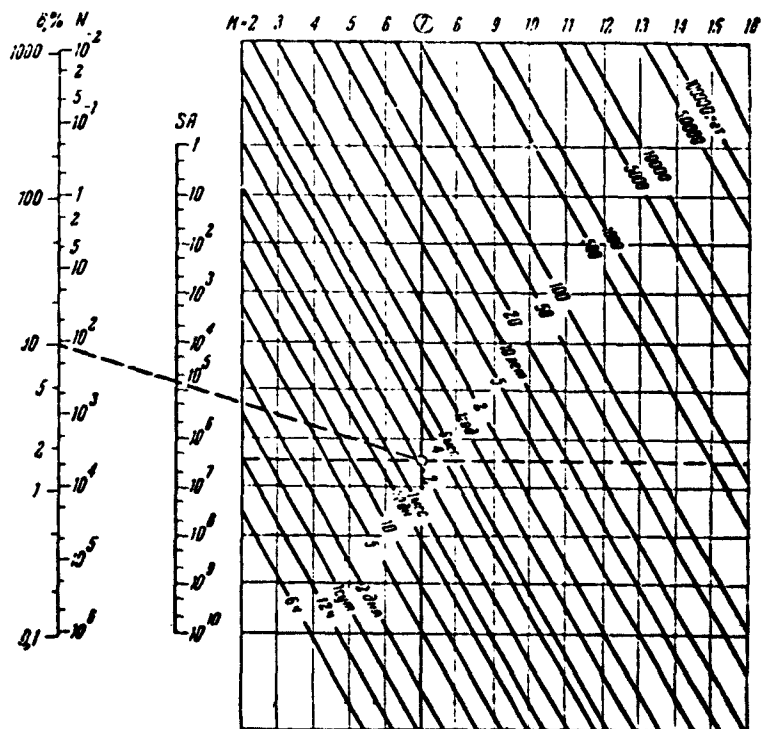
Fig. 101. Nomogram for determining the observation
period t_0 required to determine the earthquake re-
currence with a required accuracy δ in %. SA is
the product of the area of the district under ob-
servation (in km^2) and the seismic activity A~A_7.

If the seismic activity A is not computed in terms of the area

$S = 100 \text{ km}^2$, but in terms of the volume $v = 1000 \text{ km}^3$, we shall have in place of 100/SA the factor 1000/vA, where $\underline{v}$ will be measured in km^3.

Formula (104) may be used for any districts provided, naturally, that we may assume that the assumptions used in the derivation of the formula hold in these districts; for approximate estimates, naturally, there is no need for the numerical values of the parameters to coincide exactly.

In particular, this formula may be used to systematize estimates made previously for the Garm and Stalinabad districts, and presented graphically on Fig. 100. The corresponding "theoretical" points, calculated for the conditions of the Garm district ($S = 13,500 \text{ km}^2$, $A = 5.0$, $\gamma = 0.43$), as well as for the Greater and Lesser Stalinabad districts ($S = 14,300 \text{ km}^2$, $A = 0.4$, $\gamma = 0.43$; and $S = 4000 \text{ km}^2$, $A = 0.9$, $\gamma = 0.43$, respectively) are shown in Fig. 108 by the small solid circles and asterisks which, as we might expect, fall precisely along straight lines; they are arranged in proper sequence with respect to the K values (N^* is plotted along the $\underline{x}$ axis of Fig. 100). The good systematization of the observed points given by the theoretical points is evidence for the correctness of the assumed parameter values for the given districts and, in particular, for the correctness of the values taken for the constants R and γ.

In order to ease calculations making use of Formula (104), and for the sake of greater clarity in carrying out the various estimates, the corresponding nomogram of Fig. 101 has been constructed.

The first left-hand vertical scale of this nomogram is a dual scale for the relative error δ and number N of earthquakes of a given class that must be observed in order to determine the long-term mean recurrence with a given error δ. By going from one scale to the other, we obtain the relationship between δ and N satisfying Equality (95)

for R = 1.05. In performing calculations by means of the nomogram of Fig. 101, we make use, in practice, of the δ side of this scale; the N side is given only for the sake of possible comparisons.

The next, single vertical scale is calibrated in units of SA, where the district area S is given in km^2, and the seismic activity is $A = A_7$ (for K = 7).

Both of these vertical scales, together with the third scale, marked K = 7 (this number is encircled), are used to perform the operation of multiplying $(R^2/\delta^2)\cdot(100/SA)$ involved in Formula (106). This portion of the nomogram gives the relationship

$$\lg\left(\frac{t_K}{10^{\gamma(K-7)}}\right) \div \lg\left(\frac{\delta}{R}\right)^2 = \lg\left(\frac{100}{SA}\right).$$

The three terms of this equality correspond to the three functional scales mentioned, in the following sequence: t_K (for K = 7), δ (and N), and SA. The multiplication operation is reduced to the addition of logarithms, which is carried out by drawing an auxiliary line, intersecting all three scales.

For the K = 7 case, the values of t_K are read off from the vertical line K = 7 from the points at which it intersects the series of inclined lines which are labeled with values of t_K.

In order to obtain the values of t_K corresponding to other values of K, a series of vertical lines are given, labeled with appropriate numbers. We go over to these lines from the K = 7 vertical by drawing auxiliary horizontal lines. As in the K = 7 case, the values of t_K for the vertical lines K = 8, 9, 10, ..., 6, 5, 4... are read off from the points of intersection with the inclined lines labeled with values of t_K. The slope of these lines corresponds to the numerical value of the parameter $\gamma = 0.43$.

As an example, let us use the nomogram to calculate the time t_K

for the conditions of the Garm district. We assume that we are interested in the observation times t_K in this district for the various K earthquake classes which must be used in order to determine the mean recurrences $\overline{N}_{K*}$ of earthquakes for these classes with an error not exceeding $\delta = 10\%$. In this case, we should allow for the fact that in the Garm district, the area $S = 13,500 \text{ km}^2$, and the seismic activity $A_7 = 5.0$. The value SA needed for the calculations is found beforehand: $SA = 13,500 \cdot 5.0 = 6.75 \cdot 10^4$.

We now use an auxiliary line to connect the points $\delta = 10\%$ (on the first left-hand scale) and $SA = 6.75 \cdot 10^4$ (on the second scale). Where the continuation of this line intersects the vertical $K = 7$, we find from the label on the appropriate sloping line $t_K = 2$ months. This, then, is the solution to the problem under these conditions for earthquakes in the $K = 7$ class.

In order to solve this problem for other values of K, we draw an auxiliary horizontal line through the point found. From its intersection with a vertical, for example, $K = 3$, we find that in order to obtain a result accurate to within 10% for the $K = 3$ case, it is sufficient to carry out observations here over a period of one-two days. Similarly, from the intersection of this same horizontal line with the vertical line for $K = 16$ (the destructive Khait earthquake of July 1949 belongs in the $K \cong 16$ class), we find that in order to determine the mean earthquake recurrence for this class with the same 10% accuracy by means of earthquake observations for precisely this class $K = = 16$, it would be necessary to carry out observations in this district for a period of more than 1000 years.

We note that the nomogram (Fig. 101) may be used also to solve several other problems; thus, for example, it is possible to find the degree of accuracy (with what error δ_K) it is possible to determine

the mean earthquake recurrence for a specific K class if observations
in a given district (with given S and A) are assumed to have been car-
ried out over a given period t_K.

§4. SEISMIC REGIME OF THE GARM DISTRICT

There are two main trends in the study of the seismic regime of
the Garm district: a) the study of the mean earthquake-recurrence char-
acteristics for the district as a whole, and for individual sections
of it and b), the study of the time variation in the seismic regime,
its characteristics, and parameters.

Here, by the Garm district we mean a region lying between 39°15'
and 39°30' North latitude and 70°00' and 71°30' East longitude, exclud-
ing the nonseismic Southeastern corner of this rectangle. The total
area of the district under study amounts to 13,500 km². A schematic
map of the district showing its division into sections is given in
Fig. 102.

The over-all period covering the observations entering into the
treatment of the given district lasted from 1 January 1955 to 30 Novem-
ber 1956, i.e., it equaled 23 months.

Studying the Earthquake-Recurrence Characteristics

Graphs of earthquake recurrence were compiled for the district as
a whole and for its individual sections. As a rule, the analysis made
use of all earthquakes having epicenters lying within the given dis-
trict, and having energies $E = 10^K$ joules, beginning with the K = 6
class. We tended to use only low-energy earthquakes in order to exclude
the effect of seismic-station location.

The largest number of observations were used to compile a recur-
rence chart for the entire district: 2500 earthquakes ranging from K =
= 6 to K = 13. This amounted to 28% of all of the earthquakes handled
by the expedition; 72% of the earthquakes belonged to the lower energy

classes, chiefly K = 4 and K = 5.

The earthquake-recurrence graph for the entire Garm district is shown in Fig. 103. The ellipses on this graph indicate the magnitude of errors in determining the density N* of earthquake recurrence for each class separately. On the K axis, the error size is fixed,
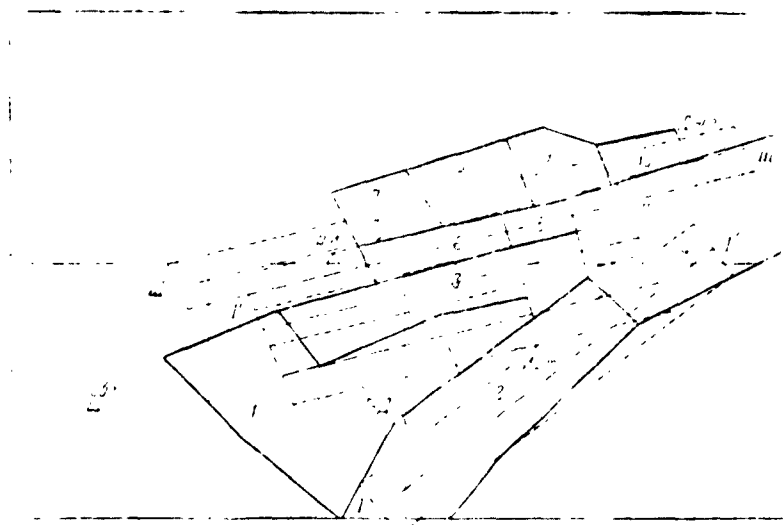
Fig. 102. Diagram showing division of Garm district into sections. Solid lines indicate section boundaries; dashed lines show boundaries and dash-dot lines axes of strips isolated for Fig. 109. The names of the sections are as follows: 1) Tovil'-Dora; 2) southern zone; 3) axial section of Peter I Range; 4) Shaklisu; 5) Tadzhikabad; 6) Nimich; 7) Kolonak; 8) Chusal; 9) Khait; 10) Dzhirgatal'.

i.e., at a half-order for E; along the N* axis are plotted the standard deviations for the mean monthly recurrence values, taken from 23 monthly observations. Table 15 gives the corresponding numerical data.

In the first line of this table, the K earthquake-energy classes are enumerated. In the following lines, the table gives the corresponding values for the following quantities: N̄, the mean monthly number of earthquakes in a given class for the entire district; N*, the earthquake-recurrence density, representing the number of earthquakes per 100 km^2 of area or per 10^3 km^3 of volume, for a one-year time interval:

TABLE 15

Mean Earthquake Recurrence for Various K Energy
Classes in Garm District, 1955-1956

	K							
	6	7	8	9	10	11	12	13
$\overline{N}$	115	60,6	18,6	7,1	3,2	0,70	0,48	0,17
N^*	10,22	5,51	1,60	0,645	0,291	0,0636	0,0436	0,0154
δ_N	23,8	11,4	37,5	44,9	49,8	169	139	230
$\delta_{\overline{N}}$	5,0	2,4	7,9	9,3	10,4	35,2	29,0	47,9

δ_N is the relative mean-square deviation of the observed monthly values N from the arithmetic mean $\overline{N}$; $\delta_{\overline{N}}$ is the relative error in the determination of the mean monthly value of the quantity $\overline{N}$ (and also N^*
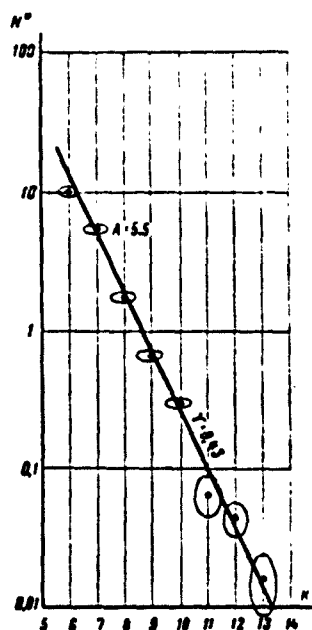
Fig. 103. Graph showing earthquake recurrence for Garm district, 1955-1956.

the following relationship holds between δ_N and $\delta_{\overline{N}}$: $\delta_{\overline{N}} = \delta_N/\sqrt{n}$, where n = 23 — the number of months in the total observation period. The quantities δ_N and $\delta_{\overline{N}}$ are given in the table in percent.

We see that for K = 6-9, the relative error $\delta_{\overline{N}}$ in the mean-monthly recurrence values $\overline{N}$ does not exceed 10%, reaching about this value for K = 10. It then rises sharply with increasing K, going to nearly 50% for K = 13. This is caused by the decrease in the number N of the earthquakes as the energy increases.

The large number of earthquakes observed makes it possible to draw a quite trustworthy average line on the recurrence graph of Fig. 103, using points for earthquakes in the seventh through tenth energy classes. There is some decrease in the number of points in class 6 with respect to the number determined by the general linear relationship, due, evidently, to the omission of some of these

weak earthquakes in the analysis of observations for border zones of the district.

On the basis of two-year (more precisely, 23-month) observations, the seismic activity for the entire Garm district amounted to $A = 5.5 \pm 0.5$, while the angular coefficient for the recurrence graph equals $\gamma = 0.43 \pm 0.05$. An estimate of the errors involved in determining the mean values of the parameters A and γ was made by comparing the monthly recurrence graphs.

Thus, the recurrence graph obtained over a two-year observation period for the Garm district quite reliably characterizes the contemporary mean seismicity of the region, to within 10%, for earthquakes of the sixth through tenth energy classes. For a direct determination of the mean recurrence for magnitude 6-7 earthquakes of class 13 to within the same 10%, it would be necessary to increase the observation period to nearly 70 years (see Fig. 100 or the nomogram of Fig. 101). In addition, the location of the observation points on the graph indicates that they fall quite well on the line, even for the two-year observation period; the line may be used for extrapolation to the stronger-earthquake region.

If an estimate of the mean seismicity for such an active district as the Garm district from class $K = 13$ earthquakes would be difficult in view of the length of time required to obtain reliable initial data, such an estimate would be impossible, in practice, for less active districts such as the Stalinabad district. Thus, in order to determine earthquake recurrence for an estimate of the seismic activity of districts, it is necessary to bring weaker earthquakes into the analysis so as to obtain a sharp increase in the total number of earthquakes observed; it is also necessary to evaluate the possibility of extrapolating the regularities obtained to the strong-earthquake region, by

studying the mean seismic-regime parameters in terms of the entire group of data.

The earthquake recurrence is determined not only for the Garm district as a whole, but also for the basic seismic zones (Northern, Central, and Southern), for individual strips, and for various localities of the district. On the corresponding graphs (Figs. 104-107), as before, the earthquake-energy classes K are plotted along the horizontal axis, and the mean monthly recurrence values N^* along the vertical axis. The various designations indicate points referring separately to 1955 and to 1956, as well as to both years together.

1. Northern zone. Table 16 gives values for the basic parameters A and γ for individual sections of the Northern Surkhob River strip.

TABLE 16

Values of the Parameters A and γ for Sections of the Northern Surkhob River Strip from 1955-1956 Observations

1 Участок	S км²	A	γ
2 Джиргаталь	144	8,4	0,45
3 Хаит	245	20,6	0,47
4 Чусал	315	9,6	0,50
5 Колонак	275	8,4	0,50

1) Section; 2) Dzhirgatel'; 3) Khait;
4) Chusal; 5) Kolonak.

When the level of the seismic activity A is examined, the Khait section stands out sharply; it is the most active section in the entire Garm district. The high activity of this section is quite stable in time: the mean-annual activity in 1955 and 1956 was nearly the same for this section — A ≅ 20. The high seismicity of the Khait section was also exhibited by observations of earlier expeditions [1, 2, 4, 83], and data from the regional seismic network over a long period of time

[11, 227].

The earthquake-recurrence graph for all four sections of the
Northern Surkhob River strip together is shown in Fig. 104a. The next
graph, Fig. 104b, characterizes the earthquake recurrence for the en-
tire Northern Surkhob zone from Garm to Dzhi:gatal'. For this zone,
$A = 6.2$ and $\gamma = 0.45$. The graph indicates a large increase in activity
during 1956 in comparison with 1955. This increase occurred chiefly
owing to the Northwestern Dzhi::atal' section, which in 1956 was
noticeably more active than in 1955. In particular, on 30 June 1956,
a class 13 earthquake occurred.

2. Central zone. Information on earthquake recurrence in sections
of this zone is given in Table 17 and on Fig. 105.

The data for the eastern regions is the most reliable. Here, ow-
ing to the partial neglect of class 6 earthquakes, the recurrence line
was drawn basically only for the three earthquake classes $K = 7-9$. The
general activity level for these sections in 1956 was somewhat less
than in 1955. The decrease in activity during 1956 was also observed
for the Tadzhikabad section, which lies in the Surkhob River strip. For

TABLE 17

Values of Parameters A and γ for Cen-
tral Seismic-Zone Sections from Ob-
servations of 1955-1956

1 Участок	S км²	A	γ
2 Шаклису	1250	4,8	0,54
3 Таджикабад	113	12,0	0,43
4 Нимич	252	7,2	0,47
5 Осевой участок хр. Петра 1 .	737	14,0	0,43
6 Товиль-Дора	1340	3,6	0,50

1) Section; 2) Shaklisu; 3) Tadzhik-
abad; 4) Nimich; 5) axial section of
Peter I Range; 6) Tovil'-Dora.

the remaining sections of this strip: in 1956, an increase in activity
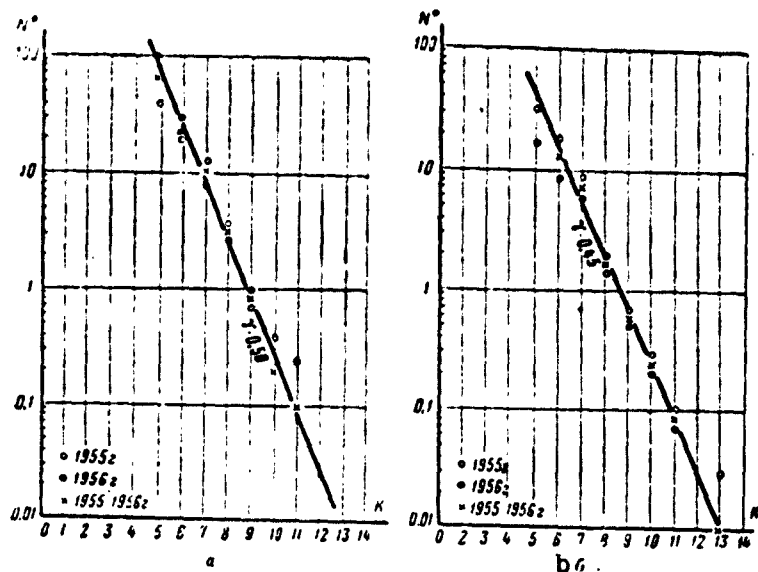
Fig. 104. Graphs of earthquake recurrence for
Northern zone. a) Northern Surkhob River strip
(Garm-Dzhirgatal'); b) entire northern Surkhob
zone.
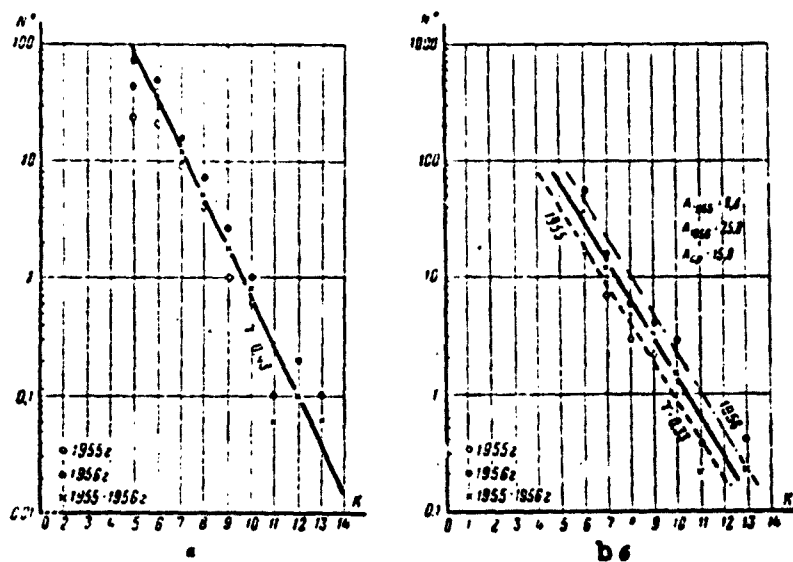
Fig. 105. Earthquake-recurrence graphs for Central
zone. a) Axial section of Peter I range; b) Chil'-
Dora district.

was observed, due chiefly to stronger earthquakes.

In 1956, there was a sharp rise in the activity of the axial por-
tion of the Peter I range (Fig. 105a). The basic role in this increase

TABLE 18

Characteristics of Seismic Activity for
Chil'-Dora District, 1955-1956

	K							
	6	7	8	9	10	11	12	13
$\bar{N}_{1955}$	3,7	1,3	0,67	0,5	0	0,083	0	0
$\bar{N}_{1956}$	12,4	3,6	1,16	0,9	0,63	0	0	0,09
δ_N	130	135	103	177	220	109	—	109
$\delta_{\bar{N}}$	27,0	27,0	20,4	37,0	45,5	220	—	220
R	3,67	2,17	1,21	1,48	1,27	1,63	—	2,26
σ_R	0,73	0,44	0,23	0,35	0,73	2,6	—	2,6

was played by the Chil'-Dora district (Fig. 105b), which falls within this section. From the end of 1955 on through the entire year of 1956, the two-year maximum number of strong class 11-13 earthquakes for the entire Garm district occurred here, as well as a considerable number of weaker earthquakes. In 1955, the activity of this district was A = = 9.6, and in 1956, it rose to A = 25. This increase in activity with respect to weak earthquakes was to a large degree due to the aftershocks of strong earthquakes. The slope angle of the recurrence curve remained practically unchanged in this case: $\gamma = 0.33$. Numerical data for this district is given in Table 18.

The K earthquake-energy classes are given in the first line of this table, and in the following lines we have the quantities: $\bar{N}_{1955}$ and $\bar{N}_{1956}$, the mean-monthly number of earthquakes for 1955 and for 1956, δ_N, the relative standard deviation of the observed monthly values of N from the arithmetic mean $\bar{N}$ for the two-year period, $\delta_{\bar{N}}$, the relative standard error in the determination of the arithmetic mean $\bar{N}$ over the two-year period (δ_N and $\delta_{\bar{N}}$ are given in percent); R, the measure of the dispersion of the earthquake recurrences with respect to the two-year data, σ_R, the standard error in the determination of the quantity R.

A very indicative characteristic of this region of unstable seis-
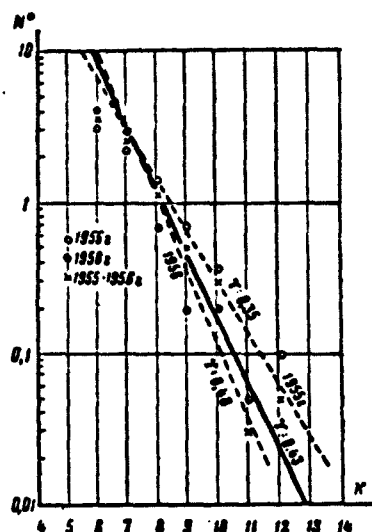
Fig. 106. Earthquake-
recurrence graphs for
the Southern zone (the
zone of the Karakul'
fault).
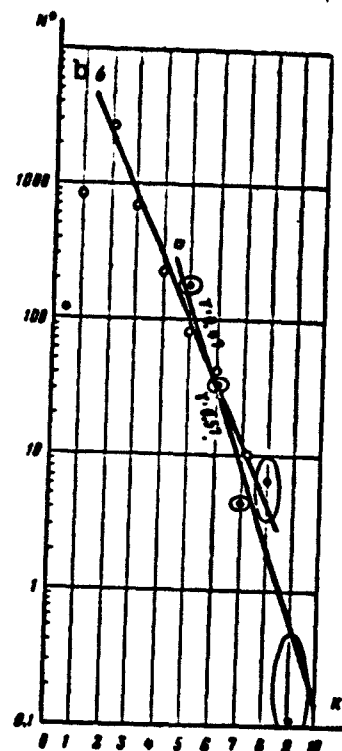
Fig. 107. Earthquake-
recurrence graphs. a)
Chusal section, 6-month
observation; b) neigh-
borhood of Chusal sta-
tion, 3 days.

micity is the behavior of R, the measure of earthquake-recurrence dis-

persion. While for the entire Garm district, the mean level of R is

close to unity, for the Chil'-Dora district, the mean value of this

quantity equals 2.0 (see Table 18).

On the whole, the entire western section of the central zone, in-

cluding the Tovil'-Dora section, is characterized, on the average,

over the two-year period by roughly the same activity A = 3.6. The

equalization in activity for these districts occurred owing to a de-

crease, during 1956, in the activity of the Tovil'-Dora section.

3. Southern zone. For the Southern seismic zone, the earthquake

recurrence (Fig. 106), on the average over the two-year period, taken

for all three sections together, is characterized by the following

values of the basic parameters: $A = 3.6$, $\gamma = 0.43$. The sections of this zone are characterized by a quite large spread of points on the recurrence curves. The lines drawn in Fig. 106 through the observation points for 1955 and 1956, differ quite sharply in their values of the parameter γ. For 1955, these values are lower ($\gamma = 0.35$), than for 1956 ($\gamma = 0.48$). Here, the activity level A for the seventh earthquake-energy class is nearly invariant in both cases. The variation in the slope of the line occurs owing to the stronger earthquakes that occurred in this zone during 1955.

Stability Evaluation for Determination of Parameters of Earthquake-Recurrence Characteristics

Such an evaluation is carried out from two points of view. First, we are interested in the possibility of determining the parameters A and γ in districts having a normal seismic regime over short periods and, second, in investigating the possibility of extrapolating recurrence curves for a normal regime to strong earthquakes. By a "normal" regime, we mean a regime whose characteristics and parameters differ little from those for the long-term average regime in the given region.

1. Evaluating stability of recurrence curves over short periods of time. To do this, special graphs of this type were constructed. For the Chusal section, such a graph was plotted from six-month observations during the first half of 1956 (Fig. 107, line $\underline{a}$). The level of seismic activity A over this period ($A = 8$) turned out to be somewhat less than the mean activity level for this section over two years ($A = 9.6$), while the parameter γ for the recurrence curve over the same period was $\gamma = 0.57$ — somewhat more than the mean value $\gamma = 0.50$ (see Table 16). The sizes of the relative errors in the recurrence determinations are shown in this graph by ellipses. As may be seen, for classes $K = 5-8$, the errors are not very large, and the average line

can in this case be drawn quite reliably. The graph obtained, on the whole, gives a rather good picture of the average seismic regime for this section.

Observations taken over a shorter period, amounting all-in-all to only three days, from 8 to 10 April 1955, were used to plot the recurrence graph (Fig. 107, line $\underline{b}$) for the area in immediate proximity to the Chusal station, on the basis of very weak recorded earthquakes, belonging to energy classes 1-7. Here, the position of the epicenters was not determined. All earthquakes recorded at the Chusal station by the MPS seismograph, having a magnification of about $5 \cdot 10^5$, showing a time difference $t_s - t_p$ in the arrival of the transverse S and longitudinal P waves not exceeding 2.5 sec were considered, i.e., those earthquakes whose hypocentral distances did not exceed roughly 20 km. The area over which the epicenters of these earthquakes were distributed amounted to about 1000 km^2.

The earthquake energies were determined from the amplitude nomogram (Fig. 47, Chapter 4). The earthquakes observed were processed in accordance with four-hour elementary time intervals. Here we have given the numbers of earthquakes in the various K energy classes observed in the separate time intervals. The bottom line of the table gives the total numbers N_Σ of earthquakes in the various classes observed over three days.

Table 19 shows the results of calculations carried out by means of the data of Table 20. Here we find the quantities: $\bar{N}$, the average, over three days, four-hour number of earthquakes in the various K classes; $\sigma_{\bar{N}}$, the standard deviation of the four-hour numbers from the mean arithmetic value $\bar{N}$; σ_N, the standard error in the determination of $\bar{N}$; δ_N and $\delta_{\bar{N}}$, the relative deviations corresponding to the absolute values of σ_N and $\sigma_{\bar{N}}$; R, the measure of the dispersion of the recur-

rences; σ_R, its standard error.

Above, we have indicated the importance of studying weak earthquakes in order to find, within short time periods, the laws governing earthquake recurrence in different districts. For the Chusal district,

TABLE 19

Characteristics of Seismic Activity in Neighborhood of Chusal Station from Three-Day Observations

	k						
	1	2	3	4	5	6	7
$\bar{N}$	4,7	7,0	4,2	1,45	0,44	0,22	0,05
s_N	2,28	2,68	2,02	1,39	0,51	0,42	0,23
$s_{\bar{N}}$	0,53	0,49	0,48	0,33	0,12	0,18	0,23
δ_N	0,48	0,30	0,48	0,96	1,16	0,19	0,42
$\delta_{\bar{N}}$	0,12	0,15	0,12	0,27	0,27	0,44	0,42
R	1,05	0,79	1,00	1,15	0,77	0,89	1,0
σ_R	0,183	0,135	0,173	0,231	0,191	0,471	0,02

despite the very short observation period — three days — the recurrence graph of Fig. 107, line b, quite well reproduces the recurrence graph of the somewhat larger district, Chusal, for a longer observation period (Fig. 107, line a). As a matter of fact, for the three-day observations we have: A = 12, γ = 0.47, while for a period of nearly two years, A = 9.6, γ = 0.50.

The quantity R is close to unity, both according to the three-day observations in Chusal, and according to the two-year observations over the entire Garm district.

The behavior of the dispersion measure R in two districts, Chil'-Dora and Chusal, is very indicative. Despite the increased activity, the regime of the Chusal district is "normal," and close to the average regime of the entire Garm district over a relatively long period of time. Here, we have a value of R close to unity, with a small spread in the individual determinations of this quantity. In the Chil'-Dora

district, an anomalously large value of R (= ~2) is observed, together with a large spread in the determinations. This "anomaly" in the seismic regime of Chil'-Dora agrees well with the fact that observations in this district over a period of many years show that the district is relatively calm, and that it is only for 1956 that a sharp rise in activity with considerable monthly fluctuations may be observed. It is clear from this example that the value of R may serve as an index of normality (R = ~1) or abnormality (R >> 1) for the seismic regime of the districts studied over the length of the observation period.

All of the earthquake-recurrence graphs given show that on the average, the slopes of the recurrence curves vary within small limits. A noticeable decrease in the value of γ will be connected, as a rule, with a rise in the district activity, mainly owing to an increase in the number of comparatively infrequent stronger earthquakes. The value of the activity A in this case may also remain substantially unchanged.

2. Evaluation of the possibility of extrapolating the recurrence curves to strong earthquakes. For this purpose, the data gathered by our expedition for weak earthquakes was plotted on a single graph (Fig. 108): 1) Garm district, 2) Stalinabad district, and 3) Chusal district; 4) data of V.I. Bune [107] for strong earthquakes in the Garm district over a 25-year period; σ) data of Gutenberg and Richter [64] for destructive shallow-focus earthquakes throughout the entire world over a period of several decades.

On this graph, the lines for weak (1) and strong (4) earthquakes for the Garm region coincide, for all practical purposes, although the different lines were plotted on the basis of different data and varying observation periods. The slope of these curves is γ = 0.43, the seismic activity is A = 5.5. The graph for the Chusal district, for the three-day period, has nearly the same slope (γ = 0.47), although

TABLE 20

Number of Weak Earthquakes in Neighborhood of Chusal Station from Three-Day Observations

1 Время наблюдения, дата, часы	K						
	1	2	3	4	5	6	7
8.IV 1955							
0—4	4	4	2	1	1	1	—
4—8	9	8	4	1	1	—	—
8—12	8	8	3	3	1	—	—
12—16	6	5	4	1	—	—	—
16—20	3	6	2	3	—	—	—
20—24	5	7	2	2	—	—	—
9.IV 1955							
0—4	2	5	4	—	—	—	—
4—8	3	7	6	—	—	—	—
8—12	4	4	3	—	—	—	—
12—16	3	7	5	1	1	—	—
16—20	7	8	9	1	—	—	—
20—24	4	8	2	4	1	1	—
10.IV 1955							
0—4	5	3	7	1	—	—	—
4—8	3	8	3	1	—	—	—
8—12	4	8	4	2	—	—	—
12—16	7	13	7	1	1	1	1
16—20	2	8	4	3	1	—	—
20—24	6	9	5	1	1	1	—
N_Σ	85	126	76	26	8	4	1

1) Observation period, date, hours.

the activity level in this case is roughly twice as great $(A = 12)$.
For the Stalinabad district, the slope is maintained, approximately,
at $\gamma = 0.47$, but $A = 0.9$. For the world as a whole, according to data
on destructive shallow-focus earthquakes [64], $\gamma = 0.45$ for the
straight-line portion of the curve, and $A = 0.03$.

The approximate constancy of the slopes, $\gamma \cong 0.45$, for the curves
of the mean earthquake recurrence is noteworthy. It is maintained over
a very wide range of earthquake-energy variation: from $K = 1$ to $K = 17$,
i.e., over 16 orders of magnitude of variation in E, for various seis-
mic-activity levels (on Fig. 108, from $A = 0.03$ to $A = 12$), for ob-
servations over different time intervals (from three days to several
decades), and for various areas investigated (from 1000 km^2 to the en-
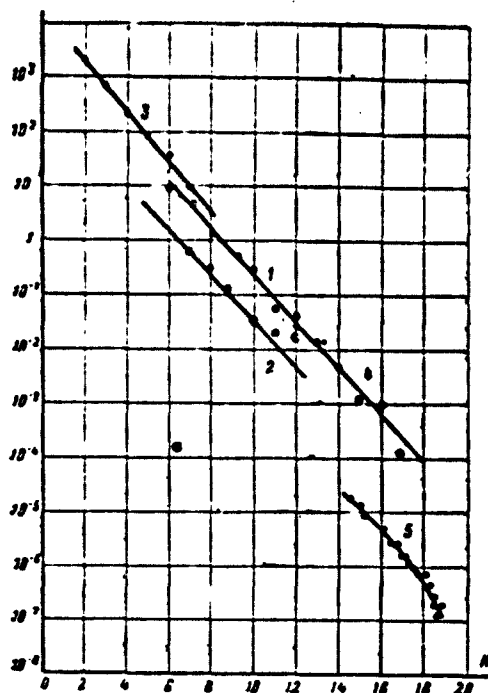
Fig. 108. Comparison of earth-
quake-recurrence graphs for
various energy ranges. 1) Garm
region, from data of TKSE; 2)
Stalinabad district; 3) neigh-
borhood of Chusal; 4) Garm dis-
trict, according to V. I. Bune;
5) entire world, shallow-focus
earthquakes, according to
Gutenberg and Richter.

tire surface of the earth).

The considerable deviations in γ from the mean value $\gamma = 0.45$ en-
countered in isolated infrequent cases may indicate, together with con-
siderable departures of R from unity, abnormality in the regime for a
given district over a given time interval. In these cases, especial
care must be exercised with respect to the evaluation of the mean seis-
mic activity of the district on the basis of comparatively brief ob-
servations.

The values of the parameters A and γ for the average seismic re-
gime for each actual district make it possible to proceed to an evalu-
ation of the possible mean recurrence (repetition frequency) of strong

earthquakes in this district, i.e., to a solution of one of the most important problems of seismic districting. In view of the fact that the recurrence graphs in a strong-earthquake region, as a rule, bend only downward, the values of A and γ for the straight-line portion of these graphs make it possible to estimate at least the maximum possible strong-earthquake recurrence.

Investigation of Time Variation in Seismic Regime

For the Garm district, this investigation was carried out in the following main directions: 1) examination of the seismic regime itself as a sequence of earthquakes having various energies in time and in space; 2) examination of the time variation in certain indices and parameters of the seismic regime; c) analysis of correlation relationships among various regime parameters that vary in time; 3) comparison of time variation in regime parameters determined from weak earthquakes with individual stronger earthquakes.

1. Examination of seismic regime in time and in space. Such an examination was carried out separately for various specially chosen sections of the Garm district. The sections were taken in the form of strips, so as to permit the plotting of space-time graphs of the seismic regime for them in the x,t plane (see §3 of this chapter for a more detailed discussion of the plotting of such graphs). Three strips about 10-12 km wide were selected. The longitudinal axes of these strips are shown on Fig. 102. Earthquakes whose epicenters fell within these bands are associated with the axial line of the section (the x coordinate). Corresponding diagrams for regime variation in time and in space are shown in Fig. 109.

Strip 1 (I-I', Fig. 102). This strip is located along the Karakul' fault. Its seismic activity is very irregular. In 1955, the number of weak earthquakes was greater to the west than to the east. Two strong

class 12 and 11 earthquakes occurred precisely in the eastern section, however, against a background of almost complete seismic calm. During 1955, a certain shift in seismic activity from west to east, toward the region in which strong earthquakes appear, was observed. The year 1956 was characterized by a uniform distribution of weak earthquakes over the entire zone.

It is noteworthy that the strong earthquake of 12 August 1959 was accompanied by almost no aftershocks, while the earthquake of 13 November 1955 was accompanied by a large number of aftershocks.

Strip 2 covers the southern slopes of the Peter I range. Two seismic districts fall within this strip: Chil'-Dora and the Ishtion district. The eastern edge of the band overlaps the first band somewhat. Within the band there are two seismic sections, separated by a zone of relative calm. The strong ($K = 13$) Chil'-Dora earthquake of 11 April 1956 fell within the western zone. A relatively high activity level is observed in both sections during the months preceding strong shocks, and it is only directly before these shocks that periods of relative calm are observed. Both shocks, western and eastern, were accompanied by considerable numbers of aftershocks.

Strip 3 falls in the axial section of the Peter I range. The activity of the entire strip, with respect to weak earthquakes, is quite uniform. Rather strong class 10 shocks occurred in 1955 in its eastern section. Throughout this entire year, there was a tendency for some shift in foci to the west. In the eastern zone of the strip, at the beginning of 1955, there was a single class 11 earthquake against a background of almost total calm. The strongest earthquake to occur in this band, falling in the twelfth energy class, occurred 22 September 1956. Prior to this earthquake, a period of relative seismic calm was also observed. Relatively few aftershocks were associated with this

earthquake. The space-time regime curves for strips 2 and 3 have been published earlier [171].

Strip 4 (II-II', Fig. 102) covers the northern slopes of the Peter I range and the left-bank portion of the valley of the Surkhob River. Within the strip, two sharp shocks of the twelfth and eleventh classes were noted at the beginning of 1956 (II-II', Fig. 109b). Prior to the earthquake of 14 January 1956, following a period of relative calm, a certain increase in activity was observed directly before the earthquake. The aftershocks for these earthquakes were small. Throughout 1955, high seismic activity was observed to the east, while in 1956, the seismic activity was distributed quite uniformly over the entire strip.

Strip 5 (III-III', Fig. 102) covers the entire valley of the Surkhob River from Dzhirgatal' to the east and roughly to the $70^{\circ}00'$ meridian in the west. The seismic activity of the strip (III-III', Fig. 109c) differs in its various sections. In the central and eastern sections, the level of activity is quite high, while to the west, across the meridian of the Yaldymych station, it drops sharply. In this section, there are only isolated extremely rare earthquakes. The strongest earthquakes of strip 5 fall into strip 4, and have been considered above. In 1955, the greatest number of epicenters was observed in the central portion of strip 5. Since the end of 1955 some tendency toward a shift in activity to the east has been observed. Throughout 1956, the seismic activity was quite uniformly manifested in the central and eastern sections of the strip.

The quantitative examination of the seismic activity for individual sections of the Garm district given above indicates that we here often see a certain decrease in activity prior to stronger earthquakes. The degree of decrease and the length of the period of relative calm dif-
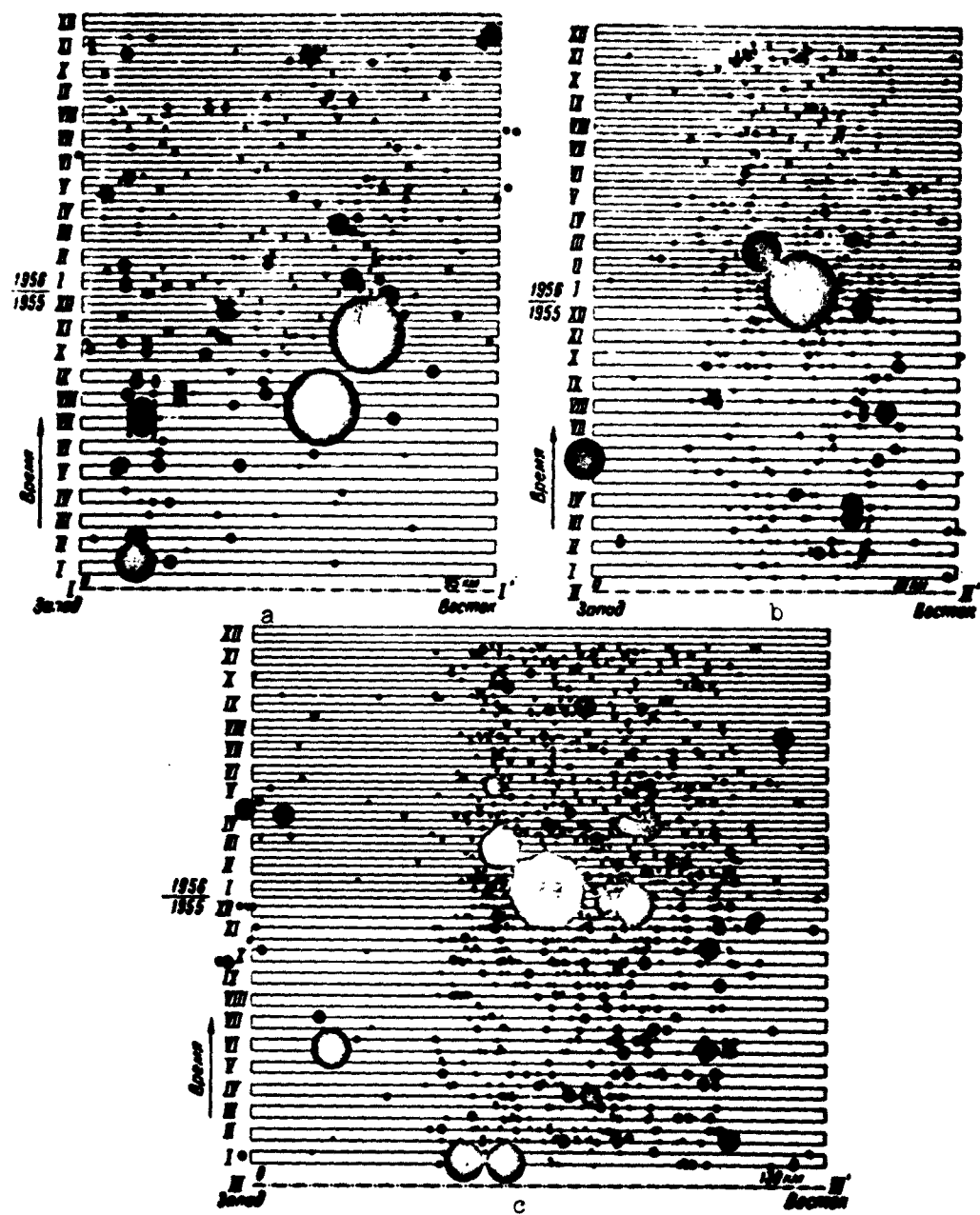
Fig. 109. Space-time seismic-regime graphs. a) Karakul' discontinuity (strip I in Fig. 102); b) Northern slopes of the Peter I range (strip II); c) Surkhob river valley (strip III). minimum energy of indicated earthquakes 10^6 joules; maximum. 10^{12} joules.

fer in different cases, and it is still very difficult to discern any quantitative relationships in this region that would indicate the imminence of a stronger shock.

The diagrams considered show clearly that in the various districts and sections rather sharp variations in seismic activity with time are observed, although the average indices of seismicity for large regions with respect to time or space may in this case vary little. As a result, a more detailed study is required in analyzing seismic activity of the time variation in the activity of individual small sections, in order to find the regularities governing activity variations in time and in space. At present, it seems that the only way of speeding up the study of this aspect of the seismic regime is the utilization of weaker earthquakes in the analysis.

2. Time variation of seismic-regime parameters. The curves of Fig. 110 were plotted for the entire Garm district; they show the time variation of the basic seismic-regime parameters, the quantities A, γ, and R; there is also the corresponding graph for the accumulation of arbitrary strains $\Sigma\sqrt{E_1}$, after Benioff, plotted in accordance with the ideas discussed in §3 of the present chapter.

The systematic decrease in activity (the calm) prior to stronger shocks is not noticeable on the Benioff graph. It is possible, provided that such phenomena do exist, that they are only local in character, and that their effect is lost owing to the degree of averaging involved here. In some cases, on the other hand, a certain increase in activity is noted on this graph prior to strong shocks. On the whole, the activity pattern for the entire district is quite uniform, according to the Benioff graph.

Let us now examine the curves $A(t)$, $\gamma(t)$, and $R(t)$, as well as the curve for the product $\Pi(t) = A \cdot \gamma \cdot R$. The points on the $A(t)$ and
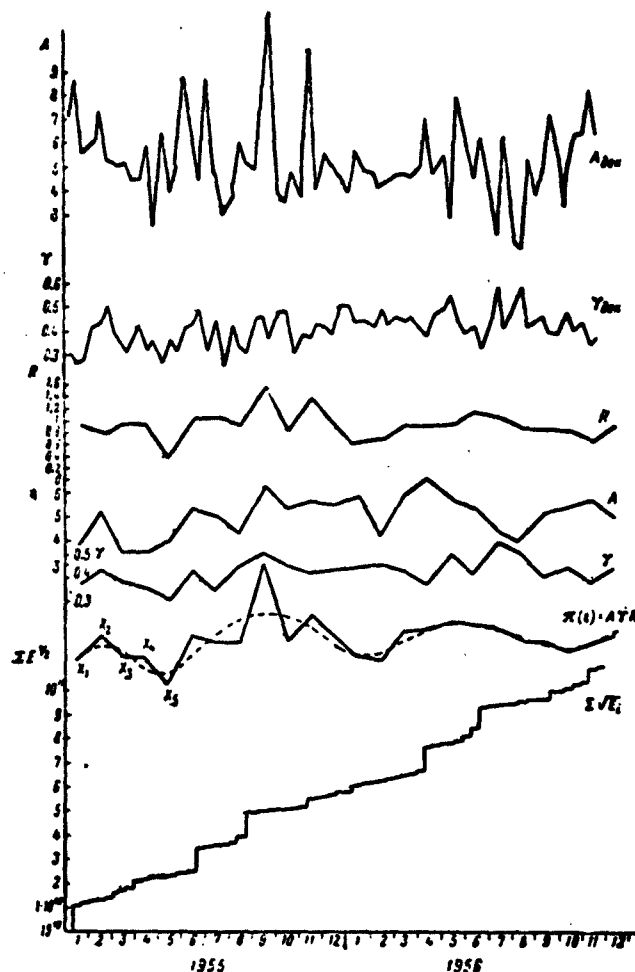
Fig. 110. Time variation in parameters
R, A from monthly data and A_{dek}, γ_{dek}
from decade data, and graph $\Pi(t) = A\gamma R$
and arbitrary-strain accumulation graph
for Garm district.

$\gamma(t)$ curves were plotted from mean monthly data and from decade data;
for R, the monthly values were used. The monthly values were also used
to plot a curve showing the time variation in the product $\Pi(t) = A \cdot \gamma \cdot R$.

We cannot find any well-defined relationships among the time vari-
ations of the corresponding quantities by direct inspection of this
group of graphs, nor can we see any connection between such variation
and the moments of appearance of stronger shocks, which are reflected
on the Benioff graph by steep steps.

In order to investigate the possible periodicity of time varia-
tions in the quantities $\Pi(t) = A \cdot \gamma \cdot R$ and $A(t)$, the data of Fig. 110
was subjected to a special analysis, using methods of mathematical
statistics [170]. Let us first consider the function $\Pi(t) = A\gamma R$. The
points X_1, X_2, X_3, ..., X_n on Fig. 110 represent the monthly values of
$\Pi(t)$. The graph takes the form of a broken curve for which a certain
periodicity strikes the eye: a repetition of maximums every 8 months.
We are now faced with the problem of whether or not to consider this
visible periodicity a manifestation of some law, or a random phenomenon,
due to the natural spread in the values of the X_i.

To solve this problem, we compute the functions $\varphi(T)$ and $\psi(T)$,
defined by the formulas

$$\varphi(T) = \sum_{i=1}^{n} \bar{X}_i \sin \frac{2\pi}{T \cdot n} i; \quad \psi(T) = \sum_{i=1}^{n} \bar{X}_i \cos \frac{2\pi}{T \cdot n} i.$$

Here $\underline{i}$ is the number of the month; $\underline{n}$ is the number of months; X_i is
the deviation of the relative monthly value of the Π_i from the mean
arithmetic value of all of the Π_i, which equals $\sum_{i=1}^{n} (\Pi_i/n)$; T is the
period with which the function repeats.

From probability theory [170], it is known that if the periodicity
is not random, the numerical value of the quantity $\sqrt{\varphi^2 + \psi^2}$ at appro-
priate values of T will be of the order of $\underline{n}$ (for sufficiently large
$\underline{n}$), while if the periodicity is random,

$$|\varphi| < 2\sqrt{\sum_{i=1}^{n} \bar{X}_i^2}; \quad |\psi| < 2\sqrt{\sum_{i=1}^{n} \bar{X}_i^2}; \quad \sqrt{\varphi^2 + \psi^2} < 2\sqrt{\sum_{i=1}^{n} X_i^2}.$$

The quantities $\varphi(T)$ and $\psi(T)$ were computed for $T = 8$ months. The
calculation yields $\sqrt{\varphi^2 + \psi^2} = 2.9$, while $2\sqrt{\sum_{i=1}^{n} X_i^2} = 4.48$, so that

$$\sqrt{\varphi^2 + \psi^2} < 2\sqrt{\sum_{i=1}^{n} X_i^2}.$$

This indicates that the periodicity observed in the curve of $\Pi(t)$ may be random in nature.

A similar calculation was carried out for the function $A(t)$ (Fig. 110). Since no dominant period T is seen on the curve for $A(t)$, the following possible values of T, in months, were tested: 36, 18, 12, 9, 7.2, and 6. The maximum value of the function $\varphi(T) = 16.77$ was obtained for $T = 12$ months; this value was far less than $2\sum_{i=1}^{n} X_i^2 = 31.48$, however. Consequently, the periodicity noted for $A(t)$ may also be accounted for through random causes.
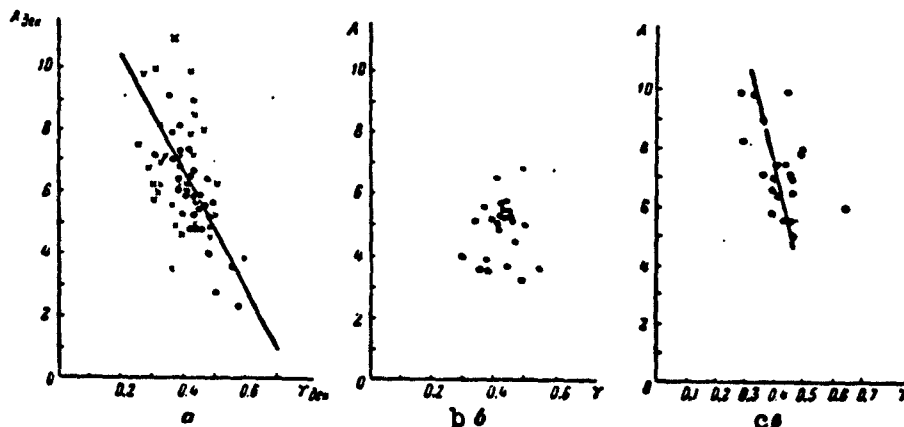
Fig. 111. Correlation function for parameters A and γ for a) Garm district, decade data; b) Garm district, monthly data; c) Peter I range district, monthly data.

3. Correlation functions for parameters A and γ. The graphs for the time variation of $A(t)$ and $\gamma(t)$, as well as $A_{dek}(t)$ and $\gamma_{dek}(t)$ (Fig. 110), do not directly display a well-defined relationship among these quantities. This does not mean, however, that such a relationship does not actually exist. A more objective examination of this problem may be carried out by constructing special correlation graphs.

Figure 111 shows graphs of the correlation between the quantities A and γ for the entire Garm district (area, $S = 13,500$ km^2 from decade (A_{dek}, γ_{dek}) and monthly (A, γ) data (Fig. 111a and b), as well as for the more localized central zone of the district, the region of the

Peter I range (area $S = 2400$ km^2, from monthly data (Fig. 111c).

The decade data for the entire Garm district (Fig. 111a) displays a clear relationship between changes in the quantities A and γ, while the relationship cannot be seen from the monthly data (Fig. 111b). In the first case, as we see, as the seismic activity A increases, the slope parameter γ for the recurrence curve decreases, i.e., a temporary increase in the activity A corresponds to a relative increase in the number of strong earthquakes. A similar relationship between A and γ is noted also for the smaller district from the monthly data (Fig. 111c). The idea arises that this inverse relationship between the time variations in the quantities A and γ does exist, but appears only in sufficiently small space-time regions.

This conclusion, however, is still not completely convincing, since it does not exclude the possibility that the observed relationship was obtained not as a result of an actually existing law-like connection between the quantities A and γ, but through the random spread in the points (Aγ), leading to special configurations having the form shown in Figs. 111a and 111c. In order to study this possibility, we check the connection between A and γ, using the so-called χ^2 criterion first for the case of Fig. 111a.

To do this, we calculate the coefficient β for the regression of γ on A, using well-known rules [170]

$$\beta_{\gamma A} = \frac{\sum_i (A_i - \bar{A})(\gamma_i - \bar{\gamma})}{\sum_i (A_i - \bar{A})^2} = 0,025.$$

Here $\bar{A}$ and $\bar{\gamma}$ are the mean values of A and γ ($\bar{A} = 6.29$, $\bar{\gamma} = 0.407$). Summation is carried out over all of the measurements for A available, and the corresponding values of γ.

We next the calculate the quantity

$$\tilde{\gamma} = \gamma_i - \beta_{\gamma A} \cdot A_i.$$

If we were now to plot a curve for the quantities A and $\tilde{\gamma}$, rather than A and γ, the region occupied by the points would be oriented roughly vertically, regardless of its previous orientation. Instead of plotting a special curve in the rectilinear coordinates A,γ, it is possible to utilize the previous graph of A,γ adding to it the oblique coordinate system $A\tilde{\gamma}$. In this system, the values of $\tilde{\gamma}$ will be constant along a line drawn to the A axis at an angle $\alpha = \arctan \beta_\gamma A$.

Let us assume that in Fig. 111a, the region of variation in A is divided into several, let us say five, intervals by horizontal strips, and the region of variation in γ into the same number of oblique strips with slope $\beta_\gamma A$ (the values of γ for which the division is made may be determined on the horizontal axis $A = 0$, where $\gamma = \tilde{\gamma}$). Then the entire region of this variation in A and $\tilde{\gamma}$ turns out to be divided into 25 quadrilaterals. We number the horizontal and oblique strips by means of a procedure that associates a pair of numbers i,j with each quadrilateral, starting from the origin. Several points fall within each such quadrilateral. If A and γ are independent, for a sufficiently large number of points, they will be distributed uniformly over the quadrilaterals. An observed nonuniformity may either be attributed to random factors or to the existence of a relationship between A and γ. In order to decide whether the pattern is random, we calculate the quantity χ^2 from the formula

$$\chi^2 = n \sum \frac{\left(\nu_{ij} - \frac{\nu_i \nu_j}{n} \right)^2}{\nu_i \nu_j},$$

where $\underline{n}$ is the total number of points on the curve (in our case $n = 63$), ν_{ij} is the number of points falling within the quadrilateral (i,j), ν_i is the number of points in the $\underline{i}$th horizontal strip, ν_j is the number of points in the $\underline{j}$th oblique strip.

The quantity χ^2 characterizes the nonuniformity in the distribu-

tion of the points over the quadrilaterals. Calculations show that $\chi^2 = 8$. Using Pearson's table [190], we find that where A and γ are independent the observed points $(A_1\tilde{\gamma}_1)$, $(A_2\tilde{\gamma}_2)$, ..., $(A_n\tilde{\gamma}_n)$ may be arranged in this fashion, or even more regularly, with a probability p = = 90%. Thus, the data shown on Fig. 111a does not indicate the existence of a definite relationship between the quantities A and γ.

A similar calculation was also carried out using the data of Graph 111c. Here it turned out that the probability p = 95%. Thus, these data also do not indicate the actual existence of a relationship between A and γ.

We note that the analysis given does not demonstrate the absence of a relationship between A and γ. It only leaves the question of the existence of such a relationship open.
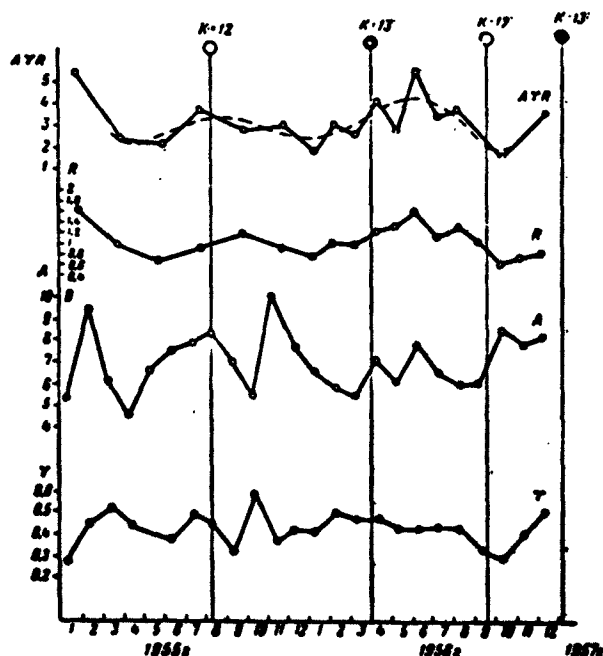
Fig. 112. Comparison of time varia-
tion in seismic-regime parameters A,
γ, and R with instants of occurrence
of stronger earthquakes for the
Peter I range district.

4. Comparison of time variation in parameters for seismic regime

with strong earthquakes. Such a comparison was carried out for the Peter I range district. The results are shown in Fig. 112. On this graph, the curves for the time variation in the parameters γ, A, and R are shown, as well as a curve for the product $\Pi = A \cdot \gamma \cdot R$ for these parameters. The appearance of stronger earthquakes on the time scale (class 12-13 with respect to energy) are indicated by vertical lines topped by circles.

We see by inspection from these graphs that there is at least an apparent connection between the variation in the curve $\Pi = A \cdot \gamma \cdot R$, which is quite similar in shape to the curve for R, and the instants of appearance of stronger earthquakes. In this case, the strong earthquakes most frequently (in 3 cases out of 4) appeared following minimum values of $\Pi = \Pi(t)$ on ascending portions of the appropriate curve. The earthquake of 22 November 1956 in the Peter I range represents an exception; it appeared at the end of a descending portion of the $\Pi(t)$ curve. The available data is insufficient to permit us to judge whether or not there is a well-defined connection between the times of appearance of relatively strong earthquakes and the time variation in the seismic-regime parameters A, γ, R, and Π. This still does not eliminate completely the possibility of the existence of a weak relationship. Far more abundant observational material would be required to find such a relationship and to establish its quantitative features should it exist.

§5. SEISMIC REGIME OF STALINABAD DISTRICT

A study of the seismic regime for the Stalinabad district was carried out by the same methods, and took the same general directions, as that of the Garm district, e.g.: 1) a study of the earthquake-recurrence characteristics, and 2) a study of the seismic-regime time variation.

The seismic-observation period used in the analysis of the Stalin-abad district differs little from the observation period for the Garm district, and amounted to 20 months: from January 1955 to August 1956, inclusive. The Stalinabad district is far less active seismically than the Garm district, however, which caused difficulty in processing the material by statistical methods: the far lower number of recorded earthquakes prevented a study of the over-all and monthly seismic-regime regularities with the desired accuracy and detail. Also, in the Stalinabad district, the station network was much more tenuous and the instrumental sensitivity, in connection with various interfering factors, was less than for the Garm district. All of these drawbacks were partially canceled by the experience gained in studying seismic-regime regularities in the Garm district. In many cases, it would have been impossible to draw definite conclusions about the Stalinabad district without a comparison with the Garm results.

The Greater Stalinabad district occupies an area lying between $38^{\circ}00'$-$39^{\circ}00'$ north latitude and $68^{\circ}00'$-$69^{\circ}30'$ east longitude. A schematic map of the Stalinabad district with the Lesser Stalinabad district outlined on it, as well as individual zones for which seismic-regime processing of materials was carried out is shown in Fig. 113. The area of Greater Stalinabad is 14,300 km^2, of Lesser Stalinabad, 4000 km^2.

Studying Earthquake-Recurrence Characteristics

Table 21 shows numerical data on earthquake recurrence for the Greater Stalinabad district for 20 months during the 1955-1956 period. In this table, the K are the earthquake-energy classes; N is the total number of earthquakes observed in a given class over 20 months; $\bar{N}$ is the mean monthly number of earthquakes; N* is the normalized earthquake recurrence (per year per 100 km^2 of area in the district); δ_N is

TABLE 21

Earthquake Recurrence in the Greater Stalinabad District

			K				
	6	7	8	9	10	11	12
N	44	63	40	13	5	2	2
$\bar{N}$	2,2	3,15	2,0	0,65	0,25	0,1	0,1
N^*	0,33	0,46	0,168	0,055	0,022	0,0084	0,0084
$\delta_{\bar{N}}$	23,0	0,14	0,14	0,20	0,48	1,0	1,0

the relative standard error in the number N. The numbers N* for $K = 6$ and 7 are computed for an area $S = 8000$ km^2, rather than 14,300 km^2 as in the case of all the remaining calculations, in view of the fact that the station network within this district is inadequate to cover all earthquakes of these classes.
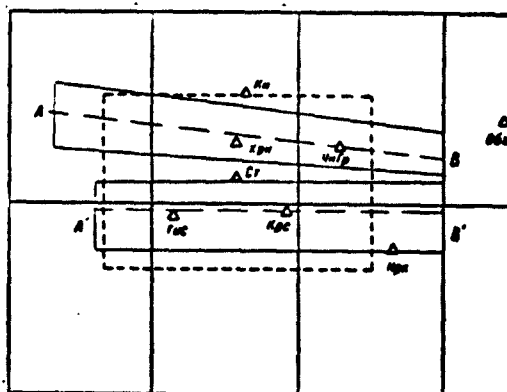
Fig. 113. Schematic map of Stalinabad district. The dashed line indicates the Lesser Stalinabad district.

Figure 114 shows earthquake-recurrence curves for the Greater and Lesser Stalinabad districts. On these graphs, as for the similar graphs of the Garm district (see Fig. 103), the ellipses indicate the magnitudes of errors in determining the recurrence N*. Here they are far greater than for the Garm district. The errors for class 11 and 12 earthquakes are especially large. This is quite understandable when we consider that over the two-year period of observations, there were all-

in-all two class 11 and 12 earthquakes here (and one class 13 earth-quake). The determination of N* for classes 7-10, for which the relative errors fluctuated from 15 to 55%, was more reliable.

For class 6, however, the relative errors again rise in comparison with classes 7-9, reaching 20-25%. In this case, the systematic errors associated with a failure to determine the focal coordinates for several earthquakes play a substantial role (without the focal coordinates, the earthquake data cannot be utilized to determine the recurrence). This may be seen from the fact that there are fewer class 6 earthquakes than class 7, despite the fact that the actual numerical relationship between these earthquake classes must be assumed to be the opposite.

The averaging line on the given graph was drawn for points of class 7-10 earthquakes, as being the most reliable data. Then the slope parameters γ for both graphs may be considered to be identical in first approximation and equal to $\gamma = 0.43$, as for the entire Garm district, while for the seismic activity the value is: for the Lesser Stalinabad district, A = 0.9, and for Greater Stalinabad, A = 0.4. The lower activity of the Greater Stalinabad district is associated with the existence of inactive sections in the southwest and northwest portions, regions not contained in Lesser Stalinabad.

For practical purposes, it is especially interesting to evaluate the seismic activity of the central portion of the Gissar Valley. The activity (see Fig. 139) is determined by the presence of strongly seismic zones along the southern and northern edges of the valley. The existence of low-seismicity zones along the northern and southern borders of Greater Stalinabad, from this point of view, is unimportant and, consequently, in further calculations it must be assumed that the seismicity of the Gissar Valley is the same as for the Lesser Stalinabad district: A = 0.9.
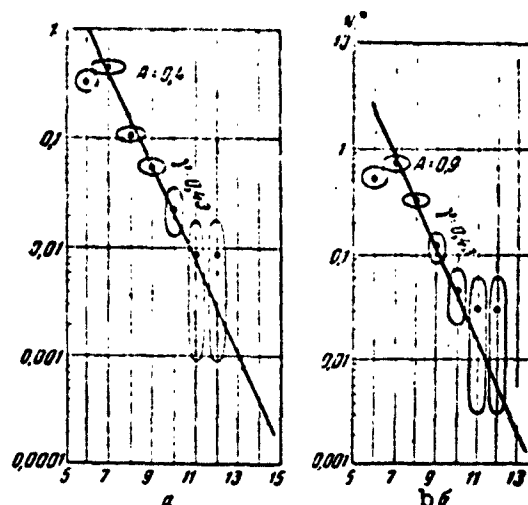
Fig. 114. Earthquake-recurrence
curves for the Stalinabad dis-
trict. a) Greater Stalinabad dis-
trict; b) Lesser Stalinabad dis-
trict.

In view of the relatively high activity of the Northern and South-
ern epicentral zones, the recurrence graphs for these areas were plot-
ted separately (Fig. 115). They include only the most representative
observations (for class 7-10 earthquakes). In plotting the averaging
lines on these graphs, they were given a slope $\gamma = 0.43$, obtained from
more reliable materials for the district as a whole. Without a more
careful choice of data from among class 6 earthquakes and, correspond-
ingly, without increasing the observation periods for stronger shocks,
it is difficult to see how closely this assumption accords with the
actual facts. If, however, the values of γ for the various zones ac-
cording to these observations remain to some degree problematical, the
value of the seismic activity A for these zones is more reliably fixed.
Thus, in 1955-1956, the activity of the Southern epicentral zone, A =
= 1.2, was greater than that of the Northern zone, A = 0.7. A more ac-
curate determination of the basic parameters A and γ of the seismic
regime for these zones is an important task of future studies on the

seismicity of the Stalinabad district.

An examination of the recurrence graphs for the Stalinabad region
and its sections gives an idea only of the mean seismic activity for
relatively large areas measuring $S = 2000-4000$ km^2 or more. Within
these areas, smaller sections may be isolated, differing quite sharply
in their activity. Thus, for example, in the Southern zone, which, on
the whole, is the most active area in the Greater Stalinabad district,
it is possible to pick out a section having small activity, such as,
for example, the section to the east of Gissar, or with higher activ-
ity, such as the districts surrounding the Karasu station (see Fig.
141).
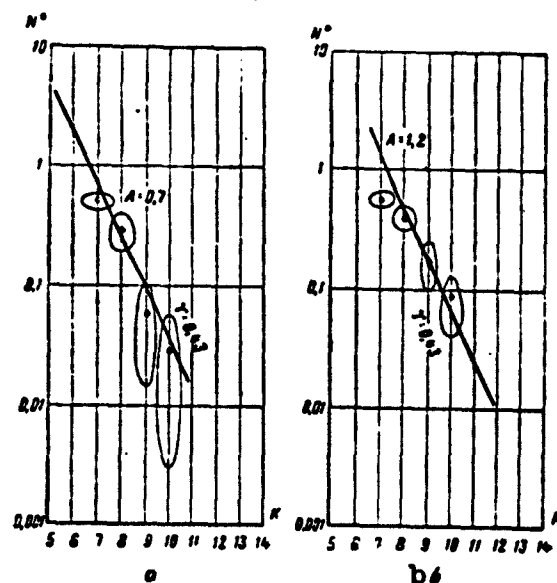
Fig. 115. Earthquake-recurrence
curves. a) Northern zone; b) South-
ern zone of Stalinabad district.

It is an indicative fact that the regime for weak shocks ($K < 7$),
recorded by a single station, will normally agree with the activity
estimate for stronger shocks ($K = 7$, 8, and 9), reflected on the seis-
mic-activity map. Thus, the Karasu station, in 1955, recorded weak
shocks ($K < 7$, where $t_s - t_p = 0.5-2.0$ sec), roughly 20 times more of-

ten than the Gissar station: 67 for Karasu, and 3 for Gissar. In the districts surrounding the Northern stations, the weak-shock activity differed less: the figures were 21 for Kon-Dora, and 15 for Khorongon. Roughly the same relationships also obtained for seismic activities determined on the basis of stronger shocks and shown on the map (Fig. 141). Thus, no contradiction was observed between relative activity estimates based upon shocks of differing forces.

Studying the Time Variation in the Seismic Regime

For the Stalinabad district, for the Northern and Southern zones separately, space-time seismic-regime curves and Benioff arbitrary-strain accumulation curves were plotted. The method used to plot these graphs was the same as those used for the Garm district.

The space-time seismic-regime curves for the Stalinabad district are shown in Fig. 116a for the Northern zone (strip along line AB on Fig. 113) and on Fig. 116b for the Southern zone (strip along line A'B' on Fig. 113). These curves show a large number of strong shocks in the Southern zone (Fig. 116b); the absence of well-defined fore-shocks on the class 6 level prior to quite severe earthquakes (22 November 1956, the magnitude 7-8 Nureksk earthquake, of class 13 energy; 18 April 1955, class 12; 4 February 1956, class 11) may also be seen from Fig. 116b; a greater uniformity in the weak-shock background in the Northern zone (Fig. 124a) than in the Southern zone (Fig. 116b) is also apparent.

An interesting feature of the Stalinabad-district seismic regime is the existence of double shocks. Double shocks for $K = 12-11$ and lower earthquake-energy classes have been noted. The time intervals between the double shocks range from one minute to 24 hours. Their foci are generally quite close together; thus, for example, the earthquakes of 4 February 1956 at 17 hr 53 min ($K = 11$) and at 17 hr 59 min ($K =$
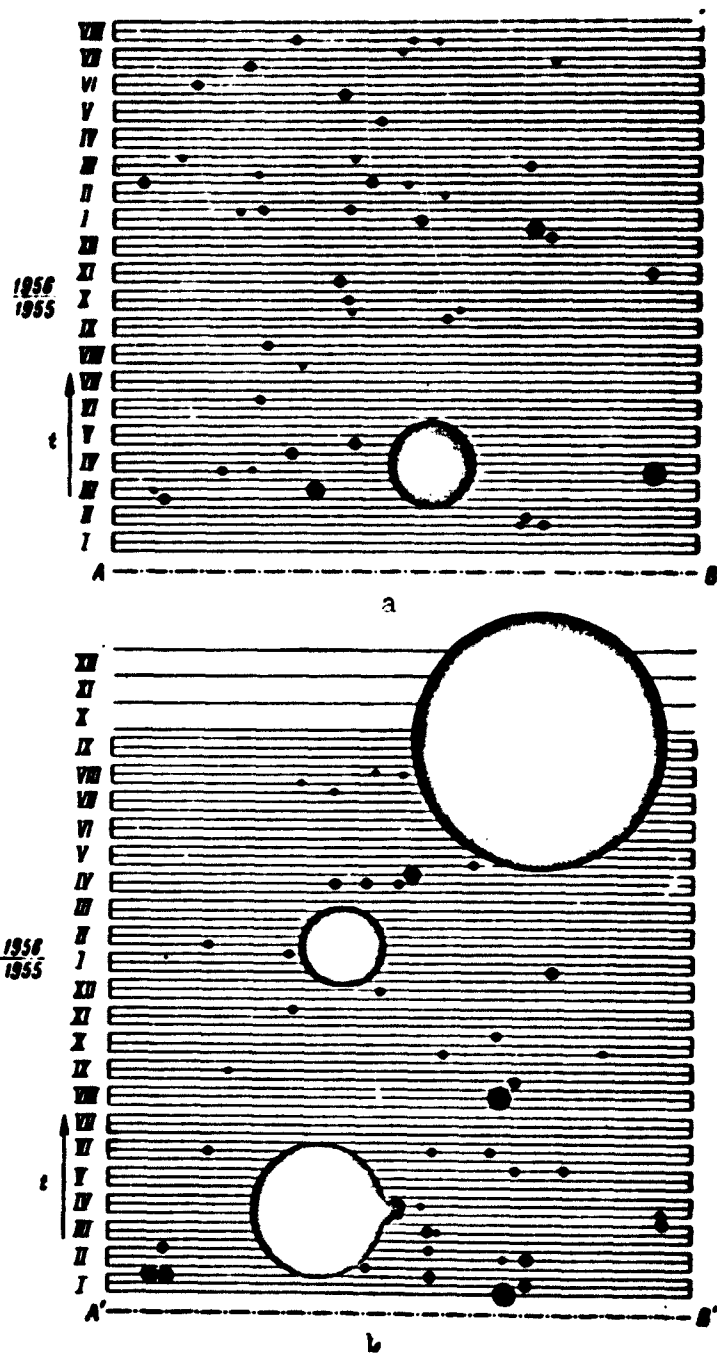
Fig. 116. Space-time seismic-regime graphs.
a) Northern zone; b) Southern zone of Sta-
linabad district.

— 11) had nearly the same focus. Sometimes, however, the foci of double

shocks are somewhat separated; thus, for example, the earthquakes of

18 April 1955 at 6 hr 54 min, K = 12, and at 16 hr 22 min, K = 12, had

foci separated by 28 km.

The arbitrary strain-accumulation graphs for the Northern and Southern zones of the Stalinabad district are shown in Fig. 117. The general nature of these curves for the given district differs from that of the Garm-district curves (Fig. 110) in that there is less uniformity in the variation, there are large steps against the background of a weaker general ascent of the curve, associated with small step-type changes. On these graphs, the greater activity of the Southern zone in comparison to that of the Northern zone, mentioned above, is quite apparent.

A study was not made of more detailed questions relating to the time variation of the seismic regime, associated with specific values of the parameters A and γ over short time intervals for the Stalinabad district. This could not be done owing to the relatively low activity of the district, the sparseness of the stations, and the moderate magnification of the seismographs ($\overline{V}$ = 12-15 thousand), which made it impossible to record weak earthquakes in sufficiently large numbers.

On the Directions for Further Research into the Seismic Regime of the Stalinabad District

Naturally, it is first of all desirable to increase the reliability of the determination of the basic parameters for the mean seismic regime in this district, A and γ. Using the method discussed previously, it is possible to determine the time required to calculate the mean earthquake recurrence N for a given K energy class to within δ = 10% (relative error). The results of calculations for the Greater (S = = 14,300 km^2; A = 0.4) and Lesser (S = 4000 km^2; A = 0.9) Stalinabad districts have been given in Fig. 100b.

On the basis of these calculations, let us estimate the time t_K required for a sufficiently reliable determination of the slope param-

eter γ of the earthquake-recurrence graph. We may assume that to do this it is necessary to have on the recurrence curve a minimum of three sufficiently reliable points that will correspond to some three consecutive energy classes K_1, K_2, and K_3. We assume that the error in the determination of the least accurate of these data, corresponding to the largest class K_3, does not exceed $\delta_N = 10\%$. The error in the determination of the remaining points, corresponding to still larger values of K, will be less, and we need not evaluate their role in the determination of γ. Then, for the conditions of the Lesser Stalinabad district, for various values of K_3, we determine the following time values: where $K_3 = 10$, $t_K = 60$ years; where $K_3 = 9$, $t_K = 20$ years; where $K_3 = 8$, $t_K = 8$ years.
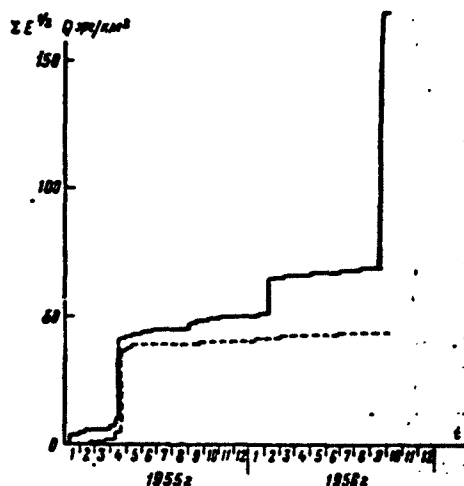
Fig. 117. Arbitrary strain-accumulation graphs for the Stalinabad district. Dashed line — Northern zone; solid line — Southern zone.

For practical reasons, we use $t_K = 8$ years as the required observation period. It is thus assumed that over this period of time, sufficiently complete observations of energy class 6, 7, and 8 earthquakes should be carried out in the Greater Stalinabad district.

This can actually be accomplished with the aid of modern observation methods, and with some concentration of the network.

The further decrease in observation periods that may be achieved by adding class 5 earthquakes, would require a substantial increase in the effective sensitivity of the seismic apparatus. In the Stalinabad district, where there is a high level of industrial and other background, the effective sensitivity may be increased by means of observations in wells about 300 meters deep. There is no difficulty in principle in carrying out such observations and, in view of the great importance of a detailed study of the seismic regime of the Stalinabad district, it is quite reasonable to organize such observations.

In addition to a reliable determination of the mean values for the basic seismic-regime parameters A and γ for the Stalinabad district, it is necessary to study the degree of stability for the seismic regime in this district, and to attempt to find possible regime variations prior to severe earthquakes.

This problem may be solved, basically, by observing the regime for still weaker shocks. Observations for class 8 or more intense earthquakes are of hardly any help in this respect. Actually, a multi-year period of observing class 8 earthquakes will permit establishment of the long-term mean-monthly recurrence value $\bar{N}_8$ with considerable accuracy, but each monthly value of N_8 will, as before, be found only roughly. This also follows from the law of earthquake-recurrence scatter $R = \delta_N \sqrt{N}$.

For the Stalinabad district, as has been shown by calculations for observation data in this district, the quantity R is close to unity, i.e., is practically the same as for the Garm district. Allowing for the fact that in Lesser Stalinabad, the mean-monthly earthquake recurrence for class 8 equals $\bar{N}_8 = 1.15$, we find from the formula

for R or for the nomogram of Fig. 101 that the error in the determination of $\bar{N}_8$ by observations over a single month alone should be close to $\delta_{N_8} = 1.0$, i.e., close to 100%. This agrees quite well with direct calculations from which values of $\delta_{N_8} = 0.76$ are obtained. Naturally, this error is far too large to permit reliable conclusions to be drawn.

Thus, in the Stalinabad district, class 8 earthquakes cannot be used with success to trace the time variation in the seismic regime by means of monthly recurrence values of $\bar{N}_8$; here it is necessary to turn to earthquakes of roughly the sixth and lower classes. This can be done at least for sections directly adjacent to stations provided with high-sensitivity apparatus. In individual points of the district, observations of this type may be carried out with the aid of temporary mobile stations.

As a result of the detailed investigations described in this chapter into the seismic regimes of the Garm and Stalinabad districts, it was possible to establish that the seismic regimes display certain general statistical regularities both in larger regions and in relatively small sections. It is very noteworthy that the parameter γ, representing the drop-off in earthquake recurrence with increasing energy, remains approximately constant over a wide range of variation in the seismic energy of the foci.

In addition to establishing the approximate constancy of the quantity γ over local regions and within a wide range of energy variation, the expedition succeeded, as a result of analysis of the observational data, in finding one more approximately constant quantity – the measure R for the dispersion of the earthquake recurrence for a "normal" seismic regime whose parameters coincide with the long-term mean values.

In isolated cases – in certain districts and in certain time intervals – quantitative deviations from the mean values and general

laws were noted. Such deviations deserve special study. Since they are
limited in extent, these deviations clearly represent no obstacle to
the utilization, primarily, of mean parameters and average laws which
are larger-scale in nature, and thus hold for the majority of cases.
This similarity in the average statistical laws, maintained over very
different energy ranges for both weak and quite strong earthquakes
clearly reflects some general property of the process that gives rise
to the group of earthquakes.

The presence of a law-like connection of statistical nature be-
tween the earthquake recurrences for various intensities, as well as
the unity of the recurrence-scatter laws over a wide range of energy
variation creates fundamental possibilities for the concrete realiza-
tion and utilization of the long-standing dreams of seismologists,
finding clear expression in the works and activities of G.A. Gamburtsev
[9]: on the basis of a relatively brief study of the seismic regime
for some given district, chiefly in the weak-earthquake regions, which
are frequently encountered, to be able to obtain data permitting judg-
ments of the possible seismicity of this district, and judgments as to
rarely occurring strong earthquakes. Together with longer-duration,
less-detailed information on the seismicity of a district, obtained by
instrumental observations of the regional and telemetering seismic sta-
tions as well as from noninstrumental descriptive data, this informa-
tion may be used to obtain more accurate and detailed seismic maps,
and to predict the mean recurrence of strong earthquakes.

As far as the prediction of individual severe earthquakes, with
respect to their location, energy, and time of occurrence, the observa-
tions of the expedition still provide no basis for solving this prob-
lem. Here, the further accumulation of factual data is necessary.

[Footnote]

285   Another term for this concept is "frequency" (G.A. Gamburt-
tsev [9]). This term is inconvenient to use here, since it
is used in a different, special sense in mathematical sta-
tistics.

[List of Transliterated Symbols]

286   ТКСЕ = TKSE = Tadshik Integrated Seismological Expedition

318   лет = let = leto = year

327   год = god = year

327   мес = mes = mesyats = month

327   дн = dn = den' = day

327   сут = sut = sutki = day

327   ч = ch = chas = hour

329   lg = log

332   Обг = Obg = Obi-Garm

332   Т-Д = T-D = Tovil'-Dora

332   Грм = Grm = Garm

332   Ялд = Yald = Yaldymych

332   Дф = Df = not identified

332   Чс = Chs = Chusal

332   Ишт = Isht = Ishtion

332   Джг = Dzhg = Dzhirgatal'

337   ср = sr = srednyy = mean

341   МПС = MPS = not identified

350   дек = dek = dekada = ten-day period

358   Кн = Kn = not identified

358   Хрн = Khrn = Khorongon

358   Чнгр = ChnGr =

[List of Transliterated Symbols (Continued)]

358   Cт = St = Stalinabad

358   Гис = Gis = Gissar

358   Крс = Krs = not identified

358   Нрк = Nrk = Nurek

358   Обг = Obg = Obi-Garm

365   epг = erg

Chapter 8

GEOLOGIC HISTORY AND PRESENT STRUCTURE OF GARM DISTRICT

The Garm district is of interest not only from the seismic but also from the geotectonic viewpoint, since the zone of contact of the Pamir and Western Tien-Shan occurs within its borders; to this day, the question of the nature of the contact zone of the Pamir and Tien-Shan appears to be one of the basic questions in the tectonics of Asia. As a result of our investigations, a new structural diagram of this territory was drawn up; it is indispensable for purposes of comparison with seismic data in order to find the factors responsible for the high degree of seismic activity of the Garm district. An annotated geological map is shown in Fig. 118.

According to V.I. Popov, V.N. Krestnikov, D.P. Rezvoy, and many others [228-231], who have studied Central Asia, geosynclinal tectonic movements occurred during the Paleozoic in the southern portion of Central Asia; they were completed at the end of the early Permian, in the Southwestern Tien-Shan territories, including the Gissar, Zeravshan, Turkestan, and Alay mountain ranges. The uplift at the end of the Hercynian orogenesis was not intense, and resulted in a gently sloping plane rather than large-scale mountain building. To the south of this territory, at the southern slopes of the western portion of the Peter I range, and the basin corresponding to the center reaches of the Obikhingou River and the Northern Pamir Range, there was a large depression, occupied by an arm of the sea. It was only at the very end of the Permian that the uplift of the central portion of the

Pamir expanded greatly to the north, and spread to the adjacent southern portion of the depression. The remaining portion of the depression continued to exist up to the beginning of the Mesozoic as a slender strip, narrowing out from West to East, and pinching out completely somewhat to the East of the 74th meridian. In the most easterly section, the depression lay where the crest of the present-day Zaalay Range is located. As it widened to the west, the depression covered the lower reaches of the Muksu River, all of the southern slope of the western portion of the present-day Peter I range, the middle and, to some extent, the lower reaches of the Obikhingou River and, still further to the West, the depression widened somewhat and turned abruptly to the South.

§1. HISTORY OF THE ALPINE TECTONIC MOVEMENTS AND THE FORMATION OF GEOLOGIC STRUCTURES IN THE GARM DISTRICT

The history of tectonic movements in the Garm district during the Mesozoic and Cenozoic Eras is reflected in a series of structural-stratigraphic and structural profiles constructed for the various periods and epochs in two structural sections. The first of these (Fig. 119) is located in the eastern portion of the Garm district, and crosses it from the Northwest to the Southeast, somewhat to the south of the Muksu River valley. The second (Fig. 120) is located in the Western portion of the Garm district, and crosses it in the same direction, passing through the city of Garm. Materials from [216, 228, 233-241] were used in reconstructing the history of the tectonic movements.

Triassic and Jurassic

During the Triassic and Jurassic, an Epihercynian platform, representing a flat land mass, existed in the northern Garm district, in the Western Tien-Shan region. In the Triassic, its southern boundary
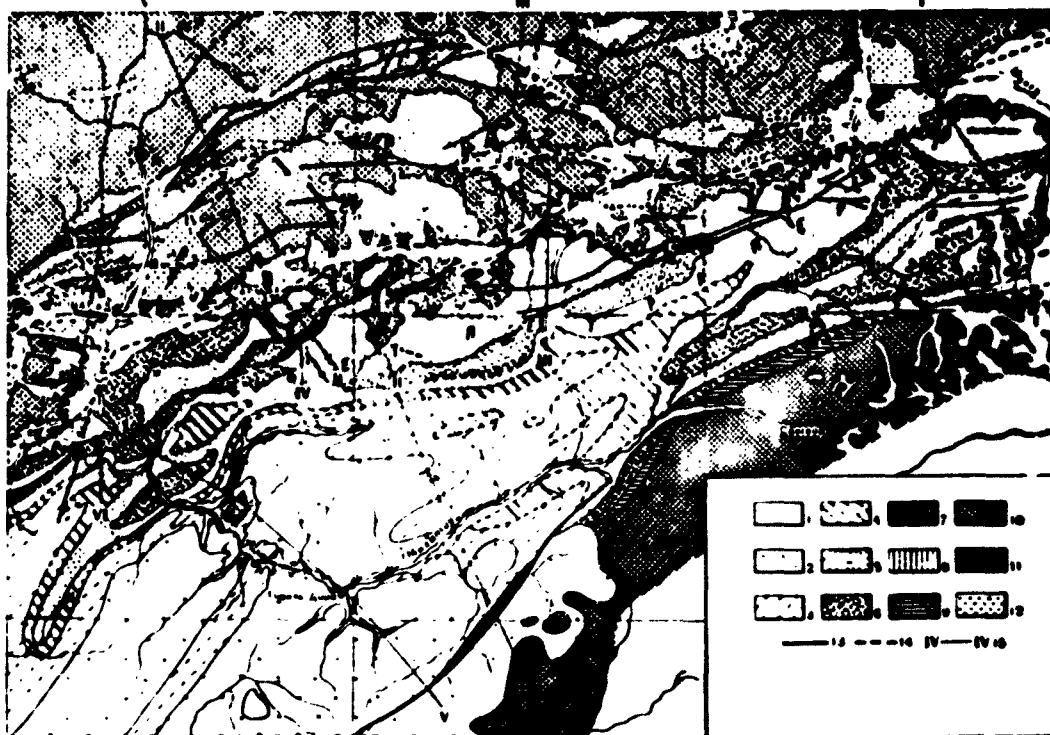
Fig. 118. Schematic geological map. 1) Quaternary deposits; 2) Upper
Neogene; 3) Upper Paleogene and Lower Neogene; 4) Lower and Middle
Paleogene; 5) Upper Cretaceous; 6) Lower Cretaceous; 7) Upper Jurassic;
8) Middle and Upper Jurassic; 9) Lower Jurassic; 10) Middle and Upper
Paleozoic; 11) Lower and Middle Paleozoic; 12) Paleozoic granitoids;
13) faults; 14) supposed faults; 15) lines of geological profiles.
A) Peter I range; B) Tovil'-Dora; C) Obikhingou; D) Surkhob; E) Novabad;
F) Garm; G) Sorbog; H) Yasman; I) Yarkhich; J) Tadzhikabad; K) Dzhir-
gatal'; L) Koksu; M) Kyzylsu; N) Muksu; O) Shaklisu; P) Sangvor.

ran roughly along the crest of the Peter I range, and was most likely
associated with a fault zone separating it from the deep and narrow
Pamir foothills trough located further to the South; the trough itself
was the margin of the Alpine intrageosyncline emerging to the East.
On the South, the intrageosyncline was bounded by a deep zone of
Paleozoic faults. In the Darvaz range, deposition had occurred by the
Paleozoic; further to the East, it is possible to speak of its exis-
tence only from the very end of the Paleozoic, or from the beginning
of the Mesozoic.

To the South of the intrageosyncline, there was the intensely
eroded uplift of the Darvaz and Northern Pamir ranges, which was an

alpine intrageanticline, inherited from the Paleozoic.

In the Pamir foothills trough, the uninterrupted Paleozoic sedimentation continued into the Mesozoic. Here, mainly terrigenous matter was deposited; its uniformity is broken in the lower Jurassic series by extrusive formations. Inasmuch as the Triassic sediments are nowhere exposed within the Garm district, we can get some idea of their composition and extent at this place on the basis of formations of the same age to the East and West of the territory under consideration. Triassic formations are conditionally assumed to exist to the East, in the Zaalay range, in the lower portion of the Mintekinskian suite, which is entirely Triassic and Early Jurassic in age [241]. This suite is 1700 m thick. It consists of continental, marine, and terrigenous extrusives, and is conformable with the eroded surface of the Lower Permian deposits. To the Southwest of the Garm district, in the Darvaz range, it can be seen that the Triassic is flat against the Permian. There is a 150-meter limestone block in its lower portion, containing guide fossils. Higher up, there are terrigenous exposures that also belong to the Lower Triassic; these exposures are 1100 m thick, and are in turn covered by the Lower Jurassic terrigenous deposits that are 750 m thick.

In the same way, there are no outcrops from the Lower Jurassic within the Garm district, if we do not consider the tufacious rocks and quartz porphyries of the Mintekinskian suite that crop out along the meridional reach of the Obikhingou River. The fact that it is necessary to project the Triassic and Lower Jurassic over a great distance (see Fig. 121), to a considerable degree makes tentative the lower portion of our structural-stratigraphic profiles for the Triassic and Jurassic periods.

During the Early Jurassic, coal-bearing deposits accumulated

within the platform region, just in individual depressions, under the swamp-like conditions that prevailed. In the Turkestan, Zeravshan, and Gissar Ranges, the deposits are no more than 700 m thick.

The Sorbulak suite, which is divided into two sections, was formed in the Pamir foothills trough in the Middle and Late Jurassic. The lower portion, whose lower boundary is not known, consists of thick quartz gravel, conglomerate, and sandstone, interbedded with small amounts of clay shales. Its apparent thickness is 1800 m. The top is conformable with the lower portion, and consists of alternating gray clay shales, coarse gray sandstones, and conglomerates with multi-colored clay shales, argillites, and siltstones. In the northern sections, lenses of gypsum are found in the upper portion. Through the South, gypsum drops out of the section, and sandstone is more abundant than shale. The apparent thickness of this part of the suite ranges up to 2000 m. Jurassic lagoonal deposits occur in the outer platform zone. Their thickness is not accurately determined, but in any case is small, of the order of 150-200 m.

Thus, we may assume that during the Triassic and Jurassic, formations about 5500 m thick were deposited to the East in the Pamir foothills trough, and up to 6500 m thick to the West. This thickness gives, in first approximation, the subsidance of the earth's crust. Since the clastic material during the time under consideration arrived almost exclusively from the South, it is established that the Darvaz and Northern Pamir uplift grew uninterruptedly. In the Late Jurassic, this uplift became slower, as indicated by the transportation of finer materials, forming sandstones, clay shales, siltstones, and argillites.

The widening of the region of sedimentation to the North all the way to the present-day Surkhob River indicates that a narrow marginal zone of the Tien-Shan platform region was also involved in the folding.
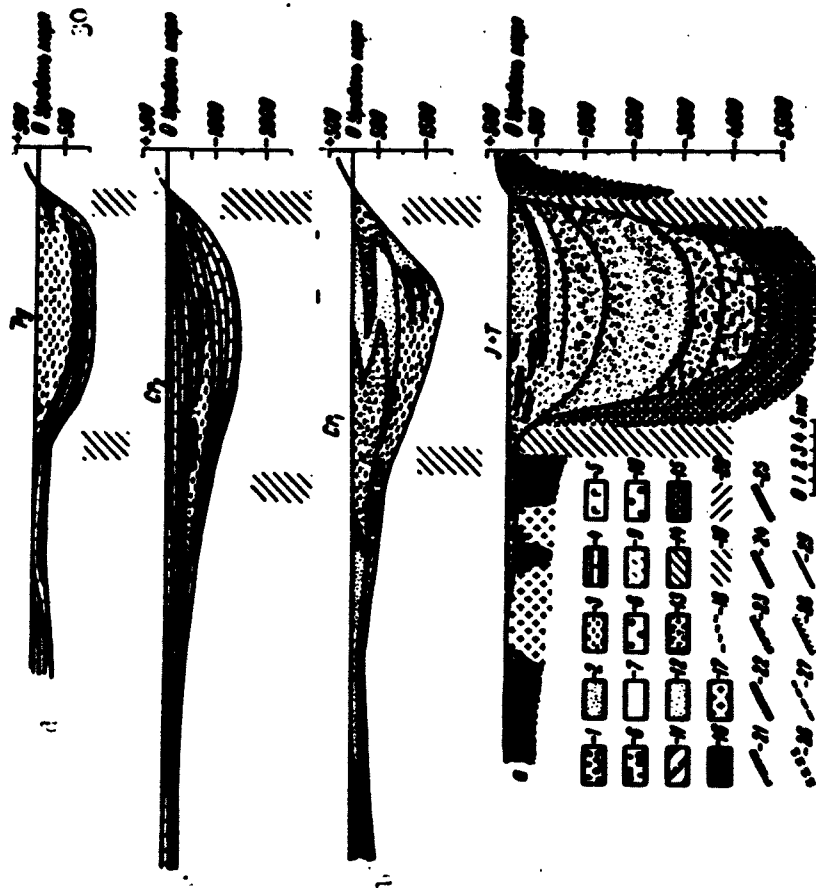
Fig. 119. Diagram showing tectonic development of eastern portion of Garm district for the Mesozoic and Cenozoic. A-d) Result of tectonic movements occurring in: a) Triassic and Jurassic periods; b) Early Cretaceous epoch; c) Late Cretaceous epoch; d) Early and Middle Paleogene; e) Late Paleogene and Neogene; f) general result of pre-Quaternary movements; g) structure created in the Early Quaternary; h) present-day structure (geological profile along line I-I, Fig. 118). Lithological nomenclature for sections: 1) Conglomerates; 2) sandstones; 3) clays and clay shales; 4) limestones and marls; 5) gypsum; 6) extrusives and their tufas; 7) Quaternary deposits; 8) Upper Neogene; 9) Upper Paleogene and Lower Neogene; 10) Upper Paleogene and Neogene, undifferentiated; 11) Lower and Middle Paleogene; 12) Upper Cretaceous; 13) Lower Cretaceous; 14) Jurassic and Triassic; 15) Middle and Upper Paleozoic; 16) Lower and Middle Paleozoic; 17) Paleozoic granitoids; 18) relics of Early Quaternary relief. Tectonic faults: A) Deep fault zones; 19) deep Paleozoic fault zones,
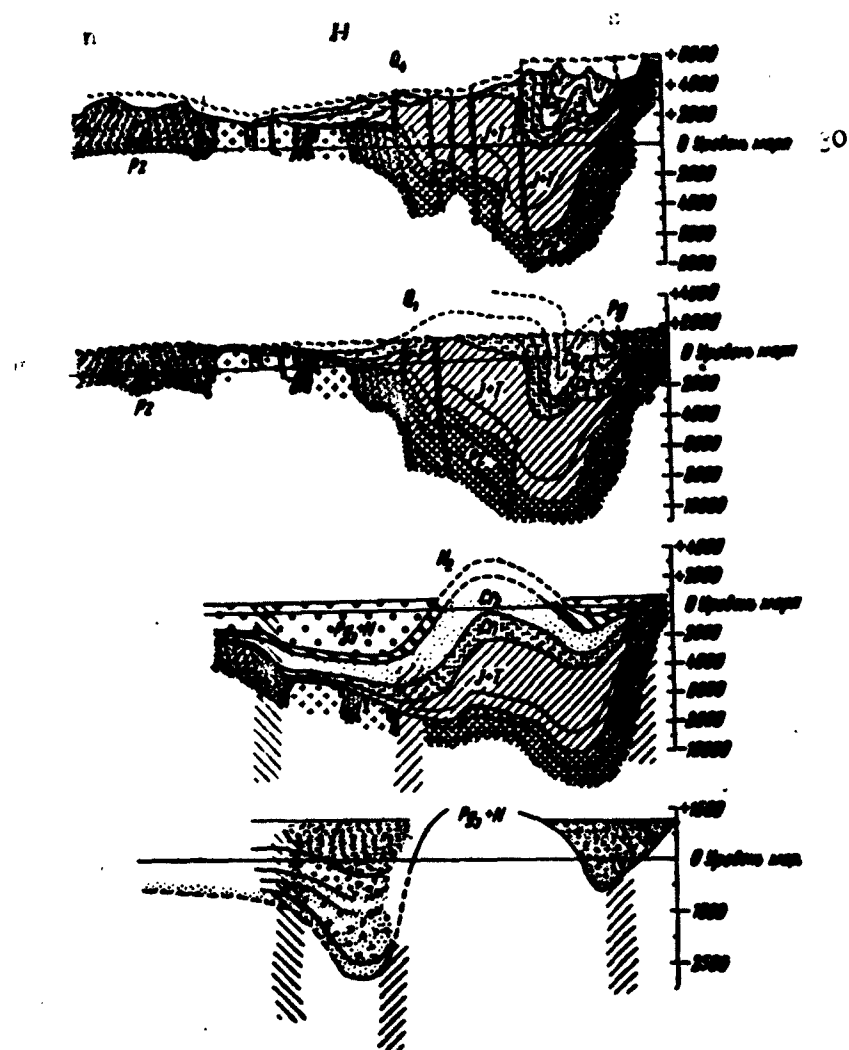
Fig. 119 caption (continued):

renewed periodically during the Mesozoic and Tertiary; 20) deep
Paleozoic fault zone, renewed in the Neogene; B) faults associated
with separate movements of zones and subzones shown on the tectonic
diagram of the Garm district (Fig. 128): 21) zones A-I relative to
zone A-II; 22) zones A-II relative to zone A-I and region B; 23)
subzones B-I-a relative to subzone B-I-b; 24) subzones B-I-b, rela-
tive to subzones B-I-a and B-I-c; 25) subzones B-I-c, relative to
B-I-b and zone A-II; 26) faults along which the direction of limb
displacement changed; 27) supposed deep faults; C) secondary faults:
28) with apparent direction of limb displacement; 29) direction of
limb displacement not known; 30) sea level. For all faults, the
heavy line is drawn from the side of the uplifted limb.

The Cretaceous

Lagoonal conditions in the formation of gypsum continued in the
platform region of the northern district at the very beginning of the
Early Cretaceous. Later, while there was a considerable expansion of
the sedimentation region to the North, deposition of multicolored
terrigenous rocks began. Just at the very end of the Early Cretaceous,
in the Albian age, to the West of Garm, in the kishlak of Shul', very
brief deposition of limestones occurred so as to form a 10-meter thick
layer among the redbeds. During the Early Cretaceous, uplifts developed
in the most northerly sections of the district, on the platform;
their destruction is explained by the transport of coarse clastic
material in a southerly direction. Within the platform boundaries,
the Lower Cretaceous is no more than 500 m thick. In the Pamir foot-
hills trough, during the entire Early Cretaceous terrigenous rocks
were deposited: conglomerates, sandstones, clays, siltstones, and
argillites colored various shades of red. The boundary between sedi-
ments of the Late Jurassic and Early Cretaceous is quite arbitrary.
N.N. Leonov believes that the upper strata of the Sorbulak suite must
belong not the the Upper Jurassic, but to the Lower Cretaceous. Judg-
ing from the maximum thickness (1800 m) of the Lower Cretaceous, the
downward movements in the trough occurred at a considerably higher

Fig. 120. Diagram of the Tectonic development of the Western Portion of the Garm region in the Mesozoic and Cenozoic (along line II-II in Fig. 118). For denotations see Fig. 119.

rate than similar movements at the edge of the platform. Finally, to the South, during the same period of time, there was a continued uplift and erosion of the Northern Pamir and Darvaz.

The sections in Figs. 119 and 120 show clearly the difference between the platform region, which drew in as it folded, but subsided little, and the Pamir foothills geosynclinal trough. The northern boundary of the trough is quite accurately marked by a sharp rise in the thickness of the Lower Cretaceous in the interfluve area in the western half of the Peter I range.

At the very beginning of the Late Cretaceous, in connection with the general descending movements that covered a considerable territory in South Asia, there began a vast transgression of the sea, and there was a considerable decrease in erosion area. Thus, in the Garm district, as in the greater part of Central Asia, carbonate deposits began to form. The source areas to the South and North were considerably depleted at this time, and yielded almost no clastic material. Only in the Turonian age, in the North, were there slight uplifts, producing argillaceous material that accumulated in the trough. The acceleration of the descending movements, commencing in the Jurassic, ceased following the Senonian age. In the Danian age, the sea regressed, and lagoonal conditions appeared over a considerable area. Throughout the entire Late Cretaceous, the Pamir foothills trough, in which the deposits are no less than 1500 m thick, continued to be the area of greatest subsidance, which was evidently particularly intensive in the Southeastern part.

Paleocene and Eocene

At the beginning of the Paleogene, a renewal of the downward movements caused a new transgression of the sea. Carbonate deposits were formed basically from the beginning of the Paleogene to the

- 407 -
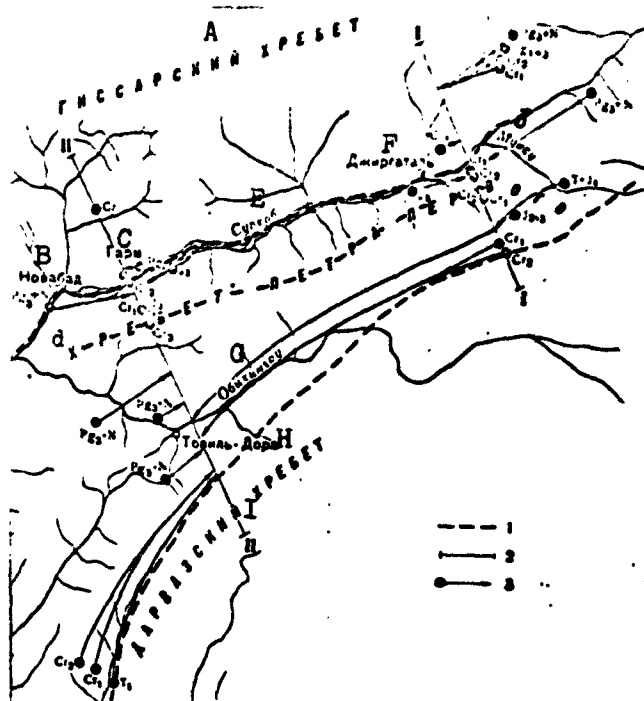
Fig. 121. Diagram showing arrangement of
stratigraphic sections used in compiling
structural-phase profiles along lines I-I
and II-II (Figs. 119 and 120). 1) Borders
of basic tectonic zones shown in Fig. 128;
2) lines of structural-phase profiles;
3) basic stratigraphic sections. A) Gissar
range; B) Novabad; C) Garm; D) Peter I
range; E) Surkhob River; F) Dzhirgatal';
G) Obikhingou; H) Tovil'-Dora; I) Darvaz
range; J) Muksu River.

Alayskian age; starting with the Turkestanian age, red marine and

lagoonal sand and clay were deposited. The latter form evidence for

the low rate of uplift in both the North and South of the Garm dis-

trict. The greatest thickness of Paleogene marine deposits in the

trough is 800 $\underline{m}$. On the interior side, on the platform, the Paleogene

marine sediments reach 350 $\underline{m}$ in thickness.

Oligocene and Neogene

In the history of tectonic movements over all of South Central

Asia and, in particular, in the Garm district, the second half of the

Fig. 122. Geological profiles along lines III-III, IV-IV, V-V, and VI-VI. For definitions of convention, see Fig. 119, for arrangement of profile lines, see Fig. 118. 1) Obikhingou River; 2) Yarkhych; 3) Yasman.

Paleogene is noted for the commencement of a new trend in movements of the earth's crust. While during the Triassic, Jurassic, Cretaceous, and the first half of the Paleogene, general downward movements, although sporadic, were predominant; during the second half of the Paleogene, however, there was an over-all sharp intensification of the role of uplifts.

Starting with the Oligocene, to the North and South of the Garm district, in the regions of the Gissar and Darvaz ranges, an intensive increase in uplifts commenced.

A great deal of coarse clastic material, conglomerates, and to a lesser degree, sand and clay deposits were brought down from the North and South into the Pamir foothills trough. The direction of transport is recorded by the occurrence of pebbles in the conglomerates of Paleozoic rocks in the Pamir and Darvaz. These deposits from the Late Paleogene and Neogene have a wide distribution in the Western and Central portions of the Garm district.

In particular individual areas, it has been established that during the Neogene, within the zone of uplift, displacements occurred along the major tectonic faults that form the boundaries of the blocks of Paleozoic rock; these displacements are reflected in the present structure. In this respect, the area north of the Obikhingou River mouth is very characteristic; here, the Upper Neogene conglomerates lie directly on the Paleozoic. North of this area, which is bordered on the North by a fault, these same conglomerates cover the entire section of the Tertiary and Cretaceous formations (Fig. 122, V-V). The great difference in the completeness of the stratigraphic columns between these two neighboring areas is due to the uplift and erosion of the Southern fault block during the Neogene. In the western part of the Garm district, within the marginal basin of the Pamir

foothills zone, the same distribution of thicknesses of sediment, in-
dicating movements of the same nature, is seen in the Neogene as was
evidenced in earlier periods. The southern part of the trough, the
intrageosyncline inherited from the Paleozoic, underwent greater sub-
sidence than the northern section, which was the margin of the Epi-
hercynian platform. The general subsidance of the basin continued to
the end of the Neogene. It has not been possible to establish the
presence of the uplifts within the basin, despite special searches
for indications of it. Different structural relationships occur in the
Zaalay range and the Alay valley, located directly to the East of the
Garm district. Here it is quite reliably established that in the
Neogene, there were major uplifts in the center of the Pamir foothills
basin, on the site of the present Zaalay range, since fragments of
Early Cretaceous red rocks were transported from South to North, into
the area of the former platform. Since at the present time, the Western
periclinal end of one such uplift of the Zaalay range, the Sorbulak,
is located in the Eastern portion of the Garm district, it must be
assumed that on the site of the Pamir foothills trough, a slight uplift
was occurring in the Eastern portion of the Garm district toward the
end of the Neogene. The growth of this uplift is marked by the Neogene
conglomerates near the mouth of the Guloma River. These differences
in the history of movements in the western and eastern portions of
the Garm district are shown in Figs. 119 and 120.

The most important feature of the movements at the end of the
Neogene was the slight subsidance of several parts of the Northern
Pamir and the Darvaz immediately adjacent to the Pamir foothills
trough. In such places, Upper Neogene gravels lie directly on the
Paleozoic. It is possible that similar movements also took place to
the North of the Pamir foothills trough zone.

To understand a number of the conclusions that will follow as to
the tectonic movements, it is very important to have a clear picture
of the nature of the relief in the Garm district at the end of the
Neogene and the beginning of the Quaternary. The history of this re-
lief begins with the deposition of marine sediments during the Paleo-
gene. During this time, a shallow, highly saline sea occupied the
Pamir foothills basin. To the North and South, in the erosion areas
in adjacent parts of the Tien-Shan and the Pamir, there was low flat
dry land from which practically no clastic material was transported.
During the uplift of the erosion area in the Late Paleogene and Neogene,
this flat relief was disected by valleys and changed gradually into a
system of tablelands similar to the mountains now existing in the
Northern Tien-Shan. Since the remnants of the ancient, slightly eroded
flat relief are still preserved in many parts of the Tien-Shan ad-
jacent to the Garm district, often with a mantle of Cretaceous deposits,
we may assume that at the end of the Neogene, before the Quaternary
uplift of the region, such remnants were considerably larger, and the
relief of the erosion areas amounted to a system of disected plateaux.
The elevation of the plateaux surface near the borders of the Garm
district was apparently no more than 1000 m, while the top of the
alluvial valley formed at the end of the Neogene in the Western portion
of the Garm district, within the Pamir foothills basin, was probably
500 m high. These two figures, 1000 and 500 m, satisfy three basic
conditions: 1) the elevation of the interstream areas at the end of
the Neogene must have been considerably less than that of the remains
of the ancient flat relief today, that is, after the general Quaternary
uplift of the entire area; moreover, the lowest known remnants within
the Garm district exist today at elevations of 1500 to 2000 m; 2) the
surface of the Neogene gravels forming an alluvial valley at the end

of the Neogene in the western portion of the Garm region should have
been considerably above sea level, where lagoonal deposits occurred at
the beginning of the Paleogene; 3) the difference in elevations of the
interfluve surfaces in the region of erosion and the surface of sedi-
mentation at the end of the Neogene in the Pamir foothills basin must
have been so great as to cause the streams to flow rapidly, so that
they carried coarse clastic material into the valley.

Quaternary Period

The following significant geological events occurred in the Garm
district during the Quaternary period: 1) within this district, area
sedimentation ceased (with the exception of river alluvia); 2) folding
in Pamir Mesozoic and Tertiary deposits; 3) a flat relief was de-
veloped, dissecting the folds, and showing no traces of substantial
further development of individual partial folds into sedimentary
blanket; 4) owing to the differential uplifting of individual tectonic
zones and sections within them, the residual mountains of the flat
Quaternary relief were uplifted to a different height; 5) as a result
of the uplifting, erosion created the present-day strongly disjointed
high-mountain relief.

It is very important to add to preliminary remarks in determining
the basic stages in the history of the Quaternary movements, and in
establishing differences in the movements of individual sections of
the Garm region.

First, in 1956, Ye.Ya. Rantsman advised us that she had observed
on the northern slope of the western half of the Peter I range out-
croppings of one surface of an ancient leveled Quaternary relief,
formed from Mesozoic and Tertiary rock within the former Pamir foot-
hills trough; the difference in heights at which the outcroppings were
observed is explained by displacements along faults occurring in the

Quaternary period. Second, the Lower Quaternary moraines, studied by Ye.Ya. Rantsman in the lower reaches of the Muksu River are located in the valley at the level of the present-day thalweg. At several points within the Garm district, the present-day channels of major rivers did not dip below the Lower Quaternary deposits. These facts were confirmed by our observations, and supplemented by additional data, obliging us to distinguish the following two basic stages in the Quaternary movements.

The first stage covers the beginning of the Quaternary period and, possibly, the very end of the Neogene period. During this time, the Pamir foothills trough was uplifted at such a rapid rate that its relief reached heights equaling those of the neighboring tectonic zones. In this connection, area sedimentation ceased within the trough; this depression ceased to be a region of accumulation of products from the disintegration of the neighboring tectonic zones, and on the whole, joined the earlier erosion regions. Destruction products from all tectonic zones were borne beyond the borders of the Garm district to the Southwest into the central portion of the Tadzhik depression. The Pamir foothills depression zone was uplifted not only absolutely but relatively as well with respect to neighboring zones. While this relative uplift of the former trough was occurring, folds and faults were forming within the Mesozoic and Tertiary rock; this was connected both directly with the relative zonal uplift and with folds in the sedimentary mantle. The folds and faults distorted the initial flat relief of the cumulative valley existing at the end of the Neogene. The partial uplifts appearing within this zone were eroded. The relationship between the rates of growth and erosion was such that a hilly relief, resembling a peneplain, was created. This peneplain, however, did not represent the end of this mountainous area's development, but corres-

ponded to its beginning. A peneplain of this type, appearing during a transition from a valley to a mountainous region, exists today to the Southwest of the Pamir foothills trough, and in the interior portion of the Tadzhik depression, adjacent to Amu-Dar'. It is also known to exist in several foothills districts of the Caucasus.

Owing to the uplift of the Pamir foothills trough zone, erosion probably was not intensive in the adjacent zones, and was replaced in part by cumulative filling up of the valley. The general level of the water sheds in the zone under consideration and in adjacent portions of neighboring zones was evidently the same. It is hard to assume that in the presence of the general increase in uplifts it would be lower than the level in the most uplifted zones at the end of the Neogene, i.e., less than 1000 m. It is more likely that the level was greater than 1000 m. Inasmuch as remnants of this relief are encountered today at heights beginning at 1500-2000 m, the level cannot be assumed to be greater than 1500 m in the Early Quaternary. In addition, remnants of the flat relief are found beyond the borders of the Pamir foothills trough zone at heights commencing at 1500 m. Thus, it is most likely that at the end of the first stage, the heights of the water sheds in the Garm district approximated to some one more or less horizontal level in all tectonic zones; this level was probably located at about 1500 m. A possible error in finding the absolute height will have no effect upon our subsequent conclusions of a seismogeological nature.

A basic feature of the second stage is the nonuniform uplifting of all tectonic zones. The heights at which outcroppings of the Lower Quaternary peneplain occur, as shown in Figs. 119 and 120, may be used to establish the fact that the greatest uplift occurred in the northern Pamir and Darwaz zone. Here, at places in which the ancient pene-

plain is already eroded, there are present-day peaks reaching 5500 m
in height. Consequently, the uplift amounted to more than 4000 m.
During i's rising, this uplift expanded somewhat to the North at the
expense of a narrow strip cut out from the Pamir foothills trough zone
by faults. These young faults displace the contemporary moraines. On
the northern slope of the western portion of the Peter I range, there
is a valley that is dammed by a fault wall that is rising today. The
shoulder of this dam is a fault surface with slickensides (Fig. 123).

The greatest uplift in the Pamir foothills trough zone occurred
to the East of the Garm region in the Zaalay range, where the relief
today reaches heights of 7000 m; in the Garm district, the maximum
heights in this zone reach only 4500 m and, consequently, here the up-
lift amounted to about 3000 m. The least uplift in the Garm district
occurs in a zone of block-dome uplift in the southern portion of West-
ern Tien-Shan on the site of the ancient platform; there was very lit-
tle uplift (500-1500 m) in the southern sections of the zone (bounded
by faults) that coincide with the present-day northern slope of the
Peter I range (Fig. 124), and with the watershed between the Surkhob
River and the more northerly Yasman and Komarou Rivers (Fig. 125).

A very important feature of the second stage consists in the fact
that these uplifts occurred in the first part of the stage, which we
date by the glaciation that occurred here. It was just at this time
that the chief rivers cut their valleys to the present-day depth. The
first of the ancient glaciations, which possibly corresponds to the
Riss glaciation or one of the stages of the Wuerm glaciation was of
the valley type. Its moraines in many places are found at levels close
to the present-day thalweg.

Subsequently, owing to the irregularity of the uplifts in time,
and the fact that they were briefly replaced by a slight subsidence,

Fig. 123. Valley partitioned by spur
formed by uplifted fault wall. The
shadow covers the slickensides sur-
face (northern slope of western sec-
tion of Peter I range).

and possibly, in part, owing to the appearance of new uplifts to the
Northwest of the Garm district, which might have elevated the general
erosion basis for the district, erosion of the bottom gave way to the
accumulation of alluvium. Maximum thickness of 120 m occurs near the
mouth of the Obikhingou River. Here it is possible to isolate two ter-
race complexes so as to fix two chief delays in the time development
of the uplift.

At the present time, the ancient alluvia of the chief rivers have
not yet been cut through to the base level in many places within the
Garm district. This means that the present-day uplift of the district
as a whole apparently does not exceed that which had been reached when
the moraines were deposited. Consequently, it may be assumed that
there was a decrease in the rate of uplift in the second portion of
the second stage in comparison with the rate during the first portion.
In addition, the terraces make it possible to establish the fact that

- 417 -

up to the end of the second stage, i.e., to the present day, individual zones and even sections within the zones have been uplifted at different rates. The smallest uplift occurred at the southern edge of the former platform at the site of the Surkhob River valley. The ancient alluvium is almost uncut by the river here. The edges of the highest terraces are only 10-20 m above the bed, and are lower in places. The flood plain of the river is broad, the bed is divided into numerous fingers, and is studded with sand bars and islands. In a portion of the valley, the bed reaches an over-all width of 1.5 km. The absence of an uplift after accumulation of the ancient alluvium is especially apparent near Khait and further to the West, almost to Garm. Here we get the impression that the mountains are "sinking" downward and are being buried by the alluvium (Fig. 125). To the West and East of this section, the terraces are somewhat higher. Near the western and eastern borders of the district they rise still further, indicating a substantial uplift of the locality. Below the mouth of the Obi-

Fig. 124. Horizontal surface on northern slope of western section of Peter I range, an outcrop of the Lower Quaternary base level.

Fig. 125. View from the right bank of the Surkhob
River, looking downstream. The Kabudkrym range is
in the middle. The Yasman valley is on the right.

khingou River, immediately beyond the western boundary of the dis-
trict, the terraces of the Vakhsh River reach heights of 100-200 m.
Near the mouth of the Muksu River, near the eastern border of the dis-
trict, the maximum terrace heights amount to 60 m.

An especially sharp variation in the vertical-movement rate may
be seen at right angles to the trend of the tectonic zones. Toward the
Northwest from the Surkhob, the terraces rise quite steeply along its
right-hand banks, extending for distances of 10-15 km, after which the
valleys become gorges with convex slopes. Here the riverbeds have been
cut far below the ancient alluvium. In many places, there are no ter-
races. Consequently, the rate of uplift of the Earth's surface to the
North of the Surkhob River rises sharply. In direct proximity to the
Surkhob, however, on the slopes of the Kabudkrym mountain massif, ac-
cording to the observations of Ye.Ya. Rantsman, the terraces are de-
veloped on a broad scale and are low in height. This indicates that
this massif has not been subject to any noticeable uplifting.

To the Southeast of the Surkhob, a considerable increase in ter-
race height may be seen within the ancient Pamir foothills trough
zone. In the eastern section of the district, the terraces of the Muk-
su River reach 120-150 m in height (Fig. 126). Further to the South,

Fig. 126. Terraces on the Muksu River.

going along the Muksu River to the northern Pamir uplift zone, we encounter a gorge that is almost devoid of terraces. This means that in this cross section of the Pamir foothills trough zone, the uplift occurred more quickly than at the edge of the platform, while at the northern edge of the Pamir zone, the uplift took place at still a higher rate.

In the western section of the region, to the Southeast of the Surkhob, a considerable elevation of terraces in the lower portion of the Obikhingou River valley is visible. On the border between the zone of the southern margin of the old platform and the zone of the ancient Pamir foothills trough, the river flows in a deep narrow gorge without terraces. Within the trough zone, however, the ancient terraces of the Obikhingou are retained throughout the greater part of the valley.

Thus, it is clear that for all sections the zone formed by the former trough clearly rose more rapidly than the margins of the old platform; here an especially intensive uplift occurred in the extreme northwestern (pre-platform) portion of the trough zone. The edge of the platform, including the Surkhob River valley, and a portion of the Kabudkrym mountain massif is an area in which the very youngest Quaternary movements occurred at slow speed. This is why it appears to be depressed with respect to the remaining sections of the district.

These differences in the movements in individual zones and sections of the Garm district during the second part of the Quaternary

period can be placed, approximately, within the past 120,000 years, if the moraines at the mouth of the Muksu River are of the Wuerm type, and within the past 230,000 years if they are of the Riss type.

The tectonic-movement curves (Fig. 127) and the geological sections (Fig. 122) clearly show the substantial difference in all of the Mesozoic and Cenozoic movements on the southern and northern slopes of the Peter I range, and thus indicate the border between the geosynclinal and platform regions.

On the basis of the data presented for the Garm district, the frequently discussed question of the nature of the border between the Pamirs and Alay (Tien-Shan) [229, 233-237, 242-246], it seems to us, should be looked into again. It is now enough to assume that Tien-Shan is a region of post-platform activation of tectonic movements on the site of an Epihercynian platform [231, 238, 247] to the South, within the Hindu Kush, Himalayas, and Pamir, there is an alpine geosynclinal region, in which there is also noticeable activation of new movements, covering, on the whole, a considerable portion of the Earth's crust. The phenomenon of activation in the Tertiary and Quaternary periods unites the former platform with the alpine geosynclinal region, and makes it difficult to draw the boundary between them. In this fact lies one of the most important features of the tectonics of South Central Asia. Thus, there is some justification for those scientists who saw no essential difference between Pamir and Alay [229, 231, 236, 246]. The difference between the former platform and the geosyncline, however, still exists, and is especially noticeable in the Mesozoic. Consequently, those scientists were right who drew a boundary between Pamir and Tien-Shan [233, 235, 240, 242]. At the present time, the essence of the Pamir – Tien-Shan boundary question lies in drawing the boundary between the geosynclinal and former platform regions. In the
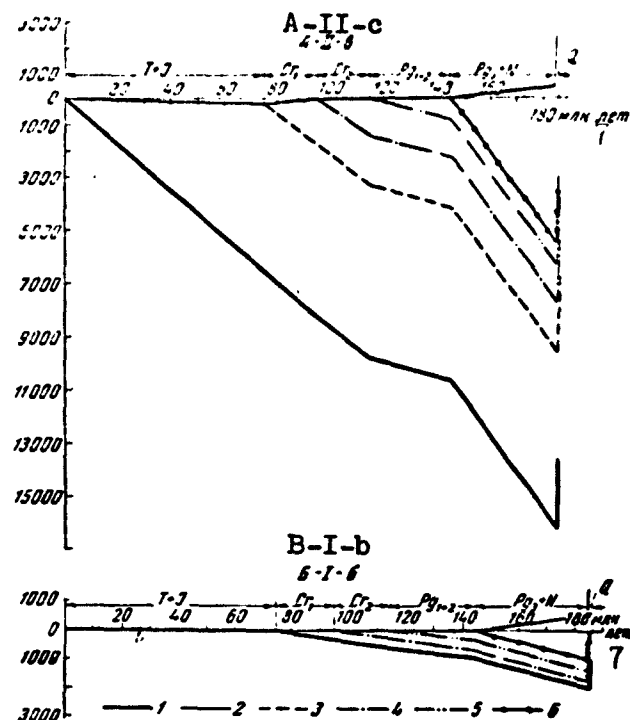
Fig. 127. Tectonic-movement curves in the Garm district during the Mesozoic and Cenozoic. A-II-c) Tovil'-Dora section; B-I-b) section between city of Garm and village of Shul'. 1) Resultant curve for tectonic movements in Mesozoic and Cenozoic (curve of tectonic movements of Paleozoic mantle); 2) curve of geomorphological representation of tectonic movement; 3) curve for tectonic movements of Lower Cretaceous sole; 4) curve for tectonic movements of Upper Cretaceous; 5) curve for tectonic movements of Lower and Middle Paleogene soles; 6) curve for tectonic movements of Upper Paleogene and Neogene soles; 7) million years.

Garm district, this boundary proves to run along the crest of the western half of the Peter I range. This is indicated by the essential difference in all Mesozoic and Cenozoic movements on the southern and northern slopes of the range, which is very well defined on the appropriate curves (Fig. 127) and on the geological profile sections (Fig.

- 422 -

122).

Using an entire set of criteria, the boundary between the platform and geosynclinal regions of the Garm district should be drawn to the East along the northern slope of the Alay range. To the Southwest of the district, it runs along the northwestern slope of the Vakhsh range, and then along the Surkh-ku range, and then turns to the Southwest toward the Tutkaul'skiy junction. From here, we should assume that it runs South into Afghanistan, approximately as shown in Fig. 129. The central section of the depression is a platform; the eastern portion is a geosynclinal depression, to the Northeast of which, in the Garm district, there is a young tectonic uplift. The western section of Tadzhik depression, in which the Mesozoic is thicker in the Kugitang range, and to the West, can be considered to be a parageosynclinal (half-platform) section. The differences in the Mesozoic and Cenozoic histories of these portions of the depression are apparently inherited from different zones of the Paleozoic geosynclinal.

The well-defined gradual development of movements along the trend of the Pamir foothills trough is noteworthy. Throughout almost the entire alpine stage, the subsidence has spread from the Southwest to the Northeast while the uplift, coming at the end of this stage, gradually moves in the opposite direction from the Northeast to the Southwest. In the Alay range, intensive uplifting and folding occurred in the Neogene. It has already become attenuated. In the Garm district, they have taken place at the beginning of the Quaternary period (in its first half), but the uplift continued to the present day. In the Southwestern portion of the trough, these processes have only begun to develop. Area accumulation of Quaternary deposits has only just ended here. Thus, the Garm district is very active from the tectonic viewpoint at the present time.
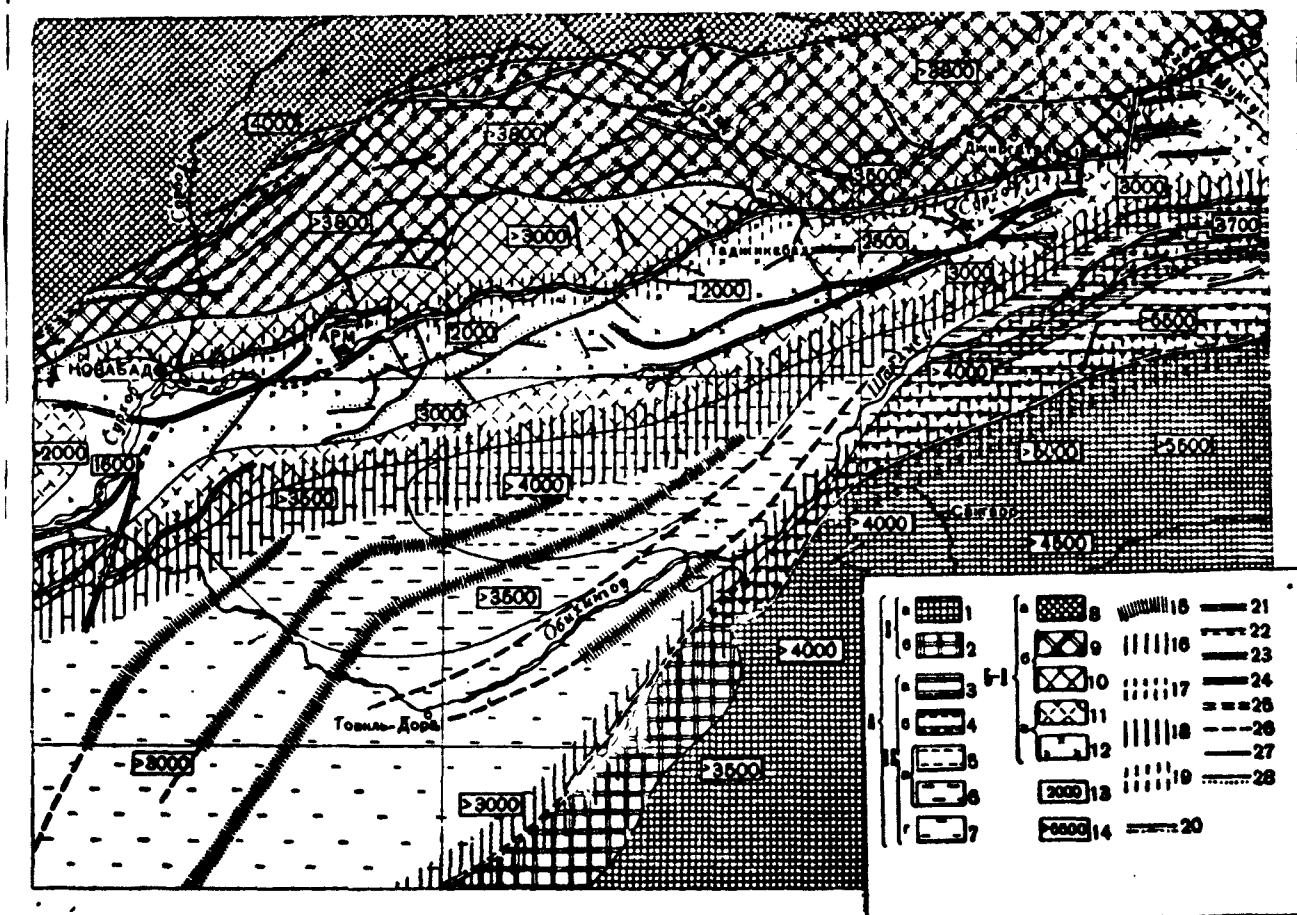
Fig. 128. Tectonic Diagram of Garm Region. A) Alpine Geosynclinal Region. I)
Zone of block-dome upheaval of Northern Pamir and Darvaz, subject to constant
and irregular upgrading during the Mesozoic and Cenozoic: 1) subzone a in
which the lower Quaternary relief is raised to a height greater than 3000-3500
m; II) zone of Pamir foothills flexure, subject to intensive sagging in the
Mesozoic and Tertiary periods, followed in the Garm region by uplift in the
East at the end of the Tertiary period, and in all sections of the region by
intensive uplift and folding in the Quaternary period;3) subzone a, Sorbulak-
skoye uplift developed in the flexure, in the Neogene; in the Quaternary
period, the southern region of the uplift became part of subzone II-b; the
Northern section detached from it by faulting became part of subzone II-c; 4)
subzone b in which the lower Quatenary relief is raised to a height of more
than 4000 m; section of flexure connected to block-dome upheaval of Northern
Pamir in the Quaternary period; 5, 6) subzone c markedly uplifted section of
flexure, ancient Quaternary relief raised to a height of more than 3500 m:
5) section of subzone in which the lower Quaternary relief is raised to a
height of more than 4000 m: 6) section of subzone in which the lower Quaternary
relief is raised to a height of more than 3500-4000 m: subzone d, section of
flexure in which the lower Quaternary relief is raised to 3000-3500 m.

- 424 -

B) Activation Region of New Movements in the Epihercynian Platform. Zone I, Southern area of Western Tien-Shan, subject to weak sinking and uplifting in the Mesozoic and Paleogene, giving way to intensive block-dome uplifting in the Neogene and Quaternary periods; highest inner subzone a in which the ancient Quaternary relief is raised to a height greater than 4000 m: 9-10) intermediate average uplifted subzone b, in regions in which the ancient Quaternary relief is raised to a height: 9) of more than 3800 m: 10) of 3000-3800 m: 11-12) the lowest outer subzone c, in which the ancient Quaternary relief is raised to a height; 11) of 2500 to 3000 m: 12) of 2000 to 2500 m: height at which relics of ancient Quaternary relief were preserved (in meters from sea level); 14) maximum altitude of contemporary watersheds, taken as the lower limit of the rise in ancient Quaternary relief (in meters from sea level)· 15) axes of anticlines in zone II. Tectonic Faults. Inherited Paleozoic plutonic fault zones along which; 16) dislocations took place in the Mesozoic and Cenozoic, primarily in one direction (the North-Western sides dropped down): 17) the shifting took place primarily in the Mesozoic and Tertiary periods in one direction (North-Western sides dropped down), while in the Quaternary period they were in the opposite direction (the same sides were elevated): 18) shifting took place in the Mesozoic and Tertiary periods in one direction (South-Eastern sides dropped down), while in the Quaternary period it took place in the opposite direction (the same sides dropped down); 19) shifting took place primarily at the end of the Neogene and Quaternary periods (the direction of the shifting of the sides varied for various faults). Faults associated with the movements of separate zones and subzones: 20) zones A-I relative to zone A-II; 21) zones A-II relative to zone A-I and region B: 22) subzones B-I-a relative to subzone B-I-b; 23) subzones B-I-b relative to subzones B-I-a and B-I-c; 24) subzones B-I-c relative to subzone B-I-b and zone A-II; 25) faults along which the direction of the shifting of the sides changed; 6) faults assumed in depth. Secondary faults: 27) with obscure direction of shifting sides; 28) with obscure direction of side shifting. For all faults, the solid line is drawn from the relatively uplifted side

§2. PRESENT-DAY STRUCTURE OF THE GARM DISTRICT

The present-day structure of the Garm district was formed over a
long period of time, differs in appearance, depending on the
stratographic surfaces we look at. Within the borders of the district,
two structural stages are clearly delimited; they differ sharply in
their physical properties. The upper stage is composed of Cenozoic and
Mesozoic deposits, and the lower stage is formed of Paleozoic blocks.
The interior structure of the upper stage differs considerably from
the interior structure of the lower stage. Also of considerable in-
terest are data on the form of two surfaces, one separating these
stages (the Paleozoic denudation surface), and the other forming the
upper boundary of the top stage (the Lower Quaternary base surface).
Thus, the description below is given in the following sequence: 1) in-
ternal structure of the lower stage; 2) shape of the surface separat-
ing the latter from the upper stage; 3) internal structure of the up-
per stage; 4) shape of its top surface.

Internal Structure of Paleozoic Formations

The constituent rocks today form three massive structural com-
plexes. Within the Paleozoic rocks of the northwestern half of the
district (within the former platform), the layers are dislocated, and
form a small anticlinorium, composed for the most part of Silurian
metamorphic schists, which in many places have been transformed into
gneisses, and have been penetrated by intrusions of Paleozoic grani-
toids. The western periclinal portion of the main anticlinorium body
is located at the western boundary of the district, at the latitude of
Garm. The eastern end of the main body lies outside the district. Evi-
dently, the hinge of the anticlinorium has experienced the greatest
uplift between Garm and Khait. It may be assumed that the southern
limb of the anticlinorium is cut at the site of the Peter I range wa-

tershed by the Petrovskaya Paleozoic fault zone; here the faults are
buried under Mesozoic deposits.

There is a synclinorium on the southern slope of the western sec-
tion of the Peter I range, composed of Late and Middle Paleozoic lime-
stones, terrigenous and extrusive rocks.

The southwestern edge of the district (the Darvaz range and the
eastern portion of the Peter I range, which turns toward the South) is
an anticlinorium in the Paleozoic structure. Large-scale intensive
folding and faulting are known to exist within it.

Shape of the Upper Surface of the Paleozoic Formations

The surface forming the top boundary of the Paleozoic rocks over
a large portion of the district cuts the layers and intrusions formed
by them, and represents an unconformity of the various Mesozoic and
Cenozoic deposits with respect to previously dislocated and denuded
Paleozoic rocks. The numerous outcroppings of this surface, as well as
the predominant bed elements and the thicknesses of the overlying Me-
sozoic and Tertiary rocks permit the basic outlines of the present-day
form of this surface to be found. This form is the total result of all
tectonic movements occurring from the beginning of the Mesozoic to the
present (Fig. 128). The Garm district includes part of the major sub-
sidence of this surface, corresponding to the Pamir foothills trough,
in which the angular unconformity between the Mesozoic and Paleozoic
vanishes. In the deepest portions of the trough, the Paleozoic surface
lies 8-12 km below sea level. The box-shaped and, evidently fault-
bounded Sorbulakskoye uplift is located within the northeastern por-
tion of the district, within the trough. In addition, the trough may
contain several other uplifts and structural ledges as illustrated
tentatively in Figs. 119, 120, 122. The deepest of the associated
faults, supposedly deep faults, are shown in Figs. 128 and 129. Two

- 431 -

steep shelves, complicated by faults separate the depression from the neighboring uplifts. One shelf — the Petrovskiy coincides with the watershed portion of the Peter I range, and the other, the Karakul', with the northwestern slope of the Darvaz range. It extends to the Northeast, intersecting the valleys of the Obikhingou and Muksu Rivers).

The present-day territory of northern Pamir and Darvaz was a continuously eroding uplift in the Mesozoic and Cenozoic. Although it contains few remnants of the surface under consideration, there is no doubt that in general it must be considered an area in which the present-day eroded surface occurs extensively. It is only in certain sections that this uplift is covered by Neogene conglomerates. One such structurally depressed section is to be found in the Garm district — the Safidaronskiy section.

Another extensive uplift of the denuded Paleozoic surface is found in the Northwest of the district. Here many Mesozoic-Paleozoic contacts are to be found. Directly to the North of the Petrovskaya shelf, bordering on the Pamir foothills trough, the Paleozoic surface is nearly horizontal. This is indicated by the flat Cretaceous beds, complicated slightly by small folds. The fact that the Paleozoic is not very far below the Earth's surface is established here independently by geological and seismic methods. We must assume that the Paleozoic is at its lowest position in the given zone in the central portion of the district. In connection with transverse flexure-type folds and faults to the East of Tadzhikabad, this surface is elevated, but still does not reach the exposed surface. To the Southwest, at the longitude of the mouth of the Obikhingou River, the Paleozoic surface rises so sharply that areal Paleozoic outcroppings appear here.

Within this structural step, there are separate sections in the
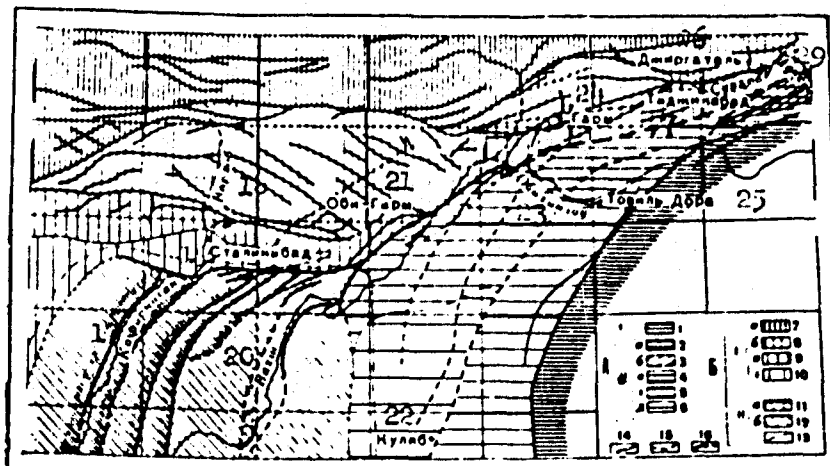
Fig. 129. Diagram showing tectonic districting of
northeastern portion of Tadzhik depression, and
its mountain frame. A) Alpine geosynclinal region;
I) Zone of block-dome uplift of northern Pamir and
Darvaz; II) Zone of Pamir foothills trough; 2)
subzone a — portion of depression uplifted inten-
sively and connected with block-dome uplift of
northern Pamir in Quaternary period; 3) subzone b
— connected with Sorbulakskoye uplift; 4, 5, 6)
subzones c, d, e, sections of depression uplifted
in Quaternary period (density of hatching indi-
cates degree of intensity of uplifting); B) Region
of post platform activation of tectonic movements;
I) Zone of block-dome uplifting in southern sec-
tion of western Tien-Shan with Epihercynian base;
7, 8, 9) subzones a, b, c (density of hatching
indicates degree of intensity of uplifting in Qua-
ternary period); 10) subzone d, relative (possibly
absolute) subsidence; II) Zone of block Tadzhik
structural depression with Epihercynian Epiproter-
ozoic base, sinking throughout the Mesozoic and
Tertiary, and subject in the Quaternary to differ-
entiated block movements; 11) subzone a, consist-
ing of blocks underlying the depression, sloping
chiefly to the West (the heavy hatching indicates
the most uplifted portions of the blocks); 12)
subzone b, consisting of blocks underlying the de-
pression, sloping chiefly to the East (the heavy
hatching indicates the most uplifted portions of
the blocks); 13) supposed Paleozoic boundary of
Epiproterozoic central massif; 14) basic zones of
tectonic faults; 15) zones of tectonic faults as-
sumed to be deep; 16) deep tectonic fault zones
bordering tectonic zones; 17) Kafirnigan; 18) Var-
zob; 19) Stalinabad; 20) Vakhsh; 21) Obi-Garm; 22)
Kulyab; 23) Obikhingou; 24) Garm; 25) Tovil'-Dora;
26) Dzhirgatal'; 27) Tadzhikabad; 28) Surkhob; 29)
Muksu.

form of blocks that have been uplifted differentially. Two systems of major branching faults with a southwesterly trend intersect the step obliquely; these are echelon faults. In addition, there are many small blocks, 10-15 km long and about 5 km wide. Their uplifted position is reflected in a blanket of Cretaceous rock in the form of long narrow anticlinal folds, frequently of box-type angular shape with steep, occasionally inverted limbs.

On the northwestern boundary of the step, along the bed of the Surkhob River (and somewhat to the North of it in the neighborhood of Garm), the next structural shelf is found, the Surkhob shelf, complicated nearly everywhere by very steep tectonic faults that merge into a single complicated fracture. To the Northwest, Paleozoic outcroppings predominate, and thus the upper surface of the Paleozoic stage must be assumed to have been uplifted roughly up to 4000 m. We next encounter outcroppings of Cretaceous rock, sloping toward the Northwest, and then cut by the next fault zone. Thus, we may speak of the existence of a second structural step to the North of the Surkhob, higher than the first step, and having the form of a gently sloping anticline. This anticline, called the Kabudkrym anticline, in general coincides with the main body of the Paleozoic anticlinorium mentioned above. The limbs of the anticline slope less than those of the anticlinorium.

Finally, the extreme Northwest of the district, which has no Mesozoic outcroppings, and in which the heights in the relief due to the Paleozoic are more than 4000 m, is considered by us to be the third and most uplifted step, where the surface under consideration (today eroded) is located at a height of more than 4000 m.

It thus appears that on the area covered by the portions of the Zeravshan, Gissar, and Karataginskiy ranges that lie within the Garm

- 430 -

district, there is a step-type limb of a dome-block bulge in the Paleozoic surface.

Internal Structure of Mesozoic and Tertiary Deposits

Within the southern stepped limb of the dome-block uplift in the southern portion of Western Tien-Shan, outcroppings of Cretaceous deposits make it possible to establish only the single major Kabudkrym anticline. Near the faults that cut it to the Northwest within the Cretaceous, we know of shallow disharmonic folded structures. In the main, the Cretaceous beds follow the shape of the Paleozoic surface.

In the next structural step to the Southeast, which coincides with the northern slope of the Peter I range, in contrast to many earlier scientists, we have found gently sloping Cretaceous beds to predominate. Another idea new with us is that the folds developed here are simple in form, and repeat the shape of the upper Paleozoic surface, which is broken up by steep faults into individual blocks shifted with respect to each other (Figs. 119, 120, 122). Directly to the West of Garm, there is a block of Paleozoic rock (Mandalyul' mountain), which is revealed by the denudation of the main portion of the anticline within the Mesozoic deposits. Some 5-10 km to the Southeast, there is a second such fold, triangular in plan, formed by Cretaceous rock. Its Paleozoic core has still not become exposed. The steep limbs of this fold are complicated by steep faults of the upthrust type. The western limb, with a North-South trend, is tilted somewhat to the West. The slope of the Runou talus runs along the trend of the limb. When we look at this slope, which reveals a section of the limb along its trend, we get the impression that the talus cuts across a recumbent synclinal fold.

On the basis of an erroneous interpretation of this outcropping, several scientists believed that within the entire structural step

- 431 -
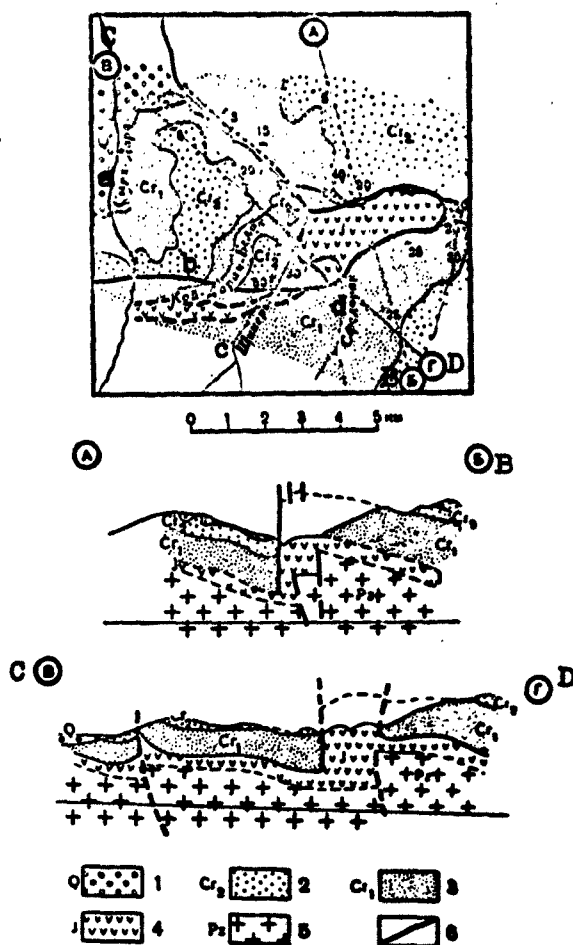
Fig. 130. Schematic geological map
and sections of the Darainushorskiy
section with intrusions of Upper
Jurassic gypsums along fault zone.
1) Quaternary gravels; 2) Upper Cre-
taceous carbonate deposits; 3) Lower
Cretaceous sandstones; 4) Upper
Jurassic gypsums; 5) Paleozoic meta-
morphic and magmatic rock; 6) tec-
tonic faults. a) Syrkh-Dara; b) Koy-
Darak Bedok; c) Shikery; d) Sfedorak.

under consideration, recumbent folds are developed, inverted to the

Northwest, and complicated by gently sloping overthrusts. As a matter

of fact, here all faults dip steeply.

The faults that cut across the Cretaceous deposits must be con-

sidered to extend to great depths, and to separate the Paleozoic blocks. In order to obtain a new idea of the internal structure in the strip under consideration it is important that the many exposures of the Jurassic in the Cretaceous should not be considered to be tectonic wedges in overthrust seams. We have established* that in many places, the Upper Jurassic gypsums have been displaced upward, forcing their way into the Cretaceous rock along the seams of steep faults (Fig. 130). It is important to note that not all the gypsums found among the Cretaceous rock are Jurassic and have forced their way along faults. There are the quite widely distributed Senoman gypsums, which are found in their natural stratographic position in the middle of the Cretaceous section. There are many Senoman gypsums at the Lyuli-Kharvi pass, where they are assumed to be Upper Jurassic.

Quite large, heavily compressed folds in the Cretaceous deposits are seen along the border that formerly separated the platform region from the Pamir foothills trough, in a narrow band stretching along the crest of the western portion of the Peter I range, and then to the Southwest, outside of the district, along the Vakhsh and Surkhob ranges. As a rule, two-three anticlines are encountered in each cross section of this strip, since echelon folds are characteristic of the entire strip. The folds are heavily compressed, frequently are Ya-fuchskiy isoclinal in form, and are overturned with a shifting direction. They are frequently overturned to the Northwest, toward the ancient platform. Proceeding along the trend of the several folds in the Obikhingou River basin, we can see how the direction of overturning can reverse itself in the same anticline. Several of the anticlines are fan folds (Fig. 122).

In the eastern portion of the district, this disharmonic fold complex, related with the northwestern border of the Pamir foothills

trough zone, vanishes.

In the Garm district, there is only the single Yafuchskiy up-thrust associated with these folds; it slopes to the Southeast at an angle of 70-80°. It is quite clearly visible in the gorge of the Obi-khingou River. It is known that there are several related faults to the Southwest of the district.

Within the Pamir foothills trough zone, the fold structure in the eastern portion of the district differs from the structure in the western portion. To the East, on the site of the ancient Mesozoic and Paleozoic depression, we see today the major Sorbulakskoye anticlinal uplift in the Mesozoic beds. In its axial section, thick Jurassic and Lower Cretaceous beds are found, sloping gently, with very steep partly overturned beds on the limbs; they give a box-like shape to the entire structure. To the East of the Muksu River, the uplift becomes wider and higher. It is one of the basic echelon uplifts, formed jointly with the Zaalay range. The Sorbulakskoye anticline takes slightly different forms in different cross sections. In the eastern section of the Garm district, in the Muksu River valley, it is asym-metric. A northwestern slope of the beds predominates. Here to the Southeast of the Sorbulakskoye uplift, there is a quite broad syn-clinal belt, formed in the Lower and Upper Cretaceous, and complicated by additional folds that are probably disharmonic with respect to the Jurassic beds. Toward the Southwest, along the tectonic-zone trend, the Sorbulakskoye uplift gradually wedges out, and the uplift becomes less and less apparent. Following the law of wedge arrangment of major folds, it gradually departs from the northwestern border of the trough zone, and stays near the southeastern edge. The narrow southwestern termination of the uplift occurs near Tovil'-Dora, where it is charac-terized by a very asymmetric shape with a gently sloping southeastern

limb, and a very steep northwestern limb, in the form of a large flexure. In exposures, it is quite plain that certain groups of Tertiary beds, disharmonically crumpled in the upper portion of the steep limb, are overturned in places toward the lower section, along which the Obikhingou River valley passes (Fig. 120). These morphological features of the Sorbulakskoye uplift tend to make us believe that far beneath the uplift there are narrow blocks, bordered by steep faults, that were forced out from the Upper Paleozoic formations in the Pamir foothills trough when they were crumpled during the Neogene and at the beginning of the Quaternary.

In the western portion of the Garm district, the Mesozoic and Tertiary beds form a synclinorium structure with a northwestern limb that sinks sharply to the Southeast, and which is complicated by the major disharmonic folds that we have mentioned. Owing to the sharp leveling off of all beds in general, this limb can be followed for a long ways to the Southeast. The axis of the synclinorium is located near its southeastern edge. The southeastern limb is narrow and slightly dislocated. As we approach Pamir, the stratification becomes simpler and simpler.

All of the folds observed in the synclinorium can be classified into two basic types. What first meets the eye are the major flexures, of which there are at least four in the section along the Obikhingou River gorge. Between their steep limbs, the beds are very nearly horizontal. Using the idea of the very probable existence of faults under the Sorbulakskoye uplift, and assuming that the flexures observed in the Garm district can be followed for a distance of several hundred kilometers to the Southwest, we must conclude that the best interpretation of the flexures is obtained if we assume that major faults in the Paleozoic base of the depression exist under them.

- 435 -

The folds of the second type are clearly disharmonic with respect
to the lower-lying Tertiary or Mesozoic beds in the section. Figure
122 shows that some of the beds are straight isoclinal anticlines with
main bodies of relatively plastic argillaceous layers or Danian or Up-
per Jurassic gypsums. Such disharmonic folds, which are very nearly of
the diapir type, are chiefly associated with the upper sections of the
major flexures just mentioned, which frequently mask the existence of
such folds.

The main flexures with "overlying" disharmonic folds are arranged
in echelon fashion, and branch out from the northwestern edge of the
Pamir foothills trough zone. Owing to the substantial difference be-
tween the internal structure of the trough zone in the eastern portion
of the district, where we find a major anticlinal uplift, and the
structure of the western portion, there must be in the central portion
of the Garm district a sharp transverse fold in the given zone, with
the hinge dipping in a southwesterly direction. To the Southwest of
the Obikhingou River, there is still another drop in all layers and
folds to the Southwest. Thus, we should take note of the step-type
character of the East-West profile in the zone under consideration.
The steps go down from the Northeast to the Southwest.

Form of the Upper Surface of Mesozoic and Tertiary Beds

The uppermost competent surface that enables us to find the
structure created during the second half of the Quaternary, is the
Lower Quaternary hilly relief. Above, we gave some justification for
the theory that the watersheds at the end of the first stage of the
Quaternary were in all parts of the Garm district located in the vi-
cinity of a single horizontal level, arbitrarily taken to be 1500 m
high.

At the present time, there are many places in various parts of

the district where it is possible to observe outcroppings of this re-lief, lying at various heights, and frequently separated by large shelves. Major alpine tectonic faults can be found quite independently of geomorphological data at the sites of such shelves from the displacements of beds of various ages. In addition, in order to see how the initially almost horizontal watershed surface was formed, we as-sume that it is possible in this district to make use of the surface that joins the present-day peaks of the mountains. Since the present-day mountains appeared owing to erosion breakdown of a plateau, their peaks lie at a height slightly below that which the surface of the eroded plateau would have had. This theory is confirmed by the fact that over sections of considerable area, the peaks are located about a single surface, regardless of the age and composition of the rock com-posing the mountains. In various sections, this surface lies at dif-ferent heights. In places, it slopes. This "present-day peak surface" we assume to be at nearly the same height (somewhat below) the water-shed surface of the already eroded Early Quaternary slightly hilly re-lief, which crops out at several places in the district.

In the northwestern portion of the district, the present-day peak surface gradually drops to the Southeast from 5000 to somewhat more than 4000 m. After the tectonic-fault belt that borders the Kabudkrym anticline on the North, this surface drops sharply to 4000 and 3800 m. It is especially low to the North of Tadzhikabad (3500 m or less). The general level of the relief then goes down sharply once again to roughly 2000-2500 m; this shelf (the Surkhob) coincides almost every-where with the bed of the Surkhob River. It is only near Garm and to the West of it that the shelf lies somewhat to the North of the Surk-hob River. It is a very important fact that Southeast of the shelf, in the lowest point of the Garm district, from the structural viewpoint,

traces of the Early Quaternary slightly hilly relief are retained.
They form a broad flat step on the northern slope of the Peter I
range. The lowest outcroppings of the ancient relief occur on the cen-
tral portion of the district, lying between the longitudes of Garm and
Khait. On the western boundary of the district, they give way to moun-
tains, worn down extensively by erosion, with a surface gradually ris-
ing to the West to 3000 m, while in the basin of the Kafirnigan River,
its remaining outcroppings are found at heights of about 3000 m. In
the eastern portion of the Garm district, the ancient relief gradually
rises to the East, reaching 3000 m at the longitude of Dzhirgatal'.

As we go to the Southeast, at right angles to the trend of the
tectonic zones, following the low strip which we have discussed, there
is a very sharp elevation in the surface of the ancient relief. In the
section before the watershed of the Peter I range, it is located at
heights greater than 3000 m, and in the highest portion of the range,
between the longitudes of Garm and Tadzhikabad, there was an uplift
that went considerably above 4000 m, since here it was eroded, and the
tops of the present peaks reach 4700 m. Thus, as we go from the tec-
tonic zone of the former platform to the zone of the former Pamir
foothills trough, there is a second sharp structural shelf (the Pe-
trovskiy). Within its boundaries there are several major steeply dip-
ping tectonic faults disturbing the ancient relief. It is important
that displacements of the Early Quaternary Relief occur in this strip
in a direction opposite to that observed in displacements of the upper
surface of the lower structural stage.

The Pamir foothills trough tectonic zone, located to the South-
west, is sharply uplifted, on the whole, in the form of a large struc-
tural step with respect to the preceding zone, while the surface of
the lower structural stage is here depressed, on the other hand. While

the remains of the ancient relief have as yet not been mapped here, we can see in advance that they should be located quite high, since the surface of the peaks does not drop below 3000 m. The highest level of the surface joining the peaks occurs near the northwestern border of the zone. From this point, it drops slightly toward the Southeast, sloping gently in this direction. In addition, the transverse strip in which the surface connecting the peaks drops to the Southwest coincides with the valley of the Obikhingou River below Tovil'-Dora.

As we approach the Muksu River from the West, the step narrows, and becomes nearly horizontal. To the East of the Muksu, beyond the border of the district, it begins to slope towards the North.

The last, most southeasterly section of the district is the next greatly uplifted step. In its southwestern portion, it is located at heights of 3500-4000 m, and rises very slightly above the preceding step. Here, in the Darvaz range, outcroppings of the Early Quaternary hilly relief may be seen. On the northwestern slope of the range, they slope toward the neighboring lower step. Toward the Northeast, the step under consideration rises steeply, and thus in this step the ancient relief proves to be eroded. The surface of the present-day peaks reaches 5500 m. In general, the given step corresponds to the ancient uplift of Northern Pamir and Darvaz. As we go from it to the preceding lower step, we encounter a massive shelf in the relief — the Karakul' shelf to the Southwest, and the Karashurinskiy shelf to the Northeast; the latter lies within the southeastern half of the Sorbulakskoye uplift. Thus, the present-day border of the Northern Pamir and Darvaz uplift in the eastern portion of the Garm district has shifted within a zone lying within the former Pamir foothills trough.

General Diagram of Present-Day Structure in the District

Comparing the data listed, we can see that in the extreme north-

eastern section of the Garm district, there is today only the lower
structural stage, formed in Paleozoic rock. Its surface, now eroded,
is high, and nearly coincides with the surface of the Early Quaternary
relief. Next, there is a large structure shelf, along which both of
these surfaces drop toward the Southeast to the lower Kabudkrym step.
On it, in places, the thin upper structural stage is preserved, formed
in Mesozoic and Tertiary deposits. Beyond this there extends the next
structural ledge — the Surkhob — in which both competent surfaces drop
sharply, and in the same way, to the Southeast. Following this, on the
northern slope of the western section of the Peter I range, there is a
structural step in which both structural stages are developed every-
where; judging from geological data alone, the upper stage here is not
very thick (to 2 km). In the following structural shelf to the South-
east, the Petrovskiy shelf, the lower competent surface is greatly de-
pressed, while the upper surface, on the contrary, rises, leading to
the next step, corresponding to the southern slope of the western por-
tion of the Peter I range. In this step, the lower surface is far
down, and the upper structural stage has a maximum thickness of 10-
15 km (according to geological data). Finally, in the most southeast-
erly shelf, which in the southwestern portion of the district is
called the Karakul' shelf, both surfaces (and especially the very low
one) rise to the Southeast to the high step of the Darvaz range, where
they run together (Fig. 131).

Summarizing all that we have said about the structure and histor-
ical tectonic movements of the Garm district, we can distinguish the
tectonic regions, zones, and subzones shown on the diagram (Fig. 129),
which has been drawn on the basis of tectonic observations alone, with
no resort to seismic data. We first of all distinguish between the re-
gions of the alpine geosyncline A and the Epihercynian platform B,

which has experienced post-platform activation of movements, beginning in the end of the Paleogene. In the geosyncline region, we find the very intensively uplifted Northern Pamir and Darvaz structures, and the Pamir foothills trough, experiencing extreme subsidence in the Mesozoic and Tertiary. During the Quaternary, this depression was up-lifted; it still was not uplifted enough to acquire the structure of an anticlinorium within the Garm district. To the East, however, in the Zaalay range, where intensive uplifting commenced as early as the Neogene, it already had a completely formed structure — that of an in-verted anticlinorium. There, the watershed surface was uplifted to 7000 m. In the Garm district, this is still an ill-defined half-in-verted anticlinorium, which has the general form of an uplift along the upper stratigraphic surfaces, and the form of a depression along the lower surfaces.

In the Epihercynian portion of the platform region, during the Mesozoic and in the beginning of the Tertiary, both subsidences and uplifts were less intensive than in the geosyncline region. In the Neogene, however, post-platform activation of movements commenced, covering many platform districts of Asia with Epihercynian (Tien-Shan), Epicaledonian (Sayany), and Epiproterozoic (Zabaykal') folded bases. The ascending movement of the southern portion of Western Tien-Shan, inherited from the Hercynian anticlinorium, was greatly intensified, and led to the formation of a major dome-block uplift with a stepped southern limb extending only in part within the Garm district. Depend-ing upon the relative uplift of the various steps, we find three sub-zones in the tectonic zone of the dome-block uplift. The subzone that touches the geosyncline border is the least uplifted. At the end of the Quaternary, the uplifting ceased almost completely (it is absent in many places at which the Surkhob River has cut into the Ancient al-

luvia). In this respect, it is somewhat like the advanced troughs, especially since this relative drop appeared only in the Quaternary, when the ascending movements extended all the way to the edge of the geosyncline, and covered the Pamir foothills trough zone, while the Northern Pamir uplift extended at the expense of the adjacent portion of the Pamir foothills trough.
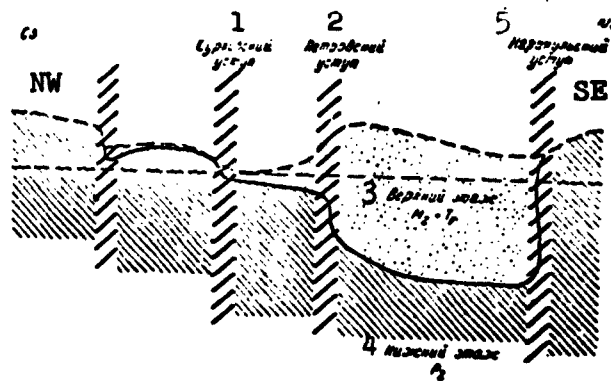
Fig. 131. Basic diagram of present-day structure of Garm district. 1) Surkhob shelf; 2) Petrovskiy shelf; 3) upper stage; 4) lower stage; 5) Karakul' shelf.

The tectonic faults shown on the map of Fig. 128 have been established from geological data alone, with no recourse to earthquake epicenters. Depending upon which deformations in the Earth's crust they are associated with, the faults are divided into three main groups. The largest faults, connected directly with deformations on the borders of very large tectonic regions and zones, produced not only by deformations of the Earth's crust, but also of the deeper mantle, are called deep fault zones. Three deep zones of steeply dipping faults are distinguished; the two oldest bordered on the Pamir foothills trough in the Paleozoic, and might have been renewed, in part, during the Mesozoic and Quaternary. The southeastern zone – the Karakul' zone – has long been known [233-236]. The southwestern zone was

the first to be isolated; it coincides with the crest of the western portion of the Peter I range, and is called the Petrovskaya zone. The faults developed in it do not emerge at the surface. In places, the directions of displacements in the deep fault zones was changed at the end of the Tertiary and in the Quaternary, owing to the uplifting of a portion of the Pamir foothills trough. This occurred with a special force on the site of the Peter I range, and beyond the borders of the Garm district, in the Zaalay, Vakhsh, and Surkh-ku ranges. Owing to the expansion of the Northern Pamir uplift to the North (in the Quaternary) from the former Karakul' deep fault zone, that ordered it, the new Karashurinskaya zone branched out, intersecting the Sorbu-lakskoye uplift, and partially assimilating the associated faults. In the Neogene and Quaternary, a third zone formed — the Surkhob deep fault zone, forming the northern border of the least uplifted, relatively depressed edge section of the ancient platform. During the formation of the given youngest deep fault zone it is possible that during this time the hidden Paleozoic faults visible in the western extension of the zone beyond the borders of the Garm district were renewed.

In addition to the deep fault zones, individual major faults visible on the surface were isolated; these faults are due to relative displacements of neighboring tectonic zones and subzones. Finally, we isolate the secondary faults within subzones. On the tectonic diagram of Fig. 128, we have especially indicated the supposed deep faults that border the variously uplifted portions of the Pamir foothills trough zone. Accurate specification of the locations of these faults requires the use of geophysical methods. On the surface, we observe only major flexures complicated by disharmonic folds.

All that we have said above with respect to faults applies to
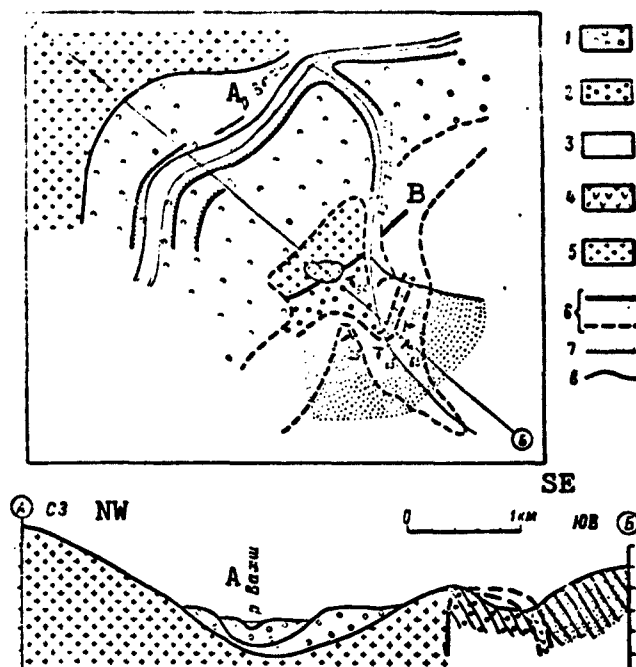
Fig. 132. Schematic geological map and section through Khodzha-AliSho. The diagram shows the narrow long graben and horst near the exposed surface of the upthrust into the wall of which Upper Jurassic gypsums have penetrated. 1) Quaternary conglomerates; 2) Pliocene loose sandstones; 3) Lower Cretaceous red sandstones; 4) Upper Jurassic gypsums; 5) Paleozoic magmatic rock; 6) tectonic faults (a — reliably established; b — supposed); 7) scarps; 8) relief contours. A) Vakhsh River; B) Khodzha-AliSho.

fractures that are longitudinal with respect to the tectonic zones. In the Garm district, they are extremely common. In addition, however, we also find here transverse faults that are less important. The transverse faults, as Fig. 128 shows, intersect the longitudinal faults belonging to the young Surkhob fault zone. In addition, they noticeably distort the Lower Quaternary base surface. It is thus clear that in the Quaternary, the transverse faults grew.

The block alpine tectonics of the Garm district are not unique, as it also is characteristic of all of Tien-Shan [248, 250]. Its importance in Paleozoic tectonics is clear in Northwestern Tien-Shan [251]. As we find it in the extremely dislocated northeastern corner of the Tadzhik depression, which is in a geosyncline, we have every reason for assuming that the tectonics of the interior platform region of the depression are based upon the same relative displacements of weakly deformed blocks. In his studies, V.V. Belousov has concentrated on the very large distribution of this type of deformation in the Earth's crust in China, the Alps, and other territories [252, 253].

Block tectonics are characteristic not only for the Neogene and Quaternary, when the present-day relief was created, and the present-day structure was determined to a considerable degree. Block-type tectonic movements constantly appeared in South Central Asia, and in other regions, and as a result the Earth's crust can be separated into numerous well-defined elementary tectonic zones [254], or as we now frequently say, structural-facial zones, whose individual features are traced over a long stretch of geological time.

§3. MECHANISM FORMING ALPINE STRUCTURE

It seems to us that the chief factor in the mechanism forming the structure characterized above is the vertical shifting of individual plastic blocks of the Earth's crust, bordered by tectonic faults, many of which run through the entire crust of the Earth. The contours of the blocks were basically determined as long ago as the Paleozoic.

Structural Results of Changes in Direction of Motion of Tectonic Zones

The direction of displacement along faults did not remain the same in all places during the Mesozoic and Cenozoic. During the Neogene and Quaternary, owing to the variation in direction of motion of the Pamir foothills trough zone, and owing to the fact that subzones

B-I-c and B-I-b (Fig. 128) (Kabudkrym anticline) did not participate in the uplifting of the adjacent subzones, the sign of movement along the faults surrounding these blocks must be reversed. At this time, there also appeared new additional faults, among which there were many transverse fractures.

Besides the very clear manifestations of a change in direction with respect to displacements of adjacent blocks that we have mentioned, established on the basis of an analysis of the general structure and movement history of the tectonic zones, there are many other structural features that indicate a change in direction of relative displacement of neighboring blocks.

1. In the Northwest, along the border of subzones B-I-a and B-I-b, cutting the Kabudkrym anticline from the Northwest, there is a fault zone within which narrow long graben are clearly visible at two points; they are formed in the Cretaceous rock (Fig. 118). The same narrow grabens formed in Tertiary beds stretched to the Southwest of the district along the Vakhsh River valley along the border of the ancient platform and the Pamir foothills trough (Fig. 132). These grabens do not seem to us to be independent tectonic zones or subzones on the same footing as those shown in Fig. 128. In these graben, we see the results of a change in direction of relative displacement of two neighboring zones or subzones. Initially, a relative uplift of one zone led to the appearance of faults on one border of the graben-to-be, and then a more rapid uplift of the other zone caused the formation of faults whose limbs had a relative displacement in the opposite direction.

2. In like manner, narrow horsts, wedge-shaped in plan, appear on the borders of two neighboring tectonic zones for which the direction of relative limb displacement remains unchanged. One such horst in
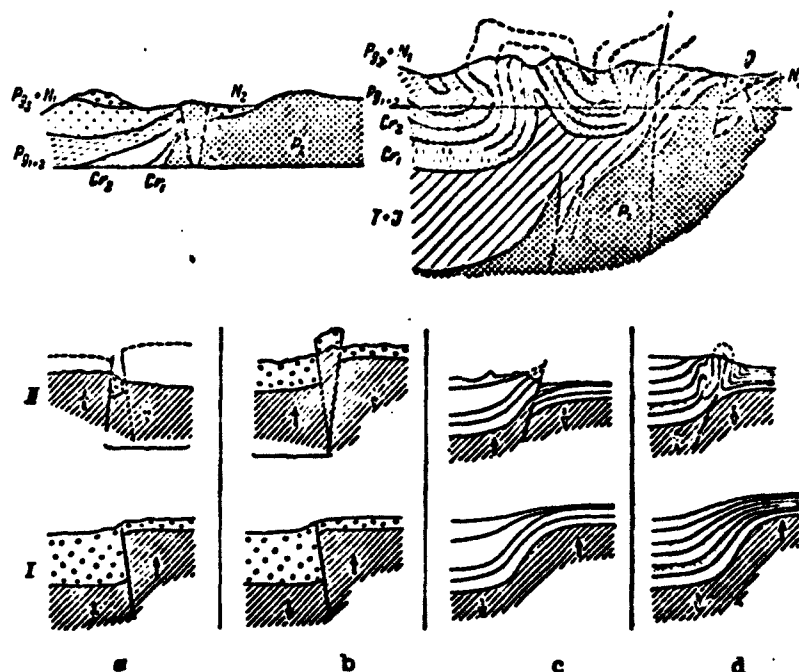
Fig. 133. Diagram of structural complications appearing on border of two tectonic zones when the direction of their relative displacement changes. a) Narrow long graben; b) narrow long horst; c) conformable upthrust; d) group of line folds. I) First stage of deformation — subsidence of left-hand tectonic zone; II) second stage of deformation — relative uplift of left-hand zone. Above are examples of a long narrow horst, conformable upthrusts, and line folds.

Permian limestones among Neogene conglomerates is found in the north-western border of the Northern Pamir and Darvaz uplift (Figs. 118 and 120).

The appearance of separate new faults when relative zone displacement direction changes, while there is no change in the direction of motion along the old fault is explained by the fact that all major faults are upthrusts sloping toward the relative uplift of the limb. With a change in direction of the relative displacement of neighboring tectonic zones, for the faults to continue to fall on the side of the

ascending limbs, it would be necessary for new slips to appear. When the old faults are used, this condition will not be satisfied (Fig. 133b).

3. Where there are major flexures (of the type separating the Pamir foothills trough zone from the platform) that have appeared as the result of a relative subsidence of their lower limbs, upthrusts may be found along which the lower limbs of the flexures are uplifted relatively. Thus there is, for example, the Yafuchskiy fault, found in the lower reaches of the Obikhingou River (Fig. 122, VI-VI). There are especially many such faults near the western border of the Garm district, and from this point they run along the Vakhsh River to the Southwest. The existence of flexures far antedating these upthrusts indicates that there were variations in the thickness of Mesozoic deposits (Fig. 133c, d).

Symptoms of Weak Additional Horizontal Compression

The formation of blocks and their vertical displacements evidently occur under the action of vertical forces, but in the presence of some horizontal compression, which determined the uniform linear extension of all zones, and the upthrust nature of the majority of faults observed.

Our attention is caught by the endurance of the echelon arrangement of young faults and folds dating back to the Neogene and Quaternary. The same type of echelon formation occurs in many other districts of Southwestern Tien-Shan and, undoubtedly, reflects some general feature of the latest deformations in a considerable portion of the Earth's crust. Evidently, there is an additional general horizontal compression directed obliquely to the trend of the tectonic zones, owing to which, an element of simple shear deformation appeared in the zones in the horizontal plane. Judging from the shape of the echelon-

type arrangement of the main faults, this must have been a left-hand shear, i.e., each zone further to the Southeast was displaced relatively at the time the faults were being produced, to the Southeast; it is possible that this displacement continues to the present day. Thus, the additional horizontal depression of tectonic zones having a southeasterly trend should lie very nearly in a North-South direction.

The Paleozoic base of the Garm district deformed and faulted as a plastic, rather than as a brittle, body under the action of vertical forces in the presence of a weak horizontal compression. Judging from the existence of curvature in the Paleozoic-Mesozoic contact surface, and the surface of the Lower Quaternary relief, the Earth's crust experienced additional plastic deformations. At places in which the deformation occurred with maximum speed, these stresses proved to be very large, and thus faults were formed here. In speaking of blocks within Paleozoic rock, we do not consider them to be absolutely rigid, but to be plastic portions of the crust, possessing a somewhat greater viscosity than the Mesozoic and Tertiary sedimentary rock. The mechanical properties of the Lower and Middle Paleozoic, which is intensely dislocated, metamorphized, penetrated by intrusions of granitoids, and located in the northwestern half of the district, should differ from the properties of the less metamorphized, weakly dislocated Upper Paleozoic rock, penetrated by fewer intrusions, deposited below the Mesozoic and the Pamir foothills trough zone.

Fold Formation Mechanism

The folded structure of the Mesozoic and Tertiary sedimentary-rock cover is thought by us not to be caused by general horizontal compression, as is frequently supposed, but by vertical movements of blocks of the Paleozoic base. Additional horizontal weak compression forces, such as those mentioned above probably act only in the Paleo-

zoic base. The main deformations in the sedimentary cover directly re-peat, basically, the vertical motion of base blocks. This type of de-formation is called a transverse fold.

Crumpling of the layers occurs only in places in the sedimentary cover under the action of the compression forces acting parallel, or nearly parallel to the beds. This crumpling reaches its greatest de-velopment along the boundary of the Pamir foothills trough zone and the platform. Here the formation of folds coincided in time with the beginning of an intensive uplift of the limb of a large flexure, bounding the trough, which had subsided greatly prior to this. The up-lifting of the trough zone led to a decrease in the length of the crumpling limb of the flexure. Isoclinal and fan-shaped disharmonic folds (Figs. 119, 120, 124, and 133c) are considered by us to be a consequence of this contraction. Such a mechanism has also been pro-posed to explain certain folds in Southern Fergana [230].

Small folds occurred with the appearance of considerable inhomo-geneity in the stressed state in stratified series experiencing the deformations mentioned above. Argillaceous, marl, and, in particular, gypsum seams were easily squeezed out of places at which there was severe compression on all sides, and were forced to points of less compression. There, small disharmonic folds were formed, and gypsums were even introduced within walls of tectonic faults. Examples of the introduction of Upper Jurassic gypsums into fault zones are shown in Figs. 130 and 132.

Materials from the literature and our field observations indicate that consideration of the folded structure as a complex of genetically different but at the same time interdependent folds and faults might be extended from the very indicative Garm district, the scene of our studies, to the territories surrounding it. The direct repetition in

the Mesozoic and Tertiary beds of the displacements and deformations that had been experienced by the surface of the Paleozoic base is the first and chief type of fold formation. This is revealed clearly not only in the Garm district, but also throughout the area of the Gissar range [231], and in the Kugitang range. We assume that the same phenomenon exists in the group of less deeply cut fault exposures between the Surkhan-Dar'ya River and the Yavanskaya valley in the Tadzhik depression [232]. The same layer folding can be noticed in the southeastern portion of the Tadzhik depression.

The folds of the second important genetic variety extend to the Southwest in the Bakhsh and Surkh-ku ranges: they are disharmonic crumblings and folds in the beds on the borders of tectonic zones (blocks) that move differently, of the type studied by us on the crest of the western portion of the Peter I range. Further on, this group of folds branches into several groups running along a group of borders between major and minor blocks in the eastern half of the Tadzhik depression, and to the southern border of the Gissar tectonic valley. As a rule, the groups of folds associated with the edges of separate blocks form raised ranges or ridges in the relief. Sharp fractures of fault boundaries of neighboring blocks cause the uplifts to appear with unexpectedly sharp turns in the fault trends. The distinctive confluence of folds having three directions in the Tutkaul'skiy junction can be explained by the fact that the arrangement of the disharmonic folds is caused by faults that are not visible on the surface, and that lie deep within the Paleozoic or even lower base.

Folds of the third type, created by flowage of material from the most "viscous" layers and even by its introduction into the walls of various faults, may be examined at many places. They are most developed where the folds of the preceding types reach maximum development.

In each section, the presence of one predominant direction of inclination of the folds and the faults directly responsible for them can be compared with the direction of relative displacement of the neighboring tectonic zones (blocks). In the Garm district, in the border group of folds in the Peter I range, overturning and upthrusting along steep upthrusts toward the side of the zone slowly ascending during fold formation predominate. The same relationship is also clear to the Southwest of the district in the Vakhsh and Surkh-ku ranges. Thus, the movement, standard in many districts, from the former depression, which later begins intensive uplifting, can be seen also in the western portion of the Tadzhik depression. Major folds, belonging to the first of the types enumerated, and forming the Kugitang, Baysuntau, Babatag, and other ranges, move up along steep faults toward the less mobile central portion of the depression with the lowest base [246]. In like manner, from the more mobile eastern portion of the depression, the folds move toward the central low-mobility section. Thus it is possible to explain the divergence of the folds in the Tadzhik depression, without resorting to the common notion of horizontal pressure on the young depression sediments from Pamir [255]. A simplification in the fold structure of the sedimentary cover of the depression directed toward Pamir is characteristic not only of the Garm district. This general law indicates that the sedimentary cover has not experienced horizontal compression from the Pamir direction at every point.

Formation of Transverse Faults

The appearance of transverse faults in the Garm district is explained by the fact that it is located in a transition area from a less uplifted portion of the Pamir foothills trough zone (to the Southwest of the Obikhingou River valley) to a more uplifted section (the Peter I and Zaalay ranges). In the Garm district, the crust of

the Earth has folded from the Southwest to the Northeast; this was accompanied by the formation of transverse faults. Since such deformation developed only in the Quaternary, the transverse faults associated with it are younger than the lower longitudinal fractures, and appear less well-developed in the district structure. The law of replacement of longitudinal faults by younger transverse faults was studied on models [256].

Form of Tectonic Zones

Finally, let us concentrate our attention on the fact that during the Mesozoic and Cenozoic, the Pamir foothills trough, separating the Pamir uplift from the Tien-Shan uplifts did not experience, within the Garm district, any contraction of its width from North to South. Consequently, the Pamir portion of the Earth's crust experienced no great displacements to the North, and did not pinch the Tadzhik depression zone between itself and the Tien-Shan uplift. This means that the curvature and complexity of shape of the Pamir and Tadzhik depression tectonic zones in plan should be considered to be primary features, rather than consequences of the deformation of the Earth's crust in later times [232]. All zones are found in their initial positions, and have not experienced major displacements horizontally. Thus, we consider false one of the most common explanations of the structure of South Central Asia in terms of horizontal pressure from the "Punjab wedge" (an angle of the Indian platform) on the Himalayan-Pamir alpine geosyncline, which is supposedly squeezed as a result against the Tien-Shan platform. We think a more correct notion of the leading role of vertical movements in the formation of the Central Asia structure is that developed long ago by V. I. Popov [228].

[Footnotes]

Manu-
script
Page
No.

402   M.V. Gzovskiy, A.V. Goryachev, V.N. Krestnikov, diagram

of Garm region, manuscript, IFZAN fund, 1954.

Chapter 9

SEISMICITY OF A DISTRICT AND COMPARISON WITH TECTONICS

The concept of seismicity comprehends both the focal activity of earthquakes, and the manifestation of such activity upon the surface of the earth.

In this connection, there are two types of data bearing upon seismicity. The first type includes information gathered with and without the aid of instruments, through modern and historical reports as to earthquake foci, territorial distribution, depths, times of appearance and energy; these data may be represented both directly and in generalized form by specification of the seismic-regime parameters, especially the seismic activity A and the parameter γ for the decrease in recurrence [frequency] with increasing earthquake energy. Second, seismicity is determined by the characteristics of ground movement during earthquakes: modern and historical reports obtained with the aid of instruments and through macroseismic observations.

Information belonging to the region lying between the two mentioned serves to characterize seismicity also; this region comprehends the transmission of seismic vibrations from the focus to the ground surface. In this area, we have information on the attenuation of energy and variation in the frequency composition of seismic waves along their propagation path from the focus to the site on the earth's surface under consideration, as well as data on the effect of the upper layers of the earth, and in particular of soil conditions, upon ground vibrations.

The preceding chapters have given much information on the seis-
micity of the district being investigated (including the Garm and
Stalinabad districts). The data given below relate chiefly to the spa-
tial distribution of seismicity; maps of earthquake epicenters and
seismic activity are presented and discussed. These seismic data are
then compared with geological data relating to the tectonic structure
of the district, and with information on tectonic movements of the
earth's crust.

§1. EPICENTER MAP

Earthquake-epicenter maps are compiled from instrument data, as
well as on the basis of isoseismal maps of strong earthquakes, obtained
from macroseismic observations. The epicenter maps are used as the
basis for comparison of seismic and geological data, for studying the
connection between weak and strong earthquakes, and to solve many
other problems. The same maps are presently in use as the basis for
maps of seismic districts, which represent the territorial distribution
of possible shock strength. The latter are widely used in connection
with the standards for construction in seismic districts (SN-8-57 [257])
in the design and construction of buildings. Naturally, the quality of
the epicenter maps determines to a considerable degree the reliability
of all conclusions based upon them.

Epicenter maps taking the form of a discrete set of points are
not the best way of representing the spatial distribution of seismicity.
The inadequacy of such a representation is especially manifest in those
extreme cases in which the epicenters are small and are scattered over
a large area with no apparent relationship, or where they are so nu-
merous as to form a solid block, in which the individual epicenters
cannot be distinguished [227]. It is impossible to draw quantitative
conclusions as to the relative seismic activity of different districts

on the basis of epicenter maps. In this connection, recent years have seen efforts to go over from maps of discrete epicenters to maps representing continuous quantities in the form of isolines: seismic-activity density, developing in a specified period of time [217, 219, 220, 221], or epicenter distribution density [11]. A further development in this direction is represented by the seismic-activity maps proposed by Yu.V. Riznichenko in connection with studies carried out by this expedition (see Chapter 7). Such maps reflect simultaneously both the spatial distribution of the epicenters and the frequency of earthquakes of various intensities, including destructive earthquakes, which considerably expands the possible field of practical application for these maps.

Methods of Plotting Epicenter Maps

Chapter 3 gives the method of determining epicenters and focal depths used to plot such a map, together with an estimate of accuracy, while the method of determining earthquake energy is discussed in Chapter 4. The basic materials for the epicenter map were the catalogs and bulletins of earthquakes compiled systematically by the expedition for all earthquakes observed commencing with the $K = 5$ energy class, and including all earthquakes of higher classes. According to the accuracy with which the focal coordinates were determined, the earthquakes were divided into classes A, B, C, and unclassified. Class A included earthquakes whose coordinates (including depth) were determined to within $\pm$1-2 km, class B corresponded to $\pm$3-5 km, class C, to $\pm$10 km. Unclassified earthquakes included those for which it was not possible to determine the depth, while the accuracy of epicenter-coordinate determination amounted to $\pm$25 km.

To compile a summary epicenter map for the Garm and Stalinabad districts, it was necessary to choose a sufficiently representative

earthquake energy class commencing with which the effect of station arrangement would have no effect upon the distribution of the epicenters noted. An analysis of registration conditions for earthquakes in the lower energy classes for these districts has shown that for the entire region studied, the K = 7 class was quite representative. It is possible to neglect these earthquakes only at the edges of the Stalinabad district and in the Obi-Garm district, where the basic mass of such earthquakes was recorded with complete reliability. This may even be seen from the recurrence graphs (Chapter 7, Figs. 103-107).

Limited use may be made of recorded earthquakes of lower classes. Thus, K = 5 earthquakes in the Garm district and K = 6 earthquakes in the Stalinabad district may be used for plotting epicenter graphs for sections that do not extend beyond the registration-range limits for the corresponding class (Fig. 134).
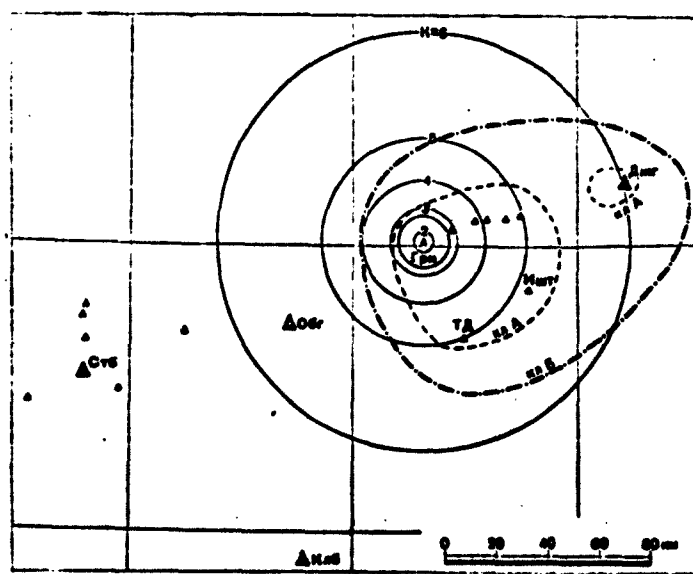
Fig. 134. Registration-range diagram for earthquakes in the lower energy classes (K = 2-6). The dashed line indicates the region for which epicenters are determined with class A accuracy; the dash-dot line, with class B accuracy,

K = 4 and K = 3 earthquakes are recorded by two-three stations, which is inadequate for reliable determination of the focal coordinates. Nonetheless, they may be used to characterize the seismic regime of small sections immediately adjacent to the stations, where the accurate position of the earthquake focus may not be known.

As we have repeatedly stated, earthquake-observation conditions were more complex in the Stalinabad district than in the Garm district: the Stalinabad district is less seismic, the station system was stretched thinner in this case, instrument sensitivity was lower due to high interference. In this connection, we give a more detailed description of the observation conditions for this district.

The basic material used in compiling the epicenter map for the Stalinabad district was obtained at the Karasu, Gissar, Khorongon, and Kon-Dora field stations. The general-purpose stations at Stalinabad, Obi-Garm, and Kulyab, could be used only to handle strong earthquakes, due to the relatively low sensitivity of the general-purpose seismic equipment (SGK and SVK seismographs), and the low scanning rate: 30 mm/min and 60 mm/min.

The seismic-station system of the Stalinabad detachment of the expedition provided a determination of the coordinates for all earthquake epicenters of the Greater Stalinabad district (see Chapter 7, Fig. 113), beginning with energy class 8. The coordinates of all weak earthquakes of K = 6 and 7 were determined only in part. They were determined more completely for the Lesser Stalinabad district (see Fig. 113). It was nearly impossible to determine the coordinates of class 5 earthquakes owing to the lack of simultaneous records at three stations for such weak shocks. The percentage of such weak earthquakes that were recorded by just a single station was quite large. Thus, for example, in 1955, the Karasu station recorded 71 earthquakes with

$(t_s - t_p)$ from 0.5 sec to 2.0 sec, but coordinates could be determined
for just the six strongest earthquakes of this group. In the 20 months
of observations covering January 1955 to August 1956, the coordinates
of 179 earthquakes were determined.

In 1956, the strong $K = 13$ earthquake north of Nurek was recorded
in the Stalinabad district (22 September at 15:54 hr). This earthquake
was accompanied by a large number of aftershocks which continued in
large numbers into 1957. In describing the seismic activity for the
1955-1956 period, we did not spend much time in analyzing these after-
shocks. The basic shock of the Norek earthquake was taken into account
in compiling the epicenter maps.

Focal-coordinate determinations in the Stalinabad district are
far less reliable than similar determinations for the Garm district:
the basic group (121 earthquakes) had epicenters located with classes
B and C accuracy. More reliable coordinate determinations were made
for earthquake foci located in direct proximity to one of the seismic
stations, as well as within the Kon-Dora—Karasu—Gissar triangle, al-
though it must be said that even in these cases it was frequency im-
possible to obtain class A accuracy ($\pm$1-2 km). Epicenter coordinate
determination reliability naturally dropped off sharply with distance
from the basic station network.

Thus, in compiling the summary earthquake-epicenter map for the
entire region studied by the expedition, including the Garm and Stal-
inabad districts, specific difficulties were encountered associated
with the somewhat lower accuracy and less detailed observations avail-
able for the Stalinabad district.

The summary epicenter map for the entire region studied, covering
the 1955-1956 period (Fig. 135) was constructed from earthquakes in
the $K = 7$-13 energy classes. Epicenters for $K = 7$ and $K = 8$ earthquakes

are combined and indicated by a common symbol on the map. Focal depths are classified on the map into the following ranges: 0-7, 8-12, 13-18, 19-25 km. To avoid complicating this map unnecessarily, information as to the accuracy of focal determination is plotted on Fig. 134, where the dashed lines indicate regions within which the determinations corresponded chiefly to the A and B precision classes; earthquakes in most of the extreme regions fell into class C or were unclassified.

General Characterization of Summary Epicenter Chart

The epicenters are distributed extremely nonuniformly within the entire region of study. The Northeastern section of the district, the southern slopes of the Gissar mountain complex, the Peter I range, and the valley of the Obikhingou River, in its middle and lower reaches, including the zone of the Karakul' fault, represents a zone of maximum epicenter density for all energy classes. In the Western section of the Alayskiy Range, there is also a zone in which epicenters are concentrated. The focal density drops off gradually toward the West, and reaches a minimum at the meridian of $69°30'$. Still further to the West — in the districts surrounding the city of Stalinabad, within the Gissar Valley and its northern and southern offshoots — it [balance of paragraph omitted in original].

The northwestern, southwestern, and southeastern portions of the district are relatively inactive. Only isolated earthquakes are observed here. To the south of the Karakul' fault, there are almost no earthquakes, with the exception of several earthquakes in the Sangvor district.

Between the Vakhsh and Pyankzh Rivers, the epicenters are concentrated along the valley of the Vakhsh River, the northwest slopes of the Vakhsh Ridge, and the southwest spurs of the Darvaza range. The central region of the area between the rivers shows only isolated foci.

The epicenter strip in the Vakhsh River valley in the Obi-Garm district turns to the West, and combines with the seismic district surrounding the city of Stalinabad. Further to the West, beyond Stalinabad, the epicenters stretch out to form a narrow band along the northern rim of the Tadzhik depression extending to Karatag. Isolated epicenters are observed along the valleys of the Vakhsh and Kafirnigan Rivers in their lower reaches.

The overwhelming majority of earthquake foci in the Garm district are located at depths of 0-10 km. To the west, in the lower reaches of the Obi-Khingou River, and the upper portion of the Vakhsh River, the focal depths are found to extend to 20 or more kilometers. Relatively great depths of 15-20 km are also characteristic of the Obi-Garm seismic region. We note that in connection with the extended nature of the Obi-Garm section it is not possible to make reliable determinations of depths for this section from the Garm and Stalinabad station systems. In the Stalinabad district, the distribution of depths varies more, but depths of 10-20 km are encountered for the most part. Thus, within the entire district studied, an over-all increase in focal depth from east to west may be noted.

Compilation of Epicenter Maps for 1955 and 1956

In addition to the summary epicenter chart for the 1955-1956 period, which we have discussed, epicenter maps were compiled separately for 1955 and for 1956 (Figs. 136 and 137), showing epicenters for earthquakes in the 9-13 energy classes. These maps give some qualitative idea as to the spatial variation in activity with time over the district studied.

It may be seen that for 1955 the seismic activity of the Garm district and the districts adjoining it on the West was quite uniform (Fig. 136). Here the strips on the map indicating earthquake-epicenter

groupings agree well with the over-all tectonic structure of the district. About the 39° parallel, there is a strip of foci lying almost directly East-West, with the eastern portion coinciding with the South Gissar zone, and extending in the west to the Obi-Garm meridian. Another strip, located almost exactly along the axial section of the Peter I range and the Vakhsh Ridge, extends at a small angle to it. This latter strip ends with the epicenter of the severe $K = 13$ earthquake of 21 August 1955, occurring to the south of Obi-Garm. From this strip, the epicenter brances to the North of Tovil'-Dora into a third strip which turns to the southwest and pinches out to the West of Tovil'-Dora. To the South there is a well-defined fourth epicenter strip which coincides with the zone of the Karakul' fault.

Severe $K = 13$ earthquakes occurred during this year in the eastern and western ends of the Garm district, and to the north of its center. They were all located in border sections of a zone of generally increased seismicity.

In 1956, the general pattern of epicenter distribution (Fig. 137) remained the same as in the preceding year, but its internal structure changed. Figure 137 shows a region of epicenter concentration extending from the northeast to the southwest; it intersects the Khait district, and pinches out in the Tovil'-Dora district. Another extended concentration of epicenters lies perpendicular to the first concentration to the northeast, somewhat west of Dzhirgatal'. The southern district along the Karakul' fault was relatively nonseismic. The epicenter distribution for this year is not easily associated with any features of the tectonic structure.

Strong $K = 13$ earthquakes occurred during 1956 in the Garm district at the northeast and southwest ends of the main earthquake strip that runs through this district. In the Stalinabad district, in the
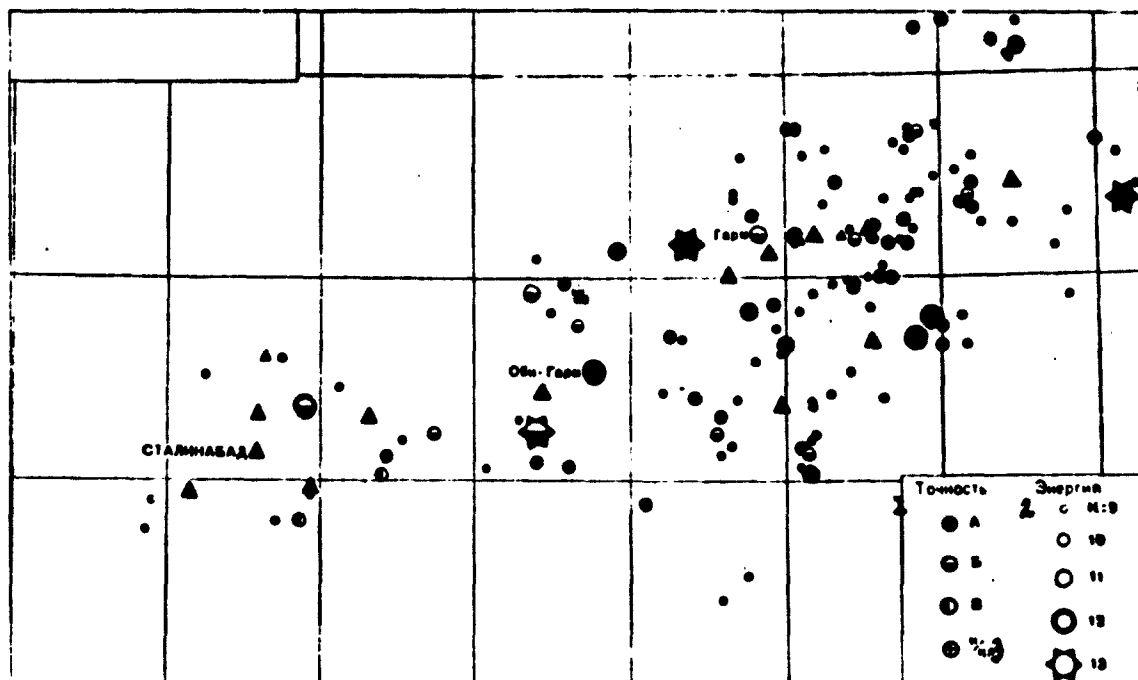
Fig. 136. Map of earthquake epicenters for the year 1955, based on earthquakes in the 9-13 energy classes. Triangles indicate seismic stations. 1) Accuracy; 2) energy; 3) unclassified.

eastern section, to the south of the previous year's concentration of epicenters in the Gayzabad district, there was also a K ≐ 13 shock, the Nurek earthquake.

This change in the structural pattern of earthquake focal distribution for the K = 9-13 classes between 1955 and 1956 indicates that in studying the details of focal distribution upon the basis of observations of earthquakes in these energy classes, objective judgments necessitate sufficiently long observation periods.

Let us concentrate in more detail on the seismicity of the Garm district alone, and then of the Stalinabad district alone, for sections that are well provided with local station networks.

Garm District

As previously (Chapter 7) we restrict our examination of the Garm
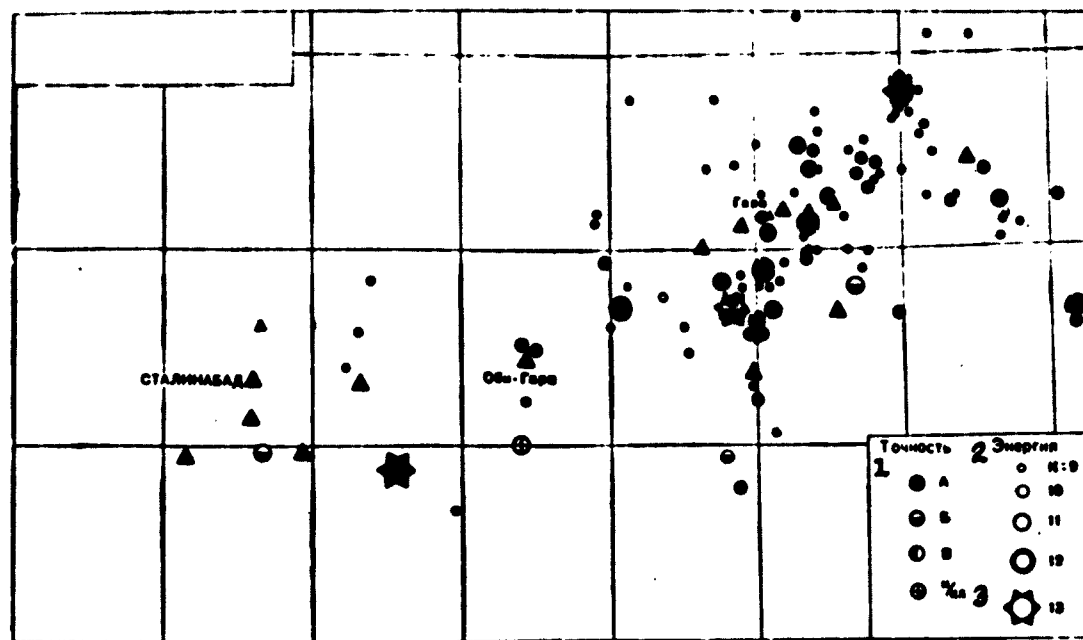
Fig. 137. Map of earthquake epicenters for year 1956, based on earthquakes of the 9-13 energy classes. 1) Accuracy; 2) energy; 3) unclassified.

district to the rectangle lying between the $70°00'-71°30'$ meridians and the $38°00'-39°30'$ parallels, excluding from this rectangle the southeastern corner in which no epicenters are observed (see Fig. 135). The over-all area of this figure amounts to 13,500 km^2. Within this district, three major independent seismic zones may be isolated: the northern (Gissar) zone, the central (Petrovskaya) zone, and the southern (Karakul') zone.

1. Gissar zone. This zone covers the entire right bank of the Surkhob River, and coincides with the Paleozoic formations of the Gissar mountain complex. The seismicity of this zone drops off at the northern slopes of the Gissar range, to the east of Dzhirgatal', and to the west of the Garm meridian. To the South, along the left bank of the Surkhob River, it is separated from the Petrovskaya zone by a section of relatively low seismicity. Within the Gissar zone, the greatest

activity is shown by the section that coincides with the Kabudkrymskiy Massif, which is bounded by the Yarkhych, Komaroy, Sorbog, and Surkhob Rivers. The central portion of the massif is less active than its border regions (Fig. 135). The epicenter strips bordering the triangular Kabudkrymskiy Massif coincide in the South with the Klebel'sberg fault, which passes along the right side of the Surkhob River valley. The greatest concentration of epicenters is observed on the northeast border of the massif, between the Yasman and Yarkhych Rivers. A strip of weak-earthquake epicenters is also noticeable on the northwestern border. It is worth noting that the severe earthquakes are found only along the borders of the massif forming, as it were, an outline of it. The epicenter concentration coincides quite well with the tectonic fault zones bordering the Kabudkrymskiy Massif. Within the Gissar zone, somewhat to the west of Dzhirgatal', there is a well-defined epicenter-concentration strip directed from North to South. The trend of this strip does not correspond with the tectonic faults for the given section of the Gissar zone, inasmuch as the majority of tectonic faults run from East to West. The remaining sections of the Gissar zone are relatively inactive.

Focal depths are shallow throughout the entire Gissar zone, and the foci lie chiefly within the first tens of kilometers. At the western end of the zone, near the Yangolyk and Garm seismic stations, and near the Klebel'sberg fault, foci ranging in depth to 35 km are observed. The nature of the earthquake vs. depth distribution may be seen from Fig. 138. The Klebels'berg fault is recorded on the sections by the increased epicenter density, and by the presence of foci at various depths within a narrow band along the Surkhob River valley.

2. The Petrovskaya zone. This zone coincides with the Peter I range. Near the divide of this range, on the northern slope, a sharp
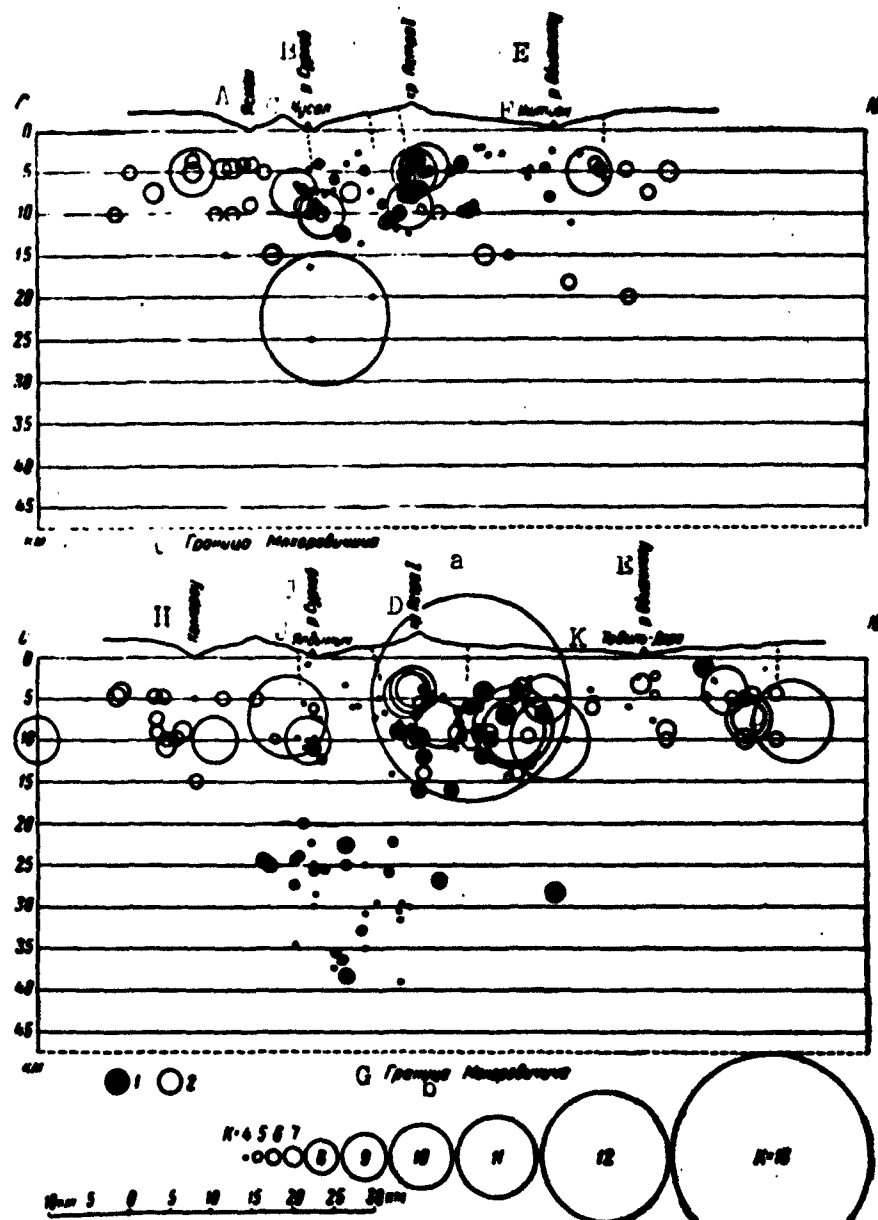
Fig. 138. Vertical sections for earthquake hypocenters
along north-south profiles. a) Chusal-Ishtion; b) Yal-
dymych-Tovil'-Dora. The size of the circles indicates
the K energy class; 1) earthquakes used to plot ver-
tical hodographs (Chapter 3); 2) remaining earthquakes.
a) Yasman; b) Surkhob River; C) Chusal; D) Peter I
range; E) Obikhingou River; F) Ishtion; G) Mohorovicic
Discontinuity; H) Komarou; I) Surkhob River; J) Yaldy-
mych; K) Tovil'-Dora.

increase in epicenter density is found. This epicenter strip, forming

extensions, also covers the southern slopes of the Peter I range at

two points: to the northeast of the Ishtion station, and in the Chil'-Dora district (to the north of the Tovil'-Dora station). These western and eastern (Chil'-Dora district) earthquake-focus concentrations runs together in the South with the epicenter strip that coincides with the Karakul' fault. Between these two concentrations, on the southern slopes of the Peter I range (between the Ishtion and Tovil'-Dora stations), no earthquake foci are observed. The eastern extension of the Peter I range beyond Tadzhikabad, in general, is relatively inactive; the number of earthquakes increases only in the extreme eastern section to the south of Dzhirgatal'. This territorial earthquake distribution in the East is clearly associated with an over-all variation in the seismic regime, since in previous years (see, for example [2, 258]), rather severe earthquakes have been observed here.

Very severe $K = 12$ and $K = 13$ earthquakes occurred in the western section of the Peter I range: the Chil'-Dora earthquake of 11 April 1956, and the earthquake in the Yaldymych district on 22 September 1956. They occurred in border portions of sections of weak-earthquake concentration. The Chil'-Dora district was the most active section of the Petrovskaya band during the 1955-1956 period.

The vast majority of earthquakes in the Peter I range are shallow, their foci lying at depths extending through the first 10 km. Depths increasing to 15-25 km have been observed, however, at the western end of the Peter I range. A local group of foci with depths ranging to 40 km is concentrated in the central section of the Peter I range, to the south of the Nimich-Yaldymych stations. In the district of the Yaldymych station, this group of deeper earthquakes joins with similar earthquakes of the Gissar zone. Isolated deeper earthquakes to the north of Tovil'-Dora have been identified on the southern slope.

3. The Karakul' zone. This zone represents the natural seismic

border for the Garm district. Its activity is substantially below that of the first two [remainder of sentence missing in original]. Stronger $K = 11$ and $K = 12$ earthquakes have been observed in two sections of this zone: to the east of Ishtion, and to the south of Tovil'-Dora. As in the other cases, relatively severe earthquakes have occurred here on the borders of the zone. In the Karakul' zone, earthquakes of various depths are found. It is possible that some tendency toward increasing depths to the east may be observed.

Stalinabad District

Here, as before, we will distinguish the Greater Stalinabad district, and the Lesser Stalinabad district included within it. Their boundaries are shown in Chapter 7, in Fig. 113. The area of the first district amounts to 14,300 km^2, and of the second district, to 4000 km^2.

The epicenter map for the Greater Stalinabad district (Fig. 139) shows all foci determined here over a twenty-month observation period (January 1955-August 1956). Although the number of weak-earthquake epicenters (for class 7 or below) clearly is too low here, all the basic features of the epicentral zones are adequately represented.

Three epicentral zones may be isolated on the map of Fig. 139: 1) the northern (line AB on Fig. 139), running along the border of the northern edge of the Gissar valley from the southern slope of the Gissar range, 2) the Takob, located to the east of the Chuyangaron station, and 3) the southern zone (line A'B' on Fig. 139), covering the southern side of the Gissar Valley and the range bordering it on the South.

The northern and southern zones are the most important. They are separated by the Gissar Valley, where the city of Stalinabad is located. In the central section of the Gissar Valley, there are fewer epicenters than in the neighboring zone; several earthquakes are noted, however,

- 469 -
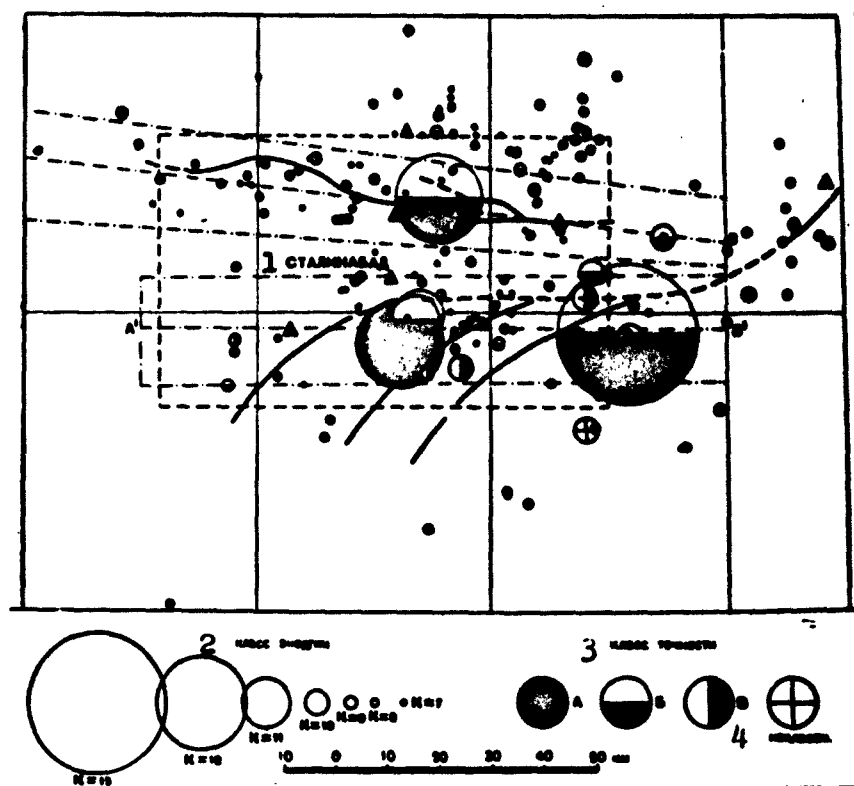
Fig. 139. Earthquake-epicenter map for the Greater
Stalinabad district, January 1955-August 1956. The
triangles indicate seismic stations. The dashed line
indicates the Lesser Stalinabad region. 1) Stalina-
bad; 2) energy class; 3) accuracy class; 4) unclass-
ified.

in direct proximity to Stalinabad. A detailed seismicity study in

the vicinity of Stalinabad is difficult because of the considerable

background of industrial interference within the city limits.

The northeastern section of the chart of Fig. 139 is relatively

inactive. It is possible that this does not represent the true situa-

tion, owing to the low sensitivity of the equipment at the Obi-Garm

station. Class 7 earthquakes cannot be determined without this station

in the given section of the chart, while the Obi-Garm station records

such earthquakes poorly. The lack of more severe shocks in this region

may be due to the short observation period. In the past, this has been
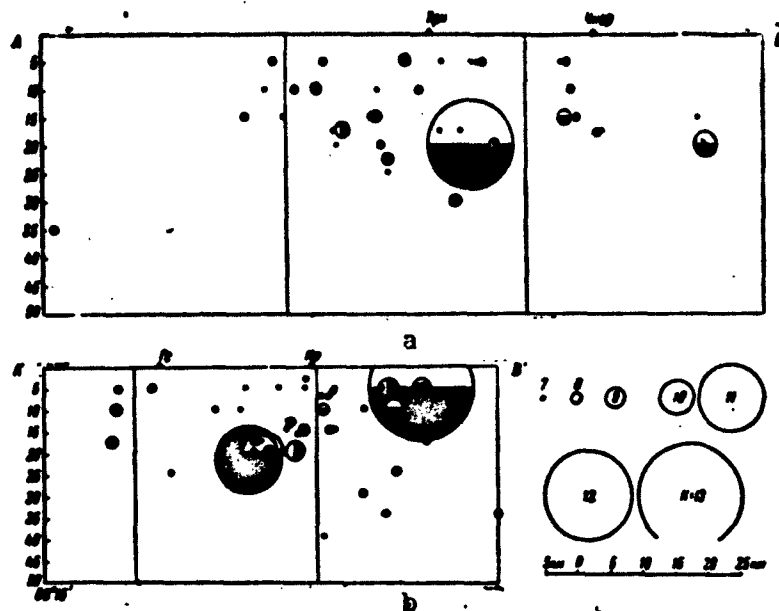
Fig. 140. Vertical sections for earthquake hypo-
centers. a) Along line AB in northern zone; b)
along line AB in southern zone. Arbitrary designa-
tions are the same as those of Fig. 139.

quite an active district [198].

The low activity of the northwest and southwest sections of the
chart clearly represents an actual condition; in any case, this does
not contradict the results of observations due to the regional network
[198] over a longer period of time (20-25 years).

Let us describe in more detail the two main epicentral zones: the
northern and southern zones.

1. The northern zone extends in a nearly east-west direction, in
the form of a chain of epicenters. The extreme epicenters to the West
fall in the Karatag district, while to the East, the epicentral bands
may be followed to the Obi-Garm district, where both zones — the north-
ern and southern — run together. The eastern boundary of the northern
zone may arbitrarily be taken along the $69^\circ 30'$ meridian. The over-all
length of this zone amounts to roughly 110 km, and it is 10-15 km wide,
on the average.

The northern epicentral zone coincides quite well with the series of tectonic faults that separate the faults of the Gissar range from the Tadzhik depression.

The section of Fig. 140 shows the depth distribution of earthquake foci in the northern zone. The northern-zone foci are located at quite different depths ranging from 5 to 30 km which, evidently, indicates the great depth of the faults with which earthquakes in this zone are associated.

In the past, very severe earthquakes have appeared in the northern zone, for example, the Karatag earthquake of 1907 [259], the Fayzabad earthquake of 1943 [260]. The present-day relatively high activity of this zone permits us to assume that earthquakes of this intensity may appear now and in the future.

2. The southern zone consists of several groups of epicenters extending from east to west from the Babatag range (in the district about the Gissar station) in the west to the $69°30'$ meridian in the east. It is possible to distinguish three groups of epicenters in this zone (from west to east): a) the Babatag zone in the district near the Gissar station; b) the Kok-Tash zone, running along the Kok-Tash ridge; c) the eastern group, which may be divided into the Fayzabad subgroup (to the north of latitude $38°30'$) and the Nurek subgroup (to the south of latitude $38°30'$). Nonetheless, such details of the intimate structure of this epicentral zone may prove to be temporary in nature (see the discussion of Figs. 138 and 139).

The southern zone and the corresponding groups of epicenters coincide with the series of ranges and associated tectonic faults that surround the Gissar Valley on the south.

Figure 140b gives a section indicating the distribution of earthquake foci in the southern zone by depth. As the figure shows clearly,

the focal depths in this zone also vary from 5 to 30 km. Within the borders of the southern zone, the earthquake foci first descend, and then ascend somewhat, in going from east to west. In the eastern portion, foci at depths of 5-10 km predominate, to the west of Karasu, the dominant depths increase to 15 km, and at the longitude of Stalinabad, they reach 20-22 km; there is then a certain decrease in depth.

In the past, the southern epicentral zone has experienced quite frequent earthquakes of intensity 7-8 (see, for example [260]). A relatively high recurrence rate for not too severe earthquakes is also shown clearly by instrument observations over longer periods of 20-25 years [198]. Historical sources reveal no catastrophic earthquakes for this zone of the Karatag or Khait type; it is possible that the peculiarities of the geological structure in this zone are responsible for this freedom from severe earthquakes.

§2. SEISMIC-ACTIVITY MAP

Method of Constructing Seismic-Activity Map

In addition to the normal epicenter map, a seismic-activity map was plotted for the entire region under study. The principles by which such charts are compiled have been discussed in Chapter 7, §2. Here we shall consider briefly the technique used in plotting the map.

The basic material used to compile the activity map consists of the standard epicenter chart, and the earthquake-recurrence graph for the district under study, normalized to time and area. Earthquakes for each of the energy classes that will be used in plotting the activity maps must be singled out by separate symbols on the epicenter map. In addition, all earthquakes must be classified by depth range, where required by circumstances, and where the observational material permits.

Earthquakes of three energy classes (K = 7, 8, and 9) were used to compile the seismic-activity map for the district investigated by

the expedition. The earthquakes were not classified by focal depths, in this case, since all foci in the given district lay within the earth's crust, and the overwhelming majority of the foci lie within a relatively small depth range (5-10 km for the Garm district, with a somewhat wider range for the Stalinabad district).

In order to go from the "discrete" epicenter map to the "continuous" map for the distribution of the seismic activity A, the initial epicenter map was divided into quarters by a grid having squares with 2.5-km sides. The intersections of this grid were the points at which the value of the activity A was determined on the basis of a calculation of the number of earthquake epicenters in the chosen energy classes that lay in the areas surrounding the given point. To delimit the areas used in the epicenter calculation, a special transparent overlay was used bearing two concentric circles with radii of 5 and 50 km drawn on tracing cloth. The center of the overlay was in turn placed over every intersection on the grid.

The numbers n_7, n_8, n_9 of epicenters for K class 7, 8, and 9 earthquakes were calculated separately for the central and ring zones of the overlay. For each K class, summation of the numbers n_K obtained for the inside zone $n_K^{(1)}$ and for the outer zone $n_K^{(2)}$ was carried out with various weighting factors: for the inside zone, the weighting factor was taken equal to $p^{(1)} = 1$, and for the outside zone, $p^{(2)} = 1/12$. The number N^*_K for the epicenter density of earthquakes in a given K class, ascribed to the center of the overlay, was calculated from the formula

$$N^*_K = \frac{p^{(1)} n_K^{(1)} + p^{(2)} n_K^{(2)}}{p^{(1)} \frac{S^{(1)}}{100} + p^{(2)} \frac{S^{(2)}}{100}}.$$

Here the number 100 (km^2) corresponds to the unit area for which the seismic activity A_7 (see Chapter 7) is calculated. Allowing for the

numerical values of the areas $S^{(1)}$ and $S^{(2)}$, as well as for the weighting factors $p^{(1)}$ and $p^{(2)}$, the preceding formula may be represented, in approximation, as

$$N_K^* = 4n_K^{(1)} + \frac{1}{3}n_K^{(2)},$$

where $K = 7$, 8, and 9.

The values of N^*_K obtained are summed with the factors m_K ($= 1$, 2.7, and 7.2), whose reciprocals equal the ratio of the numbers of earthquakes in the corresponding energy classes according to the recurrence graph for the normal slope value $\gamma = 0.43$. The result of the summation is divided by 3, the number of earthquake-energy classes utilized. Thus, we obtain the desired value of the seismic activity A_7 for each grid intersection considered

$$A_7 = \frac{1}{3}(N_7^* + 2.7N_8^* + 7.2N_9^*).$$

The distribution of the calculated values of A_7 in all intersections of the grid was generalized by drawing the isolines for the quantity A_7. For the Garm district, the lines of equal activity corresponded to the following series of values: $A_7 = 1$, 5, 10, 20, 30, 40, 50, 60, 70, 80. For the Stalinabad district, owing to the lower activity, the interval between the equal-activity lines was made smaller, and the isolines corresponded to values $A_7 = 0.5$, 1, 1.5, 2, 2.5, 3.

We note that the procedure described for the calculation may vary in detail. Thus, in [214] (see also [213, 215]), the calculation is described in which the overlay used to calculate the number of epicenters $n_K^{(i)}$ ($i = 1$, 2) used elliptical rather than circular regions, with the ellipses oriented in accordance with the dominant trends of the main tectonic structures. Both the weight factors $p^{(i)}$ and the coefficients m_K might take on other values. The principle used in the plot, however, remains exactly the same. It consists in calculating at

each point a certain mean value A of seismic activity for the area surrounding this point, and then in generalizing the pattern obtained for the distribution of the numbers A over the area by plotting a map of isolines for A.

Seismic-Activity Map for the Garm and Stalinabad Districts

Figure 141 shows a seismic-activity map for the entire district studied by the expedition, plotted by the method described above from observational data gathered during the 1955-1956 period. The same map plots the epicenters for earthquakes in the higher energy classes K = = 10-13, which were not used to calculate the activity A.

A comparison of a seismic-activity map compiled on the basis of weak earthquakes with the distribution of stronger earthquakes indicates that weak and strong earthquakes generally occur in precisely · the same regions. In addition, a more detailed consideration permits us to note that in the overwhelming majority of cases, strong earthquakes occur in border regions of increased-activity zones, corresponding to regions of weak-earthquake concentration. Naturally, this conclusion requires still further verification based upon larger quantities of material, a longer observation period, and must be verified for other seismic regions.

We may characterize the seismic-activity map in more detail, using as an example the Stalinabad district. The increased-activity zones (the Takob, northern, and southern zones) are more clearly expressed on this type of map than on an epicenter map. The Gissar Valley, which has little seismic activity, separates the northern and southern zones. Within it, the northern and southern zones are connected by a strip lying somewhat to the east of the city of Stalinabad. To the west of the city, both zones very nearly touch. Stalinabad lies in a seismic "ring," whose northern and southern sections are more active. The east-

ern section of the northern zone, adjacent to the Takob zone, appears
to be quite complicated. The latter zone is characterized by very great
activity. Although no severe earthquakes have been noted within the
Takob zone, it is not impossible that they will occur here.

The map drawn represents a first attempt at constructing a map of
seismic activity. This map is very detailed, and shows many fine points
relevant to the distribution of present-day activity. This has both a
positive and a negative aspect. From the point of view of a comparison
with geological features, the detailed map is of interest. The present
map, however, plotted on the basis of two-year observations, does not
guarantee that the details will be stable in time. It would be desir-
able for such detailed maps to be compiled upon the basis of observa-
tional material covering longer time periods.

For the purposes of seismic districting, however, such detail is
unnecessary, in general. As a matter of fact, the shocks accompanying
a severe earthquake cover a more or less considerable area, setting up,
as it were, a halo about each epicenter. The degree of smoothing or
averaging may be fixed for this map in accordance with the nature of
the focal seismic activity, so as to agree with the degree of attenua-
tion of seismic vibrations with distance from the focus. In addition,
the activity A represented on the map may be determined with an allow-
ance not only for weak earthquakes, as in the case described, but also
for all known severe earthquakes. This type of seismic-activity map
for the Garm and Stalinabad districts has been described in [214, 215].

Using Seismic-Activity Maps

Maps of seismic activity make it possible to arrive at both quali-
tative and quantitative evaluations of the seismicity of districts un-
der study.

Let us first consider the qualitative aspect. A seismic-activity
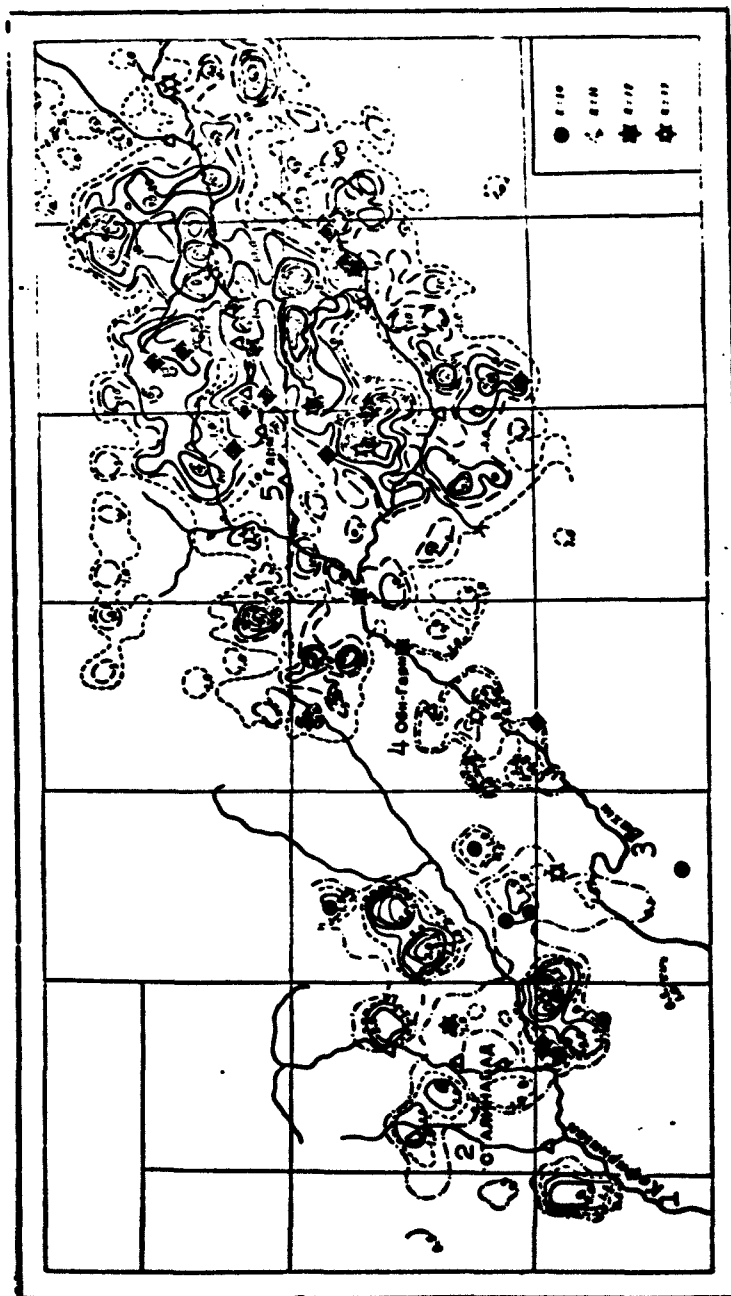
Fig. 141. Seismic-activity A_7 map of district studied by expedition based upon earthquakes of the 7-9 energy classes. Compiled by Riznichenko, Nersesov, and Bune. 1) Kafirnigan; 2) Stalinabad; 3) Vakhsh; 4) Obi-Garm; 5) Garm.

map gives an objective representation of the earthquake-epicenter distribution density, in terms of a single energy level. In this respect, it represents a somewhat improved, better grounded version of the well-known epicenter-density charts (see, for example, this type of map in the Atlas of Seismicity of the USSR [258], as well as in [187, 202, 220, 222]).

The epicenter distribution density pattern, in units of seismic activity, as in any other sensible units, makes it possible to compare zones of increased seismic activity with specific tectonic features of a district, and especially with zones of principal tectonic faults, far more graphically than is possible with the discrete epicenter maps. An activity map, supplemented by geological considerations, makes it possible to seek a well-founded qualitative picture of the relative seismicity of various sections.

The quantitative aspect of the matter is more important; this is also a special feature of the seismic-activity maps. The principal virtue of this type of chart lies in the fact that upon the basis of activity maps, together with recurrence curves, it is possible to evaluate the mean recurrence frequency, and, correspondingly, the mean recurrence periods for earthquakes of various energies and intensities.

To be completely definite in an examination of the quantitative relationships, we assume: a) that the seismic regime, on the average, does not vary in time, and b) that the relative values for the earthquake recurrence N for various energies E is independent of the seismic activity A (the question of the admissibility of such assumptions for approximate estimates, their possible limits of applicability, the conditions under which they should be discarded, we shall leave aside here; naturally, they still must be given additional study and discussion). Constant relative recurrence is equivalent to constant shape of

the recurrence curve N(E) plotted in logarithmic coordinates (Chapter 7). This makes it legitimate to shift it along the N axis, which corresponds to a change in A.

The direct quantitative interpretation of the seismic-activity map consists in the following. If at a point on the chart of interest to us, the magnitude of the seismic activity equals a specific number A_7, this indicates that in the neighborhood of this point, over an area of 100 km^2, earthquakes of the seventh energy class will recur, on the average, A_7 times each year. It is of interest to determine for the neighborhood of this point on the map, the magnitude of the earthquake recurrence N^*_K for any other class K. To do this, it is enough to set the curve N(E) on the N axis so that where K = 7, the ordinate of the point on this curve will equal A_7. Then the ordinates of all the remaining points for this curve for any other values of K will give the earthquake-recurrence values N^*_K for the corresponding energy. Using this method, a chart for the seismic activity A_7, i.e., for the earthquake recurrence where K = 7, may be converted to a chart of earthquake recurrence for any other energy classes, including the destructive earthquakes of interest to us.

In particular, if in the energy range under discussion, the angular coefficient of the graph N(E) is constant, γ = const, it is possible to go from the recurrence A_7 to any other N^*_K (in this energy range) in accordance with the formula

$$N^*_K = 10^{-\gamma(K-7)} A_7.$$

Instead of the recurrence N^*_A, it may prove clearer to consider the recurrence periods $T_K = 1/N^*_K$, i.e., the mean time intervals between earthquakes of a given K energy class.

The quantities N^*_K and T_K may be computed not only for elementary 100-km^2 areas, to which the activity A_7 refers, but for any other areas

S as well (in km^2). Thus, for example, the mean time interval T_K between two, let us say, severe earthquakes of the _K_th class over an area S may be determined from the formula

$$T_K = \frac{100}{SN_K^*}.$$

For an area S consisting of several sections S_i with various activities $A_{7,i}$, the calculation may be carried out by means of the formula

$$T_K = \frac{100}{\sum_i S_i N_{K,i}^*},$$

where the quantity $N^*_{K,i}$ is determined on the basis of the activities $A_{7,i}$ by the method described above.

For the sake of clarity, let us consider an example. On a seismic-activity map for A_7, let the isoline $A_7 = 20$ cover an area $S = 1000 \ km^2$, and let there be no other isolines in this area. This means that over the area under consideration, there are 20 x (1000/100) = 200 earthquakes of the seventh energy class each year. Let us assume for simplicity that $\gamma = const = 0.43$. The time interval between two severe earthquakes, for example, of the sixteenth energy class will in this case be

$$T_{16} = \frac{100 \cdot 10^{0.43 \, (16-7)}}{1000 \cdot 20} = 37 \ \text{years}.$$

We see that the district taken is quite dangerous from the seismic point of view. If some other district having the same area S is included within the isoline $A_7 = 1$, the mean time interval between severe class 16 earthquakes in this district will be 750 years. Consequently, the second district, should be considered to be less dangerous from the seismic point of view, and this must be taken into account in establishing the degree of seismic danger presented by both districts in seismic districting.

A seismic-activity map in A_7 isolines or any other recurrence iso-
lines may also be converted to a map in isolines of K_{max} for the great-
est energy classes of earthquakes that will recur in a given area, on
the average, no more than once in T years. Here T is any fixed time,
for example, T = 500 years (the time T may also be compared with the
mean service life of structures of a specific type [171]). The form of
such a map will approximate the form of modern seismic-district maps,
where the "maximum" force of earthquakes is indicated, although there
is no indication of the mean recurrence time T to which they corres-
pond. It is also possible to go directly from a map of K_{max} to a map
of corresponding intensities, for which it is sufficient to make use
of the well-known relationships among the energy, focal depth, and
earthquake intensity.

There is still another possibility for making use of the quanti-
tative aspect of seismic-activity charts; this lies in a comparison
with numerical values of velocity gradients for movements of the earth's
surface, determined by geological or geodesic methods, in particular,
with vertical movements. The geological aspect of this problem will be
discussed below (§4). It is reasonable to bring in quantitative geo-
logical data on movements of the earth's crust owing to the fact that
the time intervals investigated by geologists are so much greater than
those that may be taken into account on the basis of seismological
data alone. This is especially important in treating the problem of
the relationships between present-day seismicity, with its possible
variability, and long-term average seismicity.

Thus, we see, that the seismic-activity map even today may be of
considerable help in solving several fruitful problems dealing with
the establishment of the degree of seismic danger presented by a ter-
ritory. We may expect that they will serve as the basis for future,

more objective maps of seismic districts, compiled on a quantitative basis.

§3. COMPARISON OF SEISMICITY OF GARM REGION WITH ITS TECTONIC STRUCTURE

Owing to its high seismic activity, exposed nature, and the detailed geological and seismic studies that have been carried out, the region in which the expedition operated, and especially the Garm district, is very favorable for observations of the seismic regime, and for comparing seismicity with tectonics.

Here we will confine ourselves to comparing tectonic data with the seismicity of the district for only two years: 1955 and 1956. Over this period, no earthquakes having energies greater than 10^{13} joules ($K = 13$) were recorded in this district. Thus, problems associated with the most intense earthquakes, are only touched upon by our discussion.

The basic materials on the seismicity of the region under investigation, which we compared with its tectonics, consist of an epicenter map (allowing for focal depth) and a seismic-activity map.

Geological Factors Responsible for the Increased Seismicity of the Garm District

As is known, the Garm district has especially high seismicity in comparison with the surrounding districts. To elucidate the geological factors responsible for this, Fig. 142 shows a comparison of the epicenter arrangement in the district investigated by the expedition (Garm-Stalinabad) with a diagram of the basic tectonic elements of the district. An examination of this map permits us to conclude that the Garm district, i.e., the area in which a large number of earthquakes appear, coincides with a section of the Earth's crust that was deformed especially vigorously during the Quaternary. As we noted in Chapter 8, during the Quaternary period a new uplift appeared on the

site of Pamir foothills trough depression, corresponding to the western section of the Peter I range. Further to the Northeast, in the less seismic Transalayskiy Range district, this process had commenced during the Tertiary period. In the still less seismic Vakhsh Range district, lying to the Southwest, the uplift had just appeared, and developed at a slower rate than in the Garm district. The rapid growth of the new uplift within the former depression in the center of the Garm district was accompanied, in regular fashion, by a movement in the opposite direction (a so-called compensating relative subsidence) at the center of the tectonic subzone traversed by the valley of the Surkhob River. This reinforced redevelopment of strains and faults. It thus follows from the geological data that the Garm district is distinguished from the surrounding districts by the especially vigorous development of strains and faults in the Earth's crust during the Quaternary period. This clearly is the reason for the extraordinarily high seismic activity of this district. This region may be classified as an area in which rearrangement of the Earth's crustal structure is taking place. The increased seismicity of such districts has been noted before by many scientists. Thus, our explanation for the exceptionally great seismicity of the Garm district differs somewhat from that given in [238].

The Relationship of Seismicity and Fault Zones

A more detailed examination of the connection of seismicity with the tectonic structure within the Garm district itself (Fig. 143) calls attention to the quite good agreement between the location of earthquake foci for the high-energy classes (K = 12 − 13) and the deep fault zones delineated on the tectonic diagram. This is best seen in the Karakul' fault zone, and over the entire Petrovskaya zone, which in the North borders upon an alpine geosyncline region. It is quite

important that the epicenters of earthquakes having hypocenters at various depths are located within the same strips, and that there is no basis whatsoever for assuming that the fault zones responsible for earthquakes slope, regardless of whether or not these faults emerge at the Earth's surface. The entire set of seismic data supports the conclusion that all of the major faults within the Garm district, discussed in the preceding chapter, are vertical. In passing, we should note that seismic observations have been used to plot a velocity profile for the Earth's crust (see Figs. 19 and 20, Chapter 3), which confirms the fact that the sedimentary deposit under the northern slope of the Peter I range is no more than 2 — 3 km thick, while there is a sharp increase at the ridge, while under the southern slope of the range, the deposit reaches 8 — 10 km in depth. These data show that the boundary between the geosyncline region A and the Epihercynian platform region B has been properly drawn, and also supports the scheme assigned to the historical tectonic movements for the sections adjacent to this boundary, which was described in detail in the preceding chapter.

In addition to the earthquake epicenters that fall into main fault zones, concentrations of epicenters are also observed that are not associated with observed fault systems. We refer to the North-South band of epicenters to the West of Dzhirgatal'; the two epicenter bands running northwest in the Kabudkrymskiy massif, to the North of the Surkhob River; the North-South concentration of epicenters to the North of Tovil'-Dora and Ishtion. The presence of these strips is possibly associated with the appearance of a deep North-South fault trend. Such lateral faults have already been noted at the surface as a result of geological observations in other sections of the district [216].

Fig. 142. Map comparing the tectonic structure and location of earthquake foci for 1955-1956 in the eastern section of the Tadzhik depression, and its surrounding mountains. 1) Seismic station; 2) intensity eight isoseismic lines for earthquakes prior to 1955; 3) intensity seven isoseismic lines; 4-19) see 1-16 of Fig. 129, Chapter 8. Double hatching indicates lower accuracy in focal-depth determination. 1) Accuracy; 2) unclassified.

Thus, the Garm district offers confirmation of the basic coinci-
dence of earthquake epicenters and major structural elements of the
Earth's crust which are at the same time sites of maximum development
of tectonic faults. Any attempt to use this qualitative relationship
to find a more detailed connection between seismicity and the struc-
ture of the Earth's crust must meet with many difficulties.

Inadequacy of qualitative comparisons

Let us list the chief difficulties encountered in making a direct
comparison of tectonic structural data with seismicity.

There is no way of uniquely associating maximum earthquake in-
tensity with the order of boundaries for structural elements in the
Earth's crust, i.e., we cannot state that the larger the structural
element, the more intense will be the earthquakes associated with its
boundaries. Thus, at the boundary between two very large tectonic re-
gions - the geosyncline region A and the after-platform region of
movement activation B (Fig. 140, 141) - weaker earthquakes appeared
than at the boundary of the two zones A-I and A-II within region A,
or than earthquakes along the boundaries of the two subzones B-I-b and
B-I-c within region B.

The intensity of seismic processes along each boundary of a tec-
tonic region, zone, or subzone will vary very sharply. It is quite
plain from Fig. 143 that in the various sections of the same boundary,
the epicentral density will differ greatly. This is especially clear
from the examples of the boundaries A and B, A-I and A-II, B-I-b and
B-I-c.

Different earthquake forces and recurrence rates will be associ-
ated with boundaries of tectonic zones belonging to precisely the same
order of crustal structural elements. Thus, for example, there is a
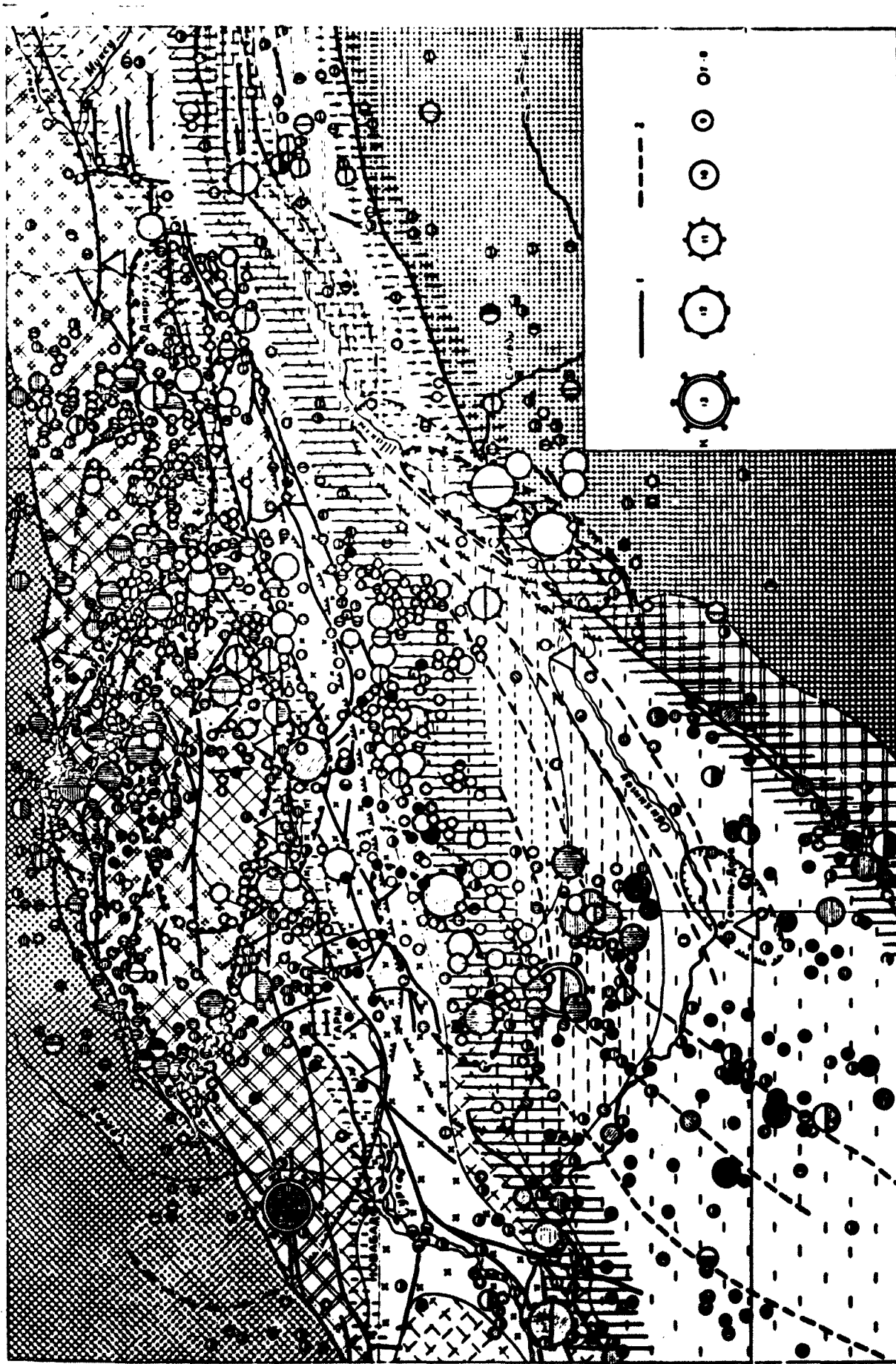substantial difference in seismicity on the orders of subzones B-I-a

Fig. 143. Comparison chart of tectonics and positions of earthquake foci for the 1955-1956 period in the Garm district (see Fig. 128, Chapter 8, and Fig. 142 of this chapter). 1) Established; 2) assumed tectonic discontinuities.

and B-I-b and subzones B-I-b and B-I-c.

Tectonic faults are frequently, although not necessarily, found at the surface in areas of epicentral concentration. Thus, it has so far not been possible to find faults along the ridge or in the upper section of the southern slope of the Peter I range about the boundary of the regions A and B, although in this area the seismicity of the boundary between regions A and B is at a maximum. From the purely geological viewpoint, it turns out that to the northwest and northeast of the Peter I range, many tectonic faults may be seen along this boundary, but the seismicity of such areas is substantially less than that on the section of border where no faults are observed on the surface.

On the one hand, earthquakes frequently appear where it has been established that there are no faults near the Earth's surface.

On the other hand, within the Garm district (and especially around it) there are many major tectonic faults, with which not a single severe earthquake is known to have been associated over the past 60 years, despite the fact that displacements along these faults occurred during the Mesozoic and Cenozoic eras.

Thus, a comparison of seismicity solely with the arrangement of borders of major structural elements in the Earth's crust having tectonic faults emerging at the surface proves to be inadequate. A merely qualitative comparison of seismicity and tectonic structure cannot yield unique conclusions.

§4. COMPARISON OF SEISMICITY OF GARM DISTRICT WITH VELOCITY GRADIENTS OF TECTONIC MOVEMENTS

In connection with the demonstrated insufficiency of direct qualitative seismic and tectonic comparisons, an attempt was made to compare the seismicity of the Garm district, in terms of a quantitative

index (seismic activity) with a quantitative tectonic characteristic (the mean velocity gradient for vertical tectonic movements). Here it is important to note that there are several factors that may have a substantial effect upon the quantitative relationship between the seismicity and the mean velocity gradient. These factors include the mechanical properties of the material in the focal region, the history of the tectonic movements and the present-day types of strains in the Earth's crust.

Determination of velocity gradients for vertical tectonic movements

We define the velocity gradient or vertical tectonic movements of the Earth's crust as the mean value for a time interval of from 75 to 300,000 years, and as the mean value of segments $l_{1,2}$, of from 2 to 5 km long, between two points (1 and 2) on the Earth's surface. For this calculation, we make use of thickness data on deposits of the same age and on the depth of deposition of a lower Quaternary erosion surface (Fig. 144). The mean velocity gradient V for vertical tectonic movements was computed as the difference of the present heights $h_1 - h_2$ (for thicknesses), determined between two points separated by $l_{1,2}$ in the direction of the greatest height (or thickness) variation, and adjusted to the distance $l_{1,2}$ and the time t (Fig. 144b).

$$| \operatorname{grad} V | = \frac{h_1 - h_2}{l_{1,2}}.$$

In addition, this same quantity was calculated from data on the present slope angle α for residual mountains of the same erosion surface (Fig. 144c).

$$| \operatorname{grad} V |_m = \frac{\operatorname{tg} \alpha}{t}.$$

For many sites at which the erosion surface has already worn down, it is only possible to indicate the lower limit of the mean gradient. The sign of the mean velocity gradient is always taken in accordance with

the diagram of Fig. 144. A more detailed exposition of methods for de-
termining movements has been published [271].
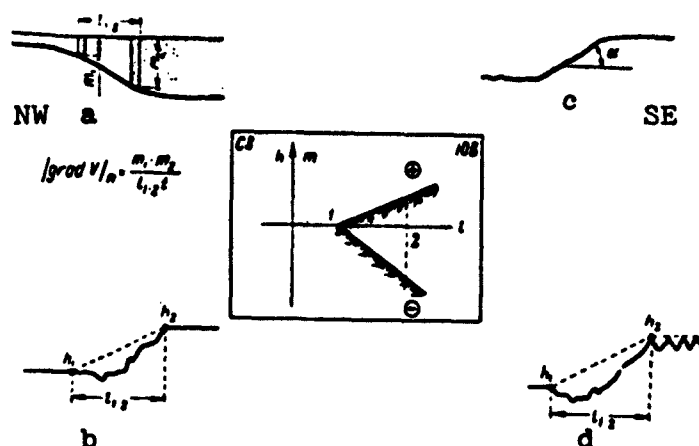
Fig. 144. Various methods for determining mean
velocity gradients of tectonic movements. a)
From stratiographic section; b) from erosion
surface; c) from deformation of erosion surface;
d) from height index marks.

The extent of the Quaternary movements was determined in accord-
ance with modern ideas [262, 263]. It was assumed that the Wuerm gla-
ciation ended 10,000 years ago and began 110,000 years ago, that the
Riss glaciation ended 170,000 years ago and began 230,000 years ago,
that the Mindel glaciation ended 370,000 years ago and commenced
470,000 years ago, and that the Quaternary period commenced 600,000
years ago.

In accordance with geological data [216], it is necessary to as-
sume that the lower Quaternary erosion surface was maintained in the
Garm district over only the first half of the Quaternary period. At the
start of the Wuerm glaciation, as a result of deformation of the
Earth's crust and processes of denudation, the relief was already
mountainous, while the lower erosion surface was cut by deep valleys.
Thus, it is most likely that the deformations distorting the shape of
what was initially a nearly horizontal erosion plane lasted about

300,000 years, and in any case, for not over 600,000 years, covering the entire Quaternary period. Since the true magnitude of t is not known, for the purposes of the calculations we assumed that t equaled the upper limit — 600,000 years. Thus, the gradient values obtained over the entire district will be too low by precisely the same factor, probably amounting to 2 — 3 in comparison with the true value. The results of calculations of the mean velocity gradient for various sections of the Garm district, carried out on the basis of materials from stratographic and structural sections (Figs. 119, 120, 121, Chapter 8), are shown in Figs. 145, 146, 147, and 148.

For the Mesozoic Era and the Tertiary Period, variation in the thicknesses of Mesozoic and Tertiary deposits within the Garm district make it possible to distinguish two main strips having a maximum mean gradient, which probably reached 10^{-8} or 10^{-9} 1/year (Figs. 145 and 146).

One of these strips — the Petrovskaya strip — corresponds to the Northwest boundary of the Pamir foothills trough (the boundary of regions A and B), and the other — the Karakul' strip — to the Southeast boundary of this trough (the boundary of the A-I and A-II zones). By the end of the Neogene Period, a third strip — the Surkhob strip — with a large mean velocity gradient had appeared on the site of the modern Surkhob River valley (Fig. 146).

The mean gradient of movement velocity can be determined with considerably greater reliability for the Quaternary Period than for the Mesozoic Era or the Tertiary Period. For the Quaternary Period, the gradient proved greatest in the same three main strips: the Surkhob to the North, the Petrovskaya in the middle, and the Karakul to the South of the district. The gradient within these strips was found from the present-day hypsographic map compiled by Ye. Ya. Rantsman, for the
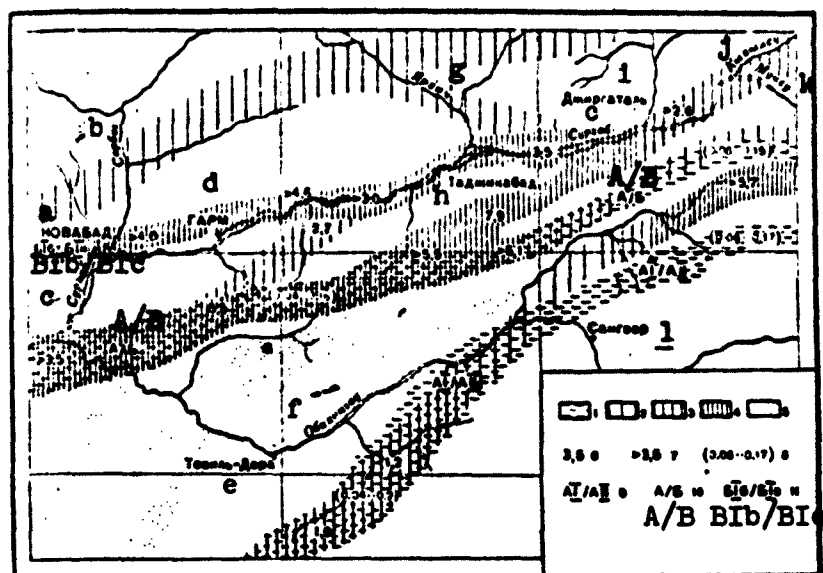
Fig. 145. Diagram showing variation in mean velocity gradient for vertical tectonic movements. The strips of maximum mean values of $|\text{grad } V|_m$ in units of 10^{-7} are: 1) for the Mesozoic Era and the Tertiary Period (0.01 — 0.2); for the Quaternary Period: 2) 0.9 — 1.1; 3) 1.2 — 3.0; 4) 3.0; 5) secondary strips of high gradients; 6) magnitude established approximately; 7) lower limit of gradient values not amenable to more accurate determination; 8) approximate value of gradient for Mesozoic Era and Tertiary Period; 9) high-gradient strip along boundary of tectonic zones A-I and A-II; 10) high-gradient strip along boundary of tectonic regions A and B; 11) high-gradient strip along boundary of tectonic subzones B-IB and B-IC. a) Novabad; b) Sorbog; c) Surkhob; d) Garm; e) Tovil'-Dora; f) Obikhingou; g) Yarkhich; h) Tadzhikabad; i) Dzhirgatal'; j) Kyzylsu; k) Muksu; l) Sangvor.

lower Quaternary erosion surface. Figure 145 shows within the main strips, sections having mean velocity gradients ranging from $0.9 \cdot 10^{-7}$ to $1.1 \cdot 10^{-7}$ 1/year; from $1.2 \cdot 10^{-7}$ to $3.0 \cdot 10^{-7}$ 1/year; and greater than $3.0 \cdot 10^{-7}$ 1/year. The mean velocity gradient for tectonic movements may be determined to within an order of magnitude, and thus a more detailed estimate, strictly speaking, is not justified, and should be made only to find the tendency in the gradient variation. It is clear
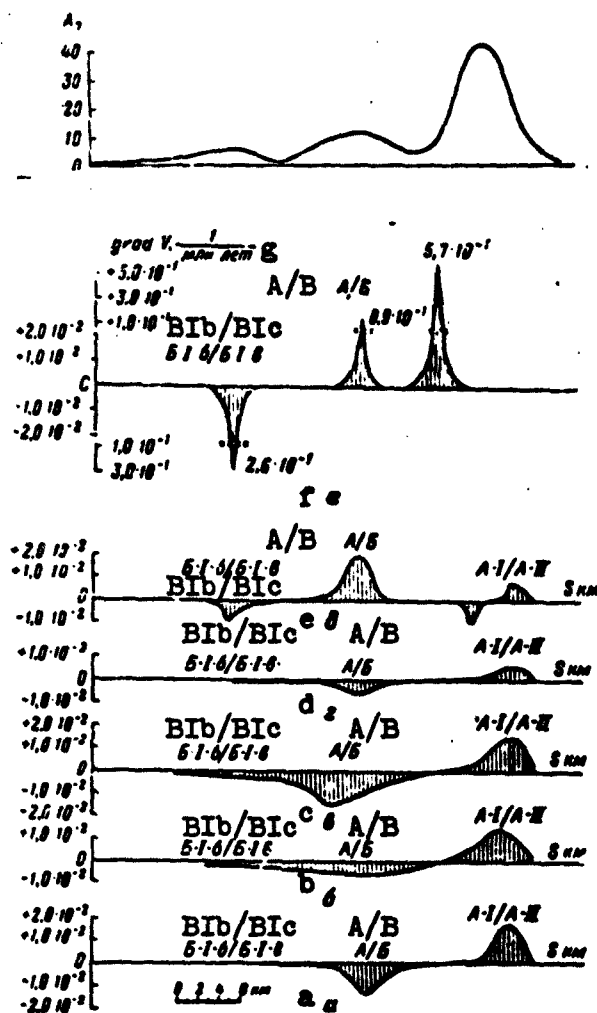
Fig. 146. Diagram showing variation in seismic activity A_7 along line I-I (Fig. 121) in eastern section of Garm region, in comparison with variation in velocity gradients for tectonic movements. a) Triassic and Jurassic; b) lower Cretaceous; c) upper Cretaceous; d) lower and middle Paleogene; e) upper Paleogene and Neogene; f) Quaternary Period; g) million years.

from these data that in the main strips, the mean velocity gradient for the Quaternary movements turns out to be greater by an order of magnitude than the mean velocity gradient for the Mesozoic Era or the

Tertiary Period. It is very important to note that in the Petrovskaya strip, in contrast to the two other main strips, the sign of the veloccity gradient for the Quaternary movements is the opposite of the sign for the Mesozoic and Tertiary movements (Fig. 148). We must note that
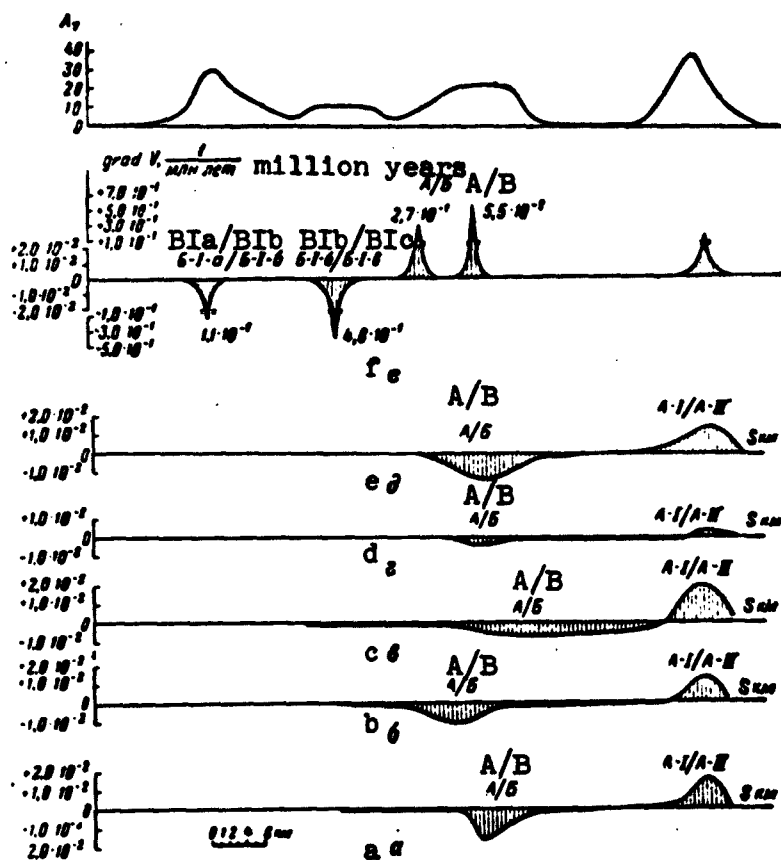
Fig. 147. Diagram showing variation in seismic activity A_7 along line II-II (Fig. 121) in western section of Garm region, as compared with variation in velocity gradients for tectonic movements (a-f, see Fig. 146).

in the eastern half of the district, in an area containing a strip of high gradients for movements occurring prior to the Quaternary, it is not possible to make such a statement for the Quaternary movements. The high gradients for Quaternary movements in this case occur somewhat to the North, in the brand new Karashurinskaya strip (Figs. 145

and 146).

In addition to the main strips, we can see several secondary strips which are isolated by their development of maximum slope angles in the Neogene deposits, the presence of major flexures, sharp folds, and tectonic faults with steep dips. It is still not possible to find
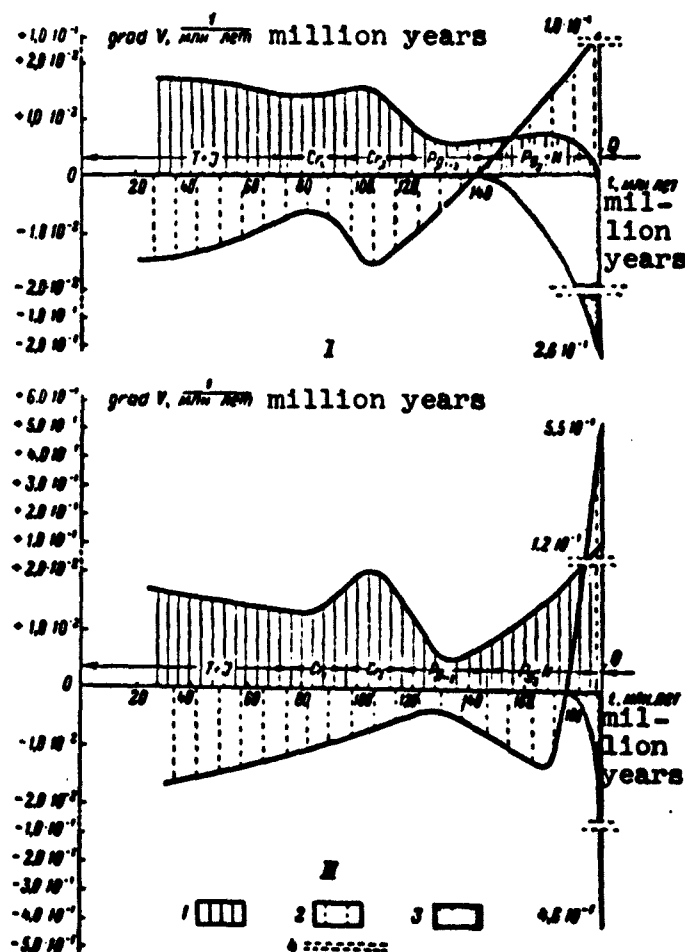
Fig. 148. Graphs showing variation in velocity gradient for tectonic movements in strips. A-I/A-II; A/B; B-I-B/B-I-c during the Mesozoic and Cenozoic Eras. I) In eastern portion of Garm region and II) in western portion of Garm district. Labels: gradient: 1) in zone A-I/A-II; 2) in zone A/B; 3) in zone B-I-b/B-I-c; 4) line indicating transition to different scale.

the mean velocity gradient for Quaternary movements within them.

In the areas between the main and secondary strips, it is possible in many places to note that the gradient reaches 10^{-8} 1/year.

Comparison of mean tectonic-movement velocity gradient for the Quaternary Period with the present-day seismic activity of the Garm district

TABLE 22

Comparison of Seismic Activity with Mean Velocity Gradient for Tectonic Movements

1 Полоса	2 Величина A_0		3 Средняя величина grad $V_{|m}$	
	4 абсолютная	5 относительная	4 абсолютная	5 относительная
6 Петровская . . .	14	4,7	5,5·10⁻⁷	3,7
7 Сурхобская . . .	10	3,3	3,5·10⁻⁷	2,3
8 Каракульская . .	3,6	1	1,5·10⁻⁷	1

1) Strip; 2) magnitude of A_7; 3) mean value of $|grad \ V|_m$; 4) absolute; 5) relative; 6) Petrovskaya; 7) Surkhob; 8) Karakul'.

Since the main bands having the maximum mean velocity gradient for Quaternary movements coincide in their boundaries with tectonic regions, zones, and subzones about which earthquake epicenters concentrate, it turns out that strips having maximum mean gradient values and strips of epicenter concentration coincide. Thus, at first glance, it appears to make no difference whether we use strips of high gradient values, or the boundaries of tectonic zones for the purposes of a comparison with the seismicity. As a matter of fact, this is not the case. So far, the boundaries of the tectonic zones have not been characterized quantitatively, and thus we have no index that may be compared with the quantitative characteristic of seismicity. The mean gradient is precisely such a quantitative characteristic of the tectonic movements on the boundary between two tectonic zones, and there-

fore a consideration of the mean velocity gradient seems to us to be a further development of those principles which have been used previously in analyzing the relationships between tectonics and the seismicity of Central Asia [238, 264-267]. The introduction of the mean velocity gradient into the discussion represents an attempt at an approximate quantitative comparison of seismicity with tectonics.

We make use of the seismic-activity map given in Fig. 141. In the first stage of the discussion, it is possible to assume for practical purposes that the slope angles of all of the recurrence curves are identical, and thus that the difference in the seismic activity A_7 of the main strips is reflected solely in the level of the recurrence curves. In order of decreasing activity, the main strips are arranged in the following sequence: Petrovskaya ($A_7 = 14$), Surkhob ($A_7 = 10$), Karakul' ($A_7 = 3$). If we take the data for the Karakul' strip at unity, then the relative activity for the Petrovskaya strip will be 4.7, and for the Surkhob strip, 3.3. These relative-activity values agree with the values obtained for the same zones of the relative mean movement-velocity gradient for the Quaternary period. On the basis of the available data (Fig. 143), for each of the three main strips, it is possible to take the following approximate values for the mean velocity gradient, in units of 10^{-7} 1/year: Petrovskaya strip — about 5.5; Surkhob strip — about 3.5; Karakul' strip — about 1.5. Taking the data for the Karakul' strip as unity, we obtain the following relative values for the mean gradient: Petrovskaya strip, 3.7; Surkhob strip, 2.3 (Table 22).

The increase in seismic activity with increasing mean velocity gradient is quite well-defined.

As we have said previously (Chapter 8), variations in the heights of river terraces indicate that after the Wuerm glaciation, i.e., dur-

ing the last 10,000 years, the plan of the tectonic movements re-
mained the same, in general, as before. Consequently, the tectonic
data obtained upon analyzing movements in the Earth's crust over an
interval of about 300,000 years, and about 10,000 years, turn out to
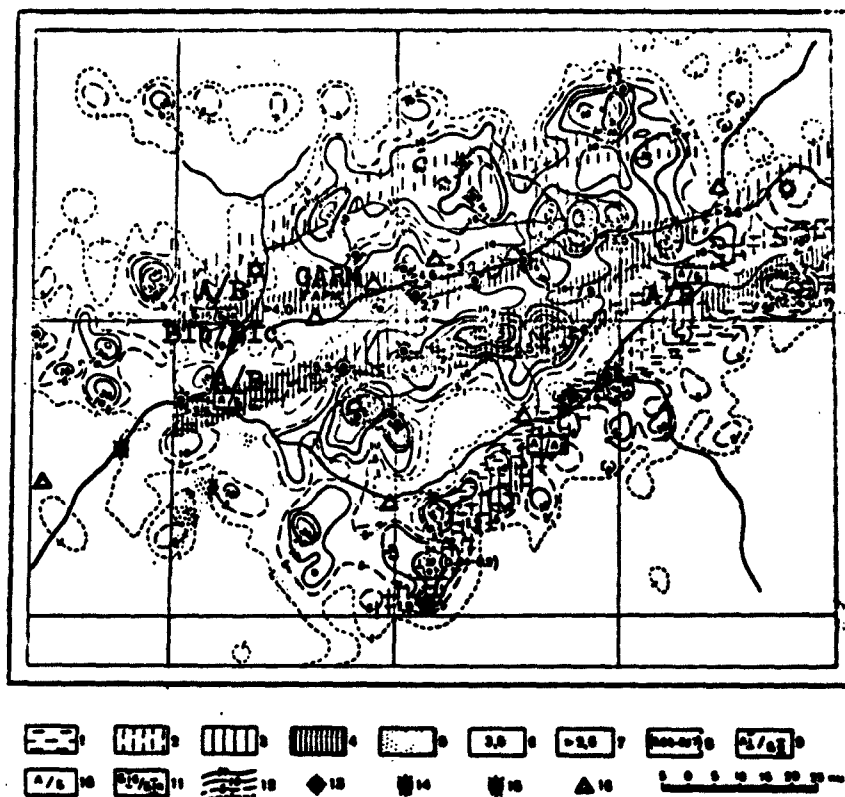
Fig. 149. Map comparing mean velocity gradient for
vertical tectonic movements with seismic activity
(1955-1956.) in Garm district. 1-11) See Fig. 143;
12) seismic-activity isolines; 13) epicenter of
K = 11 earthquakes; 14) K = 12; 15) K = 13; 16)
seismic stations.

correspond with seismic data obtained from observations made over a
two-year period.

In the spaces between the main strips that have the maximum veloc-
ity gradients for the Quaternary tectonic movements of the Earth's
crust, in the secondary strips, many sections are characterized by in-
creased seismic activity, although, on the whole, the activity is lower

here than in the main strips.

So far, we have used only the general characteristics of seis-
micity for major strips as a whole in our comparison with the tecton-
ics. It is very fruitful to compare details of seismicity and tecton-
ics within each of the strips. Such a comparison may be carried out
most clearly in accordance with a seismic-activity map (Fig. 149). In
examining any strip, we may assume that the mechanism of crustal de-
formation and the composition of the component rocks remain constant,
in first approximation, over the entire strip; thus, variations in the
mean velocity gradient must here agree well with variations in the
seismic activity.

In the lower Karakul' strip, there is a decrease in the velocity
gradient of Quaternary movements along the strip from the Southwest to
the Northeast from $1.9 \cdot 10^{-7}$ to a magnitude of the order of 10^{-8} 1/year.
In the center of the district, the younger Karashurinskaya strip
branches off from the Karakul' strip; the two strips run along together
further on; in the eastern part of the district, the gradient in the •
Karashurinskaya strip reaches $5.7 \cdot 10^{-7}$ 1/year. The spatial distribution
of the seismic activity A_7, in general, agrees with the distribution of
the mean movement velocity gradient. Within the Karakul' strip, the
magnitude of A_7 drops from the Southwest to the Northeast from 40 to 5.
At the point at which the Karashurinskaya strip branches off from the
Karakul' strip, the activity increases to 30. It becomes still greater
(up to 40) to the East, in the Muksu River basin, where the movement
velocity gradient is extremely large in the Karashurinskaya strip (Fig.
149).

In the lower Petrovskaya strip, the gradient has its maximum val-
ue at the center of the district, where it reaches $7.9 \cdot 10^{-7}$ 1/year.
Toward the western and eastern borders of the districts, the gradient

drops to 3.5 and even to $0.9 \cdot 10^{-7}$ 1/year, especially toward the East. The seismic activity A_7, which reaches 60 and 80 at the center of the district, drops to 10 and even 5 toward its borders.

In the young Surkhob strip, the maximum gradient again occurs at the center of the district, where it is more than $4.6 \cdot 10^{-7}$. Towards the West, the gradient drops off considerably. A large drop in the gradient, to $3.5 \cdot 10^{-7}$, and then to $2.5 \cdot 10^{-7}$ occurs in the eastern half of the district. The seismic activity A_7 is also at a maximum at the center of the district (to 30 - 60), and in like manner, the gradient drops off to the East. Toward the West, however, away from the center of the district, the drop in seismic activity is far sharper than the drop in the velocity gradient. Here, there is a certain discrepancy between the extremely large gradient ($4.0 \cdot 10^{-7}$ 1/year) and the exceptionally low activity, equal to 1 or less, between Garm and Novabad. This exception to the general rule is probably caused by the nonuniform nature of the tectonic movements and of the seismicity with respect to time. In evaluating the earthquake danger in the given section, the fact that it is adjacent to the Surkhob strip should be considered a more important factor than the low seismic activity which probably reflects a brief fluctuation in this quantity.

It should be emphasized, in general, that Fig. 147 shows clearly the nonuniform distribution in epicenter density within each strip. The geographical position of the separate small epicenter concentrations within each of the strips can hardly be assumed to remain stable over a period of several centuries; in any event, there is no basis for making such a statement. In view of this fact, a comparison of the mean velocity gradient with the seismic activity is best carried out by supraposing the corresponding maps, as in Fig. 149. A comparison of profiles, as in Figs. 145 and 146, may distort the quantitative rela-

tionships, which will be arbitrary owing to the great nonuniformity in the values of A_7 within the same strip. Thus, for example, in Fig. 145, the greatest maximum for A_7 turns out to lie near the boundary of the zones A-I/A-II, while the maximum mean velocity gradient for Quaternary movements in this section is shifted toward the North.

The comparisons made above deal with earthquake recurrences for energies of from 10^6 to 10^8 joules. The expedition data on weak-earthquake recurrence in the Garm district over a relatively short time interval (two years) and the data compiled by V.I. Bune [198] on strong earthquakes over a long time interval (fifty years) permits us to suppose that the linear law followed by weak-earthquake recurrence may be extended to the region of stronger earthquakes. At present, we do not have sufficient material at our disposal to answer the following two questions: a) how to determine for each section of the Earth's crust the upper limit of earthquake energy beyond which the recurrence curve cannot be extrapolated; b) whether in all cases the recurrence curve will retain its straight-line shape upon extrapolation to the high-energy region; are there any conditions under which the graph will curve so as to approach the upper energy limit? These questions are extremely important in evaluating the earthquake hazard of any territory.

Seismicity-tectonics comparison for districts adjacent to the Garm district

The seismicity of districts surrounding the Garm district, which have been studied in far less detail from the seismic-geological point of view, can be discussed only with far less definiteness. It is still possible to examine this question, however, since many data on the seismicity have been published [11, 198, 227, 268-270], while the tectonic zones traversing the Garm district spread out beyond its borders, and occupy a considerable portion of South Central Asia. The main

strips having a high mean gradient value run far beyond the borders of the Garm district (Fig. 142).

The lower Karakul' strip, which coincides with the borders of zones A-I and A-II, although running to the Southwest from the Garm district toward the city of Kulyab, is not characterized by a very great mean velocity gradient for Quaternary movements. Somewhat to the Northwest of this strip, a new strip may be noticed, running parallel through Kulyab. In this strip, we might expect some increase in the mean velocity gradient for Quaternary movements. On the Northwest, the given strip borders with the foothills of the Darvazskiy range, which is composed of Neogene deposits. The existence of several epicenters here and in the Karakul' strip confirms the possibility of increased seismic activity in these strips. The new strip that passes near Kulyab turns out to be especially hazardous. To the East of the Garm district, the Karakul' strip runs into the Translayskiy range, and runs along its southern slope. Here we cannot reasonably expect any considerable mean velocity gradient for the Quaternary and present-day movements. The quite weak seismicity of the southern slope of the Transalayskiy range accords with this notion. The Karashurinskiy strip runs along the northern slope of this same range. Here, despite the fact that the strip coincides with a high escarpment, the velocity gradient for late Quaternary movements will not, apparently be very large. The high escarpment must be related to a considerable velocity gradient for Neogene and early Quaternary movements. In the late Quaternary, there occurred the basic over-all uplift of the Transalayskiy range, together with the Pamir, Alayskaya valley, and the Alayskaya range [238]. There still were certain differences in the rate of uplift in the Alayskaya-valley and Transalayskiy-range zones, nonetheless. These differences created a specific velocity gradient, which could be the

cause for the tendency of earthquake epicenters to concentrate in a strip running along the boundary of these zones. Earthquakes are more frequent here than in the Garm district.
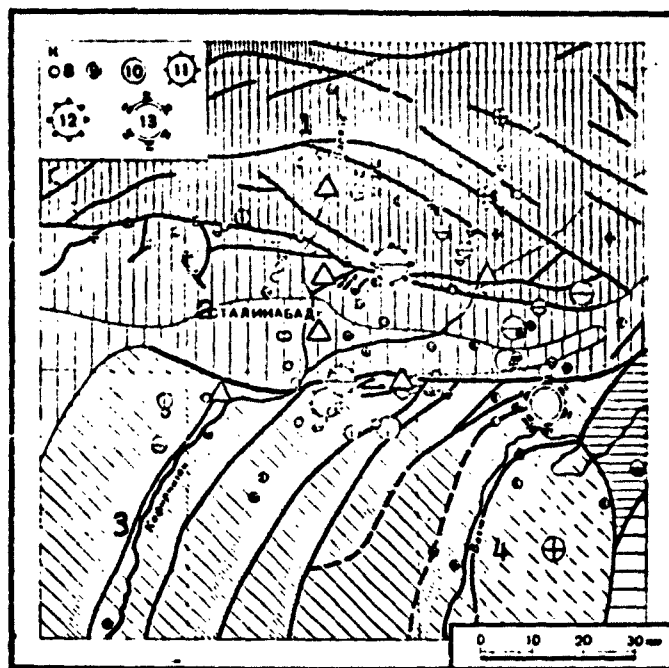
Fig. 150. Map comparing tectonics and earthquake-foci location (for the 1955-1956 period) in the Stalinabad district. The arbitrary designations in the seismic section are the same as for Fig. 142. 1) Varzob; 2) Stalinabad; 3) Kafirnigan; 4) Vakhsh.

The Petrovskaya strip, which corresponds to the boundary of the regions A and B, runs to the Southwest from the Garm district, along the Vakhsh and Surkh-ku ranges. On the section from Komsomolabad to Obi-Garm, the mean velocity gradient for the Quaternary movements is clearly less than in the Garm district, or than in the more south-westerly section. It is probably no accident that the infrequent earth-quakes appearing here are weaker than in the Garm district, or in the neighborhood of Fayzabad. To the Southwest of Fayzabad, the Petrovskaya strip forms two branches. The first branch which, tectonically speak-,

ing, is strictly similar to the Petrovskaya strip in the Garm district runs to the South toward Tutkaul' and Nurek. After crossing the Vakhsh River valley, it pinches off rapidly. Another adjoining strip runs toward the same section of Tutkaul' from the West; here, in accordance with presently known geological data, we should expect a considerabel velocity gradient. Intensive strains in the Earth's crust in the Tutkaul' section compels us to exercise great care in evaluating the earthquake hazard here. The second branch of the Petrovskaya strip, which, for convenience, is called the Ilyakska strip, runs due West along the southern slope of the Gissar valley, along the boundary of the zones B-I and B-II. This strip is in many ways similar to the Petrovskaya strip. The velocity gradient for the Quaternary movements in this strip, judging from materials furnished by M.K. Grave,* reaches 10^{-7} 1/year. Thus, it should be no surprise that the earthquake epicenters concentrate in this strip (Fig. 150). To the East of the Garm district the Petrovskaya strip, clearly, runs along the northern slope of the Transalayskiy range where it possibly borders upon or runs together with the Karashurinskiy strip.

To the West, the Surkhob strip continues to great distances from the Garm district. Judging from the relief, however, the mean velocity gradient for Quaternary tectonic movements outside of the Garm district in this strip should everywhere be small. It is precisely with this fact that we associate the lessened seismicity of this strip to the West of the Garm district (Figs. 142 and 150). To the East, the Surkhob strip clearly does not run very far.

To the West of the Garm district, in the vicinity of Stalinabad, there is still another strip having a considerable mean velocity gradient for the Quaternary movements — the Karatagskaya strip. It covers the steep northern slope of the Gissar valley, coinciding with the

boundary of the subzones B-I-b and B-I-c, where the Paleozoic rocks are in contact with the Tertiary rocks along faults (Figs. 142 and 150). In the Karatagskaya strip, there is a clear concentration of weak-earthquake epicenters. Here, in 1907, the severe Karatagskaya earthquake occurred, which had an energy of the order of 10^{16} - 10^{17} joules ($M \geq 7.5$), and the Fayzabad earthquakes of 1930 and 1943.

Thus, the city of Stalinabad turns out to be located between two strips having a considerable velocity gradient for the Quaternary movements — Ilyakska and Karatagskaya strips. Both of these strips present considerable earthquake hazard. Judging from the changes in the height of the terrace of the Kafirnigan and its right-bank tributaries,* the mean velocity gradient for the Quaternary and the Holocene movements may reach 10^{-7} 1/year in the Karatagskaya strip. If this is so, then this strip is probably extremely hazardous. In addition, in the neighborhood of Stalinabad, there are several secondary strips having an increased velocity gradient. We can determine this from the results of the geomorphological investigations of N.P. Kostenko and M.K. Grave, as well as from numerous materials obtained by geologists in Tadzhikistan. One of the secondary strips can be seen to lie within the Gissar valley. It runs toward the city from the East, and is quite broad. Another, North-South strip runs down from the North. There is a group of secondary strips to the North and to the South of the Gissar valley. These strips coincide with the boundaries of the individual subzones and blocks. The epicenters of weak earthquakes fall within these strips (Fig. 150). The large number of epicenters for earthquakes of various energies that are scattered about Stalinabad forces us to consider the entire surrounding district to be seismically active. The differentiation of this district should consist in the isolation of sections differing in energy and in earthquake recurrence with time.

The Garm district, for example, shows the direction that the investigations may take if they are to achieve this goal.

CONCLUSION

The results of the development of a method for the detailed study of seismicity, obtained upon the basis of investigations in the Garm and Stalinabad districts, which are presented in the present monograph, represent only the first results of the work of the Tadzhikistan Combined Seismological Expedition of the Institute of Physics of the Earth of the Academy of Sciences USSR and the Institute of Seismicity of the Academy of Sciences of the Tadzhikistan SSR. The work of this expedition will continue. The main goals, as before, are: the improvement of methods for detailed seismic districting and the discovery of methods for predicting severe earthquakes, based upon the study of general seismic laws, and of the conditions and causes for the occurrence of earthquakes.

Despite the incomplete nature of the investigations described above and the tentative nature of the results obtained, they may be of interest, or so it seems to us, for those seismologists who are attempting to perfect methodology, to increase the role of detailed instrumental observations, and to improve quantitative methods of processing and interpreting the material. There is no doubt that this general trend lies in the mainstream of development of modern seismology and its practical applications.

It seems to us that the methods outlined here for the quantitative determination of seismic activity, based chiefly upon instrumental observations of earthquakes over a broad range of energies, and supplemented by quantitative methods of studying tectonic movements, as well as macroseismic and other data, form the basis for the contemporary better, more objective, more detailed, more accurate, and faster me-

thods of seismic districting.

While this monograph was being prepared for press, a first, albeit perhaps far from perfect, attempt was made in one of the districts of the Soviet Union at detailed districting, making use of the principles discussed [271]. There is no doubt that other work in this direction will follow, carried out by various organizations, since a pressing need for completing work on detailed districting is felt in many districts of our country, as well as abroad. It is clearly undesirable in the majority of cases, if not in all cases, to carry out such work by the older, predominantly microseismic methods.

The development of detailed seismic investigations, in connection with problems of detailing seismic districting in separate localities, will unquestionably act to add to our knowledge of the general laws governing seismic processes, without which success is impossible in this matter. The irregular carrying out of such work, however, cannot replace long-term systematic investigations under especially selected conditions favorable to such investigations.

The continuation of fixed long-term detailed seismic observations is primarily necessary in order to clarify the as yet very little investigated problems on the maximum earthquake energy possible under given conditions, and of possible variations in seismic regimes with time.

It is necessary to broaden and perfect observations made by geological, geodesic, or other methods of present-day or past (covering various time intervals) deformations of the Earth's crust in order to obtain, basically, the quantitative data to be compared with quantitative seismicity data. In particular, we must expect from geological methods, ever better-founded materials permitting judgments as to long-term processes, that can form a basis for judging the possible

appearance of severe earthquakes in localities in which the recent seismicity has been weak, and for which the information available to seismologists as to the past seismicity level is inadequate to permit definite conclusions.

In addition, it is necessary, naturally, that investigations be carried out in several neighboring regions, and into many special questions (improvement of methods for the detailed study of the structure of the Earth's core, making use of explosives and earthquakes, study of seismic-oscillation spectra, improvement of methods for using the focal activity of earthquakes to arrive at the shocks on the ground surface in order to determine the degree of earthquake hazard, etc.). A successful solution of all of these problems (of either general or special nature) is impossible without the improvement of apparatus (and in particular, telemetering and automatic equipment) for earthquake observations, and for the instrumental processing of materials, or without the development of a theory and of laboratory experiments.

In our time, all of the increasing successes of socialist science and technology should systematically and rapidly be mastered by Soviet seismology, which is continuously improving; these advances should be adapted creatively, and should include all of the best modern facilities and methods. This is the only way in which Soviet seismology can cope with all of the problems facing it, problems of great scientific and practical importance.

Manu-
script   [Footnotes]
Page
No.

474   M. K. Grave. Rel'yef i noveyshaya tektonika tsentral'noy
           chasti Gissarskoy doliny i eye gornogo obramleniya. Rukopis',
           fondy IFZAN [Relief and Latest Tectonics of Central Portion
           of the Gissar Valley and its Mountainous Setting. Manuscript

[Footnotes (Continued)]

funds of the IFZAN not identified in standard references],
1955.

475   M. K. Grave. Ibid

REFERENCES

1. I.L. Nersesov. Opyt izucheniya mestnykh zemletryaseniy [Experience in the Study of Local Earthquakes], Candidate's Dissertation, Inst. fiziki Zemli [Institute of Terrestrial Physics], 1953.

2. D.A. Kharin, V.I. Keylis-Borok and S.D. Kogan, K metodike seysmicheskikh nabludeniy v epitsentral'noy zone i ikh inter-pretatsii [A Technique for Seismic Observations in the Epicentral Zone and Their Interpretation], Tr. Geofiz. inst. AN SSSR [Transactions of the Geophysics Institute of the Academy of Sciences of the USSR], No. 21 (148), 1953, 27-42.

3. I.L. Nersesov and L.N. Rykunov, K obrabotke mestnykh zemletrya-seniy Garmskoy Oblasti [Evaluation of Local Earthquakes in the Garm Region], Tr. Geofiz. inst. AN SSSR, No. 21 (148), 1953, 19-26.

4. D.A. Kharin and S.I. Masarskiy, Issledovaniye epitsentral'nykh oblastey pri pomoshchi regional'nykh seysmicheskikh stantsiy [Investigation of Epicentral Regions with the Aid of Regional Seismic Stations], Tr. Geofiz. inst. AN SSSR, No. 25 (152), 1954, 97-112.

5. V.I. Keykis-Borok and A.V. Vvedenskaya, Issledovaniye naprya-zheniy v ochagakh Khaitskoy epitsentral'noy zony [Investigation of Stresses in the Foci of the Khaitskaya Epicentral Zone], Tr. Geofiz. inst. AN SSSR, No. 25 (152), 1954, 113-123.

6. V.F. Bonchkovskiy, Naklony zemnoy poverkhnosti kak odin iz vozmozhnykh predvestnikov zemletryaseniy [Inclination of Earth's Surface as One Possible Precursor of Earthquakes], Tr. Geofiz. inst. AN SSSR, No. 25 (152), 1954, 134-153.

7. M.S. Antsyferov, O primenenii geoakusticheskikh metodov k resheniyu problemy prognoza zemletryaseniy [Application of Geo-acoustic Methods to Solution of the Earthquake-Prediction

Problem], Tr. Geofiz. inst. AN SSSR, No. 25 (152), 1954, 157-161.

8. V.F. Bonchkovskiy, Itogi raboty Garmskoy Ekspeditsii [Results of the Work of the Garm Expedition], Byull. Soveta po seysmologii AN SSSR [Bulletin of the Seismology Council of the Academy of Sciences USSR], 1955, No. 1, 31-39.

9. G.A. Gamburtsev, Sostoyaniye i perspektivy rabot v oblasti prognoza zemletryaseniy [Present State and Prospects of Studies in the Field of Earthquake Prediction], Byull. Soveta po seysmologii AN SSSR, No. 1, 1955.

10. G.A. Gamburtsev, Kratkoye soderzhaniye doklada "O prognoze zemletryaseniy" [Extract of Report Entitled "Earthquake Prediction"], Izv. AN SSSR, seriya geofiz. [Bulletin of the Academy of Sciences USSR, Geophysics Series], 1955, No. 3.

11. N.A. Vvedenskaya, Metodika i rezul'taty obobshcheniya nablyudeniy seti statsionarnykh seysmicheskikh stantsiy za 1950-1953 gg. [Technique and Results of Generalization of Observations from Network of Permanent Seismic Stations from 1950-1953], Izv. AN SSSR seriya geofiz., 1954, No. 6.

12. S.L. Solov'yev, K voprosu o sootnoshenii mezhdu energiyey ob-yemnykh voln i intensivnost'yu zemletryaseniy [Relationship Between Energy of Space Waves and Earthquake Intensity], Byull. Soveta po seysmologii AN SSSR, 1957, No. 6.

13. D.P. Kirnos and D.A. Kharin, Seysmograf dlya izucheniya kolebaniy sooruzheniy, seysmicheskogo effekta vzryvov i registratsii blizkikh zemletryaseniy [Seismograph for Study of Vibrations in Buildings and the Seismic Effect of Explosions and Registration of Nearby Earthquakes], "Studia geophys. et geod.", 1958, No. 2.

14. D.P. Kirnos, Nekotoryye voprosy instrumental'noy seysmologii [Certain Problems of Instrumental Seismology], Tr. Geofiz. inst.

AN SSSR, No. 27 (154), 1955.

15. V.T. Arkhangel'skiy, I.L. Nersesov, D.A. Kharin et al., Rukovod-
stvo po proizvodstvu i obrabotke nablyudeniy na seysmicheskikh
stantsiyakh SSSR [Handbook on the Conduct and Evaluation of
Observations at Seismic Stations of the USSR], Part II. Izd-vo
AN SSSR, 1954.

16. G.A. Gamburtsev and Ye. I. Gal'perin, Metodika rabot po korrelyat-
sionnomu metodu izucheniya zemletryaseniy [Technique for Correla-
tion Methods of Studying Earthquakes], Izv. AN SSSR, seriya
geofiz., 1954, No. 1.

17. G.A. Gamburtsev and Ye.I. Gal'perin, Azimutal'nyye seysmicheskiye
nablyudeniya s naklonnymi seysmografami [Azimuthal Seismic Obser-
vations With Inclined Seismographs], Izv. AN SSSR, seriya geofiz.,
1954, No. 2.

18. I.P. Pasechnik, Azimutal'naya chetyrekhkomponentnaya ustanovka
s naklonnymi seysmografami [Azimuthal Four-Component Apparatus
With Inclined Seismographs], Izv. AN SSSR, seriya geofiz., 1956,
No. 3.

19. Ye.S. Borisevich, Novyye zerkal'nyye gal'vanometry k magnito-
elektricheskim ostsillografam [New Mirror Galvanometers for
Magnetoelectric Oscillographs], Tr. Geofiz. inst. AN SSSR, No. 29
(156), 1955.

20. Ye.S. Borisevich, Vysokochastotnyye ramochnyye gal'vanometry
[High-Frequency Frame Galvanometers], Izv. AN SSSR, seriya geofiz.,
1957, No. 4.

21. I.L. Nersesov, O koeffitsiyente svyazi sistemy seysmograf-
gal'vanometr [Coupling Coefficient of Seismograph-Galvanometer
System], Tr. Geofizicheskogo inst. AN SSSR [Transaction of the
Geophysical Institute of the Academy of Sciences USSR], No. 36

(163), 1956.

22. G.V. Groshevoy and I.P. Pasechnik, Vysokochuvstvitel'nyy polevoy seysmograf MPS-1 dlya zapisi korotkoperiodnykh komponent seysmicheskikh voln [MPS-1 High-Sensitivity Field Seismograph for Recording Short-Period Seismic-Wave Components], Izv. AN SSSR, seriya geofiz., 1956, No. 10.

23. Ye.S. Borisevich, Opticheskaya sistema dlya fotozapisi kolebatel'nykh protsessov [Optical System for Photographic Recording of Vibration Processes], Izv. AN SSSR, seriya geofiz., 1957, No. 3.

24. Ye.N. Fedoseyenko and G.V. Groshevoy, Sposob kontrolya chuvstvitel'nosti i opredeleniya chastotnykh i amplitudnykh kharakteristik seysmopriyemnykh kanalov pri pomoshchi magnitoelektricheskogo generatora [Method for Checking Sensitivity and Determining Frequency- and Amplitude Characteristics of Seismic-Receiver Channels by Means of Magnetoelectric Generator], Izv. AN SSSR, seriya geofiz., 1953, No. 3.

25. L.I. Bokanenko, Opredeleniye chastotnykh i fazovykh kharakteristik elektrodinamicheskikh seysmopriyemnikov pri pomoshchi dopolnitel'noy katushki vozbuzhdeniya [Determination of Frequency- and Phase Characteristics of Electrodynamic Seismic Receivers by Means of an Auxiliary Energizing Coil], Izv. AN SSSR, seriya geofiz., 1956, No. 7.

26. P. Geyn, Kh. Lodzh and I. Stefan, Radioapparatura dlya zapisi seysmicheskikh kolebaniy s avtomaticheskim vklyucheniyem [Automatic-On Radio Apparatus For Recording Seismic Vibrations], in collection entitled Voprosy seysmicheskoy razvedki [Problems of Seismic Prospecting], IL [Foreign Literature Press], Moscow, 1953.

27. S. Omote, S. Miyamura, Y. Yamazaki. Triggered magnetic type recorder for routine seismic observations. "Bull. Earthq. Res. Inst. Tokio Univ.", 33, 3, 1955.

28. Ye.A. Rozova, Sostavleniye godografa i opredeleniye osnovnykh seysmicheskikh elementov dlya Sredney Azii [Construction of a Hodograph and Determination of Basic Seismic Elements for Central Asia], Tr. SIAN [Transactions of the Academy of Sciences Seismology Institute], 1936, No. 72.

29. G.A. Gamburtsev, Seysmicheskaya razvedka [Seismic Prospecting], 2nd Edition, 1958.

30. Yu.V. Riznichenko, Geometricheskaya seysmika sloistykh sred [Geometric Seismics of Stratified Media], Trudy ITG [Transactions of the Institute of Theoretical Geophysics], II, No. 1, 1946.

31. I.P. Kosminskaya, G.G. Mikhota and Yu.V. Tulina, Stroyeniye zemnoy kory v Pamiro-Alayskoy zone po dannym glubinnogo seys- micheskogo zondirovaniya [Structure of the Earth's Crust in the Pamiro-Alayskiy Zone According to Data of Deep Seismic Sounding], Izv. AN SSSR, seriya geofiz., 1958, No. 10.

32. B. Gutenberg. Wave velocities in the Earth crust. "Geol. Soc. Am.", Special paper, No. 62, 1955.

33. Kh. Teytel and M. T'yuv, Seysmicheskiye issledovaniya kontinen- tal'noy kory [Seismic Investigation of the Continental Crust], in collection entitled Zemnaya kora [The Earth's Crust], IL, Moscow, 1957.

34. Ye. A. Rozova, Zemletryaseniya Sredney Azii [Earthquakes of Central Asia], Tr. SIAN, 1947, No. 123.

35. P.I. Monakhov, Nekotoryye rezul'taty analiza zemletryaseniy Garmskoy oblasti [Certain Results of Analysis of Earthquakes in the Garm Region], Izv. AN SSSR, seriya geofiz., 1952, No. 2.

36. V.I. Bune and Ye. M. Butovskaya, O godografe i stroyenii zemnoy
    kory v Sredney Azii [On the Hodograph and Structure of the
    Earth's Crust in Central Asia], Tr. Geofiz. inst. AN SSSR, 1955,
    No. 30.

37. B.K. Balavadze and K.G. Tvaltvadze, Stroyeniye zemnoy kory v
    Gruzii po geofizicheskim dannym [Structure of the Earth's Crust
    in Georgia on the Basis of Geophysical Data], Izv. AN SSSR,
    seriya geofiz., 1958, No. 9.

38. F. Birch. Interpretation of the seismic structure of the crust
    in the light of experimental studies of wave velocities in rocks.
    Contributions in geophysics in honor of Beno Gutenberg. 1,
    Pergamon Press, 1959.

39. Yu.V. Riznichenko, Seysmicheskiye skorosti v sloistykh sredakh
    [Seismic Velocities in Stratified Media], Izv. AN SSSR, seriya
    geograf. i geofiz. [Bulletin of the Academy of Sciences of the
    USSR, Geography and Geophysics Series], 1947, No. 2.

40. G.A. Gamburtsev et al., Korrelyatsionnyy metod prelomlennykh
    voln [Refracted-Wave Correlation Method], Moscow, 1952.

41. Yu.V. Riznichenko, Metody massovogo opredeleniya koordinat
    ochagov blizkikh zemletryaseniy i skorostey seysmicheskikh voln
    v oblasti raspolozheniya ochagov [Methods for Large-Scale De-
    termination of Focus Coordinates of Nearby Earthquakes and
    Velocities of Seismic Waves in the Focal Region], Izv. AN SSSR,
    seriya geofiz., 1958, No. 4.

42. V.B. Sollogub, Uprugiye svoystva gornykh porod v rayone peredovykh
    progibov al'piyskikh geosinklinaley oblasti Yuga SSSR [Elastic
    Properties of Rocks in the Region of Overthrusts of the Alpine
    Geosynclinals of the Southern USSR], Tr. Inst. geol. nauk AN
    USSR, seriya geofiz. [Transactions of the Institute of Geological

Sciences Acad. Sci. UkrSSR, Geophysics Series], No. 1, Kiev, 1956.

43. Yu.V. Riznichenko and O.I. Silayeva, Opredeleniye zavisimosti skorostey rasprostraneniya uprugikh voln v obraztsakh gornykh porod ot odnorodnogo davleniya [Determination of Elastic-Wave Propagation Velocities in Rock Specimens as a Function of Homogeneous Pressure], Izv. AN SSSR, seriya geofiz., 1955, No. 3.

44. K. Wadati. Shallow and deep earthquakes. "Geophys. Mag.", 1, 4, 1927.

45. V.N. Gayskiy, K probleme obrabotki blizkikh zemletryaseniy [On the Problem of Evaluating Nearby Earthquakes], Tr. Geofiz. inst. AN SSSR, 1958, No. 20.

46. S.V. Yevseyev, K voprosu ob opredelenii epitsentrov blizkikh zemletryaseniy [On the Problem of Defining the Epicenters of Nearby Earthquakes], Trudy Geofiz. inst. AN SSSR, 1954, No. 22.

47. S.P. Golenetskiy and A.A. Treskov, Metod izokhron [The Method of Isochrones], Tr. Geofiz. inst. AN SSSR, 1953, No. 21.

48. G.A. Gamburtsev, Ob opredelenii azimuta na epitsentr pri registratsii mestnykh zemletryaseniy [On Determination of Azimuth and the Epicenter in Registration of Local Earthquakes], Dokl. AN SSSR [Proc. Acad. Sci. USSR], 87, No. 2, 1952.

49. S.I. Yeres'ko, Issledovaniye oshibok opredeleniya polozheniya ochagov krymskikh zemletryasneniy [Analysis of Errors of Position Determination on Foci of Crimean Earthquakes], Tr. Geofiz. inst. AN SSSR, 1956, No. 36.

50. I.L. Nersesov and V.A. Tokmakov, O tochnosti azimutal'nogo sposoba opredeleniya koordinat epitsentra [On the Precision of the Azimuthal Method of Epicenter-Coordinate Determination], Tr. Inst. seysmologii AN Tadzh. SSR [Transactions of the Seismology Institute of the Academy of Sciences Tadzhik SSR], 54, No. 1,

1955.

51. Yu.G. Balashko, K voprosu o metodakh obrabotki blizkikh zem-
     letryaseniy [On the Question of Methods for Evaluating Nearby
     Earthquakes], Tr. Geofiz. inst. AN SSSR, 1953, No. 20.

52. S.I. Golenetskiy and A.A. Treskov, Metod gipotsentraley [The
     Method of Hypocentrals], Tr. Geofiz. inst. AN SSSR, 1952. No. 14.

53. N.A. Vvedenskaya, O tochnosti opredeleniya polozheniya ochaga
     metodom zasechek [Precision of Focus-Position Determination by
     Intersect Method], Tr. Geofiz. inst. AN SSSR, 1955, No. 30.

54. V.S. Nenilina and Ye.F. Savarenskiy, Ob uchete geologicheskikh
     neodnorodnostey pri opredelenii polozheniya ochaga zemletryaseniya
     [On Allowance for Geological Nonuniformities in Determining the
     Positions of Earthquake Foci], Izv. AN SSSR, seriya geofiz., 1955,
     No. 1.

55. S.S. Andreyev, Metod izopoverkhnostey pri interpretatsii mestnykh
     zemletryaseni y [Isosurface Method in Interpretation of Local
     Earthquakes], Izv. AN SSSR ser. geofiz., 1954, No. 2.

56. B.B. Golitsyn, O zemletryasenii 18.2.1911 g. [On the Earthquake
     of 18 February 1911], Izv. Ross. AN [Bulletin of the Russian
     Academy of Sciences], 9, 1915.

57. H. Jeffreys. The Pamir earthquake of 1911, February 18, in rela-
     tion to the depths of earthquake foci. "Mon. Not. Roy. Astron.
     Soc., Geophys. Suppl.", 1, 2, 1923.

58. K. Sagisaka. On the energy of Earthquake. "Trans. Am. Geoph.
     Union", 36, No. 5, 1955.

59. I. Linch. The energy of local earthquakes recorded at Fordham.
     "Bull. Seism. Soc. Am.", 30, No. 4, 1940.

60. S.I. Kosenko, K voprosu o vychislenii energii zemletryaseniya
     [On the Problem of Calculating Earthquake Energies], Tr. Geofiz.

inst. AN SSSR, 1953, No. 21.

61. V.I. Bune, Ob ispol'zovanii metoda Golitsyna dlya priblizhennoy
otsenki energii blizkikh zemletryaseniy [On the Use of the
Golitsyn Method for Approximate Evaluation of the Energies of
Nearby Earthquakes], Tr. AN Tadzh. SSR, 54, 1, 1956.

62. C. Richter. An instrumental earthquake magnitude scale. "Bull.
Seism. Soc. Am.", 25, No. 1, 1935.

63. B. Gutenberg, C. Richter, Earthquake magnitude, intensity,
energy and acceleration, 1. "Bull. Seism. Soc. Am." 32, No. 3,
1942.

64. B. Gutenberg, C. Richter. Seismisity of the Earth and associated
phenomena. Princ. Univ. Press, 1954.

65. B. Gutenberg, C. Richter, B. Benioff. Progress report Seismo-
logical Laboratory Cal. Inst. of Technology, 1954. "Trans. Am.
Geoph. Un.", 36, No. 4, 1955.

66. B. Gutenberg. Amplitudes of surface waves and magnitudes of
shallow earthquakes. "Bull. Seism. Soc. Am.", 35, No. 1, 1945.

67. B. Gutenberg. Amplitudes of P, PP and S and magnitudes of shallow
earthquakes. "Bull. Seism. Soc. Am.", 35, No. 3, 1945.

68. S.L. Solov'yev, Ob energeticheskoy klassifikatsii zemletryaseniy
SSSR [Energy Classification of Earthquakes of the USSR], Disser-
tation, Inst. fiziki Zemli, 1956.

69. S.L Solov'yev, O klassifikatsii zemletryaseniy po velichine ikh
energii [Concerning a Classification of Earthquakes on the Basis
of Energy Magnitude], Tr. Geofiz. inst. AN SSSR, 1955, No. 30.

70. S.L. Solov'yev and N.V. Shebalin, Opredeleniye intensivnosti
zemletryaseniy po smeshcheniyam pochvy v poverkhnostnykh volnakh
[Determination of Earthquake Intensity from Ground Displacements
in Surface Waves], Izv. AN SSSR, seriya geofiz., 1957, No. 7.

71. Yu.V. Riznichenko, O raskhozhedenii i pogloshchenii seysmicheskikh voln [On the Divergence and Absorption of Seismic Waves], Tr. Geofiz. inst. AN SSSR, 1956, No. 35.

72. B.V. Deryagin, Fizika uprugikh voln, in book entitled Prikladnaya geofizika [Applied Geophysics], No. 2, ONTI [State Unified Publishers for Scientific and Technical Literature], 1934.

73. H. Lamb. On the propagation of tremors over the surface of an elastic solid. "Phil. Trans. Roy. Soc., A", 203, No. 1, 1904.

74. I.P. Kosminskaya, Amplitudnyye krivyye i godografy faz seysmicheskikh voln na svobodnoy granitse poluprostranstva [Amplitude Curves and Phase Hodographs of Seismic Waves on the Free Boundary of a Half-Space], Izv. AN SSSR, seriya geofiz., 1956, No. 1.

75. I.S. Berzon, Ob opredelenii pokazatelya stepeni funktsiy raskhozhdeniya dlya prelomlennykh voln po eksperimental'nym dannym [On Determination of the Divergence-Function Exponents for Refracted Waves from Experimental Data], Izv. AN SSSR, seriya geofiz., 1951, No. 4.

76. Ye.V. Karus, Pogloshcheniye uprugikh.kolebaniy v gornykh porodakh pri statsionarnom vozbuzhdenii [Absorption of Elastic Vibrations in Rocks with a Steady Disturbance], Izv. AN SSSR, seriya geofiz., 1958, No. 4.

77. B.B. Golitsyn, O zatukhanii i dispersii seysmicheskikh voln [On Attenuation and Dispersion of Seismic Waves], Izv. Akademii nauk [Bulletin of the Academy of Sciences], 6, 2, 1919.

78. Ye.F. Savarenskiy and E.A. Dzhibladze, Seysmichnost' Bol'shogo Kavkaza [Seismicity of the Greater Caucasus], Izv. AN SSSR, seriya geofiz., 1956, No. 5.

79. S.L. Solov'yev and E.A. Dzhibladze, Ob izmenenii potoka seysmicheskoy energii s epitsentral'nym rasstoyaniyem [Variation of

Seismic-Energy Flux With Epicentral Distance], Izv. AN SSSR, seriya geofiz., 1955, No. 5.

80. G.I. Petrashen', Rasprostraneniye uprugikh voln v sloisto-izotropnykh sredakh razdelennykh parallel'nymi ploskostyami [Propagation of Elastic Waves in Stratified-Isotropic Media Separated by Parallel Planes], Uchen. zap. LGU [Scientific Reports of Leningrad State University], 162, 26, 1956.

81. G.I. Petrashen' (Editor) et al., Materialy kolichestvennogo izucheniya dinamiki seysmicheskikh voln [Data on Quantitative Study of Seismic-Wave Dynamics], Vols. 1 and 2, Izd-vo LGU [Leningrad State University Press], 1957.

82. G.A. Gamburtsev, O vysokochastotnoy seysmometrii [High-Frequency Seismometry], Dokl. AN SSSR, 88, No. 5, 1953.

83. I.P. Pasechnik, K izucheniyu seysmichnosti Khaitskoy epitsen-tral'noy zony [Contribution to Study of the Seismicity of the Khaytsk Epicentral Zone], Izv. AN SSSR, seriya geofiz., 1956, No. 12.

84. L.L. Khudzinskiy and A.Ya. Melamud, Stantsiya chastotnogo analiza seysmicheskikh kolebaniy [Station for Frequency Analysis of Seismic Vibrations], Izv. AN SSSR, seriya geofiz., 1957, No. 9.

85. A.Uorsing and Dzh. Geffner, Metody obrabotki eksperimental'nykh dannykh [Methods for Evaluating Experimental Data], Chapter 13, IL, 1953.

86. Ye.F. Savarenskiy and D.P. Kirnos, Elementy seysmologii i seysmometrii [Elements of Seismology and Seismometry], Part I, 1955.

87. A.Z. Kats, K voprosu ob uchete gruntovykh usloviy pri mikro-seysmorayonirovanii [On the Problem of Correcting for Ground Conditions in Microseismic Districting], Tr. Geofiz. inst. AN

SSSR, 1955, No. 30.

88. O.D. Gotsadze, V.I. Keylis-Bcrok, I.V. Kirillova, S.D. Kogan,
T.I. Kikhtikova, L.N. Malinovskaya and A.A. Sorᵉkiy, Issledovaniye
mekhanizma zemletryaseniy [Investigation of Earthquake Mechanism],
Tr. Geofiz. inst. AN SSSR, 1957, No. 40.

89. V.I. Keylis-Borok, K voprosu ob issledovanii istochnikov,
ekvivalentnykh ochagam zemletryaseniy [On the Problem of Inves-
tigating Sources Equivalent to Earthquake Foci], Trudy Geofiz.
inst. AN SSSR, 1950, No. 9.

90. K.I. Ogurtsov, I.N. Uspenskiy and N.I. Yermilova, Nekotoryye
kolichestvennyye issledovaniya po rasprostraneniyu voln v
prosteyshikh uprugikh sredakh [Certain Quantitative Investiga-
tions of Wave Propagation in Elementary Elastic Media], Vopr.
dinam. teorii rasprostraneniya seysmicheskikh voln [Problems of
the Dynamic Theory of Seismic-Wave Propagation], Gostekhizdat
[State United Publishers for Technical and Theoretical Litera-
ture], 1957.

91. I.S. Berson, Godografy mnogokratno-otrazhennykh, otrazhenno-
prelomlennykh i prelomlenno-otrazhennykh voln [Hodographs of
Multiple-Reflected, Reflected-Refracted and Refracted-Reflected
Waves], Izv. AN SSSR, seriya geofiz. i. geogr., 1942, No. 6.

92. A.M. Yepinat'yeva, Nekotoryye tipy mnogokratnykh seysmicheskikh
voln [Certain Types of Multiple Seismic Waves], Izv. AN SSSR,
seriya geofiz., 1956, No. 1.

93. N.V. Zvolinskiy, Mnogokratnyye otrazheniya uprugikh voln v sloye
[Multiple Reflection of Elastic Waves in a Layer], Tr. Geofiz.
inst AN SSSR, 1954, No. 22.

94. Yu.V. Riznichenko, O rasseyannykh otrazhenno-prelomlennykh seys-
micheskikh volnakh [On the Scattering of Reflected-Refracted

Seismic Waves], Dokl. AN SSSR, 126, No. 4, 1959.

95. A.M. Yepinat'yeva, O summarnykh mnogokratnykh otrazhennykh
     volnakh [Resultant Multiple-Reflected Waves], Izv. AN SSSR, ser.
     geofiz., 1959, No. 8.

96. B. Gutenberg, C. Richter. Earthquake magnitude, intensity,
     energy and acceleration, II. Bull. Seism. Soc. Am., 46, No. 2,
     1956.

97. T. Tsuya (edit.). The Fukui earthquake of June 28, 1948. Report
     of the special committee, Tokyo, 1950.

98. I.S. Berzon, Ob izmenenii preobladayushchikh chastot seysmiches-
     kikh voln pri uvelichenii rasstoyaniya ot istochnika kolebaniy
     [On the Variation of Predominating Frequencies in Seismic Waves
     With Increasing Distance From the Source of Vibration], Izv. AN
     SSSR, seriya geofiz., 1956, No. 1.

99. O. Ferch and G. Shul'tse, Rasprostraneniye voln i eksperimental'-
     naya seysmika [Wave Propagation and Experimental Seismics],
     in collection entitled Voprosy seysmicheskoy razvedki [Problems
     of Seismic Prospecting], IL [Foreign Literature Press], 1953.

100. F. Evison, Novyye dannyye o rasprostranenii uprugikh voln v
     gornykh porodakh [New Data on the Propagation of Elastic Waves
     in Rocks], in collection entitled Voprosy seysmicheskoy razvedki
     [Problems of Seismic Prospecting], IL, 1953.

101. W. Regula. Untersuchungen elastischer Eigenschaften an Gesteins-
     staeben [Investigations of Elastic Properties in Rock Rods],
     Z. Geophys. [J. Geophys], 16, 1940.

102. B. Gutenberg, Vyazkost', prochnost', i vnutrenneye treniye v
     nedrakh zemli [Viscosity, Strength, and Internal Friction in
     the Interior of the Earth], in collection entitled Vnutrenneye
     stroyeniye zemli [Internal Structure of the Earth], IL, 1949.

103. F. Birch, D. Bancroft. Elasticity and internal friction in a long column of granite. Bull. Seism. Soc. Am., 28. 1938.

104. F. Berch, Dzh. Sherer and G. Speyser, Spravochnik dlya geologov po fizicheskim konstantam [Physical Constants Handbook for Geologists], Chapter 6, IL, 1949.

105. S.D. Vinogradov, M.S. Antsyferov and I.L. Nersesov, O zatuk-hanii seysmicheskikh voln pri mestnykh zemletryaseniyakh [On Attenuation of Seismic Waves in Local Earthquakes], Tr. AN Tadzh. SSR [Transactions of the Academy of Sciences Tadzhik SSR], 54, 1, 1956.

106. N.V. Shebalin, O svyazi mezhdu energiyey, ball'nost'yu, i glubinoy ochaga zemletryaseniya [On the Relationship Between Energy, Point Count, and Focus Depth of Earthquakes], Izv. AN SSSR, seriya geofiz. [Bulletin of the Academy of Sciences USSR, Geophysics Series], 1955, No. 4.

107. V.I. Bune, Sravnitel'no energeticheskaya kharakteristika seys-michnosti trekh rayonov Tadzhikistana [Energy-Comparison Charac-terization of Seismicity in Three Districts of Tadzhikistan], Dokl. AN Tadzh. SSR [Proceedings of the Academy of Sciences Tadzhik SSR], 19, 1956.

108. B. Gutenberg, C. Richter. Magnitude and energy of earthquakes. Ann. di Geofisica, 9, No. 1, 1956.

109. J. De Noyer. The energy of seismic waves. Bull. Seism. Soc. Am., 49, No. 1, 1959.

110. K. Bullen. On the size of the strained region prior to an ex-treme earthquake. Bull. Seism. Soc. Am., 45, 1955.

111. C. Tsuboi, Isostasy and maximum earthquake energy. Proc. Imp. Acad. Jap., 1940, No. 16.

112. G.P. Gorshkov, Zemletryaseniya Turkmenii [Earthquakes of Turk-

menia], Tr. Seysmol. inst. AN SSSR [Transactions of the Seismology Institute Academy of Sciences USSR], 1947. No. 122.

113. Yu.V. Riznichenko, O seysmicheskikh kvazianizotropii [Seismic Quasi-Anisotropies], Izv. An SSSR, seriya geofiz. [Bulletin of the Academy of Sciences USSR, Geophysics Series], 1949, No. 6.

114. L.M. Brekhovskikh, Volny v sloistykh sredakh [Waves in Stratified Media], Chapter 1, §6, Izd-vo AN SSSR [Academy of Sciences USSR Press], 1957.

115. L.V. Sorokin, Gravimetriya i gravimetricheskaya razvedka [Gravimetry and Gravimetric Prospecting], Gostoptekhizdat [State Scientific and Technical Publishers for the Petroleum and Mineral-Fuel Industry], 1953.

116. N.V. Shebalin, Sootncsheniye mezhdu ball'nost'yu i intensivnost'yu zemletryaseniy v zavisimosti ot glubiny ochaga [Relationship Between Point Count and Intensity of Earthquakes as Functions of Depth of Focus], Byull. Soveta po seysm. [Bulletin of the Council on Seismology], 1957, No. 6.

117. G.I. Gurevich, O dline i forme volny, voznikayushchey pri razryve [On the Length and Shape of Waves Formed on Fracture], Izv. AN SSSR, seriya geofiz., 1956, No. 3.

118. K.F. Savarenskiy, Seysmichnosti SSSR [Seismicity of the USSR], Tr. Geofiz. inst. AN SSSR [Transactions of the Geophysics Institute Academy of Sciences USSR], No. 25 (152), 1954.

119. K. Kanai, K. Osada, Sg. Yoshizawa. The relation between amplitude and the period of earthquake motion. Bull. Earth. Res. Inst., 1952, No. 31.

120. G.A. Gamburtsev, O novykh metodakh seysmicheskikh issledovaniy [New Methods of Seismic Research], Izv. AN SSSR, seriya geofiz., 1957, No. 12.

121. G.W. Housner, Properties of strong ground motion earthquakes. Bull. Seism. Soc. Am, 44, 1954.

122. H. Benioff. Mechanism and strain characteristics of White Wolf fault as indicated by aftershock sequence, Kern County. Cal., Earthquake of 1952, Bull. No. 171 Cal. Div. of Mines, 1954.

123. C. Tsuboi. Earthquake energy volume, aftershock area and strength of the Earth's crust. Journ. of Physics of the Earth, 4, No. 2, 1956.

124. J. Knopoff. Energy release in earthquake. Report to the eleventh assembly of the International Geophysical Union. Toronto, 1957.

125. A.M. Lopshits, Shablony dlya garmonicheskogo analiza [Patterns for Harmonic Analysis], Gostekhizdat [State Publishing House for Technical and Theoretical Literature], Moscow, 1945.

126. D. Skarboro, Chislennyye metody matematicheskogo analiza [Numerical Methods of Mathematical Analysis], Moscow, 1934.

127. B.F. Bonchkovskiy, Mikroseysmy i ikh prichiny [Microseisms and Their Causes], Tr. Seysmol. inst. AN SSSR, 1946, No. 120.

128. Ye.M. Butovskaya, Osobennosti zapisey Sredneaziatskikh zemletryaseniy [Peculiarities in Traces of Central Asian Earthquakes], dissertation, Geophysics Institute Academy of Sciences USSR, 1950.

129. Ye.M. Butovskaya and I.Ch. Gross, Chastotnyy analiz seysmicheskikh voln [Frequency Analysis of Seismic Waves], in collection entitled Gidrologiya i meteorologiya v Uzbekistane [Hydrology and Meteorology in Uzbekistan], Tashkent, 1955.

130. E. Uittekɪr and G. Robinson, Matematicheskaya obrabotka rezul'tatov nablyudeniy [Mathematical Evaluation of Observational Results], Gostekhizdat, 1933.

131. M.I. Rodman, Avtomaticheskiy analizator dlya zvukovykh chastot

[An Automatic Analyzer for Audible Frequencies]. Zhurn. tekhn. fiz. [Journal of Technical Physics], 5, No. 2, 1935.

132. K. Aki. Correlograms analyses of seismograms by means of a simple automatic computer, Journ. Phys. of the Earth, 4. No. 2, 1956.

133. G.V. Bereza, A.I. Slutskovskiy and M.K. Polshkov, Chastotnyy analiz seysmicheskikh kolebaniy [Frequency Analysis of Seismic Vibrations], in collection entitled Prikladnaya geofizika [Applied Geophysics], No. 11. Gostoptekhizdat, 1951.

134. V.S. Voyutskiy and A.I. Slutskovskiy, Chastotnyy analiz seysmicheskikh kolebaniy [Frequency Analysis of Seismic Vibrations], in collection entitled Prikladnaya geofizika [Applied Geophysics], No. 8. Gostoptekhizdat, 1951.

135. O.G. Shamina, Chastotnyy analiz seysmicheskikh kolebaniy [Frequency Analysis of Seismic Vibrations], Izv. AN SSSR, seriya geofiz. [Bulletin of the Academy of Sciences USSR, Geophysics Series], 1956, No. 8.

136. A.A. Karkevich, Spektry i analiz [Spectra and Analysis], Gostekhizdat, 1956.

137. V.I. Keylis-Borok, Interferentsionnyye seysmicheskiye volny v sloistoy srede [Interference Seismic Waves in a Stratified Medium], dissertation, Geophysics Institute Academy of Sciences USSR, 1951.

138. V.M. Arkhangel'skaya, Rezul'taty issledovaniya poverkhnostnykh voln [Results of Investigation of Surface Waves], dissertation, Geophysics Institute Academy of Sciences USSR, 1953.

139. G.A. Gamburtsev, O volnakh, vyzvannykh dvizhushchimsya istochnikom v tverdoy uprugoy srede [On Waves Produced by a Moving Source in a Solid Elastic Medium], Izv. AN SSSR, seriya geogr. i geofiz.

[Bulletin of the Academy of Sciences USSR, Geography and
Geophysics Series], 1946, No. 1.

140. G.S. Gorelik, Kolebaniya i volny [Vibrations and Waves], Gostekhiz-
      dat, 1950.

141. D.P. Kirnos, O vozmozhnosti vozniknoveniya sobstvennykh kolebaniy
      allyuvial'nogo sloya [On the Possibility of Appearance of Natural
      Vibrations in an Alluvial Layer], Tr. Seysmol. inst. AN SSSR,
      1945, No. 117.

142. Y. Tomoda. A simple method for calculating the correlation co-
      efficient. Journ. Phys. of the Earth, 4, 1956.

143. H. Honda, H. Ito. On the period of the P-waves and the magnitude
      of the earthquakes. Geoph. mag., XIII, No. 2, Tokyo, 1939.

144. S.V. Medvedev, Zavisimost' seysmicheskikh vozdeystviy ot periodov
      sobstvennykh kolebaniy zdaniy [Seismic Effects as Functions of
      the Natural Oscillation Periods of Buildings], Tr. Geofiz. inst.
      AN SSSR, No. 36 (163), 1956.

145. P. Byerly. The period of local earthquake waves in Central
      California. Bull. Seism. Soc. Am., 27, 1937.

146. A. Jones. The empirical studies of the seismic phenomena of
      Hawaii. Bull. Seism. Soc. Am., 28, 1938.

147. United States Earthquakes, 1951, USCGS, ser. No. 762, Washington,
      1953.

148. United States Earthquakes, 1953, USCGS, ser. No. 785, Washington,
      1955.

149. United States Earthquakes, 1954, USCGS, ser. No. 795, Washington,
      1956.

150. K.K. Zapol'skiy, Apparatura i metodika issledovaniya fizicheskikh
      kharakteristik seysmicheskikh voln v real'nykh sredakh [Apparatus
      and Technique for Investigating Physical Characteristics of

Seismic Waves in Real Media], dissertation, Institute of Earth
Physics, 1952.

151. United States Earthquakes, 1952, USCGS. Ser. No. 773. Washington.
1954.

152. V.I. Bune, O klassifikatsii zemletryaseniy po ikh sile na osnove
instrumental'nykh nablyudeniy [On a Force Classification of
Earthquakes Based on Instrumental Observations], Izv. AN SSSR.
seriya geofiz., 1956, No. 1.

153. D. Tocher. Earthquake energy and ground breakage. Bull. Seism.
Soc. Am., 48, No. 2, 1958.

154. N.A. Florensov, Katastroficheskoye zemletryaseniye v Gobiyskom
Altaye [Catastrophic Earthquake in the Gobi Altay], Priroda
[Nature], 1958, No. 7.

155. P. Bayyerli, report to the eleventh assembly of the International
Geophysical and Geodetic Union, Toronto, 1957.

156. G. Neyber, Kontsentratsiya napryazheniy [Stress Concentration],
GTI [State Technical Publications], Moscow, 1947.

157. A. Starr, Slip in a crystal and rupture in a solid due to shear.
Proc. Roy. Soc.

158. M.V. Gzovskiy, Tektonofizicheskoye obosnovaniye geologicheskikh
kriteriyev seysmichnosti [Tectonophysical Justification for
Geological Seismicity Criteria], Izv AN SSSR, seriya geofiz.,
1957, Nos. 2, 3.

159. M. Bath, H. Benioff. The aftershock sequence of the Kamchatka
earthquake of November 4, 1952. Bull. Seism. Soc. Am., 48, 1958.

160. C. Tsuboi. Notes on the mechanical strength of the Earth's crust.
Bull. Earthq. Res. Inst., Tokyo, 1933, No. 11.

161. D. Shimozuru. Elasticity of Rocks under the initial stresses with
special reference to the fracture problem. Bull. Earthq. Res.

Inst., 33, 1955.

162. O.G. Shamina, Uprugiye impul'sy pri razrushenii gornykh porod [Elastic Impulses in Fracture of Rock], Izv. AN SSSR. seriya geofiz., 1956, No. 5.

163. Yu.V. Riznichenko, O.I. Silayeva et al., Seysmoakusticheskiye metody izucheniya napryazhennogo sostoyaniya gornykh porod na obraztsakh i v massive [Seismoacoustic Methods for Study of Stressed State of Rocks in Specimens and in the Massif], Tr. Geofiz. inst. AN SSSR, 1956, No. 34.

164. S.D. Vinogradov, Akusticheskiye nablyudeniya v shakhtakh Kizilovskogo basseyna [Acoustical Observations in Shafts in the Kizilovskiy basin], Izv. AN SSSR, seriya geofiz., 1957, No. 6.

165. J.A. Sharpe. The production of elastic waves by explosion pressure. Geophysics, 1, No. 2-3, 1942.

166. G.I. Gurevich, Nekotoryye zadachi mekhaniki deformiruyemogo tela [Certain Problems in the Mechanics of the Deformable Solid], Tr. Geofiz. inst. AN SSSR, 1955, No. 31.

167. V.I. Keylis - Borok, O dinamicheskoy kharakteristike ochaga po seysmicheskim nablyudeniyam [Dynamic Characterization of the Focus on the Basis of Seismic Observations], Dokl. AN SSSR [Proceedings of the Academy of Sciences USSR], 70. No. 6, 1950.

168. L.N. Malinovskaya, Metodika opredeleniya mekhanizma zemletryaseniy [Method for Determining Earthquake Mechanism], Tr. Geofiz. inst. AN SSSR, No. 22 (149) 1954.

169. T.I. Kukhtikova, K voprosu o sopostavlenii seysmicheskikh i geologicheskikh dannyeh [On the Problem of Comparison of Seismic and Geological Data], Tr. Inst. seysmologii AN Tadzh. SSR [Transactions of the Seismology Institute, Academy of Sciences Tadzhik SSR], 71, collection II, 1957.

170. G. Kramer, Matematicheskiye metody statistiki [Mathematical Methods of Statistics], IL, Moscow, 1948.

171. Yu.V. Riznichenko, Ob izuchenii seysmicheskogo rezhima [On Study of the Seismic Regime], Izv. AN SSSR, seriya geofiz., 1958. No. 9.

172. M.W. Allen. The lunar triggering effect on earthquakes in Southern California. Bull. Seism. Soc. Am., 26, 1936.

173. C. Davison. The lunar periodicity of earthquakes. Phil. Mfg., 7, 17, 1934, 737-752.

174. A. Schuster. On lunar and solar periodicities of earthquakes. Proc. Roy. Soc., 61, 1897, 455-465.

175. S. Nakamura. Barometric and tidal effects on the occurrence of earthquakes in Kwanto district I. Jap. Journ. of Astro-Geophys., 3, 1925, 115-140.

176. S. Nakamura. Barometric and tidal effects on the occurrence of earthquakes in Kwanto district, II. Jap. Journ. of Astro-Geophys., 4, 1927, 139-165.

177. T. Matusawa, N. Nakamaty, Y. Nisikawa, Y. Yosimura, Ueber die Jahresschwankung der Erdbebenhaeufigkeit in Japan [Concerning the Annual Variation of Earthquake Frequency in Japan], Bull. Earthq. Res. Inst., Tokyo Univ., 15, 1937, 711-674.

178. E. Wanner, Zur Statistic der Erdbeben [On Earthquake Statistics]. Gerl. Beitr. Geophys. [Gerl. Contributions to Geophysics], 50, 1, 85-99, 2, 223-228, 1937.

179. V. Conrad. Die zeitliche Folge der Erdbeben und bebensausloesend Ursachen [Time Sequence of Earthquakes and Earthquake-Triggering Factors], Handbuch der Geophysik [Handbook of Geophysics], IV, 1019-1040, 1932.

180. C. Davison. Studies on the periodicity of earthquakes. London, 1938.

181. H.H. Turner. Note on the periodogram of earthquake frequency from seven years to twenty years. Brit. Assoc. Rep., Portsmouth, 1911, 332-335.

182. S. Mohorovicic. Die zwei und ein halb Jahrhundert lange Periode der Erdbeben und Klimatschwankungen [Two and a Half Centuries of Earthquakes and Climatic Fluctuations], Meteorolog. Zeitschr. [Meteorological Journal], 1921, 373-375.

183. H.H. Turner. Note on the 284-year cycle in Chinese earthquakes. Month. Not. Roy. Astr. Soc., Geophys. suppl, 1.

184. T. Terada. On the frequency of earthquakes and allied phenomenr. Proc. Tokyo Math.-Phys. Soc., 9, 1918, 515-522.

185. B. Gutenberg. Frequency of earthquakes in California. Bull. Seismol. Soc. Am., 34, 1944, 185-188.

186. B. Gutenberg and K. Rikhter, Seysmichnost' Zemli [Seismicity of the Earth], IL, Moscow, 1948.

187. T.I. Kukhtikova, V.N. Gayskiy and V.I. Bune, O seysmichnosti Tadzhikistana v 1955 g [The Seismicity of Tadzhikistan in 1955], Tr. Inst. seysmologii AN Tadzh. SSR, 41, No. II, 1957.

188. H. Benioff. Earthquake and rock creep. Bull. Seism. Soc. Am., 4, No. 1, 1951.

189. H. Benioff. Crystal strain characteristics derived from earthquake sequences. Trans. Amer. Geoph. Union, 32, No. 4, 1951, 508-514.

190. H. Benioff. Relation of the White Wolf fault to the regional tectonic pattern, Earthquakes in Kern County, California, during 1952. Bull. No. 171, Cal. Div. of Mines, 1955, 203-204.

191. H. Benioff. Global strain accumulation and release as revealed by great earthquakes. Bull. Geol. Soc. Am., 62, 1951, 331-338.

192. H. Benioff. Seismic evidence for crystal structure and tectonic activity. The crust of the earth. Geol. Soc. Amer., Special

Paper 62, 1945, 61-74.

193. H. Kawasumi. On the energy law of occurrence of Japanese earthquakes. Bull. Earthq. Res. Inst. Tokyo Univ., 30, No. 4. 1952. 319-323.

194. H. Kawasumi. Energy law of earthquake occurrence in the vicinity of Tokyo. Bull. Earthq. Res. Inst. Tokyo Univ., 30, No. 4. 1952, 325-329.

195. C. Tsuboi. Magnitude-frequency relation for earthquakes in and near Japan. Journ. Phys. of the Earth, 1, 47, 1952.

196. Z. Suzuki. A statistical study of the occurrence of small earthquakes. Science Rep. Tohoku Univ. ser. Geophys, 5, 1953.

197. C. Tsuboi. Energy accounts of earthquakes in and near Japan. Journ. Phys. of the Earth., 5, No. 1, 1957, 1-7.

198. V.I. Bune, Opyt ispol'zovaniya energicheskikh kharakteristik pri izuchenii seysmichnosti Tadzhikistana [Experience in the Use of Energy Characteristics in Study of the Seismicity of Tadzhikistan]. Izv. otd. yestestv. nauk AN Tadzh. SSR [Bulletin of the Natural Sciences Division of the Academy of Sciences Tadzhik SSR], No. 23, 1957.

199. A.D. Tskhakaya, Rezul'taty nablyudeniy Kavkazkoy seysmicheskoy ekspeditsii [Results of Observations of the Caucasus Seismic Expedition], Kvartal'nyy seysmich. byulleten' [Quarterly Seismic Bulletin], XIII, 1940, Tbilisi (Tiflis), 1947.

200. S.I. Masarskiy, Epitsentral'naya zona povtornykh tolchkov Ashkhabadskogo zemletryaseniya [Epicentral Aftershock Zone of the Ashkhabad Earthquake], Dokl. AN SSSR [Proceedings of the Academy of Sciences USSR], 74, No. 3, 1950.

201. A.S. Andreyev, S.I. Masarskiy, D.N. Rustanovich and D.A. Kharan, Issledovaniye slabykh zemletryaseniy yugo-zapadnoy Turkmenii

[Investigation of Weak Earthquakes in Southwestern Turkmenia].
Izv. AN SSSR, seriya geofiz., 1954, No. 2.

202. D.N. Rustanovich, Predvaritel'nyye rezul'taty instrumental'nogo izucheniya seysmichnosti zony Krasnopolyanskikh zemletryaseniy [Preliminary Results of Experimental Study of Seismicity in the Krasnopolyanskiy Earthquake Zone], Byull. Soveta po seysmol. [Bulletin of the Council on Seismology], 1958, No. 5.

203. N.A. Vvedenskaya and A.A. Fogel, O karte epitsentrov Severnogo Tyan' Shanya [The Epicenter Map of Northern Tyan'-Shan'], Byulleten' Soveta po seysmol., 1957, No. 3.

204. K. Aki. Quantitative prediction of earthquake. occurrence as stochastic phenomena, Journ. Physics of Earth, 2, No. 2, 1954, 63-69.

205. F. Kishinouye. Frequency distribution of the Ito earthquake swarm of 1930. Bull. Earthq. Res. Inst. Tokyo Univ., 15, 1937, 785-827.

206. H. Jeffreys. Aftershocks and periodicity of earthquakes, Gerl. Beitr. Geophys., 53, 1938, 111-139.

207. T. Nagiwara, K. Kasahara. On aftershocks accompanied the Imaichi earthquake Dec. 26, 1946. Bull. Earthq. Res. Inst. Tokyo Univ., 28, 1950, 393-412.

208. C.G. Richter. Foreshocks and aftershocks, Earthquakes in Kern County, California during 1952. Bull. 171, Cal. Divis. of Mines, 1955, 177-197.

209. K. Aki. Some problems in statistical seismology. Bull. Earthq. Res. Inst. Tokyo Univ., 8, No. 4, 1956, 205-228.

210. G.A. Gamburtsev, O korrelyatsionnykh metodakh izucheniya zemletryaseniy [Correlation Methods for Study of Earthquakes], Dokl. AN SSSR, 92, No. 4, 1953.

211. Ye.I. Gal'perin, Azimutal'nyy metod seysmicheskikh nablyudeniy [Azimuthal Method for Seismic Observations], Gostoptekhizdat. Moscow, 1955.

212. G.A. Gamburtsev, O novykh metodakh i apparature pri registratsii seysmicheskikh yavleniy [New Methods and Apparatus for Registration of Seismic Phenomena], Tr. Geofiz. Inst. AN SSSR, 1954, No. 25.

213. J.V. Riznichenko. On qualitative determination and mapping of seismic activity. Annali di Geofisica [Annals of Geophysics], XII, No. 2, 1959.

214. Yu.V. Riznichenko and I.L. Nersesov, K razrabotke osnov kolichestvennogo metoda seysmicheskogo rayonirovaniya [On Elaboration of Foundations for a Quantitative Method of Seismic Districting], Byull Soveta po seysmol. AN SSSR, 1959, No. 8.

215. Yu.V. Riznichenko and I.L. Nersesov, Povtoryayemost' zemletryaseniy i karty seysmicheskoy aktivnosti [Reproducibility of Earthquakes and Seismic-Activity Maps], Seysmich. i glyatsiol. issledov. v period MGG [Seismic and Glaciological Research During the Period of the International Geophysical Year], Izd. AN SSSR, Moscow, 1959.

216. M.V. Gzovskiy, V.N. Krestnikov, I.L. Nersesov and G.I. Reysner, Sopostavleniye tektoniki s seysmichnost'yu Garmskogo rayona Tadzhikskoy SSR [Comparison of Tectonics With Seismicity in the Garm Region of the Tadzhik SSR], Izv. AN SSSR, seriya geofiz., 1958, No. 8, 12.

217. M. Bath. Seismicity of Fennoscandia and related problems. Gerl. Beitr. z. Geophys., 63, 3, 1953.

218. S. Sponheuer, Erdbeben und Tektonic in Deutschland [Earthquakes and Tectonics in Germany], Forschungshefte [Research Notes],

7c, 1953.

219. M. Toperczer. Zur Definition der Seismizitaet [On the Definition
of Seismicity], Arch. Meteorol., Geophys. und Bioklimatol.
[Archives of Meteorology, Geophysics and Bioclimatology], A.
5, 4, 1953.

220. E. Trapp. Zur praktischen Darstellung der Seismiztaet [On
Practical Representation of Seismicity], Gerl. Beitr. z. Geophys.,
64, 2, 1954.

221. A. R. Ritsema. The seismicity of the Sunda Arc in space and time.
Indonesian Journal for Natural Science, 1954, N 1-3.

222. P.S. Amand. Two proposed measures of seismicity. Bull. Seism.
Soc. Am., 46, No. 1, 1956, 27-45.

223. M. Bath. A note on the measure of seismicity. Bull. Seism.
Soc. Amer., 46, 1956.

224. L.P.G. Koning. Earthquakes in relation to their geographical dis-
tribution, depth and magnitude. Proc. Kon. Nederl. Akad. Wer.,
55, 1952.

225. I.V. Dunin-Barkovskiy and N.V. Smirnov, Teoriya veroyatnostey
i matematicheskaya statistika v tekhnike [Probability Theory and
Mathematical Statistics in Engineering], Gostekhizdat, Moscow,
1955.

226. A. Khal'd, Matematicheskaya statistika s tekhnicheskimi prilozh-
eniyami [Mathematical Statistics with Technical Applications], IL,
Moscow, 1956.

227. Ye.A. Rozova, Raspolozheniye epitsentrov i gipotsentrov Sredney
Azii [Distribution of Epicenters and Hypocenters of Central Asia],
Tr. Geofiz. inst. AN SSSR, 1950, No. 10.

228. V.I. Popov, Istoriya depressiy i podnyatiy Zapadnogo Tyan'-Shanya
[History of Depressions and Elevations of Western Tyan'-Shan'],

Tashkent, 1938.

229. A.P. Markovskiy, O vzaimootnoshenii Pamira i Tyan'-Shanya [Inter-
     relationship Between Pamir and Tyan'-Shan'], Nauchnyye itogi TPE
     [Scientific Progress of the Tadzhikistan-Pamir Expedition], 1936.

230. A.P. Rezvoy, O nekotorykh mclodykh podnyatiyakh Yuzhnoy Fergany
     [On Certain Young Elevations of Southern Fergana], Tr. Mosk.
     geol.-razv. inst. [Transactions of Moscow Geological-Survey
     Institute], 26, 1954.

231. S.K. Ovchinnikov, Novyye danyye po geologii yuzhnogo sklona
     Gissarskogo khrebta [New Data on the Geology of the Southern
     Slope of the Gissarskiy Range], Izv. Tadzh. FAN SSSR [Bulletin
     of the Tadzhik Branch of the Academy of Sciences USSR], 1946,
     No. 11.

232. V.N. Krestnikov, Istoriya razvitiya paleozoyskoy geosinklinal'noy
     oblasti Pamira i prilegayushchikh chastey Azii [History of
     Development of the Paleozoic Geosynclinal Region of Pamir and
     Contiguous Parts of Asia], Izv. Vyssh. uchebn. zaved., Geologiya
     i Razvedka [Bulletin of the Higher Educational Institutions.
     Geology and Prospecting], 1959, Nos. 4-7.

233. I.Ye. Gubin, Geologicheskaya granitsa mezhdu Pamirom i Alayem
     [The Geological Boundary Between Pamir and Alay], Gosgeolizdat
     [State Publishing House for Literature on Geology], 1940.

234. I.Ye. Gubin, Pamir i sopredel'nyye strany [Pamir and Areas
     Bordering on it], Izv. Tadzh. FAN SSSR, 1943, No. 2.

235. I.Ye. Gubin, O glubinnom geologicheskom stroyenii territorii
     Garmskoy oblasti [On the Deep Geological Structure of the Terri-
     tory in the Garm Region], Byull. MOIP, otd. geol. [Bull. Moscow
     Soc. Naturalists, Geology Div.], No. 30 (4), 1955.

236. M.M. Kukhtikov, O tak nazyvayemoy geologicheskoy granitse mezhdu

Pamirom i Alayem-Tyan'-Shanem [On the So-Called Geological
Boundary Between Pamir and Alay/Tyan'-Shan']. Uch. zapiski TGU.
tr. fak-ta estestvennykh nauk [Scientific Reports of Tbilisi
State University, Transactions of the Natural Sciences Faculty].
IV, No. 1, 1955.

237.   M.M. Kukhtikov, Krayevyye razlomy Pamira i Darvaza [Boundary
       Faults of Pamir and Darvaz], Uch. zapiski TGU, tr. fak-ta
       yestestvennykh nauk, XII, No. 2, 1956.

238.   B.A. Petrushevskiy, Uralo-Sibirskaya platforma i Tyan'-Shan'
       [The Uralosiberian Platform and Tyan'-Shan'], Izd-vo AN SSSR,
       1955.

239.   S.N. Simakov, Voprosy stratigrafii paleogena Fergany i Tadzhikskoy
       depressii [Problems of Paleogene Stratigraphy of Fergana and the
       Tadzhik Depression], Tr. VNIGRI, novaya seriya [Trans. All-Union
       Petroleum Scientific-Research Institute for Geological Survey],
       No. 66, 1953.

240.   V.I. Solun, K voprosu o tektonike yuzhnogo Tadzhikistana [On the
       Problem of the Tectonics of Southern Tadzhikistan], Izv. Tadzh.
       FAN SSSR, 1943, No. 2.

241.   Ya. I. Shabalkin and K.N. Paffengol'd. Geologicheskaya karta
       basseyna lednika Fedchenko i r. Tanymas i Balyand-Kiik [Geological
       Map of the Fedchenko Glacial Basin and the Rivers Tanymas and
       Balyand-Kiik], Tr. TPE [Transactions of the Tadzhikistan-Pamir
       Expedition], No. XVI, 1933.

242.   O.S. Vyalov, O vzaimootnoshenii Pamira i Tyan'-Shanya [On the
       Interrelation of Pamir and Tyan'-Shan'], Izv. Tadzh. FAN SSSR,
       1943, No. 2.

243.   A.V. Grigor'yev, O tektonicheskikh strukturakh i osobennostyakh
       geologicheskogo razvitiya Alaya i Pamira [On the Tectonic Struc-

tures and Peculiarities of the Geological Development of Alay
and Pamir], Izv. TFAN SSSR [Bulletin of the Tadzhik Branch
Academy of Sciences USSR], 1946, No. 11.

244. A.P. Markovskiy, O nekotoroy zakonomernosti raspredeleniya
tektonicheskikh elementov Pamiro-Alaya [On a Certair Regularity
in the Distribution of Tectonic Elements in the Pamir-Alay
Region], Tr. TKE [Unidentified Transactions], No. IV, 1932.

245. R. Klebelsberg. Beitrage zur Geologie Westturkestans [Contribu-
tions to the Geology of Western Turkestan], Innsbruck, 1922.

246. S.A. Zakharov, Raspredeleniye po vertikali tektonicheskikh
napryazheniy v Tadzhikskoy depressii [Vertical Distribution of
Tectonic Stresses in the Tadzhik Depression], Tr. Inst. geologii
Tadzh. SSR [Transactions of the Geology Institute of the Tadzhik
SSR], 8, No. 1, 1956.

247. N.I. Nikolayev, O novom tektonicheskom etape razvitiya zemnoy
kory [On the Recent Tectonic Stage in Development of the Earth's
Crust], Byull. MOIP, otd. geol., 27, No. 3, 1952.

248. G.I. Reysner, Noveyshiye dvizheniya Alayskoy vpadiny i eye gornogo
obramleniya [Most Recent Movements of the Alay Depression and
its Mountainous Surroundings], Dokl. AN SSSR, 123, No. 6, 1958.

249. S.S. Shults',Analiz noveyshey tektoniki i rel'yef Tyan'-Shanya
[Analysis of Most Recent Tectonics and Relief of Tyan'-Shan'],
Geografizdat [State Publishing House for Literature on Geography],
1948.

250. V.N. Krestnikov, Istoriya razvitiya struktury i seysmichnost'
Tyan'-Shanya [History of Development of Structure and Seismicity
of Tyan'-Shan'], Izv. AN SSSR, seriya geol., 1954, No. 3.

251. M.V. Gzovskiy, Osnovnyye tektonofiziki i tektonika Baydzhanskogo
antiklinoriya [Basic Tectonophysics and Tectonics of the Baydzhan
Anticlinorium], Parts 1 and 2, Izd-vo AN SSSR, 1959.

252. V.V. Belousov, M.V. Gzovskiy and A.V. Goryachev, O strukture vostochnykh Al'p v svyazi s nekotorymi obshchimi tektonicheskimi predstavleniyami [On the Structure of the Eastern Alps as Rel-ted with Certain General Tectonic Conceptions], Byull. MOIP. otd. geol., 26 (1) and (2), 1951.

253. V.V. Belousov, Osnovnyye cherty tektoniki Tsentral'nogo i Yuzhnogo Kitaya [Basic Tectonic Features of Central and Southern China], Izv. AN SSSR, seriya geol., 1956, No. 8.

254. M.V. Gzovskiy, Nekotoryye osobennosti razvitiya kolebatel'nykh dvizheniy v geosinklinalyakh [Certain Peculiarities in the Development of Oscillatory Movements in Geosynclinals], Izv. AN SSSR, seriya geol., No. 6, 1948.

255. S.A. Zakharov, Stratostruktury mezokaynozoya Tadzhikskoy depressii [Stratified Structure of the Mesocenozoic in the Tadzhik Depression], Stalinabad, 1958.

256. M.V. Gzovskiy, Modelirovaniye tektonicheskikh razryvov i poley napryazheniy [Simulation of Tectonic Fractures and Stress Fields], Izv. AN SSSR, seriya geofiz., 1954, No. 6.

257. Seysmicheskiye normy po stroitel'stvu v seymoaktivnykh rayonakh [Seismic Construction Norms in Seismically Active Regions]. (SN-8-57) Moscow, 1957.

258. Atlas seysmichnosti SSSR [Seismicity Atlas of the USSR], Izd-vo AN SSSR, Moscow, 1960.

259. B. Ya. Korol'kov, Karatagskoye zemletryaseniye [The Karatag Earthquake], Izv. Russkogo geograf. ob-va, Turkestanskiy otdel [Bulletin of the Russian Geographic Society, Turkestan Division], Tashkent, 1913.

260. I.G. Gubin and L.B. Vasil'yeva, Seysmotektonicheskiye usloviya Gissarskoy doliny [Seismotectonic Conditions in the Gissar Valley],

Byull. Soveta po seyzmologii, 1956, No. 1.

261. M.V. Gzovskiy, V.N. Krestnikov and G.I. Reysner, Geologicheskiye metody opredeleniya sredney velichiny gradiyenta skorosti vertikal'nykh tektonicheskikh dvizheniy [Geological Methods for Determining Average Magnitude of Velocity Gradient in Vertical Tectonic Movements], Izv. AN SSSR, seriya geofiz., 1959, No. 8.

262. G. Bacsak. Pliozaen und Pleistozaenzeitalter im Licht der Himmelsmechanik [The Pliocene and Pleistocene Epochs in the Light of Celestial Mechanics], Acta Geol. Acad. Scient. Hungarica, 3, 4, 1955.

263. P. Krivan. Die Klimatische Gliederung des Mitteleuropaeischen Pleistozaens [The Climatic Composition of the Central European Pleistocene], Acta Geol. Acad. Scient. Hungarica, 3, 4, 1955.

264. V.V. Belousov and M.V. Gzovskiy, Tektonicheskiye usloviya i mekhanizm vozniknoveniya zemletryaseniy [Tectonic Conditions and Mechanism of Earthquake Genesis]. Tr. Geofiz. inst. AN SSSR, 1954, No. 25.

265. V.N. Krestnikov, Seysmichnost' i geologicheskoye stroyeniye na primere Severnogo Tyan'-Shanya [Seismicity and Geological Structure with Reference to the Example of Northern Tyan'-Shan'], Priroda, 1957, No. 3.

266. V.N. Krestnikov, O svyazi geologicheskikh i seysmicheskikh yavleniy Tyan'-Shanya [On the Relation Between the Geological and Seismic Phenomena of Tyan'-Shan'], Byull. Soveta po seysmologii, 1957, No. 3.

267. B.A. Petrushevskiy, Znacheniye geologicheskikh yavleniy pri seysmicheskom rayonirovanii [Significance of Geological Phenomena in Seismic Districting], Tr. Geofiz. inst. AN SSSR, 1955, No. 28.

268. N.A. Vvedenskaya, Ob ispol'zovanii instrumental'nykh nablyudeniy

nad slabymi zemletryaseniyami pri seysmicheskom rayonirovanii
[On the Exploitation of Instrumental Observations of Weak Earth-
quakes in Seismic Districting], Izv. AN SSSR, seriya geofiz..
1952, No. 2.

269. G.P. Gorshkov, Tektonicheskiye zemletryaseniya i seysmicheskoye
rayonirovaniye territorii SSSR [Tectonic Earthquakes and Seismic
Districting of the Territory of the USSR], dissertation, Insti-
tute of Earth Physics, 1947.

270. G.P. Gorshkov, Zemletryaseniya na territorili SSSR [Earthquakes
on the Territory of the USSR], Geografizdat, Moscow, 1949.

271. M.V. Gzovskiy, V.N. Krestnikov and I.L. Nersesov, Opyt primeneniya
novykh printsipov seysmicheskogo rayonirovaniya na primere basseyna
r. Naryn [Experience in the Application of New Seismic-Districting
Principles on the Example Furnished by the Naryn Basin], Izv.
AN SSSR, seriya geofiz., 1960, No. 2.

272. K.K. Zapol'skiy, Izmereniya urovnya i spektral'nogo sostava
korotkoperiodnykh mikroseysm [Measurements of Level and Spectral
Composition of Short-Period Microseisms], Tr. IFZ AN SSSR, 1960,
No. 10.

Manu- script Page No.	[List of Transliterated Symbols]
427	Стб = Stb = Stalinabad
427	Огр = Obg = Obi-Garm
427	Клб = Klb = Kulyab
427	Грм = Grm = Garm
427	ТД = TD = Tovil'-Dora
427	Ишт = Isht = Ishtion
427	Джаг = Dzhag = Dzhirgatal'
427	кл = kl = klassa = class
440	Хрн = Khrn = Khorongon
440	Чнгр = Chngr = Chuyangaron
440	Гс = Gs = Gissar
440	Кр = Kr = Karasu

DISTRIBUTION LIST

DEPARTMENT OF DEFENSE	Nr. Copies	MAJOR AIR COMMANDS	Nr. Copies
		AFSC	
		SCFDD	1
		ASTIA	25
HEADQUARTERS USAF		TDBTL	5
		TDBDP	5
AFCIN-3D2	1	SSD (SSF)	2
ARL (ARB)	1	ESD (ESY)	1
		RADC (RAY)	1
		AFSWC (SWF)	1
OTHER AGENCIES		AFMTC (MTW)	1
		AEDC (AEY)	1
CIA	1	APGC (PGF)	1
NSA	6		
DIA	9		
AID	2		
OTS	2		
AEC	2		
PWS	1		
NASA	1		
ARMY	3		
NAVY	3		
RAND	1		
SPECTRUM	1		
AFTAC (Dr. Carlson)	60		